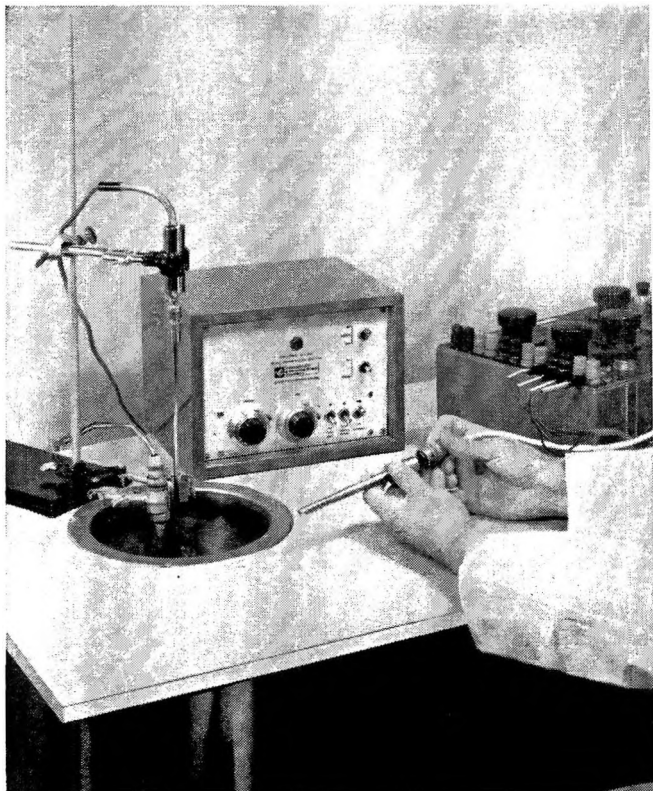


Vapor Pressure of Different Metals in the Pressure Range of 50 to 4000 Torr . . .	J. Bohdanský and H. E. J. Schins	215
Rigorous Least-Squares Estimation of Molecular Complex Equilibria. I. Single Intermolecular Complex Utilizing Spectrophotometric Data	W. E. Wentworth, Walter Hirsch, and Edward Chen	218
Paramagnetic Resonance of Metal Ions and Defect Centers in Topaz . . .	Alan C. Dickinson and Walter J. Moore	231
Polarography in a Binary Salt Solution	Thomas W. Chapman and John Newman	241
Conductance and Water Transfer in a Leached Cation Exchange Membrane	J. H. B. George and R. A. Courant	246
Some Reactions of Oxygen Atoms. II. Ethylene Oxide, Dimethyl Ether, $n\text{-C}_4\text{H}_{10}$, $n\text{-C}_7\text{H}_{16}$, and Isooctane	Grace Marsh and Julian Hecklen	250
The Thermodynamic and Physical Properties of Beryllium Compounds. X. Heats of Formation and Entropies of $\text{BeCl}_2(\text{g})$ and $\text{Be}_2\text{Cl}_4(\text{g})$	H. C. Ko, M. A. Greenbaum, M. Farber, and C. C. Selph	254
Solvent Contribution to the Electromotive Force of Ion-Exchange Membrane Cells Containing Water and Heavy Water Solutions	Jerome Greyson	259
Ion Loss by Diffusion in the Radiolysis of Gases	Cornelius E. Klots and Verner E. Anderson	265
The Electrochemical Oxidation of Arsenic(III). A Consecutive Electron Transfer Reaction . . .	Henry A. Catherino	268
The Current-Impulse Relaxation Technique and the Kinetics of Rapid Electrochemical Reactions. I. General Considerations	W. D. Weir and C. G. Enke	275
The Current-Impulse Relaxation Technique and the Kinetics of Rapid Electrochemical Reactions. II. The Electrochemical Reduction of Mercury(I)	W. D. Weir and C. G. Enke	280
On the Configuration of Polymers at the Solid-Liquid Interface	Gunther Steinberg	292
The Kinetics of the Decarboxylation of n -Hexylmalonic Acid, Cyclohexylmalonic Acid, and Oxamic Acid in Acid Media	Louis Watts Clark	302
Thermodynamics of Aqueous Mixtures of Electrolytes and Nonelectrolytes. I. Ethyl Acetate and Eight 1-1 Alkali Metal Salts at 25°	J. H. Stern and A. Hermann	306
Thermodynamics of Aqueous Mixtures of Electrolytes and Nonelectrolytes. II. Transfer of Nitromethane from Water to Seven 1-1 Chlorides and Perchlorates at 25°	J. H. Stern and A. Hermann	309
Polymer Nuclear Magnetic Resonance Spectroscopy. XII. The Stereoregularity of Polyvinyl Chloride and Its Dependence on Polymerization Temperature	F. A. Bovey, F. P. Hood, E. W. Anderson, and R. L. Kornegay	312
Electrical Conductance of Salts in Liquid Iodine. I. Iodide Donor Solutes	Dorothy J. Bearcroft and Norman H. Nachtrieb	316
Relaxation Spectra of Some Uranyl and Vanadyl Complexes in Aqueous Solution	P. Hurwitz and K. Kustin	324
Oxygen Quenching of Acriflavine Phosphorescence	J. L. Rosenberg and Frederick S. Humphries	330
Electron Paramagnetic Resonance Studies of Vitamin K and Vitamin E Quinones	John M. Fritsch, Shankar V. Tatwawadi, and Ralph N. Adams	338
Infrared Spectra of Carbon Monoxide Adsorbed on Some Evaporated Metal Films	J. F. Harrod, R. W. Roberts, and E. F. Rissmann	343



Rosemount Baths maintain stable temperatures for the most critical calibrations

Rosemount calibration baths are designed to meet some of the toughest temperature calibration requirements ever encountered. Extreme stability and uniformity, wide temperature range, fast temperature change and operating convenience ensure precise sensor calibrations.

There are three variable temperature models and a constant temperature ice bath. A variety of coolants and bath media are used for set points from -250°F to $+750^{\circ}\text{F}$. Calibration zones are large and unobstructed.

Uses include calibration of temperature sensors, determination of temperature coefficients of temperature-sensitive devices, and experiments where extreme temperature stability is essential.

Full information and complete technical data furnished on request.

SPECIFICATIONS				
	Model 910A	Model 913	Model 910K	Model 911
Range	-50 to $+500^{\circ}\text{F}$	-250 to $+750^{\circ}\text{F}$	-250 to $+750^{\circ}\text{F}$	—
Stability	$\pm 0.015^{\circ}\text{F}$	$\pm 0.010^{\circ}\text{F}$	$\pm 0.015^{\circ}\text{F}$	$\pm 0.002^{\circ}\text{F}$
Coolant	Dry Ice	LN_2	Various liquids	Ice



4900 West 78th Street
Minneapolis, Minnesota 55435

CAREER APPOINTMENT

SURFACE AND PHYSICAL CHEMISTRY

Assistant Research Director

Foster D. Snell, Inc., one of the nation's leading independent chemical laboratories and for 45 years a major force in new chemical product development, now offers an outstanding career opportunity to an experienced physical chemist. You will direct projects and will be required to meet clients and sell Snell services.

The industrial projects and problems with which you deal will require an excellent theoretical background in physical and surface chemistry, proficiency in performing experimental studies, and experience in supervision and reporting. You should have a PhD and 3-5 years experience (or a lesser degree and 10 years) in industrial R & D, preferably dealing with product development in adhesives, cosmetics, cleaners, pharmaceuticals and/or food products.

Please send your resume in confidence to: Mr. Paul H. Luke

FOSTER D. SNELL, Inc.

A Subsidiary of

BOOZ-ALLEN

APPLIED RESEARCH Inc.

29 West 15th Street, New York, N.Y. 10011

An equal opportunity employer M&F

Ion-Molecule Reactions in the Gas Phase

ADVANCES IN CHEMISTRY NO. 58

Interactions between ions and molecules are more common than had been suspected, as shown by new tools and techniques, such as tandem mass spectrometers and pulsed radiolysis. They are the cause of many chemical transformations in such energetic systems as:

- flames
- electrical discharges
- high energy radiation
- light

Eighteen papers survey the methods and results of studies on such systems.

336 pages with index cloth bound (1966) \$8.50 postpaid in U.S., plus 20 cents in PUAS and foreign.

Set of L.C. cards free with library orders.

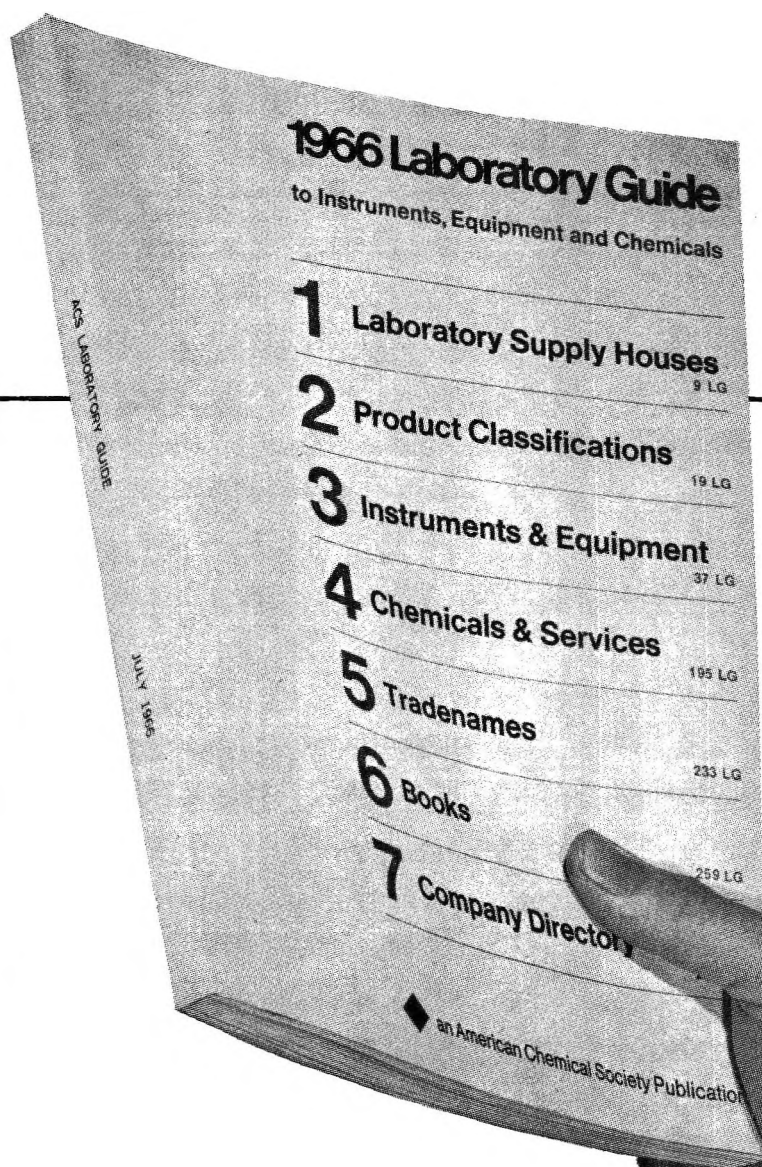
Order from: Special Issues Sales
American Chemical Society
1155 Sixteenth St., N.W.
Washington, D. C. 20036

Phase Equilibria in Solutions of Liquid Sulfur. II. Experimental Studies in Ten Solvents: Carbon Disulfide, Carbon Tetrachloride, Benzene, Toluene, o-Xylene, Naphthalene, Biphenyl, Triphenylmethane, <i>cis</i> -Decalin, and <i>trans</i> -Decalin	John A. Larkin, Jeffrey Katz, and Robert L. Scott	352
The Enthalpy of Dissociation of Nitrogen Trifluoride	G. C. Sinke	359
The Enthalpy of Reaction of Sulfur and Nitrogen Trifluoride	Lynn C. Walker	361
The Monomer-Dimer Equilibria of Liquid Aluminum Alkyls. I. Triethylaluminum	Martin B. Smith	364
A Study of the Chemiluminescence from Oxygen Atom-Hydrazine Flames	K. H. Becker and K. D. Bayes	371
Low-Pressure Physical Adsorption and Electron Microscope Study of the Surface of Annealed Pyrolytic Graphite	L. B. Harris, J. B. Hudson, and S. Ross	377
Pulse Radiolysis Studies. IX. Reactions of the Ozonide Ion in Aqueous Solution	W. D. Felix, Bonnie L. Gall, and Leon M. Dorfman	384
The Kinetics of Oxalate Ion Pyrolysis in a Potassium Bromide Matrix	K. O. Hartman and I. C. Hisatsune	392
The Kinetics of Calcium Oxalate Pyrolysis	F. E. Freeberg, K. O. Hartman, I. C. Hisatsune, and J. M. Schempf	397
A Study of the Adsorption of Thiourea on Mercury by Chronocoulometry	Brian Case and Fred C. Anson	402
SCF-MO Calculations of Heteroatomic Systems with the Variable- β Approximation. II. Electronic Spectra of Hydroxy Aza-aromatic Molecules	Kichisuke Nishimoto and Leslie S. Forster	409
Estimations of the Dispersion and Polar Force Contributions to Heats of Immersion and Interaction Energies of Organic Molecules with Rutile and Graphon Surfaces	J. A. Lavelle and A. C. Zettlemoyer	414
The Dialysis of Sodium Dodecyl Sulfate, Its Activity above the Critical Micelle Concentration, and the Phase Separation Model of Micelle Formation.	Mohammad Abu-Hamdiyyah and Karol J. Mysels	418
Reactions of 40-kev Tritiated Ions with Solid Organic Compounds	Sergio Ascoli, Fulvio Cacace, Giordano Giacomello, and Elvira Possagno	427
Spectroscopic Moments and the Question of d Orbital Participation in the Elements of Groups IV and VII	W. Kenneth Musker and George B. Savitsky	431
Cation Exchange across Ion-Exchange Membranes	A. S. Tombalakian, C. Y. Yeh, and W. F. Graydon	435
Self-Diffusion in Simple Fluids	John A. Palyvos and H. Ted Davis	439

NOTES

Hydrogen-Bonding Interaction between Alcohols and Ethylene Trithiocarbonate	Sadhan Kumar De and Santi R. Palit	444
Mass Spectrometric Studies at High Temperatures. XIV. The Vapor Pressure and Dissociation Energy of Silver Monofluoride.	K. F. Zmbov and J. L. Margrave	446
On the Application of the Scaled Particle Theory to Aqueous Solutions of Nonpolar Gases	A. Ben-Naim and Harold L. Friedman	448
Improved Theoretical Calculation of the Stability Ratio for Colloidal Systems	D. N. L. McGown and G. D. Parfitt	449
The Proton Magnetic Resonance Spectra of Ammonia Nickel Cyanide Clathrates	Kimiko Umemoto and Steven S. Danyluk	450
Effect of Pretreatment on the Two-Dimensional Condensation of Adsorbed Krypton on Alkali Chlorides	T. Takaishi and Masashi Saito	453
Gibbs Equation for the Adsorption of Charged Micelles	D. K. Chattoraj	455
Gaseous Oxides and Oxyacids of Iodine and Xenon: Mass Spectra	Martin H. Studier and John L. Huston	457
Concerning the Spectroscopic Determination of the Structure of Water	Gerhard Boettger, Hartwig Harders, and Werner A. P. Luck	459

ACS Laboratory Guide



The definitive directory to research instruments, chemicals, services, books, equipment and tradenames.

Issued annually in July, used daily to...

FIND WHO SELLS WHAT
INQUIRE ABOUT PRODUCTS
LOCATE SALES OFFICES
CREATE BIDDER'S LISTS
CONTACT VENDORS
PLACE ORDERS

COMMUNICATIONS TO THE EDITOR

High-Energy Induced Isomerization of Stilbene in Benzene Solution . . .	Robert R. Hentz, K. Shima, and Milton Burton	461
Identification of a Specific Mode of Oxidation in the Radiolysis of the Purine Bases in Oxygenated Aqueous Solution . . .	John Holian and Warren M. Garrison	462
Thermodynamic Limiting Laws for Impurities in Semiconductors	W. W. Harvey	463
Hydrodynamic Shear Stress and the Tensile Strength of Covalent Bonds	Cyrus Levinthal and Peter F. Davison	464
A 2:1 Solid-State Complex of HMB·TCNE	Bobby Hall and J. Paul Devlin	465

AUTHOR INDEX

- Abu-Hamdiyyah, M., 418
 Adams, R. N., 338
 Anderson, E. W., 312
 Anderson, V. E., 265
 Anson, F. C., 402
 Ascoli, S., 427

 Bayes, K. D., 371
 Bearcroft, D. J., 316
 Becker, K. H., 371
 Ben-Naim, A., 448
 Boettger, G., 459
 Bohdansky, J., 215
 Bovey, F. A., 312
 Burton, M., 461

 Cacace, F., 427
 Case, B., 402
 Catherino, H. A., 268
 Chapman, T. W., 241
 Chatteraj, D. K., 455
 Chen, E., 218
 Clark, L. W., 302
 Courant, R. A., 246

 Danyluk, S. S., 450

 Davis, H. T., 439
 Davison, P. F., 464
 De, S. K., 444
 Devlin, J. P., 465
 Dickinson, A. C., 231
 Dorfman, L. M., 384

 Enke, C. G., 275, 280

 Farber, M., 254
 Felix, W. D., 384
 Forster, L. S., 409
 Freeberg, F. E., 397
 Friedman, H. L., 448
 Fritsch, J. M., 338

 Gall, B. L., 384
 Garrison, W. M., 462
 George, J. H. B., 246
 Giacomello, G., 427
 Graydon, W. F., 435
 Greenbaum, M. A., 254
 Greyson, J., 259

 Hall, B., 465

 Harders, H., 459
 Harris, L. B., 377
 Harrod, J. F., 343
 Hartman, K. O., 392, 397
 Harvey, W. W., 463
 Hecklen, J., 250
 Hentz, R. R., 461
 Hermann, A., 306, 309
 Hirsch, W., 218
 Hisatsune, I. C., 392, 397
 Holian, J., 462
 Hood, F. P., 312
 Hudson, J. B., 377
 Humphries, F. S., 330
 Hurwitz, P., 324
 Huston, J. L., 457

 Katz, J., 352
 Klots, C. E., 265
 Ko, H. C., 254
 Kornegay, R. L., 312
 Kustin, K., 324

 Larkin, J. A., 352

 Lavelle, J. A., 414
 Levinthal, C., 464
 Luck, W. A. P., 459

 Margrave, J. L., 446
 Marsh, G., 250
 McGown, D. N. L., 449
 Moore, W. J., 231
 Musker, W. K., 431
 Mysels, K. J., 418

 Nachtrieb, N. H., 316
 Newman, J., 241
 Nishimoto, K., 409

 Palit, S. R., 444
 Palyvos, J. A., 439
 Parfitt, G. D., 449
 Possagno, E., 427

 Rissmann, E. F., 343
 Roberts, R. W., 343
 Rosenberg, J. L., 330
 Ross, S., 377

 Saito, M., 453

 Savitsky, G. B., 431
 Schempf, J. M., 397
 Schins, H. E. J., 215
 Scott, R. L., 352
 Selph, C. C., 254
 Shima, K., 461
 Sinke, G. C., 359
 Smith, M. B., 364
 Steinberg, G., 292
 Stern, J. H., 306, 309
 Studier, M. H., 457

 Takaishi, T., 453
 Tatwawadi, S. V., 338
 Tombalakian, A. S., 435

 Umemoto, K., 450

 Walker, L. C., 361
 Weir, W. D., 275, 280
 Wentworth, W. E., 218

 Yeh, C. Y., 435

 Zettlemyer, A. C., 414
 Zmbov, K. F., 446

THE JOURNAL OF PHYSICAL CHEMISTRY

Registered in U. S. Patent Office © Copyright, 1967, by the American Chemical Society

VOLUME 71, NUMBER 2 JANUARY 16, 1967

Vapor Pressure of Different Metals in the Pressure Range of 50 to 4000 Torr

by J. Bohdanský and H. E. J. Schins

CCR-Euratom, Direct Conversion Group, Ispra, Varese, Italy (Received October 3, 1966)

The vapor pressure of Cs, Rb, Na, Li, Sr, Ca, Tl, Bi, Ba, Pb, and Ag was measured in the pressure range of 50 to 4000 torr. The method used for these experiments is relatively independent of impurity concentration. All measured values for the different metals follow regression lines. The constants of these lines are listed as well as the boiling points and the latent heats of vaporization. The experimental data are compared with those in the literature.

Introduction

Recently, a new method for vapor pressure measurements was described by the authors¹ which allows measurements in the pressure range of atmospheres at high temperature (up to 2000°). Data for Ag, Pb, Li, and Cs were published previously.¹ This paper contains additional results for Na, Rb, Ca, Sr, Ba, Tl, and Bi. Some of the measured values (*e.g.*, Na, Cs, and Rb) are in good agreement with recent experimental data.²⁻⁴ For the other metals discussed here, large discrepancies exist in the literature or no experimental data are available.⁵

Experimental Arrangement

The experimental arrangement has been described elsewhere¹ and will be discussed only briefly here. The vapor pressure of the metal is measured in a closed tube containing the test material. The tube is held in a vertical position and heated at the lower end (in our experiments with an RF coil). The upper end is connected by a small tube to an argon pressure vessel in order to fix a certain argon pressure in the tube. During operation, the inert gas is pushed into the upper part of the tube by the vapor flow of the liquid metal

under test. This vapor flow is established by a continuous evaporation of the test metal in the heated section, and by a continuous condensation of the metal on the tube walls which are cooled by radiation. The inert gas and vapor interface is visible by a sharp change in the temperature of the tube (Figure 1).

The hot part of the tube has a constant temperature corresponding to the vapor pressure. This temperature was measured by a thermocouple or by a pyrometer. Under stationary conditions, the vapor pressure is equal to the gas pressure which can be measured outside the tube. Both measured values are used to determine the vapor pressure-temperature relation of the test material.

Impurities. This method involves a continuous distillation of the test material and hence a certain amount of purification. Therefore, the influence of impurities

(1) J. Bohdanský and H. E. J. Schins, *J. Appl. Phys.*, **36**, 3683 (1965).

(2) F. Tepper, A. Murchison, J. Zelenak, and F. Rochlich, ORNL 3605-1 (1964), p 26.

(3) P. Y. Achener, ORNL 3605-1 (1964), p 3.

(4) S. Sowa, *Nucleonics*, **21**, 76 (1963).

(5) A. N. Nesmeyanov, "Vapor Pressure of the Chemical Elements," Elsevier Publishing Co., Amsterdam, 1963.

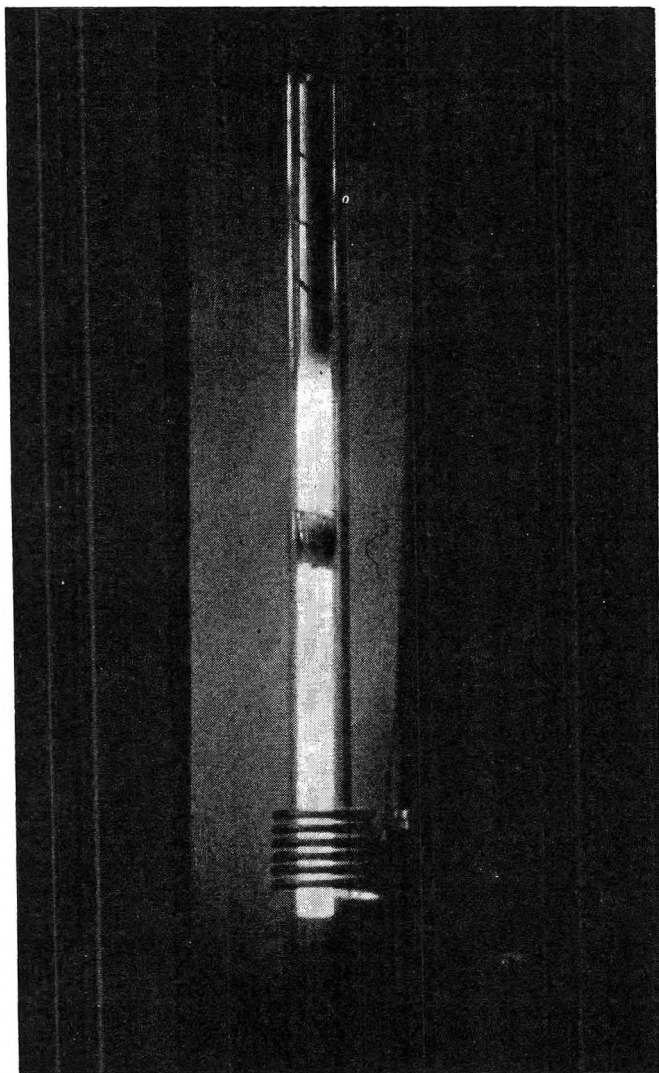


Figure 1. Tube used for vapor pressure measurements shown during operation. A shielded thermocouple is fixed in the hot part.

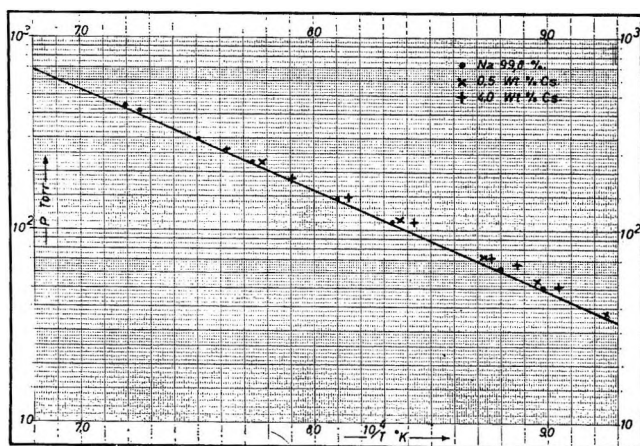


Figure 2. Vapor pressure of pure sodium (99.8%) vs. temperature, for impurity contents of 0.5 and 4 wt % Cs, respectively.

should be small. This was checked by measurements on Na having 0.5 and 4 wt % Cs (Figure 2) as an impurity.

Even in the case of high impurity content, the values, especially at higher pressure, do not deviate much from the values for the pure metal. The major difference in the case of high impurity concentration is a rather large transition zone between the hot and the cold parts of the tube. Impurities of lower vapor pressure do not influence the results. This was verified on a system of Cs having a 1 wt % Na impurity content.

Thermodynamic Equilibrium. During operation there is a continuous evaporation and flow of vapor which condenses mainly in the hot part of the tube. This means that all data are taken slightly out of thermodynamic equilibrium. Therefore, the influence of the vapor flow rate on the vapor pressure was checked. The vapor pressure was measured at constant temperature and different ratios of vapor flow to sound velocity (from $1/1000$ to $1/10$). No influence could be found. Due to this fact, we may assume that the system is in equilibrium with respect to the vapor pressure.

Results

The measured data for the different materials are given in Table I. In Table II, the purities of the tested materials are indicated.

The data for the different metals could easily be fitted to an analytical expression of the form

$$\log p = A - \frac{B}{T} \quad (1)$$

where p is in torr and T is in degrees Kelvin. The constants A and B are listed in Table III. This list also includes the temperature at the boiling point and the heat of vaporization at this temperature, calculated by the Clausius-Clapeyron relation.

Discussion

During the last 3 years, vapor pressure measurements in the pressure range of a few atmospheres have been published²⁻⁴ for Cs, Rb, and Na. In all cases the boiling point method was used in a carefully stabilized furnace. A comparison of our experiments with these measurements demonstrates the simplicity of our method. Previous results are in good agreement with our values.

A critical presentation of earlier measurements was given by Nesmeyanov,⁵ who gave values for all elements discussed here. In most cases, however, his calculations are based on data in the low-pressure range. Our measurements agree with these values except for

Table I: Vapor Pressure of Different Metals at Various Temperatures

Metal	P , torr (T , °K)						
Cs	50 (723)	100 (769)	200 (819)	500 (897)	1104 (979)	2240 (1064)	3680 (1137)
Rb	52 (750)	100 (793)	200 (844)	500 (925)	1105 (1000)	2210 (1080)	3680 (1153)
Na				515 (1116)	1102 (1198)	2215 (1290)	4380 (1390)
Li		102 (1374)	200 (1442)	500 (1557)	1111 (1674)	2210 (1786)	3640 (1881)
Sr	20 (1217)	50 (1314)	100 (1389)	360 (1527)	500 (1588)	1485 (1760)	2210 (1840)
Ca	20 (1313)	31 (1350)	100 (1477)	300 (1616)	600 (1728)	1103 (1830)	2210 (1960)
Tl	22 (1312)	52 (1417)	105 (1487)	200 (1557)	500 (1670)	1103 (1778)	1845 (1862)
Bi		49 (1501)	98 (1575)	200 (1659)	552 (1794)	1103 (1892)	1840 (1982)
Ba	20 (1496)	50 (1600)	100 (1702)	200 (1810)	500 (1984)	600 (2024)	
Pb		52 (1628)	100 (1710)	198 (1800)	500 (1945)	1105 (2084)	1472 (2148)
Ag	41 (1965)	50 (1990)	60 (2015)	70 (2040)	100 (2085)	150 (2150)	1840 (2177)

Table II: Purity of Metals Used

Metal	Supplier	Purity	Remarks
Cesium	Merck, Darmstadt, Germany	99.5%	Impurity mostly Na 0.1%
Rubidium	Leytess, New York, N. Y.	99.8%	
Sodium	Merck	99.8%	Pro analysis: K, 0.1%; Ca, 0.05%
Lithium	Leytess	99.9%	
Strontium	Leytess	99.5%	Ba, Ca, Mg all <0.2%
Calcium	Leytess	99.999%	
Thallium	Leytess	99.999%	
Bismuth	Leytess	99.9999%	
Barium	Degussa, Hanau, Germany	99%	Main impurity Mg
Lead	Johnson-Matthey, London	99.999%	Spectr. standardized
Silver	Johnson-Matthey	99.999%	Spectr. standardized

Table III: The Constants of the Regression Lines, the Boiling Point, and the Heat of Vaporization at the Boiling Point for Different Metals

Metal	A , (p in torr)	B , (T in °K)	T_B , °K	ΔH_v , cal/mole
Cs	6.88	3,750	939	17.2
Rb	7.05	4,010	962	18.3
Na	7.46	5,290	1156	24.2
Li	7.67	7,740	1613	35.4
Sr	7.35	7,370	1649	33.7
Ca	7.48	8,110	1762	37.1
Tl	8.24	9,260	1726	42.4
Bi	8.25	9,860	1838	45.1
Ba	7.04	8,590	2063	39.3
Pb	7.83	9,970	2018	45.6
Ag	8.06	12,720	2450	58.3

Ba and Bi. In both cases the author mentioned the uncertainty of the basic experimental data. In the case of Ba, the impurity content may have influenced our

data. However, the large discrepancy between our data and his extrapolation cannot be explained.

Experimental data on Ag,^{6,7} Na,⁴ and Ca⁸ agree relatively well with our results. Also, the measured⁹ boiling points of Bi, Pb, and Tl are in accordance with our measurements. Li, Sr, Tl, Bi, Ba, and Pb have been measured here for the first time in the whole pressure range or only unreliable values exist.⁵

Acknowledgment. We are obliged to Dr. Neu for his encouragement and interest in this work. We are also indebted to Dipl.-Phys. Gammel of Brown, Boveri Cie, Heidelberg, Germany, who contributed to several measurements and to R. van Wijk and H. Waldmann, also from Brown Boveri Cie. for their assistance in performing the experiments.

(6) J. Fischer, *Z. Anorg. Allgem. Chem.*, **219**, 367 (1934).

(7) P. D. Zavitsanos, *Rev. Sci. Instr.*, **35**, 1061 (1964).

(8) H. Hartmann and R. Schneider, *Z. Anorg. Allgem. Chem.*, **180**, 275 (1929).

(9) W. Leitgetel, *ibid.*, **202**, 305 (1932).

Rigorous Least-Squares Estimation of Molecular Complex Equilibria. I.

Single Intermolecular Complex Utilizing Spectrophotometric Data

by W. E. Wentworth, Walter Hirsch, and Edward Chen

University of Houston, Houston, Texas 77004 (Received January 20, 1966)

Under the assumption that the experimental measurements are independent, the rigorous least-squares adjustment of spectrophotometric data to a 1:1 molecular complex is presented. This differs from previous investigations in one or more of the following ways: (1) the spectrophotometric and concentration measurements can be properly weighted if the errors in the observations are known; (2) the exact calculation of the complex concentration is carried out; (3) all parameters including the molar extinction coefficients of the molecular species can be properly included in the adjustment; (4) the propagation of error including the covariance terms is calculated. A technique reported earlier in the literature is applied to this type of calculation which effectively enhances convergence of the iterative procedure. Convergence generally occurs rapidly. Finally, the use of spectrophotometric data from several wavelengths is incorporated in a general least-squares adjustment to obtain estimates of the molar extinction coefficients and the equilibrium constant. A significant reduction of error is obtained by combining data from several wavelengths.

Introduction

In recent years there has been an increased interest in the investigation of molecular complexes, many of which may involve several complex species in equilibrium. Several experimental techniques can be employed in these studies, but one of the most convenient and commonly used is spectrophotometric measurements. In order to obtain reliable estimates of the numerous equilibrium constants and hence thermodynamic properties of the molecular complexes, it is generally necessary to have precise experimental observations in addition to a careful evaluation of the data. To accomplish the latter, generally a rigorous least-squares adjustment can be employed. Two of the primary advantages of this adjustment are a convenient statistical test for the "goodness of fit" to the selected mathematical model and an estimate of the errors in the desired parameters.

Generally speaking, there are two groups of investigators who are concerned or involved with the determination of thermodynamic properties of complexes: (1) those interested in inorganic complex systems and (2) those dealing primarily with organic complexes.

The two groups have problems which are similar, but since different instrumentation is applicable to the two problems, there are also dissimilarities. Since potentiometric measurements are generally more precise than spectrophotometric information, it is preferable to utilize potentiometric measurements wherever applicable in the study of inorganic systems. Molecular complexes generally are studied in inert solvents such as saturated hydrocarbons; since ions are not involved in the reactions, potentiometric measurements are not applicable. For this reason other less precise techniques must be employed, such as spectrophotometry. A further disadvantage in using spectrophotometric measurements is that it is necessary to determine the molar extinction coefficients for each of the absorbing species. This introduces additional parameters to be evaluated in the reduction of the data and further diminishes the precision in the determination of the desired equilibrium constants. As will be shown later, the errors can be diminished by using spectrophotometric data from several judiciously selected wavelengths.

The purpose of the first paper in this series is to de-

scribe in detail the least-squares adjustment to the simple AB equilibrium using spectrophotometric data. The manner in which estimates of the molar extinction coefficients of the reacting species should be incorporated in the general least-squares adjustment is given. Also, a simplified but rigorous method of combining data from different wavelengths to get the best estimates for the equilibrium constant and the molar extinction coefficients is given. In each of these cases estimates of only a single parameter are involved.

The intent of this series of papers is not to consider all possible molecular equilibria, but rather to present examples which describe various techniques of setting up the rigorous least-squares adjustment. With this background it is anticipated that any individual investigator can readily set up the least-squares adjustment for his specific problem. In later papers of this series the problems of dimerization, multiple complex equilibria, and the combination of estimates of more than one parameter will be presented.

Graphical Evaluation of Equilibrium Systems

As in the past, the numerous graphical procedures which can be employed to analyze data for the desired parameters are still of great importance. These graphical procedures vary considerably according to the type of equilibria suspected to occur, the type of data used to examine the system, and finally the assumptions which may be necessary to simplify the functional relationship so that a graphical analysis can be carried out. There are several limitations that can be stated in general concerning graphical solutions, and these will be given shortly. In order to carry out a nonlinear least-squares adjustment, one must have initial approximations for the parameters in order to initiate an iterative procedure. With better initial approximations for these parameters the convergence is better guaranteed and generally will proceed more rapidly. Graphical solutions can be used to give these first approximations of the parameters. Furthermore, a graphical presentation of the experimental data is generally helpful in examining data and is recommended even after a least-squares adjustment of the data has been carried out.

It is not the intent of this paper to review, criticize, or evaluate the various graphical procedures. Reference should be made, however, to a paper by Tamres¹ where he considers the various graphical procedures for evaluating the equilibrium constant for a 1:1 molecular complex. Tamres considers the interaction with the solvent in addition to evaluating the errors arising from the assumptions necessary for some graphical procedures.

The limitations of graphical solutions in the order of significance according to the authors' viewpoint are as follows. (1) It is difficult to obtain reliable estimates of errors in the parameters. (2) Sometimes it is difficult to decide whether there is a good fit of the data to the proposed functional relationship. (3) In complicated problems frequently only a portion of the data is used to evaluate a given parameter, say by extrapolation to some point. This may limit the precision with which a parameter can be evaluated from the data. (4) Considerable effort may be expended in arriving at justifiable assumptions to get the equations in a form with which they can be conveniently plotted. (5) The graphical solution may be time consuming compared to the task of punching the input data and subsequent use of an electronic computer. Many of these limitations are overcome by a rigorous least-squares adjustment if one assumes that the random errors do belong to a normal distribution and that bias or systematic errors are accounted for properly. It might be stated at this point, however, that the effort put into the programming of the rigorous least-squares adjustment is probably not justified unless there are numerous sets of data which are to be analyzed according to this functional relationship.

Least-Squares Application to Equilibrium Systems

The application of a least-squares adjustment to complex chemical equilibrium systems was first presented by Rydberg and Sullivan in 1959 using solvent extraction data.^{2,3} With these data, as in the case of potentiometric data,⁴ a single functional relationship between the observations and parameters could be obtained. This makes a least-squares adjustment quite straightforward. As Sillén has pointed out, in studying more complicated systems it is not always possible to reduce the relationships to a single function.⁴ A similar problem is encountered using spectrophotometric data in only moderately complicated equilibrium systems. The complexity arises from the fact that generally measurements are made of absorption arising from more than one species simultaneously. In order to solve the least-squares problem in which a single functional relationship cannot be obtained, Sillén has developed a numerical technique which he calls "pitmapping." In addition to this advantage over the so-called usual least-squares method, this

(1) M. Tamres, *J. Phys. Chem.*, **65**, 654 (1961).

(2) J. Rydberg and J. C. Sullivan, *Acta Chem. Scand.*, **13**, 186 (1959).

(3) J. C. Sullivan, J. Rydberg, and W. F. Miller, *ibid.*, **13**, 2023 (1959).

(4) L. G. Sillén, *ibid.*, **16**, 159 (1962).

numerical solution of the least-squares adjustment will converge more readily than the Gauss method. Some years ago, Levenberg suggested a damped least squares whereby the sum of the squares of the corrections to the parameters is also minimized in order to enhance convergence.⁵ The usual least-squares method has been modified by several authors⁶⁻⁸ which enables the iterative procedure to be convergent in addition to increasing the rate of convergence. In a more recent publication, Sillén has presented a procedure to increase the rate of convergence for the "pitmapping" procedure.⁹ Also in a recent paper, Lansbury, *et al.*, use a weighted least-squares adjustment to inorganic metal complex equilibria and properly minimize errors in both potentiometric and volumetric measurements.¹⁰ Their procedure is basically the same as that employed in this work.

In our work, the general least-squares adjustment as presented by Deming^{11,12} has been used which employs a first-order Taylor expansion in order to obtain a linear function of the parameters. The theory of the method was reviewed and the application to two chemical problems was given in earlier papers.^{13,14} The nomenclature in this paper will follow closely that in Deming's book.

The least-squares adjustment of spectrophotometric data to a somewhat simple equilibrium was presented by Rabideau and Kleine.¹⁵ A single nonlinear function was obtained and a first-order Taylor expansion was used. The computer program used was taken from a general report on least squares.¹⁶ In this report some doubt was expressed concerning Deming's treatment of errors in more than one variable, but no specific details were given.

Although there has been an extensive use of computers and least-squares adjustment to inorganic complex systems, a similar type of analysis of molecular complex systems has not been too apparent in the literature. To the author's knowledge, the only extensive work of this type is that of de Maine and co-workers. Their methods have been presented in two recent texts.^{17,18} In the work of de Maine, *et al.*, the least-squares principle is used; however, there is apparently a reluctance toward weighting the data, and, furthermore, in complex equilibria the errors in previously determined parameters are not propagated on the new least-squares adjustment. Many times this oversight can lead to an optimistic estimate of errors. In our work an attempt is made to adhere rigorously to the least-squares principle and to consider the general propagation of random errors of all data points.

In the programs of de Maine, *et al.*, an editing procedure is used to eliminate so-called bad data points

which are defined as data points with residuals exceeding a maximum permitted error. Also, provision is made to edit data external to the computer. The only comment to be made here is that editing of data is generally a difficult procedure and one must always guard against the possible elimination of good data points which will appear to be bad because of a poor model for the system being chosen. In our programs all editing is controlled external to the computer. The program does examine the residuals and will carry out a least-squares re-minimization with a single questionable data point removed. The residuals and σ_{ext}^2 ¹¹⁻¹⁴ are printed out from both least-squares adjustments, and this information is used to decide whether editing is necessary. Seldom has it been necessary to edit data.

In a text by Briegleb¹⁹ on electron donor-acceptor complexes, a procedure is given for the determination of the equilibrium constant for a 1:1 complex using spectrophotometric data at several wavelengths. Briegleb attempts to find some "average" absorbance due to the complex using the data at different wavelengths. He states, "The average value is not an improvement over the measured data. However, a single point which deviates from the average and is not valid for some reason can be recognized and neglected in the calculation." It is very difficult to determine the final propagation of error by his procedure. The final step is a least-squares adjustment to an equation linear with respect to two constants which in turn are related to the molar extinction coefficient and equilibrium constant. This least-squares adjustment is carried out rigorously except that the covariance term has been

(5) K. Levenberg, *Quart. Appl. Math.*, **2**, 164 (1944).

(6) G. E. P. Box, *Bull. Inst. Intern. Statistique*, **36**, 215 (1958).

(7) H. O. Hartly, *Technometrics*, **3**, 269 (1961).

(8) T. G. Strand, D. A. Kohl, and R. A. Bonham, *J. Chem. Phys.*, **39**, 1307 (1963).

(9) L. G. Sillén, *Acta Chem. Scand.*, **18**, 1085 (1964).

(10) R. C. Lansbury, *et al.*, *J. Chem. Soc.*, 1896 (1965).

(11) W. E. Deming, "Statistical Adjustment of Data," John Wiley and Sons, Inc., New York, N. Y., 1943.

(12) W. E. Deming, "Statistical Adjustment of Data," Dover Publications, New York, N. Y., 1964.

(13) W. E. Wentworth, *J. Chem. Educ.*, **42**, 96 (1965).

(14) W. E. Wentworth, *ibid.*, **42**, 162 (1965).

(15) S. W. Rabideau and R. J. Kleine, *J. Phys. Chem.*, **64**, 680 (1960).

(16) R. H. Moore and R. K. Ziegler, "The Solutions of the General Least Squares Problem with Special Reference to High-Speed Computers," Report LA-2367, Oct 15, 1959.

(17) P. A. de Maine and R. D. Seawright, "Digital Computer Programs for Physical Chemistry," Vol. I, The Macmillan Co., New York, N. Y., 1963.

(18) P. A. de Maine and R. D. Seawright, ref 17, Vol. II.

(19) G. Briegleb, "Electronen-Donator Acceptor Komplexe," Springer-Verlag, Berlin, 1961.

neglected in the final expression for the error in the equilibrium constant.

Mention should also be made of a paper by Conrow, *et al.*,²⁰ on the computation of association constants from spectrophotometric data and an analysis of errors. They have employed a least-squares adjustment with the same approach given by Coburn and Grunwald.²¹ This is basically the same idea used by Sillen which was mentioned previously; however, Sillen has considered more complicated equilibria with more parameters to be determined and hence his procedure is necessarily more complex. In the paper by Conrow, *et al.*, a long discussion of the propagation of errors was presented. We do not particularly disagree with any of the conclusions reached in this discussion; however, when their procedure for the least-squares adjustment is used, the analysis of error propagation becomes unnecessarily awkward. In the procedure presented in this paper, the error propagation is obtained along with the normal calculation of the parameters. Furthermore, errors originating from the concentration and/or the absorbance measurements are readily taken into consideration in our rigorous adjustment. Errors in both these measurements have not been considered in the procedure by Conrow, *et al.*²⁰

Finally, in a recent paper, Person²² discusses the possible questionable reliability of the formation constants of weak complexes. He considers the graphical solutions using the well-known Benesi-Hildebrand and Scott equations. Again, we do not question or dispute Person's conclusions, but the resulting error in the formation constant could be found simply by carrying out a rigorous least-squares adjustment. The results are generally considered unreliable when the error in the formation constant is on the order of magnitude of the formation constant.

Single AB Equilibrium Using Data at One Wavelength

The simplest equilibrium possible to study is the single 1:1 complex between A and B.



The equilibrium expression can be written as

$$K = \frac{[AB]}{[A][B]} \quad (2)$$

where one generally assumes that the ratio of activity coefficients remains constant and is incorporated into K . Usually this is a satisfactory assumption for molecular complexes arising from nonelectrolytes at low concentrations. In a spectrophotometric investigation of the equilibrium one generally assumes the

absorption law holds for each of the individual absorbing species.

$$\rho = -\log T = \rho_0 + l\{\epsilon_A[A] + \epsilon_B[B] + \epsilon_{AB}[AB]\} \quad (3)$$

ρ is the absorbance or optical density, T is the transmittance, l is path length, ϵ_j are the molar extinction coefficients, and ρ_0 is the measured difference in absorbance between the cells filled with solvent. The initial quantities of A and B added to our solution generally are also known. In some of our experimental work the varying amounts of B are added titrimetrically. The expressions for the relationship between the initial concentrations of A and B, a and b , respectively, and the actual equilibrium concentrations $[A]$, $[B]$, and $[AB]$, are

$$\frac{c_A V_0}{V_0 + V_B} K_T = a = [A] + [AB] \quad (4)$$

$$\frac{c_B V_B}{V_0 + V_B} K_T = b = [B] + [AB] \quad (5)$$

where K_T is a correction factor to take into account the solvent expansion from the temperature at which the solutions were prepared to the temperature of the equilibrium mixture. C_A is the initial concentration of A in the volume V_0 before B is added. C_B is the concentration of B in the added volume V_B .

Equations 2-5 define the system mathematically. The unknown parameters in this case are K , ρ_0 , ϵ_A , ϵ_B , and ϵ_{AB} . The concentrations $[A]$ and $[B]$ can be eliminated from eq 2, 4, and 5

$$K = \frac{[AB]}{(a - [AB])(b - [AB])} \quad (6)$$

This is a simple quadratic expression for $[AB]$; the real positive root applicable to the problem is

$$[AB] = \frac{1}{2}[(a + b + K^{-1}) - \sqrt{(a + b + K^{-1})^2 - 4ab}] \quad (7)$$

Equation 3 can likewise be expressed in terms of $[AB]$ by use of eq 4 and 5.

$$\rho = \rho_0 + l\{\epsilon_A(a - [AB]) + \epsilon_B(b - [AB]) + \epsilon_{AB}[AB]\} \quad (8)$$

Then the condition equations are of the form

$$F = \rho - \rho_0 - l\{\epsilon_A a + \epsilon_B b + (\epsilon_{AB} - \epsilon_A - \epsilon_B)[AB]\} \quad (9)$$

(20) K. Conrow, G. D. Johnson, and R. E. Bowen, *J. Am. Chem. Soc.*, **86**, 1025 (1964).

(21) W. C. Coburn and E. Grunwald, *ibid.*, **80**, 1318, 1322 (1958).

(22) W. B. Person, *ibid.*, **87**, 167 (1965).

where [AB] is obtained from eq 7 and a and b are obtained from eq 4 and 5. With these substitutions in eq 9, F is a function of the observations ρ_i , V_{B_i} , and the desired parameters ϵ_A , ϵ_B , ϵ_{AB} , K_{AB} , and ρ_0 . Here we have assumed that measurements of V_0 , C_A , and C_B can be made with extreme accuracy compared to the errors of the other observations. This accuracy could be attained by weighing all solutions rather than relying on volumetric accuracy.

The least-squares solution to this problem is now a very straightforward procedure. All that remains is to take the partial derivatives with respect to the observations and the parameters, define the weights of the observations, and then set up the normal equations. With suitable first approximations for the parameters, solve for the corrections to the parameters, and, with the new approximations for the parameters, iterate the procedure until convergence is obtained. A discussion of the problem of convergence will follow this section. Before considering the general case with all five parameters, let us restrict the problem by assuming that ϵ_A and ϵ_B are well known and can be considered free of error. This would be the situation if A and B were nonabsorbing or their absorbances were quite small compared to the complex AB at the selected wavelength. We will call this case I and consider the general case under case II.

Case I. AB Equilibrium Assuming ϵ_A and ϵ_B Free of Error. In our spectrophotometric studies we have employed a Beckman DU and have assumed that the error in the transmittance remains constant and independent of the magnitude of the transmittance. Since the transmission scale is read directly, this assumption is justified. With double-beam absorbance recording spectrophotometers, where the absorbance is measured directly, a different error propagation must be considered.²³ A complete discussion of the different types of spectrophotometric errors is given by Hughes.²⁴ If we assign the variance of unit weight, σ_0^2 , equal to $(0.434)^2\sigma_T^2$, where σ_T^2 = variance in transmittance, then the weight of the absorbance will be

$$W_{\rho_i} = \frac{\sigma_0^2}{\sigma_{\rho_i}^2} = \frac{(0.434)^2\sigma_T^2}{\left(\frac{\delta\rho}{\delta T}\right)^2\sigma_T^2} = T_i^2 \quad (10)$$

The variance in V_B , $\sigma_{V_{B_i}}^2$, is assumed to be constant and has been determined to be on the order of magnitude of 10^{-6} ml². This value will vary depending upon the type of titrator used. Using the value given above, the weight of the volume measurement will be

$$W_{V_{B_i}} = \frac{\sigma_0^2}{\sigma_{V_{B_i}}^2} = (0.434)^2 10^6 \sigma_T^2 \quad (11)$$

From this point on, the least-squares solution is quite straightforward and Deming's book^{11,12} should be consulted. For a briefer exposition of the theory and an application to some chemical problems, two papers could be read.^{13,14} The nomenclature in this paper will conform to that used in those references.

It is necessary to obtain the partial derivatives of eq 9 with respect to the observations, designated by a subscript to F . Then L_i is given by

$$L_i = \frac{F_{\rho_i}^2}{W_{\rho_i}} + \frac{F_{V_{B_i}}^2}{W_{V_{B_i}}} = \frac{1}{T_i^2} + \frac{F_{V_{B_i}}^2}{(0.434)^2 10^6 \sigma_T^2} \quad (12)$$

The desired parameters in this case are ρ_0 , ϵ_{AB} , and K , and it is also necessary to take the partial derivatives of eq 9 with respect to these parameters. Again the partial derivatives are designated by a subscript.

The function F evaluated with the initial approximations, ρ_0^0 , ϵ_{AB}^0 , K^0 , is designated by F^0 and the normal equations are then as shown in eq 13. The

$$\begin{bmatrix} \frac{F_{\rho_0 i}^2}{L_i} & \frac{F_{\rho_0 i} F_{\epsilon_{AB} i}}{L_i} & \frac{F_{\rho_0 i} F_{K i}}{L_i} \\ & \frac{F_{\epsilon_{AB} i}^2}{L_i} & \frac{F_{\epsilon_{AB} i} F_{K i}}{L_i} \\ & & \frac{F_{K i}^2}{L_i} \end{bmatrix} \begin{bmatrix} \Delta\rho_0 \\ \Delta\epsilon_{AB} \\ \Delta K \end{bmatrix} = \begin{bmatrix} \frac{F_{\rho_0 i} F_i^0}{L_i} \\ \frac{F_{\epsilon_{AB} i} F_i^0}{L_i} \\ \frac{F_{K i} F_i^0}{L_i} \end{bmatrix} \quad (13)$$

3×3 matrix is symmetric and the lower terms have been left out for clarity.

Again ref 11-14 describe how an iterative procedure is set up which hopefully is convergent until a suitable criterion is satisfied. In this work we have used $\Delta\sigma_{\text{ext}}^2 \leq 10^{-3}\sigma_0^2$ where $\Delta\sigma_{\text{ext}}^2$ is the difference in successive σ_{ext}^2 . Also, the error propagation onto the desired parameters has been fully described in the above references.

As one can readily see, the rigorous least-squares adjustment is quite straightforward. The advantages in this procedure over graphical or less rigorous procedures are as follows.

(1) Errors in both observations ρ_i and V_{B_i} can be taken into account and their relative importance or contribution can be found in the two terms of L_i in eq 12.

(2) No approximations in the equilibrium expression eq 6 are needed.

(3) The errors in the desired parameters can be obtained from the inverse of the 3×3 coefficient matrix in eq 13.

(23) W. Slavin, *Appl. Spectry.*, **19**, 32 (1965).

(24) H. K. Hughes, *Appl. Opt.*, **2**, 937 (1963).

(4) To investigate how well the data fit the model proposed, in this case a simple 1:1 complex, an F test can be applied using σ_{ext}^2 and σ_0^2 .

Many 1:1 molecular complexes are weak enough that one may simplify the equilibrium expression. If the constituent B in this case is added in excess over A, then one can make the approximation $[B] \approx b$ and

$$K = \frac{[AB]}{(a - [AB])b} \tag{14}$$

In this expression $[AB]$ is not a quadratic function and the partial derivatives of eq 9 are grossly simplified.

Many investigators do not collect their data by titrating in one of the constituents, but rather prepare solutions of concentration a_i and b_i . In this case one would consider errors in these observations and the L_i term would become

$$L_i = \frac{F_{\rho_i}^2}{W_{\rho_i}} + \frac{F_{a_i}^2}{W_{a_i}} + \frac{F_{b_i}^2}{W_{b_i}} \tag{15}$$

The remaining calculations in the least-squares adjustment would be identical. If the errors in a_i and b_i were sufficiently small, the last two terms of eq 15 could be dropped. However, it is not always obvious when these may be dropped unless these terms are compared with $F_{\rho_i}^2/W_{\rho_i}$.

Finally, a comment should be made about including ρ_0 as a parameter. Generally, most investigators neglect this term in that a value of this constant can be obtained directly by observing the solvent *vs.* reference absorption. If this reading were known with absolute certainty this would be satisfactory. However, generally only one reading is taken and this observation is subject to error as is any other absorbance

measurement. For this reason it should be carried as an adjustable parameter.

Case II. AB Equilibrium Considering Errors in ϵ_A and ϵ_B . When ϵ_A and/or ϵ_B are of a magnitude such that their uncertainty will contribute a significant error to F in eq 9, they should be carried as adjustable parameters. Expanding the least-squares adjustment to include these parameters simply requires that the partial derivatives

$$F_{\epsilon_{A_i}} = -l[A]_i \tag{16}$$

$$F_{\epsilon_{B_i}} = -l[B]_i$$

be evaluated and the normal equations expanded to five equations with five corrections of the parameters to be evaluated. The concentrations $[A]_i$ and $[B]_i$ can be calculated from eq 4, 5, and 7. However, there is more to the problem than this since generally ϵ_B and ρ_{0B} are determined from absorbance measurements of solutions with varying concentrations of only A or B. Since these are independent sets of measurements, one should include zero absorbance measurements as before. Let us designate these as ρ_{0A} and ρ_{0B} for each of the sets of data. In a general least-squares adjustment one would include all of the observations and expand the matrix to a 7×7 . Shortly a reduction of this matrix back to a 5×5 matrix will be presented. For brevity, let us consider the inclusion of only ϵ_A and ρ_{0A} as parameters, giving a 5×5 matrix which will shortly be reduced to a 4×4 . The same procedure could be applied to ϵ_B and ρ_{0B} as we will consider for ϵ_A and ρ_{0A} .

The normal equations would then be of the form shown in eq 17 where the summations over j refer to the data with solutions containing only A. In order to simplify the following discussion, let us represent the elements of the matrix by eq 18 where the super-

$$\begin{bmatrix} \sum \frac{F_{\rho_{0A_j}}^2}{L_j} & \sum \frac{F_{\rho_{0A_j}} F_{\epsilon_{A_j}}}{L_j} & 0 & 0 & 0 \\ \left(\sum \frac{F_{\epsilon_{A_j}}^2}{L_j} + \sum \frac{F_{\epsilon_{A_1}}^2}{L_1} \right) & \sum \frac{F_{\epsilon_{A_j}} F_{\rho_{0j}}}{L_j} & \sum \frac{F_{\epsilon_{A_j}} F_{\epsilon_{AB_j}}}{L_j} & \sum \frac{F_{\epsilon_{0j}} F_{K_j}}{L_j} & \\ 0 & \sum \frac{F_{\rho_{0j}}^2}{L_j} & \sum \frac{F_{\rho_{0j}} F_{\epsilon_{AB_j}}}{L_j} & \sum \frac{F_{\rho_{0j}} F_{K_j}}{L_j} & \\ 0 & & \sum \frac{F_{\epsilon_{AB_j}}^2}{L_j} & \sum \frac{F_{\epsilon_{AB_j}} F_{K_j}}{L_j} & \\ 0 & & & \sum \frac{F_{K_j}^2}{L_j} & \end{bmatrix} \begin{bmatrix} \Delta \rho_{0A} \\ \Delta \epsilon_A \\ \Delta \rho_0 \\ \Delta \epsilon_{AB} \\ \Delta K \end{bmatrix} = \begin{bmatrix} \sum \frac{F_{\rho_{0A_j}} F_j^0}{L_j} \\ \sum \frac{F_{\epsilon_{A_j}} F_j^0}{L_j} + \sum \frac{F_{\epsilon_{A_1}} F_1^0}{L_1} \\ \sum \frac{F_{\rho_{0j}} F_j^0}{L_j} \\ \sum \frac{F_{\epsilon_{AB_j}} F_j^0}{L_j} \\ \sum \frac{F_{K_j} F_j^0}{L_j} \end{bmatrix} \tag{17}$$

$$\begin{bmatrix} {}^i b_{11} & {}^i b_{12} & 0 & 0 & 0 \\ & {}^i b_{22} + {}^i b_{22} & {}^i b_{23} & {}^i b_{24} & {}^i b_{25} \\ & & {}^i b_{33} & {}^i b_{34} & {}^i b_{35} \\ & & & {}^i b_{44} & {}^i b_{45} \\ & & & & {}^i b_{55} \end{bmatrix} \begin{bmatrix} \Delta\rho_{0A} \\ \Delta\epsilon_A \\ \Delta\rho_0 \\ \Delta\epsilon_{AB} \\ \Delta K \end{bmatrix} = \begin{bmatrix} {}^i C_1 \\ {}^i C_2 + {}^i C_2 \\ {}^i C_3 \\ {}^i C_4 \\ {}^i C_5 \end{bmatrix} \quad (18)$$

scripts *i* and *j* refer to the summations over the different sets of data. If one solves the first of the five linear equations for $\Delta\rho_{0A}$ and substitutes into the second equation, then upon rearranging

$$\left(\frac{{}^i b_{11} {}^i b_{22} - {}^i b_{12}^2}{{}^i b_{11}} + {}^i b_{22} \right) \Delta\epsilon_A + {}^i b_{23} \Delta\rho_0 + {}^i b_{24} \Delta\epsilon_{AB} + {}^i b_{25} \Delta K = \frac{{}^i b_{11} {}^i C_2 - {}^i b_{12} {}^i C_1}{{}^i b_{11}} + {}^i C_2 \quad (19)$$

Since the first column elements of the remaining three equations are zero, we have reduced the matrix to a 4×4 .

If one considers the least-squares solution for ρ_{0A} and ϵ_A from absorbance measurements of solutions with varying concentrations of only A, then

$$\begin{bmatrix} {}^j b_{11} & {}^j b_{12} \\ & {}^j b_{22} \end{bmatrix} \begin{bmatrix} \Delta\rho_{0A}' \\ \Delta\epsilon_A' \end{bmatrix} = \begin{bmatrix} {}^j C_1 \\ {}^j C_2 \end{bmatrix} \quad (20)$$

The primes are used to differentiate between the similar parameters from the general solution. Expressions for $\Delta\epsilon_A'$ and $\sigma_{\epsilon_A'}^2$ can be readily obtained.¹¹⁻¹⁴ The weight of ϵ_A' can be calculated from $W_{\epsilon_A'} = \sigma_0^2 / \sigma_{\epsilon_A'}^2$ and the weighted correction to ϵ_A' from $W_{\epsilon_A'} \Delta\epsilon_A'$.

Substituting these into (19) our system of four linear equations becomes (21) where the superscript *i* has

$$\begin{bmatrix} (b_{22} + W_{\epsilon_A'}) & b_{23} & b_{24} & b_{25} \\ & b_{33} & b_{34} & b_{35} \\ & & b_{44} & b_{45} \\ & & & b_{55} \end{bmatrix} \begin{bmatrix} \Delta\epsilon_A \\ \Delta\rho_0 \\ \Delta\epsilon_{AB} \\ \Delta K \end{bmatrix} = \begin{bmatrix} C_2 + W_{\epsilon_A'} \Delta\epsilon_A' \\ C_3 \\ C_4 \\ C_5 \end{bmatrix} \quad (21)$$

been dropped since now all *b* coefficients consist of sums over *i*. In an analogous manner, one can see how the W_{ϵ_B} and $W_{\epsilon_B} \Delta\epsilon_B'$ could be included and the original 7×7 matrix reduced to a 5×5 matrix. This general least-squares solution should give the propagation of the errors in ϵ_A and ϵ_B upon the determination of the desired ϵ_{AB} and *K*. In our work, one of the complexing species does not absorb and we have included only ϵ_A as a parameter.

The significance of this treatment is not restricted to this type of study. In general, if one is introducing uncorrelated parameters, such as ϵ_A and ϵ_B , into a least-squares solution for which there is another estimate of the parameter from some other experiment, then this same basic procedure can be followed. This other experiment does not even have to arise from the same type of instrumentation; *e.g.*, infrared and ultraviolet spectrophotometric measurements can be used together. Of course, one must always have reliable estimates of the errors in the parameters. The introduction of more than one parameter whose errors are correlated will be considered in the second paper of this series.

An example of this least-squares adjustment is presented in Table I. The hydrogen-bond complex between phenol and triethylamine was studied by ultraviolet spectrophotometry. The values of the parameters are given for the corresponding iterations, designated by *m*. The values for *m* = 0 are the initial approximations, and the procedure used for obtaining these is given in the next section. The first set of iterations assumes ϵ_A is a known quantity and carries ρ_0 , ϵ_{AB} , and K_{AB} as parameters. The rapid convergence should be noted. Convergence was essentially accomplished at the end of two iterations, the third iteration simply confirming that convergence had occurred. *S* is the weighted sum of squared residuals.¹³ The criterion of convergence is a change in $\sigma_{ext}^2 = S/(n - 3)$ less than $10^{-3} \sigma_0^2$. The numbers have been rounded off to indicate the precision of the parameters within the estimated error. The calculations were performed on an IBM 7094 in the floating point mode, which carried approximately eight significant decimal digits.

The second set of data includes ϵ_A as a parameter. The error in ϵ_A , as determined from pure A data, is $\sigma_{\epsilon_A} = \pm 12.45$. As one would expect, the error in ϵ_A is decreased in the general least-squares adjustment whereas the errors in the other parameters increase. In this specific example the change in errors is small since ϵ_A is small compared to ϵ_{AB} . In other situations it could be much more significant. The data used in these calculations are also tabulated in Table I. The ΔT values given are the differences between the ob-

Table I: Least-Squares Adjustment of Ultraviolet Spectrophotometric Data for the Study of Phenol-Triethylamine Equilibrium^a

<i>m</i>	ϵ_A	ρ_0	ϵ_{AB}	<i>K</i>	$S \times 10^6$
0	462.10	0.03000	2266.2	17.63	1.003
1	462.10	0.03161	2287.5	17.07	0.7856
2	462.10	0.03160	2288.0	17.08	0.7839
3	462.10	0.03160 ± 0.001	2288.0 ± 38.3	17.08 ± 0.64	0.7838
0	462.10	0.03160	2288.0	17.08	0.7816
1	461.28	0.03133	2289.5	17.07	0.8492
2	461.28	0.03185	2286.2	17.09	0.7822
3	461.28 ± 12.4	0.03186 ± 0.004	2286.2 ± 45.7	17.09 ± 0.66	0.7822

V_B (ml)	<i>T</i>	ΔT	$[A](10^6),$ <i>M</i>	<i>T</i>	ΔT
0.000	0.660	0.0002	0.000	0.812	-0.0017
0.100	0.625	-0.0010	2.277	0.795	0.0008
0.200	0.597	-0.0007	4.270	0.780	0.0025
0.300	0.574	0.0001	6.028	0.762	-0.0011
0.400	0.553	-0.0006	7.591	0.751	0.0005
0.500	0.538	0.0017	8.989	0.739	-0.0004
0.600	0.523	0.0017	10.248	0.729	-0.0006
0.700	0.510	0.0017			
1.000	0.478	-0.0006			
1.200	0.462	-0.0024			
1.400	0.454	0.0007			
1.600	0.442	-0.0028			
1.800	0.440	0.0019			
2.000	0.430	-0.0030			
2.500	0.426	0.0009			
3.000	0.424	0.0019			

^a $V_0 = 10.0$ ml, $l = 1.000$ cm, $C_B = 0.2645$ M, $\epsilon_B = 0.00$, $\sigma_T^2 = 4.0 \times 10^{-8}$, $\sigma_{V_B}^2 = 1.0 \times 10^{-8}$, $C_A = 3.2986 \times 10^{-4}$ M, $K_T = 0.9777$, and $\sigma_{ext}^2 = 3.46 \times 10^{-6}$.

served transmittances and the least-squares line. These are not truly the residuals in *T* since errors are being considered in V_B as well.^{11,12} The *T*'s and ΔT 's in the columns following V_B are for the molecular complex data. The *T* and ΔT columns following the [A] column are for the pure A data.

It is pertinent to point out that it is not always necessary to include all of the parameters. Frequently A (and/or B) is nonabsorbing at the selected wavelength and one would set ϵ_A (and/or ϵ_B) equal to zero. Also, it is possible that ϵ_{AB} would be zero. For example, if one follows hydrogen-bond complex formation by observing the absorbance at the monomer O-H stretching frequency, the corresponding absorbance of the complex species is sufficiently removed from the monomer so that ϵ_{AB} can be set equal to zero. It is always of value to reduce the number of parameters wherever possible, since the remaining parameters can then be determined with greater precision.

Convergence of the Iterative Procedure

As mentioned earlier in the section entitled Least-Squares Application to Equilibrium Systems, many

authors have experienced divergence of the iterative process using the Taylor series expansion truncated at the first-order term. In order to overcome this problem in our work, care has been taken to obtain good first approximations in addition to selecting the magnitude of the correction to give a minimum sum of the weighted residuals. Initially ρ_0 is taken from the data point where $V_B = 0$ and ϵ_A is determined from the data on solutions containing only A. Then, using the Benesi-Hildebrand equation

$$\frac{al}{\rho - \rho_0 - \epsilon_A a} = \frac{1}{K(\epsilon_{AB} - \epsilon_A)} \frac{1}{b} + \frac{1}{\epsilon_{AB} - \epsilon_A} \quad (22)$$

a linear least-squares adjustment is carried out to obtain ϵ_{AB} and *K*. Since the equation is linear with respect to $1/K(\epsilon_{AB} - \epsilon_A)$ and $1/(\epsilon_{AB} - \epsilon_A)$, there is no problem of convergence.

These first approximations ϵ_A^0 , ρ_0^0 , ϵ_{AB}^0 , and *K*⁰, are put into the general least-squares program to obtain the corrections to the parameters along with *S*, sum of the weighted squared residuals, which will be designated as *S*₁. After applying one-half the cor-

rection and the full correction to the parameters, S is recalculated each time and will be designated as S_2 and S_3 , respectively. If one assumes that S is a quadratic function of the magnitude of the corrections,⁶ the minimum S is given by

$$R_m = \frac{1}{2} + \frac{S_1 - S_3}{4(S_1 - 2S_2 + S_3)} \quad (23)$$

where R_m is the fraction of correction which yields the minimum S . This correction, *e.g.*, $\epsilon_A = \epsilon_A^0 - R_m \Delta \epsilon_A$, is applied and the same process repeated. This procedure is carried out for two corrections to the parameters. From our experience, this procedure of finding the minimum S tends to decrease the probability for divergence. However, we have also observed that it decreases the rate of convergence. For this reason this minimization process is limited to a few cycles and then the full correction is applied to the parameters. The number of cycles to which this minimization procedure is to be applied is read into the program with each set of data. Generally only two or three cycles are necessary.

In order to show the advantage in this interpolation procedure, the same data as in Table I were recalculated using poor first-order approximations which would display any difficulty in convergence. A convenient manner in which poor first approximations can be introduced in our program is to select a poor value of ρ_0 . A value of -0.06 in contrast to the previously used $+0.03$ was used. In our program the least-squares adjustment considering the three parameters ρ_0 , ϵ_{AB} , and K is carried out first and after convergence the final adjustment considering ϵ_A as a parameter is commenced. The values of the parameters for the various iterations are given in Table II. Again the m refers to the iteration. The iteration count is restarted after convergence with the three parameters is accomplished. Calculation of the first set of data was carried out without the previously discussed interpolation procedure. It will be noted that convergence was accomplished; however, the convergence was not approached in a smooth or monotonic manner. Rather, the approximations alternated low, then high, etc., about the final values. More frequently, one experiences divergence and often a negative K approximation is obtained. When this occurs, there is no hope of convergence since the calculated concentrations are imaginary numbers. The calculations were also carried out using the interpolation procedure previously discussed. The interpolation procedure was applied for five iterations (indicated by an asterisk) and then the full corrections were applied. It should be noted that

Table II: Convergence of the Iterative Procedure Using the Interpolation Technique

m^a	ϵ_A	ρ_0	ϵ_{AB}	K	$S \times 10^6$
0	462.10	-0.0600	1,803.2	93.25	576.8
1	462.10	0.03864	1,637.8	3.19	4523.3
2	462.10	0.03394	-10,813.3	57.70	9575.9
3	462.10	0.03305	1,867.7	63.54	2298.4
4	462.10	0.03609	1,794.5	12.19	1123.8
5	462.10	0.03174	2,162.0	19.82	6.846
6	462.10	0.03167	2,274.0	16.96	1.724
7	462.10	0.03159	2,287.7	17.08	0.7813
8	462.10	0.03159	2,287.8	17.08	0.7816
1	461.28	0.03133	2,289.5	17.07	0.8493
2	461.28	0.03185	2,286.2	17.09	0.7822
3	461.28	0.03186	2,286.2	17.09	0.7822
0	462.10	-0.06000	1,803.1	93.25	576.8
*1	462.10	-0.03112	1,754.7	66.88	284.8
*2	462.10	-0.01212	1,759.6	50.03	149.8
*3	462.10	0.00081	1,798.8	39.12	85.02
*4	462.10	0.00987	1,859.0	31.89	51.43
*5	462.10	0.01656	1,932.5	26.87	31.77
6	462.10	0.03215	2,181.3	15.84	73.94
7	462.10	0.03159	2,282.2	17.20	0.8027
8	462.10	0.03159	2,287.9	17.07	0.7815
9	462.10	0.03159	2,287.8	17.07	0.7816
*1	462.10	0.03159	2,287.8	17.08	0.7814
*2	462.10	0.03159	2,287.8	17.08	0.7813
*3	462.11	0.03159	2,287.8	17.08	0.7814
*4	462.10	0.03159	2,287.8	17.08	0.7813
*5	462.11	0.03159	2,287.8	17.08	0.7815
6	462.28	0.03133	2,289.5	17.07	0.8505
7	461.28	0.03185	2,286.2	17.09	0.7819
8	461.28	0.03185	2,286.2	17.09	0.7822

^a The entries designated with an asterisk, an interpolation procedure.

in this case the convergence was accomplished with the approximations gradually approaching the final values.

Single AB Equilibrium Using Data at Several Wavelengths

The purpose of this section is to show how one can rigorously carry out a least-squares adjustment for an AB equilibrium utilizing spectrophotometric measurements from several wavelengths. The complexity of the problem will then be reduced to a calculation which is only slightly more involved than reducing data at a single wavelength. In order to simplify the mathematical presentation in this section, let us assume we have determined ϵ_A and ϵ_B accurately as in case I previously discussed. The extension to include ϵ_A and ϵ_B as parameters is straightforward and the same result is obtained. Also, for the present assume that there are data at only three wavelengths with which to determine ϵ_{AB} and ρ_0 at each of the wavelengths

along with the equilibrium constant. The extension to any number of wavelengths will again become obvious.

The condition equations for each of the different

wavelengths will all contain the equilibrium constant K as a parameter, but at each wavelength there will be a characteristic ϵ_{AB} and ρ_0 . If we let $i, j, \text{ or } k$ represent the index for the data at the three wavelengths,

$$\begin{bmatrix}
 \sum \frac{F_{K_i} F_{K_i}}{L_i} + \sum \frac{F_{K_j} F_{K_j}}{L_j} + \sum \frac{F_{K_k} F_{K_k}}{L_k} & \sum \frac{F_{K_i} F_{\epsilon_{1i}}}{L_i} & \sum \frac{F_{K_i} F_{\rho_{01i}}}{L_i} & \sum \frac{F_{K_j} F_{\epsilon_{2j}}}{L_j} & \sum \frac{F_{K_j} F_{\rho_{02j}}}{L_j} & \sum \frac{F_{K_k} F_{\epsilon_{3k}}}{L_k} & \sum \frac{F_{K_k} F_{\rho_{03k}}}{L_k} \\
 \sum \frac{F_{K_i} F_{\epsilon_{1i}}}{L_i} & \sum \frac{F_{\epsilon_{1i}} F_{\epsilon_{1i}}}{L_i} & \sum \frac{F_{\epsilon_{1i}} F_{\rho_{01i}}}{L_i} & 0 & 0 & 0 & 0 \\
 \sum \frac{F_{K_i} F_{\rho_{01i}}}{L_i} & \sum \frac{F_{\epsilon_{1i}} F_{\rho_{01i}}}{L_i} & \sum \frac{F_{\rho_{01i}} F_{\rho_{01i}}}{L_i} & 0 & 0 & 0 & 0 \\
 \sum \frac{F_{K_j} F_{\epsilon_{2j}}}{L_j} & 0 & 0 & \sum \frac{F_{\epsilon_{2j}} F_{\epsilon_{2j}}}{L_j} & \sum \frac{F_{\epsilon_{2j}} F_{\rho_{02j}}}{L_j} & 0 & 0 \\
 \sum \frac{F_{K_j} F_{\rho_{02j}}}{L_j} & 0 & 0 & \sum \frac{F_{\epsilon_{2j}} F_{\rho_{02j}}}{L_j} & \sum \frac{F_{\rho_{02j}} F_{\rho_{02j}}}{L_j} & 0 & 0 \\
 \sum \frac{F_{K_k} F_{\epsilon_{3k}}}{L_k} & 0 & 0 & 0 & 0 & \sum \frac{F_{\epsilon_{3k}} F_{\epsilon_{3k}}}{L_k} & \sum \frac{F_{\epsilon_{3k}} F_{\rho_{03k}}}{L_k} \\
 \sum \frac{F_{K_k} F_{\rho_{03k}}}{L_k} & 0 & 0 & 0 & 0 & \sum \frac{F_{\epsilon_{3k}} F_{\rho_{03k}}}{L_k} & \sum \frac{F_{\rho_{03k}} F_{\rho_{03k}}}{L_k}
 \end{bmatrix} \times$$

$$\begin{bmatrix}
 \Delta K \\
 \Delta \epsilon_1 \\
 \Delta \rho_{01} \\
 \Delta \epsilon_2 \\
 \Delta \rho_{02} \\
 \Delta \epsilon_3 \\
 \Delta \rho_{03}
 \end{bmatrix}
 \begin{bmatrix}
 \sum \frac{F_{K_i} F_{i^0}}{L_i} + \sum \frac{F_{K_j} F_{j^0}}{L_j} + \sum \frac{F_{K_k} F_{k^0}}{L_k} \\
 \sum \frac{F_{\epsilon_{1i}} F_{i^0}}{L_i} \\
 \sum \frac{F_{\rho_{01i}} F_{i^0}}{L_i} \\
 \sum \frac{F_{\epsilon_{2j}} F_{j^0}}{L_j} \\
 \sum \frac{F_{\rho_{02j}} F_{j^0}}{L_j} \\
 \sum \frac{F_{\epsilon_{3k}} F_{k^0}}{L_k} \\
 \sum \frac{F_{\rho_{03k}} F_{k^0}}{L_k}
 \end{bmatrix} \tag{24}$$

$$\begin{bmatrix}
 {}^i b_{11} + {}^j b_{11} + {}^k b_{11} & b_{12} & b_{13} & b_{14} & b_{15} & b_{16} & b_{17} \\
 & b_{21} & b_{22} & b_{23} & 0 & 0 & 0 \\
 & b_{31} & b_{32} & b_{33} & 0 & 0 & 0 \\
 & b_{41} & 0 & 0 & b_{44} & b_{45} & 0 \\
 & b_{51} & 0 & 0 & b_{54} & b_{55} & 0 \\
 & b_{61} & 0 & 0 & 0 & 0 & b_{66} & b_{67} \\
 & b_{71} & 0 & 0 & 0 & 0 & b_{76} & b_{77}
 \end{bmatrix}
 \begin{bmatrix}
 \Delta K \\
 \Delta \epsilon_1 \\
 \Delta \rho_{01} \\
 \Delta \epsilon_2 \\
 \Delta \rho_{02} \\
 \Delta \epsilon_3 \\
 \Delta \rho_{03}
 \end{bmatrix}
 =
 \begin{bmatrix}
 {}^i C_1 + {}^j C_1 + {}^k C_1 \\
 C_2 \\
 C_3 \\
 C_4 \\
 C_5 \\
 C_6 \\
 C_7
 \end{bmatrix} \tag{25}$$

the normal equations will be of the form shown as (24). In order to simplify the nomenclature for the following reduction in the matrix, let us rewrite (24) as eq 25 where the presubscripts $i, j,$ and k indicate the summations over the data at the individual wavelengths. The presubscripts are missing when it is obvious from equations of (24) over which data the summation is made.

We will now show that the ΔK obtained from the general solution in equations of (25) is simply the weighted average of the ΔK 's determined with data at each of the individual wavelengths. This is a result which one probably would have expected. However, it will also be shown that the $\Delta\epsilon$ for the various wavelengths from the general solution can be obtained by solving only a system of three equations. In other words, we will reduce the 7×7 matrix to a 3×3 matrix and in general with data at n wavelengths reduce a $2n + 1$ system of equations to three equations. Obviously, one can see the great advantage from a computational standpoint.

Solving the last two equations of (25) for $\Delta\epsilon_3$ and $\Delta\rho_{03}$ in terms of ΔK , eq 26 and 27 are obtained

$$\begin{bmatrix} b_{66}b_{67} \\ b_{67}b_{77} \end{bmatrix} \begin{bmatrix} \Delta\epsilon_3 \\ \Delta\rho_{03} \end{bmatrix} = - \begin{bmatrix} b_{16} \\ b_{17} \end{bmatrix} \Delta K + \begin{bmatrix} C_6 \\ C_7 \end{bmatrix} \quad (26)$$

$$\begin{bmatrix} \Delta\epsilon_3 \\ \Delta\rho_{03} \end{bmatrix} = - \frac{1}{|B_{67}|} \begin{bmatrix} b_{77} & -b_{67} \\ -b_{67} & b_{66} \end{bmatrix} \begin{bmatrix} b_{16} \\ b_{17} \end{bmatrix} \Delta K + \frac{1}{|B_{67}|} \begin{bmatrix} b_{77} & -b_{67} \\ -b_{67} & b_{66} \end{bmatrix} \begin{bmatrix} C_6 \\ C_7 \end{bmatrix} \quad (27)$$

where $|B_{67}|$ is the determinant of the 2×2 matrix in (25). The first equation of (25) can be written as

$$\begin{aligned} & (b_{11} + {}^i b_{11})\Delta K + b_{12}\Delta\epsilon_1 + \dots + b_{15}\Delta\rho_{02} + \\ & {}^k b_{11}\Delta K + [b_{16}b_{17}] \begin{bmatrix} \Delta\epsilon_3 \\ \Delta\rho_{03} \end{bmatrix} = {}^i C_1 + {}^j C_1 + {}^k C_1 \quad (28) \end{aligned}$$

Let us consider only the terms involving the summations over k in eq 28. Substituting eq 27 into 28

$$\begin{aligned} & {}^k b_{11}\Delta K + \frac{1}{|B_{67}|} [b_{16}b_{17}] \begin{bmatrix} b_{77} & -b_{67} \\ -b_{67} & b_{66} \end{bmatrix} \begin{bmatrix} b_{16} \\ b_{17} \end{bmatrix} \Delta K = \\ & {}^k C_1 - \frac{1}{|B_{67}|} [b_{16}b_{17}] \begin{bmatrix} b_{77} & -b_{66} \\ -b_{67} & b_{67} \end{bmatrix} \begin{bmatrix} C_6 \\ C_7 \end{bmatrix} \quad (29) \end{aligned}$$

Partially expanding (29) and factoring out $1/|B_{67}|$, we get

$$\begin{aligned} & \frac{1}{|B_{67}|} \left\{ {}^k b_{11} |B_{67}| - [b_{16}b_{17}] \begin{bmatrix} b_{77}b_{16} - b_{67}b_{17} \\ -b_{67}b_{16} + b_{66}b_{17} \end{bmatrix} \right\} \Delta K = \\ & \frac{1}{|B_{67}|} \left\{ {}^k C_1 |B_{67}| + [-b_{16}b_{77} + b_{17}b_{67} + \right. \\ & \left. b_{16}b_{67} - b_{17}b_{66}] \begin{bmatrix} C_6 \\ C_7 \end{bmatrix} \right\} \quad (30) \end{aligned}$$

Equation 30 can be written in terms of matrices

$$\frac{1}{|B_{67}|} \begin{bmatrix} {}^k b_{11} & b_{16} & b_{17} \\ b_{16} & b_{66} & b_{67} \\ b_{17} & b_{67} & b_{77} \end{bmatrix} \Delta K = \frac{1}{|B_{67}|} \begin{bmatrix} {}^k C_1 & b_{16} & b_{17} \\ C_6 & b_{66} & b_{67} \\ C_7 & b_{67} & b_{77} \end{bmatrix} \quad (31)$$

Now if one considers the least-squares solution using data only at the wavelength for which we have represented the summations over k , the normal equations in terms of the nomenclature of eq 25 are

$$\begin{bmatrix} {}^k b_{11} & b_{16} & b_{17} \\ b_{16} & b_{66} & b_{67} \\ b_{17} & b_{67} & b_{77} \end{bmatrix} \begin{bmatrix} \Delta K_k \\ \Delta\epsilon_3 \\ \Delta\rho_{03} \end{bmatrix} = \begin{bmatrix} C_1 \\ C_6 \\ C_7 \end{bmatrix} \quad (32)$$

Solving for ΔK_k , σK_k^2 , and hence W_{K_k} ,¹¹⁻¹⁴ it can be shown that

$$W_{K_k} \Delta K_k = \frac{1}{|B_{67}|} \begin{bmatrix} {}^k C_1 & b_{16} & b_{17} \\ C_6 & b_{66} & b_{67} \\ C_7 & b_{67} & b_{77} \end{bmatrix} \quad (33)$$

Substituting W_{K_k} and (33) into (31)

$$W_{K_k} \Delta K = W_{K_k} \Delta K_k \quad (34)$$

If one similarly solves eq 4 and 5, and 2 and 3, of eq 25 and makes the appropriate substitution into the first equation of (25), one obtains the result

$$\Delta K = \frac{W_{K_i} \Delta K_i + W_{K_j} \Delta K_j + W_{K_k} \Delta K_k}{W_{K_i} + W_{K_j} + W_{K_k}} \quad (35)$$

This states that the least-squares estimate of ΔK or hence K is simply the weighted average of the K 's determined with data at each wavelength.

However, the solution for $\Delta\epsilon$ at each wavelength is not so obvious. Let us consider the calculation of $\Delta\epsilon$ from eq 25. If we solve eq 6 and 7, and 4 and 5, in (25) and again substitute into the first equation of (25), we have a system of three equations (36). From

$$\begin{bmatrix} b_{11} + W_{K_j} + W_{K_k} & b_{12} & b_{13} \\ b_{12} & b_{22} & b_{23} \\ b_{13} & b_{23} & b_{33} \end{bmatrix} \begin{bmatrix} \Delta K \\ \Delta \epsilon_1 \\ \Delta \rho_{01} \end{bmatrix} = \begin{bmatrix} C_1 + W_{K_j} \Delta K_j + W_{K_k} \Delta K_k \\ C_2 \\ C_3 \end{bmatrix} \quad (36)$$

one can now readily solve for the corrections to the parameters. The application to the calculation of $\Delta \epsilon_2$ and $\Delta \epsilon_3$ is of a similar form where the sum of W_K from data at the other wavelengths is added to the remaining b_{11} term and $W_K \Delta K$ to the remaining C_1 term. Thus we can see that the rigorous solution of the original $(n + 1)$ system of normal equations is reduced to the solution of three equations. Of course, one must solve the system of three equations $2n$ times.

For an example of combining absorption data at different wavelengths to establish an AB equilibrium, data from Briegleb's book¹⁹ have been selected (p 216, Tables 89 and 93). The results of the least-squares calculations are given in Table III. The K and ϵ_A values are estimates of the parameters using the data at the individual wavelengths. The general least-squares estimate of the equilibrium constant, obtained from the weighted average of the K 's from data at each wavelength, is $\bar{K} = 0.319 \pm 0.047$. Using the procedure described earlier, the general least-squares estimates of the molar extinction coefficients are given in the final column designated by $\bar{\epsilon}_{AB}$. The reduction in errors in the estimates of K and the ϵ_{AB} should be noted.

The molar extinction coefficients are plotted in the absorption spectra of Figure 1. The horizontal lines above and below a data point indicate the magnitude of the standard deviation in the ϵ_{AB} value before com-

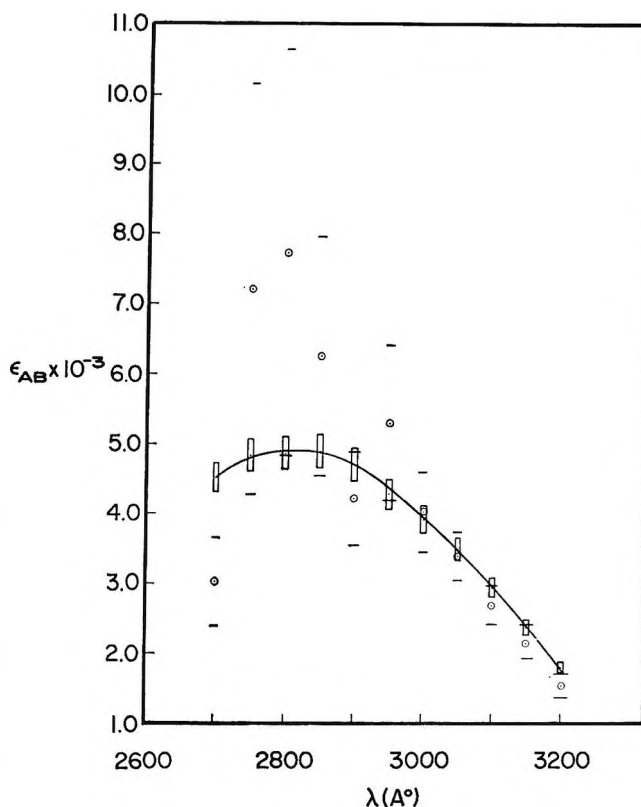


Figure 1. Absorption spectra of trinitrobenzene-benzene electron donor-acceptor complex: \circ , reduction of data at a single wavelength; \square , reduction using data at all wavelengths.

binning data at the various wavelengths. The standard deviations of ϵ_{AB} 's after combining the data are indicated by the height of the rectangle encompassing the ϵ_{AB} values. An error of $\sigma_T = \pm 0.002$ was assumed and apparently was a reasonable choice. One will observe that the error limits generally encompass the smooth curve drawn for the charge-transfer absorption band. Also, the errors in the estimates of the ϵ_{AB} using the data at individual wavelengths generally encompass the smooth curve drawn. The advantage in using a general least-squares adjustment is very obvious from the data graphed in Figure 1.

Table III: Determination of Trinitrobenzene-Benzene Complex Using Data from Multiple Wavelengths

	γ	$K + \sigma_K$	$\epsilon_{AB} + \sigma_{\epsilon_{AB}}$	$\bar{\epsilon}_{AB} + \sigma_{\bar{\epsilon}_{AB}}$
1	3200	0.3948 ± 0.060	1547.8 ± 168	1803.5 ± 79.8
2	3105	0.3573 ± 0.050	2171.2 ± 232	2367.9 ± 10.9
3	3100	0.3584 ± 0.048	2700.3 ± 280	2954.4 ± 14.0
4	3050	0.3299 ± 0.048	3403.0 ± 340	3497.5 ± 16.9
5	3000	0.3094 ± 0.054	4029.3 ± 573	3932.6 ± 19.0
6	2950	0.2456 ± 0.061	5318.4 ± 1111	4282.6 ± 20.8
7	2900	0.3663 ± 0.076	4226.1 ± 676	4718.9 ± 22.9
8	2850	0.2375 ± 0.076	6266.3 ± 1714	4908.0 ± 24.0
9	2800	0.1840 ± 0.078	7753.0 ± 2888	4877.5 ± 23.7
10	2750	0.1963 ± 0.092	7221.8 ± 2935	4843.1 ± 23.3
11	2700	0.5904 ± 0.208	3032.1 ± 627	4525.8 ± 21.3

Least-Squares Estimation of Thermodynamic Parameters of AB Complex

In order to determine the thermodynamic parameters, the following well-known expressions are employed.

$$\Delta G^\circ = -RT \ln K \quad (37)$$

$$-\frac{1}{R} \left(\frac{\partial(\Delta G^\circ/T)}{\partial(1/T)} \right)_P = \left(\frac{\partial(\ln K)}{\partial(1/T)} \right)_P = \frac{-\Delta H^\circ}{R} \quad (38)$$

$$\Delta G^\circ = \Delta H^\circ - T\Delta S^\circ \quad (39)$$

where ΔG° is the change in standard free energy. Generally, for molecular complex formation ΔH° is assumed constant within a given temperature interval and integration of eq 38 then gives a function which is linear between the variables $\ln K$ and $1/T$

$$\ln K = -\frac{\Delta H^\circ}{RT} + C \quad (40)$$

where C is the constant of integration. Substitution of eq 37 into 39 yields an expression similar to (40) where the constant, C , would be identified with $\Delta S^\circ/R$. This is expected since the assumed constancy of ΔH° within the temperature range infers that $\Delta C_p^\circ = 0$ for the complex formation and this in turn necessitates that ΔS° be constant.

$$\ln K = -\frac{\Delta H^\circ}{RT} + \frac{\Delta S^\circ}{R} \quad (41)$$

Therefore, if ΔH° and ΔS° are assumed constant, the equation to be adjusted to the data is eq 41 with ΔH° and ΔS° as parameters.

Of course the K 's are not measured directly, but are derived from a least-squares adjustment of the appropriate spectrophotometric data. If the absorbances are restricted to a single wavelength, then eq 13 or 21 is the appropriate normal equation for the adjustment at a given temperature. Data from multiple wavelengths could likewise be used to obtain the best estimate of K as discussed in the previous section.

With the K and σ_K values at the various temperatures, the least-squares adjustment of eq 41 is carried out in the conventional manner.¹¹⁻¹⁴ Equation 41 can be written in the form of a condition equation

$$F = \ln K + \frac{\Delta H^\circ}{RT} - \frac{\Delta S^\circ}{R} \quad (42)$$

The normal equations are

$$\begin{bmatrix} \sum \frac{F_{\Delta H_1^\circ} F_{\Delta H_1^\circ}}{L_i} & \sum \frac{F_{\Delta H_1^\circ} F_{\Delta S_1^\circ}}{L_i} \\ \sum \frac{F_{\Delta H_1^\circ} F_{\Delta S_1^\circ}}{L_i} & \sum \frac{F_{\Delta S_1^\circ} F_{\Delta S_1^\circ}}{L_i} \end{bmatrix} \begin{bmatrix} \Delta(\Delta H^\circ) \\ \Delta(\Delta S^\circ) \end{bmatrix} = \begin{bmatrix} \sum \frac{F_i^\circ F_{\Delta H_1^\circ}}{L_i} \\ \sum \frac{F_i^\circ F_{\Delta S_1^\circ}}{L_i} \end{bmatrix} \quad (43)$$

If one does not wish to assume $\Delta C_p^\circ = 0$, the next higher approximation would be the assumed constancy of ΔC_p° . Under this assumption the thermodynamic expression becomes

$$R \ln K = -\frac{\Delta H^\circ_{298}}{T} - \frac{\Delta C_p^\circ}{T}(T - 298) + \Delta S^\circ_{298} + \Delta C_p^\circ \ln \frac{T}{298}$$

The reference temperature of 25° has been selected. In this case there are three parameters to be evaluated, namely ΔH°_{298} , ΔS°_{298} , and ΔC_p° . The least-squares procedure described earlier can be simply applied to this nonlinear equation, giving estimates of the parameters and the associated errors. Estimates of ΔH° and ΔS° at other temperatures can be calculated from

$$\Delta H^\circ = \Delta H^\circ_{298} + \Delta C_p^\circ(T - 298)$$

$$\Delta S^\circ = \Delta S^\circ_{298} + \Delta C_p^\circ \ln \frac{T}{298}$$

In calculating the errors in ΔH° and ΔS° it should be emphasized that the terms involving the covariances $\sigma_{\Delta H^\circ_{298}, \Delta C_p^\circ}$ and $\sigma_{\Delta S^\circ_{298}, \Delta C_p^\circ}$ should not be left out. This can be a very important contribution as pointed out in earlier publication.^{13,14}

Application to Other Chemical Systems

It should be emphasized that the technique of combining data from various sources, as developed in this paper, has important application to other chemical systems. Essentially, we have obtained an estimate of a parameter and its associated error from another source of data and rigorously included this information in the least-squares adjustment. For example, an estimate of the equilibrium constant using data from all other wavelengths was first evaluated, and this estimate was included in the least-squares adjustment of the data at the single wavelength, giving better estimates of the molar extinction coefficient and the equilibrium constant. In a similar manner, an estimate of a parameter from a completely different type of instrumentation could be incorporated into the least-squares adjustment. In a complicated analysis of kinetic data this should probably occur frequently. In this case, an estimate of a rate constant, obtained by another investigator, could be included in the least-squares analysis of the data. This presupposes that the other investigator has also obtained a reliable estimate of error in the parameter.

In our laboratory an application of this technique to a completely different chemical problem has already been completed.²⁵ In this case, different compounds

(25) W. E. Wentworth, E. Chen, and J. E. Lovelock, *J. Phys. Chem.*, **70**, 445 (1966).

should exhibit a linear relationship between two variables with different slopes but possibly with very nearly the same intercept. In order to improve on the precision of the slopes, a common intercept was assumed in the general least-squares adjustment using data for all compounds. Using the technique developed in this paper, the $n + 1$ square matrix ($n =$ number of compounds) which would ensue from the general solution was reduced to the solution of $2n \times 2$ matrices.

Acknowledgments. The authors express their appreciation to the Robert A. Welch Foundation for the financial support of this work. Also, one of the authors (E. C.) is the recipient of a NASA Traineeship for predoctoral work in chemistry and is grateful for this assistance. Finally, we wish to express our appreciation to Miss Marie Cobb for hand calculations and assistance in preparing the programs and to Miss Elsie Bryan for assistance in preparing the manuscript.

Paramagnetic Resonance of Metal Ions and Defect Centers in Topaz

by Alan C. Dickinson and Walter J. Moore

Chemical Laboratory, Indiana University, Bloomington, Indiana¹ (Received January 25, 1966)

Electron paramagnetic resonance (epr) of Fe^{3+} impurities in colorless topaz was measured at 77 and 300°K with X-band frequencies. The most intense peaks occurred at g values greater than 2 and were split by hyperfine interaction with two fluoride ions. It was determined that Fe^{3+} substitutes for Al^{3+} in nearly octahedral sites. The principal axis of the paramagnetism was close to a threefold axis of the octahedron. Second- and fourth-order axial and second-order rhombic components dominated the spin Hamiltonian with values: $D = -9.699$, $E = 2.503$, and $F = 0.800$ Gc/sec. The epr spectrum of yellow topaz showed an octet of peaks near $g = 2$ due to V^{4+} and several broad peaks at lower fields due to Cr^{3+} . On heating to 500°, yellow topaz became pink and blue topaz became colorless, in both cases with the loss of epr peaks near $g = 2$. Irradiation of all samples produced an amber-yellow color and gave rise to several peaks near $g = 2$. These heat and irradiation-sensitive peaks were assigned to various types of electronic defect centers.

Topaz may be classified as a mineral of the individual silicate type. Its empirical formula is $\text{Al}_2\text{F}_2\text{SiO}_4$. It commonly occurs in high-temperature veins probably formed in igneous intrusions in the presence of fluoride and water vapor. As a result, some of the fluoride is usually replaced by hydroxyl giving it the variable composition, $\text{Al}_2(\text{F},\text{OH})_2\text{SiO}_4$. Topaz samples from various locations have been shown to contain from 15 to 20% fluorine,^{2a} and the presence of hydroxyl has been clearly demonstrated by the absorption spectrum in the near-infrared,^{2b} which is dominated by the OH peak at 2.745 μ . This variable composition also has an effect on such physical properties as refractive indices,

specific gravity (3.4–3.6), and the large optic axial angle ($2V = 48$ to 65°). In spite of the conditions of its formation, topaz decomposes above 1200° to mullite, with the loss of silicon tetrafluoride and water. This fact has caused difficulty for the artificial preparation of the mineral, and only polycrystalline topaz has ever been synthesized. Electrical conductivity becomes

(1) This work was supported by the U. S. Atomic Energy Commission.

(2) (a) A. N. Winchell, "Elements of Optical Mineralogy," John Wiley and Sons, Inc., New York, N. Y., 1953; (b) W. Lyon and E. L. Kinsey, *Phys. Rev.*, **61**, 482 (1942).

appreciable at elevated temperatures and is believed to be due to the mobility of fluoride and hydroxyl ions.³

Natural topaz has an orthorhombic crystal structure with a perfect cleavage parallel to the (001) plane. The space group was determined by Leonhardt⁴ to be D_{2h}^{16} (Pnma). The crystal structure was first proposed by Pauling⁵ and determined in detail by Alston and West.⁶ The oxygen and fluoride ions are close packed in a manner which is neither purely hexagonal nor cubic. The unit cell contains four of the structural units, $Al_2F_2SiO_4$. Each silicon ion is surrounded tetrahedrally by four oxygens which are shared only with aluminum ions. The environment of the aluminum is octahedral, involving four oxygen and two fluoride ions. The latter are on adjacent rather than opposite corners of the octahedron. These octahedra occur in pairs along the *c* axis with two oxygens shared. The fluorines are shared between diagonal rather than adjacent aluminums. Because of the presence of the fluorines and the bonding involved in the crystal, the local symmetry of the aluminum ion is considerably less than octahedral. As an effect of the fluorines, there are eight nonequivalent aluminum sites, whereas only four nonequivalent silicon sites are present. The crystal structure contains, in addition to three twofold planes and axes of symmetry, an inversion center which further reduces the number of nonequivalent sites to four and two for aluminum and silicon, respectively.

The various shades of yellow topaz found chiefly in Minas Gerais, Brazil, are those most prized in gem stones. Colorless and blue topaz are also quite common and crystals of rose and other colors are known. Although these colors have always been attributed to small amounts of impurity ions, there has been no general agreement on the ions responsible. Wild and Liesegang⁷ attributed the pink color to chromium and the blue to lithium and iron. Howard⁸ suggested that the yellow color was due to chromium, blue to iron, and pink to vanadium. Lemlein and Melankholin,⁹ however, believed that the yellow was caused by Fe^{3+} and the blue by Fe^{2+} . Grum-Grzhimailo¹⁰ also proposed that iron caused the yellow color but believed the color of rose topaz to be due to Cr^{3+} .

Heat treatment and irradiation under various conditions have been shown to have profound effects on the color of topaz. In general, colors are lost on heating from 400 to 750°. Blue topaz is completely bleached in this way, while a pink tint remains in samples which were originally yellow. Irradiation, on the other hand, tends to produce or intensify the coloration. Clear blue and pink samples acquired a deep yellow, while yellow topaz became dark orange to smoky brown. In almost

all cases these irradiation-produced colors were lost on heating or on exposure to sunlight.

In recent years much information has been obtained about the nature and possible applications of similar impurity and color centers in minerals such as sapphire, amethyst, and ruby by use of the technique of electron paramagnetic resonance (epr).¹¹⁻¹³ The present work was an attempt to attack the mysteries of color centers connected with the unusual symmetries found in the topaz structure by use of the epr technique.

Experimental Section

Spectrographic Analyses. Samples of colorless topaz used for epr measurements were cut from three larger pieces which were originally from Brazil, Japan, and Russia. The last two contained some small blue regions. A piece of yellow and blue Brazilian topaz provided the colored samples. Fragments from each piece were analyzed spectrographically by Huffman Microanalytical Laboratories of Wheatridge, Colo., with results given in Table I.

Apparatus and Methods. Optical absorption spectra in the visible region were measured on a Cary Model 14 spectrometer. The basic epr instrument was a Varian Model V-4500 spectrometer with a Varian 22.5-cm rotating magnet and magnet power supply. The field was self-regulated through the Hall-effect crystal probe of a V-FR2503 "Fieldial" and was modulated at 100 kc/sec. The microwave source was a klystron operating in the X-band at approximately 9.5 Gc/sec. Room-temperature measurements were made with the crystal mounted with Duco cement on the end of a quartz rod and suspended in one of three cavity assemblies. A single rectangular cavity (V-4531) made of gold-plated brass operated in the TE_{102} mode with a minimum unloaded *Q* of 7000. By attaching to this a similar cavity, a dual rectangular cavity (V-4532) was obtained which operated in the TE_{104}

(3) C. Doelter, *Z. Anorg. Chem.*, **67**, 394 (1910).

(4) J. Leonhardt, *Z. Krist.*, **59**, 261 (1924).

(5) L. Pauling, *Proc. Natl. Acad. Sci. U. S.*, **14**, 603 (1928).

(6) N. A. Alston and J. West, *Proc. Roy. Soc. (London)*, **A121**, 358 (1928).

(7) G. O. Wild and R. E. Liesegang, *Centr. Mineral. Geol.*, **385** (1923).

(8) J. W. Howard, *J. Chem. Educ.*, **12**, 153 (1935).

(9) G. G. Lemlein and N. M. Melankholin, *Tr. Inst. Kristallogr. Akad. Nauk SSSR*, **6**, 245 (1951).

(10) S. V. Grum-Grzhimailo, *Zap. Vses. Mineralog. Obshchestva*, **82**, 142 (1953).

(11) H. F. Symmons and G. S. Bogle, *Proc. Phys. Soc. (London)*, **79**, 468 (1962).

(12) T. I. Barry, P. McNamara, and W. J. Moore, *J. Chem. Phys.*, **42**, 2599 (1965).

(13) E. O. Schulz-DuBois, *Bell System Tech. J.*, **38**, 271 (1959).

Table I: Spectrographic Analyses of Topaz Samples (% by wt)

	Sample no., origin, color							
	IA, Brazil, colorless	IB, Brazil, colorless	IC, Brazil, colorless	II, Brazil, yellow	III, Brazil, yellow	IV, Brazil, blue	V Japan, colorless	VI, Russia, colorless- blue
Boron	0.001	0.001	0.002	0.0005	0.001	0.003	0.0001	0.0015
Calcium	0.008	0.005	0.014	0.020	0.012	0.015	0.008	0.010
Chromium	0.035	0.105
Copper	0.0001	0.0001	0.0005	0.003	0.0005	0.0002	0.006	0.0005
Gallium	0.001	0.001	0.0015	0.001	0.0019	0.0017
Germanium	0.012	0.010	0.011	0.012	0.002	0.008	0.013	0.010
Iron	0.008	0.004	0.008	0.005	0.001	0.002	0.003	0.005
Lead	0.02	0.015
Magnesium	0.10	0.08	0.009	0.004	0.011	0.004	0.002	0.005
Silver	0.0006	0.0004
Sodium	0.006	0.007	0.0014	0.001	0.001	0.002	0.0010	0.0015
Strontium	0.002
Titanium	0.006	0.005	0.0001	0.045	0.001	...	0.0001	0.0001
Vanadium	0.002	0.002
Zirconium	0.016	0.015	0.008

mode. The third assembly was an aluminum rotating cavity (V-4533). Measurements at 77°K were accomplished by means of a quartz dewar inserted in one of the rectangular assemblies. The crystal was immersed in liquid nitrogen in the narrow, unsilvered portion of the dewar inside the cavity.

A Harvey-Wells Model G-502 precision nmr gaussmeter and a Hewlett-Packard Model 524 electronic counter were employed for measurement of the field. The frequency of the cavity was determined by measuring the field at which absorption occurred for certain standards, whose g values were accurately known, through use of the relation $h\nu = g\beta H$. The most frequently used standard was a speck of DPPH whose g value was 2.0036 ± 0.0002 . The frequency could be varied within a small range (9.1–9.5 Gc/sec) by loading the cavity with quartz tubes.

Experimental samples of topaz were cut from the natural specimens with a diamond saw, and were ground and polished on an MD & R master faceting machine. Those crystals used exclusively for optical work were small rectangular plates varying in thickness from 0.09 to 0.16 cm. The epr samples were mostly rectangular parallelepipeds whose volume varied from about 0.03 to 0.2 cc. These were cut and ground with each side normal to one of the three crystal axes. Rough orientation was obtained from the external form of the natural sample, and more accurate orientation was determined by extinction in the polarizing microscope. The deviation of each side was less than 0.5° from the normal. With the crystal mounted on the flat end of a quartz rod the final orientation was achieved in the

epr cavity by superposition of peaks from nonequivalent sites when a twofold crystal axis was brought parallel to the direction of the magnetic field.

Two mechanisms were available for changing the angle of the crystal axes relative to the direction of the magnetic field. The crystal itself could be rotated by means of a chuck and dial assembly equipped with a vernier allowing an accuracy of $\pm 0.2^\circ$. Alternatively, when the rotating cavity was used, the magnet could be rotated throughout the required 180° range and the angle could be read to about the same accuracy. Spectra taken with the magnetic field parallel to principal crystal directions were recorded by a Varian G22-A dual channel recorder. The angular variation of the most intense features could be followed on the oscilloscope. Recorder traces taken at usually 5° intervals were required to follow the weaker peaks.

Spectra. The simplest spectra were those taken along crystal axes, as all octahedral sites were equivalent with respect to the magnetic field at these orientations. Figure 1 shows typical spectra of the colorless, blue, and yellow topazes taken at room temperature with the magnetic field parallel to the [001] axis of the crystal. All features were quite weak, requiring high settings of the spectrometer for their observation.

In the spectra of colorless samples, the most intense feature (labeled c) was a triplet with a separation of 24.6 gauss, an average line width of about 9.8 gauss, centered about a g value of approximately 4.2. Features labeled a and b at lower fields, while partially masked in the orientation shown, were also triplets, although peak b was later found by analysis of its

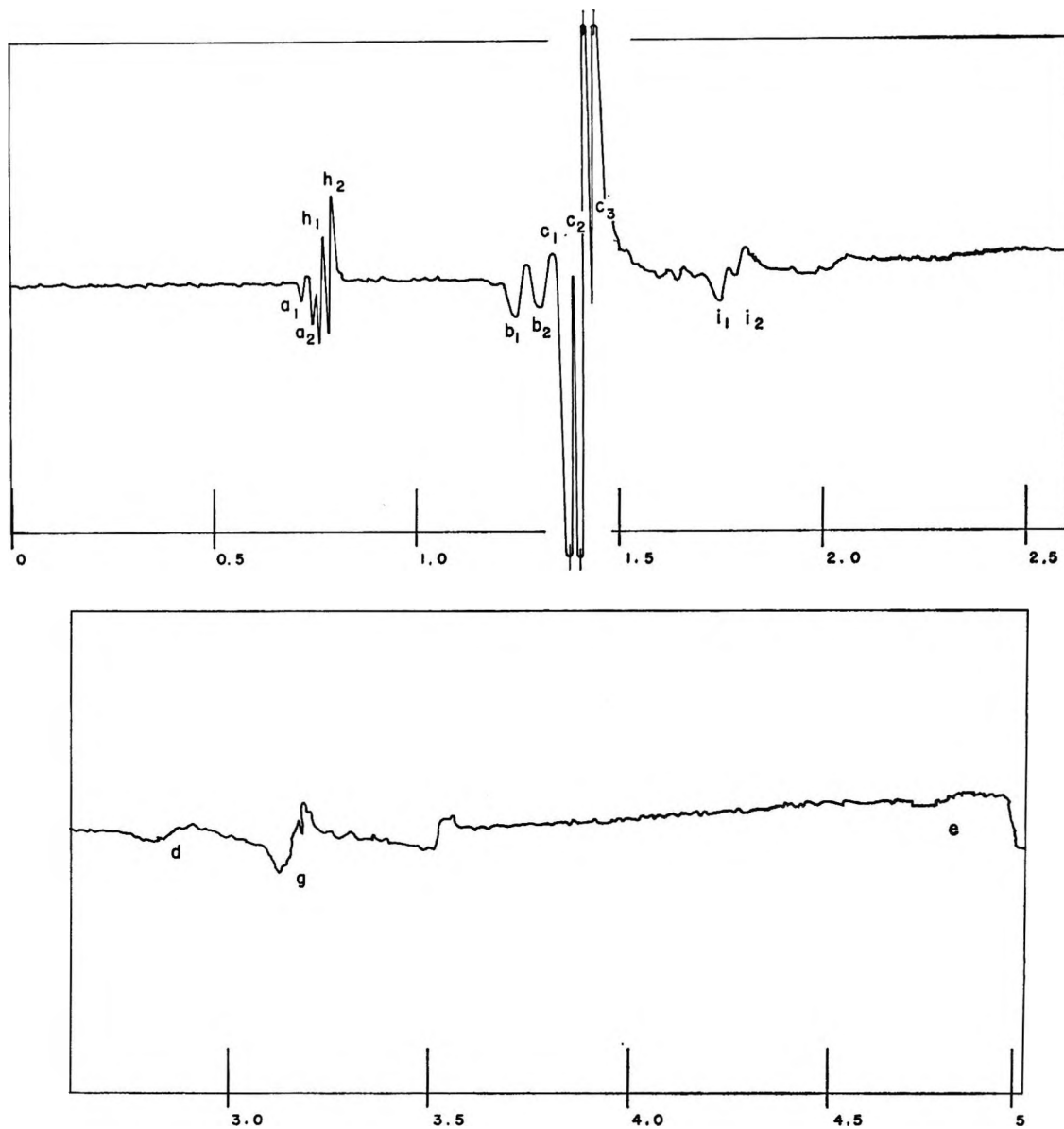


Figure 1a. Epr spectrum of colorless topaz, 77°K (sample E11). $H \parallel c$ axis. Field in kilogauss.

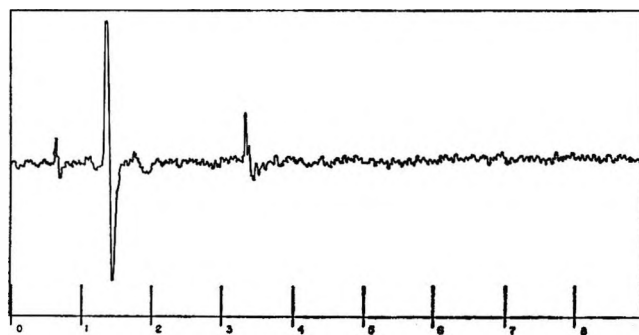


Figure 1b. Epr spectrum of blue topaz, 300°K (sample E5). $H \parallel c$ axis.

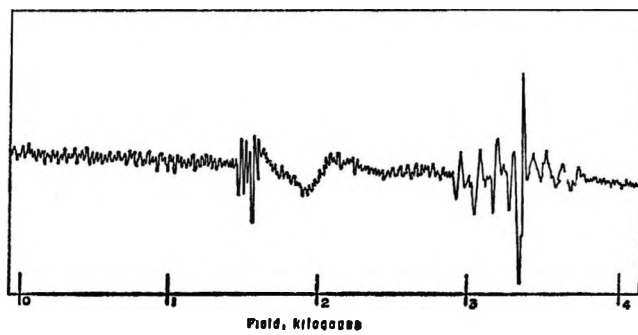


Figure 1c. Epr spectrum of yellow topaz, 300°K (sample E4a). $H \parallel b$ axis.

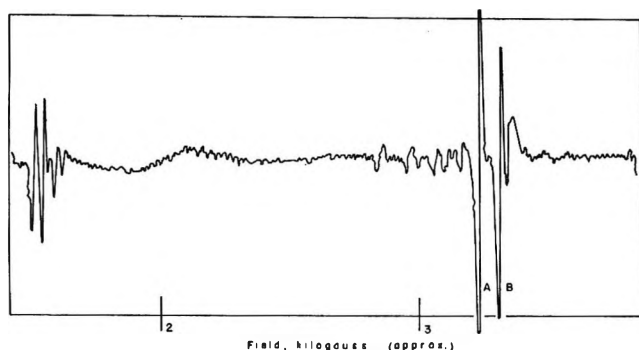


Figure 1d. Epr spectrum of yellow topaz, 77°K (sample E4a). $H \parallel b$ axis.

angular variation not to be a member of the set of peaks which includes the other triplets. Features d, e, and f, however, did follow the same angular variation pattern as the triplets although any hyperfine structure (hfs) they might have shown was unresolved, owing to their large line width, from 59 to 98.5 gauss at 77°K. The colorless samples also showed a set of doublets, including features h and i, as well as others seen at different orientations. Finally, one weak feature appeared at a g value close to 2.0. Colorless samples from different geographical locations gave essentially the same spectra, with slight differences in the intensities of certain peaks.

The epr spectra of blue topaz (Figure 1b) were quite similar to those of colorless topaz, again with slight differences in intensities. The most characteristic feature of these spectra was the appearance of rather intense peaks at $g = 2$, the sharpest of these being somewhat anisotropic.

The yellow samples, on the other hand, had entirely different epr spectra (Figure 1c) from those of either colorless or blue samples. Intense peaks did occur at a g value of about 2, but the major one had a nearly isotropic g value of 1.95 and was surrounded by several small, moderately sharp peaks. The features characteristic of colorless and blue topaz were indistinguishable among several broad and sharp peaks at effective g values ranging from about 3 to 4.5.

The effect of viewing spectra at liquid nitrogen temperature was, in general, to increase the signal-to-noise ratio by at least a factor of 2 and in some cases to decrease the line width of the peaks. Spectra of yellow topaz, however, revealed some unexpected results at 77°K. While most features increased from three to five times in intensity, the sharp $g = 2$ peak increased by about 25 times (Figure 1d). Moreover, one peak at a slightly higher field increased by about 263 times its room-temperature intensity and a smaller

peak which had been of negligible intensity at room temperature appeared at slightly lower fields. These unusually large increases were not accompanied by any noticeable change in line width but were strongly anisotropic.

Heat Treatment and Irradiation. Crystals were heated in air inside a Vycor tube which was inserted midway into a small cylindrical furnace. A colorless sample was annealed for about 2 days at nearly 1000° and showed a slight increase in epr peak intensity. A small crystal of blue topaz was heated for half-hour periods at 100° intervals from 200 to 1000°. By 400° the color had been completely bleached and there was no further change.

The behavior of yellow topaz on heating was more complex. A gradual transition from yellow to pink was complete after heating at 500°. At higher temperatures, the crystal was colorless while heated but regained its color on cooling. The color regained became gradually more yellow as higher temperatures were used. The visible spectrum of the untreated crystal was dominated by two peaks, at about 4100 and 5600 Å. As the heating progressed, the intensity of both peaks decreased and both clearly split into doublets. Thus after heating yellow topaz to 500°, its color and optical spectrum were remarkably similar to those of chromium in ruby.¹⁴

The intense epr peaks near $g = 2$ dropped off with heating to a negligible intensity after the 500° treatment. On further heating, however, they began to return. This behavior indicated a relationship between these $g = 2$ peaks and the yellow color. The smaller peaks surrounding these showed a slight increase in intensity with heating up to 500° and a decrease with heating beyond that range. Other peaks either stayed essentially the same or exhibited a non-uniform behavior except for one low-field peak which, after heating to 1000°, increased by a factor of about 3 while a neighboring peak decreased by a factor of 6. In all cases, heating at lower temperatures could not influence the intensities of peaks produced by the 1000° heating.

Samples of all three types of topaz were γ -irradiated with about 5×10^6 r from a Co⁶⁰ source. The colorless sample developed a pale amber-yellow color and a moderately intense epr peak at $g = 2.068$. The blue sample, which had been bleached by heating at 1000°, also gained a faint amber-yellow tint and an epr peak at $g = 2.094$. This peak was broader than the original $g = 2$ peak and was split by a great deal of hyperfine structure. The yellow sample, which had also been

(14) C. P. Poole, *Phys. Chem. Solids*, **25**, 1169 (1964).

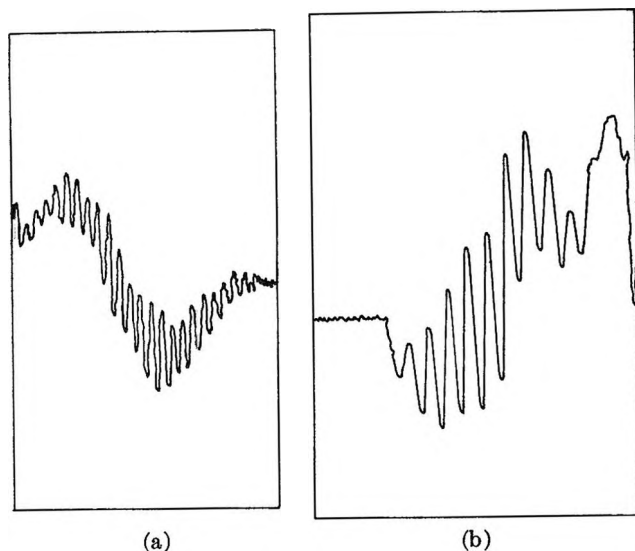


Figure 2. Epr peak of center F in irradiated topaz. (a) Sample E7, $H \parallel z$ axis, 300°K . (b) Sample E4a, $H \parallel b$ axis, 77°K .

treated at 1000° , became a deep yellow-orange. An epr peak at $g = 2.096$ appeared in the yellow sample and was split by hfs similar to that of the blue (Figure 2). In addition, all epr peaks of the yellow topaz increased in intensity after the irradiation, and two of the original peaks of the crystal before heat treatment reappeared. The colors produced by irradiation were bleached by heating to 500° for 30 min and the crystals regained the appearance produced by the 1000° heating of the natural crystals.

Discussion

Identification of Centers. The chief problem in the case of colorless topaz was to identify and establish the nature of the center which gave rise to the triplets and those epr peaks which behaved on angular variation in the same manner as the triplets. Their insensitivity to heat treatment and irradiation as well as their widely varying effective g values indicated that they arose from some paramagnetic impurity rather than from electronic defects in the crystal structure. From the spectrographic analyses the only impurities which might have paramagnetic ions were titanium, zirconium, copper, and iron; only zirconium and iron were present in appreciable concentrations. The multiplicity of epr peaks and the similarity of their effective g -values to those of Fe^{3+} in glass¹⁵ led to the tentative conclusion that the Fe^{3+} ion was responsible for the triplets. If Fe^{3+} was substituted at a normal Al^{3+} site, the two surrounding fluoride ions, each with nuclear spin $1/2$, would explain the superhyperfine triplet structure.

Several experiments were undertaken to provide more evidence for this assignment. Attempts at the synthesis of topaz and the use of endor technique at 77°K gave no profitable results. Correlation of epr peak intensities with impurity concentrations in samples of different origins suggested titanium or iron as the cause but not zirconium or copper (Table II). These results could not be considered conclusive partly because the concentration values used included total iron and not just Fe^{3+} , which would have appeared in the epr spectra. When a sample of colorless topaz was heated to 960° for 66 hr in contact with a coating of Fe_2O_3 , almost all epr peaks exhibited an increase of about 33%. This constituted the most conclusive evidence that Fe^{3+} was responsible for the resonances. Similar heating without the Fe_2O_3 caused a slight increase in peak intensities, perhaps due to an oxidation of Fe^{2+} to Fe^{3+} . The corresponding peaks observed in blue topaz were thus also attributed to Fe^{3+} .

The doublets also appeared to be associated with the iron content. It is possible that their patterns arise from an Fe^{3+} ion in an octahedral site in which only one fluoride ion is present. This would be particularly feasible in the case where all other neighbors were oxygen. In the case of a substitutional hydroxyl group, the nuclear spin of the proton might upset this idea although its distance from the Fe^{3+} ion would probably preclude this interaction. A less likely cause might be an interstitial site close to a single $I = 1/2$ ion.

The presence of chromium in yellow topaz to the extent indicated by the analyses should allow an epr spectrum from Cr^{3+} to be seen, as in ruby.¹⁶ Several rather wide peaks at low fields seemed by their behavior and positions to belong to such a spectrum. The unique set of small peaks near the value of $g = 2$ were linked to vanadium present only in the yellow samples. An octet of peaks with a uniform separation of about 142 gauss centered about a g value of 2 clearly indicated that the ion responsible was V^{4+} .

The remaining epr peaks were those at a g value of approximately 2. These were in some way affected by heating or irradiation or both. The fact that hfs was almost completely lacking indicated that all these centers consisted of systems with one unpaired electron. The sharp decrease in intensity on heating to about 500° correlated so well with the loss of yellow that this color must be caused by one or more of these $g = 2$ centers. The remaining pink tint is probably the color due to chromium, as is true in ruby. The yellow color and

(15) T. Castner, Jr., G. S. Newell, W. C. Holton, and C. P. Slichter *J. Chem. Phys.*, **32**, 668 (1960).

(16) J. E. Geusic, *Phys. Rev.*, **102**, 1252 (1956).

epr peaks which return on further heating, however, appear to be permanent and thus different from the original yellow color centers. The irradiation-produced centers, on the other hand, could be bleached by moder-

ate heating and thus could be related to the color centers of the natural crystals.

One peak which appeared after irradiation, however, contained a great deal of hfs and was clearly not one

Table II: Correlation of Epr Peak Intensities with Impurity Concentration in Topaz Samples

Peak	Iron		Titanium		Zirconium		Copper	
	ρ	No. of samples	ρ	No. of samples	ρ	No. of samples	ρ	No. of samples
a ₂	0.069	5	0.269	4	-0.369	4	-0.106	5
c ₂	0.645	6	0.884	5	0.376	5	-0.062	6
d	0.420	5	0.751	4	-0.031	4	-0.195	5
e	0.320	6	0.607	5	-0.105	5	-0.164	6

Table III: Summary of Proposed Epr Centers in Topaz

(a) Impurity Centers

Proposed center	Site	Occurrence	Epr characteristics			
			No. of primary peaks	Hyperfine splitting	Super-hyperfine splitting	Optical spectra
Fe ³⁺	Octahedral	Colorless and blue	5 (max)	Not observed	Triplet, separation 24.6 gauss	
Fe ³⁺	Octahedral (one fluorine) or interstitial	Colorless, blue, and yellow	3 (max)	Not observed	Doublet, separation 23.5 gauss	2400 A
V ⁴⁺	Tetrahedral	Yellow	1	Octet, separation 142 gauss	Not observed	
Cr ³⁺	Octahedral	Yellow	6 (max)	Unresolved	Unresolved	4050 A 5600 A

(b) Defect Centers

Name of center	Type	Occurrence	Production	Destruction	g Value	Epr characteristics		
						Hyperfine splitting	Intensity change at 77°K	Possible relation to color
A	Electron	Yellow	Natural	Heating to 500°	a -Axis 1.88 b -Axis 1.96	None	Increases	Natural yellow
B	Electron	Yellow	Natural	Heating to 500°	a -Axis 1.94 b -Axis 1.92	None	Increases	Natural yellow
X	Hole	Yellow, blue, and colorless	Natural	Heating to 500°	2.01	None	Disappears (in yellow crystal)	Blue
Y	Hole	Yellow	Heating to 500°	Not achieved	2.005	None	Increases	Unknown
Z	Electron	Yellow	Heating to 1000°	Not achieved	1.925	None	Increases (?)	Heated yellow
F	Hole	Yellow, blue, and colorless	Irradiation	Heating to 500°	2.09	11-22 lines, separation 6.4 gauss	Increases	Irradiated yellow

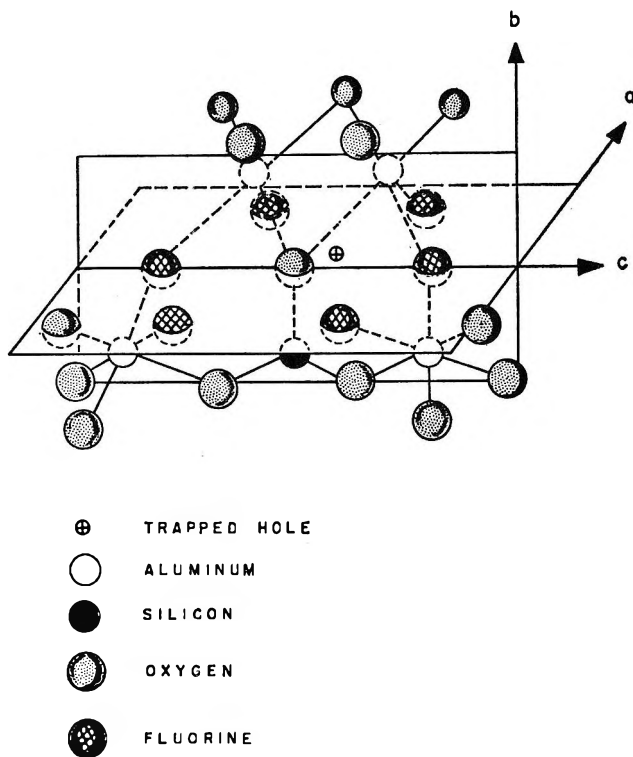


Figure 3. Diagram of model proposed for radiation-produced color center, F , in topaz.

of the original centers. After the work of Van Wieringen and Kats¹⁷ on silicate glasses it might be suggested that those centers with g values less than 2 be attributed to electrons while those with g values greater than 2 be attributed to holes. It seems possible that the radiation-produced center with much hfs, at a g value of 2.09, could be caused by the presence of a hole on that oxygen of a silicon tetrahedron which is coplanar with and surrounded hexagonally by six fluoride ions in the (010) crystal plane. This center is depicted in Figure 3. A summary of all proposed epr centers in topaz is given in Table III.

Description of the Fe^{3+} Center. The angular variation of the triplets in the epr spectra of colorless topaz showed a very strong axial dependence. Two sets of angular-variation data were required to fix the orientation of the principal axis of the paramagnetism. The first was a rotation with the magnetic field in the (100) crystal plane. A minimum was reached for the peaks in question at a point 25° from the [001] axis in this plane. Next the magnetic field was rotated in the plane perpendicular to this first symmetry direction. A further minimum was reached for all peaks considered at 22.5° away from the first point. At this ultimate minimum, the paramagnetic or z axis was parallel to the direction of the magnetic field. Figure

4 shows the magnetic and crystal axes. At this point one of the four nonequivalent sites exhibited five peaks at a minimum with respect to magnetic field strength. These five peaks were labeled a, c, d, e, and g in Figure 1a. Peak b did not exhibit a minimum at this point and later computer treatment of the data confirmed the assumption that peak b does not arise from the Fe^{3+} center in question. A further rotation in the plane perpendicular to the z axis gave evidence of further anisotropy showing that the paramagnetic site is not purely axial.

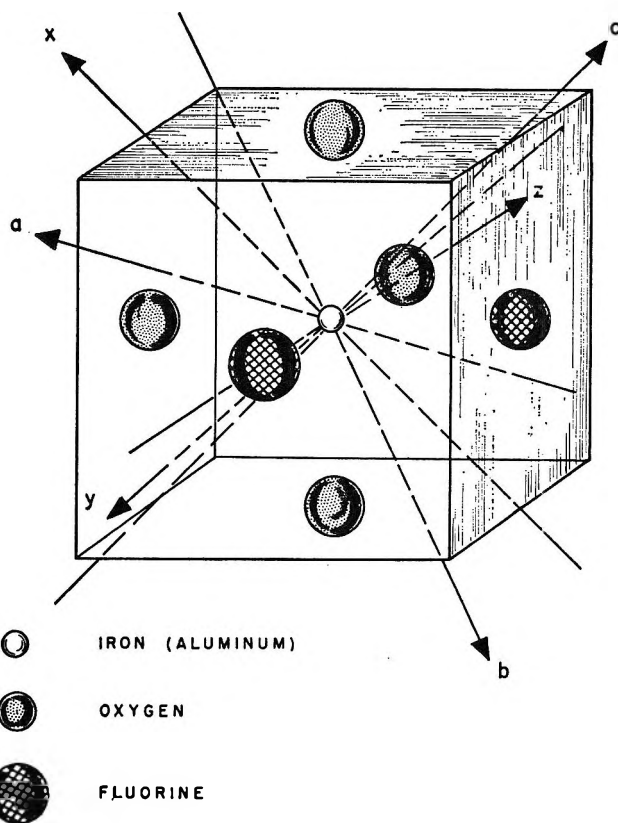


Figure 4. Octahedral topaz site showing crystal axes, a , b , c , and paramagnetic axes, x , y , z .

In order to assign these peaks to the corresponding transitions of the Fe^{3+} ion, the change in the positions of the peaks on variation of cavity frequency was measured. The results indicated that transitions a and c were between diverging levels of a $\pm M_s$ type, most likely $\pm 5/2$ and $\pm 3/2$, respectively. Transitions d and e were between converging levels before and after crossing (or repulsion), respectively.

(17) J. S. Van Wieringen and A. Kats, *Philips Res. Rept.*, 12, 432 (1957).

The most general spin Hamiltonian applicable to this problem is

$$\mathcal{H} = g\beta H \cdot S + B_2^0 O_2^0 + B_2^2 O_2^2 + B_4^0 O_4^0 + B_4^2 O_4^2 + B_4^4 O_4^4 + AI \cdot S$$

where B = coefficient, including crystal field parameters and O = operator equivalent, subscripts 2 = second-order term and 4 = fourth-order term, and superscripts 0 = axial term, 2 = rhombic term, and 4 = cubic term, and A = superhyperfine splitting factor, I = nuclear spin angular momentum quantum number, and S = electron spin angular momentum quantum number. Because of the symmetry of the site it was expected that the terms $B_2^0 O_2^0$ and $B_2^2 O_2^2$ would dominate the spin Hamiltonian. After preliminary calculations to determine the approximate magnitude of the axial effect, the spin Hamiltonian was diagonalized in the axial term. In this form the complete spin Hamiltonian was

$$\begin{aligned} \mathcal{H} = & g\beta H \cos \theta S_z + \frac{1}{2}g\beta H \sin \theta \cos \psi (S_+ + S_-) - \\ & \frac{1}{2}g\beta H \sin \theta \sin \psi (S_+ + S_-) + \\ & D[S_z^2 - (1/3)S(S+1)] + (E/2)[S_+^2 + S_-^2] + \\ & [(F-a)/180]\{35S_z^4 - [30S(S+1) - 25]S_z^2 - \\ & 6S(S+1) + 3S^2(S+1)^2\} + \\ & (c/12)\{7S_z^2 - S(S+1) - 5\}(S_+^2 + S_-^2) + \\ & (S_+^2 + S_-^2)[7S_z^2 - S(S+1) - 5] + \\ & (a\sqrt{2}/36)[S_z(S_+^3 + S_-^3) + (S_+^3 + S_-^3)S_z] \end{aligned}$$

where D = second-order axial parameter, E = second-order rhombic parameter, F = fourth-order axial parameter, c = fourth-order rhombic parameter, a = cubic parameter, θ = the angle between the z axis and the magnetic field, and ψ = the angle between the x axis and the projection of the magnetic field on the xy plane (eliminated with the imaginary terms in analysis). It was assumed throughout that $g = 2.0036$, which is the value for DPPH and which has been observed to be correct for Fe^{2+} .¹⁸

Calculations were done on a CDC 3600 computer using a modified form of a program developed for this purpose by Howell and Barry. The most accurate experimental data were the positions of peaks a, c, d, and e at room temperature measured at the first minimum (22.5° away from the z axis). By using these transitions in the computer treatment, the best fit to the experimental data was obtained with the following assignments (a, c, d, e, and f).

$$+5/2 \rightarrow -5/2 \quad (\text{a})$$

$$+3/2 \rightarrow -3/2 \quad (\text{c})$$

$$+5/2 \rightarrow -3/2 \quad (\text{d})$$

$$+5/2 \rightarrow -3/2 \quad (\text{e})$$

$$+5/2 \rightarrow -1/2 \quad (\text{f})$$

These data were thus used to calculate the values of the spin Hamiltonian parameters. The results were

$$D = -9.699 \pm 0.0005 \text{ Gc/sec}$$

$$E = +2.503$$

$$F = +0.800$$

The negative value of D puts the $\pm 5/2$ levels lowest at zero field, thus explaining the fact that certain theoretically less forbidden transitions were not in fact seen. Limited intensity comparison at 77°K confirmed the sign of D . It was found that the sign of E and F must be opposite to that of D to give the best fit. No improvement was obtained with values of c or a greater than 0.0001 Gc/sec . With the cited values of the parameters, the standard deviation of the four energy differences from the actual frequency of the cavity, 9.2813 Gc/sec , was 0.688% .

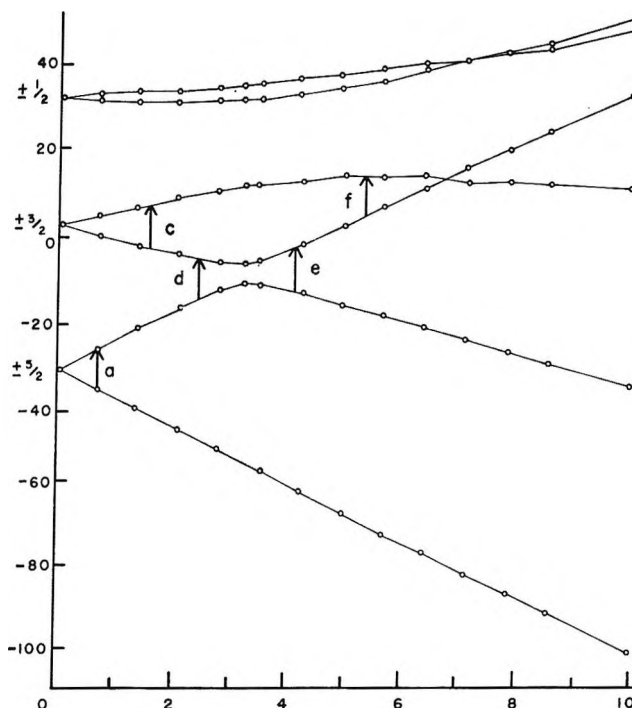


Figure 5. Energy-level diagram of Fe^{2+} in topaz at 300°K . $\theta = 0^\circ$. (Observed transitions are labeled.)

(18) S. Geschwind, *Phys. Rev.*, 121, 363 (1961).

Table IV: D/E Values for Fe^{3+} in Various Crystals

Crystal	Symmetry	D/E
TiO_2 (rutile)	Octahedral	9.2 ^a
SiO_2 (amethyst)	Tetrahedral	5.43 ^b
Al_2SiO_5 (kyanite)	Octahedral	5.17 ^c
MgWO_4	Octahedral	-3.95 ^d
Topaz	Octahedral	-3.87 ^e
Al_2BeO_4 (chrysoberyl)	Octahedral	-1.08 ^f
SiO_2 (glass)	Tetrahedral	$\leq 0.05^g$

^a D. L. Carter and A. Okaya, *Phys. Rev.*, **118**, 1485 (1960).

^b D. R. Hutton, *Phys. Rev. Letters*, **12**, 310 (1964). ^c G. J.

Troup and D. R. Hutton, *Brit. J. Appl. Phys.*, **15**, 1493 (1964).

^d M. Peter, *Phys. Rev.*, **113**, 801 (1959). ^e This paper. ^f V. M.

Vinokurov, M. M. Zaripov, V. G. G. Stepanov, Yu. E. Pol'skii,

G. K. Chirkin, and L. Ya. Shekun, *Soviet Phys.-Solid State*, **3**,

1797 (1962). ^g T. Castner, Jr., G. S. Newell, W. C. Holton,

and C. P. Slichter, *J. Chem. Phys.*, **32**, 668 (1960).

The parameter values were checked by calculating the energy differences of the various transitions using some less accurate sets of experimental data. In all cases standard deviations were less than 6%.

Finally, the eigenvalues were calculated for various fields at the positions of the two minima. The resulting energy level diagram for the z -axis direction is given in Figure 5.

The ratio of axial to rhombic spin Hamiltonian parameters gives a view of the purity of the axial or rhombic splitting. A D/E value close to 1 would indicate a distortion which is neither axial nor rhombic purely and may correspond to extremely broad resonances.¹⁹ While the D/E value alone gives little indication of the magnitude of the distortion, it is usually in highly distorted symmetries that an E term becomes at all appreciable. Table IV gives some D/E values reported for Fe^{3+} in various crystals. For Fe^{3+} in sapphire, however, no appreciable E term has been reported.

The superhyperfine splitting parameter, A , due to the interaction with the fluorine nuclei could be calculated from the observed triplet splitting of the $3/2 \rightarrow -3/2$ peak. Its value was $8.58 \times 10^{-4} \text{ cm}^{-1}$. This is

consistent with values obtained from the epr spectra of vanadium and chromium ions in alkali fluoride crystals,²⁰ $A = 7.1 \times 10^{-4}$ and $9.4 \times 10^{-4} \text{ cm}^{-1}$, respectively. The interaction has been explained as due to a slight covalent bonding, wherein the 3d wave function of the metal ion is augmented by the admixture of fluorine terms. The superhyperfine interaction of electrons with neighboring nuclei is usually about an order of magnitude less than the hyperfine interaction of the electrons with their own nuclei.

Conclusions

It seems quite evident that the triplet epr peaks in colorless and blue topaz are due to Fe^{3+} ions in substitutional Al^{3+} sites where the presence of two fluoride ions gives rise to the observed superhyperfine splitting. The symmetry of the site is similar to that of Fe^{3+} in sapphire. The principal axis of the paramagnetism does not fall along one of the threefold axes of the octahedron, however, but is directed slightly away from it toward the two fluorines. As a result, the site is much less symmetrical with a higher axial field parameter, a much lower cubic field parameter, and an appreciable rhombic parameter. This large distortion results in the large values of zero field splitting, 34.628 and 30.250 Gc/sec, which might make this material more suitable than sapphire for certain maser applications.

It also seems apparent that in colored topaz not the yellow but the pink produced by heating is caused by chromium. Both the natural yellow and blue and the heated and irradiated yellow are related to certain electronic defect centers in the crystal structure. In addition, there are similar centers which are not necessarily directly related to colors except perhaps as precursors. These facts not only may help to clear up several puzzles as to the origin of colors in topaz, but may provide a foundation for geochemical studies of the origin and formation of such gem stones.

(19) T. Castner, Jr., G. S. Newell, W. C. Holton, and C. P. Slichter, *J. Chem. Phys.*, **32**, 668 (1960).

(20) T. P. P. Hall, W. Hayes, R. W. H. Stevenson, and J. Wilkens, *ibid.*, **38**, 1977 (1963).

Polarography in a Binary Salt Solution

by Thomas W. Chapman and John Newman

Inorganic Materials Research Division, Lawrence Radiation Laboratory, and Department of Chemical Engineering, University of California, Berkeley, California (Received March 2, 1966)

The instantaneous current and the average current to a dropping mercury electrode in a binary salt solution are calculated. At very small times the instantaneous current depends only on the ohmic drop and varies as $t^{1/2}$, whereas at sufficiently large times and voltages a limiting current is reached which varies as $t^{1/6}$. The average current over a drop lifetime is not well represented by the limiting-current approximation of the Ilkovič equation if either the drop life or the applied voltage is too small. However, the current is always directly proportional to the bulk concentration of the reactant for a given voltage and drop life.

Introduction

Polarographic analysis with a dropping mercury electrode is usually carried out in the presence of a large excess of indifferent, nonreacting electrolyte. This serves both to reduce the ohmic potential drop in the solution and to reduce the effect of the electric field on the movement of reacting ionic species. For a sufficiently large applied potential, the current to the drop is limited by the rate of diffusion and convection and corresponds to a zero concentration of the reactant at the surface. For the total cathodic current in this case Ilkovič^{1,2} and Mac Gillavry and Rideal³ have obtained the expression

$$I_D = 4nF\gamma^2c_\infty\sqrt{7\pi D_i/3}(t^{1/6}) \quad (1)$$

where $4\pi\gamma^3/3$ is the constant volumetric flow rate of mercury through the capillary, F is Faraday's constant, c_∞ is the bulk concentration, D_i is the diffusion coefficient of the reactant, and n is the number of electrons consumed when one reactant ion or molecule reacts. The radius r_0 of the drop grows with the cube root of time

$$r_0 = \gamma t^{1/3} \quad (2)$$

For discharge of cations from a solution containing only two ionic species, a limiting current is still obtained and is still proportional to the one-sixth power of time. The total limiting current, given by Lingane and Kolthoff,⁴ is

$$I_L = I_D\sqrt{D/D_+}/(1 - t_+) \quad (3)$$

where t_+ is the cation transference number, $D = D_+D_-(z_+ - z_-)/(z_+D_+ - z_-D_-)$ is the diffusion coefficient of the salt, and z_+ and z_- are the charge numbers of the cation and anion. Ionic migration in this case of cation discharge enhances the limiting current so that $I_L > I_D$. For example, for a symmetric electrolyte and a transference number of 0.5, $I_L = 2I_D$.

For solutions of intermediate compositions, the limiting current follows a similar time dependence and has been calculated for several cases by Newman.⁵ The effect of ionic migration on limiting currents has been discussed qualitatively by the early polarographers.^{1,6} If there is insufficient indifferent electrolyte, the current due to one discharging species will produce an electric field which enhances the limiting current for a second discharging species.

The low electrical conductivity associated with the absence of supporting electrolyte can also lead to an ohmic potential drop in the solution which prevents the attainment of a limiting current, at least in the initial stage of the growth of the drop. The ohmic resistance for flow of current to a sphere of radius r_0 in a medium of uniform conductivity κ is $1/4\pi\kappa r_0$.

(1) D. Ilkovič, *Collection Czech. Chem. Commun.*, **6**, 498 (1934).

(2) D. Ilkovič, *J. Chim. Phys.*, **35**, 129 (1938).

(3) D. Mac Gillavry and E. K. Rideal, *Rec. Trav. Chim.*, **56**, 1013 (1937).

(4) J. J. Lingane and I. M. Kolthoff, *J. Am. Chem. Soc.*, **61**, 1045 (1939).

(5) J. Newman, *Ind. Eng. Chem. Fundamentals*, **5**, 525 (1966).

(6) I. Šlendyk, *Collection Czech. Chem. Commun.*, **3**, 385 (1931).

Hence, for an applied potential V , the total current can be no larger than

$$I = 4\pi\kappa\tau_0 V = 4\pi\kappa\gamma V t^{1/2} \quad (4)$$

For small values of t , this value is less than the limiting diffusion-migration current, and the effect becomes particularly important for solutions of low conductivity.

For polarographic analysis the applied potential is essentially constant over the drop life, and the current will at first follow eq 4. As the drop grows, the current and the concentration must adjust themselves so that the various overpotentials, including concentration overpotential, surface overpotential, and ohmic drop, balance the applied voltage.

Levich⁷ has already treated this problem for a binary electrolyte. However, he assumed a constant concentration at the surface of the drop and thus missed the ohmic limitation at short time represented by eq 4. His work also contains a number of mathematical errors which obscure the analysis. With some generosity, his result can be expressed as

$$I = I_L(c_\infty - c_0)/c_\infty \quad (5)$$

where c_0 is the assumed constant concentration at the surface and depends upon the applied potential. This current is proportional to $t^{1/2}$ and represents an asymptote for large values of t . Equation 5 does reproduce the limiting current of Lingane and Kolthoff for a large applied potential.

Physical Basis for the Analysis. It is assumed that the solution can be treated as a dilute electrolytic solution; *i.e.*, the diffusion coefficients and activity coefficients are taken to be constant and the molar flux of an ionic species is expressed as

$$N_i = -z_i(D_i/RT)Fc_i\nabla\Phi - D_i\nabla c_i + v c_i \quad (6)$$

where v is the fluid velocity and Φ is the electrostatic potential. The concentration of the reactant in a solution of a single salt then obeys the equation of convective diffusion

$$\frac{\partial c}{\partial t} + v \cdot \nabla c = D \nabla^2 c \quad (7)$$

where D is again the diffusion coefficient of the salt.

For simplicity and clarity, let the growing mercury drop be an amalgam with an initial concentration c_s of the discharged reactant, and let the applied potential V refer to the potential of the growing drop relative to an amalgam reference electrode also of concentration c_s and located at a large distance from the capillary electrode. The applied potential V can then be expressed as

$$V = \frac{RT}{F} \frac{z_+ - z_-}{-z_+z_-} t_- \ln \frac{c_0}{c_\infty} - \frac{RT}{z_+F} \ln \frac{c_{s0}}{c_s} + \int_{r_0}^{\infty} \frac{i_r}{\kappa} dr \quad (8)$$

where i_r is the radial current density, c_0 is the concentration in the solution near the surface, and c_{s0} is the concentration in the mercury amalgam near the surface. Equation 8 is the potential of a concentration cell with transference plus the ohmic potential drop in the solution. The surface overpotential associated with the electrode reaction has been ignored.

The concentration in the solution differs from the bulk value c_∞ only in a thin region near the surface. If in this region the concentration is approximated by a linear profile

$$c = c_0 + (c_\infty - c_0)y/\delta \text{ for } 0 < y < \delta \\ c = c_\infty \text{ for } y > \delta \quad (9)$$

where

$$y = r - r_0 \quad (10)$$

then the integral in eq 8 can be evaluated, and the equation simplifies to (*cf.* ref 8)

$$V = \frac{RT}{F} \frac{z_+ - z_-}{-z_+z_-} \left[\ln \frac{c_0}{c_\infty} + t_+ \left(1 - \frac{c_0}{c_\infty} \right) \right] - \frac{RT}{z_+F} \ln \frac{c_{s0}}{c_s} - \frac{I}{4\pi\kappa_\infty r_0} \quad (11)$$

(Levich⁷ uses the crude approximation of taking $c = c_0$ in a region of thickness δ . See also editor's note to his section 52.)

The analysis of Ilkovič^{1,2} applies to a drop growing radially with no tangential velocity and to a thin diffusion layer which becomes thicker with time but is thin compared to the radius of the drop. The same approximation can be introduced in the present analysis so that the equation of convective diffusion, eq 7, becomes

$$\frac{\partial c}{\partial t} - \frac{2y}{r_0} \frac{dr_0}{dt} \frac{\partial c}{\partial y} = D \frac{\partial^2 c}{\partial y^2} \quad (12)$$

or

$$\frac{\partial c}{\partial t} - \frac{2y}{3t} \frac{\partial c}{\partial y} = D \frac{\partial^2 c}{\partial y^2} \quad (13)$$

A similar equation applies inside the sphere, but with the diffusion coefficient D_s of the discharged reactant in mercury.

(7) V. G. Levich, "Physicochemical Hydrodynamics," Prentice-Hall, Inc., Englewood Cliffs, N. J., 1962, Section 110.

(8) J. Newman, "The Effect of Migration in Laminar Diffusion Layers," UCRL-16665, Lawrence Radiation Laboratory, Berkeley, Calif., Feb 1966.

Finally the derivatives of concentration at the surface, both inside and outside the drop, are related to the total current by the expression

$$\frac{I}{4\pi r_0^2} = \frac{nFD}{1-t_+} \left. \frac{\partial c}{\partial y} \right|_{y=0_+} = nFD_s \left. \frac{\partial c}{\partial y} \right|_{y=0_-} \quad (14)$$

Derivation of Concentration at the Surface. In this section we obtain an integro-differential equation from which the surface concentration can be determined. Equation 13 can be reduced to the transient heat conduction equation

$$\frac{\partial c}{\partial \tau} = D \frac{\partial^2 c}{\partial z^2} \quad (15)$$

by means of the variables

$$z = t^{1/2}y \text{ and } \tau = (3/7)t^{3/2} \quad (16)$$

The solution to eq 15 satisfying the conditions

$$\begin{aligned} c &= c_\infty \text{ at } \tau = 0 \\ c &= c_\infty \text{ at } z = \infty \\ c &= c_0(\tau) \text{ at } z = 0 \end{aligned} \quad (17)$$

is⁹

$$c = c_\infty + \frac{2}{\sqrt{\pi}} \int_{z/\sqrt{4D\tau}}^{\infty} \left[c_0 \left(\tau - \frac{z^2}{4Dx^2} \right) - c_\infty \right] e^{-x^2} dx \quad (18)$$

The concentration $c_0(\tau)$ at the surface is still to be determined. The derivative of the concentration at the surface can be evaluated from this solution and substituted into eq 14 to yield

$$\frac{I}{4\pi r_0^2} = -\frac{nFt^{1/2}}{1-t_+} \sqrt{\frac{D}{\pi}} \int_0^\tau \frac{c_0'(x) dx}{\sqrt{\tau-x}} \quad (19)$$

In a similar manner, the solution for the amalgam inside the drop gives

$$\frac{I}{4\pi r_0^2} = nFt^{1/2} \sqrt{\frac{D_s}{\pi}} \int_0^\tau \frac{c_{s0}'(x) dx}{\sqrt{\tau-x}} \quad (20)$$

By equating expressions 19 and 20 and integrating, one can relate c_{s0} to c_0

$$c_{s0} - c_s = \frac{\sqrt{D/D_s}}{1-t_+} (c_\infty - c_0) \quad (21)$$

An integro-differential equation for the surface concentration can now be obtained by substituting eq 19 and 21 into the potential relation 11. The result is

$$\begin{aligned} V = \frac{RT}{F} \frac{z_+ - z_-}{-z_+z_-} \left[\ln \frac{c_0}{c_\infty} + t_+ \left(1 - \frac{c_0}{c_\infty} \right) \right] - \\ \frac{RT}{z_+F} \ln \left(1 + \frac{\sqrt{D/D_s}}{1-t_+} \frac{c_\infty - c_0}{c_s} \right) + \\ \frac{nF\gamma t}{\kappa_\infty(1-t_+)} \sqrt{\frac{D}{\pi}} \int_0^\tau \frac{c_0'(x) dx}{\sqrt{\tau-x}} \end{aligned} \quad (22)$$

Solution for the Concentration and the Current. We shall obtain the solution when the concentration variation inside the mercury drop can be neglected and eq 22 can be written

$$\begin{aligned} \frac{-z_+z_-}{z_+ - z_-} \frac{FV}{RT} = \ln \frac{c_0}{c_\infty} + t_+ \left(1 - \frac{c_0}{c_\infty} \right) - \\ \frac{-z_+z_-}{z_+ - z_-} \frac{nF^2\gamma t}{RT\kappa_\infty(1-t_+)} \sqrt{\frac{D}{\pi}} \int_0^\tau \frac{c_0'(x) dx}{\sqrt{\tau-x}} \end{aligned} \quad (23)$$

The form of this equation suggests that most of the parameters can be eliminated by the use of appropriate dimensionless variables. For the potential and the concentration the choice is clear

$$E = \frac{z_+z_-}{z_+ - z_-} \frac{FV}{RT} \text{ and } C = \frac{c_0}{c_\infty} \quad (24)$$

Note that E is now positive while V is negative. Equation 23 then becomes

$$-E = \ln C + t_+(1-C) + \frac{N\gamma t}{\sqrt{\pi D}} \int_0^\tau \frac{C'(x) dx}{\sqrt{\tau-x}} \quad (25)$$

where

$$N = \frac{-z_+z_-}{z_+ - z_-} \frac{nF^2Dc_\infty}{RT(1-t_+)\kappa_\infty} \quad (26)$$

The dimensionless parameter N is related to the relative importance of concentration overpotential and ohmic drop in balancing the applied voltage. For a dimensionless time variable we choose

$$\theta = \sqrt{3\pi D/7} t^{1/2} / N\gamma \quad (27)$$

With this variable, eq 25 can be written

$$-E = \ln C + t_+(1-C) + \int_0^1 \frac{dC}{d\eta} \Big|_{\eta=\theta\psi} \frac{d\psi}{\sqrt{1-\psi^2}} \quad (28)$$

where C is now a function of θ .

From eq 11 it now becomes apparent that an appropriate choice for the dimensionless current would be

$$J = \frac{3(1-t_+)I}{28nF\gamma^3c_\infty N} \quad (29)$$

(9) H. S. Carslaw and J. C. Jaeger, "Conduction of Heat in Solids," Clarendon Press, Oxford, 1959, pp 62, 63.

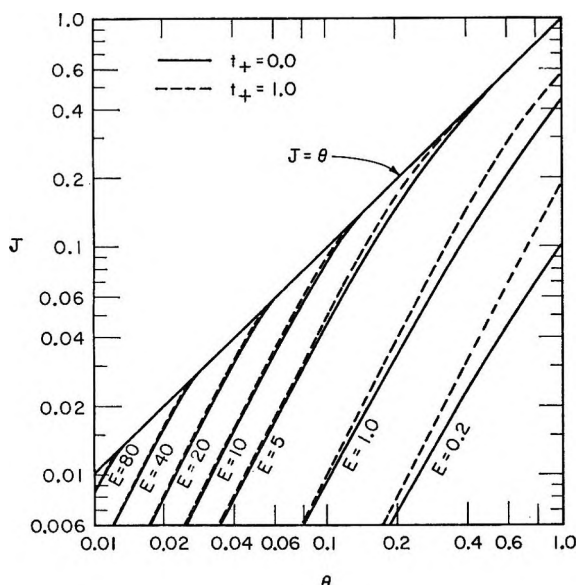


Figure 1. The reduced instantaneous current to the drop as a function of dimensionless time, dimensionless applied voltage, and cation transference number.

With this choice, eq 11 becomes

$$J = \theta^2 [E + \ln C + t_+(1 - C)] \quad (30)$$

Now C can be obtained as a function of θ from eq 28, and the dimensionless current can then be obtained from eq 30. For small times, C can be expanded as a power series in θ

$$C = 1 - E\theta + a_2\theta^2 + a_3\theta^3 + \dots \quad (31)$$

with then

$$J = E\theta^2 + e_3\theta^3 + e_4\theta^4 + \dots \quad (32)$$

The first term of these equations corresponds to eq 4, and the applied voltage is opposed only by the ohmic potential drop in the solution. The coefficients a_i and e_i are functions of the parameters E and t_+ .

At very large times, C will be a constant, given implicitly by the equation

$$-E = \ln C + t_+(1 - C) \quad (33)$$

and the current will be given by eq 5, where c_0 is determined from eq 33. For a large applied potential the limiting dimensionless current is

$$J = \theta \quad (34)$$

corresponding to eq 3.

Using the small time expansion introduced in eq 31 we have calculated the dimensionless current to the drop for various values of E and for values of θ up to 1. The results are shown in Figure 1. It is seen

that the value of the transference number has only a small effect on the current, particularly at large voltages, in which case the effect vanishes in both the small and large time limits. The current varies with θ^2 or $t^{1/3}$ at small times and then changes over to a θ or $t^{1/3}$ dependence at large times, the transition being earlier the greater the applied potential.

The significant quantity for comparison with experiment is usually not the instantaneous current but rather the current averaged over the lifetime of a drop. This average current is defined as

$$\bar{I} = \frac{1}{T} \int_0^T I dt \quad (35)$$

where T is the drop life.

The solution for the instantaneous current has been integrated to obtain the average current to the drop. The results are shown in Figure 2 where the dimensionless average current \bar{J} , defined analogously to J , is plotted vs. dimensionless drop life $\Theta = \theta_{\text{final}}$ with the dimensionless voltage and t_+ as parameters. For a typical experiment Θ is on the order of 0.1–0.5. Also, for a 1–1 electrolyte an applied voltage of 1 v corresponds to $E = 19.5$. The line $\bar{J} = 6\Theta/7$ is the limiting current result corresponding to eq 3 and represents the large-time, large-voltage asymptote. The value of the transference number has little effect on the average current particularly for reasonably large voltages. Curves for values of t_+ between 0 and 1 fall between the two curves.

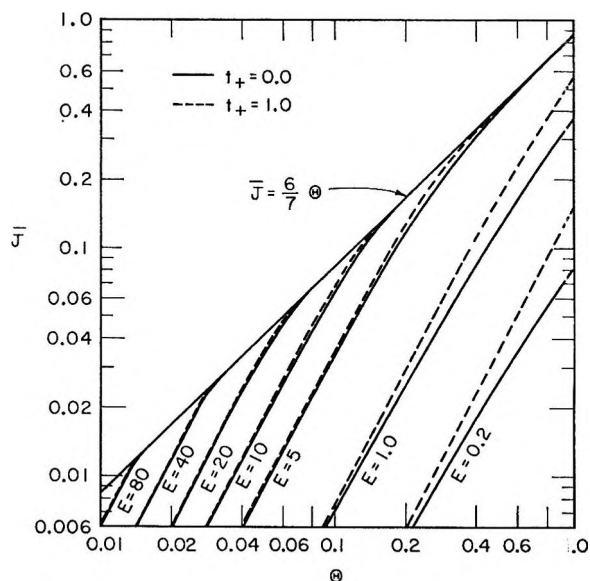


Figure 2. The reduced average current to the drop as a function of dimensionless drop life, dimensionless applied voltage, and cation transference number.

This analysis has been developed for a two-electrode polarographic technique where the reference electrode is far from the working electrode. If the applied voltage is controlled by a potentiostat which employs a probe reference electrode very close to the drop, the upper limit of the integral in eq 8 would be no longer infinity but rather the radial position of the reference electrode. The probe would still be outside the diffusion layer, which is at most 10^{-3} to 10^{-2} cm thick in these experiments, so that the approximation used to evaluate the integral would not be invalidated. The only change in the analysis necessitated by the use of a probe is the introduction of a factor of $\zeta/(\zeta + r_0)$ in the last term in eq 23 where ζ is the distance of the tip of the probe from the surface of the drop.

The introduction of this time-dependent factor in eq 23 complicates the solution of the problem. However, since the factor would normally vary from unity down to 0.7–0.6 over the lifetime of a drop, it should not greatly change the results of the analysis as stated. Its effect on the measured average current would be essentially the same as that of an increase in the conductivity of the bulk solution.

We have neglected the effects on the transient current behavior of certain electrode phenomena. If the electrode is not reversible as we have assumed, it is necessary to include the overpotential involved with the electrode reaction in the boundary condition formulated in eq 8.

In addition to the Faradaic current calculated, a capacitive current must also flow as the drop grows in order to charge the double layer on the newly formed mercury-solution interface. The magnitude of this capacitive current can be estimated by considering the charging of a spherical capacitor of double-layer capacity K . The total voltage is made up of the double-layer voltage and the ohmic drop

$$V = V_{dl} + V_{ohm} \quad (36)$$

Since the total voltage is constant

$$-\frac{dV_{ohm}}{dt} = \frac{dV_{dl}}{dt} = \frac{i}{K} = \frac{I}{4\pi r_0^2 K} \quad (37)$$

Differentiation of the expression for the ohmic loss to a sphere

$$V_{ohm} = I/4\pi\kappa_\infty r_0 \quad (38)$$

yields

$$\frac{dV_{ohm}}{dt} = \frac{1}{4\pi\kappa_\infty r_0} \left(\frac{dI}{dt} - \frac{1}{3} \frac{I}{t} \right) \quad (39)$$

Substitution of eq 37 into eq 39, integration, and application of eq 38 as an initial condition for I with $V_{ohm} = V$ yield eq 40.

$$I = 4\pi\kappa_\infty\gamma V t^{1/3} \exp\left(-\frac{3\kappa_\infty t^{2/3}}{2\gamma K}\right) \quad (40)$$

The ratio of this ohmically limited charging current to the total ohmically limited current at small times is

$$\exp(-3\kappa_\infty t^{2/3}/2\gamma K)$$

For the typical values of the parameters $\gamma = 0.1$ cm/sec^{1/3}, $K = 30 \mu\text{f}/\text{cm}^2$, and $\kappa_\infty = 0.01(\text{ohm cm})^{-1}$, this ratio is $e^{-5 \times 10^{-2} t^{2/3}}$, where t is in seconds. Since we need not concern ourselves with extremely short times, the capacitive current may be considered negligible compared to the Faradaic current.

A discussion of the effect of the solution resistance on the capacitive current in electrochemical kinetics studies, where it is not negligible, has been given recently by Oldham.¹⁰ Also Delahay has made a more thorough investigation of the contributions of Faradaic and capacitive currents in transient electrode processes.¹¹

Conclusions

For $E > 20$ and $\Theta > 0.07$ the limiting-current approximation provides a good representation of the average current. However, for $E = 10$ the approximation is not very accurate unless $\Theta > 0.2$, and it becomes much less accurate for smaller voltages and shorter times. Therefore, the correct interpretation of experimental data obtained under circumstances where values of drop life or applied voltage may be necessarily small or where instantaneous current is measured directly requires consideration of the detailed results of this analysis.

A further conclusion of this work follows from eq 29 and 30. The right side of eq 30 is dimensionless and independent of c_∞ . Therefore, since N is independent of c_∞ for dilute solutions, the current I is always proportional to the bulk concentration of the reactant, even during the transient concentration behavior. This is the characteristic of all polarographic situations which gives the method its great usefulness as a quantitative analytical tool.

The phenomena considered here for a binary electrolyte also occur in a supported electrolyte. However, because of the higher conductivity, the transient effects are of much shorter duration and therefore insignificant in that case.

Acknowledgment. This work was supported by the U. S. Atomic Energy Commission.

(10) K. B. Oldham, *J. Electroanal. Chem.*, **11**, 171 (1966).

(11) P. Delahay, *J. Phys. Chem.*, **70**, 2373 (1966).

Conductance and Water Transfer in a Leached Cation-Exchange Membrane

by J. H. B. George and R. A. Courant

Arthur D. Little, Inc., Cambridge, Massachusetts (Received March 11, 1966)

Specific conductance and water transfer have been determined for a variety of cations in a polystyrene-sulfonate cation-exchange membrane substantially free of co-ions. The measurements were made at three temperatures, 10, 25, and 40°, and equivalent conductances and energies of activation for conduction were calculated. Not surprisingly, it was found that equivalent conductances in the membrane are lower than in free aqueous solution, the difference being much greater for multivalent ions. Among ions of a given class, such as the alkali metals or alkaline earths, the equivalent conductances go through a maximum with increasing atomic number instead of increasing continuously as in free solution. The corresponding activation energies show a minimum. This behavior is interpreted as being due to a balance between increased mobility as the hydration of the cation decreases and an increased degree of ion association with the exchange groups of the membrane. Water transfer per equivalent of charge decreases as the charge of the cation increases although it is nearly constant per mole of ions transferred. It is little affected by temperature but increases markedly at very low current densities. This latter phenomenon may be due to utilization of only the larger pores in the membrane.

Introduction

Ion-exchange membranes have some interesting characteristics as electrolytically conductive systems. When they are in equilibrium with sufficiently dilute solutions (generally 0.01 *N* and lower), virtually all the mobile ions are of one sign, and values for the equivalent conductance of the counterions can be derived directly from the experimental data. Another feature is the transport of water which accompanies the passage of ions through the membrane, caused partly by ionic hydration and partly by electroosmotic transfer. A comparison of the observed conductances of ions in membranes and in free aqueous solution shows, not surprisingly, that ions are much less conductive in membranes. Part of this is clearly due to the obstructive effect of the polymer chains of the membrane, and Despic and Hills¹ and Meares^{2,3} have employed expressions involving the volume fraction of the resin in the membrane to estimate its magnitude. The most remarkable feature of membrane conductances, however, is the wide differences shown by ions according to their charge type. While the equivalent conductances of the majority of monovalent, divalent, and trivalent cations in free aqueous solution are equal to within

10–20% or so, very large differences are observed in the membrane phase. Thus Rosenberg, George, and Potter⁴ found values of 12.5, 2.7, and 0.7, respectively, for the equivalent conductances of potassium, barium, and lanthanum in a polystyrene-sulfonate membrane. The objective of the present work was to study the conductance and water transfer accompanying the transport of a wide variety of ion species through a single cation exchange membrane in order to characterize their dependence on ion size and charge type. All measurements were made with the membrane in equilibrium with solutions sufficiently dilute, 0.01 *N*, so that the counterions were the only conductive species in the membrane and at three temperatures, 10, 25, and 40°, in order that activation energies might be calculated for the conduction processes.

(1) A. Despic and G. J. Hills, *Discussions Faraday Soc.*, **21**, 150 (1956).

(2) J. S. Mackie and P. Meares, *Proc. Roy. Soc. (London)*, **A232**, 485, 498 (1955).

(3) P. Meares, *J. Polymer Sci.*, **20**, 507 (1956).

(4) N. W. Rosenberg, J. H. B. George, and W. D. Potter, *J. Electrochem. Soc.*, **104**, 111 (1957).

Experimental Procedures

The cation-exchange membrane selected for the transport measurements was the commercially available Nepton CR-61, Type AZL 183, and was supplied by Ionics, Inc., Watertown, Mass. The CR-61 family of membranes has a polystyrene base and sulfonate exchange groups. Individual members vary in the degree of cross-linking with divinylbenzene. The particular membrane selected had a high divinylbenzene content, approximately 40%, and was prepared by techniques described in the patent literature.⁵ The membranes are light yellow, approximately 0.07 cm thick, and are supported on an inert backing (in this case a loosely woven Dynel cloth).

Conversion of the membrane to the various ionic forms was carried out by repeated equilibration with approximately 2 *N* solutions of the appropriate chloride or nitrate followed by thorough washing with deionized water to remove absorbed electrolyte. For certain costly chemicals, the conversion was carried out electrolytically by containing the solution on one side of the membrane and passing a small current through it. It was found that passage of a quantity of electricity equivalent to twice the capacity of the membrane sample was generally sufficient to ensure complete conversion.

Before its conductivity and water transfer were measured, the membrane was characterized for capacity, water content, and specific volume by standard methods.⁶

Conductance Measurements. The conductance measurements were made in a lucite cell consisting of two equivalent electrode sections fitting closely into a cylindrical sleeve. Circular platinized platinum electrodes parallel to the plane of the membrane were embedded in each section and slightly recessed so that neither was in contact with the membrane. The shoulders of the sections fitted closely together, keeping the electrodes at a constant distance from each other (approximately 0.4 cm) when no membrane was present. The diameter of the electrodes and thus of the exposed membrane sample was approximately 1.0 cm. Resistance measurements were made with and without the membrane in a 0.01 *N* solution of the chloride or nitrate of the ion under investigation. According to the analysis of Barrer, Barrie, and Rogers,⁷ refraction of the lines of current flow would cause a lowering in the apparent resistance of the order of 4% in a conductance cell with these dimensions. The actual experimental results were not, however, corrected for this effect.

The conductance determinations were made with a Campbell-Shackleton bridge which has been described

elsewhere.⁸ Temperature control was attained by use of oil baths, the temperature of which was observed never to deviate from the set value by more than 0.02° at 25° and 0.05° at 10 and 40°. A plastic bag was placed around the cell to prevent the cell and its contents from being contaminated by oil from the bath.

The effect of frequency on the experimentally determined membrane conductances was investigated. With sodium ions in the membrane the conductance rose gradually by about 7% as the frequency was increased from 60 to 1000 cps. It subsequently remained almost constant as the frequency was further increased to 10,000 cps and gradually fell by about 2–3% between 10,000 and 50,000 cps. Since the effect of frequency thus appeared to be small, 1000 cps was used as the standard for all measurements.

The precision of this technique for the measurement of ionic conductivity in the membrane improved with an increase in membrane resistance. For the less conductive multivalent ions the spread in experimental values among half a dozen samples was never greater than about ±3%. For the more conductive monovalent ions, the spread was somewhat greater, on the order of ±5%. Nonuniformity of the membrane samples is believed to account for the lack of greater precision.

Water-Transfer Measurements. Water-transfer measurements were made in a two-compartment Lucite apparatus—the donating chamber, which was stirred vigorously, having a volume of approximately 750 ml, and the receiving chamber, having a volume of approximately 100 ml. A circular sample of membrane, with a diameter of 7 cm, separated the two compartments and was prevented from buckling by perforated Lucite sheets. The exposed membrane area was 12.5 cm². Volume changes were determined by observing with a cathetometer the liquid level in a glass capillary leading from the smaller chamber. A current of 2.5 ma was passed between large, flat silver–silver chloride electrodes giving a current density of 0.2 ma/cm² of exposed membrane surface. The correction for change in volume at the electrodes was too small to be significant. All measurements were carried out in constant-temperature oil baths and as an additional check on the constancy of the temperature, a platinum–platinum–rhodium thermocouple was immersed in the

(5) J. T. Clarke (Ionics, Inc.). U. S. Patents 2,730,768 and 2,731,411 (1956).

(6) F. Helfferich, "Ion Exchange," McGraw-Hill Book Co., Inc., New York, N. Y., 1962, Chapter 4.

(7) R. M. Barrer, J. A. Barrie, and M. G. Rogers, *Trans. Faraday Soc.*, **58**, 2473 (1962).

(8) R. A. Horne and G. R. Frysinger, *J. Geophys. Res.*, **68**, 1967 (1963).

Table I: Membrane Equivalent Conductances, Activation Energies, and Water Transfer

Ionic form of membrane	λ_m , cm ² ohm ⁻¹ equiv ⁻¹ 25°	λ_m/λ_0^a 25°	E_a , kcal/mole			Water transfer, ^b mole/faraday		
			Membrane	Soln at infinite dilution ^a	Difference	10°	25°	40°
Li ⁺	2.19	0.057	5.46	4.13	+1.33	20.6	19.6	17.1
Na ⁺	2.82	0.058	5.39	3.87	+1.52	13.3	14.0	13.8
K ⁺	5.31	0.072	3.69	3.47	+0.22	10.7	10.1	9.7
Rb ⁺	3.81	0.049	4.00	3.38	+0.71	7.9	7.7	8.1
Cs ⁺	1.86	0.019	4.15	3.33	+0.82	8.9	8.5	6.6
NH ₄ ⁺	5.32	0.072	4.69	3.86	+0.83	14.4	12.5	14.8
Tl ⁺	3.04	0.041	4.73	16.4	11.5	6.4
Mg ²⁺	0.689	0.013	4.87	3.92	+0.95	5.5	3.4	2.5
Ca ²⁺	0.989	0.016	4.46	3.92	+0.54	7.2	6.8	6.4
Sr ²⁺	0.844	0.014	4.82	4.04	+0.78	6.3	4.8	3.2
Ba ²⁺	0.749	0.012	4.80	4.23	+0.57	5.4	4.5	3.1
La ³⁺	0.219	0.003	4.00	4.64	-0.64	3.9	2.3	2.0

^a Values for λ_0 and its temperature coefficient taken from R. A. Robinson and R. H. Stokes, "Electrolyte Solutions," 2nd ed, Butterworth and Co., Ltd., London, 1959. ^b At 0.2 ma/cm².

receiving chamber. Even so, the precision in the experimental values, some half dozen per ion at each temperature, was only about $\pm 10\%$.

Results

The capacity of the Nepton CR-61 membrane was found to be 2.45 mequiv/g and 1.77 mequiv/ml of surface dried membrane. These figures include the Dynel backing material, reported by the manufacturer to constitute about 36% of the weight of the completely dry membrane. Capacity determinations in various ionic forms differed by less than 2%. Water content data, expressed as a weight percentage of water in the wet membrane (surface dried and including backing), were: Li⁺, 36.9; Na⁺, 36.4; K⁺, 35.7; Rb⁺, 32.2; Cs⁺, 32.7; NH₄⁺, 36.0; Tl⁺, 37.8; Mg²⁺, 35.5; Ca²⁺, 35.2; Sr²⁺, 32.8; La³⁺, 32.5.

The results of the conductivity measurements, expressed as equivalent conductances λ_m at 25° and energies of activation E_a calculated from the temperature coefficients, are shown in Table I. Over the limited temperature range, 10–40°, the Arrhenius plots showed little deviation from linearity. Ratios of λ_m to λ_0 , the limiting equivalent conductances of the ions in free aqueous solution, and values of E_a calculated from the temperature coefficients of λ_0 are also included.

Table I also contains the results of the water-transfer measurements at 10, 25, and 40° expressed as mole/faraday.

Discussion

The results of the conductance measurements expressed in Table I show very clearly the effect of ionic charge on the mobility of ions in the membrane.

For example, the values of λ_m at 25° for the monovalent ions vary from 1.86 for cesium to 5.32 for ammonium; the values for the bivalent ions, which are much more similar, range from 0.69 for magnesium to 0.99 for calcium while the value for lanthanum, the only trivalent ion studied, is as low as 0.22. Values of λ_0 for all these ions fall in the range from 38.7 for lithium to 77.8 for rubidium and are not directly related to charge type. It thus appears that λ_m/λ_0 decreases by a factor of about 4 for each unit increase in the charge of the ion.

These data are generally similar to earlier results obtained by Manecke and Otto-Laupenmühlen⁹ for a phenol-formaldehyde-based sulfonate membrane. The work of Spiegler and Coryell¹⁰ and of Grubb¹¹ also showed marked differences in λ_m between alkali metal cations and ions of bivalent metals such as zinc, calcium, and copper in membranes of this type.

Consideration of the values of λ_m for the monovalent ions separately leads to some interesting observations. Values increase from lithium through sodium to potassium, but then decrease to rubidium and cesium. This behavior contrasts with that in free aqueous solution where λ_0 increases monotonically from lithium to cesium. The behavior in solution is interpreted as being due to the decrease in hydration as the crystallographic radius of the cation increases. In the membrane phase, ion hydration is likely to be lower than in solution because of the more limited supply of water.

(9) G. Manecke and E. Otto-Laupenmühlen, *Z. Physik. Chem. (Frankfurt)*, **2**, 336 (1954).

(10) K. S. Spiegler and C. D. Coryell, *J. Phys. Chem.*, **57**, 687 (1953).

(11) W. T. Grubb, *ibid.*, **63**, 55 (1959).

The water content determinations show that only approximately 11 water molecules are present in the solution for every equivalent of exchange capacity. Coulombic forces will be much stronger because of the lower dielectric constant and the high ionic concentration in the membrane. The increase in λ_m from lithium to potassium may thus be due to decreasing ionic hydration as in free aqueous solution, and the subsequent decrease from potassium to cesium reflects increasing ion association with the exchange groups as a consequence of the diminished hydration cover of the counterions. The same general phenomenon seems to occur also in the bivalent ions in this series although the range

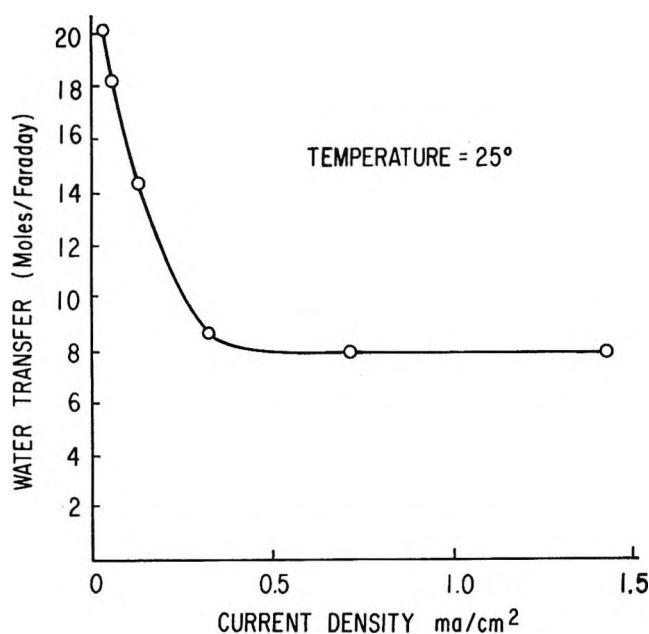


Figure 1. Water transfer in sodium form of Nepton CR-61 as a function of current density.

of values is not so great in this case. At 25°, for example, λ_m values increase from 0.69 for magnesium to a maximum of 0.99 for calcium and then decrease to 0.84 for strontium and 0.75 for barium. Corresponding values for λ_0 in free aqueous solution show a continuous, if small, increase throughout this series of bivalent ions.

Activation energies for the conductance process in the membrane are significantly greater than the values for free solution. The increase in activation energy is undoubtedly related to the interaction of the hydrated ions with the membrane structure and particularly the effect of coulombic interaction with the exchange groups. Among the alkali metal cations, the activation energies for conductance in the membrane appear to decrease from lithium to potassium and then in-

crease for rubidium and cesium, the inverse order of the λ_m values.

It is doubtful whether the water-transfer measurements presented in Table I have much absolute significance although their relative values are believed to be self-consistent. The measurements were carried out at very low current densities (approximately 0.2 ma/cm²) in order to minimize osmotic effects due to concentration polarization in the unstirred receiving solution. However, it became apparent that the water transfer per faraday was in fact a function of the current density, as is demonstrated in Figure 1 for some measurements on the sodium form of the membrane at 25°. It can be seen that the water transfer is extremely high at low current densities but falls to a relatively constant value at current densities above about 0.5 ma/cm². This effect has also been observed in phenolsulfonic membranes by Lakshminarayanaiah,¹² who suggested that transport might be taking place only in the larger pores of the membrane at the lower current densities. The water-transfer coefficient through these large pores is likely to be higher than the average value which obtains when a reasonably high current density is used.

The data indicate that water-transfer coefficients generally decrease somewhat with increasing temperature. Water transfer per faraday is about twice as great for monovalent ions as for bivalent ions and four times as great for the trivalent ion lanthanum. The numbers, in fact, suggest that to a first approximation the water transfer is almost the same per mole of ions transferred. Among the monovalent ions, the water-transfer coefficients decrease very substantially from lithium to potassium and are then roughly constant. A great deal of the water transferred with the lithium and sodium ions must be water of hydration. The relatively low values of water transfer for the bivalent and trivalent ions may be some indication that they are less hydrated in the membrane than in free aqueous solution. Thus, while it is not possible to develop any quantitative treatment for the effects of variable hydration and ion association on the conductance and transfer of ions in the membrane, the experimental results do provide broad support for an interpretation in these terms of the gross differences in behavior between ions of different charge types.

Acknowledgment. This work was supported by Contract No. 14-01-0001-372 with the Office of Saline Water, U. S. Department of the Interior.

(12) N. Lakshminarayanaiah, *Proc. Indian Acad. Sci.*, **A55**, 200 (1962).

Some Reactions of Oxygen Atoms. II. Ethylene Oxide, Dimethyl

Ether, $n\text{-C}_4\text{H}_{10}$, $n\text{-C}_7\text{H}_{16}$, and Isooctane¹

by Grace Marsh and Julian Heicklen²

Aerospace Corporation, El Segundo, California 90045 (Received March 30, 1966)

Oxygen atoms $\text{O}(^3\text{P})$ were generated from the mercury-sensitized decomposition of N_2O in the presence of C_3F_6 and a sample gas at 34, 70, and 125°. The C_3F_6 and sample gas compete for the oxygen atoms. From the competition, the Arrhenius parameters were found, and they are tabulated. The sample gases used were ethylene oxide, dimethyl ether, $n\text{-C}_4\text{H}_{10}$, $n\text{-C}_7\text{H}_{16}$, and isooctane (2,2,4-trimethylpentane).

I. Introduction

Some reaction rates of oxygen atoms with hydrocarbons have been summarized by Cvetanović.³ One of the cleanest methods of producing $\text{O}(^3\text{P})$ atoms is the mercury-sensitized photolysis of N_2O . This technique has been used in this laboratory to study oxygen atom reactions with C_3F_6 and C_2F_4 .⁴⁻⁶ With C_2F_4 the only oxygen-containing product is CF_2O ; from C_3F_6 , CF_2O and CF_3CFO are produced. Thus by monitoring these products when mixtures of either C_2F_4 or C_3F_6 and a hydrocarbon are present, relative rate constants can be obtained. In part I of this series,⁵ a number of rate constants were found by this method. In the present paper, C_3F_6 is used in competition with ethylene oxide, dimethyl ether, $n\text{-C}_4\text{H}_{10}$, $n\text{-C}_7\text{H}_{16}$, and isooctane (2,2,4-trimethylpentane) to obtain Arrhenius parameters.

II. Experimental Section

A. Chemicals. The compounds used in this experiment were Matheson Coleman and Bell N_2O , dimethyl ether, and $n\text{-C}_4\text{H}_{10}$, Peninsular ChemResearch Co. C_3F_6 , and Eastman Organic Chemicals $n\text{-C}_7\text{H}_{16}$, ethylene oxide, and Spectrograde isooctane (2,2,4-trimethylpentane). All compounds were degassed through a spiral trap at -196° . Gas chromatographic analysis indicated no appreciable impurities.

B. Apparatus. *In situ* infrared analysis was employed to monitor the changes in the 5.12- and 5.30- μ bands representing, respectively, CF_2O and CF_3CFO . The vacuum manifold, X-shaped cell, and optical arrangement have been described previously.⁴⁻⁶

C. Procedure. Mixtures of C_3F_6 and a sample gas were placed in the reaction cell. The total pressure did not exceed 150 mm except with ethylene oxide, whose low rate constant necessitated greater pressures. Then 470–530 mm of N_2O was added. After a short period of time to allow for gas diffusion, an initial scan of the 5.12- and 5.30- μ bands was taken. The gas mixture in the reaction cell was irradiated for a fixed period of time. The product bands grew linearly with time. Three minutes after illumination ended, the final scan of the same region was obtained. Whenever the rate of formation of N_2 was required, the gases in the reaction cell were allowed to expand through a -196° trap to a McLeod gauge. The pressure of the noncondensable gas (N_2) was measured, and predetermined expansion factors were used to calculate the rate of formation of N_2 .

The extinction coefficients used to convert optical density to pressure were established previously.⁵

III. Relative Reaction Rates

Oxygen atoms $\text{O}(^3\text{P})$ are obtained by the reactions³

(1) Supported by the U. S. Air Force under Contract No. AF 04(695)-669.

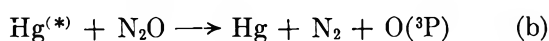
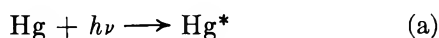
(2) To whom request for reprints should be addressed at Materials Sciences Laboratory, Aerospace Corp., P. O. Box 95085, Los Angeles, Calif.

(3) For a review, see R. J. Cvetanović, *Advan. Photochem.*, **1**, 15 (1963).

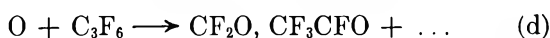
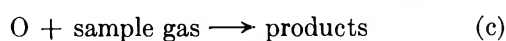
(4) D. Saunders and J. Heicklen, *J. Am. Chem. Soc.*, **87**, 4062 (1965).

(5) D. Saunders and J. Heicklen, *J. Phys. Chem.*, **70**, 1950 (1966).

(6) D. Saunders and J. Heicklen, *J. Am. Chem. Soc.*, **87**, 2088 (1965).



The possibility of the excited mercury atom reacting with the other species present is minimized by the use of high pressures of N_2O in relation to the other species. Two competing reactions are present with mixtures of C_3F_6 and a sample gas



The ratio of rate constants k_c/k_d is expressed by

$$\frac{k_c}{k_d} = \left[\frac{\gamma R(\text{N}_2) - R(\text{RO})}{R(\text{RO})} \right] \frac{[\text{C}_3\text{F}_6]}{[\text{sample gas}]} \quad (1)$$

Table I: Relative Rate Constants for $\text{O}(^3\text{P})$ with Ethylene Oxide and C_3F_6 ; $[\text{N}_2\text{O}] = 500 \pm 31$ mm

$[\text{C}_3\text{F}_6]$, mm	$[\text{C}_2\text{H}_4\text{O}]$, mm	$R(\text{N}_2)$, μ/min	$R(\text{RO})$, μ/min	k_c/k_d
$T = 307^\circ\text{K}$				
1.96	44	54	30	0.033
3.9	117	54	25	0.038
3.8	149	54	20.5	0.041
4.1	164	54	21	0.040
3.2	157	54	18.2	0.040
2.8	172	54	19.3	0.029
2.3	182	54	13.2	0.038
4.4	184	54	16.8	0.052
1.94	220	54	8.3	0.048
2.1	179	54	13.4	0.035
1.85	74	54	19.1	0.045
1.31	176	11.1	1.85	0.038
2.2	167	11.4	2.6	0.044
				$\text{Av} = 0.040 \pm 0.004$
$T = 343^\circ\text{K}$				
3.8	109	134	67	0.034
4.6	182	163	70	0.033
4.0	220	146	54	0.031
3.1	202	175	44	0.045
2.3	204	175	39	0.038
1.10	175	171	26	0.035
1.40	193	160	29	0.033
				$\text{Av} = 0.036 \pm 0.003$
$T = 398^\circ\text{K}$				
3.5	223	133	38	0.039
2.6	225	139	29	0.044
1.86	205	129	28	0.033
4.2	171	124	57	0.029
4.4	165	121	57	0.029
1.99	113	121	45	0.020
1.36	178	152	25	0.040
1.8	156	6.2	1.68	0.031
				$\text{Av} = 0.034 \pm 0.005$

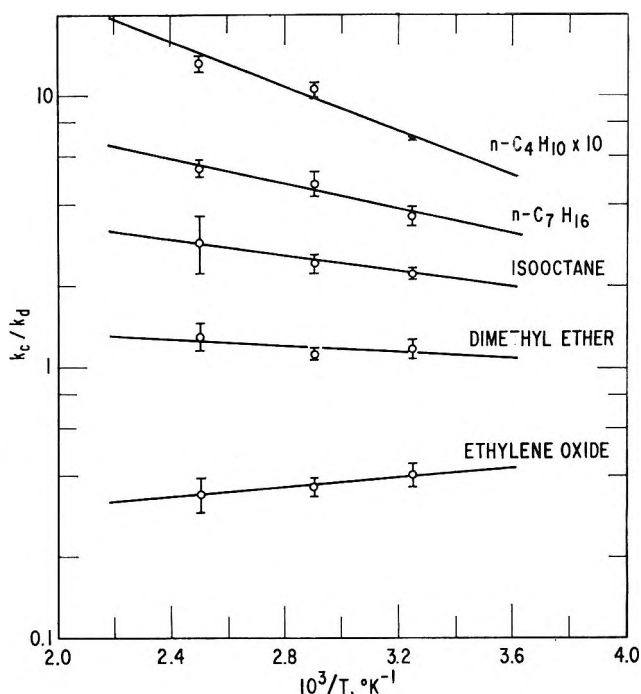


Figure 1. Semilog plots of k_c/k_d vs. reciprocal temperatures for various gases.

Table II: Relative Rate Constants for $\text{O}(^3\text{P})$ with Dimethyl Ether and C_3F_6 ; $[\text{N}_2\text{O}] = 505 \pm 12$ mm

$[\text{C}_3\text{F}_6]$, mm	$[\text{CH}_3\text{OCH}_3]$, mm	$R^0(\text{RO})^a$, μ/min	$R(\text{RO})$, μ/min	k_c/k_d
$T = 307^\circ\text{K}$				
4.6	39.8	44	3.6	1.30
11.5	27.0	44	11.9	1.28
13.0	20.0	44	16.2	1.10
10.5	38.5	44	10.0	0.92
11.0	62.0	44	5.4	1.24
11.2	19.6	29	9.5	1.15
8.5	40.0	100	15.3	1.18
				$\text{Av} = 1.17 \pm 0.09$
$T = 343^\circ\text{K}$				
8.6	14.4	50	17.9	1.08
17.0	38.0	50	14.4	1.10
14.0	40.0	48	11.0	1.19
12.0	18.0	48	18.4	1.07
24.0	23.0	46	22	1.18
				$\text{Av} = 1.12 \pm 0.05$
$T = 398^\circ\text{K}$				
6.3	15.7	87	21	1.23
6.8	11.2	79	23	1.52
10.0	10.0	66	31	1.17
14.7	13.3	56	28	1.12
15.0	48.0	56	9.8	1.46
				$\text{Av} = 1.30 \pm 0.15$

^a Determined by separate runs.

Table III: Relative Rate Constants for O(³P) with *n*-C₄H₁₀ and C₃F₆; [N₂O] = 499 ± 14 mm

[C ₃ F ₆], mm	[C ₄ H ₁₀], mm	<i>R</i> ⁰ (RO), ^a μ/min	<i>R</i> (RO), μ/min	<i>k_c/k_d</i>
<i>T</i> = 307°K				
25.5	26	43	25	0.70
13.2	26.3	40	17.0	0.68
13.0	38.0	35	12.4	0.68
12.5	47.5	33	9.0	0.72
12.5	58.5	32	7.5	0.69
Av = 0.69 ± 0.01				
<i>T</i> = 343°K				
13.0	23.0	202	68	1.12
11.5	33.5	190	45	1.11
14.0	59.5	178	33	1.04
10.0	71.5	205	26	0.98
Av = 1.06 ± 0.05				
<i>T</i> = 398°K				
10	11.5	233	86	1.50
11	19.5	222	66	1.32
12.5	37.0	211	42	1.34
13.0	51.5	200	35	1.21
13.3	74.7	177	23	1.18
Av = 1.31 ± 0.08				

^a Determined by separate runs.**Table IV:** Relative Rate Constants for O(³P) with *n*-C₇H₁₆ and C₃F₆; [N₂O] = 512 ± 13 mm

[C ₃ F ₆], mm	[C ₇ H ₁₆], mm	<i>R</i> ⁰ (RO), ^a μ/min	<i>R</i> (RO), μ/min	<i>k_c/k_d</i>
<i>T</i> = 307°K				
42.2	13	105	48	3.8
26.3	12	105	43	3.1
16.3	9.7	105	32	3.9
12.0	12.0	105	23	3.5
11.0	22.0	105	12.2	3.8
Av = 3.6 ± 0.3				
<i>T</i> = 343°K				
8.0	10.0	118	23	3.3
9.4	16.6	118	10.2	5.8
9.8	14.5	118	16.0	4.3
21.4	12.6	118	28	5.4
47.5	16	118	45	4.8
46.5	10.5	118	57	4.8
Av = 4.7 ± 0.5				
<i>T</i> = 398°K				
7.4	6.6	172	35	4.4
24.2	12.2	172	46	5.4
29.5	10	172	62	5.3
46.5	10	172	74	6.0
9.2	17.2	172	14.4	5.9
Av = 5.4 ± 0.4				

^a Determined by separate runs.

where *R*(RO) is the sum of the rates of CF₂O and CF₃-CFO formation and γ is $\Phi(\text{CF}_2\text{O}) + \Phi(\text{CF}_3\text{CFO})$ in the absence of a sample gas. The previously reported values⁵ are 1.00, 0.90, and 0.78, respectively, at 24, 70, and 125°. (Actually the data in ref 5 show some trend with the C₃F₆ pressure at 125°. However more recent work in our laboratory has established the invariance of γ with C₃F₆ pressure.)

Equation 1 was used to compute *k_c/k_d* when the sample gas was ethylene oxide. During these runs it was found that the *R*(N₂) remained constant from run to run. Thus $\gamma R(\text{N}_2)$ could be replaced by *R*⁰(RO), the value of *R*(RC) with no sample gas present. The values for *R*⁰(RO) were obtained in separate runs. This procedure gave more consistent results and was used with the other sample gases.

The rate data are listed in Tables I-V for the various sample gases. The ratio of rate constants *k_c/k_d* is essentially independent of exposure time, absorbed intensity, and pressures of the reactants. The average values at each temperature are plotted vs. reciprocal temperature on the semilog plot in Figure 1. Reasonably straight lines can be drawn through the data; the Arrhenius parameters are tabulated in Table VI.

A. Ethylene Oxide. Ethylene oxide reacts very

much more slowly with oxygen atoms than do the other compounds in spite of the fact that the activation energy for the ethylene oxide reaction is small. Consequently the slowness of the reaction results from an unusually low preexponential factor, which means that reaction only occurs for a very limited angle of attack. It would seem that hydrogen atom abstraction might occur with almost any angle of attack. The low preexponential factor then suggests that perhaps the reaction involves ring opening to form CH₂O.

It is interesting to compare the rate data for ethylene oxide with cyclopropane.⁵ At room temperature the rate constants of these two molecules with oxygen atoms are similar, that of ethylene oxide being slightly smaller. The Arrhenius parameters (*A* = 0.19 × 10⁹ l./mole sec, *E* = 3.4 kcal/mole) for *c*-C₃H₆ are larger, but its preexponential factor is still very small. Perhaps it too reacts by ring opening.

B. Dimethyl Ether. The reaction of oxygen atoms with dimethyl ether has been studied by Takezaki, Kawasaki, and Mori.⁷ They believe that the initial

(7) Y. Takezaki, H. Kawasaki, and S. Mori, International Conference on Photochemistry, Tokyo, 1965.

Table V: Relative Rate Constants for O(³P) with Isooctane (2,2,4-Trimethylpentane) and C₃F₆; [N₂O] = 505 ± 14 mm

[C ₃ F ₆], mm	[C ₈ H ₁₈], mm	R ^o (RO), ^a μ/min	R(RO), μ/min	k _o /k _d
T = 307°K				
15.8	14.2	130	46	2.0
8.6	11.4	130	33	2.2
6.5	10.5	130	29	2.1
9.0	22.1	130	20.5	2.2
6.1	27.9	130	12.2	2.7
8.3	6.5	130	48	2.2
				Av = 2.2 ± 0.1
T = 343°K				
7.5	8.7	146	39	2.4
25	12.0	132	57	2.8
6.9	11.4	146	34	2.0
7.5	20.5	146	19.7	2.4
20	15	146	53	2.2
				Av = 2.4 ± 0.2
T = 398°K				
6.0	15.0	170	16.6	3.7
25.4	12	170	85	2.0
9.8	20.9	170	20	3.5
9.1	10.9	170	41	2.6
11.2	7.5	170	71	2.2
11.2	8.4	170	46	3.6
				Av = 2.9 ± 0.7

^a Determined by separate runs.

to us to be much too large. On the other hand, our preexponential factor is about as small as could be reasonably expected. The true Arrhenius parameters probably lie between the two sets of values.

C. *Alkanes.* There is still some controversy concerning the products of the reaction of oxygen atoms with alkanes. The Canadian workers^{3,8} believe the reaction to be hydrogen atom abstraction, whereas Wright⁹ and Avramenko and his co-workers¹⁰ believe that carbon-carbon bonds cleave and that carbonyl compounds are formed directly. Our work sheds no light on the mechanism. However, hydrogen atom abstraction seems more reasonable to us.

It is interesting to note that the Canadian groups both get the same value for the room temperature constant for O + *n*-C₄H₁₀ and that Wright and the Avramenko school get similar values for this rate constant, but that a discrepancy of greater than a factor of 3 exists between the two schools. Our room-temperature value lies intermediate. Azatyan, Nalbandyan, and Tsui¹¹ get the highest value of all; however their preexponential factor seems impossibly high. It also seems to us that the preexponential factor of Elias⁸ is abnormally large. Fortunately, however, all four determinations of the activation energy are in excellent agreement.

Isooctane and *n*-heptane are molecules of particular interest because they are used for standards of combustion. Isooctane has an octane rating of 100 and *n*-

Table VI: Rate Constant Data for O(³P) Reactions

Sample gas	E _a - E _d , kcal/mole	k _o × 10 ⁻⁹ at 25°, l./mole sec	A _o × 10 ⁻⁹ , l./mole sec	E _c , kcal/mole	Ref
Ethylene oxide	-0.4	0.00077	0.0160	1.8	This work ^a
Dimethyl ether	0.3	0.021	1.43	2.5	This work ^a
<i>n</i> -C ₄ H ₁₀	1.9	0.021	63	4.7	7
		0.012	12.0	4.1	This work ^a
		0.024	30	4.2	8
		0.027	3 ^b
		0.0066	9
		0.067	80	4.2	11
<i>n</i> -C ₇ H ₁₆	1.1	0.0078	8.0	4.1	10
		0.062	16.4	3.3	This work ^a
		0.039	5.2	2.9	This work ^a

^a Assuming k_d = 7.7 × 10⁸ exp(-2200/RT) l./mole sec; see ref 5. ^b Assuming a rate constant for ethylene of 6 × 10⁸ l./mole sec. at 25°.

reaction is hydrogen atom abstraction. Their room-temperature rate constant agrees exactly with ours. Using some crude approximations they estimated the Arrhenius parameters and obtained values that differ from ours. Their preexponential factor seems

(8) L. Elias, *J. Chem. Phys.*, **38**, 989 (1963).

(9) F. Wright, *Symp. Combust., 10th, Univ. Cambridge, Cambridge, Engl., 1964*, 387 (1965).

(10) L. I. Avramenko, R. V. Kolesnikova, and G. I. Savinova, *Izv. Akad. Nauk SSSR Otd. Khim. Nauk*, **17**, 976 (1963).

(11) V. V. Azatyan, A. B. Nalbandyan, and M. Y. Tsui, *Dokl. Akad. Nauk Arm. SSR*, **36**, 23 (1963).

heptane has an octane rating of zero. Their reaction rate constants with oxygen are not too different, that of *n*-heptane being somewhat larger. Thus it appears that the octane rating is not influenced by the rate of oxygen atom reactions.

The Arrhenius parameters are now reasonably well known for oxygen atom reactions with several alkanes: CH₄, C₂H₆, C₃H₈, *n*-C₄H₁₀, *n*-C₇H₁₆, and *i*-C₈H₁₈ (isooctane). The preexponential factors lie between 3.5 and 16×10^9 l./mole sec. The activation energies

decrease as the complexity of the alkane is enhanced. The "best" values for the activation energies are 7.3, 4.3, 3.8, 4.1, 3.3, and 2.9 kcal/mole, respectively, for the above-mentioned hydrocarbons. It should be realized though, that for molecules with nonequivalent hydrogen atoms, the activation energies are averages for the various possible reactions.

Acknowledgment. The authors wish to thank Mrs. Barbara Peer for assistance with the manuscript.

The Thermodynamic and Physical Properties of Beryllium Compounds. X.

Heats of Formation and Entropies of BeCl₂(g) and Be₂Cl₄(g)¹

by H. C. Ko, M. A. Greenbaum, M. Farber,

Rocket Power Research Division, Pasadena, California

and C. C. Selph

Air Force Rocket Propulsion Laboratory, Edwards, California (Received April 29, 1966)

Transpiration studies were performed to determine the thermodynamic properties and composition of the vapor over solid beryllium chloride in the temperature range from 623 to 683°K. By means of an iterative procedure the data obtained from the transpiration studies were coupled with the data previously obtained by means of torsion and gravimetric effusion experiments in the temperature range 440–600°K. The heats of formation obtained for BeCl₂(g) and Be₂Cl₄(g) were -84.3 ± 1.5 and -196.3 ± 1.0 kcal/mole for $\Delta H_{f, 298}$, respectively. A second-law value of 92.5 ± 1.0 cal/deg mole was obtained for S°_{298} of Be₂Cl₄(g).

Introduction

Several experimental studies on the composition of the vapors over condensed BeCl₂ have been reported with results remaining controversial. Rahlfs and Fischer^{2a} suggest that near the boiling point the major species is BeCl₂ dimer. Buchler and Klemperer^{2b} found evidence for (BeCl₂)₂ up to 500° and 1 atm. Ryabchikov and Tikhinskii³ concluded from a mass spectrometer study that in the range 496–578°K the

concentration of dimer was 0.5–1.5% of the total vapor, but this conclusion neglects the possible contribution

(1) This work was sponsored by the Air Force Rocket Propulsion Laboratory, Research and Technology Division, Air Force Systems Command, U. S. Air Force, Edwards Air Force Base, Calif., under Contract AF 04(611)-7414.

(2) (a) O. Rahlfs and W. Fischer, *Z. Anorg. Allgem. Chem.*, **211**, 349 (1933); (b) A. Buchler and W. Klemperer, *J. Chem. Phys.*, **29**, 121 (1958).

(3) L. N. Ryabchikov and G. F. Tikhinskii, *Fiz. Metal. i Metalloved.*, **10**, 635 (1960); *Chem. Abstr.*, **55**, 1198d (1961).

to the BeCl_2^+ peak due to fragmentation of the dimer. The extent of this contribution cannot definitely be established because the appearance potentials of monomer and dimer are virtually identical. Previously experiments were performed at this laboratory⁴ employing both torsion and gravimetric effusion methods to study the vapor species over crystalline BeCl_2 in the temperature range of 440–600°K. The values obtained for the torsion data and gravimetric data (assuming the vapor consisted of monomer only) were $\log p = -(7260 \pm 90)/T + (9.39 \pm 0.20)$ and $\log p = -(7200 \pm 90)/T + (9.39 \pm 0.18)$, respectively. The equation obtained from the gravimetric data would agree with that for the torsion data if an average molecular weight of 140 were employed. However, on the basis of the experimental precision of these data, this was not done and the species were assumed to be nearly completely monomer and second- and third-law heats of sublimation of 33.1 ± 0.5 and 32.1 kcal/mole were calculated. Thus the several published results by experimental methods including mass spectrometry, manometry, and effusion yield a heat of sublimation for the monomer agreeing within 1–3 kcal.

Although evidence points to the existence of dimeric species in the vapor, insufficient data have been reported to enable a determination of its heat of formation and entropy. This present work was undertaken in an attempt to obtain these thermal functions for the dimer $\text{Be}_2\text{Cl}_4(\text{g})$. A series of transpiration experiments was performed over a temperature range of 623–683°K. The data of the transpiration, torsion, and gravimetric effusion experiments were combined to obtain thermal functions and approximate composition of the vapors over solid BeCl_2 .

Experimental Section

Apparatus. The apparatus consisted of a Monel furnace tube of 1.25-in. i.d. and 32 in. long. Heating of the furnace was accomplished by ceramic electrical heating half-units, 24 in. long, around the tube. The transpiration tube was also constructed of Monel 4 in. long and of 1 in. o.d. One end of the tube was welded to a 0.25-in. o.d. tube so that gas could be passed through the tube. The other end of the transpiration tube was fitted to a screw-tight cap. An orifice approximately $1/16$ in. in diameter and $1/16$ in. deep was drilled through the center of the cap and another hole approximately $3/16$ in. in diameter and $1/4$ in. deep was drilled into the end of the cap (off center) to accommodate the thermocouple. A nickel boat about 3.5 in. long containing the sample was inserted into the transpiration tube by opening the screw cap. A trap was used to prevent

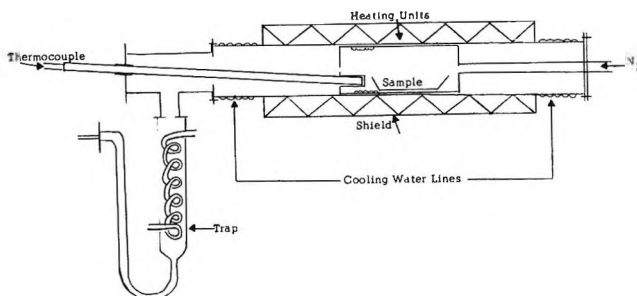


Figure 1. Apparatus for the study of the vaporization of BeCl_2 .

any gas species from being exposed to the atmosphere. Figure 1 shows a diagram of the apparatus.

All handling of the BeCl_2 samples was carried out inside the drybox. Dry nitrogen was used as the carrier gas. A chromel–alumel thermocouple was used as the temperature-sensing element. A saturable reactor was used along with a Leeds & Northrup recorder with controller unit, a K3 potentiometer, and a DC null detector for temperature control. The temperature of the furnace can be controlled to within approximately 0.05°.

Procedure. Samples of high-purity, crystalline BeCl_2 were transferred in a drybox from a tightly sealed bottle (which was kept in the drybox at all times) to the boat. The boat was then placed in a weighing bottle which was closed. Weighing of the sample, boat, and bottle was carried out rapidly on an Ainsworth Right-a-Weigh single-pan semimicro balance outside the drybox. The nickel boat containing the sample was then rapidly placed in the reaction chamber and immediately purged with dry nitrogen.

The flow rate of the dry nitrogen was adjusted to the desired level with an accurately calibrated flowmeter. The furnace temperature was then brought to the desired point and automatically controlled to $\pm 0.05^\circ\text{K}$ throughout the run. The duration of all the runs was 1.0–1.5 hr. At the conclusion of the run the furnace was cooled while maintaining the flow of carrier gas. At room temperature the nickel boat was removed from the furnace, placed in the weighing bottle, and the entire assembly was weighed. At least two runs were made at every temperature.

Since the time of heating the furnace to the reaction temperature and cooling it back to room temperature was significant in comparison to the total reaction time, it was necessary to make corrections for the amount of BeCl_2 lost during the nonequilibrium periods. This was accomplished by heating a sample of $\text{BeCl}_2(\text{s})$ having approximately the same weight as the one used

(4) M. A. Greenbaum, R. E. Yates, and M. Farber, *J. Phys. Chem.*, **67**, 1802 (1963).

in the actual run to the reaction temperature and then cooling it immediately. The weight loss of $\text{BeCl}_2(\text{s})$ occurring in the process was subtracted from the total weight loss observed in the actual runs. These corrections were also made in duplicate. The weight losses of $\text{BeCl}_2(\text{s})$ observed in both the actual runs and in the correction determination were highly reproducible. It was necessary to use $\text{BeCl}_2(\text{s})$ samples of similar size for both the runs and corrections because of a small amount of water present in the $\text{BeCl}_2(\text{s})$. Thus the heat-up and cool-down corrections also included the corrections for the H_2O present in the sample and consequently their magnitudes were dependent upon the total mass of sample. It was demonstrated independently that all water is rapidly removed (by conversion to $\text{HCl} + \text{BeO}$ *via* reaction with BeCl_2) from the sample of $\text{BeCl}_2(\text{s})$ by heating to much lower temperatures ($\sim 475^\circ\text{K}$) than were employed in this study.

The choice of a suitable flow rate for use in the present investigations was made after a study of the effect of carrier gas flow rate on the weight loss of $\text{BeCl}_2(\text{s})$. Flow studies were made at 623°K (the lowest temperature in the study) and at 668°K to establish a flow rate which would ensure saturation of the carrier gas with the beryllium chloride vapor. Table I shows

Table I: Effect of $\text{N}_2(\text{g})$ Flow Rate on Weight Loss of BeCl_2 at 668°K

Flow rate, cc/min	Weight loss, mg/1.25 hr	Weight loss/cc, mg/1.25 hr
5.6	267	47
8.4	370	44
11.5	460	40
16.2	640	40
		Av 43

Table II: Data for the Vaporization of $\text{BeCl}_2(\text{s})$

T , $^\circ\text{K}$	Time, hr	Total wt loss, mg		Wt loss of heat-up and cool- down correction, mg	
623	1.5	68.3	66.0	18.1	
643	1.5	133.5	139.6	35.3	
648	1.5	214.4	220.2	46.0	
653	1.5	267.7	272.3	63.9	59.9
658	1.5	331.2	340.3	86.6	90.8
663	1.5	432.1	429.5	109.0	
668	1.25	464.3	455.9	131.4	126.5
673	1.0	496.4	509.0	165.0	158.2
678	1.0	619.5	631.6	195.7	197.3
683	1.0	764.5	749.7	244.2	238.5

the constancy of the weight loss per unit volume at flow rates ranging from 5.6 to 16.2 cc/min. Therefore an average flow rate of 11.5 cc/min was chosen for the investigation. The data obtained for the experiments performed in the temperature range of 623 – 683°K are reported in Table II.

Discussion

Since the analysis of transpiration data required knowledge of the vapor molecular weight, the uncertainty in the dimer:monomer ratio discussed earlier causes some interpretational difficulties. In the present treatment the transpiration experiments described above have been combined with earlier torsion-effusion experiments conducted here at lower temperatures.⁴ The treatment involved is tedious but is the natural outcome of attempts to avoid drawing conflicting conclusions from the two sets of data. The result is a general picture of how the vapor composition would have to vary with temperature in order to produce the weight losses and torsion pressures actually found.

If the transpiration results are interpreted in terms of monomer, then the derived vapor pressure is over three times higher than what would be predicted from extrapolations of the torsion-effusion pressures. If interpreted as dimer they are still 75% too great. This indicates curvature of the total pressure curve and is most probably due to ascendancy of dimer at the higher temperatures.

Initially the transpiration experiments were interpreted in terms of the dimer with a weight loss correction for the monomer being derived by assuming that the torsion-effusion studies were experiencing only monomer formation. This assumption proved incompatible with the thermodynamic functions which resulted for the dimer. These functions predict significant dimerization even at the lower temperatures of the torsion-effusion study (471 – 510°). The monomer thus contributes only part of the pressure in the torsion-effusion range and must be less stable than was thought previously.

The initial dimer functions thus are also affected—but not greatly so—since the assumed monomer correction was not large and apparently should have been smaller. The absence of a temperature range where one of the species can be neglected makes further interpretation difficult, but the above discussion suggests an approach. Essentially the function for dimer and monomer were synthesized by an iteration back and forth between the two temperature regimes. Dimer was obtained from transpiration and monomer from torsion-effusion, employing sliding correction

Table III: Transpiration Data (Flow Rate = 11.5 cc/min)

T , °K	Time, hr	Total wt loss, mg	Wt. loss of heat-up and cool-down correction, mg	Cor wt loss, mg	Rate of wt loss, mg/hr	Wt loss assumed for monomer, mg/hr	Wt loss due to dimer, mg/hr	p dimer, atm	ΔH (3rd law), kcal
623	1.5	67.2	18.1	49.1	32.8	3.0	29.8	0.00630	35.60
643	1.5	140.0	35.3	104.7	69.8	6.0	63.8	0.01360	35.60
648	1.5	217.3	46.0	171.3	114.2	7.5	106.7	0.02303	35.23
653	1.5	270.0	61.9	208.1	138.7	9.3	129.4	0.02777	35.31
658	1.5	335.8	88.7	247.1	164.7	10.9	153.8	0.03282	35.23
663	1.5	430.8	109.0	321.8	214.5	13.3	201.2	0.04245	35.11
668	1.25	460.1	129.0	331.1	264.9	16.0	250.5	0.05226	35.06'
673	1.0	502.7	161.6	341.1	341.1	18.7	322.4	0.06620	34.97
678	1.0	625.6	196.5	429.1	429.1	22.4	406.7	0.08198	34.90
683	1.0	757.1	241.4	515.7	515.7	29.3	486.4	0.09621	34.89
									35.19 ± 0.2

Table IV: Thermodynamic Properties for Vaporization Studies

	$\text{BeCl}_2(\text{c}, \alpha \text{ form}) = \text{BeCl}_2(\text{g}) (\text{M})$	
	$2\text{BeCl}_2(\text{c}, \alpha \text{ form}) = \text{Be}_2\text{Cl}_4(\text{g}) (\text{D})$	
	2nd law	3rd law
$\Delta H_M^{471^\circ\text{K}}$		$32.20 \pm 1.5 \text{ kcal}$
$\Delta H_M^{298^\circ\text{K}}$		$33.00 \pm 1.5 \text{ kcal}$
$\Delta H_f^{298^\circ\text{K}}(\text{BeCl}_2(\text{g}))$		$-84.33 \pm 1.5 \text{ kcal/mole}$
$\Delta H_D^{663^\circ\text{K}}$	$36.00 \pm 1.0 \text{ kcal}$	$35.11 \pm 0.2 \text{ kcal}$
$\Delta H_D^{298^\circ\text{K}}$	$38.38 \pm 1.0 \text{ kcal}$	$37.49 \pm 0.2 \text{ kcal}$
$\Delta H_f^{298^\circ\text{K}}(\text{Be}_2\text{Cl}_4(\text{g}))$	$-196.29 \pm 1.0 \text{ kcal/mole}$	$-197.18 \pm 0.2 \text{ kcal/mole}$
$\Delta S_D^{663^\circ\text{K}}$	$48.04 \pm 1.0 \text{ cal/deg}$	
$\Delta S_D^{298^\circ\text{K}}$	52.99 cal/deg	
$S^{298^\circ\text{K}}(\text{Be}_2\text{Cl}_4(\text{g}))$	$92.51 \text{ cal/deg mole}$	$91.51 (\text{JANAF})^a \text{ cal/deg mole}$

^a See ref 5.

terms for monomer and dimer which are updated from one iteration to the next.

The weight loss correction in grams for monomer, g_M , is calculated from the total weight loss, g_T , and the assumed vapor pressure in atmospheres of monomer, p_M , using the equation

$$g_M = \frac{M_M n_c + \frac{M_M}{M_D} g_T}{\frac{p_T}{p_M} + \frac{M_M}{M_D} - 1} \quad (1)$$

where M_M and M_D are the molecular weights of monomer and dimer, respectively; p_T is total pressure (atmospheres); and n_c is the number of moles of carrier gas. This equation is derived by substituting

$$n_{\text{total}} = n_c + \frac{g_D}{M_D} + \frac{g_M}{M_M}$$

into the equation $p_M = (n_M/n_{\text{total}})p_T$ and rearranging. It thus accounts for the volume contributed by both monomer and dimer to the carrier gas. Substituting the values of M_M and M_D into eq 1 and also noting that $n_c = pV/RT = [(1)(11.5)(60)]/[(82.05)(298)] = 0.02821 \text{ mole/hr}$ results in

$$g_M = \frac{4.51 + g_T}{\frac{2}{p_M} - 1} \quad (2)$$

The vapor pressure of monomer, p_M , was arrived at by iteration as noted above. The iteration was begun by assuming that the p_M could be obtained from the equation

$$\log p_M = -(7260/T) + 9.39 \quad (3)$$

which is the least-squares fit of the torsion-effusion pressures. These pressures result in monomer weight loss

corrections of $\sim 30\%$ to the transpiration results. That this correction is too great is revealed when the resulting dimer functions are used to derive dimer pressures in the torsion-effusion range. Monomer is seen to account for only about 30% of the pressure calculated for by eq 3.

A much smaller monomer correction is called for in the next iteration. This is provided by a third-law calculation assuming that the pressure of monomer is only one-third of the total pressure at the lowest torsion-effusion temperature (471°K).

After several iterations, consistency is obtained. The weight losses obtained for monomer are given in column 7 of Table III. In summary, the concentration of dimer is found to vary between 65% at 471°K and 90% at 683°K. Based on these concentrations the heats and entropies are calculated in Table IV. The thermal functions, heat capacities, and entropies employed in these calculations are the estimated values listed in the current JANAF tables.⁵

Conclusions

Although great care was taken in reducing the data for the establishment of the vapor composition, the results should be used with caution. This treatment is sensitive to slight inaccuracies in the data. The concentration of monomer is especially sensitive since it appears as the difference between one number and another which is only 35% greater. Thus a 35% change in the torsion-effusion pressures would either double the monomer or dispose of it entirely. The

situation with the dimer is much more encouraging since the transpiration results needed only a small monomer correction. Indeed there is excellent agreement between second- and third-law heats derived for the dimer. A large error in the vapor composition has only a small effect on the heat of vaporization. The assumption of all monomer for the vapor composition in the low pressure data⁴ yielded a $\Delta H_v^{298^\circ\text{K}}$ of 32.1 kcal/mole for the monomer as compared to the value of 33.0 ± 1.5 kcal/mole reported in Table IV. Therefore, the effects of probable error in the data are represented by the error limits attached to the data in the table.

Some confidence is gained in the data when it is noted that a generally similar conclusion may be derived by combining the torsion-effusion pressures with the gravimetric effusion measurements also given in ref 4. Pairing these studies gives an average molecular weight of the saturated vapors of about 140 in the torsion-effusion range. This lends weight to the high dimerization concluded from the present data.

A further confirmation of the existence of almost all dimer in the high-temperature range can be obtained by an analysis of the entropy values derived from consideration of the data as all dimer in one case or all monomer in the other. If one considers the data to apply to monomer, the value obtained is 6–8 cal/deg mole higher than all previously reported values for S°_{298} of $\text{BeCl}_2(\text{g})$.

(5) "JANAF Thermochemical Tables," Sept 30, 1965.

Solvent Contribution to the Electromotive Force of Ion-Exchange Membrane Cells Containing Water and Heavy Water Solutions¹

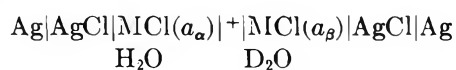
by Jerome Greyson

Atomics International Division of North American Aviation, Inc., Canoga Park, California
(Received May 9, 1966)

An investigation of solvent influence on ion-exchange membrane cell emf values has been carried out. In an earlier work it was assumed that solvent-transport contributions to the emf of such cells containing heavy and normal water ionic solutions could be neglected and the emf values were related to the entropy of transfer of salts between the isotopic solvents. A simple theory is presented which allows an experimental evaluation of the magnitude of the solvent contribution. It is found to be nonnegligible. Values are given for the solvent effect in anion membranes separating chloride ions and cation membranes separating sodium and potassium ions. Although the emf contribution to the total cell potential is not negligible, it has negligible effect on the calculated entropy of transfer. This results because the transfer process is dominated by the enthalpy of transfer rather than the free energy.

Introduction

Because of current interest in sea water desalination, renewed interest in the influence of dissolved species on the structure of water has been stimulated. Several papers have appeared recently in which the differences in properties between heavy and normal water solutions have been attributed to the influences of dissolved species on structure.²⁻⁷ This writer² reported the results of a series of measurements of the electrical potential of ion-exchange membrane electrochemical cells of the type



where the symbol $|+|$ is a cation-exchange membrane, M is a cation, and the subscripted a 's are the salt activities in the respective cell compartments. With the assumption that the contribution to the cell potential resulting from solvent transport could be neglected, the author related the emf values to the partial molal free energy and entropy of transfer of the salts between the solvents. The resulting values of free energy and entropy indicated a spontaneous transfer of salt from D₂O to H₂O and an associated decrease in entropy in the transfer process. The entropy values were in-

terpreted as evidence for support of Frank's model for the structure of water and the effect thereon by the dissolved ionic salts.⁸ That is, since heavy water was considered to be more structured than normal water, it suffered a somewhat greater disrupting effect by structure-breaking ions. The ions then, in transferring from heavy to normal water, experienced a decrease in entropy. Since the publication of that report, the several papers which have reported comparisons of the properties of heavy water solutions with those of normal water solutions have confirmed that interpretation.^{3,5,7} Of particular interest was the report by Kerwin in collaboration with Frank in which entropies obtained from solubility measurements of NaCl and KCl in D₂O were compared with those obtained from the emf measurements.³ Although the solubility

(1) Supported by the U. S. Department of the Interior, Office of Saline Water, Research Division.

(2) J. Greyson, *J. Phys. Chem.*, **66**, 2218 (1962).

(3) R. E. Kerwin, Ph.D. Thesis, University of Pittsburgh, 1964.

(4) A. Ben-Naim, *J. Chem. Phys.*, **42**, 1512 (1965).

(5) R. L. Kay and D. F. Evans, *J. Phys. Chem.*, **69**, 4216 (1965).

(6) G. C. Kresheck, H. Schneider, and H. A. Scharaga, *ibid.*, **69**, 3132 (1965).

(7) Y. C. Wu and H. L. Friedman, *ibid.*, **70**, 166 (1966).

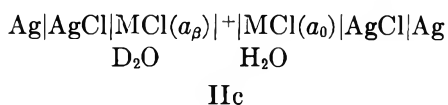
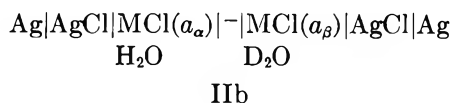
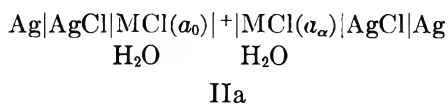
(8) H. S. Frank and E. W. Evans, *J. Chem. Phys.*, **13**, 507 (1945).

data yielded somewhat higher values for the transfer entropy than did the emf measurements, they were in agreement with regard to the order of the values, *i.e.*, $\Delta S_{\text{KCl}} > \Delta S_{\text{NaCl}}$, indicating that KCl was the more structure-breaking salt.

It would seem then that measurement of the emf values of ion-exchange membrane cells containing heavy and normal water solutions can provide a technique for investigating ionic influences on water structure. In view of the somewhat higher entropies obtained from solubility data, however, Frank⁹ suggested that the neglect of solvent transport in these cells might be a questionable assumption. Furthermore, Kerwin³ pointed out that the conclusions derived from the cell measurements depended upon thermodynamically nonrigorous interpretations of ion-exchange membrane junction potentials. The purpose of this paper therefore is twofold. The first is to report the results of a series of measurements which place the interpretation of the cell emf values on firmer thermodynamic ground. The second is to report on an investigation of the validity of the assumption that solvent transport resulted in a negligible contribution to the cell emf. As will be shown, although the emf contribution due to solvent transport is not negligible, it is of such magnitude that the conclusions of the original paper remain valid.

Theory

It will be convenient to consider the cell configurations shown in Table I. It should be noted that the cells are not independent. That is, one can separate any aqueous phase in any cell into two parts and reconnect them with the electrode system $\text{AgCl}|\text{Ag}|\text{AgCl}|\text{Ag}$ with no resultant change in the cell process and no net change in the emf. Therefore one could rewrite cell II, for example, as a series connection of the three cells



Cell IIb is exactly cell III in Table I while in the series connection of IIa and IIc the inverse process of that which would occur in cell I of Table I will be generated

by current flow. Since the emf of cell II is equal to the series connection of IIa, IIb, and IIc, it is also equal to the difference in emf between cells III and I, *i.e.*, $E_{\text{II}} = E_{\text{III}} - E_{\text{I}}$. Using the same arguments one can show that $E_{\text{V}} = E_{\text{I}} - E_{\text{III}}$ and $E_{\text{IV}} = 0$. Of course, if one neglects solvent effects then analysis of the cells in Table I, *i.e.*, passage of an equivalent of electricity and examination of the associated free energy changes, will reveal that cell III should exhibit zero emf values. Thus cell II should yield an emf equal and opposite to that of cells V and I. With nonnegligible solvent effects, however, the relations between the various cells are not trivial. They are also independent of any processes underway within the membrane junctions themselves. Measurements of the emf values of the various cell configurations therefore provided a method of testing the thermodynamic reliability of the cell data.

Table I: Ion-Exchange Membrane Cell Configurations^a

$\text{Ag} \text{AgCl} \text{MCl}(a_\alpha) \text{H}_2\text{O} \text{MCl}(a_\beta) \text{D}_2\text{O} \text{AgCl} \text{Ag}$
I
$\text{Ag} \text{AgCl} \text{MCl}(a_0) \text{H}_2\text{O} \text{MCl}(a_\alpha) \text{H}_2\text{O} \text{MCl}(a_\beta) \text{D}_2\text{O} \text{MCl}(a_0) \text{H}_2\text{O} \text{AgCl} \text{Ag}$
II
$\text{Ag} \text{AgCl} \text{MCl}(a_\alpha) \text{H}_2\text{O} \text{MCl}(a_\beta) \text{D}_2\text{O} \text{AgCl} \text{Ag}$
III
$\text{Ag} \text{AgCl} \text{MCl}(a_0) \text{H}_2\text{O} \text{MCl}(a_\alpha) \text{H}_2\text{O} \text{MCl}(a_\beta) \text{D}_2\text{O} \text{MCl}(a_0) \text{H}_2\text{O} \text{AgCl} \text{Ag}$
IV
$\text{Ag} \text{AgCl} \text{MCl}(a_0) \text{H}_2\text{O} \text{MCl}(a_\alpha) \text{H}_2\text{O} \text{MCl}(a_\beta) \text{D}_2\text{O} \text{MCl}(a_0) \text{H}_2\text{O} \text{AgCl} \text{Ag}$
V

^a The symbol $||$ refers to an anion-exchange membrane and a_0 is the activity of the salt in the electrode compartments of the three-membrane cells. The other symbols are defined in text.

Further, in the analysis which follows and in which solvent transport is considered, it will be shown that each of these cell configurations displays an emf value which is a linear combination of terms, each of which is characteristic only of salt or solvent transfer. The values of the solvent transfer terms will in addition be shown to be experimentally accessible.

The analysis is based on an analysis of ion-exchange membrane cells which was presented originally by Scatchard.¹⁰ Starting with Scatchard's equation for the

(9) H. S. Frank, personal communication.

(10) G. Scatchard, *J. Am. Chem. Soc.*, **75**, 2883 (1953).

emf of a voltaic cell and specifying symmetric Ag|AgCl electrodes and uni-univalent salts one gets

$$\frac{Ef}{RT} = \frac{E^{\circ}f}{RT} + \ln a_{\text{Cl}^{-}\alpha} - \ln a_{\text{Cl}^{-}\beta} - \int_{\alpha}^{\beta} \sum_i t_i d \ln a_i \quad (1)$$

The symbols R and T have their usual significance, f is the faraday, E° is the standard potential resulting from all processes underway in the cell, and a_i is the activity of the species i . The transference numbers t_i are mass transport numbers and include the transport of neutral species.¹¹ They represent the number of moles of species i which pass through the cell in the direction of positive current when a faraday of electricity passes from left to right in the cell. The mass transport number of a negative species is therefore negative. The integral over $t_i d \ln a_i$ extends over the composition range from α to β . The electrical transport number Γ_i , the fraction of current carried by the species i , is $z_i t_i$ where z_i is the charge on the species. The electrical transport number is therefore positive for charged species and zero for neutral species. For the cell configurations shown in Table I the integral in eq 1 can be written

$$\int_{\alpha}^{\beta} \sum_i t_i d \ln a_i = \int_{\alpha'}^{\beta'} \left\{ t_{\text{M}^{+}} d \ln a_{\text{M}^{+}} + t_{\text{Cl}^{-}} d \ln a_{\text{Cl}^{-}} + t_{\text{W}} d \ln a_{\text{W}} + t_{\text{D}} d \ln a_{\text{D}} \right\} \quad (2)$$

where t_{D} and t_{W} are the solvent-transference numbers for heavy and normal water, respectively, and the primes indicate the compositions of the extreme cell compartments.

The sum of the electrical transport numbers can be written as

$$\Gamma_{\text{M}^{+}} + \Gamma_{\text{Cl}^{-}} = z_{\text{M}^{+}} t_{\text{M}^{+}} + z_{\text{Cl}^{-}} t_{\text{Cl}^{-}} = 1$$

Thus

$$t_{\text{Cl}^{-}} = t_{\text{M}^{+}} - 1 \quad (3)$$

Also, by definition one can write

$$t_i = \frac{\mu_i m_i}{\sum_j z_j \mu_j m_j} = \frac{\mu_i m_i}{I} \quad (4)$$

where μ_i and m_i are the mobility and concentration, respectively, of the species i . Substituting eq 3 into the second term on the right-hand side of eq 2 and eq 4 into the last two terms one gets

$$\int_{\alpha}^{\beta} \sum_i t_i d \ln a_i = \int_{\alpha'}^{\beta'} \left\{ 2t_{\text{M}^{+}} d \ln a_{\text{MCl}} - d \ln a_{\text{Cl}^{-}} + \frac{\mu_{\text{W}} m_{\text{W}}}{I} d \ln a_{\text{W}} + \frac{\mu_{\text{D}} m_{\text{D}}}{I} d \ln a_{\text{D}} \right\} \quad (5)$$

where a_{MCl} is the mean activity of the salt. If eq 5, with the second term integrated, is substituted into eq 1, the result is

$$\frac{Ef}{RT} = \frac{E^{\circ}f}{RT} - \int_{\alpha'}^{\beta'} \left\{ 2t_{\text{M}^{+}} d \ln a_{\text{MCl}} + \frac{\mu_{\text{W}} m_{\text{W}}}{I} d \ln a_{\text{W}} + \frac{\mu_{\text{D}} m_{\text{D}}}{I} d \ln a_{\text{D}} \right\} \quad (6)$$

For the single-membrane configurations of cells I and III eq 6 can be solved in the following way: since $a_i = \gamma_i m_i$ where γ_i is the activity coefficient of the species i , the last two terms in eq 6 may be written

$$\int_{\alpha}^{\beta} \frac{\mu_{\text{W}} d(\gamma_{\text{W}} m_{\text{W}})}{\gamma_{\text{W}} I} \quad \text{and} \quad \int_{\alpha}^{\beta} \frac{\mu_{\text{D}} d(\gamma_{\text{D}} m_{\text{D}})}{\gamma_{\text{D}} I} \quad (7)$$

One would expect that solvent activity coefficients and mobilities will not depend significantly upon isotopic composition. Therefore one writes

$$\int_{\alpha=m_{\text{W}}}^{\beta=0} \frac{\mu_{\text{W}} d(\gamma_{\text{W}} m_{\text{W}})}{\gamma_{\text{W}} I} = -\frac{\mu_{\text{W}} m_{\text{W}}}{I} = -t_{\text{W}} \quad (8)$$

and

$$\int_{\alpha=0}^{\beta=m_{\text{D}}} \frac{\mu_{\text{D}} d(\gamma_{\text{D}} m_{\text{D}})}{\gamma_{\text{D}} I} = \frac{\mu_{\text{D}} m_{\text{D}}}{I} = t_{\text{D}} \quad (9)$$

Substituting 8 and 9 into eq 6 and integrating the remaining term over the appropriate composition range one obtains

$$\frac{Ef}{RT} = \frac{E^{\circ}f}{RT} - 2t_{\text{M}^{+}} \ln \frac{a_{\text{MCl}}^{\beta}}{a_{\text{MCl}}^{\alpha}} - (t_{\text{D}} - t_{\text{W}})^{+} \quad (10)$$

where the activities in the respective cell compartments are indicated by the superscripts. Equation 10, it should be noted, is independent of the nature of the membrane but applied to cell I (as the + superscript indicates) it shows that the emf contains a contribution resulting from the difference between the transport numbers of the two solvents.

For cell III, containing an ideal anion membrane, $t_{\text{M}^{+}} = 0$. Further, no net solute-transfer process which leads to an emf contribution can occur. Thus, applying eq 10 to cell III results in

$$\frac{Ef}{RT} = -(t_{\text{D}} - t_{\text{W}})^{-} \quad (11)$$

where the superscript - indicates an anion membrane. Equation 11 predicts that cell III will exhibit an emf which is dependent upon solvent transport and which is independent of the concentration of salts bounding the membrane.

(11) A. J. Staverman, *Trans. Faraday Soc.*, **48**, 176 (1952).

Finally, as was shown above, $E_{II} = E_{III} - E_I$ and $E_V = E_I - E_{III}$. That is, one can write for the triple-membrane cells containing ideal membranes

$$\frac{Ef}{RT} = - \left[\frac{E^\circ f}{RT} - 2 \ln \frac{a_{MCl}^\beta}{a_{MCl}^\alpha} - (t_D - t_w)^+ + (t_D - t_w)^- \right] \quad (12)$$

for cell II and

$$\frac{Ef}{RT} = \frac{E^\circ f}{RT} - 2 \ln \frac{a_{MCl}^\beta}{a_{MCl}^\alpha} - (t_D - t_w)^+ + (t_D + t_w)^- \quad (13)$$

for cell V.

One can see from these equations that, as stated earlier, the various contributions to the cell emf are additive. For $\beta = \alpha$ the emf is simply the standard emf plus a term characteristic of solvent transport. Having the value of E° for the process (from solubility and activity coefficient measurements for example) one can obtain the solvent transport terms *via* measurements of cells I, II, or V. Alternatively, one can obtain the solvent transport term in anion membrane cells directly *via* eq 11. Also one could, as a rederivation of eq 10 will verify, obtain the solvent transport contribution to the emf of cation membrane cells by using a cell I configuration and cation reversible electrodes.

We have made measurements of the emf values of the five different cell configurations containing solutions of LiCl, NaCl, KCl, and $(CH_3)_4NCl$. The results of the measurements have been interpreted in the following sections according to the preceding arguments.

Experimental Section

Procedure. The experimental procedure was substantially the same as that described in the original paper.² Membranes were clamped between No. 15 "O" ring joints which in turn were sealed to vertical tubes which served as the cell compartments. Membranes were supplied by the Ionac Chemical Co. and were designated by them as MA-3475 XL anion membranes and MC-3470 XL cation membranes. A Rubicon slide wire potentiometer, wired in series with the cell and with a Leeds and Northrup high-impedance null detector, was used to measure the emf. Measurements were carried out in an air thermostat controlled at $22 \pm 0.50^\circ$.

Solution Preparation. As in the original paper, solutions were prepared by weight to concentrations varying $\pm 10\%$ around 0.1 aquamolal. Aquamolality is defined as moles of salt per 55.5 moles of solvent and

places heavy and normal water solutions in thermodynamically comparable states.^{3,12} The salts were reagent grade and were used as received. Heavy water (99.88 mole %) was supplied by the Atomic Energy Commission's Savannah River Operations Office. Its specific resistivity was 5×10^6 ohms cm and it was used without further purification.

Calculations. Solution activities were calculated from the composition with the aid of an expression for the activity coefficient γ

$$\ln \gamma = Am^{1/2}/(1 + m^{1/2}) + Bm$$

due to Guggenheim and Turgeon¹³ and with the assumption that the tabulated "B" values given by those authors were applicable to heavy water solutions.¹⁴ The constant A in the equation, which was evaluated for each of the solvents, is the Debye-Hückel limiting law constant. The measured emf values were plotted *vs.* the logarithm of the calculated activity ratios and the value of the standard emf for the cell was calculated from the intercept with the ordinate at $\lg(a_\beta/a_\alpha) = 0$. At least nine different concentration ratios were measured for each of the salts except $(CH_3)_4NCl$ for which only three were measured. For the alkali halides, at least two different pairs of concentrated stock solutions were prepared independently and working solutions were prepared therefrom.

Results and Discussion

The results are displayed in Table II. Values of the intercept, E° , and the slope of the graph of E *vs.* $\log(a_\beta/a_\alpha)$ were obtained from least-square analysis of the data for the various activity ratios. The values of E° are shown with their root-mean-square deviation from the least-square line.

For ideal membranes, *i.e.*, $t_{M^{+}} = 1$ and $t_{M^{-}} = 0$, where the superscript indicates the membrane type, one should obtain a slope of 117 mv when silver chloride electrodes are used at 22° . Table II shows that, except for KCl in cell II, the least-square slopes varied no more than about 5% from ideal. For KCl in cell II, the slope was about 10% lower than ideal and may have resulted from a leaky membrane. It can be shown easily that the slope is also proportional to the number of equivalents of salt transferred across the cells for an equivalent of electricity passed. The

(12) Aquamolality was used first by Kerwin³ and then by Wu and Friedman⁷ to designate these concentration units.

(13) E. A. Guggenheim and J. Turgeon, *Trans. Faraday Soc.*, **51**, 747 (1955).

(14) Kerwin³ has shown that activity coefficients calculated for molality apply equally to aquamolality and that alkali chloride activity coefficients in heavy and normal water solutions become equal at concentrations lower than 1 aquamolal.

Table II: Standard Emf and Slope of Emf vs. $\log(a_\beta/a_\alpha)$ Graph^a

Cell type Salt	I		I		III		IV		V	
	E° , mv	Slope, mv	E° , mv	Slope, mv	E° , mv	Slope, mv	E° , mv	Slope, mv	E° , mv	Slope, mv
LiCl	4.5 ± 0.2	114	-1.4 ± 0.2	-110	3.2 ± 0.1	4	0 ± 0.3	...	1.3 ± 0.3	116
NaCl	6.2 ± 0.2	116	-2.6 ± 0.2	-117	3.1 ± 0.1	3	0 ± 0.3	...	2.9 ± 0.3	119
KCl	6.8 ± 0.2	115	-4.0 ± 0.2	-105	3.4 ± 0.2	3	0 ± 0.3	...	3.6 ± 0.4	110
(CH ₃) ₄ NCl	5.1 ± 0.1	119	-1.6 ± 0.1	-117	3.1 ± 0.1	2	0 ± 0.3	...	2.0 ± 0.1	115

^a Data were calculated from a least-square analysis of measured cell potentials except for cell IV the values of which are averages of random checks of several different activity ratios.

intercepts therefore should be divided by $(f/2RT) \times$ slope to obtain the actual value of E° . Potassium chloride, in cell II, is the only salt for which a slope was obtained which was significantly lower than ideal and the value of E° shown in Table II has been corrected for the nonideality of the membrane.

It is to be noted, in examining values of E° in Table II, that for each of the salts the same following general results are obtained. Cells II and V exhibit values of E° essentially equal in magnitude but opposite in sign. Cell IV, in random checks of several different activity ratios for each salt, yields no emf within the estimated uncertainty of the measurements. And finally the difference between the cell I emf and the cell V emf is, within the experimental uncertainty, equal to the emf observed in the cell III configuration. These results are in accord with the relations presented earlier, *i.e.*, that $E_{II} = E_{III} - E_I$ and $E_V = E_I - E_{III}$ and indicate that the membrane cells do indeed yield good thermodynamic data.

The data of Table II also show that the least-square slope resulting from cell III measurements for each of the salts is nearly zero, indicating concentration independence. This result is in agreement with eq 11. The deviation from zero undoubtedly arises from the nonideality of the anion membrane. Further, according to eq 11, the emf values obtained for cell III are a direct measure of the contribution to the cell potential resulting from solvent transport. Therefore, this anion membrane, used to separate solutions of chloride ions, displays a solvent effect amounting to about 3 mv. To this author's knowledge, no such clear-cut demonstration of solvent contributions to membrane cell emf values has been made before. It is also noteworthy that all of the cell III emf values are equal within the experimental uncertainty. Thus solvent transport for a given anion through an anion membrane is independent of the nature of the cation. Although such independence is probably to be expected, it has not heretofore been demonstrated.

The emf values for cell I according to eq 10 each contain a term for solvent effect in the cation membrane which is not directly accessible from these measurements. Equation 10 can be used though to calculate the solvent effect by substitution of known values of E° . Kerwin³ has given the values of the standard free energy of transfer of NaCl and KCl from D₂O to H₂O as -116 and -121 cal/mole, respectively (corresponding to 5.02 and 5.26 mv, respectively). Using these values and cell I data for NaCl and KCl one gets 1.2 and 1.5 mv, respectively, as the solvent transport effect in the cation membrane used in these measurements.

One is tempted to compare the relative values of sodium, potassium, and chloride ions. However, it should be emphasized that although the value for sodium is lower than that of potassium, the difference is of the order of the experimental uncertainty. The chloride value is not comparable because it applies to a positively charged membrane. Of more importance to the content of this paper are the values of the solvent effects relative to the measured cell potentials and their resulting contribution to the calculated transfer entropies.

In Table III we have listed values of the entropy for the transfer of LiCl, NaCl, and KCl from heavy to normal water. The numbers in the first three columns were calculated by combining membrane cell data (disregarding solvent effects) with heat of transfer data from Lange and Martin.¹⁶ First column values result from averaging the emf data of cells II and V. The second and third column values result from cell I data. In column III the results of the original work² are reproduced for comparison since a somewhat different membrane was used. In the fourth column, Kerwin's³ values for the transfer entropy are shown. These were obtained by combining the heat data of Lange and Martin¹⁶ with solubility values of NaCl and KCl in heavy and normal water. As such,

(15) H. E. Lange and W. Martin, *Z. Elektrochem.*, **42**, 662 (1936).

Table III: Entropy of Transfer of MCl from D₂O to H₂O

Salt	$-\Delta S$, cal/mole deg cells II and V	$-\Delta S$, cal/mole deg cell I	$-\Delta S$, cal/mole deg ref 2	$-\Delta S$, cal/mole deg Kerwin ^a
LiCl	1.31	1.08	1.03	...
NaCl	1.51	1.25	1.23	1.32
KCl	1.59	1.35	1.27	1.47

Kerwin's numbers contain no solvent transfer contributions. It will be noted that solvent transfer does not seriously affect the entropy values calculated from the cell potentials or the agreement with Kerwin. This is true for the case of two different cation membranes (columns II and III) and for the case where the effect results from the combination of both anion and cation membranes (column I and see eq 12 and 13). Such results are obtained because the transfer process is dominated by the enthalpy of transfer. That is, a change of 1 mv in the cell potential corresponds to a change of about 0.08 cal/mole deg. Thus the total emf values measured for these cells correspond to only a few tenths of a cal/mole deg compared to 1-2 cal/mole deg for the transfer process. Since the solvent-transfer contribution amounts to only 20-25% of the

measured potential, it contributes only in a minor way to the calculated transfer entropy. The remainder of the measured emf is attributable to solvent structural differences though and the cells do provide a technique to investigate ion influence on structure.

As a final point, it is interesting to note that eq 10 predicts that the solvent-transfer contribution to the cell emf will be positive. Solvent transport results from movement of the ion with its primary solvation sheath and from the viscous drag of the solvated ion. Since one would not expect the size of the primary solvation sheath to be affected by isotopic composition, the difference in transport numbers of the two solvents probably results from differences in the viscous drag. Normal water is about 20% more mobile (less viscous) than D₂O. Thus one is led to expect $t_w > t_D$. Since it is not likely that solution of any salt could invert the viscosity ratio of heavy and normal water, the solvent contribution to the cell I emf should always be positive. The positive emf values observed for cell III are confirmation of this argument. Furthermore, a positive error in the value of the standard potential will always lead to a more positive value for the apparent standard entropy. Thus the less negative values obtained from the cell I measurements compared to Kerwin's values have physical justification.

Ion Loss by Diffusion in the Radiolysis of Gases¹

by Cornelius E. Klots and Verner E. Anderson

Health Physics Division, Oak Ridge National Laboratory, Oak Ridge, Tennessee (Received May 20, 1966)

Expressions are presented for calculating the role of surface neutralization in gases homogeneously irradiated in spherical vessels. It is found that diffusion will be ambipolar in typical situations. Comparison with experiments suggests that uncontrolled effects, probably thermal convection currents, apparently enhance the role of surface neutralization beyond that calculated.

It has been recognized for some time that the site at which neutralization occurs can have a bearing on the chemical products from gas-phase radiolyses. The clearest indication of this is seen in the effect of weak externally applied electric fields on the various chemical yields.^{2a} More recently dose-rate effects have been plausibly interpreted in terms of a similar alteration of the neutralization mechanism.^{2b} Thus at low radiation intensities it is suggested that charged particles diffuse to the vessel wall prior to neutralization; at much higher intensities bimolecular volume combination can occur. LET effects in gases may be accorded a similar interpretation in terms of effective dose rates.³

It should be useful to have explicit formulas from which the fraction of ions terminating at each site can be calculated at a given set of experimental conditions. This would facilitate not only the evaluation of existing data but the design of experiments in which laboratory parameters are deliberately varied so as to encompass both modes of neutralization. Simple order-of-magnitude considerations suggest that the fraction of volume recombination, f , is given by

$$f/(1-f)^2 = \kappa^2 \quad (1)$$

where the dimensionless parameter κ is defined by

$$\kappa^2 = R^4 I \alpha / D_+ D_-$$

in which R is a characteristic dimension of the radiation vessel, I is the rate of ion-pair generation per unit volume, α is the bimolecular recombination coefficient, and D_+ and D_- are appropriate diffusion coefficients. In what follows below we shall see that κ does indeed emerge as a convenient analytic parameter although eq 1 itself is neither unambiguous nor particularly accurate.

The model to be considered is both tractable and quite general. It has been investigated, for example, in connection with certain photochemical⁴ and pyrolytic⁵ reactions. The gas is assumed to be under uniform irradiation in a spherical vessel of radius R . Since volume recombination is being considered the treatment is limited, it would appear,⁶ to pressures less than about 200 atm, above which parent-ion recapture sets in. Ions reaching the walls are assumed to be neutralized there without reflection. It is further assumed that the charged species of a given sign are of one type; thus, if the medium is capable of electron attachment, this is presumed to occur quite rapidly before the free electrons diffuse significantly. Finally, the treatment below will assume a steady state.

One has for the fluxes

$$\Gamma_+ = -\nabla D_+^0 n_+ + E \mu_+ n_+$$

$$\Gamma_- = -\nabla D_-^0 n_- - E \mu_- n_-$$

in which D_i^0 , μ_i , and n_i are, respectively, ionic diffusion coefficients, mobilities, and concentrations. The first two are related at the low fields of present concern by

$$D_i^0 = \mu_i kT/e$$

(1) Research sponsored by the U. S. Atomic Energy Commission under contract with Union Carbide Corp.

(2) (a) H. Essex, *J. Phys. Chem.*, **58**, 42 (1954); (b) T. W. Woodward and R. A. Back, *Can. J. Chem.*, **41**, 1463 (1963).

(3) R. A. Back, T. W. Woodward, and K. A. McLaughlan, *ibid.*, **40**, 1380 (1962).

(4) R. M. Noyes, *J. Am. Chem. Soc.*, **73**, 3039 (1951).

(5) R. M. Marshall and C. P. Quinn, *Trans. Faraday Soc.*, **61**, 2671 (1965).

(6) S. G. ElKomoss and J. L. Magee, *J. Chem. Phys.*, **36**, 256 (1962).

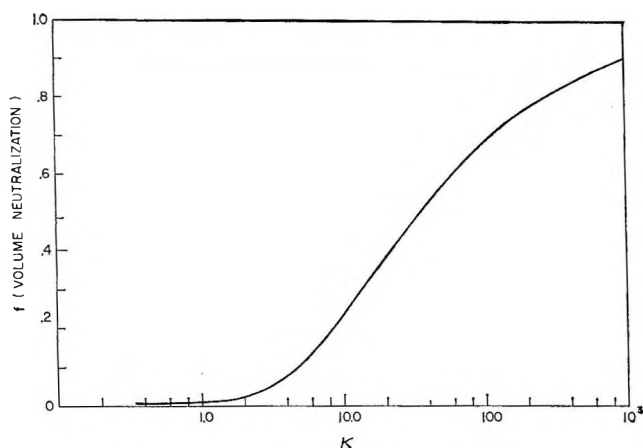


Figure 1. The fraction of ion pairs terminating in the volume as a function of the parameter κ (defined in the text).

The space-charge electric field is given by

$$\nabla \mathbf{E} = (e/\epsilon_0)(n_+ - n_-)$$

Finally matter conservation gives

$$I = \alpha(n_+)(n_-) - \nabla \Gamma_i = 0 \quad (2)$$

Our method of solution will be to assume that, for the ions of either sign, a well-defined diffusion coefficient exists, independent of position, defined by

$$\Gamma_i = -D_i \nabla n_i$$

This is clearly correct in the absence of a space charge when $D_i = D_i^0$ and is also correct in the ambipolar or high space-charge limit when

$$D_+ = D_- = D_a = 2D_+^0 D_-^0 / (D_+^0 + D_-^0)$$

It follows, in intermediate situations, from the further assumption of proportionality discussed by Allis.⁷ Utilizing the result $D_+ n_+ = D_- n_-$ and the substitutions

$$\eta = \frac{\alpha R r n_+}{D_-} = \frac{\alpha R r n_-}{D_+}$$

$$\xi = r/R$$

Equation 2 may be transformed into dimensionless form

$$(d^2 \eta / d\xi^2) + \kappa^2 \xi - \eta^2 / \xi = 0 \quad (3)$$

with a convenient set of boundary conditions

$$\eta(\xi = 0) = \eta(\xi = 1) = 0$$

Equation 3 has been solved numerically with a CDC-1604 computer to get the flux at the wall and thus f , the fraction of ion pairs combining within the volume

as a function of the single parameter κ . The relation obtained is displayed in Figure 1. The severe limitations of eq 1 will be evident.

It remains now only to show how the "effective diffusion coefficients" D_i can be obtained. From its definition D_- is given at the center ($\xi = 0$) by

$$D_- / D_-^0 = 1 + \frac{e^2}{\epsilon_0 k T} \frac{n_-(n_+ - n_-)}{\nabla^2 n_-} \quad (4)$$

With manipulation and use of the identity

$$D_- / D_-^0 + D_+ / D_+^0 = 2$$

this rearranges to

$$D_- / D_a = \frac{D_-^0 + [2e^2 D_+^0 D_-^0 / \epsilon_0 \alpha k T] F(\kappa)}{D_a + [2e^2 D_+^0 D_-^0 / \epsilon_0 \alpha k T] F(\kappa)} \quad (5)$$

where $F(\kappa) = (\eta/\xi)^2 / [\kappa^2 - (\eta/\kappa)^2]_{\xi=0}$, a function of κ only. The form of eq 5 follows one of Allis and brings out the limiting values of D_- . Evaluation of $F(\kappa)$ from the machine solutions indicates

$$F(\kappa) \simeq \kappa^2 / 36 \quad (6)$$

This simple result, together with eq 4 and 5, permits the evaluation of the effective diffusion coefficients at any value of κ . Via a reiterative procedure, κ and thus the fraction of volume recombination appropriate to the experimental conditions may be deduced.

The simple form of $F(\kappa)$ in eq 6 may also be obtained from a variational treatment of eq 3 using as trial function a solution appropriate to small recombination.⁸ We find, in fact, that it holds quite well for $\kappa \leq 25$. This is entirely sufficient since insertion in eq 5 of parameters appropriate to pressures about 1 atm indicates that diffusion is ambipolar down to the lowest values of κ of interest. Only under quite pathological conditions is there apt to be any ambiguity in the "effective diffusion coefficients" for $\kappa > 25$. This result, that gas-phase radiolyses are almost always conducted under ambipolar conditions, may be examined in another light. Consideration of eq 5 shows that diffusion will be ambipolar so long as $R > l$ where l is the Debye length. Since this condition holds quite typically, gas-phase radiation chemistry may legitimately be thought of as a sort of plasma chemistry.

The boundary condition $\eta(\xi = 1) = 0$ is, as is well known, an oversimplification. At a plane boundary one has for the outward and inward fluxes, respectively

(7) W. P. Allis, "Handbuch der Physik," Vol. XXI, Springer-Verlag, Berlin, p 397 ff.

(8) R. H. Ritchie, private communication.

$$\Gamma_i^+ = \frac{3n_i D_i}{4\lambda_i} - \frac{D_i}{2} \frac{dn_i}{dr}$$

$$\Gamma_i^- = \frac{3n_i D_i}{4\lambda_i} + \frac{D_i}{2} \frac{dn_i}{dr}$$

where λ_i is a mean-free path.

Then defining a surface accommodation or sticking coefficient by

$$a = 1 - \Gamma_i^-/\Gamma_i^+$$

one obtains for a more correct boundary condition ($\xi = 1$)

$$d\eta/d\xi = \eta \left[\frac{3R}{2\lambda_i} \left(\frac{a}{a-2} \right) + 1 \right] \quad (7)$$

Thus η will vanish within a few mean-free paths of the boundary unless a is very small. Use of eq 7 can only increase the extent of volume neutralization beyond that calculated above. The available experimental data hardly justify any such concern, as we shall now see.

A comparison of the present results with the systematic investigation of Back, *et al.*,^{2b} is invited. We estimate, as outlined in the Appendix, D_+^0 and D_-^0 in propane at his densities to be 3×10^{-2} and 2×10^2 cm²/sec, respectively. With $\alpha \sim 10^{-7}$ cc/ion sec and $R \sim 3$ cm, his data indicate surface neutralization at dose rates where, according to Figure 1, neutralization should have been almost entirely within the bulk volume. A simple reconciliation can be achieved only by assuming improbably low values of α . Nevertheless the correctness of Back's interpretation seems indisputable; his data are of the form of Figure 1 and are consistent with other investigations.⁹ It is the lack of quantitative agreement with the present calculations which is disappointing.

While there is some ambiguity in the geometry of Back's irradiation vessel, another origin of the discrepancy is suggested by a consideration of some recent work of Bone, *et al.*¹⁰ Using dose rates much higher than even the highest of Back, *et al.*, these authors present evidence that neutralization occurs predominantly at the walls. This apparent incompatibility among the experimental results and the failure of the present model to describe them can be most simply understood in terms of a role of convection currents, especially at large radiation intensities. Similar effects seem to arise in photochemistry⁴ and are extremely difficult to encompass in any theoretical model. Temperature gradients will thus, we suggest, have to be

minimized if it is ever desirable to eliminate or control the extent of surface neutralization.

Acknowledgment. The authors wish to acknowledge several useful discussions with Dr. R. H. Ritchie and Dr. H. C. Schweinler.

Appendix

Ionic diffusion coefficients can apparently be calculated with sufficient accuracy from the simplified Langevin formula for ionic mobilities at standard temperature and pressure

$$\mu_i = 35.9(\alpha M)^{-1/2} [\text{cm}^2/\text{v sec}]$$

where α is the polarizability of a bulk molecule in units of a_0^3 (where a_0 is the Bohr radius) and M is the reduced mass, in atomic units, of the ion-neutral pair. Correction of this standard mobility to the appropriate experimental density and application of the Nernst-Einstein relation should then yield a quite acceptable estimate of D_i^0 .

Understandably no such formula is available for electron-transport parameters. Nevertheless examination of drift-velocity data indicates^{11,12} electron diffusion coefficients are, with rare exceptions, in the range $1-4 \times 10^2$ cm²/sec at standard conditions. Thus uncertainty is quite acceptable since, as noted above, diffusion will usually be ambipolar, or nearly so, and thus insensitive to D_-^0 .

By far the greatest source of uncertainty in calculations of the present sort lies in estimating the second-order neutralization coefficient. Little in the way of generalizations can be offered. Recent measurements of electron-molecular ion combinations indicate $\alpha \sim 2 \times 10^{-7}$ to 2×10^{-6} cc/ion sec.¹³⁻¹⁵ No pressure dependence of these coefficients has been established. The mechanism of ion-ion neutralization is somewhat more complicated^{16,17} but effective second-order combination coefficients in the above range are again indicated.

(9) G. R. A. Johnson and J. M. Warman, *Trans. Faraday Soc.*, **61**, 1709 (1965).

(10) L. I. Bone, L. W. Sieck, and J. H. Futrell, *J. Chem. Phys.*, **44**, 3667 (1966).

(11) G. S. Hurst, L. B. O'Kelly, E. B. Wagner, and J. A. Stockdale, *ibid.*, **39**, 1341 (1963).

(12) T. L. Cottrell and I. C. Walker, *Trans. Faraday Soc.*, **61**, 1585 (1965).

(13) H. J. Oskam and V. R. Mittelstadt, *Phys. Rev.*, **132**, 1445 (1963).

(14) W. H. Kasner and M. A. Biondi, *ibid.*, **137**, A-317 (1965).

(15) R. C. Gunton and T. M. Shaw, *ibid.*, **140**, A-756 (1965).

(16) B. H. Mahan and J. C. Person, *J. Chem. Phys.*, **40**, 392 (1964).

(17) T. S. Carlton and B. H. Mahan, *ibid.*, **40**, 3683 (1964).

The Electrochemical Oxidation of Arsenic(III). A Consecutive Electron-Transfer Reaction

by Henry A. Catherino

Department of Chemistry, University of Michigan, Ann Arbor, Michigan (Received May 23, 1966)

Analysis of $\log i$ vs. E curves for the electrochemical oxidation of arsenic(III) in 1.0 M perchloric acid shows two well-defined linear sections in the potential region where concentration polarization effects are negligible. This observation is inconsistent with mechanisms involving a single transition state. The experimental results show excellent agreement with the theoretical predictions based on a mechanism involving two consecutive one-electron-transfer steps. The simplest mechanism assignable to the reaction is $\text{As(III)} \leftrightarrow \text{As(IV)} \leftrightarrow \text{As(V)}$. These findings provide evidence in support of the existence of the intermediate As(IV) which has been postulated from kinetic effects observed in homogeneous solution studies.

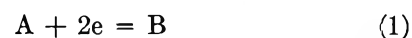
Introduction

The principles developed in the study of electrochemical kinetics have provided a powerful tool for elucidating the mechanisms of electrode reactions.¹ Essentially, each fundamental step can be considered as involving an activation energy barrier. The charge-transfer step, however, is characterized by the unique quality of having a potential-dependent activation energy barrier. Consequently, *via* the application of varying applied potentials, the electrochemical effects caused by changes in the rate-determining step can be studied.

Two distinct methods² of approaching the problem of consecutive electron-transfer processes can be identified: (a) the steady-state method and (b) the quasi-equilibrium method. The former method equates the rates of each of the conceivable steps through a steady-state approximation. The solution of these equations is tedious and, as a result, little has been done in applying this method. The latter approach assumes that a single rate-determining step exists. The rate constants of the preceding and subsequent steps are assumed to be large and can be thought of as being at equilibrium. This approach is readily amenable to mathematical formulation. In the discussion which follows, the steady-state method is applied with the modification that all chemical steps are taken to

be at equilibrium as in the quasi-equilibrium method. The approach has as its purpose the formulation of a mathematical expression which takes into account a possible change in the rate-determining step attributable solely to a sequence of consecutive charge-transfer steps.

Expressions have been derived describing the possible current-voltage curves obtainable at microindicator electrodes for the three simplest mechanistic sequences of an over-all electrode reaction written as³



The intermediate, if any, is taken to be of short chemical half-life and of low concentration so as not to be isolable by ordinary chemical means. These mechanisms are (I) a two-electron-transfer step *via* a single activated complex, (II) two consecutive one-electron-transfer steps, and (III) two discrete one-electron-transfer steps wherein the intermediate disproportionates rapidly.

It is assumed in these mechanisms that all other steps preceding and subsequent to the electron-transfer re-

(1) P. Delahay, "Double Layer and Electrode Kinetics," Interscience Publishers, Inc., New York, N. Y., 1965.

(2) B. E. Conway, "Electrode Processes," Ronald Press Co., New York, N. Y., 1965, p 109.

(3) J. Jordan and H. Catherino, *J. Phys. Chem.*, **67**, 2241 (1963).

action are fast. Unfortunately, mechanism I has a current-voltage (CV) curve identical with special cases of mechanisms II and III and therefore cannot be unambiguously determined by voltammetric methods. An example of mechanism III is the thallic-thallos electrode reaction in perchloric acid on a clean platinum electrode.^{3,4} The discussion which follows will be limited to an electrode reaction involving mechanism II.

Originally, Vetter⁵ derived an expression for the current-voltage curve peculiar to an electrode reaction proceeding *via* two consecutive one-electron-transfer steps in terms of apparent exchange currents. Later, a similar expression was derived in a paper by Catherino and Jordan⁴ in terms of specific rate constants. Vetter's derivation is, no doubt, simpler to use in an operational sense. The other derivation, however, makes clear certain fundamental chemical principles that are implied in Vetter's equation. Below is the essence of this derivation together with its conclusions.

Theoretical Section

An expression for the voltammetric wave resulting from mechanism II



can simply be derived by noting that the cathodic and anodic current contributions are given by

$$i_o = F A k_{3,2} a^0_3 + F A k_{2,1} a^0_2 \quad (4)$$

$$i_a = -F A k_{1,2} a^0_1 - F A k_{2,3} a^0_2 \quad (5)$$

where F is the faraday, A is the electrode area, k is the electrochemical rate constant whose subscript indicates the reaction to which it refers, and a is the activity of the electroactive species where the subscript indicates the electroactive species to which it refers and the superscript zero refers to the location at the electrode surface.

The activity of the intermediate S_2 is eliminated by applying the steady-state requirement, rate of formation of S_2 = rate of decomposition of S_2

$$k_{3,2} a^0_3 + k_{1,2} a^0_1 = k_{2,3} a^0_2 + k_{2,1} a^0_2 \quad (6)$$

The potential dependencies of these heterogeneous rate constants are

$$k_{3,2} = k^0_{3,2} \exp(-\alpha_{3,2})(E - E^{\circ}_{3,2}) \frac{F}{RT} \quad (7)$$

$$k_{2,3} = k^0_{3,2} \exp(1 - \alpha_{3,2})(E - E^{\circ}_{3,2}) \frac{F}{RT} \quad (8)$$

$$k_{2,1} = k^0_{2,1} \exp(-\alpha_{2,1})(E - E^{\circ}_{2,1}) \frac{F}{RT} \quad (9)$$

$$k_{1,2} = k^0_{2,1} \exp(1 - \alpha_{2,1})(E - E^{\circ}_{2,1}) \frac{F}{RT} \quad (10)$$

where k^0 is the specific rate constant defined when $E = E^{\circ}$, α is the transfer coefficient having a value $0 < \alpha < 1$, R is the gas constant, and T is the absolute temperature.

These expressions were used so as to define each of the electron-transfer steps in terms of a specific rate constant and an applicable standard potential. Although these standard potentials are unknown, they must be related by the restriction imposed by the law of conservation of energy

$$2E^{\circ}_{3,1} = E^{\circ}_{3,2} + E^{\circ}_{2,1} \quad (11)$$

In order to take into account the effect of concentration polarization, the mass transport restrictions are given as

$$i = \pm n F A m (a - a^0) \quad (12)$$

where \pm is used depending on the cathodic or anodic direction of the current, n is the number of faradays involved per mole, and m is the mass transport coefficient. A limiting current is defined when a^0 becomes negligible compared to a

$$i_1 = \pm n F A m a \quad (13)$$

Combining these relationships and eliminating the activity terms, the following expression is obtained

$$i = \frac{\frac{k_{3,2} k_{2,1}}{m_3} i_{1,c} + \frac{k_{1,2} k_{2,3}}{m_1} i_{1,a}}{k_{2,3} + k_{2,1} + \frac{k_{3,2} k_{2,1}}{m_3} + \frac{k_{1,2} k_{2,3}}{m_1}} \quad (14)$$

where the potential dependence of the rate constants is given by eq 7-10. $i_{1,c}$ is the cathodic limiting current and $i_{1,a}$ is the anodic limiting current. The preceding equation describes all of the possible CV curves for a reaction involving two consecutive one-electron-transfer steps where the intermediate is of very small concentration in order that 6 will hold.

An important observation is made when a qualitative assignment of standard potentials is attempted. Thermodynamically, it is clear that $E^{\circ}_{3,2}$ cannot be greater than or equal to $E^{\circ}_{2,1}$ as this would require that the intermediate have a large equilibrium concentration. This is inconsistent with the requirement that S_2 be an intermediate of low concentration. Therefore

$$E^{\circ}_{3,2} < E^{\circ}_{2,1} \quad (15)$$

(4) H. Catherino and J. Jordan, *Talanta*, 11, 159 (1964).

(5) K. J. Vetter, *Z. Naturforsch.*, A7, 328 (1952); A8, 323 (1953).

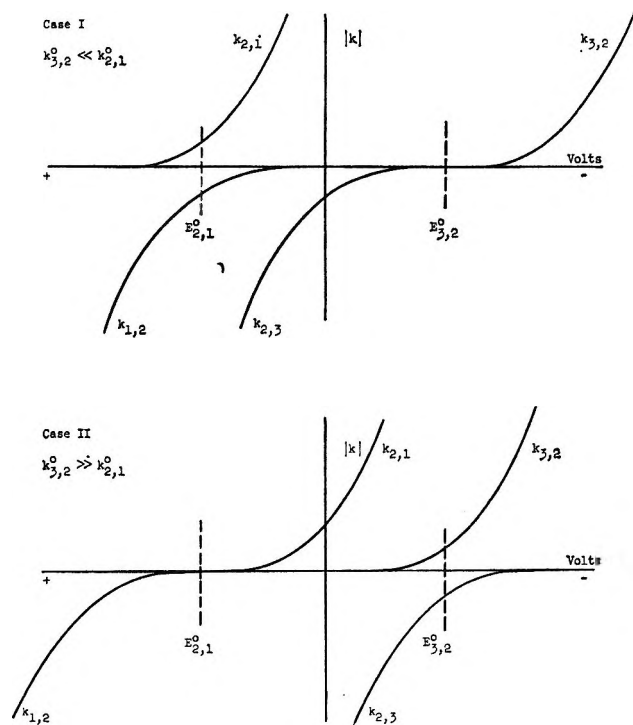


Figure 1. Relative magnitudes of the electrochemical rate constants for each of the steps of a consecutive electron-transfer sequence. The potential of the origin is the standard potential of the over-all reaction, $E_{3,1}^0$. The y axis represents the magnitude of the electrochemical rate constant. This value is always positive. The magnitudes above and below the x axis refer to increasing k for the cathodic and anodic electrode processes.

and consequently, it follows that the intermediate is unstable with respect to disproportionation. This argument was made by Heyrovsky in attempting to interpret oscillographic data obtained from multiple electron-transfer reductions.⁶ Two reasons based on kinetic considerations can be given to explain the nonoccurrence of the disproportionation reaction: (a) the steady-state concentration of the intermediate is very small so as to favor the first-order electrode reaction rather than the second-order disproportionation and (b) the activation energy of the disproportionation is large.

The current-voltage curve equation describes the possible forms of the CV curves consistent with this mechanism. In this connection, Riddiford has pointed out that often various mechanisms can yield identical CV curves thus making such comparisons meaningless.⁷ It is important then to pick out only those cases where a unique effect results and this can best be done by looking at an irreversible CV curve in the region where concentration polarization is negligible. By solving eq 4-6 to eliminate a_2 and the contribution

from the reverse reactions, the following Tafel equations are obtained applicable to totally irreversible waves: cathodic

$$\ln i_c = \ln 2FAa_3 + \ln \frac{k_{3,2}k_{2,1}}{k_{2,1} + k_{2,3}} \quad (16)$$

anodic

$$\ln (-i_a) = \ln 2FAa_1 + \ln \frac{k_{1,2}k_{2,3}}{k_{2,1} + k_{2,3}} \quad (17)$$

where the potential dependence of k is given by eq 7-10.

Of interest are the limiting cases wherein $k_{2,1} \gg k_{2,3}$ and $k_{2,1} \ll k_{2,3}$ in eq 16 and 17. This may be best demonstrated by a diagram of rate constant magnitude vs. potential as shown in Figure 1. This diagram is a sketch of k vs. E as given in eq 7-10 with the restriction of (15). The relative magnitude of k for each electron-transfer step at an applied potential is a means of identifying the rate-determining step. In the case of the cathodic Tafel region described by eq 16, case I ($k_{3,2}^0 \ll k_{2,1}^0$) shows that $k_{2,1} \gg k_{2,3}$ so that $S_3 \rightarrow S_2$ is the rate-determining step at negative (reducing) potentials. Since $k_{2,1} \gg k_{2,3}$ at these potentials

$$\frac{k_{3,2}k_{2,1}}{k_{2,1} + k_{2,3}} \rightarrow \frac{k_{3,2}k_{2,1}}{k_{2,1}} = k_{3,2} \quad (18)$$

then the applicable equation describing the foot of the curve occurs in the usual Tafel form

$$\ln i_c = \ln 2FAa_3k_{3,2} - \alpha_{3,2}(E - E_{3,2}^0)\frac{F}{RT} \quad (19)$$

In case II ($k_{3,2}^0 \gg k_{2,1}^0$) where $k_{3,2}$ becomes substantially large, $k_{2,1}$ and $k_{2,3}$ reverse their relative magnitudes so that two separate and distinct situations can exist: (a) at larger reducing potentials, $k_{2,3} < k_{2,1}$ so that

$$\frac{k_{3,2}k_{2,1}}{k_{2,1} + k_{2,3}} \rightarrow \frac{k_{3,2}k_{2,1}}{k_{2,1}} = k_{3,2} \quad (20)$$

in which case the curve is given in the usual Tafel form given in eq 19, and (b) at smaller reducing potentials, $k_{2,3} > k_{2,1}$

$$\frac{k_{3,2}k_{2,1}}{k_{2,1} + k_{2,3}} \rightarrow \frac{k_{3,2}k_{2,1}}{k_{2,3}} \quad (21)$$

and consequently, an unusual Tafel-like equation results

$$\ln i_c = \ln 2FAa_3 + \ln \frac{k_{3,2}k_{2,1}}{k_{2,3}} \quad (22)$$

(6) J. Heyrovsky, *Discussions Faraday Soc.*, 1, 220 (1947).

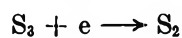
(7) A. C. Riddiford, *J. Chem. Soc.*, 1175 (1960).

or, by substituting and rearranging

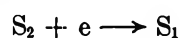
$$\ln i_o = \ln 2FAa^0_3k^0_{2,1} +$$

$$(E^{\circ}_{3,2} - \alpha_{2,1}E^{\circ}_{2,1})\frac{F}{RT} - (1 + \alpha_{2,1})E\frac{F}{RT} \quad (23)$$

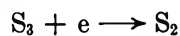
Evidently, a plot of $\ln i$ vs. E under the conditions present in case II should yield two linear portions having the slopes $-(1 + \alpha_{2,1})(F/RT)$ at smaller reducing potentials and $-\alpha_{3,2}(F/RT)$ at larger reducing potentials. These conclusions are basically identical with those of Vetter.⁵ However, the physical interpretation of this inflection is evident from Figure 1. That is, at less reducing potentials, the step



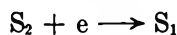
is at equilibrium and



is rate determining with the requirement that S_2 is of small concentration and at steady state. At more reducing potentials



is rate determining, whereas



is fast.⁸

It is apparent from Figure 1 that cases I and II are actually identical when rotated 180° around an axis perpendicular to the origin. Consequently, the same arguments can be given for the anodic Tafel region occurring at positive (oxidizing) potentials. In case I at lower oxidizing potentials

$$\ln(-i_a) = \ln 2FAa^0_1k^0_{3,2} - (1 - \alpha_{3,2})E^{\circ}_{3,2}\frac{F}{RT} - E^{\circ}_{2,1}\frac{F}{RT} + (2 - \alpha_{3,2})E\frac{F}{RT} \quad (24)$$

and at higher oxidizing potentials as well as always in case II

$$\ln(-i_a) = \ln 2FAa^0_1k^0_{2,1} +$$

$$(1 - \alpha_{2,1})(E - E^{\circ}_{2,1})\frac{F}{RT} \quad (25)$$

Some important observations are that (1) if the inflected Tafel slope occurs on one wave, it will not occur on the other and (2) the inflection will occur on the wave whose first electron-transfer step has the largest specific rate constant.

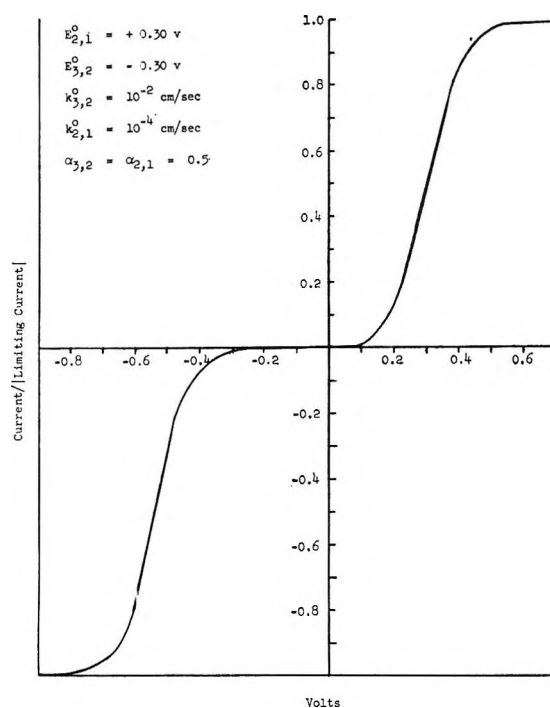


Figure 2. A current-voltage curve calculated on the basis of an assumed mechanism having two consecutive electron-transfer steps.

Computer solutions for the shape of the current-voltage curve were obtained for various values of the kinetic parameters α , k^0 , and E° . A curve illustrating the effect characteristic of two consecutive one-electron-transfer steps is seen in Figure 2. The curve shown is totally irreversible allowing measurements on the foot of the waves to be converted directly to a Tafel plot. The anodic and cathodic Tafel plots are shown in Figures 3 and 4. The two linear portions on the cathodic Tafel plot are solely characteristic of mechanism II. This effect, as mentioned earlier, is obtained whenever (a) the composite wave is irreversible and (b) the specific rate constant for one electron-transfer step is sufficiently different from the other. Generally, the inflected Tafel slope is seen when the specific rate constants vary by at least two orders of magnitude. When the specific rate constants are of the same size, the current-voltage curve is consistent with the three mechanisms given earlier.

(8) Should $k_{3,2}^0 \gg k_{2,1}^0$ so that $k_{2,1}$ will be less than $k_{3,2}$ at all reducing potentials, no inflection in the Tafel curve will be observed. If this is the case, the concentration of the intermediate will continually increase at reducing potentials until (a) a substantial concentration gradient will exist between the electrode and the bulk of the solution causing a loss of the intermediate by mass transport away from the electrode and (b) the steady-state assumption will not be applicable. Such a situation violates the original model and so is not applicable in this analysis.

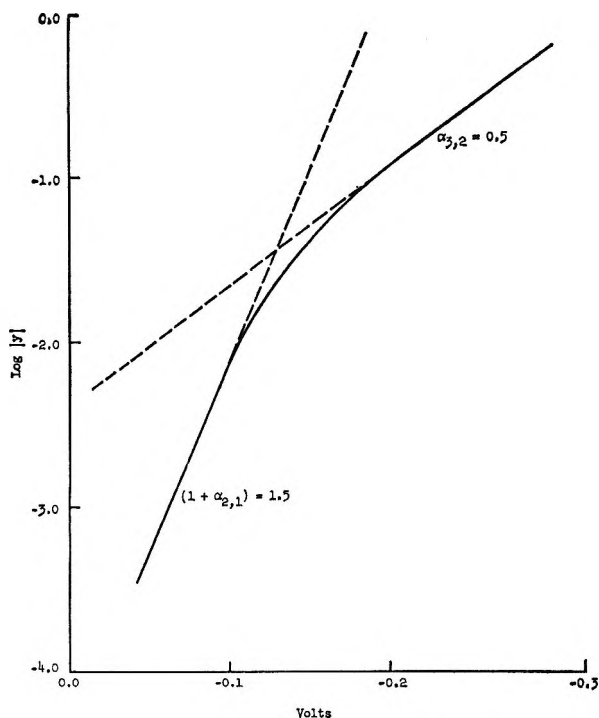


Figure 3. A Tafel plot of the foot of the cathodic portion of the calculated current-voltage curve shown in Figure 2 where $y = \text{current}/|\text{limiting current}|$.

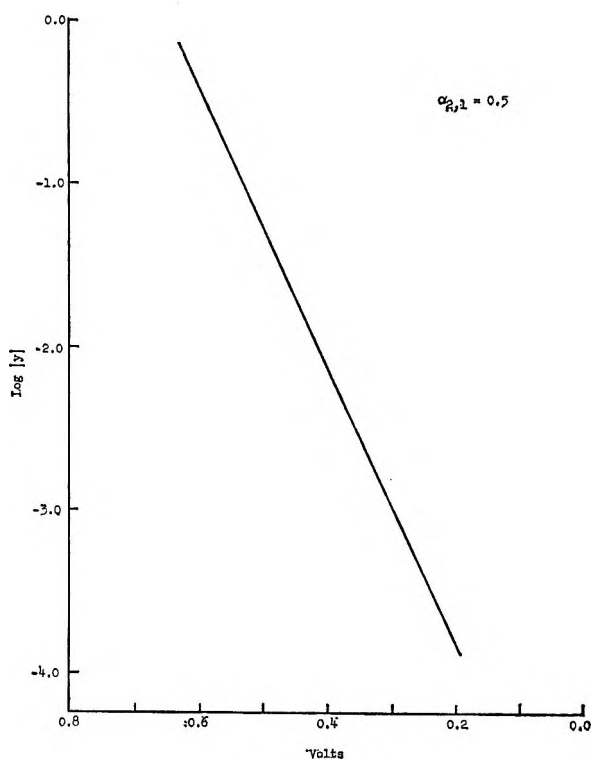


Figure 4. A Tafel plot of the foot of the anodic portion of the calculated current-voltage curve shown in Figure 2 where $y = \text{current}/|\text{limiting current}|$.

The conclusions of this analysis are in complete agreement with the criteria given by Hurd,⁹ whose study was based on Vetter's equation for consecutive single-electron-transfer steps. These criteria are (a) two well-defined linear logarithmic portions of the Tafel curve must be obtained, (b) agreement between the relative sizes of the exchange currents, and (c) agreement between the transfer coefficients. In terms of specific rate constants, essentially identical statements could be made.

In the application of these criteria it is important to consider the possible effects caused by abrupt changes in the electric field of the double layer.¹ It was assumed in the derivation that the influence of the double-layer field was either negligible or constant over the range of potentials wherein the measurements are made. This assumption is reasonable when the supporting electrolyte concentration is 0.1 *M* or greater and the potential region studied does not include the potential of zero charge. Should these conditions be absent, the double-layer field will undergo a considerable change causing substantial variations in the electrochemical rate constants, inconsistent with eq 7-10. Under these conditions, conclusions based on the above-mentioned criteria must be reviewed with caution.

Experimental Section

The experimental technique employed was hydrodynamic voltammetry. The details of this technique were described earlier.¹⁰ Since the studies were performed on the foot of the wave where concentration polarization is negligible, strict control of the solution flow was not necessary. A platinum microindicator electrode was used. It was pretreated by ignition to red heat and, after cooling, was used to scan the range of potentials 0.5-1.4 v until reproducible curves were obtained. Two preliminary scans were needed. A saturated silver-silver chloride electrode with a barrier sleeve compartment was used as a reference electrode. The added compartment served to eliminate possible contamination caused by diffusion to and from the reference electrode.

The current-voltage curves were recorded with the ORNL controlled-potential voltammeter, Model 1988A (Indiana Instruments, Inc.), in conjunction with a Photovolt recorder, Model 43. The scan rate used was 100 mv/min toward positive potentials. The experiments were carried out at 25.0°. Reagent grade chemicals and conductivity water were used.

Theoretical current-voltage curves, based on the ex-

(9) R. M. Hurd, *J. Electrochem. Soc.*, **109**, 327 (1962).

(10) J. Jordan, *Anal. Chem.*, **27**, 1708 (1955).

pression for the consecutive one-electron-transfer step mechanism described earlier, were computed by the IBM 7090 computer on the campus of the University of Michigan.

Discussion of Results

Figure 5 shows the anodic wave resulting from the oxidation of arsenic(III) at a platinum microelectrode in 1.0 M perchloric acid. The appearance of the minimum in the region corresponding to the plateau of the wave is caused by the passivating influence of the formation of platinum oxide.¹¹ In the following discussion, only the foot of this wave will be considered where concentration polarization is negligible and the electron-transfer reaction is rate determining. It is important to note that arsenic(V) is not reducible anywhere in the range of potentials accessible for study at the platinum electrode. Furthermore, As(V) is not reduced on a mercury cathode whose range of accessible potentials exceeds that of platinum toward reducing potential.¹² Evidently, if a measurement of the specific rate constant were made assuming a single-step mechanism from the anodic and cathodic reactions at the standard potential of the arsenic-arsenious couple, +0.56 v *vs.* nhe (+0.36 v *vs.* ssce), the measurement from the hypothetical reduction reaction would be very large as compared to that determined from the anodic wave. For a single-stage two-electron transfer to occur, it is mandatory that the specific rate constant calculated from the anodic and cathodic waves be identical. Therefore, from an inspection of the data, the observed discrepancy in the relative overpotentials of the anodic and cathodic processes, when compared with reference to the standard potential,

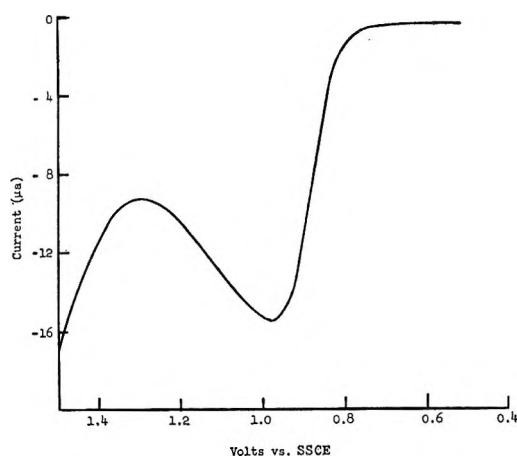


Figure 5. An experimental current-voltage curve of millimolar arsenic(III) in 1.0 M perchloric acid under a forced convective mass transport. The direction of scan was toward positive potentials.

would be *prima facie* evidence for a process involving consecutive electron-transfer steps.¹³

A direct identification of the mechanism is made by comparing the arsenic oxidation wave with the unique

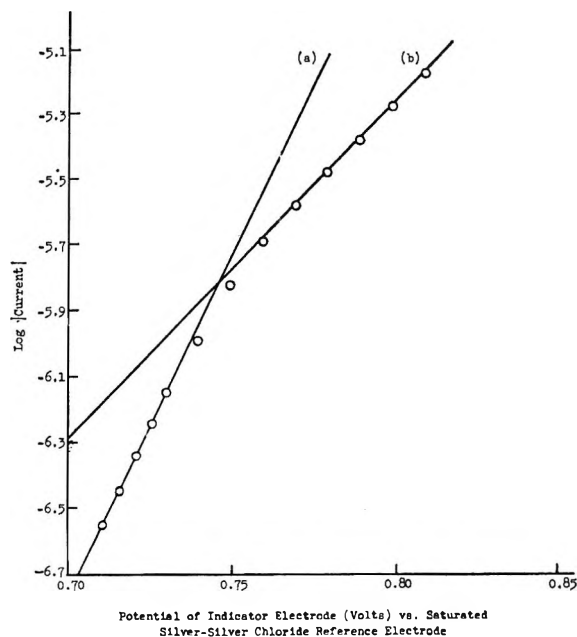
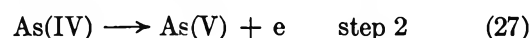
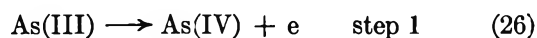
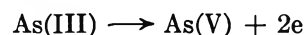


Figure 6. A Tafel plot of the foot of the arsenic oxidation wave showing two discrete linear portions. Correction was made for the residual current.

effects predicted by the kinetic equation for the following assumed mechanism



with the over-all reaction



The most prominent characteristic of this mechanism is that the wave having the smaller overpotential should have an inflected Tafel slope (*vide supra*). The Tafel curve for the oxidation of arsenic(III) is shown in Figure 6. It has been shown earlier that the slope of the curve at smaller currents should be

$$\frac{(2 - \alpha_{5,4})F}{2.3RT} = \text{slope } a \quad (28)$$

(11) V. A. Zakharov and O. A. Songina, *Zh. Fiz. Khim.*, **38**, 767 (1964).

(12) L. Meites, "Polarographic Techniques," Interscience Publishers, Inc., New York, N. Y., 1965, p 656.

(13) K. J. Vetter, "Transactions of the Symposium on Electrode Processes," E. Yeager, Ed., John Wiley and Sons, Inc., New York, N. Y., 1961, p 65.

and at higher currents

$$\frac{(1 - \alpha_{4,3})F}{2.3RT} = \text{slope } b \quad (29)$$

where the subscripts refer to the energy barrier of a particular electron-transfer step. Since α can only have a value between 1 and 0, the quantity $(2 - \alpha_{5,4})$ must have a numerical value between 1 and 2 and $(1 + \alpha_{4,3})$ must have a numerical value between 0 and 1. If these slopes are analyzed as having the empirical form

$$\frac{(1 - \beta)nF}{2.3RT} = \text{slope} \quad (30)$$

the experimental data yield at lower currents

$$(1 - \beta)n = 1.3 \pm 0.1$$

and at higher currents

$$(1 - \beta)n = 0.6 \pm 0.1$$

on the basis of a sample of ten determinations. These values were found to be unaffected in the concentration range 5.0×10^{-4} to 1.0×10^{-2} M As(III) and in the flow-velocity range 5–100 cm/sec. It therefore follows that the specific rate constant for step 1 is very much larger than that for step 2, *i.e.*, $k_{4,3}^0 \gg k_{5,4}^0$. In addition, the appropriate standard potentials are related as

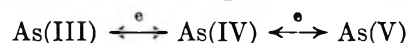
$$E_{5,4}^0 < E_{4,3}^0$$

which requires that arsenic(IV) be unstable with respect to disproportionation. Evidently, the disproportionation reaction is not the kinetically preferred reaction path under the experimental conditions. The criteria established by Hurd on the basis of computer studies of Vetter's equation (*vide supra*) are also satisfied by the experimental data.¹⁴

The literature documenting the influence of the double layer on electrochemical reactions provides convincing arguments demonstrating that an abrupt alteration in the electric field of the double layer can cause a change in the electrochemical rate constants as mentioned earlier. Under certain conditions, the observed inflection in the Tafel curve could be interpreted as resulting from double-layer effects. The experimental conditions are such that this interpretation, although possible, is improbable and is merely speculative. That is, the characteristic conditions which would warrant the suspicion of an abrupt change in the double layer are absent: (1) the range of potentials where the results obtained are considerably distant from the potential of zero charge; (2) the supporting electrolyte concentration is high and is known not to be specifically adsorbed to any great extent; and (3) although nothing is known about the affinity of arsenic(III)

toward specific adsorption, its low concentration and chemical characteristics would not be suggestive of such behavior.

The arsenic(IV) intermediate has been postulated on the basis of kinetic data obtained from experiments in homogeneous solutions.^{15,16} These studies together with the electrochemical evidence presented within provide a powerful argument for the existence of the As(IV) species. A comparison between the results of these investigations provides a consistent picture of the chemical properties of the intermediate under the considerably different experimental conditions. The only inconsistency between the homogeneous and the electrochemical results is the effect of oxygen on the data. In solution As(IV) appears to react preferentially with dissolved oxygen rather than with any other oxidant present. The electrochemical results, however, were independent of the presence of oxygen. This absence of any detectable effect may be rationalized in the following manner. Since the potential range of 0.5–1.4 v *vs.* s.sce was scanned repeatedly, the platinum surface contained an oxide film. It is sometimes helpful to consider the surface in the potential range of interest (the Tafel region) as a half-reduced oxide, Pt(OH)₂, according to Feldberg.¹⁷ In any event, an oxygen-containing species will be present at the electrode surface as the result of the oxidation of platinum at positive potentials. Furthermore, this surface oxidation will occur independently of the presence of dissolved oxygen (*i.e.*, H₂O is oxidized). Since the As(IV) exists only at the electrode surface, it could react with the surface film. Consequently, the reaction would be independent of dissolved oxygen. This would, however, suggest a more complex mechanism for the over-all oxidation process. For the purpose of simplicity the surface oxide can be considered as part of the electrode proper so that the mechanism of the electrode reaction can be given succinctly as



Acknowledgment. This investigation was supported in part by a grant from the Horace H. Rackham School of Graduate Studies of the University of Michigan. The author also acknowledges the facilities made available by the Computing Center at the university. The author acknowledges the assistance of Matthew J. Raszka who helped put this manuscript into its final form.

(14) H. A. Catherino, *J. Phys. Chem.*, **70**, 1338 (1966).

(15) M. Daniels, *ibid.*, **66**, 1473 (1962).

(16) R. Woods, I. M. Kolthoff, and E. J. Meehan, *J. Am. Chem. Soc.*, **86**, 1698 (1964).

(17) S. W. Feldberg, C. G. Enke, and C. E. Bricker, *J. Electrochem. Soc.*, **110**, 826 (1963).

The Current-Impulse Relaxation Technique and the Kinetics of Rapid Electrochemical Reactions. I. General Considerations

by W. D. Weir¹ and C. G. Enke

Frick Chemical Laboratory, Princeton University, Princeton, New Jersey (Received May 31, 1966)

The current-impulse relaxation technique, which extends the time domain experimentally accessible to kinetic investigations and permits direct assessment of charge-transfer kinetics without mass-transport polarization of the interphase, is described. The electrochemical system is displaced from equilibrium by a constant current impulse of restricted duration relative to the system relaxation time. From the slope of the charging curve and the value of the applied current density the differential capacitance is directly calculated; the subsequent relaxation of the overpotential is directly related to the kinetics of the faradaic process through which relaxation proceeds. By drastic restriction of the coulombic content of the impulse and reduction of the time interval before relaxation data are acquired, the kinetic parameters of the charge-transfer process are found without correction for mass-transport contributions. As a consequence of its conceptual and experimental simplicity, the technique offers operational and interpretive advantages over other methods.

Introduction

A dominant characteristic of the development of the study of the rates and mechanisms of electrochemical reactions through the past decade has been the introduction of techniques by which ever more rapid processes may be investigated. The fundamental problem in the extension of these techniques to the investigation of very rapid electrochemical processes is the difficulty of discrimination between the kinetic effects of charge-transfer and mass-transport processes. Satisfactory resolution of this problem requires the establishment of well-defined boundary conditions in the electrode-electrolyte interphase, appropriate to the direct application of a solution to the corresponding boundary-value problem for the mass-transport contribution to the over-all process.

The step-functional transient relaxation techniques² offer distinct limitations in imposing the definition of boundary conditions required for the study of very rapid reactions, and they involve practical difficulties of observation of the resulting system response at sufficiently brief intervals following the perturbation. That both of these limitations might be avoided if the perturbation was an impulse rather than a step function was recognized in the proposals of Reinmuth

and Wilson³ and of Delahay^{4,5} that the charge-step technique⁶ be applied to the study of rapid electrochemical reactions. In a charge-step experiment, the potential of the electrochemical cell under study is observed in response to a very brief impulse of undefined form but of known coulombic content. Because for a sufficiently abrupt pulse the transient impedance of the capacitive double layer is quite small relative to the partially resistive faradaic impedance, the double layer is charged to a new potential before appreciable

(1) To whom correspondence should be addressed at Department of Chemistry, Harvard University, Cambridge, Mass. 02138.

(2) For a thorough review, see P. Delahay, *Advan. Electrochem. Electrochem. Eng.*, **1**, 233 (1961). A more recent appraisal is given by W. H. Reinmuth, *Anal. Chem.*, **36**, 211R (1964).

(3) W. H. Reinmuth and C. E. Wilson, *ibid.*, **34**, 1159 (1962); W. H. Reinmuth, *ibid.*, **34**, 1272 (1962).

(4) P. Delahay, *ibid.*, **34**, 1161 (1962).

(5) P. Delahay, *J. Phys. Chem.*, **66**, 2204 (1962).

(6) P. Delahay and D. M. Mohilner, *J. Am. Chem. Soc.*, **84**, 4247 (1962); P. Delahay and D. M. Mohilner, *J. Phys. Chem.*, **66**, 959 (1962); P. Delahay, *ibid.*, **67**, 135 (1963). It is to the study of adsorption processes, with which these papers deal, that the technique owes an alternative (if not generally applicable) name, the "coulostatic" method. The more satisfactory designation "charge-step" is also due to Delahay, although its use was not preferred by him.

charge is consumed by the faradaic process. If the impulse is applied in such a manner that the cell is decoupled from the pulse source upon termination of the impulse, the double-layer capacitance is effectively in series only with the faradaic impedance and dissipation of the excess charge of the double layer can occur only as charge is consumed progressively by the electrode reaction. The relaxation of the overpotential from the initial value imposed by the impulse as the system approaches equilibrium is directly related to the kinetics of the reaction through which relaxation proceeds.

If the duration of the coulombic impulse is restricted to a time quite small relative to the relaxation time constant, the boundary conditions at the initiation of relaxation are well defined on the time scale of the relaxation process. Because the perturbation is of impulse rather than step-functional form, no ohmic correction of the overpotential response observed during relaxation is required. The very large ohmic drop across the cell during the interval of the impulse may drive the detector amplifier into saturation, however, and its recovery may be slow; extended transient oscillation due to stray inductance and capacitance present in cells of conventional design and to coupling capacitance also may prohibit reliable measurements for a significant interval following the impulse. Each of the published kinetic investigations in which the charge-step technique has been applied has demonstrated this restriction from measurements at short times: the experimental studies of Zn(II)-Zn(Hg) by Delahay and Aramata⁷ and by Hamelin⁸ and those of Bi(III)-Bi(Hg) by Hamelin⁹ graphically depict measurements to 5 μ sec. Reinmuth and Wilson³ reported satisfactory relaxation behavior at times greater than 2 μ sec following an impulse.

This prohibition from short time measurements imposes a distinct upper bound upon the rate of processes which can be examined. For adequate sensitivity and to assure applicability of the mass-transport equations, measurements of response must be initiated at times of the order of the time constant of the relaxation process. For a simple R-C model of the electrode process, as appropriate to the description of a small-amplitude relaxation through a simple charge-transfer reaction, assuming a nominal differential capacitance of 20 μ f cm⁻², a 2- μ sec time constant for the discharge of a univalent ion corresponds to a maximum value for the apparent exchange current of approximately 0.2 amp cm⁻². The restriction from short time measurements also necessitates an extended extrapolation of the observed response to $t = 0$ for the determination of the perturbation overpotential η_0 . The resulting uncertainty in η_1 is reflected in the value calculated for the differential

capacitance and leads to a substantial uncertainty in the calculated apparent exchange current.

The current-impulse relaxation technique was conceived to permit direct assessment of differential capacitance and to extend the time domain accessible to impulse relaxation measurements.

The Current-Impulse Relaxation Technique

In a current-impulse relaxation experiment, electrode potential is observed as a function of time in response to a constant-current pulse of brief duration; the technique is a direct but significant refinement of the charge-step technique in which a rectangular coulombic pulse replaces the "pseudoderivative" pulse of the charge-step method as the forcing function.

The response to such a perturbation may most conveniently be analyzed in terms of an equivalent linear network consisting of the electrolyte resistance, R_e , in series with the parallel combination of the capacitance of the double layer, C_1 , and the faradaic impedance. The faradaic impedance, in the time domain, is a series combination of charge-transfer resistance, R_c , and time-dependent mass-transport impedance, $Z_m(t)$. In the short time limit, or for negligible perturbation, the mass-transport contribution to the faradaic impedance vanishes, and the customary simplified network results. The behavior of the parallel arms is described by the equation

$$i_p = C_1(d\eta/dt) + \eta/R_c \quad (1)$$

where i_p is the external (pulse) current, η the overpotential, and t the time. The contribution of the electrolyte resistance, R_e , in series with the parallel arms is specified by the expression

$$\xi = i_p R_e + \eta \quad (2)$$

where ξ is the observable displacement of the cell potential from its equilibrium value. From the initiation of the constant-current impulse, charging response is given by

$$d\xi/dt = d\eta/dt = (i_p/C_1) \exp(-t/R_e C_1) \quad (3)$$

At the instant of impulse termination ($t = T$) the ohmic component of the observed potential vanishes, and only the perturbation overpotential, symbolized by η_0 , remains

$$\eta_0 = i_p R_c [1 - \exp(-T/R_e C_1)] \quad (4)$$

If following the impulse the cell is essentially at open circuit, the observed response must be simply

$$\xi = \eta = \eta_0 \exp[-t/R_e C_1] \quad (5)$$

(7) P. Delahay and A. Aramata, *J. Phys. Chem.*, **66**, 2208 (1962).

(8) A. Hamelin, *Compt. Rend.*, **257**, 1709 (1963).

(9) A. Hamelin, *ibid.*, **259**, 362 (1964).

where the origin at the time axis is redefined at the instant of impulse termination.

During the current pulse, the slope of the charging curve, $d\xi/dt$, must be i_p/C_1 for measurement times much less than the time-constant product $R_c C_1$; from the experimentally observed linear charging slope in the short time limit and the measured value of the impulse current, the differential capacitance is directly calculated.¹⁰ The capacitance can also be estimated from the relaxation plot, as with the charge-step method. Determination of R_c is made directly from the relaxation response of the system: a plot of $\ln \xi$, against t yields a slope $-(1/R_c C_1)$; with the value of C_1 assessed from the charging slope, R_c is calculated. Because this analysis requires only a determination of the slope of the logarithmic plot, and not its intercept at $t = 0$, there is no need for precise experimental definition of $t = 0$. Over the small excursions of potential for which the analysis is valid, the current-overpotential characteristic may be linearized; the charge-transfer resistance is then

$$R_c = \nu_d R T / n f i_a^0$$

where ν_d is the stoichiometric number for the rate-determining step, R is the gas constant, T the absolute temperature, n the number of electrons per unit advancement of the over-all electrochemical reaction, f the faraday, and i_a^0 represents the apparent exchange current density. Where this simple model is applicable, the exchange current density of a process is directly calculated from the value of R_c obtained from relaxation data if a value of n/ν_d is assumed or evaluated (*e.g.*, by analysis of the current overpotential characteristic over an extended potential range). Analysis of the dependence of exchange current density upon the concentration(s) of the reactant species in accordance with an electrochemical reaction-order treatment yields a value for the transfer coefficient of the charge-transfer reaction.

Application of an analysis which neglects the contribution of mass transport to the faradaic impedance requires that the concentrations of reactant and product be constrained to negligible changes in the course of a relaxation measurement. This requirement is implemented in the current-impulse technique by a drastic restriction of the quantity of charge transferred in each experiment and by a substantial reduction in the time interval between pulse termination and acquisition of the first reliable relaxation data.

Experimental Considerations

Operationally, a current-impulse relaxation experiment requires first that the charge density of the test

electrode be abruptly changed from its equilibrium value by a constant-current impulse of time duration negligible with respect to the time constant of the relaxation process in such a way that the cell is essentially at open circuit when the charging is completed, and second, that some means be available for observation of the resulting displacement of the electrode potential and its relaxation as the system approaches equilibrium.

To supply the current impulse to the cell, a fast-rise dc-coupled pulse generator with high output impedance and moderately high output voltage capability is required. The instrument used in exploratory studies was the General Radio 1217-B pulse generator with its associated 1201-B power supply. The dc component normally present at the positive output of this instrument was removed by a simple diode clamp. The pulse generator was coupled to the cell through a 1-kilohm load resistor to assure constant impulse current and two 1N-914 switching diodes with polarity appropriate to pass a pulse but to reject counterflow of current. This method of coupling offers the additional advantage relative to capacitive coupling of substantially decreasing the settling time of the series $R-L-C$ loop to which the input circuit is equivalent. The settling time increases with increasing LC product for the loop; with diode coupling L is the inductance of cell leads and electrode geometry and C is essentially the decoupling diode interelectrode capacitance, 5 pf or less, while for capacitive coupling the inductance is equivalent but the capacitance becomes that of the coupling capacitor, typically of the order of 500 pf. The decreased settling time with diode coupling manifests itself in substantially abbreviated post-impulse ringing.

With this input arrangement, current pulses continuously variable in amplitude from 0 to 20 ma and of duration as brief as 100 nsec were applied to the cell.

The overpotential response to the constant-current perturbation was amplified by a Tektronix 1121 amplifier (rise time 21 nsec). Although the limitation of its first amplification stage is nominally 10 mv, the unit recovers quickly from overload. The amplified signal was cabled to a Tektronix 535A sweep-delay oscilloscope with a type H plug-in preamplifier (rise time 31 nsec). The delayed trigger output pulse of the oscilloscope was used to trigger the pulse generator and the

(10) Measurement of the "initial slope" of the overpotential response of a system to a constant-current pulse, first reported by F. P. Bowden and E. K. Rideal, *Proc. Roy. Soc. (London)*, **A120**, 59, 80 (1928), has been extensively applied in determinations of differential capacitance in the presence of irreversible or quasi-reversible electrochemical reactions. The present technique simply extends this procedure to the class of highly reversible processes.

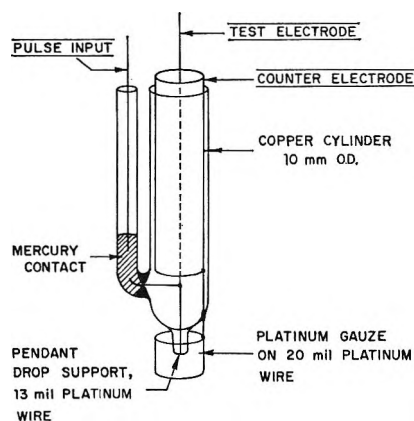


Figure 1. Low-inductance two-electrode probe with auxiliary pulse input for current-impulse relaxation measurements.

experiment was controlled by the oscilloscope time base "A." Single-sweep triggering was employed to avoid significant polarization.

With this system, an over-all deflection sensitivity as great as $50 \mu\text{V cm}^{-1}$ was achieved on a 100-nsec cm^{-1} time base. With appropriate calibration, current, overpotential, and time can be measured with an accuracy of 1%. Charging curves and relaxation response were recorded photographically with a Tektronix 350/C 35-mm camera system using Kodak Tri-X (ASA 400) film.

The transient response observed during and following an abrupt perturbation of a reactive system is relatively sensitive to the effects of stray capacitance and inductance, which may increase rise time and introduce extended ringing; to optimize response, an adaptation of the coaxial two-electrode configuration proposed by Blomgren, Inman, and Bockris¹¹ was employed. The two-electrode probe is illustrated in Figure 1. The pulse current is applied through the auxiliary contact to the test electrode, with the shield held at ground, and the response is observed between the inner conductor and the shield. In principle, there is no inductive coupling between the pulse input lead and the potential-measuring part of the system since the output lead is external to the shield. The mutual inductance between the shield and the inner conductor and the self-inductance of the shield cancel with the result that the over-all inductance of the cell is reduced to that of the loop: test electrode-counter electrode-shield.

The effect of electrolyte resistance upon the observed current-impulse response also may be substantial; as a consequence of the high current level of the impulse, the detection system is subjected to a voltage pulse which may be many times the magnitude of the

overpotential to be observed subsequent to the impulse (for $R_e = 5$ ohms, for example, up to 100 mv). Although iR compensation would provide the most direct solution to this problem, the recovery time of the detection system for overloads of such brief duration was of the order of 200 nsec, so an iR compensation scheme was not required.

The system 10–90% rise time was less than 100 nsec; however, overshoot and transient ringing due to uncompensated inductance and stray capacitance prohibited reliable ($\pm 100 \mu\text{V}$) observation of relaxation for an interval of up to 400 nsec following termination of the current pulse. Ringing was evident only following the pulse and did not obscure charging response. With excessive overload of the 1121 amplifier, however, the charging slope is suppressed, and care must be taken that the input attenuation is adequate to eliminate this distortion. System noise was observed to be of the order of $50 \mu\text{V}$ peak-to-peak; no interference by line frequency noise is possible over the time scale of a measurement.

Applicability and Scope

The unique advantage of the current-impulse relaxation technique has been identified as its capability for assessing the kinetic parameters of an electrochemical charge-transfer reaction directly, without correction for mass-transport polarization of the electrode-electrolyte interphase. The compatibility of a strict limitation of the charge passed in an experiment with the generation of experimentally significant response can be demonstrated in terms of the capabilities of the measurement system described.

If one estimates that the magnitude of the perturbation overpotential, η_0 , must be 5 mv to assure accurate relaxation measurements, a perfectly polarizable electrode with a differential capacitance of $20 \mu\text{f cm}^{-2}$ will require a 1×10^{-7} coulomb cm^{-2} impulse to assume this overpotential. This corresponds, for deposition of a univalent ion from solution, to approximately 0.05% of a monolayer, assuming 10^{15} deposition sites cm^{-2} . Even with this quite conservative estimate of the detection sensitivity, the polarization should introduce only a negligible mass-transport contribution to the observed overpotential at short times. Because the effects of mass-transport polarization are relatively more pronounced at longer times, examination of a semilogarithmic plot of the relaxation data for linearity permits immediate confirmation that these effects are inappreciable in the time interval of observation.

The maximum rate of an electrochemical reaction

(11) E. Blomgren, D. Inman, and J. O'M. Bockris, *Rev. Sci. Instr.*, **32**, 11 (1961).

which can be investigated with the current-impulse relaxation technique may be directly calculated. Two sets of limiting conditions are involved, the minimum conditions for adequate assessment of the value of C_1 during charging and the condition of a sufficient overpotential at the time of impulse termination to permit satisfactory analysis of the relaxation response. If one assumes that a satisfactory "initial slope" determination of the capacitance can be made if the time constant of the relaxation process, $R_c C_1$, is greater than twice the duration T of the impulse (cf. eq 3), the requirement $T > 0.2 \mu\text{sec}$ based upon a typical 80-nsec system rise time yields directly the over-all condition $0.2 \mu\text{sec} < 0.5 R_c C_1$, or $R_c C_1 > 0.4 \mu\text{sec}$. The specification that the time constant of the process must be greater than $0.4 \mu\text{sec}$ is also compatible with the $0.4\text{-}\mu\text{sec}$ interval following pulse termination before reliable relaxation data can be recorded: the overpotential at one time constant must be η_0/e , or for $\eta_0 = 5 \text{ mv}$, almost 2 mv , which is certainly adequate to assure accurate measurements. For a nominal differential capacitance of $20 \mu\text{f cm}^{-2}$ the restriction on the relaxation time constant corresponds to a minimum charge-transfer resistance of 0.02 ohm cm^2 . What might be a more severe limitation on the minimum value of R_c arises as a consequence of the 20-ma maximum pulse current of the apparatus described. Applying the condition $T < 0.5 R_c C_1$ to eq 4

$$\eta_0 < i_p R_c [1 - \exp(-0.5)] = 0.4 i_p R_c$$

if, as before, a minimum value of 5 mv is required for η_0 , then $i_p R_c > 0.0125 \text{ v}$. For $i_p = 20 \text{ ma}$, this places a minimum value of 0.625 ohm on R_c . With an impulse current of 20 ma applied to an electrode of surface area 0.01 cm^2 , $R_c \geq 0.00625 \text{ ohm cm}^2$, corresponding, for η/ν_d assumed to be unity, to a maximum exchange current density of approximately 4 amp cm^{-2} . Thus within the range of parameters experimentally attainable with commercial instrumentation, the current-impulse technique permits determinations of the kinetic parameters for electrochemical reactions about one order of magnitude more rapid than have been investigated with other transient relaxation methods.

The simplicity and power of the current-impulse relaxation technique promote its applicability to a wide range of problems in electrochemical kinetics and the elucidation of the mechanisms of electrode processes. The direct determination of differential capacitance in conjunction with kinetic measurements suggests application of the technique to the study of the dynamic properties of the electrochemical double layer and the influence of the double layer upon charge-transfer kinetics. Work is proceeding in each of these areas and detailed examinations of the kinetics of model metal deposition and oxidation-reduction reactions are underway.

Acknowledgment. The authors gratefully acknowledge support of this work by the National Science Foundation.

The Current-Impulse Relaxation Technique and the Kinetics of Rapid Electrochemical Reactions. II. The Electrochemical Reduction of Mercury(I)¹

by W. D. Weir² and C. G. Enke

Frick Chemical Laboratory, Princeton University, Princeton, New Jersey (Received May 31, 1966)

The electrochemical reduction of mercury(I) has been examined with the current-impulse relaxation technique. The differential capacitance of the mercury-electrolyte interface was observed to rise sharply with increasing anodic electrode potential, in striking agreement with the measurements of Sluyters-Rehbach and Sluyters. Impulse relaxation determinations of exchange current density were in substantial agreement with those of other transient relaxation methods. Two significant anomalies appeared in the investigation: dependence of differential capacitance calculated from impulse charging curves upon current density and significant deviation from linearity in reaction-order plots for high concentrations. A model appropriate to the description of transient relaxation processes which involve adsorbed reactant and/or intermediate is developed. Analysis of the dynamic behavior of this transient equivalent network resolves the anomalous observations of this investigation and suggests the cause of the marked disparity between the kinetic results of the transient and the periodic relaxation techniques for this system. The mechanistic consequences of the observed relaxation kinetics are considered.

Introduction

The electrochemical reduction of mercury(I) presents three particularly engaging aspects. First, the system Hg(I)-Hg(0) has long been regarded as the prototype of a highly reversible electrochemical system; the intrinsic rate of the electrodeposition-dissolution process is comparable to that of any other heterogeneous charge-transfer process which has been examined. Second, a number of studies by both transient and periodic relaxation techniques have yielded an array of disparate values for the kinetic parameters of the process; in particular, a persistent discrepancy between the transient results taken together and the results obtained with the periodic techniques appears unresolved. No entirely satisfactory estimates of the charge-transfer parameters of the process have been identified, and too few credible mechanistic inferences have been drawn from the available data. Third, the differential capacitance of a mercury-electrolyte interface is strongly potential-dependent in the anodic potential

region, as has been demonstrated in the work of Sluyters-Rehbach and Sluyters;³ the kinetic and mechanistic consequences of the observed anodic increase in capacitance have not as yet been considered.

The current-impulse relaxation technique, which was described in part I, is uniquely appropriate as an experimental approach to this problem.⁴ Direct current-impulse determination of differential capacitance permits confirmation of the faradaic impedance results of the Sluyters and obviates the use of an assumed capacitance value in calculations of kinetic parameters. The capability which the technique offers for drastically limited polarization of the interphase and short time

(1) Part I: W. D. Weir and C. G. Enke, *J. Phys. Chem.*, **71**, 275 (1967).

(2) To whom correspondence should be addressed at Department of Chemistry, Harvard University, Cambridge, Mass. 02138.

(3) M. Sluyters-Rehbach and J. H. Sluyters, *Rec. Trav. Chim.*, **83**, 967 (1964).

(4) W. D. Weir, Dissertation, Princeton University, Princeton, N. J., 1965; University Microfilms, Inc., Ann Arbor, Mich., 1966.

observation of the resulting transient assures direct estimates of charge-transfer kinetics. Finally, the internal checks of the technique provide a useful diagnostic for complications of the mechanistic scheme of the process which are not reflected in the results of earlier investigations.

Experimental Section

Reagents. ACS reagent quality mercury metal, obtained from Metal Salts Corp., Hawthorne, N. J., was used without further purification. Solutions were prepared from analytical reagent red mercuric oxide and bidistilled "lead-free" reagent perchloric acid. Distilled water used in the preparation of solutions and in cell rinsing was obtained by redistillation, from sodium hydroxide solution, of water obtained from a two-stage conductance water still. Nitrogen gas used to purge cell solutions of oxygen was treated in an all-glass purification train and passed into the cell *via* stopcocks. The gas was dried over calcium chloride, passed through an oven containing copper turnings at 350° to remove traces of oxygen and through a multiple-element trap containing activated coconut charcoal at liquid nitrogen temperature, and presaturated by dispersion through unimolar perchloric acid.

Solutions. Aqueous perchloric acid for use as a constant ionic medium was assayed volumetrically at $1.000 \pm 0.005 M$. A stock solution of mercurous perchlorate was prepared by reduction of a determinate solution of mercuric oxide in 1.00 M perchloric acid with mercury metal. This solution was assayed gravimetrically as the chloride at $0.0505 \pm 0.0004 M$. Working solutions were prepared by volumetric dilution with 1.00 M perchloric acid and stored over mercury. Solutions were treated by filtration through purified activated charcoal, but they were not pre-electrolyzed as it was considered unlikely that any of the trace impurities could influence the kinetic results by competitive reaction on the time scale of the impulse relaxation experiments. Each solution was thoroughly purged of dissolved oxygen prior to a series of determinations.

Cell and Electrodes. The coaxial electrode system described in part I was used to extend measurements to short times. The counter electrode was a lightly platinized cylinder of platinum gauze of 10-mm diameter and 4-cm² geometric area. The test electrode lead terminated in a 13-mil platinum wire which was sealed into the Pyrex sheath and polished flat. No attempt was made to taper the pendant drop support in view of the calculations of De Levie⁵ and the absence of dispersion found by Barker⁶ with a blunt dropping mercury electrode at 1.6 MHz. The drop contact was

prepared according to Ramaley, Brubaker, and Enke.⁷ A Pyrex cell with ground fittings was constructed to accommodate this electrode system, a dropping capillary, a transfer spoon of TFE, and a gas inlet. The dropping capillary was fed from a constant-head reservoir and pendant drop area was reproducible to within 1%, as determined by differential capacitance measurements; measurements extended to 1 hr after drop suspension confirmed that alternation of interfacial structure by adsorption of tensides was experimentally negligible. A fresh mercury drop was suspended for each charging and relaxation determination. Estimates of the drop area at 25.0° corresponding to each solution concentration⁸ were secured by calculation of the spherical area from the appropriate average drop mass; no correction for the area of the drop contact, estimated to have been about 4% of the spherical area of a drop, was made. The spherical drop area in $1.03 \times 10^{-3} M$ solution was similarly determined for several temperatures from 5 to 45° for use in calculations of the temperature dependence of differential capacitance and exchange current density. All reported capacitance and exchange current values are normalized to unit area. The temperature of the cell solution was maintained by a Tamson T-9 bath to within 0.04° of the set point.

Instrumentation. The instrumentation for the current-impulse relaxation measurements reported here was that described in part I. All oscilloscope and amplifier calibrations were maintained within 0.5%. Determinations of pulse current for calculation of differential capacitance were made by interposing a 10-ohm, 0.5% resistor between the electrode shield and the connection to the grounding system and measuring the voltage drop across it produced by a 0.5- μ sec current pulse.

Results

Estimates of differential capacitance were obtained for seven concentrations from 2.06×10^{-5} to $5.15 \times 10^{-3} M$ $Hg_2(ClO_4)_2$ in 1.00 M $HClO_4$ by two methods:

(5) R. De Levie, *J. Electroanal. Chem.*, **9**, 117 (1965).

(6) G. C. Barker in "Transactions of the Symposium on Electrode Processes," E. Yeager, Ed., John Wiley and Sons, Inc., New York, N. Y., 1961, pp 325-367.

(7) L. V. Ramaley, R. L. Brubaker, and C. G. Enke, *Anal. Chem.*, **35**, 1088 (1963).

(8) Because the interfacial tension of a mercury-electrolyte interface is strongly dependent upon the potential difference across it, the mass of a mercury droplet at detachment from a dropping capillary, which is proportional to the interfacial tension, must be potential-dependent. Because the electrode potential of mercury in contact with a solution of a soluble mercurous salt is determined by the mercurous ion concentration, a separate drop-mass determination and surface area calculation must be made from each solution concentration.

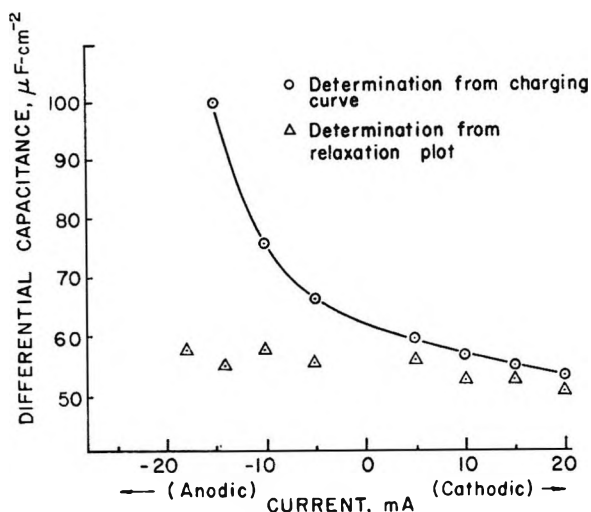


Figure 1. Representative plot of differential capacitance estimates against impulse current, for $1.03 \times 10^{-3} M \text{Hg}_2(\text{ClO}_4)_2$ in $1.00 M \text{HClO}_4$ at 25.0° .

first, by direct calculation from the initial slope of the charging curve and the value of the constant charging current, and second, by extrapolation of the relaxation data on a plot of $\log \eta$ against t to determine η_0 and calculation of the capacitance from this value and the coulombic content (current \times pulse duration) of the pulse. Although the charging curves over a $2\text{-}\mu\text{sec}$ current pulse were well-defined and exhibited little curvature, comparison of charging curves at different concentrations revealed a steep initial curvature over the first portion of the charging curve for concentrations above $5 \times 10^{-4} M \text{Hg}_2(\text{ClO}_4)_2$. The initial curvature was more prolonged the higher the concentration, and was more evident with lower than with higher cathodic current density. This observation will be discussed below; as a point of procedure, the "initial slopes" upon which capacitance calculations were based were determined in such a way as to disregard the sharp initial curvature.

Estimates of differential capacitance obtained with the direct technique exhibit one immediately striking feature—dependence upon the current density at which the determination was carried out. Further, the estimates secured by the two techniques were at variance with one another for concentrations above $2.06 \times 10^{-4} M \text{Hg}_2(\text{ClO}_4)_2$. These two effects are illustrated by the typical data of Figure 1. These data, for $1.03 \times 10^{-3} M \text{Hg}_2(\text{ClO}_4)_2$, show strong dependence of differential capacitance calculated from anodic charging curves on the magnitude of the charging current, increasing with increasing anodic current, while for cathodic charging, the capacitance shows a distinct but decreasing trend with increasing cathodic

Table I: Values of Differential Capacitance and Apparent Exchange Current Density for Solutions of Varying Concentration of $\text{Hg}_2(\text{ClO}_4)_2$ in $1.00 M \text{HClO}_4$ at 25.0°

Concn, mole l. ⁻¹	C (relaxa- tion), μf cm^{-2}	C (charg- ing), μf cm^{-2}	i_a^0/C , amp f^{-1}	i_a^0 (charg- ing), amp cm^{-2}	i_a^0 (relaxa- tion), amp cm^{-2}
2.06×10^{-5}	29.1	31.2	677	0.0212	0.0197
1.03×10^{-4}	34.8	32.9	2060	0.0678	0.0717
2.06×10^{-4}	36.0	35.6	2895	0.103	0.104
5.15×10^{-4}	43.5	45.5	4180	0.190	0.182
1.03×10^{-3}	56.3	62.5	4860	0.304	0.274
2.06×10^{-3}	75.6	112	5910	0.662	0.447
5.15×10^{-3}	205	464	5910	2.7 \pm	1.21

current. Capacitance estimates obtained by extrapolation of relaxation data, while necessarily of poor precision (typically, as in this case, $\pm 10\%$) due to the uncertain extrapolation, were lower and exhibited no marked increase with decreased cathodic or increased anodic current. Upon the presumption (which will be justified in terms of a model which permits description of this behavior) that the single appropriate differential capacitance estimate of either procedure for a given concentration is that corresponding to the zero-current intercept of its current-dependent values, for the data of Figure 1 one estimates graphically C -(charging) = $62.5 \pm 0.7 \mu\text{f cm}^{-2}$ and C -(relaxation) = $56.3 \pm 0.6 \mu\text{f cm}^{-2}$.

Similarly, "zero-current" estimates of the differential capacitance were obtained for each of the other solutions by both procedures. Current dependence of capacitance values obtained from charging curves was most pronounced for the most concentrated solution, progressively less severe for decreasing concentrations, and practically unobservable for concentrations in the $10^{-5} M$ range. Dependence of capacitance values obtained from relaxation plots upon pulse current was in every case slight and of marginal significance in view of the scattering of the data. The normalized "zero-current" values from the two procedures are summarized in Table I.

The values determined from charging slopes are shown in Figure 2 in comparison with the values calculated by Sluyters-Rehbach and Sluyters from their "complex plane" analysis of faradaic impedance data.^{3,9} The agreement in form of these capacitance-potential profiles is substantial, and because the capacitance values of Sluyters-Rehbach and Sluyters are reported

(9) The equivalent electrode potentials were calculated taking $\phi_M^0 = 0.789 \text{ v}$ against the standard hydrogen electrode and with a mean ionic activity coefficient $\gamma_{\pm} = 0.676$.

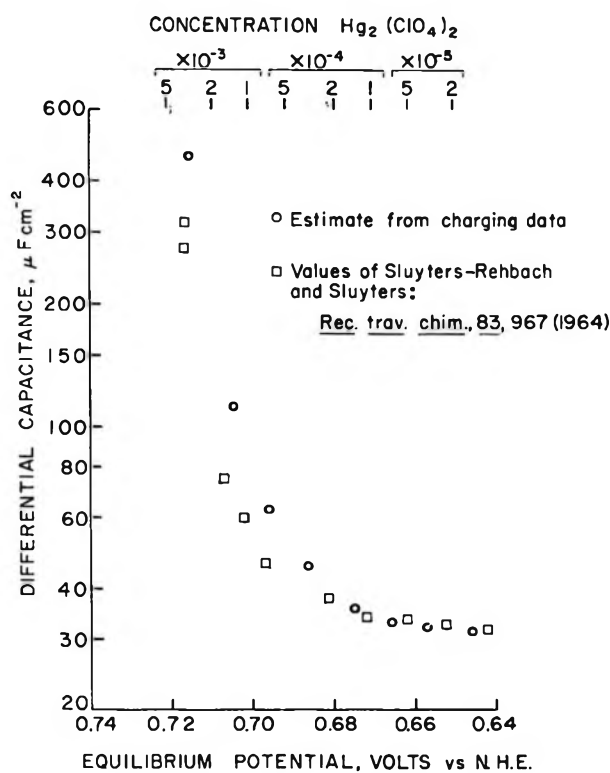


Figure 2. Plot of differential capacitance from impulse-charging data in 1.00 M HClO₄ at 25.0° against Hg₂(ClO₄)₂ concentration and calculated equilibrium potential, to compare the data of Sluyters-Rehbach and Sluyters.

for measured potentials of a cell with transference, the discrepancy of the profiles might be simply the result of a constant liquid junction potential included in their measured cell potentials.

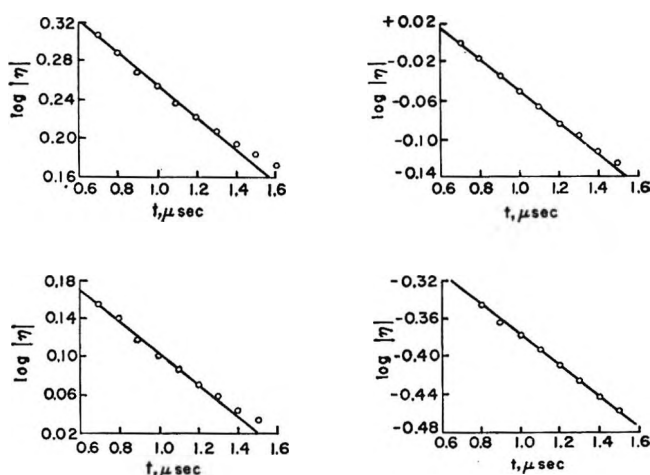


Figure 3. Typical cathodic semilogarithmic relaxation plots for 1.03×10^{-3} M Hg₂(ClO₄)₂ in 1.00 M HClO₄ at 25.0°, with constant pulse duration of 200 nsec: (a) upper left, 20.0 ma; (b) lower left, 15.0 ma; (c) upper right, 10.0 ma; and (d) lower right, 5.0 ma.

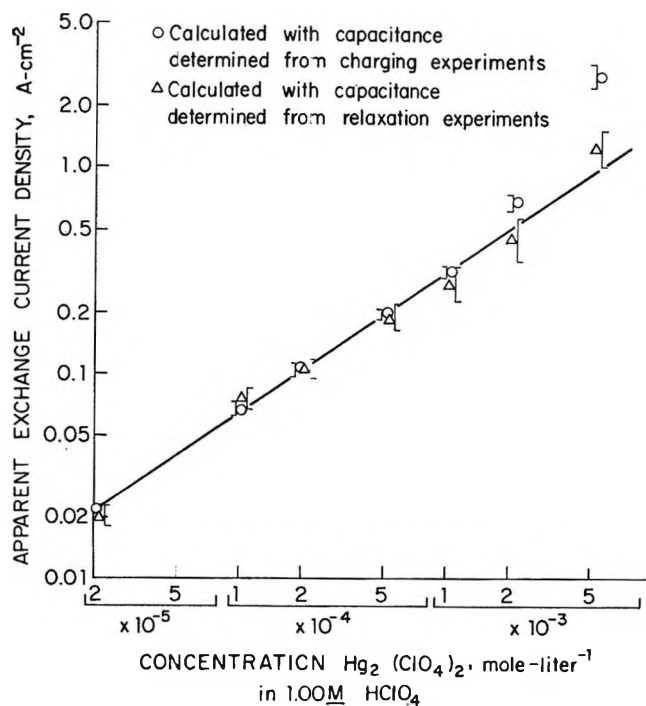


Figure 4. Reaction-order plot for electrochemical reduction of mercury(I) in 1.00 M HClO₄ at 25.0°.

Typical semilogarithmic relaxation plots for 1.03×10^{-3} M mercurous perchlorate in 1.00 M perchloric acid at 25.0° are illustrated in Figure 3. It is apparent that as the current level of the impulse is increased, deviation from linearity in the semilogarithmic plots appears at long times. Slopes of these were taken over the interval where strict linear behavior was observed or, in the case of low concentrations at high current levels, where slight curvature was persistent, as the limiting slope at short times. That this procedure yields consistent results was confirmed at low and at high concentration by comparison of calculated values of exchange current for several currents at constant pulse duration and for several pulse durations at a single current level.

In Table I are summarized values of the quotient i_0^a/C for each of the seven solutions; each entry is an average of three or more determinations, typically in agreement within 5%. The apparent exchange current densities calculated from the values of i_0^a/C and the two sets of differential capacitance values appear in the right-hand columns.

A reaction-order plot of these data is given in Figure 4. It shows excellent linearity in the low concentration region for both sets of data, but marked systematic departure from linearity is evident at higher concentrations for the points corresponding to the capacitance values determined in charging experi-

ments. The significance of this anomalous behavior will be discussed at length below. The slope of the reaction-order plot established at low and intermediate concentrations is 0.68 ± 0.02 . On the basis of the reaction-order treatment applicable to a simple $R-C$ equivalent network, this corresponds to an apparent transfer coefficient of $\alpha_a = 0.32 \pm 0.02$. From the i_a^0 values and α_a an apparent standard rate constant $k_a^0 = 0.019 \pm 0.002 \text{ cm sec}^{-1}$ is calculated.

A temperature dependence study was conducted with $1.03 \times 10^{-3} M$ mercurous perchlorate in $1.00 M$ perchloric acid to establish a value for the experimental enthalpy of activation. The results of the study were as follows: for $T = 5, 15, 25, 35,$ and 45° , $i_a^0 = 0.212, 0.246, 0.274, 0.292,$ and $0.351 \text{ amp cm}^{-2}$. A plot of $\log i_a^0$ vs. $1/T$ exhibited a slope of -490 K° from which an experimental enthalpy of activation of $2.2 \pm 0.2 \text{ kcal mole}^{-1}$ was calculated. This value is in excellent agreement with the result of Gerischer and Krause,¹⁰ $2.0 \pm 0.5 \text{ kcal mole}^{-1}$.

Discussion

The kinetic results of the present investigation and of previous studies¹⁰⁻¹⁵ of the electrochemical reduction of mercury(I) are summarized in Table II. Because of the strong dependence of the calculated standard rate constant upon the apparent transfer coefficient, the results may best be compared in terms of exchange current density at a specified reactant concentration. This comparison among the entries of the last column of Table II reveals that the exchange current density determined by the current-impulse relaxation technique is higher than that found with any of the other transient methods except the galvanostatic technique of Birke and Roe.¹⁶ This observation is in accord with the *ab initio* expectation that inadequate correction for mass-transport impedance in transient techniques should lead to low estimates of exchange current density; circumvention of the necessity for mass-transport correction in the present investigation should result in higher and, presumably, more satisfactory results. The estimate obtained from periodic relaxation measurements remains inexplicably higher than those of the transient techniques, however.

Despite the substantial concordance of the results of the present investigation with previous work, *ab intra* they exhibit anomalies which provide compelling evidence of mechanistic complexity inadequately described by the postulated $R-C$ equivalent network. The hypothesis that the anomalous observations might be consequences of nonfaradaic nonlinearity arising from the strong potential dependence of differential capacitance at anodic potentials was considered, how-

ever. A significant variation in differential capacitance through the overpotential range of impulse response would produce substantial differences in form between cathodic and anodic charging transients, specifically, divergence from linearity in the positive sense for cathodic charging and in the negative sense for anodic charging; the complete absence of positive inflection in the cathodic charging transients and the closely comparable form of anodic and cathodic transients was taken as evidence that the anomalies could not be rationalized as consequences of nonlinearity.

A Transient Equivalent Network. A model which encompasses the observations classified as anomalous from the standpoint of the simple $R-C$ model must rationalize the deviation from linearity revealed in the electrochemical reaction-order plot at high reactant concentrations and the observed dependence of differential capacitance values obtained by constant-current charging upon current density. A model which resolves these anomalies and explains the untoward discrepancy between the estimates of kinetic parameters obtained by periodic and transient relaxation measurements is postulated here, based upon previous treatments of the contributions of adsorbed reactants, intermediates, and products to the ac impedance of a faradaic process.

The kinetic consequences of adsorption of reactant were first examined by Laitinen and Randles,¹⁷ based upon the proposal of a mechanism in which two independent charge-transfer processes take place in parallel, one involving the discharge of "adsorbed" reactant at the surface and the other the discharge of "nonadsorbed" reactant from solution. In the equivalent network which represents this mechanism, two faradaic discharge paths shunt the double-layer

(10) H. Gerischer and M. Krause, *Z. Physik. Chem.* (Frankfurt), **14**, 184 (1958).

(11) H. Gerischer and K. Staubach, *ibid.*, **6**, 118 (1956).

(12) H. Matsuda, S. Oka, and P. Delahay, *J. Am. Chem. Soc.*, **81**, 5077 (1959).

(13) H. Imai and P. Delahay, *J. Phys. Chem.*, **66**, 1108 (1962).

(14) M. Sluyters-Rehbach and J. H. Sluyters, *Rec. Trav. Chim.*, **83**, 967, 983 (1964).

(15) R. L. Birke and D. K. Roe, *Anal. Chem.*, **37**, 450, 455 (1965).

(16) The results of these authors are rendered somewhat uncertain by the necessity of an extended extrapolation of η vs. $t^{1/2}$ data based upon a very few experimental points in the kinetically useful time interval identified by their analysis of the mass-transport and double-layer charging problems. This uncertainty is confirmed by the nonlinearity of a reaction-order plot constructed with their reported exchange current densities for the three concentrations of mercurous perchlorate for which determinations were made. That the exchange current densities found by this technique are somewhat higher than those found by current-impulse relaxation determination need not be regarded as significant. Cf. W. H. Reinmuth, *Anal. Chem.*, **38**, 270R (1966).

(17) H. A. Laitinen and J. E. B. Randles, *Trans. Faraday Soc.*, **51**, 54 (1955).

Table II: Comparison of the Present Kinetic Results with the Results of Previous Studies of the Electrochemical Reduction of Mercury(I) at 25.0^o^a

Investigator(s)	Technique	Ref	Apparent transfer coeff	Std rate const, cm sec ⁻¹	Apparent exchange current density 1.0 × 10 ⁻⁴ M, amp cm ⁻²
Gerischer and Staubach	Faradaic impedance	11	0.3 ± 0.2(C)	...	0.16
Gerischer and Staubach	Potentiostatic	11	0.4 ± 0.1	...	0.07
Gerischer and Krause	Double-pulse galvanostatic	10	0.30 ± 0.03	0.011(C)	0.13
Matsuda, Oka, and Delahay	Double-pulse galvanostatic	12	0.30 ± 0.02(C)	0.021(C)	0.25
Imai and Delahay	Faradaic rectification	13	0.28 ± 0.03	1.3	13
Sluyters-Rehbach and Sluyters	Faradaic impedance	14	≥0.46
Birke and Roe	Modified galvanostatic	15	0.25 ± 0.05	0.06(C)	0.38
Weir	Current-impulse	...	0.32 ± 0.02	0.019	0.30

^a Results designated (C) were not reported by the respective authors but are calculated from their data.

capacitance: the conventional solution discharge path through series charge-transfer resistance and Warburg impedance; and a path corresponding to discharge of adsorbate, with series charge-transfer resistance, R_a , and capacitance, C_a . An incremental displacement, $d\phi_M$, of the potential of the test electrode from equilibrium must correspond to a change in the ratio of the two oxidation states of the adsorbate and, because the model assumes that adsorption and desorption processes are negligibly slow relative to charge transfer, a finite quantity of charge dq_a must be transferred through R_a to effect the surface concentration changes required to permit relaxation to the new equilibrium state. The differential quotient $dq_a/d\phi_M$ defines the capacitance, C_a , which, because no mass transport processes are implicated, must be frequency-independent.

The effect of reactant adsorption upon the faradaic impedance was reconsidered by Llopis and co-workers¹⁸ and later by Senda and Delahay¹⁹ for the case of a single discharge path involving adsorbed reactant where the adsorption process may be comparable in rate to the charge-transfer reaction. The equivalent network to which these treatments correspond is that of Figure 5a. In this representation the significance of C_a and R_a is that of the Laitinen and Randles model; however, shunting C_a is a series path consisting of Warburg impedance and frequency-independent resistance, R_s . The element R_s relates to the kinetics of the adsorption process and, presumably, charge transfer and coupled chemical steps, if any, preceding the adsorption of intermediate. For sufficiently restricted

perturbations of the system, all of the components may be considered to behave as linear elements.

While both the Laitinen-Randles and Llopis-Senda-Delahay networks describe plausible mechanisms for heterogeneous oxidation-reduction processes, the latter model is more appropriate for the description of electrodeposition processes. A number of converging lines of evidence, both experimental and speculative, indicate that adsorption of a reactant or intermediate species may substantially reduce the apparent activation energy of metal deposition processes.²⁰ If adsorption of reactant or intermediate is possible, the contribution of discharge of nonadsorbed species to the observed rate of the over-all process will be small and, for a substantial difference of activation energies, negligible relative to the rate of discharge *via* adsorbed species. The faradaic impedance model of Llopis and co-workers and Senda and Delahay is, then, an appropriate point of departure for the synthesis of an analogous model for the analysis of transient relaxation processes even though the alternative direct discharge path is not considered.

Transformation of the ac model, Figure 5a, into a form suitable for the interpretation of rapid dc transients is accomplished directly when the Warburg impedance, which arises from a frequency domain analysis, is replaced by its time domain analog, a time-

(18) J. Llopis, J. Fernández-Biarge, and M. Pérez Fernández, *Electrochim. Acta*, 1, 130 (1959).

(19) M. Senda and P. Delahay, *J. Phys. Chem.*, 65, 1580 (1961).

(20) B. E. Conway and J. O'M. Bockris, *Electrochim. Acta*, 3, 340 (1961).

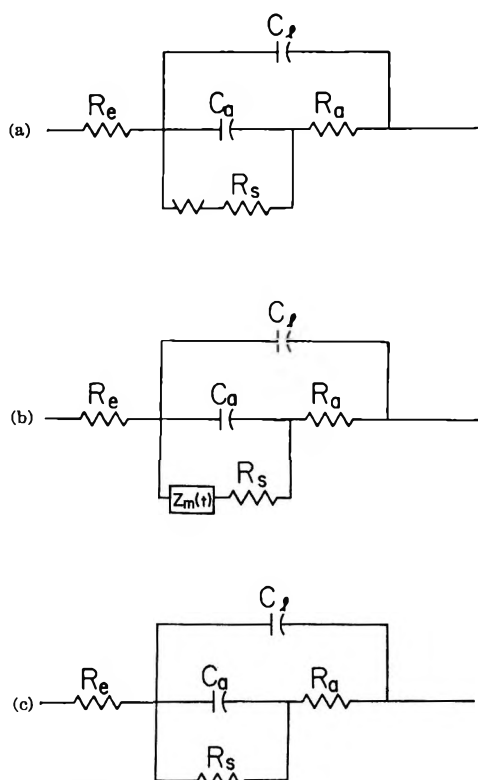


Figure 5. Adaptation of the ac model to describe transient relaxation processes: (a) the ac model of Llopis, *et al.*, and Senda and Delahay; (b) the time domain equivalent network applicable to dc analysis; (c) the simplified transient equivalent network, in the limit $t \rightarrow 0$. The circuit elements are as follows: R_e , electrolyte resistance; R_a , charge-transfer resistance for discharge of adsorbate; R_s , resistive element representing the kinetic consequences of o_2^- adsorption and coupled charge transfer or chemical processes; C_1 , electrochemical double-layer capacitance; and C_a , capacitance due to adsorbate discharge.

dependent mass-transport impedance, $Z_m(t)$. The resulting dc equivalent network is represented in Figure 5b. It has been demonstrated that on the time scale of current-impulse relaxation experiments the effects of mass-transport polarization are eliminated or at least minimized so that, as a quite reasonable approximation, $Z_m(t) = 0$ as $t \rightarrow 0$. The simplified transient equivalent network is represented in Figure 5c.²¹ Justification of the appropriation of the ac model and of its adaptation to the dc transient case by analogy must rest with the congruence of predictions based upon the transient model with experimental observations.

Linear Analysis of the Transient Equivalent Network. Before the dynamic behavior of this model is formally described, it will be useful to examine, in a qualitative way, the response of the model to short duration constant-current charging and subsequent relaxation.

The configuration of the equivalent network, Figure 5c, suggests immediately that for constant-current charging the two capacitors, C_1 and C_a , are effectively in parallel. The capacitance determined from a constant-current charging experiment will be their sum, $C_1 + C_a$, if R_a is negligible and R_s is sufficiently large that leakage across C_a is negligible.²² Charging of C_a corresponds, as in the ac case, to changing the surface concentration of a reactant or intermediate in equilibrium with the substrate metal by virtue of the charge-transfer process represented by R_a ; the charge q_a on capacitor C_a is exactly equivalent to the quantity of charge transferred and represents, in chemical terms, the deficit or excess of that reactant or intermediate relative to its surface concentration at equilibrium.

If C_1 and C_a charge in parallel (C_1 directly and C_a through R_a), at the instant of termination of the charging current the potential differences across C_1 and C_a differ by the magnitude of the ohmic drop across R_a immediately prior to the cessation of the impulse. Because R_a is small with respect to R_s , the capacitors can equalize their potential differences rapidly by charging in series through R_a . The direction of charging must be such that the charge on C_1 and its potential difference decrease while the charge on C_a increases with the consequence that the faradaic process represented by R_a is further advanced; the charge q_a on C_a increases since leakage across R_s must be presumed to be negligible on this time scale. When this charging process is complete, the potential difference across the two capacitors must be equal and the capacitors are effectively in parallel across R_s because, as R_a is much smaller than R_s , its effect upon the charging of R_s by C_1 is negligible.

The subsequent discharge process may be conceptually resolved into two components: the discharge of C_1 through the series combination R_s and R_a and the discharge of C_a through R_s alone. The discharge of C_1 through R_s and R_a corresponds to the complete sequence of steps comprising the mechanism: adsorption of reactant or, after a preceding charge-transfer step,

(21) The network will be designated a *transient* equivalent network to avoid the suggestion that it is in any sense applicable to the description of stationary-state dc processes. Its appropriateness is assured whenever $Z_m \rightarrow 0$, in the high frequency limit for periodic perturbations as in the short time limit for dc transient measurements.

(22) In any case, the capacitance assessed from a charging experiment of reasonable duration will be larger than C_1 unless R_a is quite large. It is appropriate that the assumption $R_s \gg R_a$ is made since R_a includes processes (adsorption of reactant, discharge of solvated reactant and adsorption of the intermediate, or volume chemical reaction coupled to the adsorption or discharge process) which are, in general, energetically less favored than those included in R_s (discharge of desolvated reactant or intermediate and rapid assimilation of product into the structure of the liquid metal).

of intermediate and subsequent discharge of the adsorbed species. It may be identified with the relaxation process of a simple R - C equivalent network. As the discharge of C_1 takes place and the overpotential decays, the concentration of adsorbed reactant or intermediate must change to remain in equilibrium with the decaying potential; it is the process by which the concentration of adsorbate changes that the discharge of C_a through R_s alone describes. Because $R_a \ll R_s$, the over-all process can be described as discharge of C_1 and C_a in parallel through R_s .

This qualitative survey of the response of the model suggests that the analysis of its dynamic behavior can be resolved into three discrete and simple problems.

(a) Parallel charging of C_1 and C_a by a charging current i_c is given by

$$(d^2\eta/dt^2) + [(C_a + C_1)/R_a C_a C_1](d\eta/dt) - i_c/R_a C_a C_1 = 0 \quad (1)$$

The solution with the appropriate boundary conditions, $\eta_{t=0} = 0$ and $(d\eta/dt)_{t=0} = i_c/C_1$, is

$$\eta = [i_c/(C_a + C_1)]t + \frac{i_c R_a C_a^2 / (C_a + C_1)^2 \times [1 - \exp[-t(C_a + C_1)/R_a C_a C_1]]}{(C_a + C_1)^2} \quad (2)$$

The quantity of interest experimentally is the charging slope $(d\eta/dt)$ given by

$$d\eta/dt = i_c/(C_a + C_1) + [i_c C_a / (C_a + C_1) C_1] \times \exp[-t(C_a + C_1)/R_a C_a C_1] \quad (3)$$

so for $t = 0$, $(d\eta/dt) = i_c/C_1$ and for $t \rightarrow \infty$, $(d\eta/dt) = i_c/(C_a + C_1)$. The transition from the initial slope, i_c/C_1 , to the normal slope, $i_c/(C_a + C_1)$, is governed by the time constant $R_a C_{\text{series}}$, where C_{series} represents the series equivalent of C_1 and C_a .

(b) Series discharge of C_1 into C_a through R_a at open circuit is given by

$$(d^2\eta/dt^2) + [(C_a + C_1)/R_a C_a C_1](d\eta/dt) = 0 \quad (4)$$

The solution is subject to the boundary conditions $\eta_{t=0} = \eta_0$ and $\eta_0 = \delta_0 + i_a R_a$ where i_a is the charging current which flowed through R_a prior to cessation of the impulse and δ_0 is the potential difference across C_a at $t = 0$. The solution

$$\eta = \eta_0 - [i_a R_a C_a (C_a + C_1)] \times [1 - \exp[-t(C_a + C_1)/R_a C_a C_1]] \quad (5)$$

exhibits the anticipated property of going to a non-zero value $\eta_0' = \eta_0 - i_a R_a C_a / (C_a + C_1)$ as $t \rightarrow \infty$. If C_a is small, the process of series charging through R_a

requires only a small quantity of charge and $\eta_0' \approx \eta_0$. The time constant of the discharge is $R_a C_{\text{series}}$.

(c) Open circuit discharge of parallel C_1 and C_a through R_s is given by

$$(d\eta/dt) - [1/R_s(C_a + C_1)]\eta = 0 \quad (6)$$

the solution of which, subject to the boundary condition $\eta_{t=0} = \eta_0'$, is

$$\eta = \eta_0' \exp[-t/R_s(C_a + C_1)] \quad (7)$$

The time constant of the discharge is $R_s C_{\text{parallel}}$.

Identification of Characteristic Time Constants. In the discussion of (a) it was concluded that the time constant of the exponential transition from the charging of C_1 alone to the charging of C_1 and C_a in parallel is $R_a C_{\text{series}}$; in (b) it was found that the series charging process has the identical time constant. The time constant of the parallel discharge process considered in (c) is $R_s C_{\text{parallel}}$.

A reexamination of the morphology of the charging curves as a function of concentration, as described above, permits an assessment of the relation of these time constants to the time domain of the charging and relaxation experiments. It was noted that a steep inflection in the charging curves became evident with concentrations greater than $5.15 \times 10^{-4} M$ mercurous perchlorate. If this initial curvature can be identified with the transition from charging of C_1 alone to parallel charging of C_1 and C_a , it can be suggested that at the higher concentrations the time constant $R_a C_{\text{series}}$ encroaches upon the time domain of the charging experiments; at lower concentrations, where the charging curves exhibit no initial curvature, if the parallel capacitance $(C_a + C_1)$ is assessed, the time constant $R_a C_{\text{series}}$ must be less than the rise time of the response to the constant-current charging pulse. That $(C_a + C_1)$ and not C_1 alone is assessed by constant-current charging may be established by comparison of the results of the charging determinations with the ac impedance measurements of Grahame²³ which, for 1.0 M HClO_4 but in the absence of added $\text{Hg}_2(\text{ClO}_4)_2$, should be identifiable with C_1 . These results are given in Table III. For the lower concentrations the two sets of results are in close agreement, while for higher concentrations their discrepancy is substantial. Values of C_a calculated by difference based upon identification of the charging capacitance with $(C_a + C_1)$ and of Grahame's results with C_1 are given also. By this identification, as C_a increases with increasing concentra-

(23) D. C. Grahame, *Chem. Rev.*, **41**, 441 (1947). The data cited are read from Figure 6. The zero point of the rational potential scale for nonabsorbing electrolytes is -0.20 v against the standard hydrogen electrode.

Table III: Capacitance Values at 25.0° for Solutions of Varying Concentrations of $\text{Hg}_2(\text{ClO}_4)_2$ in 1.00 M HClO_4

Concn, mole l. ⁻¹	Potential vs. N.H.E., v	$C_1 + C_a$ (charging)	C_1 (Grahame)	C_a (calcd)
	2.06×10^{-5}	0.646	31.2	30.5
5.15×10^{-5}	0.657	32.0	31.0	1.0
1.03×10^{-4}	0.666	32.9	31.5	1.4
2.06×10^{-4}	0.675	35.6	32.0	3.6
5.15×10^{-4}	0.687	45.5	32.5	13
1.03×10^{-3}	0.696	62.5	33.0	29
2.06×10^{-3}	0.705	112	34.0	78
5.15×10^{-3}	0.716	464

tion of $\text{Hg}_2(\text{ClO}_4)_2$, the time constant, $R_a C_a C_1 / (C_a + C_1)$, which for $C_a \leq C_1$ is controlled principally by C_a , must increase sharply in magnitude. At 1.03×10^{-3} M $\text{Hg}_2(\text{ClO}_4)_2$, the appearance of prolonged initial curvature in the charging curves indicates that the time constant corresponding to this concentration approaches the time domain of the impulse. The initial curvature should, as observed, be more prolonged the larger the concentration.

Interpretation of Reaction-Order Deviation. The anomalous deviation from the linear slope of the reaction-order plot at the higher concentration levels can now be readily interpreted. If the time constant $R_a C_{\text{series}}$ is within the time domain of the relaxation experiments, typically $0.4 \mu\text{sec} < t < 1.2 \mu\text{sec}$, the observed relaxation must be the result of mixed series and parallel discharge, leading to a higher apparent relaxation rate than would be observed for parallel discharge only. The time constant for this enhanced relaxation rate will correspond neither to $R_a C_{\text{series}}$ nor to $R_a C_{\text{parallel}}$ and, as a consequence, the capacitance determined from a semilogarithmic extrapolation of the relaxation data will correspond neither to C_{series} nor to C_{parallel} . The apparent exchange current density values calculated from the time constants for mixed discharge must be larger than anticipated for parallel discharge through R_a alone, and the deviations of the corresponding logarithmic values from the slope of the reaction-order plot established at low and intermediate concentrations result. The observed deviation from linearity may be considered to represent the first stage of a transition from rate control on the time scale of the relaxation observation by the time constant, $R_a(C_a + C_1)$, to control by $R_a C_a C_1 / (C_a + C_1)$. The onset of this transition, as reflected in the initial curvature of the charging curves and the departure from linearity in reaction order plots at higher concentrations, is strikingly revealed in the disparity between

charging and relaxation estimates of capacitance (see Table I). Comparison of these estimates over a significant range of reactant concentration provides a sensitive diagnostic for mechanistic complexity described by the transient model.

Interpretation of Current Dependence of Capacitance. These arguments resolve the first of the two anomalies identified among the results of the current-impulse relaxation study of mercury electrodeposition; the second, the dependence of differential capacitance determined by constant-current charging upon the magnitude of the current density, yields also to analysis in terms of the transient network. The solution to the problem of parallel charging of C_1 and C_a at constant current given above carries no explicit current dependence for $C_a + C_1$; however, Gileadi and Conway²⁴ have advanced a compelling argument for current dependence of a capacitive element which here corresponds to C_a , maintaining that the potential at which C_a is determined is not the equilibrium potential but rather a potential displaced from it by the ohmic drop across R_a . Because the capacitance is strongly potential-dependent, the contribution of C_a to the measured capacitance must be dependent upon its charging current; where C_a is negligible relative to C_1 , little or no current dependence of the assessment of parallel capacitance should be apparent, while where C_a makes a substantial contribution to the total capacitance, the over-all current dependence may be appreciable. This hypothesis is fully supported by the charging data of the present investigation. It has been noted that the current dependence of charging capacitance was most pronounced for the most concentrated solution (for which the estimate of C_a is greatest), progressively less severe for decreasing concentration to intermediate concentrations (where the contribution of C_a becomes slight), and unobservable for low concentrations (where the relative magnitude of C_a is negligible). On the strength of this argument it should be clear that the most significant estimate of $(C_a + C_1)$ is that determined in the zero-current limit of either anodic or cathodic charging, where the potential determining the magnitude of C_a is the equilibrium potential. The agreement of the resulting estimates with the data of Sluyters-Rehbach and Sluyters³ suggests the appropriateness of this procedure; that these authors ascertained $(C_a + C_1)$ and not C_1 alone is suggested by the time scale to which their measurements correspond (for 1000 Hz, 0.5 msec) and by their acknowledgment of a concentration-dependent contribution to the capacitance as-

(24) E. Gileadi and B. E. Conway in "Modern Aspects of Electrochemistry," J. O'M. Bockris and B. E. Conway, Ed., Butterworth Inc., Washington, D. C., 1964, No. 3, pp 413-415.

essed by their technique for the Tl(I)-Tl(Hg) electrode.²⁵

The details of the morphology of the charging curves may be further clarified in terms of the current dependence argument. It was observed that the initial curvature which was apparent at high concentrations of $\text{Hg}_2(\text{ClO}_4)_2$ was more pronounced at low cathodic current densities than at higher current levels. It has been established that the initial curvature is to be identified with the time constant $R_a C_{\text{series}}$, an increase in the magnitude of $R_a C_{\text{series}}$ rendering the initial curvature more pronounced. Increasing C_a results in an increase in the time constant and, since the current dependence of C_a is greater when C_a is larger, current dependence of the time constant increases as the time constant increases. Because C_a decreases with increasing cathodic current density (see Figure 1), the time constant and the initial curvature should decrease with increasing current, as observed; this dependence of initial curvature upon current density should be greatest where C_a and the time constant are greatest, at high concentrations, also as observed.

Transient vs. Periodic Relaxation Measurements. The transient model thus provides a complete interpretation of the results of the present investigation which were, on the basis of the simpler R - C model, anomalous. Attention must now turn to a final but not insignificant consequence of the transient model; its anticipation, under the assumption of inequality of R_s and R_a , of the marked disparity between the kinetic parameters determined by the transient relaxation techniques and those secured by faradaic impedance or rectification measurements.

The time domain analysis of the model which has been described may be summarized in the identification of two characteristic relaxation times, τ_1 and τ_2 , corresponding to the series and parallel discharge processes and evaluated in terms of the time constants $\tau_1 = R_a C_{\text{series}}$ and $\tau_2 = R_s C_{\text{parallel}}$. The relaxation process initiated by a perturbation, periodic or transient, will correspond, over a specified interval in the time domain, to one, the other, or both of these relaxation times depending upon their resolution in time. The relaxation process observed on the time scale presently accessible for current-impulse relaxation measurements has been identified, for the Hg(I)-Hg system, with τ_2 at low concentrations. For periodic techniques, an analysis in the frequency domain identifies two characteristic relaxation frequencies, ω_1 and ω_2 , which are reciprocals of the relaxation times, τ_1 and τ_2 . At low frequency a periodic technique will assess the process represented by ω_2 , corresponding to the longer relaxation time, τ_2 , while at very high fre-

quencies the process represented by ω_1 , analogous to τ_1 , must be assessed. In terms of the transient network, the assignment of ω_2 to low frequency and ω_1 to high frequency measurements arises from recognition that at limitingly low frequencies, the admittance of C_a is small and the faradaic impedance assessed must be essentially R_s , while in the high frequency limit, the admittance of C_a is appreciable and, for $R_a \ll R_s$, the measured impedance corresponds to R_a . For the faradaic rectification technique, as exemplified in the study of Imai and Delahay,¹³ at 50 MHz the conjugate time is 2×10^{-8} sec. In terms of the relative magnitudes of the time constants τ_1 and τ_2 identified by current-impulse measurements at high concentrations of $\text{Hg}_2(\text{ClO}_4)_2$, this time domain must certainly be that of τ_1 .

If the transient techniques assess $R_s(C_a + C_1)$, and hence the rate of processes represented within R_s , and the periodic techniques establish the rates of processes represented within R_a , the disparity between transient and relaxation estimates of the rate of electrochemical reduction of mercury(I) is resolved subject to the condition that $R_s \gg R_a$. The identifications proposed provide the following estimates for R_s and R_a for $2.06 \times 10^{-4} M$ mercurous perchlorate in unimolar perchloric and at 25.0° : based on an interpolation of the data of Imai and Delahay, $i_a^0 = 3.86$ amp cm^{-2} , $R_a = 0.003$ ohm cm^2 ; from the present investigation, $i_a^0 = 0.103$ amp cm^{-2} , $R_s = 0.125$ ohm cm^2 . The difference in estimated values of R_s and R_a assures the validity of the assumed inequality $R_s \gg R_a$ upon which the simplified treatment of relaxation response was based.

Mechanistic Conclusions

The facility with which the transient equivalent network provides a description of the kinetics of the electrochemical reduction of mercury(I) over a wide range of reaction concentration and an extended time domain suggests that certain provisional mechanistic conclusions might be drawn. The mechanism upon which the model is explicitly based is one in which reactant or intermediate is adsorbed in the interphase; whether reactant or intermediate is adsorbed, R_s includes any unit steps which occur in solution and the adsorption process itself, while R_a represents the surface processes occurring subsequent to adsorption. It has been observed that kinetic determinations both of R_s (by current impulse and other transient relaxation techniques) and of R_s (by faradaic rectification and impedance measurements at high frequencies) lead

(25) M. Sluyters-Rehbach, B. Timmer, and J. H. Sluyters, *Rec. Trav. Chim.*, **82**, 553 (1963).

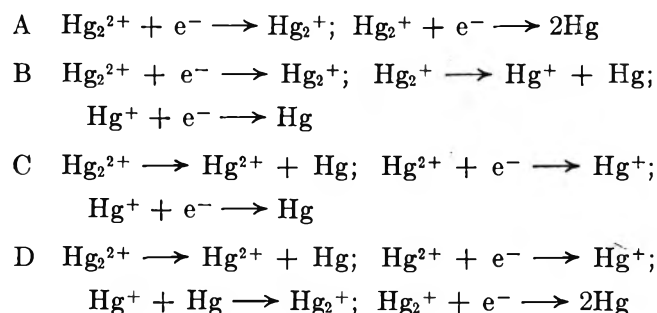
to linear electrochemical reaction-order plots with fractional slopes. If adsorption were the rate-controlling unit step within R_s , a well-defined reaction-order slope would not be anticipated, so a rate-controlling coupled chemical or charge-transfer step must be postulated. A fractional reaction order for the case of a rate-determining chemical step coupled to the adsorption process would require a fractional chemical reaction order; because none of the solution reactions which have been proposed for the mercury(I)-perchlorate system are of fractional order in mercury(I), this possibility will not be considered further. Because the reduction of dimeric mercury(I) is a two-electron process, the alternative of a coupled rate-determining charge-transfer step requires that the over-all process be described by two single-electron steps: first the discharge of solvated reactant from the outer Helmholtz plane and adsorption of the intermediate (both represented within R_s), followed by discharge of the desolvated intermediate from the inner plane of closest approach (represented within R_a).

Independent evidence for a successive charge-transfer mechanism may be adduced to support this postulated scheme. In terms of an electrochemical reaction-order treatment appropriate to the description of successive charge-transfer reactions, the complete current density overpotential characteristic determined by Gerischer and Krause¹⁰ has been analyzed.²⁶ The diagnostics of the treatment permit three conclusions to be drawn: that the mechanism of electrodeposition of mercury(I) includes two charge-transfer steps; that the first of these is hindered relative to the second; and that the initial reactant is either Hg_2^{2+} or a species with which it is in equilibrium and which, by virtue of that equilibrium, varies in concentration in direct proportion to the concentration of Hg_2^{2+} . The transfer coefficient for the slow first step is determined from the data of Gerischer and Krause and this treatment to be $\alpha_1 = 0.58$, leading to a predicted slope of 0.71 for the reaction-order plot, in excellent agreement with the experimental values, 0.70 ± 0.03 of Gerischer and Krause and 0.68 ± 0.02 of the present investigation. Further evidence is suggested by the correlation between adion formation and the observed increase in capacitance in the anodic region which has been considered by Watts-Tobin.²⁷

In terms of the model then, R_s represents faradaic impedance due to adsorption, prior charge transfer, and perhaps coupled chemical reaction, and R_a represents that corresponding to discharge of adsorbed intermediate and to coupled surface processes. A well-defined reaction order for each set of processes should be determined for such a scheme when coupled

volume reaction is rapid or absent, adsorption is rapid, and the effect of surface reaction, if present, is negligible. This set of conditions is not at all unreasonable in the case of the present system, for which the substrate metal provides a homogeneous surface at which no rate-limiting diffusion to growth sites should be observed. The presence of a coupled chemical reaction, if first order in reactant mercury(I) and rapid relative to the discharge of its product, cannot be detected for a mechanistic scheme of this type—at the very short times or high frequencies at which its rate control might be evident, the measurement is in the time domain of the relaxation time, τ_1 , not that of τ_2 to which R_s corresponds. If such a coupled reaction is present in the mechanism for reduction of mercury(I), it is most probably the disproportionation of dimeric mercury(I), which has been estimated to be extremely rapid.²⁸ No estimate has been made of the rate of the adsorption process.

A complete set of four noncyclic reaction sequences may be framed, based upon three intermediates (Hg_2^+ , Hg^+ , and Hg^{2+}), and eight unit steps relating these intermediates to reactants and products and involving only single-electron charge-transfer steps



where any intermediate following the first of the two charge-transfer steps may be adsorbed. Examination of these mechanisms with respect to their capability of supporting a high rate of over-all reaction under anodic and cathodic polarization suggests, however, that C and D are implausible. For these mechanisms the coupled disproportionation of the mercurous dimer must be a volume reaction and it may be argued, as was first suggested by Gerischer and Krause, that the very low ($\sim 10^{-7}$ g-atom l.⁻¹)²⁹ concentration of metal atoms in solution would render the reverse reaction subject to abrupt concentration polarization. That no evi-

(26) W. D. Weir, to be published.

(27) R. J. Watts-Tobin, *Phil. Mag.*, **6**, 133 (1961).

(28) R. L. Wolfgang and R. W. Dodson, *J. Phys. Chem.*, **56**, 872 (1952).

(29) H. C. Moser and A. F. Voigt, *J. Am. Chem. Soc.*, **79**, 1837 (1957).

dence of this is found, even at high current densities, suggests that C and D are not appropriate mechanistic descriptions of the process. Each of the two remaining sequences, A and B, is capable of supporting a high rate of charge transfer and a choice between them on the basis of the adsorption model or the results of the current-impulse relaxation experiments appears impossible.

Extensive studies of several rapid electrodeposition

reactions are being undertaken to establish the generality of this interpretation of the kinetic complexity discovered for the electrochemical reduction of mercury(I).

Acknowledgment. The authors gratefully acknowledge support of this work by the National Science Foundation.

On the Configuration of Polymers at the Solid-Liquid Interface¹

by Gunther Steinberg²

Shell Development Co., Emeryville, California (Received June 9, 1966)

The adsorption of polylauryl methacrylate (PLMA) and some vinylpyridine-containing alkyl methacrylates (PAPM) onto iron powder was studied. Use of carbon-14-labeled polymers permitted determination of the amount adsorbed by solution depletion and/or by direct assay. The loop model for the configuration of these polymers is inferred from the results of experiments with several systems: (1) each polymer from toluene and *n*-decane, the better and poorer solvent, respectively; (2) sequential, two-step adsorption of one polymer from each of the solvents; (3) sequential adsorption of two polymers from the same and from different solvents; (4) determination of the effect of increasing the methylvinylpyridine (MVP) comonomer concentration and lowering the molecular weight in type 3 experiments; and (5) competitive adsorption of PLMA and PAPM. PAPM acts as a spotwise adsorbing polymer and was able to sorb on iron surfaces already covered to saturation by PLMA with only minor displacement of PLMA. Polymer adsorption could be maximized by adsorption of PLMA followed by PAPM, both from decane. At 25% MVP comonomer, the total amount of polymer at the surface was twice that of the isotherm values of either polymer alone. When PAPM is allowed to saturate the surface first, essentially no PLMA is adsorbed in step two. It is postulated that a uniformly adsorbing polymer like PLMA forms loops to accommodate itself to the available surface sites. Relatively little looping over the covered areas is expected. For spotwise adsorbing polymers of the PAPM type, increasing loop size is postulated, together with a decrease in the number of polymer segments from each chain at the interface, with increasing surface coverage. The longest loops attaching to the surface as saturation is approached would be sorbed exclusively *via* strongly held pyridine groups. Ultimate film thickness would be a function of molecular weight and spacing of the polar groups and the solvent. The polymer density as a function of the distance from the surface is postulated to decrease slowly for the first 50–300 Å and then rapidly, with a small number of loops extending far from the surface, exerting the viscometric effects noted by Öhrn and others.

Introduction

The configuration of polymers at the solid-liquid interface has been the subject of considerable interest for both fundamental and practical reasons since the mode of adsorption of polymers has an important bearing on corrosion, adhesion, dispersancy, and flocculation. The first model suggested by Jenkel and Rumbach³ proposed loops or single point attachment to account for the amount of polymer adsorbed at a solid surface. A theoretical approach to the problem was that by Frisch, Simha, and Eirich,^{4–9} who presented a statistical analysis of polymer adsorption from solution for flexible, random, homogeneous

polymer coils in the presence of a reflecting barrier. The scope of this treatment was extended by Higuchi.¹⁰

(1) Presented in part at the 151st National Meeting of the American Chemical Society, Pittsburgh, Pa., March 1966.

(2) To whom correspondence should be addressed at Stanford Research Institute, Menlo Park, Calif.

(3) E. Jenkel and B. Rumbach, *Z. Elektrochem.*, **55**, 612 (1951).

(4) H. L. Frisch, R. Simha, and F. R. Eirich, *J. Chem. Phys.*, **21**, 365 (1953).

(5) R. Simha, H. L. Frisch, and F. R. Eirich, *J. Phys. Chem.*, **57**, 584 (1953).

(6) H. L. Frisch and R. Simha, *ibid.*, **58**, 507 (1954).

(7) H. L. Frisch, *ibid.*, **59**, 633 (1955).

(8) H. L. Frisch and R. Simha, *J. Chem. Phys.*, **24**, 652 (1956).

(9) H. L. Frisch and R. Simha, *ibid.*, **27**, 702 (1957).

(10) W. I. Higuchi, *J. Phys. Chem.*, **65**, 487 (1961).

Silberberg¹¹ criticized this treatment for not being satisfactorily formulated, and treated separately the surface that contains the adsorbed segments of the polymer and the adjacent layers in the solution. A narrow distribution of loop sizes was assumed, and the polymer was essentially treated as a freely linked chain. More recently, Hoeve, DiMarzio, and Peyser¹² presented another statistical mechanical treatment for polymers adsorbed at solid surfaces. The chains were assumed to have resistance to bending, and surface coverage was assumed to be low enough so that interaction of polymer molecules with each other might be neglected. The resulting theory predicts large loops and few units adsorbed for small adsorption free energies and small loops and more units adsorbed for larger adsorption free energies when the chains are sufficiently flexible. Further important refinements in the theoretical treatments have been introduced by DiMarzio and McCrackin,¹³ who considered the number of contacts of the chain with the surface using a model of a molecule tied down at one end of a reflecting barrier, which does not allow runs of adsorbed segments. Roe,¹⁴ on the other hand, has extended the treatment of the model of sequences of polymer chain segments in and out of the surface. Both of these papers comment on the importance of the chain ends, which according to Roe can constitute up to 70% of the chain length at the transition between strong and weak adsorption. Roe also concludes that thick films, when they exist at all, should be ascribed to these dangling ends of the polymer chains.

A number of pertinent experimentally oriented papers have appeared since the present studies were completed. Eirich and co-workers¹⁵ have developed additional data on the thickness of adsorbed layers and the resulting hydrodynamically effective thicknesses or dimensions of dispersed particles and capillaries. The configuration deduced from this work is that of polymers (polystyrene, vinyl acetate, methyl methacrylate) adsorbed at solid-liquid interfaces in the form of "monolayers" of molecular coils whose dimensions are proportional to the free coils in that particular solution. Stromberg¹⁶ and co-workers have measured the film thickness of polystyrene in liquid environments by ellipsometry. It was found that the molecules initially adsorbed are more extended than the later arrivals that must compete for a steadily decreasing number of adsorption sites. Further interpretation of the data postulates a recoiling of the chains, leading to greater extension from the surface, and resulting in an eventual conformation very similar to that of a random coil.

Fontana^{17,18} studied the number of segments at the

silica-solution interface by infrared techniques with some polymers quite similar to those used in this work. Preferential attachment of the polar groups in the polymer and a 2.5-fold increase in the amount of polymer adsorbed were found when long polyglycol chains were substituted into an alkyl methacrylate polymer. Significantly, this was accompanied by a fourfold decrease in the number of ester groups attached to the silica surface hydroxyls *via* hydrogen bonds.

Adsorption of polyvinyl alcohol on several substrates and measurement of the surface potential to follow polymer-surface interactions, together with a radio-tracer determination of the amount adsorbed, have been reported by Gottlieb.¹⁹ A region in which the surface potential is independent of surface coverage was found corresponding to apparent adsorption with only a small fraction of the segments at the interface. The theory postulated on the basis of the surface potential results states that the surface is first covered by a number of polymer groups which is independent of the solvent with almost all of the polar groups oriented and in contact with the surface; subsequent polymer adsorption is determined by the configuration of the polymer in solution. This adsorption to vacant sites on the surface would result in the bulk of the polymer being on top of the initial layer of oriented polymer.

A similar model was suggested by Peterson and Kwei,²⁰ who postulated essentially two-dimensional adsorption followed by an "overfilm" of polymer molecules with at least some segments in contact with the surface.

A general review covering the adsorption of polymers from solution was recently published by Patat²¹ which, together with Silberberg's¹¹ paper, constitutes the most inclusive survey of the recent work.

Experimental Section

Materials. The iron powder adsorbent was grade N.F., reduced by hydrogen (J. T. Baker Chemical Co.,

- (11) A. Silberberg, *J. Phys. Chem.*, **66**, 1872, 1884 (1962).
- (12) C. A. J. Hoeve, E. A. DiMarzio, and P. Peyser, *J. Chem. Phys.*, **42**, 2558 (1965).
- (13) E. A. DiMarzio and F. L. McCrackin, *ibid.*, **43**, 539 (1965).
- (14) R. J. Roe, *ibid.*, **43**, 1591 (1965); *Proc. Natl. Acad. Sci. U. S.*, **53**, 50 (1965).
- (15) F. Rowland, R. Bulas, E. Rothstein, and F. R. Eirich, *Ind. Eng. Chem.*, **57** (No. 9), 46 (1965).
- (16) R. R. Stromberg, D. J. Tutas, and E. Passaglia, *J. Phys. Chem.*, **69**, 3955 (1965).
- (17) B. J. Fontana, *ibid.*, **67**, 2360 (1963).
- (18) B. J. Fontana and J. R. Thomas, *ibid.*, **65**, 480 (1961).
- (19) M. H. Gottlieb, *ibid.*, **64**, 427 (1960).
- (20) C. Peterson and T. K. Kwei, *ibid.*, **65**, 1330 (1961).
- (21) F. Patat, E. Killman, and C. Schliebener, *Fortschr. Hochpolymer. Forsch.*, **3**, 332 (1964).

Type 2228), all of the same lot number. Batches were extracted with hot benzene for 5–7 days, dried in air, outgassed in 10 or 25-g lots in special thin-bottomed vials for 2 hr at 100 and 275° each at 10^{-5} torr, and sealed. The surface area was determined by BET methods using krypton or nitrogen adsorption, as well as by stearic-1- C^{14} acid adsorption from solution. Gas adsorption data varied over the time of this study but without a pattern, averaging $0.3 \text{ m}^2/\text{g}$.

Toluene solvent was Analytical Reagent grade and was used without further purification; *n*-decane was Phillips Pure grade, 99 mole %, percolated through a silica gel column stored over Molecular Sieve 4A and protected from moisture.

Polymers were prepared by free-radical polymerization in oil. The products were freed of solvent by precipitation with methanol or by dialysis.²²

Polylauryl methacrylate- C^{14} (PLMA- C^{14}) was prepared from lauryl-1- C^{14} methacrylate (Nuclear Research Chemicals, Orlando, Fla.). Inactive PLMA was prepared by identical procedures.

The poly(alkyl methacrylate)-methylvinylpyridine copolymer (PAPM- C^{14}) was prepared by direct programmed copolymerization of lauryl-1- C^{14} methacrylate, other alkyl methacrylates, and methylvinylpyridine (MVP). PAPM-1 is a commercially produced material equivalent to PAPM- C^{14} . PAPM-2 has a somewhat lower pyridine content and lower molecular weight. PAPM-3 is a 25% pyridine content polymer. The distribution of MVP in the labeled polymer was uniform as determined from the constant ratio of radioactivity to optical absorbance at 2685 Å in PAPM- C^{14} diluted with PAPM-1. Since the order of magnitude of the molecular weights and the solution behavior are of importance in polymer adsorption the available data are shown in Table I. Predominance of very low molecular weight species would result in greater mobility of polymer molecules.

Adsorption experiments in duplicate or triplicate

were run in centrifuge tubes with Polyseal screw-cap closures. The iron powder was introduced to the solution by breaking the vials under the surface of the liquid. Losses of material by transfer or evaporation were negligible as monitored by separate tracer experiments. Tubes were agitated during a run by end-over-end rotation. Polymer adsorption was determined by measuring solution depletion using both aliquots and assay of the total C^{14} remaining in solution (material balance). Analysis was accomplished by liquid scintillation counting or ultraviolet spectroscopy using the pyridine peak at 2685 Å (in decane solutions). Occasional checks on the amount of C^{14} polymer actually on the iron were made by combusting the powder, collecting the CO_2 in benzylamine-ethanol-toluene scintillation solvent, and assaying. Corrections for amounts withdrawn were made on all rate runs.

Competitive studies were carried out in two modes: (1) for simultaneous competitive adsorption, in which two components were present at the time the fresh iron powder was exposed to the solution; and (2) for sequential competitive adsorption, in which the first adsorbate was allowed to equilibrate with the adsorber and the iron was washed with *n*-heptane, which did not desorb any polymer, and was subsequently exposed to the second polymer solution. In the sequential competitive mode, one variation with a significant difference was also used. Upon completion of the first step of the adsorption, the iron was exposed to a solution of both polymers; *i.e.*, the solution concentration of the first adsorbate was maintained in the second step.

Adsorption rates were determined by two methods: usually 50 ml of solution was used, either in stirred three-necked flasks or large culture tubes, and samples were withdrawn at predetermined times. In order to minimize the cumulative volume error, the experiment was designed to withdraw 0.50 ml of sample using pipets calibrated to deliver when the last drop is blown out. Prior to sampling, the iron powder was either settled with the aid of a magnet or centrifuged for 1 min.

For following the initial adsorption of C^{14} polymers with time, in toluene solution a nonsampling technique was devised that allowed obtaining more points in the first 30 min of an experiment. At the same time, long-term changes could be measured without depleting the solution. For these experiments, a single-channel liquid scintillation counter²³ was adapted to view glass

Table I: Properties of Polymers

	PLMA- C^{14}	PLMA	PAPM- C^{14}	PAPM-1
Mol wt				
Light scattering	1.3×10^6		1.2×10^6	
Osmometric	1.1×10^6		1.3×10^6	
Sedimentation	2.7×10^6		1.5×10^6	
diffusion				
Viscosity				8×10^6
Intrinsic viscosity in				
<i>n</i> -Decane	0.48	0.55	0.28	0.42
Toluene		0.74		0.97

(22) G. Steinberg, unpublished results; similar to the procedure of M. Hill, American Chemical Society Division of Petroleum Chemistry, Preprints 5 (No. 3), 1960, p 115.

(23) T. S. Hodgson, B. E. Gordon, and M. E. Ackerman, *Nucleonics*, 16 (No. 7), 89 (1958).

vials from the side. Using terphenyl scintillator in toluene, the 1-in. multiplier phototube counted 20 ml of solution in a 25 × 150-mm tube with an efficiency of 25%. In use, the polymer solution is placed into the tube, terphenyl is added to a concentration of 5.1 g/l., and a zero time reading of radioactivity is obtained. Iron powder is introduced by breaking the sealed vial under the surface of the solution. As soon as possible, the iron is settled and another reading is taken. The tube was then removed, placed on a shaker, and readings of activity remaining in solution were taken at intervals. Preliminary work showed that terphenyl does not interfere with the adsorption of either small or large molecules from solutions.

Results and Discussion

Polymer Adsorption Isotherms. The adsorption isotherms for all of the polymers used in this study typically rise very rapidly to a plateau at concentrations of less than 0.2 mg/ml. Saturation values, A_s , representing at least 24-hr adsorption figures, are presented in Table II. As noted previously by other workers,

Table II: Polymer Adsorption on Iron Powder: Experimental and Calculated

System, 22°	A_s , isotherm value at satn	"a" from eq 1	A_s/a
PAPM-C ¹⁴ -toluene-iron	0.286
PAPM-C ¹⁴ -decane-iron	0.399	0.444	0.90
PAPM-1-decane-iron	0.356	0.411	0.90
PLMA-C ¹⁴ -decane-iron	0.362	0.398	0.91
PLMA-C ¹⁴ -toluene-iron	0.223	0.244	0.91
PAPM-3-decane-iron	0.395	0.462	0.86

the adsorption data fit the Langmuir type I isotherm even though Langmuir theory is inappropriate because the assumptions made do not apply. Moreover, systematic deviations at very low concentrations have been demonstrated for polyvinyl acetate.²⁴ However, for comparison, the limiting saturation adsorption "a" values were calculated from the linear Langmuir equation

$$C/A = (1/ab) + (C/a) \quad (1)$$

and are compared to A_s in Table II. "A" is the amount adsorbed in mg/g, "C" the concentration (mg/ml), and "a" and "b" are constants for each system. Each "a" term was calculated by a multiple regression analysis program using all of the adsorption data available at the end of this work. Since adsorption

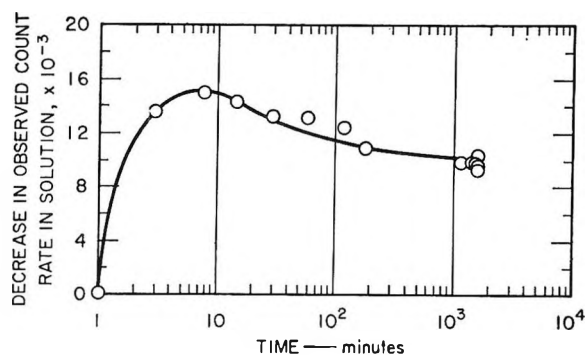


Figure 1. Adsorption as a function of time: PLMA-C¹⁴ in toluene.

with time data were also available, the 24-hr values could be assumed to be quite close to saturation. The proximity of the ratio $A_s/a:1$ is remarkable, especially in view of the discussion by Molyneux,²⁵ who found that the "a" value might be in error by a factor up to 2 at low surface coverage when calculated for large molecules.

Adsorption Rates. Attachment of the chain to the surface by many segments favors the adsorption of high polymers from most solutions. While the rate of diffusion of polymer to the surface decreases with increasing molecular weight,²⁶ initial rates of adsorption of PAPM and PLMA were found to be quite rapid, with 50–75% of the final amount, A_s , adsorbed in 2 min. Adsorption was 85–95% complete in 4 hr and no changes could be detected between 24 and more than 100 hr. Precise determination of initial rates is quite difficult by conventional sampling techniques normally employed to estimate the time required to reach saturation, and the alternate nonsampling method was used, though this is restricted to use with radioactive polymers in toluene solution. When sufficient points are obtained in the first 60 min, the amount adsorbed from toluene as a function of time is seen to reach a maximum, subsequently decreasing to the eventual apparent saturation value, A_s . This phenomenon was observed both with polymers (Figure 1) and with stearic acid on iron adsorbent. In the stearic acid experiments, the peaks are very sharp, reach a maximum, and return to a smooth increase with time in 1 min. For the polymer case, the following explanation is advanced: coils approach the interface, partially uncoil, or adsorb with only a few segments of the chain in the surface. A rather large bulk of polymer is thus held to the surface and is

(24) J. Koral, R. Ullman, and F. R. Eirich, *J. Phys. Chem.*, **62**, 641 (1958).

(25) P. Molyneux, *Nature*, **202**, 368 (1964).

(26) S. Claesson, *Discussions Faraday Soc.*, **7**, 321 (1949).

Table III: PLMA and PAPM Adsorbed in One or Two Steps

Polymer	Solvent		Amt adsorbed, mg/g of Fe		Total polymer, mg/g of Fe
	Step 1	Step 2	Step 1	Step 2	
PLMA-C ¹⁴	Toluene	...	0.223	...	0.223
PLMA-C ¹⁴	Decane	...	0.362	...	0.362
PLMA-C ¹⁴	Toluene	Decane	0.208	0.156	0.364
PLMA-C ¹⁴	Toluene	Decane	0.235	0.129	
PAPM-C ¹⁴	Toluene	...	0.286	...	0.286
PAPM-C ¹⁴	Decane	...	0.400	...	0.400
PAPM-C ¹⁴	Toluene	Decane	0.286	0.219	0.506

essentially counted as being out of the solution since concentration is determined by measuring depletion from solution. As the polymer continues to uncoil and adsorb, some coils will be displaced by their neighbors. Since the initial major coverage is rapid, many of the loosely held coils will return to the bulk solution, resulting in an increase in the detectable concentration. A similar peaking has been observed by Stromberg¹⁶ for high molecular weight polystyrene in cyclohexane at 100 min while following the increase in in "rms film thickness" in a presumably unstirred system.

There is some difference in the adsorption with time as a function of solvent. It appears that from decane any "overshoot" adsorption occurs more rapidly. Toluene, being a better competitive adsorbent, would be displaced more slowly by adsorbing polymer. Also, fewer polymer segments are active in the interface in this solvent, thus adding a mass effect.

Stepwise Adsorption of Polymer. These polymers follow the generally observed result that adsorption is favored from a poorer solvent; *i.e.*, adsorption is greater from decane than from toluene (see Table II). The observed differences in A_s are attributed qualitatively to greater area required by the better solvated, swollen polymer as well as to changes in the solvent-surface interaction.²⁷ The latter is essentially a competition for the surface between the solvent and the polymer segment functional group. Once adsorbed from a particular solvent, polymers generally do not desorb appreciably in that solvent because the multiplicity of adsorbing sites energetically favors adsorption, resulting in very small desorption rate constants. On changing the environment of adsorbed PLMA from toluene to decane (the poorer solvent), the PLMA should become more surface active, and additional polymer would be adsorbed. Qualitatively, the area per segment may also decrease as the PLMA is desolvated, conceivably resulting in additional available surface.

Accordingly, PLMA-C¹⁴ was adsorbed to saturation onto iron powder from toluene, and the iron powder was rinsed with *n*-heptane to remove the residual adhering liquid film. The heptane rinse had been shown not to remove any adsorbed PLMA. The iron was subsequently shaken with a solution of PLMA in *n*-decane. Adsorption was again allowed for the usual 24 hr and the amount adsorbed was determined. The results and comparison with direct, one-step adsorption (Table III) show that the same adsorption value is reached by either route.

A similar two-step experiment with PAPM-C¹⁴ resulted in considerably greater adsorption in two steps than in a single-step adsorption from decane.

The results for PLMA may be explained by considerations of polymer activities and changes in free energies that favor polymer adsorption. However, additional factors may complicate the picture because of the postulated change in polymer configuration with increasing surface coverage (discussed below).

The marked differences between amount adsorbed in one- and two-step experiments for PAPM are interpreted differently even though the kinetic and thermodynamic arguments still hold. A major difference exists between PLMA and PAPM in that the latter is a "spotwise adsorbing" polymer. This is meant to define a polymer molecule containing a fraction of segments spaced along the chain that are much more strongly sorbed to the surface than the rest of the copolymer segments. As a result, the change of solvent could result in additional adsorption, but in two possible modes: (1) adsorption of the molecules by runs of segments on the surface as pictured for PLMA and (2) a looping overlayer adhering to the surface primarily *via* its more strongly adsorbed pyridine groups, similar to the suggestion of Gottlieb.¹⁹ A spotwise adsorbing overlayer will increase the average film thickness and the long loops would presumably

(27) S. Ellerstein and R. Ullman, *J. Polymer Sci.*, **55**, 123 (1961).

Table IV: Two-Step Adsorption of PLMA and PAMP

Polymer	Solvent		Amt adsorbed, step 1, mg/g of Fe	Amt desorbed, mg/g of Fe	Amt adsorbed, step 2, mg/g of Fe	Total polymer, mg/g of Fe
	Step 1	Step 2				
(1) PLMA (2) PAMP-C ¹⁴	Decane	Toluene	(Inactive)	Estd ~35%	0.315	Estd 0.55
(1) PLMA-C ¹⁴ (2) PAMP-1	Decane	Decane	0.336 ^a	0.112	0.410	0.640
(1) PAMP-1 (2) PLMA-C ¹⁴	Decane	Decane	0.458	0.05	0.05	0.462

^a Represents saturation level.

be able to exert the typical viscometric effects observed as a consequence of polymer adsorption.¹⁵ An additional driving force for such adsorption behavior may be provided by the heterogeneous surface of the oxide-coated iron powder with a distribution of acidity on sites that could then preferentially adsorb acid (or conjugate acid) and basic functional groups.

The model of polymer adsorption on such surfaces, as it is developed here, postulates that the methacrylate groups have occupied most of the conveniently spaced surface sites, the rest being less favorable to ester linkages in the chain. However, the more strongly adsorbing pyridine groups may still anchor sections of the chain to the surface, resulting in loops spotwise adsorbed.

Two-Step Adsorption of Two Different Polymers. Such a model would predict that iron powder precoated with PLMA would permit additional adsorption of PAMP under conditions where no additional PLMA could adsorb. The reverse, PLMA adsorbing over or on a surface which has been precoated with PAMP, would not be expected to occur since the latter polymer would occupy both the ester and pyridine adsorbing sites in the surface lattice. PAMP would be expected to adsorb on the PLMA precoated surface from either

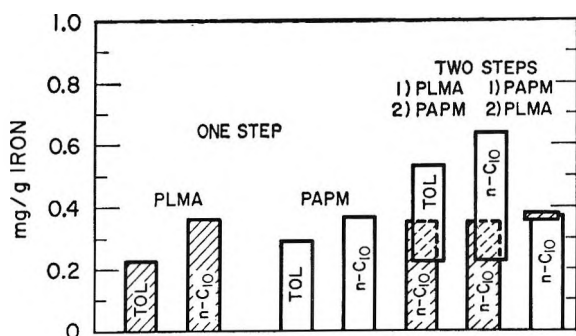


Figure 2. Adsorption of polymers from solution.

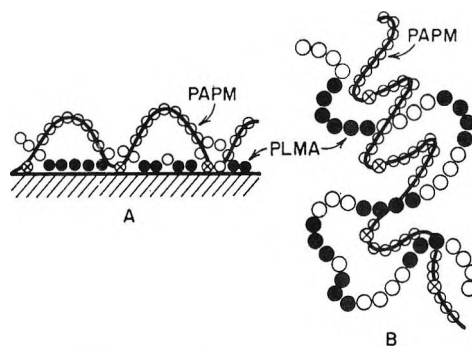


Figure 3. Solution adsorption model: two steps: 1, PLMA; 2, PAMP.

solvent, the amount again being a function of the solvent. The results of such two-step experiments are presented in Table IV. Figure 2 compares the amount of each polymer adsorbed from toluene and decane in single-step experiments and the two-step experiments with two polymers. The overlap between the bars of steps one and two in the latter experiments denotes the desorption of the first polymer by the one in the second solution. The amount of PAMP which adsorbs on a PLMA precoated surface is equivalent to that which deposits on a fresh iron surface. This result is in agreement with the predictions of the postulated model. A conceptual illustration of the mode of adsorption of PAMP on a PLMA precoated surface is shown in Figure 3, where PAMP is shown to be adsorbed primarily but not only by its pyridine groups, most of the remainder of the molecule extending as loops of varying lengths into the solution.

Effect of Concentration and PAMP Type on the Polymer Adsorbed in Step Two. When the concentration of the polymer adsorbed in the second step is varied, it is found that a new isotherm can be constructed plotting the amount of PAMP (or the total polymer) adsorbed vs. the PAMP concentration in

step two (Figure 4 and Table V). The desorption of preadsorbed polymer is somewhat dependent on the concentration of the second polymer solution at these levels.

When a PLMA-precoated surface is presented with PAMP-3, of higher MVP content than PAMP-1, greater adsorption results despite their nearly equal mean isotherm adsorption values (see Table II). All

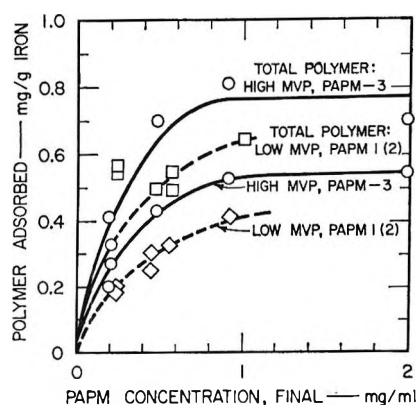


Figure 4. Two-step adsorption: 1, PLMA; 2, PAMP.

of these "step 2" adsorptions were carried out at final concentrations which are on the concentration plateau level for the polymer when by itself with fresh iron surfaces; however, precoating changes the surface, and the polymer is forced into a different configuration on adsorption.

Alternative interpretations may be advanced to account for the increased adsorption by the lower molecular weight but higher MVP content PAMP-3. The more frequent spacing of the pyridine groups in PAMP-3 may enable it to adsorb at more of the re-

maining vacant surface sites, resulting in a more closely packed "overlayer" and occupying more adsorption sites. PAMP-1 could then be expected to form longer loops and cover these sites less efficiently. The concentration dependence seems to favor this interpretation. If the polymer overlayers were to adsorb in solution configuration, the more polar PAMP-3 may be expected to be more compact and fit better into the vacant, approachable areas of the surface.

Competitive Polymer Adsorption. Competitive adsorption with PLMA and PAMP present simultaneously in varying ratios gives the now expected results. The film composition is governed by the relative surface activity of the two polymers. The solution and film composition for experiments run at constant initial PLMA concentration are given in Table VI. Samples were taken at 24 and 72 hr to reflect changes that might occur because of displacement of adsorbed polymer. Maximal adsorption is observed under conditions where PLMA has the best chance to reach the surface, at low PAMP concentration. If the rates of adsorption are assumed to be approximately comparable, an interpenetrating overlayer again seems to be formed. This occurs to a lesser extent when the two polymers are present at equal concentration and not at all when PAMP predominates, as is reflected in the total amount of polymer present. Changes in film composition between 24 and 72 hr indicate some competitive displacement of PLMA in the presence of PAMP. The net increase in total polymer with time in the two-component system can be related to the slower rate of adsorption of PAMP when it is confronted with a partly PLMA-precoated surface.

Polymer Desorption Displacement. The literature on polymer adsorption abounds in reports of a apparent

Table V: PAMP Adsorption over PLMA as a Function of Concentration and Type

Polymer-solvent		Amt adsorbed, mg/g		PAMP	Amt	%	Total
Step 1	Step 2	Step 1	Step 2	concn, C_i , mg/ml	desorbed, step 2	step 2	polymer, mg/g
PLMA-decane	PAMP-C ¹⁴ -toluene	Inactive	0.310	0.90	~0.55 ^b
PLMA ^a -decane	PAMP-1-decane	0.427	0.195	0.306	0.0696	16.0	0.552
PLMA ^a -decane	PAMP-1-decane	0.422	0.204	0.693	0.0884	20.1	0.538
PLMA ^a -decane	PAMP-1-decane	0.336	0.416	0.90	0.112	33	0.640
PLMA ^a -decane	PAMP-2-decane	0.339	0.279	0.45	0.080	25	0.529
PLMA ^a -decane	PAMP-3-decane	0.340	0.206	0.21	0.132	61	0.333 ^c
			0.275				0.411
PLMA ^a -decane	PAMP-3-decane	0.397	0.425	0.472	0.126	32	0.696
PLMA ^a -decane	PAMP-3-decane	0.397	0.534	0.91	0.124	31	0.807
PLMA ^a -decane	PAMP-3-decane	0.331	0.548	2.0	0.145	56	0.693 ^c

^a C¹⁴-labeled. ^b From experiments with PLMA-C¹⁴. ^c Final PLMA concentration of step 1 maintained during step 2; in all other runs precoated iron was washed with heptane.

Table VI: Simultaneous Competitive Adsorption of PLMA and PAM (Decane)

Sample time, hr	PLMA ^a adsorbed, mg/g of Fe	PAPM adsorbed, mg/g of Fe	Total polymer, mg/g of Fe	PAPM:PLMA ratio	
				Solution	Film
24	0.208	0.302	0.510		
72	0.185	0.342	0.527	1:2	2:1
24	0.143	0.314	0.457		
72	0.113	0.377	0.490	1:1	3:1
24	0.03	0.34	0.370		
72	0.03	0.34	0.370	10:1	10:1

^a Initial solution concentration of PLMA constant at 0.26 mg/ml.

irreversibility. However, successful equilibration has been reported by Ellerstein²⁷ for methyl methacrylate in benzene and benzene-acetonitrile mixtures on iron powder substrate; by adjusting the solvent apparent reversibility was attained. Experiments reported here indicate a certain degree of displacement under com-

petitive conditions that could possibly be attributed to the presence of low molecular weight species. Displacement of the polymer from iron by the original solvent is generally very small in the time allotted. However, only very small increases in adsorption energy with increasing molecular weight would be reflected in very great decreases in the rate of displacement.

A series of experiments was performed to survey the effect of molecular weight, polymer composition, and solvent medium on the desorption or displacement of PLMA-C¹⁴ by PAPM and PAPM-C¹⁴ by the higher pyridine content PAPM-3.

PLMA adsorbed from toluene, when equilibrated with fresh solvent several times for 24-72 hr each for a total of 148 hr, will desorb to the extent of 30%. Initial rate is rapid but levels off after 12-24 hr. Most of the material desorbed comes off in the first solvent treatment. If a competing polymer (PAPM) is added to such a solution, more PLMA is desorbed very rapidly in the first 30 min followed by a low but measurable desorption rate.

Table VII: Polymer Desorption

Adsorption system, 22°	Desorption system	Time, hr	% desorbed
PLMA-C ¹⁴ - <i>n</i> -C ₁₀ -Fe	PAPM-1-toluene	221	35.4
PLMA-C ¹⁴ - <i>n</i> -C ₁₀ -Fe	PAPM-1-toluene	221	57.1 ^a
PLMA-C ¹⁴ - <i>n</i> -C ₁₀ -Fe	(1) Toluene		
	(2) PAPM-3-toluene	114	53.4
PLMA-C ¹⁴ - <i>n</i> -C ₁₀ -Fe	(1) Toluene		
	(2) PAPM-3-toluene	114	34.8
PLMA-C ¹⁴ - <i>n</i> -C ₁₀ -Fe	PAPM-1- <i>n</i> -C ₁₀	100	27.6
PLMA-C ¹⁴ - <i>n</i> -C ₁₀ -Fe	PAPM-1- <i>n</i> -C ₁₀	100	53.8
PLMA-C ¹⁴ - <i>n</i> -C ₁₀ -Fe	(1) Toluene	20	17.5
	(2) PAPM-2- <i>n</i> -C ₁₀	89	11.2
			28.6
PLMA-C ¹⁴ - <i>n</i> -C ₁₀ -Fe	(1) Toluene	24	17.6
	(2) PAPM-2- <i>n</i> -C ₁₀	89	11.2
			28.6
PLMA-C ¹⁴ - <i>n</i> -C ₁₀ -Fe	PAPM-3- <i>n</i> -C ₁₀	118	45.3
PLMA-C ¹⁴ - <i>n</i> -C ₁₀ -Fe	PAPM-3- <i>n</i> -C ₁₀	118	44.1
PLMA-C ¹⁴ -toluene-Fe	(1) Toluene	72	
	(2) PAPM-1-toluene	120	42.8
PLMA-C ¹⁴ -toluene-Fe	<i>n</i> -C ₇ only, not agitated	196	<1
PLMA-C ¹⁴ -toluene- <i>n</i> -C ₁₀ -Fe,	PAPM-1-toluene	144	33.3
two-step adsorption	PAPM-1-toluene	144	35.9
PLMA-C ¹⁴ -toluene- <i>n</i> -C ₁₀ -Fe,	PAPM-1-toluene	288	29.8
two-step adsorption	PAPM-1-toluene	288	28.0
PLMA-C ¹⁴ -toluene- <i>n</i> -C ₁₀ -Fe,	PAPM-1- <i>n</i> -C ₁₀	172	17.6 ^b
two-step adsorption	PAPM-1- <i>n</i> -C ₁₀	172	18.8
PAPM-C ¹⁴ - <i>n</i> -C ₁₀ -Fe	Acetonitrile	121	1.38
PAPM-C ¹⁴ - <i>n</i> -C ₁₀ -Fe	Acetonitrile	121	2.85
PAPM-C ¹⁴ - <i>n</i> -C ₁₀ -Fe	PAPM-3- <i>n</i> -C ₁₀	141	30.6
PAPM-C ¹⁴ - <i>n</i> -C ₁₀ -Fe	PAPM-3- <i>n</i> -C ₁₀	141	30.0
PAPM-C ¹⁴ - <i>n</i> -C ₁₀ -Fe	PAPM-1- <i>n</i> -C ₁₀	(48)	~4
PAPM-C ¹⁴ - <i>n</i> -C ₁₀ -Fe	PAPM-1- <i>n</i> -C ₁₀		

^a Value probably high because of solvent evaporation. ^b Per cent of second-step adsorption: A, 45.5%, B, 57.2%.

Table VIII: Two-Step Adsorption of (1) Polymer and (2) Stearic-9,10-H³ Acid on Iron Powder

Polymers	Step 1		Step 2			Polymer remaining, mg/g	Total organics, mg/g		
	Adsorbed, mg/g	Time, hr	Stearic acid adsorbed, mg/g	Time, hr	Polymer desorbed, mg/g				
PAPM-C ¹⁴ - <i>n</i> -C ₁₀ ^a	0.401	48	0.877	24	0.253	0.148	1.025		
			0.920	48	0.267 (67%)			0.134	1.055
PLMA-C ¹⁴ - <i>n</i> -C ₁₀ ^a	0.420	24	0.860	24	0.271	0.149	1.008		
			0.876	116	0.281			0.140	1.015
			0.919	194	0.283 (67%)			0.137	1.056
			0.351	24	0.117			0.321	0.672
PLMA-C ¹⁴ - <i>n</i> -C ₁₀ ^b	0.438	92	0.364	72	0.127	0.311	0.675		
			0.409	141	0.129 (30%)			0.309	0.718
			0.759						
Stearic acid, max adsorption from extrapolated linear Langmuir plot			0.759						

^a Iron powder rinsed free of polymer solution after step 1. ^b Final polymer solution concentration maintained in step 2.

PLMA precoated on iron will desorb or be displaced at very high initial rates when treated with PAPM-1 or PAPM-3. After the first 2-4 hr the rate drops off steadily, but daily increments of desorbed polymer are readily measurable after 10 days.

A summary of some of the competitive desorption experiments performed is given in Table VII. (Some of the lack of agreement between duplicates is a reflection of poor agreement on initial adsorption, while others are cumulative errors caused by a large number of samples taken and loss of solvent.)

In practice it is found that a strongly competing species can displace much of the polymer depending on its polarity, its molecular weight, and the solvation of the displaced species—*i.e.*, the net change of free energy. Failure of all of the polymer to be desorbed may be accounted for by one of the following: the high molecular weight species remaining on the surface, differences in the fraction of segments in the interface of equivalent molecules adsorbed at different times, or the interpenetrating "overlayer" postulated here assisting in anchoring the polymer to the surface. The amounts of polymer involved in these experiments precluded comparison of the molecular weight of the desorbed portion with the original polymer. Failure of acetonitrile to displace PAPM from the iron powder may simply be an unfavorable solvent-surface and solvent-polymer interaction relative to the polymer-surface interaction.

Maximal polymer is displaced from the surface when the competing species can essentially chemisorb on the surface. When iron powder precoated with either PLMA or PAPM is exposed to a solution of stearic acid that is sufficient to saturate the surface when alone, 67% of the polymer is displaced in 48 hr (Table

VIII). The total amount of stearic acid that is adsorbed on the polymer-precoated surface is greater than a monolayer on clean iron powder by about 20%. Stearic acid isotherm adsorption values are quite stable with time, indicating that there is no progressive soap formation. Some interaction with the polymer seems to occur which is not specific for the pyridine group in PAPM. When the solution concentration of the polymer (PLMA) is maintained, it can compete for vacated adsorption sites on the available surface. Apparently, the polymer is then usually not bound because an insufficient number of segments make contact at the interface.

The Configuration and Thickness of Adsorbed Polymer Films. Polymers at the solid-liquid interface have been reported to be present in all configurations. Polyisobutylene at the carbon-benzene interface²⁸ was reported to be flat, with every CH₂ group present in the interface. At the other extreme, coverage by random coils effectively approximating a layer of oblate or prolate spheroids^{15,24} have been postulated. Though the need to consider the nature of the surface, the composition of the polymer, and the solvent has been discussed, their effects on the configuration of polymer has had only limited consideration until recently.^{13,14}

Most studies have utilized homopolymers though some have actually been mixtures, *e.g.*, partly hydrolyzed poly(vinyl acetate)²⁴ and poly(methyl methacrylate).²⁷ Silberberg¹¹ has made excellent progress toward developing a model which takes most of these

(28) J. S. Binford and A. M. Gessler, *J. Phys. Chem.*, **38**, 1376 (1959).

factors into consideration and he attempts to correlate the model generally with the available data.

This study has utilized two closely related polymers—one homogeneous and the other containing strongly sorbed copolymer segments spaced along the chain—in order to test the previously favored random coil adsorption model. The inference from these results is that spotwise adsorption to the surface through an existing adsorbed polymer layer occurs under these conditions resulting in some long loops.

The results of two-step adsorption of PLMA from two solvents, in conjunction with the observations of Stromberg¹⁶ and Gottlieb,¹⁹ argue that the first polymer molecules arriving at a surface uncoil and adsorb in an extended configuration. Initially, the fraction of segments adsorbed at the interface, p , presumably approaches 1. As the surface coverage, θ , increases, the configuration progressively changes, approaching the random coil configuration. At the same time, the formation of an overlayer may commence because the remaining surface now has a more limited distribution of adsorption sites for runs of polymer segments. The resulting loops constitute entanglement and interpenetration of the adsorbed molecules. Desorption and displacement results presented above are evidence of the mobility and rearrangement that can take place even after a polymer has adsorbed. Equivalent molecules which arrived at the surface at very different times and therefore have appreciably different values of p would exhibit great differences in desorption behavior (equivalent to appreciable differences in molecular weight at constant p).

While these arguments are inconclusive for the homogeneous PLMA, the model of interpenetrating loops fits very well to the results of two-step adsorption of PAPM and the sequential adsorption of PLMA followed by PAPM. The results of Fontana¹⁷ with his spotwise adsorbing alkyl methacrylate-polyglycol methacrylate support this model.

Further adsorption of polymer—while the *net* number of segments at the surface remains constant, as determined by surface potential measurements¹⁹—is also best accommodated by the interpenetrating loop hypothesis. (It is possible that the poly(vinyl acetate)

used in that study contained a small fraction of free hydroxyl groups.)

For conditions where polymer can aggregate in solution because of hydrogen bonding and poor solvation,²⁹ which has been investigated further by Smith,³⁰ adsorption is most likely to occur in solution configuration or a modified (compressed) form. This would be the other extreme of the models recently proposed.

The models for polymer configuration at the solid-liquid interface must account for the viscometric behavior of coated particles, capillaries,³¹ and surfaces.¹⁵ The effective thickness of polymer films on particles has an important place in the stabilization of colloids according to Fontana,¹⁷ Romo,³² and the earlier work of Van der Waarden,³³ though Fowkes³⁴ recently discussed an electric charge mechanism. The most generally explored hypothesis is that of the effect of adsorbed random coils in which the effective thickness is proportional to the square root of the molecular weight.^{15,16}

The model of large loops originating from spotwise adsorbing polymers allows an alternative explanation. It has been postulated here that the loops grow longer with increasing θ . Consequently, there would be an effective polymer concentration gradient with distance from the surface through the adjoining phase of short loops. The concentration can be expected to drop off sharply with distance from the surface and with increasing loop size, eventually reaching solution concentration. The region of approach to solution concentration could represent the "effective viscometric thickness" of the adsorbed polymer film.

Acknowledgments. The author wishes to thank J. Beardmore for preparation of the C¹⁴-labeled polymers.

(29) F. M. Fowkes, M. J. Schick, and A. Bondi, *J. Colloid Sci.*, **15**, 531 (1960).

(30) M. L. Smith, to be published.

(31) O. E. Öhrn, *Arkiv Kemi*, **12**, 397 (1958).

(32) L. A. Romo, *J. Phys. Chem.*, **67**, 386 (1963).

(33) M. Van der Waarden, *J. Colloid Sci.*, **5**, 317 (1950); **6**, 443 (1951).

(34) F. M. Fowkes, F. W. Anderson, and R. J. Moore, Abstracts, 150th National Meeting of the American Chemical Society, Atlantic City, N. J., Sept 1965, p 281.

The Kinetics of the Decarboxylation of *n*-Hexylmalonic Acid, Cyclohexylmalonic Acid, and Oxamic Acid in Acid Media

by Louis Watts Clark

Department of Chemistry, Western Carolina College, Cullowhee, North Carolina 28723
(Received June 13, 1966)

Kinetic data are reported for the decarboxylation of *n*-hexylmalonic acid (mp 105°), cyclohexylmalonic acid (mp 180°), and oxamic acid (mp 210°) in hexanoic acid and octanoic acid. Comparison of the results obtained in this research with previously published data on malonic acid (mp 135°) and oxanilic acid (mp 150°) indicates that the isokinetic temperatures for the various reaction series are the same as the melting points of the reactants and that the free energy of activation for the various reactions at the melting point of the reactant is a constant and is equal to approximately 31.1 kcal/mole.

Kinetic studies have been carried out previously on the decarboxylation of malonic acid in the molten state as well as in solution in a large number of fatty acids.¹ The activation parameters for these reactions are listed in Table I and shown graphically in Figure 1. The slope of the line in Figure 1 is 408°K or 135°C. This is the so-called isokinetic temperature of the reaction series; *i.e.*, the temperature at which the rate constants of all the reactions conforming to the line are equal.² It is also the melting point of malonic acid. This means that at its melting point, the rate of decarboxylation of malonic acid is not affected by the presence of acidic solvents.³ The intercept of the isokinetic temperature line on the zero entropy of activation axis yields ΔF° , the free energy of activation of all the reactions in the particular series at the isokinetic temperature.⁴ In Figure 1 this value turns out to be 31.1 kcal/mole. If $\Delta F^\ddagger_{135^\circ}$ is calculated by means of the equation

$$\Delta F^\ddagger = \Delta H^\ddagger - T\Delta S^\ddagger$$

for the various systems shown in Table I, the result in every case is very close to the value of 31.1 kcal/mole as shown in the last column in the table.

Kinetic data for the decarboxylation of several acids in the molten state are listed in Table II. The free energies of activation of the various reactants at their respective melting points are shown in the last column. It is surprising to note that in spite of the

Table I: Activation Parameters for the Decarboxylation of Malonic Acid in the Molten State and in Several Fatty Acids^a

Solvent	ΔH^\ddagger , kcal/ mole	ΔS^\ddagger , eu/ mole	$\Delta F^\ddagger_{135^\circ}$, kcal/ mole
Pivalic acid	38.7	18.3	31.2
Melt	35.8	11.9	31.0
Octanoic acid	34.83	8.9	31.19
Propionic acid	33.6	6.1	31.11
Isovaleric acid	32.56	3.57	31.10
Hexanoic acid	32.5	3.2	31.20
Pentanoic acid	32.2	2.4	31.20
Benzoic acid	30.4	-1.8	31.14
β -Mercaptopropionic acid	30.3	-1.9	31.08
Heptanoic acid	29.7	-3.4	31.1
Decanoic acid	26.6	-11.0	31.1
(+)-1,2-Methylpentanoic acid	26.45	-11.1	31.0

^a Reference 1.

wide variation in the values of the activation parameters and the range of melting points, the free energy of activation at the melting point is the same for each reactant and is equal to approximately 31.1 kcal/mole.

(1) L. W. Clark, *J. Phys. Chem.*, **68**, 3048 (1964).

(2) S. L. Friess, E. S. Lewis, and A. Weissberger, Ed., "Technique of Organic Chemistry," Vol. VIII, 2nd ed, Part I, Interscience Publishers, Inc., New York, N. Y., 1961, p 207.

(3) L. W. Clark, *J. Phys. Chem.*, **67**, 526 (1963).

(4) J. E. Leffler, *J. Org. Chem.*, **20**, 1202 (1955).

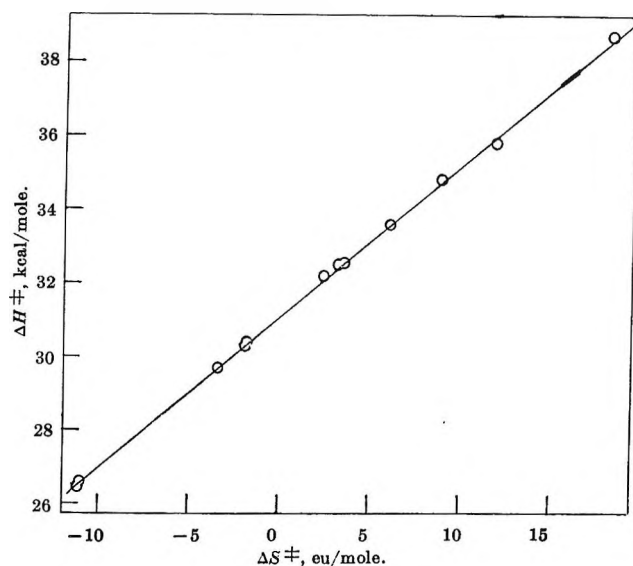


Figure 1. Enthalpy vs. entropy of activation plot for the decarboxylation of malonic acid in the molten state and in several fatty acids. Slope of line: 408°K or 135°C .

Table II: Activation Parameters for the Decarboxylation of Several Acids in the Molten State

Reactant	Mp, $^{\circ}\text{C}$	ΔH^{\ddagger} , kcal/mole	ΔS^{\ddagger} , eu/mole	$\Delta F^{\ddagger}_{\text{mp}}$, kcal/mole
Oxanilic acid ^a	150	40.1	21.4	31.05
Malonic acid ^b	135	35.8	11.9	31.0
Methylmalonic acid ^c	135	35.0	9.6	31.08
<i>n</i> -Hexylmalonic acid ^d	105	32.2	2.8	31.14
<i>n</i> -Butylmalonic acid ^e	105	32.2	2.9	31.10

^a L. W. Clark, *J. Phys. Chem.*, **66**, 1543 (1962). ^b L. W. Clark, *ibid.*, **67**, 138 (1963). ^c L. W. Clark, *ibid.*, **70**, 2523 (1966). ^d L. W. Clark, *ibid.*, **67**, 2602 (1963). ^e L. W. Clark, *ibid.*, **68**, 587 (1964).

These results suggest the possibility that compounds related to malonic and oxanilic acids may exhibit behavior in acidic solvents analogous to that of the parent compounds; *i.e.*, (1) they may have isokinetic temperatures equal to their melting points, and (2) they may have the same free energies of activation at their melting points as does malonic acid, namely, 31.1 kcal/mole. In order to test this hypothesis, three acids were selected differing widely in melting points (*n*-hexylmalonic acid, mp 105° , cyclohexylmalonic acid, mp 180° , and oxamic acid, mp 210°) and their rates of reaction were carefully measured at several temperatures in two high-boiling fatty acids (hexanoic and octanoic acid). The results of this investigation, which are reported herein, leave no doubt as to the validity of the hypothesis which prompted it.

Experimental Section

Reagents. The *n*-hexylmalonic acid and cyclohexylmalonic acid used in this research were obtained from Distillation Products Industries, Rochester, N. Y. The cyclohexylmalonic acid melted sharply at 180° (corrected) and was used as purchased. The *n*-hexylmalonic acid had a melting range of 103 – 106° when received. After recrystallization from benzene it was found to melt sharply at 105° (corrected). The oxamic acid was obtained from Matheson Coleman and Bell, Norwood, Ohio. It melted sharply at 210° (corrected) and was used as purchased. The hexanoic and octanoic acids were reagent grade. The samples used in the decarboxylation experiments were freshly distilled at atmospheric pressure immediately before use.

Apparatus and Technique. Details of the apparatus and technique have been described previously.⁵

In each experiment a weighed sample of the reactant was introduced in the usual manner into the reaction flask containing 95 ml of solvent. The weight used was that which was required to furnish exactly 40.0 ml of CO_2 at STP on complete reaction calculated on the basis of the actual molar volume of CO_2 at STP, namely, 22,267 ml. For *n*-hexylmalonic acid this is 0.3361 g, for cyclohexylmalonic acid, 0.3382 g, and for oxamic acid, 0.1600 g. All experiments were carried out in an atmosphere of dry CO_2 .

Results

For each reactant at least two decarboxylation experiments were carried out in each solvent at each

Table III: Apparent First-Order Rate Constants for the Decarboxylation of *n*-Hexylmalonic Acid, Cyclohexylmalonic Acid, and Oxamic Acid in Two Fatty Acids

Reactant	Hexanoic acid		Octanoic acid	
	Temp, $^{\circ}\text{C}$ (cor)	$k \times 10^4$, sec ⁻¹	Temp, $^{\circ}\text{C}$ (cor)	$k \times 10^4$, sec ⁻¹
<i>n</i> -Hexylmalonic acid	137.87	2.82	135.09	2.06
	143.63	4.84	146.36	5.90
	154.80	13.3	149.75	7.97
	157.33	16.56	154.80	12.4
Cyclohexylmalonic acid	140.17	2.74	140.60	2.32
	150.23	7.06	150.49	6.30
	160.23	17.22	160.59	16.15
Oxamic acid	138.93	3.23	138.83	3.11
	149.81	8.54	149.06	7.81
	158.88	18.64	157.49	16.38

(5) (a) L. W. Clark, *J. Phys. Chem.*, **60**, 1150 (1956); L. W. Clark, *ibid.*, **70**, 627 (1966).

Table IV: Comparison of Activation Parameters for the Decarboxylation of Several Unstable Acids in the Molten State and in Solution

Solvent	<i>n</i> -Hexylmalonic acid, mp 105°			Malonic acid, mp 135°			Oxanilic acid, mp 150°			Cyclohexylmalonic acid, mp 180°			Oxamic acid, mp 210°		
	ΔH^\ddagger , kcal/ mole	ΔS^\ddagger , eu/ mole	$\Delta F^\ddagger_{105^\circ}$, kcal/ mole	ΔH^\ddagger , kcal/ mole	ΔS^\ddagger , eu/ mole	$\Delta F^\ddagger_{135^\circ}$, kcal/ mole	ΔH^\ddagger , kcal/ mole	ΔS^\ddagger , eu/ mole	$\Delta F^\ddagger_{150^\circ}$, kcal/ mole	ΔH^\ddagger , kcal/ mole	ΔS^\ddagger , eu/ mole	$\Delta F^\ddagger_{180^\circ}$, kcal/ mole	ΔH^\ddagger , kcal/ mole	ΔS^\ddagger , eu/ mole	$\Delta F^\ddagger_{210^\circ}$, kcal/ mole
Melt	32.2 ^a	2.8	31.14	35.8 ^a	11.9	31.0	40.1 ^a	21.4	31.05						
Hexanoic acid	31.24	0.54	31.1	32.5 ^a	3.2	31.2				31.82	1.94	31.09	30.5	-1.25	31.1
Octanoic acid	30.75	-1.0	31.14	34.83 ^a	8.9	31.19	36.73 ^a	13.3	31.1	33.7	5.61	31.16	30.5	-1.25	31.1

^a Reference 1.

constant temperature selected. Each reaction was measured at three or four different temperatures over a 20° range. All the reactions gave good first-order kinetics in both solvents over the greater portion of the reaction.

Average rate constants, calculated in the usual manner from the slopes of the logarithmic plots, are shown in Table III. The parameters of the absolute reaction rate equation based upon the data in Table III are shown in Table IV. Included for comparison are corresponding data previously published for malonic acid and oxanilic acid.

Discussion

In Table IV it will be observed that for the first three reactants the acidic solvent lowers both the enthalpy and entropy of activation of the decarboxylation reaction. This is consistent with the proposed mechanism of the reaction⁶ since the fatty acids are weaker acids (and therefore stronger bases in the Lewis sense) than malonic acid. It will be observed also that, in the molten state and in identical solvents, the substituent on malonic acid lowers both the enthalpy and entropy of activation of the reaction. The effect of the cyclohexyl group, however, is less than that of the *n*-hexyl group. In octanoic acid the enthalpy of activation for the decarboxylation of oxamic acid is considerably less than that for the oxanilic acid reaction. The reverse is true for these two reactions in basic solvents.⁷

The most interesting feature of Table IV is the comparison of the free energies of activation of the various reactions at the melting points of the reactants (the third column in each section). For each of the five reactants shown, in the molten state (where data are available) as well as in the fatty acids, it will be observed that the free energy of activation at the melting point of the reactant is constant (equal to approximately 31.1 kcal/mole) as was noted previously in the case of malonic acid (see Table I). In the case of the decarboxylation of oxanilic acid, oxamic acid, and malonic acid and its derivatives, in the molten state and in

solution in fatty acids, these results indicate that the isokinetic temperature is the same as the melting point of the reactant and that the free energy of activation at the melting point is constant (equal to approximately 31.1 kcal/mole).

It is interesting to note that the melting points of the acids shown in Table IV (as well as in Table II) increase by integral multiples of 15°.

It has been noted previously that numerous reaction series formed by the decarboxylation of a large number of compounds in various homologous solvents exhibit isokinetic temperatures beginning at 105° and increasing by integral multiples of 15°.⁸

These results indicate that the numbers associated with these melting points and isokinetic temperatures are natural constants pointing to some sort of fundamental interrelationship of chemical reactivity. High melting points are indicative of strong attractions between the units composing the crystal lattice. Similarly, high isokinetic temperatures would be expected to be associated with strong mutual attractions between the electrophile-nucleophile pairs of the transition state.

The reactants listed in Table IV and Table II may be regarded as belonging to either of two groups of compounds: (1) α -keto acids (oxamic and oxanilic acids) and (2) β -keto acids (malonic acid and its derivatives). It is interesting to speculate whether or not the results of the present research may apply to other α - and β -keto acids. If so, then a compound such as *o*-nitrophenylpyruvic acid (mp 120°) should have a free energy of activation at 120° of 31.1 kcal/mole and an isokinetic temperature of 120° in acidic solvents. Unstable acids belonging to other homologous series (e.g., α -amino acids) should show analogous behavior; i.e., the free energy of activation at the melting point should be constant (but not necessarily the same as

(6) G. Fraenkel, R. L. Belford, and P. E. Yankwich, *J. Am. Chem. Soc.*, **76**, 15 (1954).

(7) L. W. Clark, *J. Phys. Chem.*, **65**, 1460 (1961).

(8) L. W. Clark, *ibid.*, **70**, 1597 (1966).

for the keto acids) and isokinetic temperatures in acid media should be equal to their melting points. If such results are established a great deal of insight will be gained in regard to chemical reactivity. Furthermore, the rates of a vast number of reactions of theoretical as well as practical interest under all kinds of conditions may be calculated without recourse to experimentation.

In the case of the decarboxylation of the high-melting cyclohexylmalonic acid (mp 180°) in the fatty acids, k_{180° may be calculated by use of the absolute reaction rate equation⁴ assuming an average value of $\Delta F^\ddagger_{180^\circ}$ to be 31.1 kcal/mole. When this is done, the rate constant at 180° turns out to be 0.0094 sec⁻¹ corresponding to a half-life of 73 sec. Similar calculations for oxamic acid (mp 210°) yield k_{210° equal to 0.086 sec⁻¹ corresponding to a half-life of only 8 sec. These results evidently would apply also to the decarboxylation of the molten acids at their melting points. These rates are too rapid for accurate measurement with the apparatus employed in this research.

It should be pointed out that the decarboxylation of malonic acid in alcohols,^{9,10} cresols,¹¹ and aniline and its derivatives¹² forms three separate reaction series all having the same isokinetic temperature as that for the reaction in fatty acids (namely, 135°) but with different values of ΔF° (see ref 4). However, not all reaction series involving decarboxylation show isokinetic temperatures corresponding to the melting points of the substrates. For example, the isokinetic temperature of the reaction series formed by the decarboxylation of oxanilic acid (mp 150°) in ethers is 135° (see Table IV). Similarly, the isokinetic temperature of the reaction series consisting of the decarboxylation of *n*-butylmalonic acid (mp 105°) in cresols is 150° (see Table VI). The interesting fact remains, however, that the various isokinetic temperatures

shown by all the reaction series under discussion appear to differ from one another by integral multiples of 15°. It is hoped that a theoretical explanation of these puzzling results will soon be forthcoming.

Table V: Activation Parameters for the Decarboxylation of Oxanilic Acid in Ethers^a

Solvent	ΔH^\ddagger , kcal/mole	ΔS^\ddagger , eu/mole	$\Delta F^\ddagger_{135^\circ}$, kcal/mole
<i>n</i> -Amyl ether	28.3	-6.6	31.0
β -Chlorophenetole	31.3	0.7	31.0
Phenetole	32.6	4.0	31.0
Anisole	35.6	11.1	31.07
Dibenzyl ether	36.8	14.2	31.0
<i>n</i> -Hexyl ether	40.1	22.1	31.0

^a L. W. Clark, *J. Phys. Chem.*, **66**, 1453 (1962).

Table VI: Activation Parameters for the Decarboxylation of *n*-Butylmalonic Acid in Cresols^a

Solvent	ΔH^\ddagger , kcal/mole	ΔS^\ddagger , eu/mole	$\Delta F^\ddagger_{150^\circ}$, kcal/mole
Phenol	36.2	13.0	30.7
<i>p</i> -Cresol	24.0	-15.8	30.7
<i>m</i> -Cresol	29.7	-2.3	30.7

^a L. W. Clark, *J. Phys. Chem.*, **68**, 587 (1964).

Acknowledgment. Acknowledgment is made to the donors of the Petroleum Research Fund, administered by the American Chemical Society, for support of this research.

(9) L. W. Clark, *J. Phys. Chem.*, **64**, 508 (1960).

(10) L. W. Clark, *ibid.*, **64**, 677 (1960).

(11) L. W. Clark, *ibid.*, **67**, 526 (1963).

(12) L. W. Clark, *ibid.*, **62**, 79 (1958).

Thermodynamics of Aqueous Mixtures of Electrolytes and Nonelectrolytes.

I. Ethyl Acetate and Eight 1-1 Alkali Metal Salts at 25°

by J. H. Stern and A. Hermann

Department of Chemistry, California State College at Long Beach, Long Beach, California 90804
(Received June 28, 1966)

Partial molal enthalpies of transfer of ethyl acetate from water to eight aqueous 1 *m* alkali halides and nitrates were determined *via* calorimetry at 25°. The enthalpies of transfer range from 204 to -66 cal/mole and were combined with free energies calculated from activity coefficient data to yield partial molal entropies of transfer. The entropies are negative for transfer to seven of the eight electrolytes and range from -0.50 to 0.10 cal/mole deg. A partial explanation of the values in terms of changes in solution structure is proposed. The enthalpies also fix the temperature variation of the activity coefficient of the nonelectrolyte in the electrolyte solutions.

I. Introduction

Activity coefficients of nonelectrolytes of low solubility in aqueous salt solutions have been useful in examining theoretical predictions on electrolyte–nonelectrolyte interactions. Such activity coefficients have been reported for many systems.¹

In many cases the solubility of the nonelectrolyte in aqueous solution decreases and its activity coefficient increases when an electrolyte is added. This phenomenon is known as “salting-out” and is of importance in fields from physical chemistry to biochemistry. For example, it affects the equilibrium concentrations of nonelectrolytes distributed between aqueous solutions and other phases immiscible in water. This is directly related to extraction processes and to the passage of nonelectrolytes across phase boundaries in biochemical systems.

The interaction between electrolytes and nonelectrolytes also affects a variety of thermodynamic studies of nonelectrolyte reactions such as heats of complexing and neutralization carried out in aqueous electrolyte solutions.² Such heats are dependent on the nature and concentration of the supporting electrolyte.

There are several empirical equations that express the activity coefficient of the nonelectrolyte as a function of the electrolyte concentration. The simplest and most frequently used is³

$$\log \gamma_3 = k_{32}m_2 \quad (1)$$

where γ_3 = activity coefficient of the nonelectrolyte solute “3” in the electrolyte solution of molality m_2 , relative to the standard state of the solute in pure water. k_{32} = salting coefficient or ion–nonelectrolyte interaction parameter. The linear relation between $\log \gamma_3$ and m_2 has been observed for many electrolyte systems over wide ranges of electrolyte concentration.

Several theories of ion–nonelectrolyte interactions analogous to the Debye–Hückel limiting theory for ion–ion interactions have been proposed. Those of Debye and MacAulay⁴ and later of Debye⁵ predict as a limiting behavior a first-power dependence of $\log \gamma_3$ on m_2 in agreement with eq 1. The theories are based on the change in coulombic interaction as a result of a decrease in the dielectric constant of the solvent when the nonelectrolyte is added. The order of magnitude of the observed effects is predicted, but their specific nature is not satisfactorily accounted for. These theories are developed and critically discussed by

- (1) (a) F. A. Long and W. F. McDevit, *Chem. Rev.*, **51**, 119 (1952); (b) M. Randall and C. F. Failey, *ibid.*, **4**, 271 (1927); (c) H. S. Harned and B. S. Owen, “The Physical Chemistry of Electrolytic Solutions,” 3rd ed, Reinhold Publishing Corp., New York, N. Y., 1958, p 531.
- (2) P. Paoletti, J. H. Stern, and A. Vacca, *J. Phys. Chem.*, **69**, 3759 (1965); P. Paoletti, A. Vacca, and D. Arenare, *ibid.*, **70**, 193 (1966).
- (3) G. N. Lewis and M. Randall, “Thermodynamics,” revised by K. S. Pitzer and L. Brewer, McGraw-Hill Book Co., Inc., New York, N. Y., 1961, p 584.
- (4) P. Debye and J. MacAulay, *Physik. Z.*, **26**, 22 (1925).
- (5) P. Debye, *Z. Physik. Chem.*, **130**, 55 (1927).

Harned and Owen⁶ and by Edsall and Wyman.⁷ Interactions other than coulombic are also possible.¹ It is likely, however, that the interactions which require the addition of a specific interaction term to the Debye-Hückel limiting equation also give rise to excess thermodynamic properties of mixed electrolytes⁸ and are at least partly responsible for the specific nature of the salting effects. It may be noted that the salting coefficient, k_{32} , has a similar functional dependence on the activity coefficient and electrolyte molality as does B , the second virial or specific interaction coefficient in the extended form of the Debye-Hückel limiting equation.⁹

The salting-out of ethyl acetate has been the subject of extensive study.¹ Aside from tabulations of k_{32} and γ_3 almost no other related thermodynamic information for this nonelectrolyte and others in such systems has been reported to date. From the activity coefficients one may calculate the partial molal free energy of transfer.

Consider the isothermal transfer of ethyl acetate from pure water to an aqueous electrolyte solution "MX" at molality m_2



If $\overline{\Delta F}_3$ is the partial molal free energy change, then for a transfer at constant composition

$$\overline{\Delta F}_3 = RT \ln \gamma_3 \quad (3)$$

The partial molal enthalpy of transfer, $\overline{\Delta H}_3$, was determined from the separate and direct measurement of the heats of solution of small quantities of ethyl acetate in pure water, ΔH_3° , and the aqueous electrolyte solution, ΔH_3 , respectively, so that

$$\overline{\Delta H}_3 = \Delta H_3 - \Delta H_3^\circ \quad (4)$$

No calorimetric enthalpies of transfer appear to have been published to date. A value of $\overline{\Delta H}_3$ of less than 100 cal/mole calculated from the vapor phase equilibration measurements of Brewer, Simonson, and Tong¹⁰ for mesityl oxide in 1 *m* NaCl at 20 and 25° is smaller than the experimental error. An estimate of 1400 cal/mole was possible for mesityl oxide in 1 *m* NaNO₃ and NaClO₄ from distribution experiments at 25 and 30°.

The partial molal enthalpy of transfer, $\overline{\Delta H}_3$, together with $\overline{\Delta F}_3$, yields the corresponding partial molal entropy

$$\overline{\Delta S}_3 = (\overline{\Delta H}_3 - \overline{\Delta F}_3)/T \quad (5)$$

Almost no values of $\overline{\Delta S}_3$ have been published. Frank and Evans¹¹ calculated some entropies for N₂O based

on γ_3 values at 15 and 25° in alkali halide solutions¹² from

$$\overline{\Delta S}_3 = -R \ln \gamma_3 - RT[\partial \ln \gamma_3 / \partial T]_P = -[\partial \overline{\Delta F}_3 / \partial T]_P \quad (6)$$

Values for the change in partial molal entropy are of great importance in the present study since they may be considered as quantitative criteria for the structural changes accompanying the transfer of ethyl acetate from water to various aqueous electrolyte solutions. It is difficult to make meaningful theoretical predictions on the magnitude or sign of $\overline{\Delta S}_3$ since these require assumptions about the temperature variation of functions of dielectric constants in the absence of such data.¹¹

II. Experimental Section

The calorimeter has been described previously.⁸ Its accuracy was rechecked *via* measurements of the heat of solution of crystalline KCl in water, and the agreement with the most recently recommended value¹³ was excellent. Sealed glass ampoules with small quantities of ethyl acetate were crushed against the bottom of the dewar containing 450 g of water or aqueous salt solution, respectively. All runs were carried out at 25.00 ± 0.10°.

Materials. All AR grade salts were kept at elevated temperatures for at least 12 hr prior to weighing and were dissolved to the desired molality with weighed quantities of distilled CO₂-free water. The bromide and iodide salts were dried under vacuum at 40°. Ethyl acetate, AR grade, was further checked for purity by vapor phase chromatography.

III. Results and Discussion

The enthalpy of solution of ethyl acetate in water (ΔH_3°) is -2229 ± 9 cal/mole based on 23 runs. The enthalpies of solution of ethyl acetate in 1 *m* electrolyte solutions (ΔH_3) are shown in Table I. Variations in the amount of pure ethyl acetate per run and consequently in the low final concentrations (ranging approximately from 0.002 to 0.008 *m*) gave essentially

(6) See ref 1c, pp 80, 536.

(7) J. T. Edsall and J. Wyman, "Biophysical Chemistry," Vol. I, Academic Press Inc., New York, N. Y., 1958, p 263.

(8) J. H. Stern and C. W. Anderson, *J. Phys. Chem.*, **68**, 2528 (1964).

(9) See ref 3, p 318.

(10) L. Brewer, R. Simonson, and L. K. J. Tong, *J. Phys. Chem.*, **65**, 420 (1961).

(11) H. S. Frank and M. W. Evans, *J. Chem. Phys.*, **13**, 507 (1945).

(12) W. Geffcken, *Z. Physik. Chem.*, **49**, 257 (1904).

(13) S. R. Gunn, *J. Phys. Chem.*, **69**, 2902 (1965); G. Somsen, J. Coops, and M. W. Tolck, *Rec. Trav. Chim.*, **82**, 231 (1963).

Table I: Enthalpies of Solution of Ethyl Acetate in 1 *m* Aqueous Electrolyte Solutions (ΔH_3)

Electrolyte	$-\Delta H_3$, cal/mole	No. of runs
KCl	2179 \pm 4	4
KBr	2216 \pm 3	2
KI	2295 \pm 9	4
KNO ₃	2195 \pm 4	4
NaCl	2025 \pm 9	6
NaBr	2121 \pm 10	6
NaNO ₃	2096 \pm 9	3
LiCl	2159 \pm 8	4

Table II: Summary of $\overline{\Delta F}_3$, $\overline{\Delta H}_3$, and $\overline{\Delta S}_3$

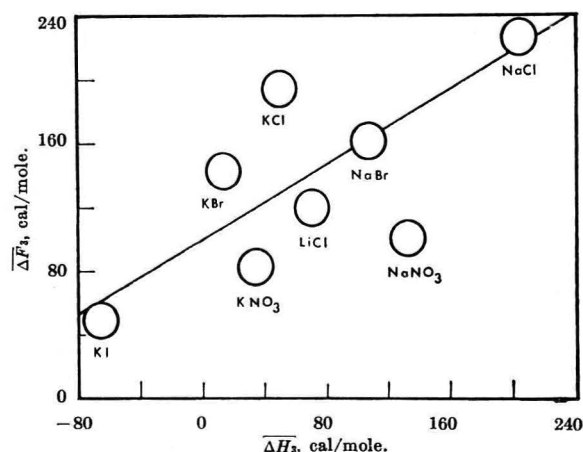
Electrolyte	$\overline{\Delta F}_3$, cal/mole	$\overline{\Delta H}_3$, cal/mole	$\overline{\Delta S}_3$, cal/mole deg
KCl	195	50	-0.50
KBr	143	13	-0.45
KI	50	-66	-0.40
KNO ₃	82	34	-0.15
NaCl	227	204	-0.10
NaBr	163	108	-0.20
NaNO ₃	101	133	+0.10
LiCl	120	70	-0.15

constant heats within the limits of the standard deviations associated with all average values. The overall estimated experimental error is ± 10 cal/mole.

Partial molal free energies, enthalpies, and entropies of transfer are shown in Table II.

An examination of the thermodynamic properties in Table II indicates the following trends for the potassium and sodium salts. All $\overline{\Delta F}_3$ are positive. Those for potassium salts are lower than for the corresponding sodium salts. This order from electrolyte to electrolyte has been found to hold approximately for other nonelectrolytes as well. The $\overline{\Delta H}_3$ for the potassium and sodium salts fall into two groupings, with the latter being more endothermic. All heats are positive except for that of potassium iodide.

It may be observed that the entropies of transfer, $\overline{\Delta S}_3$, for seven of the eight electrolytes are negative. The salting-out may in part be explained by postulating that the ions are preferentially solvated by the higher dielectric constant component, in this case, water. The nonelectrolyte molecules in the neighborhood of the ions would thus be deprived of access to water. One may interpret this as an "unmixing" effect which would tend to lower the partial molal entropy of the nonelectrolyte in accord with the observed negative values of $\overline{\Delta S}_3$.

**Figure 1.** Correlation of $\overline{\Delta H}_3$ with $\overline{\Delta F}_3$.

The effect of ion solvation may also be a function of ion size. The smaller chloride is thought to immobilize the water structure more due to its specific size and localized charge density and hence make relatively less water available for dissolving the nonelectrolyte than the larger iodide or nitrate ions.¹¹ A decrease of $\overline{\Delta S}_3$ with decreasing ion size would be expected. Such a trend is discernible, particularly for the potassium salts. It is recognized that the complicated nature of interactions makes assignment of any trend to ion size speculative. Many more nonelectrolyte systems will have to be investigated before the effect of ion size on $\overline{\Delta S}_3$ can be established. In this context it may also be noted that $\overline{\Delta S}_3$ together with $\overline{\Delta H}_3$ for the sodium and potassium salts falls approximately into two groups. It is possible that this is due to differences in interaction between the cations and the negative carbonyl oxygen of the polar ethyl acetate.

One may examine the relationship between $\overline{\Delta S}_3$ and the change in interaction. If $\overline{\Delta S}_3$ is simply and smoothly related to $\partial \ln \gamma_3 / \partial T$ (eq 6) then $\overline{\Delta S}_3$ should be simply related to $\overline{\Delta F}_3$. This would lead to a similar relationship between $\overline{\Delta F}_3$ and $\overline{\Delta H}_3$. A plot of $\overline{\Delta H}_3$ vs. $\overline{\Delta F}_3$ should reveal whether any correlation exists. This approach is analogous to that of Pitzer and Brewer¹⁴ who show a plot of the partial molal enthalpies and free energies of dilution for a variety of 1-1 electrolytes. Figure 1 indicates some degree of correlation, although the scatter of experimental points from the least-squares line suggests that the correlation is neither simple nor smooth.

The enthalpy of transfer leads to the fixing of the temperature derivative of the activity coefficient, γ_3 , and consequently k_{32} since

$$\partial \ln \gamma_3 / \partial T = -\overline{\Delta H}_3 / RT^2 \quad (7)$$

(14) See ref 3, p 396.

In all cases except for KI, the heats were endothermic. This gives rise to a negative temperature dependence for γ_3 and k_{32} and thus the solutions tend toward ideality as the temperature increases.

Acknowledgment. The authors express deepest appreciation to Professor Leo Brewer for fruitful discussion and encouragement of this study and the U. S. Army Research Office (Durham) for financial support.

Thermodynamics of Aqueous Mixtures of Electrolytes and Nonelectrolytes.

II. Transfer of Nitromethane from Water to Seven 1-1 Chlorides and Perchlorates at 25°

by J. H. Stern and A. Hermann

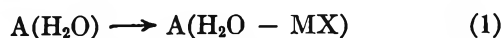
Department of Chemistry, California State College at Long Beach, Long Beach, California 90804
(Received September 27, 1966)

Partial molal enthalpies of transfer of nitromethane from water to aqueous 1 *m* solutions of LiCl, NaCl, KCl, CsCl, HClO₄, LiClO₄, and NaClO₄ were determined *via* calorimetry at 25°. The enthalpies of transfer range from -239 to 247 cal/mole and were combined with free energies calculated from salting coefficient data to yield partial molal entropies of transfer. For the chlorides, the entropies and enthalpies decrease regularly with increasing cation size from 0.2 to -0.7 cal/mole deg between LiCl and CsCl, respectively. For the three perchlorates, the entropies are all positive and remain constant with a value of 1.1 cal/mole deg.

I. Introduction

Mixtures of strong electrolytes and nonelectrolytes in aqueous solutions form an important part of many systems and physicochemical processes whose diversity ranges from physiological fluids to desalination. The interactions in such solutions are very complex, and their nature is not well understood.^{1,2} Further advances are hampered by a lack of data.

This paper is the second in a series reporting on the changes in thermodynamic properties when the isothermal transfer



takes place under the following conditions: 1 mole of a nonelectrolyte, A, at molality m_3 is transferred from

a large quantity of water to a large quantity of a solution of A at m_3 containing an electrolyte, MX, at molality m_2 .

The first contribution describes the partial molal heats and free energies and entropies for the transfer of ethyl acetate from water to a variety of aqueous 1 *m* alkali halides and nitrates.³

Other than extensive collections of activity coefficients for a wide variety of nonelectrolytes in aqueous electrolyte solutions very little related thermodynamic

(1) F. A. Long and W. F. McDevit, *Chem. Rev.*, **51**, 119 (1952).

(2) H. S. Harned and B. B. Owen, "The Physical Chemistry of Electrolytic Solutions," 3rd ed, Reinhold Publishing Corp., New York, N. Y., 1953, p 80.

(3) J. H. Stern and A. Hermann, *J. Phys. Chem.*, **71**, 306 (1967).

information has been reported for such systems. The activity coefficients are commonly determined *via* measurements of solubilities, distribution of the nonelectrolyte solute between the aqueous salt solution and an immiscible phase, and vapor pressures.¹ The activity coefficient of the nonelectrolyte γ_3 , hereafter called component 3, may be expressed as a function of the electrolyte and nonelectrolyte concentrations m_2 and m_3 , respectively, by the equation⁴

$$\log \gamma_3 = k_{32}m_2 + k_{33}m_3 \quad (2)$$

where γ_3 = the activity coefficient of the nonelectrolyte solute "3" in the electrolyte solution relative to the hypothetical 1 *m* standard state of the solute in pure water, k_{32} = the salting or ion–nonelectrolyte interaction coefficient, and k_{33} = the self-interaction coefficient. This parameter is usually negative and of the same order of magnitude as k_{32} . When m_3 is much lower than m_2 the self-interaction contribution to γ_3 becomes so small that it may be neglected. When γ_3 is greater than unity salting out takes place with a reduction of solubility and when γ_3 is less than 1, salting in with enhanced solubility in the salt solution occurs. The relation between $\log \gamma_3$ and the concentration of the electrolyte has been found to be linear for a variety of nonelectrolyte–electrolyte combinations.⁵ The salting coefficients have a small range of values for nonelectrolytes from such solutes as nitrous oxide to ethyl acetate.⁶ The salt effects are, however, quite specific and the order from salt to salt is generally similar.

Numerous examples of salting out have been reported. Instances of salting in are not so common. Electrolytes that salt in include large aryl sulfonates,⁷ alkyl pyridium halides,⁸ and quaternary ammonium halides.⁹ Data for salting in with simpler 1–1 salts are not as readily available. Perchlorates are among the few inorganic salts with negative k_{32} values. For example, perchloric acid salts in helium,⁶ argon, and mesityl oxide.¹⁰ Nitromethane¹¹ was found to be strongly salted in by perchloric acid and the perchlorates of lithium and sodium. It may be noted that Haugen and Friedman¹¹ also measured solubilities of some perchlorates and other 1–1 salts in aqueous solutions of nitromethane and investigated the relationship between k_{32} and k_{23} . The latter pertains to the reverse effect of a nonelectrolyte on the activity coefficient of the electrolyte γ_2 . The equality $k_{23} = k_{32}$ was found to hold as required for constant k values by the Gibbs–Duhem equation.¹² It was thus possible to obtain the activity coefficient of the electrolyte from experimentally obtained values of γ_3 and in this way calculate the free energies of transfer of electrolytes from water to aqueous solutions containing nitromethane. The

corresponding free energy of transfer of nitromethane from water to aqueous salt solutions may be obtained directly from γ_3

$$\overline{\Delta F}_3 = RT \ln \gamma_3 \quad (3)$$

The partial molal enthalpy of transfer $\overline{\Delta H}_3$ may be determined by the difference between the heat of solution of nitromethane in aqueous salt solution, ΔH_3 , and in pure water, respectively, ΔH_3° , with both heats measured to approximately the same low final concentration m_3

$$\overline{\Delta H}_3 = \Delta H_3 - \Delta H_3^\circ \quad (4)$$

The partial molal enthalpy of transfer $\overline{\Delta H}_3$ together with $\overline{\Delta F}_3$ yields the corresponding partial molal entropy

$$\overline{\Delta S}_3 = \frac{\overline{\Delta H}_3 - \overline{\Delta F}_3}{T} \quad (5)$$

II. Experimental Section

The calorimeter has been described previously.¹³ Sealed glass ampoules with small quantities of nitromethane were crushed against the bottom of the dewar containing 450 g of water or salt solution, respectively. All runs were carried out at $25.00^\circ \pm 0.10$.

Materials. Lithium chloride (Fisher), NaCl and KCl (Mallinckrodt), LiClO₄ and NaClO₄ (G. F. Smith), and CsCl (British drug houses) were all AR grade and were dissolved to 1 *m* concentrations with distilled CO₂-free water. Perchloric acid (Mallinckrodt) was prepared from concentrated AR stock solution and standardized *via* titration with THAM (Fisher). Nitromethane, Spectroquality reagent (Matheson Coleman and Bell) was checked for purity (99.8%) by vapor–liquid chromatography.

III. Results and Discussion

The enthalpies of solution of nitromethane in water, ΔH_3° , and in 1 *m* electrolyte solutions, ΔH_3 , are shown

(4) L. Brewer, T. R. Simonson, and L. K. J. Tong, *J. Phys. Chem.*, **65**, 420 (1961).

(5) See ref 2, p 531.

(6) See ref 2, p 736.

(7) J. Steigman and J. Lando, *J. Phys. Chem.*, **69**, 2895 (1965).

(8) V. F. Sergeev and L. Eskarazva, *Zh. Obshch. Khim.*, **32**, 2958 (1962).

(9) J. O'M. Bockris, J. Bowler-Reed, and J. A. Kitchener, *Trans. Faraday Soc.*, **47**, 184 (1951).

(10) G. N. Lewis and M. Randall, "Thermodynamics," revised by K. S. Pitzer and L. Brewer, McGraw-Hill Book Co., Inc., New York, N. Y., 1961, p 586.

(11) G. R. Haugen and H. L. Friedman, *J. Phys. Chem.*, **60**, 1363 (1956).

(12) See ref 10, pp 572, 586.

(13) J. H. Stern and C. W. Anderson, *J. Phys. Chem.*, **63**, 2528 (1964).

Table I: Enthalpies of Solution of Nitromethane in Water (ΔH_3°) and in 1 M Aqueous Electrolyte Solutions (ΔH_3)

H ₂ O	ΔH_3° ^a	mmoles of nitromethane
	634	5.012
	626	3.822
	635	7.197
	619	7.244
	Mean: 629 ± 3 ^b	
Electrolyte	ΔH_3	mmoles of nitromethane
LiCl	763	7.764
	746	7.666
	755	6.313
	735	6.998
	747	7.514
	743	7.712
	Mean: 748 ± 4	
NaCl	709	7.964
	722	6.296
	704	6.343
	713	6.166
	Mean: 712 ± 4	
KCl	468	7.391
	474	8.136
	492	6.452
	476	7.772
	509	7.837
	460	5.168
	505	7.946
	Mean: 484 ± 7	
CsCl	384	7.741
	397	8.177
	Mean: 390 ± 7	
HClO ₄	772	9.225
	769	7.927
	769	8.658
	782	9.900
	Mean: 773 ± 3	
LiClO ₄	878	7.005
	875	8.088
	Mean: 876 ± 2	
NaClO ₄	875	8.151
	858	8.198
	851	7.599
	Mean: 861 ± 7	

^a All enthalpies in cal/mole. ^b Standard deviation of the mean.

in Table I. The mean value of ΔH_3° (629 cal/mole) measured to low final concentrations ranging from 0.016 to 0.008 *m* is in very good agreement with that calculated from NBS tables¹⁴ of 0.63 kcal/mole for the

Table II: Summary of $\overline{\Delta F}_3$, $\overline{\Delta H}_3$, and $\overline{\Delta S}_3$

Electrolyte	$\overline{\Delta F}_3$, cal/mole	$\overline{\Delta H}_3$, cal/mole	$\overline{\Delta S}_3$, cal/mole deg
LiCl	70	119	0.2
NaCl	76	83	0
KCl	12	-145	-0.5
CsCl	-27	-239	-0.7
HClO ₄	-199	144	1.1
LiClO ₄	-95	247	1.1
NaClO ₄	-106	232	1.1

enthalpy of solution in water to the higher final concentration of 0.12 *m*. The enthalpies thus appear to remain essentially constant below 0.12 *m*. The overall estimated error is ± 12 cal/mole.

Partial molal free energies from Table III of ref 11 are shown in Table II with enthalpies and entropies.

The thermodynamic properties in Table II indicate the following notable trends: the free energy of transfer $\overline{\Delta F}_3$ to the halides appears to generally decrease with increasing cation size. It is positive for three of the four salts studied. It is thought that the salts are preferentially solvated with water molecules. Thus the availability of water for the nonelectrolyte is decreased. Consequently the free energy of the latter may rise; the largest change to be expected is that with the cation having the highest charge density. Apparently the larger and more poorly hydrated ions have the opposite effect on the nonelectrolyte so that the free energy of the nonelectrolyte decreases and its solubility increases.¹⁵

For the chlorides, $\overline{\Delta H}_3$ and $\overline{\Delta S}_3$ decrease regularly with increasing cation size. The same trend in $\overline{\Delta S}_3$ was observed with nitrous oxide,^{15b} acetic acid,¹⁶ and appears to be present with ethyl acetate.³ The entropies of many more such systems will have to be investigated before the effect of ion size can be established. It may also be noted that there is a high degree of uncertainty in the lower values of $\overline{\Delta S}_3$ since they are calculated by the difference of two numbers of similar magnitude and varying accuracy.

For transfer to the perchlorates, all $\overline{\Delta H}_3$ and $\overline{\Delta S}_3$ are positive with the latter remaining constant. Their

(14) "Selected Values of Chemical Thermodynamic Properties," National Bureau of Standards Technical Note 270-1, Part I, p 116, U. S. Government Printing Office, Washington, D. C., Oct 1, 1965.

(15) For discussions related to the structure of ionic solutions and its effect on dissolved nonelectrolytes see (a) R. M. Diamond, *J. Phys. Chem.*, **67**, 2513 (1963); and (b) H. S. Frank and M. G. Evans, *J. Chem. Phys.*, **13**, 507 (1945).

(16) J. H. Stern and A. Hermann, to be published.

magnitude indicates a large positive contribution to $\overline{\Delta S}_3$ by the perchlorate ion. Assignment of the values and trends of these entropies in terms of changes in the solution structure and of ionic additive contributions to the thermodynamic properties¹¹ will not be attempted at this time.

The enthalpy of transfer fixes the temperature derivative of γ_3 , since

$$\frac{\partial \ln \gamma_3}{\partial T} = \frac{-\overline{\Delta H}_3}{RT^2} \quad (6)$$

When $\overline{\Delta H}_3$ is endothermic, γ_3 tends to decrease with increasing temperature. Two possibilities now arise depending on whether $\gamma_3 > 1$ (salting out) or $\gamma_3 < 1$ (salting in). In the former case the tendency toward

salting out will decrease with temperature and the nonelectrolyte–electrolyte system will tend toward the behavior of the nonelectrolyte–pure water system. With $\gamma_3 < 1$, the trend will be toward more salting in away from the behavior in the nonelectrolyte–pure water system.

When $\overline{\Delta H}_3$ is exothermic the trends are reversed. However, since all heats of transfer are small (less than 250 cal/mole), the change of γ_3 with temperature is very low. For example, a $\overline{\Delta H}_3$ of 100 cal/mole indicates that $\gamma_3^{26^\circ}/\gamma_3^{25^\circ}$ is only 0.998.

Acknowledgments. The authors wish to thank O. Brown and D. Fagerburg for assisting with this study and the U. S. Army Research Office (Durham) for financial assistance.

Polymer Nuclear Magnetic Resonance Spectroscopy. XII.¹ The Stereoregularity of Polyvinyl Chloride and Its Dependence on Polymerization Temperature

by F. A. Bovey, F. P. Hood, E. W. Anderson, and R. L. Kornegay

Bell Telephone Laboratories, Inc., Murray Hill, New Jersey 07971 (Received July 11, 1966)

The high-resolution nmr spectrum of poly- α - d_1 -vinyl chloride is interpreted in terms of tetrad configurational sequences of monomer units. The stereochemistry of polymers prepared over a 178° temperature range is determined. It is found that there is a tendency toward a more syndiotactic structure at lower temperature, but that the dependence on temperature is relatively small.

Introduction

High-resolution nmr spectroscopy has been applied to the study of the stereochemical configuration of polyvinyl chloride by a number of investigators.^{2–11} The nmr study of the model substances *meso*- and *dl*-2,4-dichloropentane^{12–15} and the three diastereoisomeric 2,4,6-trichloroheptanes^{15,16} has aided the understanding of the polymer spectra but has also produced some

confusion and disagreement. This has centered mainly about the interpretation of the β -methylene proton

(1) Previous paper in this series: F. A. Bovey, F. P. Hood, III, E. W. Anderson, and L. C. Snyder, *J. Chem. Phys.*, **42**, 3900 (1965).

(2) (a) U. Johnsen, *J. Polymer Sci.*, **54**, S6 (1961); (b) F. A. Bovey and G. V. D. Tiers, *Chem. Ind. (London)*, 1826 (1962).

(3) R. Chujo, S. Satoh, T. Ozeki, and E. Nagai, *J. Polymer Sci.*, **61**, S12 (1962).

spectrum, which appears as five peaks at 60 Mc/sec. Johnsen^{2a} interpreted these as two overlapping triplets centered at 7.78 and 7.96 τ (in chlorobenzene at 160°), corresponding to *meso* and *racemic* methylene groups, respectively. Tincher,⁴ being aware that the *meso* methylene groups are heterosteric,^{17,18} *i.e.*, that the protons in each are nonequivalent and should exhibit different chemical shifts, challenged Johnsen's view and interpreted the β -methylene resonance as the *AB* part of an *ABX*₂ spectrum with a triplet *racemic* resonance superimposed. This appeared to gain support from the observation of Doskocilova¹² that the methylene protons in *meso*-2,4-dichloropentane differ substantially in chemical shift (*ca.* 0.25 ppm in CCl₄). However, Bovey and Tiers^{2b} and Bovey, *et al.*,⁵ found that the decoupled β -proton spectrum and the poly- α -*d*₁-vinyl chloride spectrum showed singlets for the *meso*-methylene protons rather than the expected *AB* quartet, although small extraneous peaks appeared which were not obviously explainable. On the basis of 100-Mc/sec spectra, Tincher⁷ adopted Johnsen's interpretation and suggested that the extraneous peaks might arise from branch points. Thus, the *meso*- β -methylene protons must on this view be regarded as fortuitously equivalent in chemical shift although differing in chemical shift in the pentane model. Exactly analogous observations have been made for isotactic polystyrene and *meso*-2,4-diphenylpentane.¹ Shimanouchi, *et al.*,¹⁵ have found a difference of only 0.10 ppm for the methylene protons of the "isotactic" 2,4,6-trichloropentane, and this presumably would decrease rapidly toward zero as the chain is lengthened.

Yoshino and Komiyama⁸ have recently shown that the spectrum of poly- α -*cis*- β -*d*₂-vinyl chloride exhibits the ten different chemical shifts expected if one can discriminate all six of the β -methylene tetrad resonances.^{5,18} According to their assignment the central β -protons in all three of the *meso* tetrads are heterosteric, but the nonequivalence is substantial only for the *rmr* tetrad. The presence of geminal coupling tends to concentrate intensity at the center of the band, and this effect is accentuated by the fact that the *mean* chemical shift for each heterosteric pair of protons is nearly the same for all *meso* tetrads. This is also true for the one heterosteric and two homosteric *racemic* tetrads. Thus, tetrad resonances can be most clearly demonstrated in the α , β -*d*₂ polymer. We shall show that they also give rise to the small extra peaks in the poly- α -*d*₁-vinyl chloride spectrum.

In this paper, we interpret the 60-Mc/sec poly- α -*d*₁-vinyl chloride spectrum in terms of Yoshino's assignments, slightly modified. The calculated *racemic/meso* ratio is altered somewhat from that derived from

previous interpretations in terms of strict or near equivalence of the protons.^{2,5} Spectra of free-radical polymers prepared over a wide temperature range are then interpreted on the assumption of Bernoulli trial statistics to give the differential enthalpy and entropy for isotactic and syndiotactic monomer placement in chain propagation.

Experimental Section

The monomer is that described previously^{2b,5} and was polymerized in 10% (v/v) cyclohexanone solution in sealed ampoules at -78, 0, 50, and 100°; Co⁶⁰ γ irradiation was employed to initiate polymerization

Table I

Polymerization temp, °C	$[\eta]^{26^\circ}$	\bar{M}_v
0	0.352	13,000
50	0.130	3,550
100	0.065	<i>ca.</i> 1,440

at the two lowest temperatures and azobisisobutyronitrile at the others. Spectra were obtained at 150° using 10-15% (wt/vol) solutions of polymer in chlorobenzene containing 2% of tetramethylsilane as internal reference. A Varian HA-60 spectrometer was employed.

Molecular weights were estimated from intrinsic viscosity measurements in cyclohexanone using the

- (4) W. C. Tincher, *J. Polymer Sci.*, **62**, S148 (1962).
- (5) F. A. Bovey, E. W. Anderson, D. C. Douglass, and J. A. Manson, *J. Chem. Phys.*, **39**, 1199 (1963).
- (6) S. Satoh, *J. Polymer Sci.*, **A2**, 5221 (1964).
- (7) W. C. Tincher, *Makromol. Chem.*, **85**, 20 (1965).
- (8) T. Yoshino and J. Komiyama, *J. Polymer Sci.*, **B3**, 311 (1965).
- (9) O. C. Bockman, *ibid.*, **A3**, 3399 (1965).
- (10) B. Schneider, J. Stokr, D. Doskocilova, M. Kolinsky, S. Sykora, and D. Lim, *Intern. Symp. Macromol. Chem.*, Prague, 1965, preprint P 599.
- (11) K. C. Ramey, *J. Phys. Chem.*, **70**, 2525 (1966).
- (12) D. Doskocilova, *J. Polymer Sci.*, **B2**, 421 (1964).
- (13) D. Doskocilova and B. Schneider, *Collection Czech. Chem. Commun.*, **29**, 2290 (1964).
- (14) P. E. McMahon and W. C. Tincher, *J. Mol. Spectry.*, **15**, 180 (1965).
- (15) T. Shimanouchi, M. Tasumi, and Y. Abe, *Makromol. Chem.*, **86**, 43 (1965).
- (16) D. Doskocilova, J. Stokr, B. Schneider, H. Pivcova, M. Kolinsky, J. Petranek, and D. Lim, *Intern. Symp. Macromol. Chem.*, Prague, 1965, preprint P 5.
- (17) F. A. Bovey and G. V. D. Tiers, *J. Polymer Sci.*, **44**, 173 (1960).
- (18) F. A. Bovey, *Pure Appl. Chem.*, in press.
- (19) I. Rosen, P. H. Burleigh, and J. F. Gillespie, *J. Polymer Sci.*, **54**, 31 (1961).

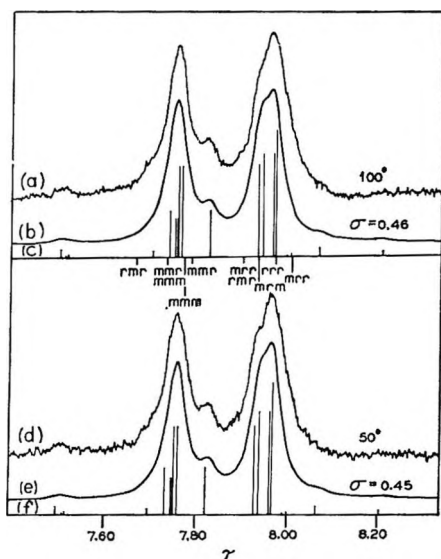


Figure 1. Calculated and experimental nmr spectra of poly- α - d_1 -vinyl chloride prepared at varying temperatures of polymerization: a, observed spectrum of 100° polymer; b, calculated spectrum of 100° polymer with line width of 2.5 cps; c, "stick" spectrum corresponding to b; d, observed spectrum of 50° polymer; e, calculated spectrum of 50° polymer with line width of 2.5 cps; f, "stick" spectrum corresponding to e. On the abscissa of spectra a, b, and c are shown the chemical shifts of the six tetrads. For the rrr and mrm tetrads, the markers occur at the actual line position. For the rmr, mrr, mmm, and mrr tetrads, the protons appear as AB quartets and the markers are at the true chemical shifts rather than the observed line positions.

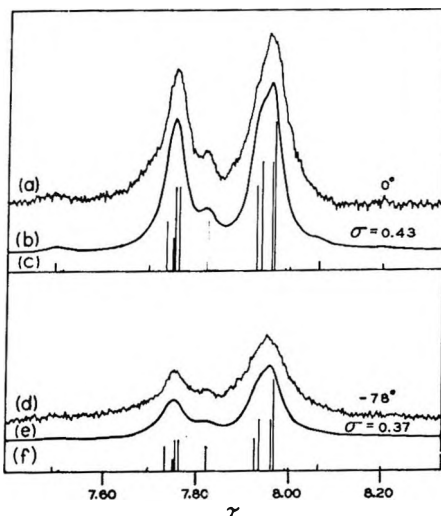


Figure 2. Nmr spectra of poly- α - d_1 -vinyl chloride: a, observed spectrum of polymer prepared at 0°; b, calculated spectrum of the 0° polymer with line width of 2.5 cps; c, "stick" spectrum corresponding to b; d, observed spectrum of -78° polymer; e, calculated spectrum of -78° with line width of 3.2 cps; f, "stick" spectrum corresponding to e.

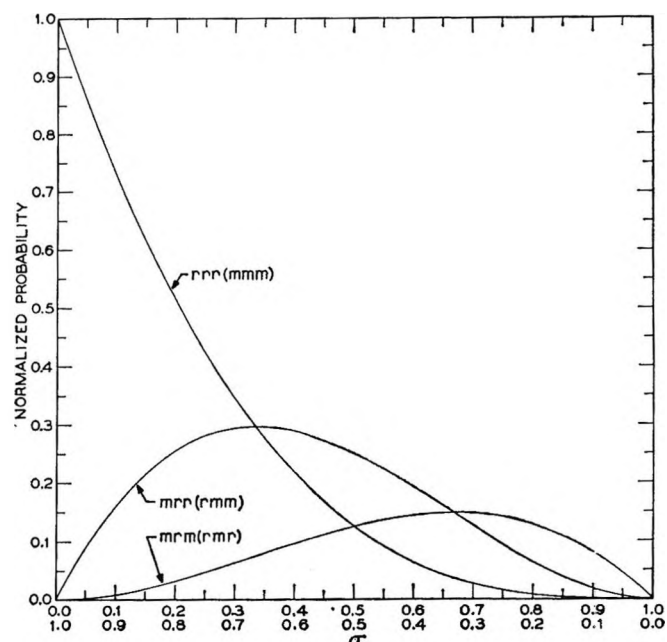


Figure 3. Tetrad probabilities for Bernoulli trial vinyl polymer chains. For rrr, mrr, and mrm, the upper σ scale is used; for mmm, rmm, and rmr the lower σ scale is used.

relationship of Rosen, *et al.*¹⁰ The results are given in Table I. The molecular weight of the polymer prepared at -78° was not determined as it was found to have become insoluble after a period of some months.

The calculated spectra (Figures 1 and 2) were obtained from a computer program which allows one to sum (in any desired proportion) any number of nmr spectra having a total of up to 10^4 transitions. The spectra are displayed by a Stromberg-Carlson 4020 microfilm printer as previously described.¹

Spectra were calculated for 14 values of σ ranging from 0.35 to 0.48. For each spectrum tetrad spectra were summed up in the proportions given by Figure 3, which is based on the assumption of Bernoulli trial statistics.^{1,5,8} A true line width of 2.5 cps was found to give the best match of calculated and observed spectra and was used for all spectra except that of the -78° polymer [Figure 2(e)] for which a line width of 3.2 cps was employed.

To obtain σ values, calculated and observed spectra can be matched in an approximate manner by visual inspection, but a more reliable estimate can be obtained by comparison of ratios of peak maxima in both the calculated and observed spectra. These are found to be insensitive to the assumed true line width over the probable experimental range of line widths. (It should be emphasized that the ratio of the low-field maximum to the sum of the heights of both peaks is

not equal to σ in these spectra; this would be true only if the spectra were much simpler, consisting of a single peak for each dyad.)

Experimental Results

In Figure 1 are shown spectra obtained for polymers prepared at -78 , 0 , 50 , and 100° . The upfield peak increases in intensity relative to the major low-field peak as the temperature of polymerization is decreased; the "extraneous" peak at 7.83τ does not appear to change greatly in intensity. In Figures 1 and 2, the observed spectra are compared to spectra calculated using the computer program described in the previous section. We have employed Yoshino's assignments, with minor modifications in the $7.9\text{-}\tau$ region, reasonable in view of the differing solvents used. The tetrad chemical shift assignments are as follows (in τ): rmr

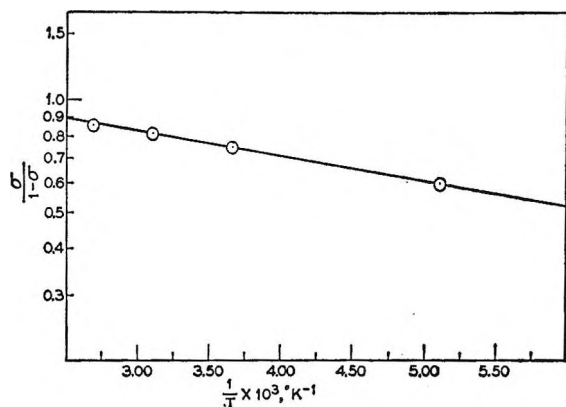


Figure 4. Arrhenius plot of $\sigma/(1 - \sigma)$ for poly- α - d_1 -vinyl chloride prepared at varying temperatures of polymerization (-78 to 100°).

H_a 7.67, H_b 7.89; mmr H_a 7.73, H_b 7.79; mmm H_a 7.73, H_b 7.77; mrm 7.92; rrr 7.96; mrr H_a 7.89, H_b 8.00. The geminal coupling of 14.0 cps (actually negative, but this does not affect these spectra) is taken from the results for *meso*-2,4-dichloropentane.^{12,13} The peak at 7.83τ is part of the rmr tetrad quartet. Similar quartets are constructed for the mmm, mmr, and mrr tetrads; the rrr and mrm tetrads are homosteric.^{8,18} We believe this interpretation accounts well for the observed resonances, although weak peaks corresponding to branch points are not necessarily excluded.⁷

The *meso* and *racemic* intensities were estimated by comparison to the calculated spectra in the manner described in the Experimental Section. From this analysis, the following values of σ were obtained:

-78° , 0.37; 0° , 0.43; 50° , 0.45; 100° , 0.46. From these data and eq 1 and 2²⁰

$$\Delta(\Delta H_p^\ddagger) = \Delta H_i^\ddagger - \Delta H_s^\ddagger = R \partial \ln [\sigma/(1 - \sigma)] / \partial (1/T) \quad (1)$$

$$\Delta(\Delta S_p^\ddagger) = \Delta S_i^\ddagger - \Delta S_s^\ddagger = R \ln [\sigma/(1 - \sigma)] + \Delta(\Delta H_p^\ddagger)/T \quad (2)$$

It is found that

$$\Delta(\Delta H_p^\ddagger) = 310 \pm 20 \text{ cal}$$

$$\Delta(\Delta S_p^\ddagger) = 0.6 \pm 0.1 \text{ eu}$$

The Arrhenius plot is shown in Figure 4.

Discussion

Fordham, *et al.*,²¹ estimated a value of 600 cal for $\Delta(\Delta H_p^\ddagger)$ for vinyl chloride propagation. Germar, *et al.*,²² have reported infrared and nmr data showing a much greater dependence of σ on temperature than we find in this study; the discrepancies are mainly in the data for polymers prepared at low temperatures. Both of these groups of investigators appear to have overestimated $\Delta(\Delta H_p^\ddagger)$. On the other hand, Bovey and Tiers,^{2b} on the basis of preliminary temperature dependence results, judged $\Delta(\Delta H_p^\ddagger)$ to be less than 200 cal, clearly an underestimate.

The only other free-radical polymer for which $\Delta(\Delta H_p^\ddagger)$ and $\Delta(\Delta S_p^\ddagger)$ have been reported is polymethyl methacrylate.^{20,23,24} These results do not agree perfectly but indicate values of approximately 1000 cal and 1 eu, respectively. For polyisopropyl and polymethyl acrylate values of *ca.* 0 cal for $\Delta(\Delta H_p^\ddagger)$ and *ca.* -1.4 eu for $\Delta(\Delta S_p^\ddagger)$ have been deduced.^{2b}

Polyvinyl chloride prepared at temperatures of *ca.* 100° approaches an atactic configuration. Most previous estimates have placed the proportion of syndiotactic sequences somewhat higher than this. The syndiotactic placement probability increases measur-

(20) F. A. Bovey, *J. Polymer Sci.*, **46**, 59 (1960).

(21) J. W. L. Fordham, P. H. Burleigh, and C. L. Sturm, *ibid.*, **20**, 251 (1956).

(22) H. Germar, K. H. Hellwege, and U. Johnsen, *Makromol. Chem.*, **60**, 106 (1963).

(23) T. G. Fox and H. W. Schnecko, *Polymer*, **3**, 575 (1962).

(24) Y. Kato and A. Nishioka, *Bull. Chem. Soc. Japan*, **37**, 1614 (1964).

(25) C. Schuerch, W. Fowells, F. P. Hood, and F. A. Bovey, unpublished observations. Matsuzaki, *et al.* (K. Matsuzaki, T. Uryu, K. Tameda, and M. Takeuchi, *Kogyo Kagaku Zasshi*, **68**, 1466 (1965), and private communication), find a *negative* $\Delta(\Delta H_p^\ddagger)$ for free radical methyl acrylate polymerization. This discrepancy requires further study.

ably as the polymerization temperature is decreased but hardly sufficiently to account for the alteration in polymer properties,²¹ particularly the enhanced crystallizability. Decreased branching^{2b,26,27} or decreased molecular weight⁹ may be the explanation, but this has not yet been clearly established.

Acknowledgment. The authors are indebted to Mrs. M. Y. Hellman for the molecular weight determinations.

(26) J. D. Cotman, Jr., *Ann. N. Y. Acad. Sci.*, **57**, 417 (1953).

(27) M. H. George, R. J. Grisenthwaite, and R. F. Hunter, *Chem. Ind. (London)*, 1114 (1958).

Electrical Conductance of Salts in Liquid Iodine. I. Iodide Donor Solutes¹

by Dorothy J. Bearcroft and Norman H. Nachtrieb

Institute for the Study of Metals and Department of Chemistry, The University of Chicago, Chicago, Illinois (Received July 18, 1966)

Molten iodine has a specific electrical conductance of 1.21×10^{-5} ohm⁻¹ cm⁻¹ at 140°, and its temperature coefficient is negative ($dx/dT = -4.25 \times 10^{-8}$ ohm⁻¹ cm⁻¹ deg⁻¹). Salts such as potassium iodide and thallos iodide are quite soluble in liquid iodine, and their behavior suggests that the transport mechanism is ionic in both the pure solvent and in solutions. A mechanism is proposed in which iodine dissociates into I⁺ and polyiodide ions, with the transfer of I⁻ from the latter to iodine molecules providing the majority carrier process. Iodide ion donors, such as potassium iodide and thallos iodide, are present in dissociated form, as ion pairs, and as higher ion multiples. Equilibrium constants for the electrolytic dissociation of iodine and the various equilibria involving the solute ions are given.

Introduction

Electrical conductance studies in liquid iodine began in 1835, when Inglis reported² his experiments and demonstrated them in a lecture to the Chemical Section of the British Association of Science at Bristol in the following year. The first important quantitative work was carried out in 1906 by Lewis and Wheeler,³ who measured the conductance of potassium iodide in liquid iodine. Since that time, the principal interest in the electrical transport properties of the liquid halogens and their solutions has been shown by Russian investigators, beginning in 1904 with Plotnikov^{4a} and continuing with Fialkov^{4b} and their co-workers until 1959.

Pure liquid iodine has a relatively low electrical conductivity, exceeding that of water, nevertheless, by

several orders of magnitude. Its dielectric constant is of intermediate magnitude (11.08 at 118.1°)⁵ and the halogen is consequently a moderately good solvent for polar molecules and some ionic salts. These include alkali metal iodides, but interestingly enough the other halides of these cations are only very sparingly soluble. For these reasons, iodine is an interesting solvent in which to study the equilibrium and transport properties of dissolved iodides.

(1) Based upon a dissertation submitted by D. J. Bearcroft in partial fulfillment of the requirements for the Ph.D. degree in chemistry.

(2) J. Inglis, *Phil. Mag.*, **7**, 441 (1835); **9**, 450 (1836).

(3) G. N. Lewis and P. Wheeler, *Z. Physik. Chem.*, **56**, 179 (1906).

(4) (a) V. A. Plotnikov, *ibid.*, **48**, 220 (1904); (b) J. A. Fialkov and F. D. Shevchenko, *Zh. Obshch. Khim.*, **22**, 1101 (1952).

(5) A. Jaglieski, *Bull. Intern. Acad. Polonaise, Ser. A*, 327 (1932).

Experimental Section

Apparatus. Conductance measurements were made by the conventional alternating current bridge method with a high-precision Leeds and Northrup Co. shielded Jones bridge and variable frequency oscillator, and with an oscilloscope for null detection. No frequency-dependent polarization effects were observed, and the data reported were obtained at 2000 cps. Dip-type cells of two different designs were used, one of which is illustrated in Figure 1. Construction was of Pyrex glass, with spirally wound tungsten electrodes sealed into glass lead-in tubes. There was no visual evidence of attack upon the electrodes by iodine, nor were there detectable changes in weight of test pieces in prolonged contact with molten iodine. A similar cell with tantalum electrodes gave results which were identical with those for tungsten electrodes. Cells with graphite electrodes performed erratically, however, and were discarded early in the study. The cells were equipped with a third leg having a porous fritted glass disk sealed into the lower portion. Its purpose was to facilitate the addition of solutes to the cell and to mix the result-

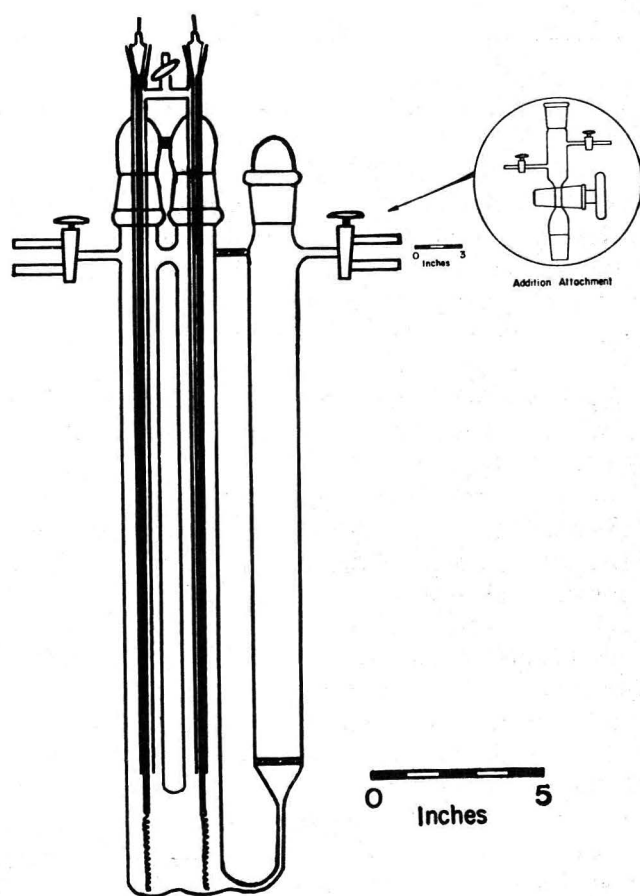


Figure 1. Conductance cell.

ing iodine solutions by repeated transfer through the fritted disk under applied nitrogen gas pressure.

Calibration of the cells was carried out at room temperature with 0.0100 *N* potassium chloride on the basis of Kohlrausch's⁶ values for the specific conductance. The centinormal solution was prepared from distilled water and recrystallized potassium chloride (Fisher Certified reagent grade). The cell constant for the cell which was used for most of the measurements was 0.3964 cm⁻¹. No correction was applied for the thermal expansion of the cell in its use with liquid iodine solutions because the uncertainty in the conductance of pure iodine is a much larger source of error.

The cells were heated by immersion in a stirred bath of molten salt composed of 17 mole % sodium nitrate, 30 mole % lithium nitrate, and 53 mole % potassium nitrate. Temperature was controlled by manual regulation of the current in the bath heater elements, and was readily maintained within close limits because of the high heat capacity of the salt bath. Nitrogen gas, used both to maintain an inert atmosphere above the liquid iodine solutions and to transfer them from the mixing compartment to the conductance cell, was purified by passage through a copper-diatomaceous earth column⁷ at 250° to remove oxygen and through concentrated sulfuric acid to remove moisture.

Materials. Early in the study, resublimed iodine of commercial reagent grade quality was found to leave a brown residue on the fritted glass disk of the mixing compartment, and spectrographic analysis showed it to contain boron, aluminum, magnesium, silicon, manganese, iron, nickel, copper, zinc, molybdenum, silver, tin, antimony, and lead. Their removal was accomplished by digestion of 1-lb lots of iodine with 1-2 l. of distilled water on a steam bath for 3 hr, following which the iodine was recovered by filtering the cooled solution, drying the crystals over phosphorus pentoxide, and finally subliming the solid. This procedure appeared to be effective in removing water-soluble and nonsublimable impurities, and brown residues were no longer seen on the glass frit. Further evidence of the efficacy of the purification method was obtained by concentrating the aqueous filtrate from the digestion of the iodine crystals and adding a small volume of silver nitrate solution. The resulting silver iodide and the residue obtained from evaporating the supernatant to dryness were examined spectrographically and found to contain boron, aluminum, magnesium, silicon, manganese, iron, nickel, copper, zinc, and tin in amounts

(6) F. Kohlrausch, L. Holborn, and H. Diesselhorst, *Wied. Ann. Physik*, **64**, 417 (1898).

(7) F. R. Meyer and G. Ronge, *Z. Angew. Chem.*, **52**, 637 (1939).

that corresponded within experimental uncertainty, with those found in the original brown residue. Sublimation of the purified iodine was carried out in an apparatus consisting of an electrically heated glass tube to contain the iodine crystals and a water-cooled finger condenser.

The source and state of purity of the solutes are as follows.

KI: Baker's Analyzed reagent grade was recrystallized from distilled water.

TI: MacKay 99.9% thallos iodide was used without purification for one experiment and high-purity thallium metal for another. Spectrographic analysis gave for TI: Cu, 0.01%, Pb, 0.01%, Mg, 0.001%, Si, 0.001%, and for TII: Ni, Cu, Zn, Ag, and In, 0.01% each.

AgI: Fisher Certified reagent grade. Spectrographic analysis gave Mg, Fe, and Cu, 0.01% each.

Cu: The source was copper wire, whose spectrographic analysis indicated 0.001% Ag.

Operation. For the conductance measurements, 400 g of purified iodine was weighed into the mixing compartment of the cell and melted by immersion of the vessel in the ternary eutectic salt bath at approximately 140°. Nitrogen gas was applied to transfer the iodine through the glass frit into the electrode compartment and allowed to continue bubbling to remove possible traces of moisture from the iodine. The direction of nitrogen flow was then reversed to return the iodine to the mixing compartment. This process of moving the iodine from one compartment to the other with nitrogen was alternated with resistance measurements until a constant value was obtained.

The cell design was highly satisfactory for experiments in which the solute dissolved readily in iodine. For those salts which dissolved slowly, it was less satisfactory because it was difficult to keep a large volume of liquid iodine in contact with the undissolved solute over a long period of time.

Results

Pure Iodine. Published values^{8,9} for the specific conductance of pure liquid iodine range from 0.6 to $6.0 \times 10^{-5} \text{ ohm}^{-1} \text{ cm}^{-1}$ at 140°. The average of the best values from this study is $1.21 \times 10^{-5} \text{ ohm}^{-1} \text{ cm}^{-1}$ at this temperature. Trace impurities may cause large changes in the specific conductance in either a positive or a negative direction, depending upon their nature. Although the iodine used in this study is believed to be of very high purity, there is no proof of this beyond the fact that the brown residue found in commercial sublimed reagent grade material is absent from the purified iodine and the recovery of the metallic ele-

Table I: Temperature Dependence of Liquid Iodine Conductance

T , °C	R , ohms	κ , ($\text{ohm}^{-1} \text{ cm}^{-1}$) $\times 10^5$
139.0	33,310	1.1971
141.0	33,554	1.1813
141.8	33,705	1.1759
142.5	33,870	1.1703
143.0	33,934	1.1681
143.8	34,014	1.1653
144.3	34,150	1.1607
146.0	34,311	1.1552
Iodine Mixed with Nitrogen		
145.9	34,163	1.1602
146.2	34,131	1.1613
143.8	33,906	1.1690
143.0	33,825	1.1718
142.8	33,799	1.1727
142.1	33,710	1.1758
141.6	33,633	1.1785
140.0	33,463	1.1845
138.9	33,365	1.1880
Iodine Mixed with Nitrogen		
138.6	33,380	1.1874
137.0	33,233	1.1927

ments in this residue in the wash water as described earlier.

Table I and Figure 2 show the temperature dependence of the specific conductance of liquid iodine in a typical experiment over the interval 137–146°, with an average value of $-0.00425 \times 10^{-5} \text{ ohm}^{-1} \text{ cm}^{-1} \text{ deg}^{-1}$ for the temperature coefficient. Rabinowitsch's value ($-0.0237 \times 10^{-5} \text{ ohm}^{-1} \text{ cm}^{-1} \text{ deg}^{-1}$) is considerably larger.

Potassium Iodide Solutions. The potassium iodide-iodine system was thoroughly studied by Lewis and Wheeler³ with a cell of different design. Table II shows the present results, along with the low concentration data from one experiment of Lewis and Wheeler. The agreement between the two sets of data is excellent. Potassium iodide is very soluble in liquid iodine, and is the best conductor studied to date.

Thallium(I) Iodide Solutions. The thallium-iodine system was studied using both thallium(I) iodide and thallium metal. The data are presented in Table III, and the small discrepancy between the results for the two solutes in the low concentration region is probably due to an error in the concentration of thallium(I) io-

(8) M. Rabinowitsch, *Z. Physik. Chem.*, **119**, 83 (1926).

(9) W. A. Plotnikov, J. A. Fialkov, and W. P. Tschalij, *ibid.*, **A172**, 307 (1935).

dide in the thallium metal run. Thallium metal oxidizes readily in air, and even with rapid handling a sample of a few milligrams acquires an appreciable oxide layer.

Thallium(I) iodide is much less soluble in liquid iodine than is potassium iodide. The concentration given for point number eight of the thallium(I) iodide run corresponds to the total quantity of TII added, but not all of the salt dissolved. From an extrapolation of

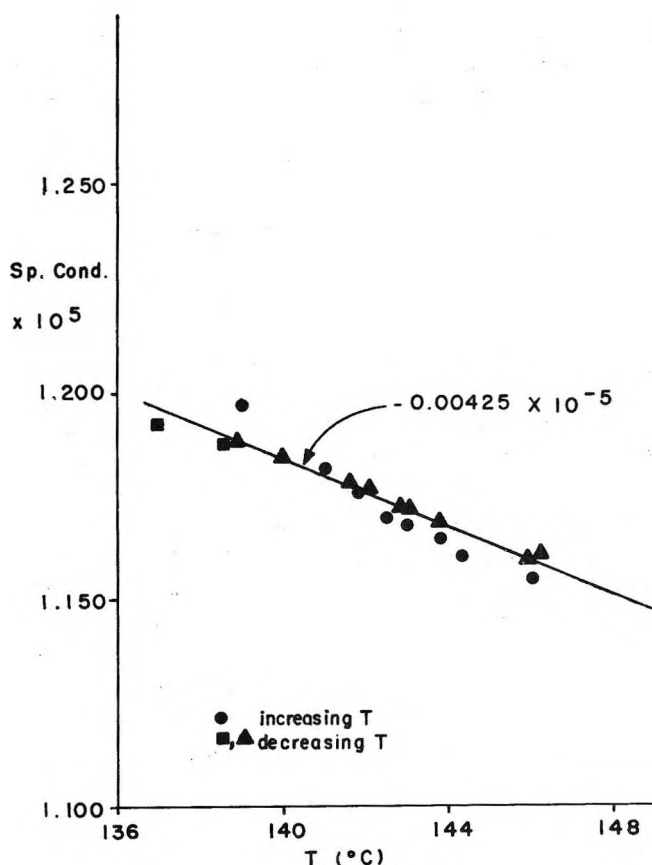


Figure 2. Specific conductance of liquid iodine vs. temperature.

the conductance curve as well as a visual estimate of the amount of undissolved thallium(I) iodide, the solubility was estimated to be $2.34 \pm 0.08 \times 10^{-3}$ mole fraction at 140° .

Silver Iodide Solutions. Silver iodide is very slightly soluble in liquid iodine, and dissolves at a very slow rate. Two attempts were made to obtain quantitative data for the silver iodide-iodine system and the results, which can be considered as only semiquantitative, are shown in Figure 3. At 140° , the specific conductances corresponding to 0, 1.24×10^{-4} , and 3.30×10^{-4} mole of AgI/l. of solution are: $\kappa = 1.246 \times 10^{-5}$, 1.368×10^{-5} , and $1.552 \times 10^{-5} \text{ ohm}^{-1} \text{ cm}^{-1}$, respectively.

Table II: Conductance of Potassium Iodide-Iodine Solutions at 140°

Wt of KI(g)	Wt of I_2 (g)	C_{KI} , M	κ , ($\text{ohm}^{-1} \text{ cm}^{-1}$) $\times 10^5$
0	400.0	0	1.676
0.0733	400.0	4.286×10^{-3}	11.99
0.1673	400.0	9.778×10^{-3}	22.23
0.4961	400.0	2.896×10^{-2}	66.27
0.8190	400.0	4.775×10^{-2}	129.9

Data of Lewis and Wheeler^a

0	100	0	2.16
0.0135	100	3.158×10^{-3}	9.70
0.0246	100	5.751×10^{-3}	14.1
0.0471	100	1.101×10^{-2}	24.0
0.0688	100	1.608×10^{-2}	34.0
0.0901	100	2.105×10^{-2}	45.5
0.206	100	4.804×10^{-2}	133.0

^a G. N. Lewis and P. Wheeler, *Z. Physik. Chem.*, **48**, 220 (1906).

Table III: Conductance of Thallous Iodide-Iodine Solutions at 140°

Wt of Tl(g)	Wt of I_2 (g)	C_{TlI_2} , M	κ , ($\text{ohm}^{-1} \text{ cm}^{-1}$) $\times 10^5$
0	400.0	0	1.180
0.0015	405.6	7.027×10^{-5}	1.401
0.0025	409.1	1.161×10^{-4}	1.548
0.0556	413.9	2.552×10^{-3}	4.042
0.0871	417.5	3.963×10^{-3}	5.649
0.2040	422.8	9.165×10^{-3}	10.66
0.3573	428.1	1.585×10^{-2}	16.84
0.4958	432.9	2.174×10^{-2}	22.64
0.7381	436.1	3.211×10^{-2}	34.60

Wt of TII(g)	Wt of I_2 (g)	C_{TII} , M	κ , ($\text{ohm}^{-1} \text{ cm}^{-1}$) $\times 10^5$
0	400.0	0	1.230
0.0103	405.2	2.987×10^{-4}	1.903
0.0236	408.8	6.764×10^{-4}	2.528
0.0700	412.6	1.987×10^{-3}	4.254
0.1378	416.5	3.879×10^{-3}	6.261
0.2526	420.6	7.036×10^{-3}	9.142
0.4396	426.8	1.207×10^{-2}	13.42
0.7525	431.1	2.043×10^{-2}	21.15
1.4382	437.9	3.840×10^{-2}	40.77

Copper(I) Iodide Solutions. A small sample of high-purity copper (6.7 mg) was added to 400 g of liquid iodine. After 2 hr, the copper was still plainly visible on the frit, and the conductance had increased by only 1%. No attempt was made to prepare copper(I) iodide, but presumably it would behave in much the same manner as silver iodide.

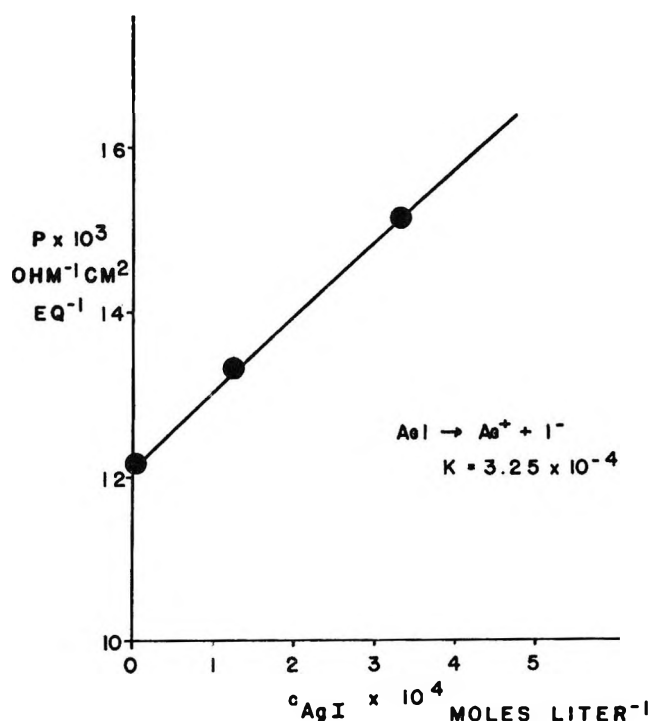


Figure 3. Conductance of silver iodide-iodine solutions at 140°.

Antimony(III) Iodide Solutions. The antimony-iodine system was previously studied by Plotnikow, *et al.*,¹⁰ but not at low concentrations. Their data were expressed in terms of antimony(V) iodide. The phase diagram of the antimony-iodine system¹¹ does not show the existence of antimony(V) iodide, however, and if it exists in liquid iodine its concentration must be small relative to antimony(III) iodide. In addition, when the conductance cell containing the antimony-iodine solution was allowed to stand overnight, orange crystals appeared on the vessel walls. The color and melting point of these crystals corresponded to those reported for antimony(III) iodide.¹¹ Conductivity data for this system are listed in Table IV.

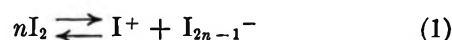
Table IV: Conductance of Antimony(III) Iodide-Iodine Solutions at 140°

Wt of Sb(g)	Wt of I ₂ (g)	C _{SbI₃} , M	κ , (ohm ⁻¹ cm ⁻¹) × 10 ⁴
0	400.0	0	1.038
0.0035	400.0	2.792×10^{-4}	1.035
0.0067	400.0	5.343×10^{-4}	1.036
0.0145	400.0	1.156×10^{-3}	1.042
0.0257	400.0	2.050×10^{-3}	1.044
0.0535	400.0	4.267×10^{-3}	1.050
0.0630	400.0	5.025×10^{-3}	1.054

Sulfur Solutions. At the conclusion of each run, the electrode assembly was removed from the cell and the molten iodine was poured into an ice-filled crystallizing dish. The cell was then flamed to remove all but the smallest traces of iodine. The remaining iodine was removed with an aqueous solution of sodium thiosulfate. As a result of this procedure, free sulfur was often formed, and although care was exercised to remove it, it seemed desirable to determine the effect of sulfur on the electrical conductivity of iodine. The sulfur used in this study was prepared from sodium thiosulfate. It was added to iodine in the amounts indicated in Table V, and measurements were made in the normal manner. The solubility of sulfur in liquid iodine was found to be $(4.5 \pm 0.2) \times 10^{-5}$ mole fraction at 139° on the basis of S₈ molecules. At this concentration, the specific conductance has increased by 9.4%. On this basis, it appears that the cell-cleaning procedure is unlikely to have introduced large errors into the measurement of the conductances of other solutes.

Discussion

The foregoing experiments may be interpreted in a self-consistent manner on the basis of a simple ionic model. No direct evidence exists concerning the conduction mechanism in pure liquid iodine, but the effects of dissolved salts upon the electrical conductance strongly suggest that the solvent dissociates into positive and negative ions. Conceivably, an electron hopping process might be involved, but in the absence of Hall coefficient or carrier injection data to support such a speculation, we propose a conduction mechanism in which the charge carriers are cations and anions derived from equilibria of the type



The I₃⁻ ion, with $n = 2$, is probably the stablest polyiodide species in liquid iodine as it is in aqueous solution, but I₅⁻, I₇⁻, and I₉⁻ are known in the crystalline state and may exist at low concentration or in the form of weak aggregates in the melt. There appears to be no evidence for polynuclear iodine cations.

We imagine that anionic species dominate the charge transport process by a Grotthuss-like mechanism, in which I⁻ is transferred from I_{2n-1}⁻ ions to neighboring I₂ molecules on collision. It seems reasonable to suppose that polyiodide anions have considerably higher apparent mobilities than cations if such a transfer process is involved, and we accordingly assume

(10) V. A. Plotnikow, J. A. Fialkov, and W. P. Tschalij, *Zh. Obshch. Khim.*, **6**, 273 (1936).

(11) F. M. Jager and H. J. Doornbosch, *Z. Anorg. Chem.*, **75**, 261 (1912).

that to a first approximation the mobilities of all cations are small by comparison and equal among themselves. To the extent that larger anionic aggregates than I_3^- are present, the translational entropy for eq 1 will be negative. Even though they are present at much lower concentration than I_3^- , they may account for the small negative temperature coefficient of the conductance which is found. This is not an essential part of our argument, however, and for simplicity we need only consider the ionic dissociation of iodine to be formally



just as in aqueous solution, where the degree of hydration of the proton is neglected in mass law calculations. The dissociation constant for eq 2 is designated K .

For convenience, we define a quantity, P , to be $10^3 \kappa$. Then for pure iodine

$$P_{I_2} = P^+ + P^- = [I^+] \Lambda_{I^+} + [I^-] \Lambda_{I^-} \quad (3)$$

where the Λ 's are the ionic equivalent conductances (approximated by their limiting values, Λ_0) and the square bracketed quantities refer to concentrations in equivalents per liter. Tables II-V list concentrations which have been calculated on the assumption that the solution densities do not differ appreciably from that of pure iodine (3.884 g ml⁻¹ at 140°).¹² Since in pure

Table V: Conductance of Sulfur-Iodine Solutions at 140°

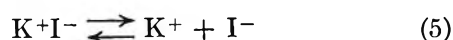
Wt of S(g)	Wt of I ₂ (g)	Mole fraction of S ₂ /(S ₂ + I ₂)	κ , (ohm ⁻¹ cm ⁻¹) × 10 ⁶
0	400.0	0	8.72
0.0013	400.0	3.22×10^{-6}	8.74
0.0051	400.0	1.26×10^{-5}	8.78
0.0180*	400.0	4.45×10^{-5}	9.54

* Solubility limit.

iodine, $[I^+] = [I^-]$, it follows that

$$P_{I_2} = [I^-](\Lambda_{0I^+} + \Lambda_{0I^-}) = [I^-] \Lambda_{0I_2} \quad (4)$$

We may now evaluate Λ_{0I_2} and K by use of the conductance data for very dilute solutions of potassium iodide in iodine on the basis of the previous assumption that all cation equivalent conductances are essentially equal (specifically, $\Lambda_{0K^+} = \Lambda_{0I^+}$), and that potassium iodide ion pairs are in equilibrium with dissociated potassium ions and iodide ions



The conductance due to potassium iodide is equal to the sum of the conductances of K^+ and I^-

$$P_{KI} = P_{K^+} + P_{I^-} =$$

$$[K^+]_{KI} \Lambda_{0K^+} + [I^-]_{KI} \Lambda_{0K^+} = [I^-]_{KI} \Lambda_{0KI} \quad (6)$$

Moreover, on the assumption that $\Lambda_{0K^+} = \Lambda_{0I^+}$, $\Lambda_{0KI} = \Lambda_{0I_2}$. The total conductance of a solution of potassium iodide in iodine is then

$$P = P_{KI} + P_{I_2} =$$

$$\Lambda_{0I_2}([I^-]_{I_2} + [I^-]_{KI}) = \Lambda_{0I_2}[I^-]_{total} \quad (7)$$

From the law of mass action

$$[I^+][I^-]_{total} = K[I_2] = K_2 \quad (8)$$

$$[K^+][I^-]_{total}/[K^+I^-] = K_{KI} \quad (9)$$

Material balance requires that

$$[I^-]_{total} = [I^-]_{I_2} + [I^-]_{KI} \quad (10)$$

$$[K^+I^-] + [K^+] = c_{KI} \quad (11)$$

$$[K^+] = [I^-]_{KI} \quad (12)$$

$$[I^+] = [I^-]_{I_2} \quad (13)$$

Equations 8, 10, and 13 lead to

$$K_2 = [I^-]_{I_2}([I^-]_{I_2} + [I^-]_{KI}) \quad (14)$$

Equations 9, 10, 11, and 12 lead to

$$K_{KI} = \frac{[I^-]_{KI}([I^-]_{I_2} + [I^-]_{KI})}{c - [I^-]_{KI}} \quad (15)$$

To simplify, let $x = [I^-]_{I_2} + [I^-]_{KI} = [I^-]_{total}$, and $y = [I^-]_{KI}$. Then eq 7, 14, and 15 become

$$P = x \Lambda_{0I_2} \quad (16)$$

$$x(x - y) = K_2 \quad (17)$$

$$xy/(c - y) = K_{KI} \quad (18)$$

Eliminating x and y from (18) by means of (16) and (17) gives

$$K_{KI} = \frac{P[P^2 - \Lambda_{0I_2}^2 K_2]}{\Lambda_{0I_2}^2 [cP\Lambda_{0I_2} - P^2 + \Lambda_{0I_2}^2 K_2]} \quad (19)$$

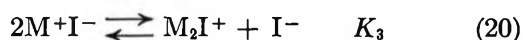
For pure iodine, $y = 0$, and $K_2 = x^2 = P_0^2/\Lambda_{0I_2}^2$. Our best value for $P_0 = 1.21 \times 10^{-2}$ ohm⁻¹ cm² l.⁻¹, and hence $K_2 = 1.464 \times 10^{-4}/\Lambda_{0I_2}^2$. Equation 19 may now be evaluated for K_{KI} and Λ_{0I_2} from the data in Table I. This leads to $K_2 = 1.047 \times 10^{-7}$, $K_{KI} = 8.49 \times 10^{-5}$, and $\Lambda_{0I_2} = 37.4$ ohm⁻¹ cm² equiv⁻¹. For this purpose, values of c and P in the lowest concentration range were used.

(12) T. Nayder. *Bull. Intern. Acad. Polonaise, Ser. A*, 231 (1934).

Table VI: Ion-Pair Dissociation Constants (K_1) in I_2 at 140°

$M^+I^- \rightleftharpoons M^+ + I^-$	
KI	8.49×10^{-3}
TlI	1.24×10^{-3}
AgI	3.25×10^{-4}
SbI ₃	5.39×10^{-7}

This interpretation of the conductance measurements applies to all solutes of the type M^+I^- that furnish I^- ion by dissociation. Table VI lists the dissociation constants obtained for salts at low concentration in liquid iodine at 140° . At higher concentrations, these solutes exhibit positive deviations of conductance, indicating that further ion-producing equilibria come into prominence



Thus in the case of potassium iodide, the conductance data may be fitted to higher concentrations by considering three simultaneous equilibria

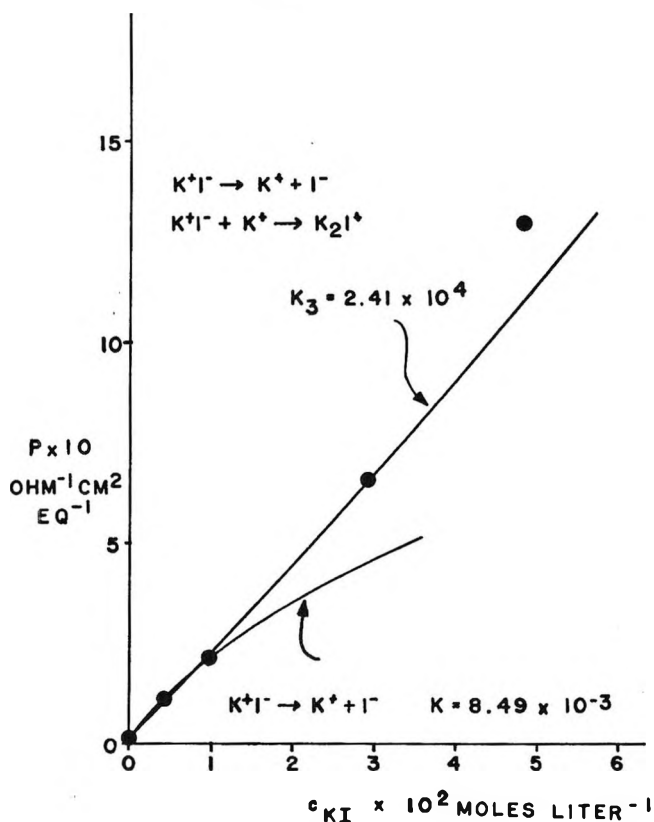
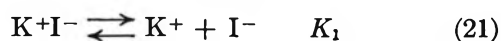
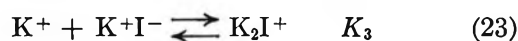
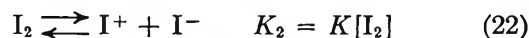


Figure 4. Conductance of potassium iodide-iodine solutions at 140° .



Combining these equilibrium equations gives

$$K_3 = \frac{(K_1 - x)[K_1(cx - x^2 + K_2) - x^3 + K_2x]}{K_1(cx - 2x^2 + 2K_2)^2} \quad (24)$$

Equation 24 does not yield constant values for K_3 when these are evaluated from the K_1 values of Table VI, together with the total iodide ion concentration, x , derived from the conductance data. In all probability this is because yet another ion-pair equilibrium should be considered



We have not attempted to include this equilibrium, because even eq 24 is fourth degree in x , and the data probably do not warrant this test.

Instead, we have noted that eq 24 may be rewritten in the form

$$c^2 = \frac{c}{x} \left[4(x^2 - K_2) + \frac{(K_1 - x)}{K_3} \right] + \left[\frac{4(x^2 - K_2)^2}{x^2} + \frac{(K_1^2 - x^2)(x^2 - K_2)}{K_1K_3x^2} \right] = c \quad (26)$$

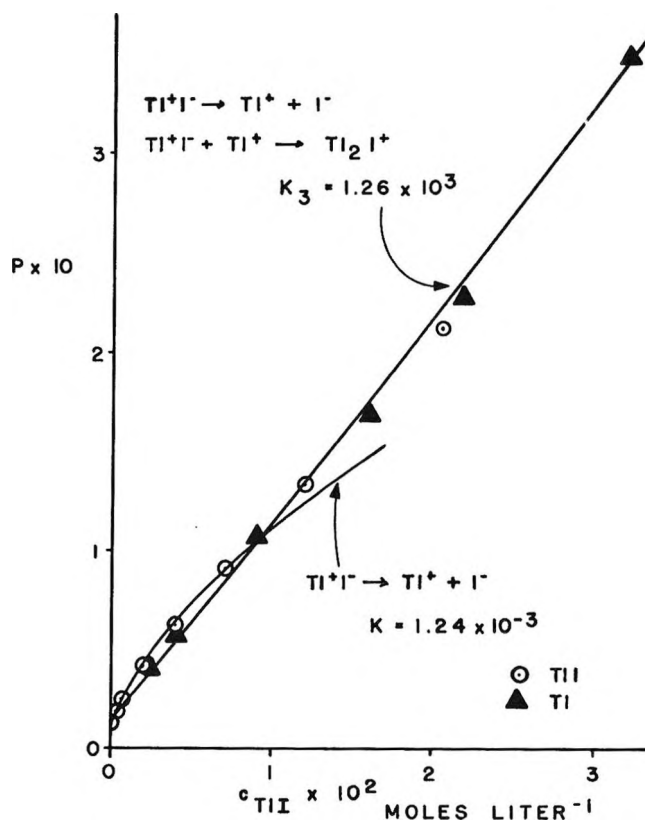


Figure 5. Conductance of thallous iodide-iodine solutions at 140° .

whose asymptotic behavior at low solute concentration is tractable. In pure iodine, $x^2 = K_2$, and eq 26 reduces to $c^2 - c(K_1 - x)/K_3x = 0$. The roots of this equation are $c = 0$ and $c = (K_1 - x)/K_3x$. In pure iodine, the concentration of the dissolved species is clearly zero, so that for a comparison of the theoretical and experimental conductance curves, those roots of eq 26 must be selected which converge to zero as x^2 approaches K_2 . With this restriction in mind and with the K_1 's tabulated in Table VI, various values of K_3 were used to calculate theoretical conductance curves. Such curves were little better than those for the K_1 equilibria alone.

On the other hand, if both roots of eq 26 are required to converge to zero, then $(K_1 - x)$ must converge to zero and K_1 must equal $K_2^{1/2}$. When K_3 values are chosen for each system with this restriction, the agreement between the calculated and experimental data is reasonably good. Triple ion formation constants (K_3) for K_2I^+ and Tl_2I^+ in iodine at 140° are 2.41×10^4 and

1.26×10^3 , respectively, and the curves of Figures 4 and 5 were constructed from them. It should be noted that for both systems the limiting behavior at very low salt concentration is adequately represented by the simple ion-pair equilibrium: $M^+I^- \rightleftharpoons M^+ + I^-$. This is also true for silver iodide, whose solubility in iodine is very slight (Figure 3). At higher concentrations of potassium iodide or thallos iodide, the calculated curves which include the next stage of ion pairing (K_3) follow the experimental data quite well. At still higher salt concentrations, the experimental data lie above the calculated curves, and suggest that other ion-pair equilibria should be included.

Acknowledgment. This study was supported in part of the Air Force Office of Scientific Research under Grant Number AF-AFOSR-624-64 with the University of Chicago and by the Advanced Research Projects Agency under Contract No. SD-89.

Relaxation Spectra of Some Uranyl and Vanadyl Complexes in Aqueous Solution^{1a}

by P. Hurwitz^{1b} and K. Kustin

Department of Chemistry, Brandeis University, Waltham, Massachusetts 02154 (Received July 18, 1966)

The temperature-jump method has been used to determine the kinetics of the reaction of UO_2^{2+} ion with monochloroacetate, sulfate, acetate, and thiocyanate and of VO^{2+} ion with thiocyanate. The UO_2^{2+} ion forms higher order complexes with the first three of these ligands, whereas for uranyl and vanadyl only the thiocyanate monocomplex is important. Bimolecular rate constants at 20° and the given ionic strength for formation of the 1-1 uranyl complex are: SO_4^{2-} , $180 M^{-1} \text{sec}^{-1}$ at $\mu = 0.15 M$; $\text{ClCH}_2\text{COO}^-$, $110 M^{-1} \text{sec}^{-1}$ at $\mu = 0.15 M$; SCN^- , $290 M^{-1} \text{sec}^{-1}$ at $\mu = 1.2 M$; CH_3COO^- , $1050 M^{-1} \text{sec}^{-1}$ at $\mu = 0.15 M$. For the reaction between vanadyl and thiocyanate the rate constant is $160 M^{-1} \text{sec}^{-1}$ at 20° and $\mu = 0.2 M$. Substitution labilizes the water molecules still bound to the oxo ion, so that further substitution is speeded up. The effect, however, is not as pronounced as for divalent transition metal ions. Complexation rates for uranyl ion are most nearly typical of 3+ ions. No clear-cut correlation between the formation rate constant and ligand basicity could be demonstrated for either cation. The principal effect the oxo ion has on the rate of complexation is exerted by the rather high positive charge density on the metal, especially for uranyl. The site of nucleophilic attack on vanadyl may play a role in the kinetics of substitution.

Introduction

Many aspects of the aqueous chemistry of simple metal ions are shared by oxo ions. One of these features is the general rapidity of ligand substitution into the inner hydration sphere. Another characteristic of metal ions exhibited even more pronouncedly by oxo ions is the formation of polynuclear species. In the past, these effects acted as deterrents to systematic rate studies of these ions in solution although their equilibrium properties and chemistry in other phases have been thoroughly examined.² Recently the temperature-jump,³ dissociation field,⁴ and pressure-jump⁵ techniques have been used to expand our understanding of the dynamical aspects of equilibrium in uranyl and vanadyl systems.

By utilizing the temperature-jump method and working for the most part at low pH values in order to suppress formation of polynuclear species, it has been possible to gain some further information on the kinetics of complexation of these two oxo ions. In particular, the following reactions were studied: uranyl ion with monochloroacetate, sulfate, acetate, and thiocyanate; and vanadyl with thiocyanate. Fortunately, the stability constants for all of the systems are well described

by Ahrland for the uranyl complexes⁶⁻¹⁰ and by Garner for the vanadyl complex of thiocyanate.¹¹

Experimental Section

The temperature-jump apparatus used for the present experiments is described elsewhere.¹² The rate con-

(1) (a) This investigation was supported in part by Public Health Service Research Grant GM-08893-04 from the National Institute of General Medical Sciences, Public Health Service, and in part by National Science Foundation Grant GP-1745. (b) Department of Chemistry, University of Massachusetts, Boston, Mass. 02116.

(2) F. A. Cotton and G. Wilkinson, "Advanced Inorganic Chemistry," Interscience Publishers, Inc., New York, N. Y., 1962, Chapter 32.

(3) M. P. Whittaker, E. M. Eyring, and E. Dibble, *J. Phys. Chem.*, **69**, 2319 (1965).

(4) J. F. Spinner and A. Patterson, Jr., *ibid.*, **69**, 513 (1965).

(5) H. Strehlow and H. Wendt, *Inorg. Chem.*, **2**, 6 (1963).

(6) S. Ahrland, *Acta Chem. Scand.*, **3**, 783 (1949).

(7) S. Ahrland, *ibid.*, **5**, 1151 (1951).

(8) S. Ahrland, *ibid.*, **5**, 199 (1951).

(9) S. Ahrland, *ibid.*, **3**, 1067 (1949).

(10) E. W. Davies and C. B. Monk, *Trans. Faraday Soc.*, **53**, 442 (1957).

(11) S. C. Furman and C. S. Garner, *J. Am. Chem. Soc.*, **73**, 4530 (1951).

(12) P. Hurwitz and K. Kustin, *Inorg. Chem.*, **3**, 823 (1964).

Table I:^a Metal and Metal Indicator Blank Experiments^b

[UO ₂ ²⁺]	[KNO ₃]	pH	λ , m μ	Result	Indicator, type and concn
0.025	0.05	1.0	410	No chemical relaxation	UO ₂ ²⁺
0.025	0.05	2.0	410	No chemical relaxation	UO ₂ ²⁺
0.025	0.05	4.1	410	No chemical relaxation	UO ₂ ²⁺
0.01	0.03	1.70	525	No chemical relaxation	Metacresol purple, total concn = 2×10^{-5}
0.01	0.03	2.30	525	No chemical relaxation	Metacresol purple, total concn = 3×10^{-5}
0.01	0.03	2.70	525	$\tau = 5.6$ msec	Benzyl orange, total concn = 2×10^{-5}
0.01	0.03	4.0	590	$\tau = 5.3$ msec	Bromochlorophenol blue, total concn = 2×10^{-5}
[VO ²⁺] ^c					
0.056	...	1.55	580	No chemical relaxation	VO ²⁺
0.051	...	1.55	600	No chemical relaxation	Thymol blue, total concn = 2×10^{-5}

^a All concentrations in *M*. ^b Control experiments with ligand showed no observable effects. ^c No KNO₃ required.

stants are given for a temperature of $20^\circ \pm 1$. Although individual oscillograms could be evaluated to yield relaxation times with a relative error of $\pm 10\%$ the uncertainties inherent in the treatment of the data extend the error range to $\pm 25\%$ in many cases.

As in most applications of the temperature-jump method the change in absorbancy is oscilloscopically recorded and photographed.¹³ In this case, however, the shift to the new equilibrium could be followed directly without employing coupled indicators by utilizing the fact that each of the various complexes absorbed considerably more light at a given wavelength than did the uncomplexed ion. For uranyl, the monochloroacetate complexes were followed at 436 m μ , the sulfate complexes at 440 m μ , the acetate complexes at 475 m μ , and the thiocyanate complex at 500 m μ . For vanadyl, detection was carried out at 580 m μ .

Reagent grade uranyl nitrate hexahydrate, monochloroacetic acid, and sodium acetate were purchased from the Fisher Scientific Co., reagent grade potassium thiocyanate from Baker and Adamson Products, and reagent grade potassium sulfate from the J. T. Baker Chemical Co. The uranyl salt required drying in a desiccator over concentrated sulfuric acid before it could be used.

Each solution was prepared by weighing out appropriate amounts of metal nitrate and ligand, then diluting to a known volume with doubly distilled water. An inert electrolyte such as potassium nitrate was not required to adjust the ionic strength of each reaction mixture because the concentrations of the reactants were sufficiently high to ensure proper Joule heating in the cell. (In many cases, the minimum concentration

of reactants which produced a detectable effect resulted in an ionic strength greater than 0.1 *M*. Since these concentrations differed from ligand to ligand uniformity of ionic strength could not be achieved. The effect of this inconsistency on the final conclusions is not significant.) Each solution was brought to the desired pH by dropwise addition of dilute NaOH and/or dilute HNO₃.

The importance of blank or control experiments in systems where hydrolysis and polymerization may occur cannot be overemphasized. For this reason, coupled pH indicators as well as the metal ions themselves were followed in the blank determinations. The results are given in Table I. It will be noted that an effect was detected for uranyl at pH 3 and higher. This effect (which was in agreement with a previous observation³) did not interfere with the evaluation of the relaxation times in the pH range of this study since it was significantly shorter than the relaxational process associated with complexation.

Results

The treatment of relaxation data with specific reference to multi-step metal-ligand association has been given by Hammes and Steinfeld.¹⁴ In the following we shall indicate the salient features of this analysis, pointing out the specific instances in which the conditions of this study necessitate a change in the mathe-

(13) M. Eigen and L. De Maeyer in "Techniques of Organic Chemistry," Vol. VIII, Part 2, A. Weissberger, Ed., John Wiley and Sons, Inc., New York, N. Y., 1963.

(14) G. G. Hammes and J. I. Steinfeld, *J. Am. Chem. Soc.*, **84**, 4639 (1962). Cf. also ref 13.

Table II:^a Relaxation Spectra of Vanadyl^b and Uranyl^c Thiocyanate at 20°

[VO ²⁺] ₀	[SCN ⁻] ₀	[VO ²⁺]	[SCN ⁻]	[VOSCN ⁺]	pH	τ_{obs} , msec	k_1 , M ⁻¹ sec ⁻¹	k_{-1} , sec ⁻¹
0.0502	0.0499	4.55×10^{-2}	4.52×10^{-2}	4.72×10^{-3}	1.70	11.1	171	74
0.0502	0.0506	4.54×10^{-2}	4.58×10^{-2}	4.80×10^{-3}	0.97	10.6	179	78
0.0301	0.0302	2.83×10^{-2}	2.84×10^{-2}	1.85×10^{-3}	1.70	15.6	130	57
$pK_L \ll 1$, $K_{ML} = 2.3$; ^d ref 11						Average: 160 ± 20 ; 70 ± 8		
[UO ₂ ²⁺] ₀	[SCN ⁻] ₀	[UO ₂ ²⁺]	[SCN ⁻]	[UO ₂ SCN ⁺]				
0.2784	0.5264	0.1396	0.1876	0.1388	2.00	7.4	260	49
0.0111	0.0131	1.0×10^{-2}	1.2×10^{-2}	1.1×10^{-3}	2.00	18.9	251	47
0.2784	0.5257	0.1398	0.1871	0.1386	2.00	5.9	325	51
0.2784	0.5257	0.1398	0.1871	0.1386	2.65	6.1	316	50
$pK_L \ll 1$, $K_{ML} = 5.3$; ref 10						Average: 290 ± 30 ; 54 ± 8		

^a All concentrations in M. ^b The approximate ionic strength is 0.2 M. ^c The approximate ionic strength is 1.2 M. ^d K_{ML} determined experimentally at an ionic strength of ~ 0.2 M and 20°.

mathematical representation of the relaxation spectra. (Charges will be neglected in writing the reactions and equations.)

(A) UO_2SCN^+ and $VOSCN^+$. The simplest system to consider is a single-step reaction of the type

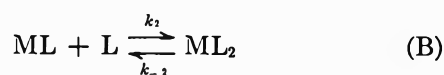


for which the reciprocal of the relaxation time is given by

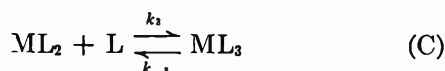
$$1/\tau = k_{-1} + k_1[(M) + (L)] \quad (1)$$

where k_{-1} and k_1 are the unimolecular and bimolecular dissociation and association rate constants, M is either UO_2^{2+} or VO^{2+} , and L is SCN^- (or anyone of the ligands subsequently treated). The data and rate constants for these systems are given in Table II.

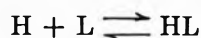
(B) $UO_2CH_2ClCOO^+$ and UO_2SO_4 . In many solutions, concentrations could be adjusted so that only a single reaction was of kinetic importance. The two possibilities to warrant our consideration in addition to reaction A are



and



The reciprocal relaxation time would then have the same form as eq 1, the subscript now being 2 or 3 and M replaced by ML or ML_2 , respectively, where required. Unlike thiocyanate, however, the other ligands studied can be protonated in solution. The appropriate equilibrium



must be included in the computation of the relaxation time. Doing so leads to a factor of $1 + a$ dividing the concentration of metal or complex in eq 1 in which

$$a = \frac{\delta(HL)}{\delta(L)} = \frac{(H)}{K_L + (L)} \quad (2)$$

where K_L is the acid dissociation constant of the ligand. The expression for the reciprocal of the relaxation time is now

$$1/\tau = k_n \left[\frac{(ML_{n-1})}{1 + a} + (L) \right] + k_{-n} \quad (3)$$

If the ligand is completely dissociated, then K_L would be very large with respect to unity, so that in the limit of complete ligand acid dissociation a becomes zero and eq 3 reduces to eq 1

$$\lim_{K_L \rightarrow \infty} \left[\frac{\delta(HL)}{\delta(L)} \right] = 0$$

Before proceeding to a consideration of multi-step reactions, we should like to point out that eq 3 is applicable to the uranyl monochloroacetate and sulfate systems, but not to the acetate system. Nevertheless, the treatment with respect to the outstanding feature shared by these three systems, namely, coupling, in which steps A, B, and C all contribute to the relaxation spectrum, applies to the acetate as well. The general solution to the rate equations for multi-step reactions has been given in two of the references previously cited (ref 13 and 14). The relaxation times of the system are found by solving the matrix equations

$$|\mathbf{K}|\delta x\rangle = |1/\tau|\delta x\rangle \quad (4)$$

which is satisfied by the secular determinant

$$|\mathbf{K} - (1/\tau)\mathbf{I}| = 0 \quad (5)$$

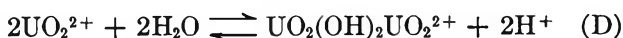
Table III:^a Relaxation Spectra of Uranyl Complexes at 20^b

[UO ₂ ²⁺] ₀	[(L) + (HL)] ₀	[UO ₂ ²⁺]	[L]	[ML]	[ML ₂]	[ML ₃]	pH	τ_{obs} , msec	τ_{calcd} , msec	
Monochloroacetate										
*4.010 × 10 ⁻²	0.6077	2.23 × 10 ⁻²	2.79 × 10 ⁻²	1.50 × 10 ⁻²	2.64 × 10 ⁻³	1.73 × 10 ⁻⁴	1.36	2.22	21.4	
4.028 × 10 ⁻²	0.7015	7.99 × 10 ⁻³	9.65 × 10 ⁻²	1.85 × 10 ⁻²	1.13 × 10 ⁻²	2.54 × 10 ⁻³	1.90	27.8	...	
4.012 × 10 ⁻²	1.275	1.36 × 10 ⁻²	5.78 × 10 ⁻²	1.88 × 10 ⁻²	6.85 × 10 ⁻³	9.26 × 10 ⁻⁴	1.35	16.7	16.0	
6.010 × 10 ⁻²	0.1915	4.92 × 10 ⁻²	8.76 × 10 ⁻³	1.03 × 10 ⁻²	5.72 × 10 ⁻⁴	1.17 × 10 ⁻⁵	1.37	155.0	...	
*4.010 × 10 ⁻²	0.6077	1.63 × 10 ⁻²	4.61 × 10 ⁻²	1.80 × 10 ⁻²	5.24 × 10 ⁻³	5.65 × 10 ⁻⁴	1.60	17.8	...	
pK _L = 2.66, K _{ML} = 24.0, K _{ML₂} = 6.31, K _{ML₃} = 2.34; ref 7.										
Sulfate										
*4.026 × 10 ⁻²	0.2011	5.54 × 10 ⁻³	7.14 × 10 ⁻²	1.98 × 10 ⁻²	9.80 × 10 ⁻³	5.08 × 10 ⁻³	1.90	22.2	...	
4.006 × 10 ⁻²	9.063 × 10 ⁻²	1.46 × 10 ⁻²	2.83 × 10 ⁻²	2.06 × 10 ⁻²	4.04 × 10 ⁻³	8.29 × 10 ⁻⁴	1.88	44.5	...	
6.018 × 10 ⁻²	6.684 × 10 ⁻²	3.14 × 10 ⁻²	1.62 × 10 ⁻²	2.55 × 10 ⁻²	2.86 × 10 ⁻³	3.35 × 10 ⁻⁴	1.865	97.0	96.6	
*4.026 × 10 ⁻²	0.2011	1.23 × 10 ⁻²	3.50 × 10 ⁻²	2.15 × 10 ⁻²	5.20 × 10 ⁻³	1.32 × 10 ⁻³	1.35	35.6	...	
pK _L = 1.92, K _{ML} = 50.1, K _{ML₂} = 6.92, K _{ML₃} = 7.25; ref 8.										
Acetate										
[UO ₂ ²⁺] ₀	[(L) + (HL)] ₀	[UO ₂ ²⁺]	[L]	[M ₂]	[ML]	[ML ₂]	[ML ₃]	pH	τ_{obs} , msec	τ_{calcd} , msec
4.010 × 10 ⁻²	0.1200	3.37 × 10 ⁻³	1.19 × 10 ⁻²	1.88 × 10 ⁻³	9.62 × 10 ⁻³	1.09 × 10 ⁻²	1.24 × 10 ⁻²	4.07	77.7	74.1
*4.005 × 10 ⁻²	0.3610	3.69 × 10 ⁻³	1.19 × 10 ⁻²	4.70 × 10 ⁻³	1.06 × 10 ⁻²	1.20 × 10 ⁻²	1.37 × 10 ⁻²	3.23	38.9	39.7
6.020 × 10 ⁻²	0.1005	1.93 × 10 ⁻²	4.28 × 10 ⁻³	4.88 × 10 ⁻³	1.98 × 10 ⁻²	8.09 × 10 ⁻³	3.31 × 10 ⁻³	3.50	95.0	...
6.004 × 10 ⁻²	0.1024	1.96 × 10 ⁻²	4.25 × 10 ⁻³	4.60 × 10 ⁻³	1.99 × 10 ⁻²	8.08 × 10 ⁻³	3.28 × 10 ⁻³	3.52	122.0	...
*4.005 × 10 ⁻²	0.3610	1.52 × 10 ⁻³	1.83 × 10 ⁻²	2.20 × 10 ⁻³	6.66 × 10 ⁻³	1.16 × 10 ⁻²	2.02 × 10 ⁻²	3.45	31.2	...
pK _L = 4.59, K _D = 1.2 × 10 ⁻⁶ , K _{ML} = 240, K _{ML₂} = 95.5, K _{ML₃} = 95.5; ref 9.										

^a All concentrations in *M*. ^b An approximate ionic strength of 0.15 *M* was maintained for the monochloroacetate, sulfate, and acetate systems.

Here **K** is the matrix of coefficients for the linearized rate equations, δx is the column vector, $[\delta x_i]$, representing the displacements of the components, and **I** is the unit matrix. The more rapid protolytic reaction coupled to the complexation enters into this reaction scheme as it did for the single-step reactions. For the uranyl with acetate, which was studied at higher pH values, another complication manifests itself.

(C) $UO_2CH_3COO^+$. Up to now, the dimerization of uranyl, which becomes significant at a pH of about 3.5 and above, has been ignored. For the reaction



we define¹⁵

$$K_D = \frac{(M_2)(H)^2}{(M)^2} = 1.2 \times 10^{-6}$$

where *M*₂ represents the dimer. This reaction adjusts to the new equilibrium more rapidly than the complexation reactions actually being studied (see Table I and ref 4). Its presence will therefore modify the concentrations appearing in the linearized rate equations. As before, the metal or metal-complex concentrations will be divided by a suitable factor, in this case, $1 + \alpha$. The acetate concentration will be divided by a factor $1 + \beta$, where

$$\beta = \frac{2\delta(M_2)}{\delta(M)} \quad (6)$$

These terms are explicitly

$$\alpha = \frac{4K_D(M)[(L) + (H)] + (H)^2[4(M_2) + (H)]}{(H)^2[K_L + (L)] + 4K_L[K_D(M) + (M_2)(H)]} \quad (7)$$

and

$$\beta = 4 \left\{ \frac{K_D(M)[(L) + K_L + (H)] + (M_2)(H)^2}{(H)[(H)^2 + (H)[K_L + (L)] + 4K_L(M_2)} \right\} \quad (8)$$

In the absence of appreciable dimer α should reduce to a and β should be zero. Examination of eq 7 and 8 shows that

$$\lim_{K_D, (M_2) \rightarrow 0} \left[\frac{\delta(HL)}{\delta(L)} \right] = \frac{(H)^3}{(H)^2[K_L + (L)]} = \frac{(H)}{K_L + (L)} = a$$

and

$$\lim_{K_D, (M_2) \rightarrow 0} 2 \left[\frac{\delta(M_2)}{\delta(M)} \right] = 0$$

(D) *Evaluation of Relaxation Spectra for Multi-Step Reactions.* The experimental conditions and relaxation times for uranyl with monochloroacetate, sulfate, and acetate are listed in Table III. A trial

(15) C. F. Baes, Jr. and N. J. Meyers, *Inorg. Chem.*, **1**, 780 (1962).

and error method was used to find the best set of rate constants for calculating the relaxation times according to eq 5. The measured and calculated relaxation times are shown for comparison. The concentrations of the various species at equilibrium were calculated with the aid of an IBM 1620 computer.

In interpreting the relaxation data, it is important to determine which species, whether L or HL, or both, contribute to the relaxation spectra. Inclusion of the reaction with HL into the rate equations results in additional terms in the final expression for the reciprocal of the relaxation time. These additive terms are proportional to hydrogen ion concentration. A number of systems showing this type of behavior have been examined, of which some studies by Cavasino may be cited.¹⁶ In general, protonated ligands show smaller complexation rate constants than the corresponding deprotonated ligand. Qualitative studies were performed for each of the three ligands (the experiments that are marked with asterisks) to determine which species was principally responsible for the observed effect.

The procedure that was followed consisted of varying the pH of two identical initial experiments such that the assignment of rate constants remained nearly the same. The observed changes in the relaxation time of each system appeared to correlate with changes in L and not with HL. That is, lowering the hydrogen ion concentration, which favors the formation of L at the expense of HL, resulted in a shorter relaxation time. Alternately, raising the hydrogen ion concentration, which did not favor the formation of L, resulted in a longer relaxation time.

Obtaining a solution of the matrix equation for the case of coupled reactions is difficult when the eigenvalues are close together. For many of the systems in Table III resolution of the relaxation spectrum was not possible; consequently, for these experiments no entry appears in the column labeled τ_{calcd} . The rate constants derived from the uranyl experiments showing higher order complexing are listed in Table IV.

Table IV: Rate Constants of Uranyl Complex Reactions at 20°

Ligand	$M^{-1} \text{ sec}^{-1}$			Sec^{-1}		
	k_1	k_2	k_3	k_{-1}	k_{-2}	k_{-3}
Acetate	1050	800	200	4.4	8.4	2.1
Monochloroacetate	110	240	80	4.4	38.0	34.0
Sulfate	180	300	160	3.6	43.0	22.0

Discussion

The formation of complexes between simple bivalent metal ions and sterically favorable ligands is usually controlled by the water exchange rate of the aquated metal ion with the ligand having a minimal influence.¹⁷ Ions with high charge to radius ratios, which may be divalent ions of small size like Be^{2+} or more highly charged ions like Fe^{3+} , tend to have slower, ligand-dependent rates of complex formation. We have endeavored to determine which situation prevails for the dipositive, oxygen-containing uranyl and vanadyl ions. Let us begin with uranyl.

The magnitude of the k_1 rate constants for the four ligands studied runs from $110 M^{-1} \text{ sec}^{-1}$ for chloroacetate to $1050 M^{-1} \text{ sec}^{-1}$ for acetate as shown in Tables II and IV. This range lies below that observed for the bivalent transition metal ions, being comparable to values obtained for ferric ion complexation.¹⁸ Moreover, the nature of the incoming ligand affects the rate of substitution, a point to which we shall return after a more detailed consideration of k_1 relative to k_2 and k_3 .

For chloroacetate and sulfate k_2 is greater than k_1 . This effect is readily understood, since previous studies have shown that substitution of negatively charged ligands into the inner coordination sphere loosens the binding between the central cation and the remaining coordinated waters.¹⁴ Since the mechanism is complicated, however, certain assumptions have to be made in order to derive the same trend between k_2 and k_3 . Specifically, the ion-pair association constant for reactions B and C would have to be known. The procedure usually employed is to calculate this value from theory, a process too uncertain for these systems. Roughly, the trend seems to prevail. The fact that k_2 is less than k_1 for acetate may reflect the screening of charge due to the unbound hydrophobic end of the acetate ion.¹⁹ This effect would be reflected in the ion pair formation constant for this and the next step. Essentially, then, the most significant feature of these results concerns the relative slowness of the substitution, as reflected in the k_1 rate constants, and we take up this point again.

Numerous studies have shown that in the crystal, the characteristic structure for uranyl is a unit con-

(16) F. P. Cavasino, *J. Phys. Chem.*, **69**, 4380 (1965); *Pic. Sci.*, **35** (II-A), 1120 (1965).

(17) M. Eigen, *Ber. Bunsenges. Physik. Chem.*, **67**, 753 (1963).

(18) M. Eigen and R. G. Wilkins, "Mechanisms of Inorganic Reactions," R. F. Gould, Ed., American Chemical Society, Washington, D. C., 1965, p 55.

(19) J. I. Steinfeld and G. G. Hammes, *J. Phys. Chem.*, **67**, 928 (1963).

taining a more or less linear O-U-O axis with a roughly hexagonal equatorial plane at right angles to this axis.² It seems clear that f orbitals participate in the bonding, accounting for both the relatively strong U-O axial bonds, and the over-all geometric configuration.^{20,21} In one of the earlier papers concerned with the role of f orbitals in the bonding of uranium and the transuranic elements, Connick and Hugus consider charge distribution in the uranyl ion and its effect on the entropy of the ion.²² Their conclusion that "... a uranyl ion appears as a +3 ion to waters about its equator. . ." is in accord with the kinetic experiments reported on here.

There remains, then, the question of the ordering of the k_1 rate constants with regard to properties of the ligands studied. To effect a comparison, it is necessary to "normalize" the charge effect, so that the divalent sulfate can be compared with the univalent ions. Therefore, if we divide the rate constants for the univalent ions by $2 M^{-1}$ and the rate constant for sulfate ion by $10 M^{-1}$ (approximate values for the ion-pair formation constants at these temperatures and ionic strengths¹⁴), we obtain the order $\text{CH}_3\text{COO}^- > \text{SCN}^- > \text{ClCH}_2\text{COO}^- > \text{SO}_4^{2-}$. This series would correlate with decreasing pK, and hence basicity, were it not for thiocyanate. The same would be true for the correlation with the stability constant K_{ML} if it were normalized, again with the exception of SCN^- . What is really of importance here, however, is how strong a nucleophile the ligand is with regard to this cation. Since thiocyanate is known to form complexes rather frequently with most metal ions,²³ we feel justified in surmising that the above ligand order of decreasing rate of substitution is also consistent with decreasing nucleophilic character.

Whether or not there is an influence of ligand properties on the kinetics of substitution depends upon the mechanism. In particular, the formation of a transition state of reduced coordination number by a dissociation mechanism would be ligand independent, while formation of a transition state of expanded coordination number by a displacement mechanism should be ligand dependent.²⁴ An *a priori* choice between the two mechanisms would be difficult to make because the effectiveness of a ligand field in splitting electron levels for 5f electrons is not on the same order of magnitude as for 3d and 4d electrons;²⁵ consequently, a change in coordination number need not signify appreciable loss in crystal field stabilization energy. On the basis of the experimental evidence, however, we conclude that the displacement mechanism predominates.

In contrast to the uranyl studies, for which no other values were available, the vanadyl thiocyanate study may be compared to a previous investigation, namely, the pressure-jump study in which the kinetics of reaction between VO^{2+} and SO_4^{2-} were measured.⁵ For these ions, the recombination rate constant is about $10^4 M^{-1} \text{sec}^{-1}$, while the SCN^- rate constant is $160 M^{-1} \text{sec}^{-1}$. The pK of HSCN is less than 1 while the pK of HSO_4^- is 1.92.⁷ Therefore, a displacement type of mechanism with dependency on the ligand basicity seems to be indicated.

For both the VO^{2+} and the UO_2^{2+} kinetic studies with thiocyanate, the pH dependence was examined and within experimental accuracy none was found. A pH dependence was found for the SO_4^{2-} experiment. This kind of behavior would imply that the appearance of a pH dependence depends on whether or not the ligand has an appreciable pK value, that is, a value at least greater than unity, unless, of course, the effect is to be associated solely with hydroxyl ion catalysis.

As in the case of the uranyl ion, the structure of vanadyl complexes as exemplified by the acetylacetonate is known.² It has a square pyramidal structure with the vanadium atom above the center of the basal square of oxygens. Thus, an alternative explanation for the vanadyl results is possible.

It may well be that two different processes are being observed in these studies. Attack by the ligand at the open, basal side of the square pyramidal complex may have been observed in one system. In the other, substitution may have been initiated at the apical side of the complex. At this time it does not seem feasible to determine which of the two is the more rapid.

Indeed, it is possible that further fast reaction studies on these ions will disclose other relaxational processes in the range between 10 msec and the diffusion-controlled relaxation time for ion-pair formation of about 10 nanosec. Furthermore, the anisotropic structures of the oxo ions can give rise to many different interactions with the solvent, of which association between the negatively charged oxygen ends of the O-U-O axis and water is an interesting possibility.

(20) C. A. Coulson and G. R. Lester, *J. Chem. Soc.*, 3650 (1956).

(21) S. P. McGlynn and J. K. Smith, *J. Mol. Spectry.*, **6**, 164 (1961); cf., however, R. L. Belford, *J. Chem. Phys.*, **34**, 318 (1961), for another point of view on f-orbital participation.

(22) R. E. Connick and Z. Z. Hugus, Jr., *J. Am. Chem. Soc.*, **74**, 6012 (1952).

(23) See ref 2, p 314.

(24) F. Basolo and R. G. Pearson, "Mechanisms of Inorganic Reactions," John Wiley and Sons, Inc., New York, N. Y., 1958, p 108.

(25) R. A. Satten, C. L. Schreiber, and E. Y. Wong, *J. Chem. Phys.*, **42**, 162 (1965).

Oxygen Quenching of Acriflavine Phosphorescence¹

by J. L. Rosenberg and Frederick S. Humphries

Department of Chemistry, University of Pittsburgh, Pittsburgh, Pennsylvania (Received July 19, 1966)

Neutral aqueous solutions of acriflavine (3,6-diamino-10-methylacridinium chloride) do not obey Beer's law because of the formation of dimers. The dissociation constant of the dimer at 25° was found to be 5.0×10^{-3} mole/l. The nonexponential decay of phosphorescence of silica gel adsorbates of acriflavine was shown to be resolvable into two first-order processes, having decay constants at 25° of 24 and 5.0 sec⁻¹. These components on the gel are identified as dimer and monomer, respectively. The decay constants are independent of oxygen pressure although the phosphorescence intensity may be reduced in oxygen to less than 10%. These results are explained by a static quenching model, in which oxygen forms a relatively nonphosphorescent complex with the ground state of the dye. The formation constant of the complex was found to be 2.5×10^3 or 3.2×10^4 mm⁻¹ for the dimer or monomer, respectively. Quenching is believed to occur by an energy redistribution within the excited state of the complex followed by an escape of oxygen with an appreciable fraction of the excitation energy. There is a small probability, especially for the dimer, that the energy redistribution will not occur and that an uncomplexed dye triplet can be formed from the excited complex.

Introduction

The quenching of dye phosphorescence by molecular oxygen is a well-known process. In most cases the quenching leads to a pure deexcitation, and in a few cases it leads to a photooxidation reaction with identifiable products. The primary photochemical event is still incompletely understood. This study was undertaken to learn more about the direct interaction of oxygen with excited aromatic molecules and to correlate the observed facts with the electronic structure of these substances.

The system chosen for the study was a silica gel adsorbate of the acridine dye, acriflavine. The lifetime of the triplet state of the dye in the gel approaches 1 sec under vacuum and is long enough to allow a study of the details of the decay process with conventional oscilloscopic techniques. The triplet state can be monitored by two separate emission processes: (a) the β -phosphorescence, representing the direct triplet to ground transition, with a maximum intensity at 560 m μ , and (b) the α -phosphorescence, representing the delayed transition to the ground state from the first excited singlet state repopulated by a thermal activation from the triplet state, with a maximum intensity at 510 m μ .

Results

Acriflavine Solutions. The present work was all done with acriflavine (3,6-diamino-10-methylacridinium chloride) separated from proflavine by the method of Gailliot.² Previous experimental work on adsorbates of acriflavine on silica gel had shown the nonuniform nature of the dye.^{3,4} We therefore decided to study aqueous solutions of acriflavine, the previously reported metachromasy of which⁵ suggested an analog to the nonuniformity of the dye on gels. Aqueous solutions of acriflavine were studied from 10^{-6} to 10^{-3} M. Their absorption spectra were recorded with a Spec-

(1) This article is based upon a dissertation submitted by F. S. Humphries in partial fulfillment of the requirements for the Ph.D. degree at the University of Pittsburgh, Oct 1964. The work was supported by National Science Foundation Grant GP-4268 and by the Air Force Cambridge Research Laboratories, Office of Aerospace Research, under Contract No. AF19(604)-8354 with the University of Pittsburgh. Computations were partly supported by National Science Foundation Grant G-11309 to the Computing Center of the University of Pittsburgh. This was presented at the 150th National Meeting of the American Chemical Society, Atlantic City, N. J., Sept 1965.

(2) M. Gailliot, *Quart. J. Pharm. Pharmacol.*, **7**, 63 (1934)

(3) J. L. Rosenberg and D. J. Shombert, *J. Am. Chem. Soc.*, **82**, 3252 (1960).

(4) S. Kato and M. Koizuma, *Bull. Chem. Soc. Japan*, **30**, 27 (1957).

(5) N. Mataga, *J. Inst. Polytech. Osaka City Univ.*, **4C**, 189 (1953).

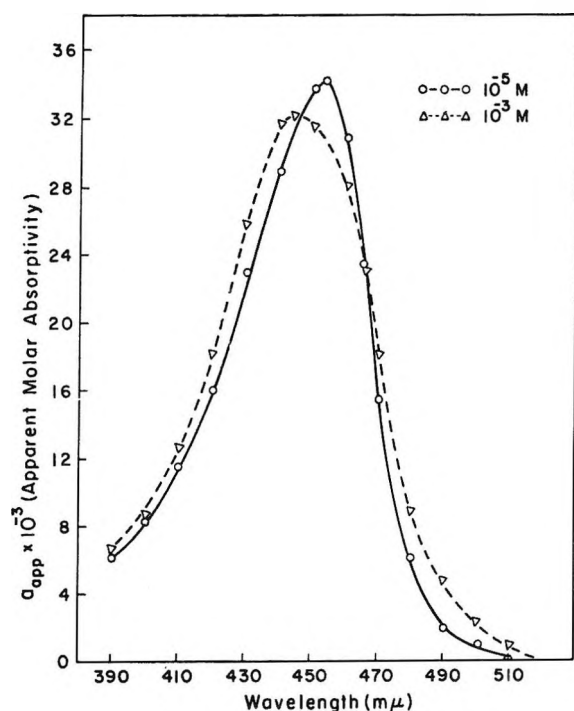


Figure 1. Absorption spectra of dilute and concentrated aqueous solutions of acriflavine.

tronic 505 spectrophotometer. All measurements were made within the pH range 6–11, within which no change in ionization could be detected spectrophotometrically. Beer's law was obeyed exactly from 10^{-6} to $5 \times 10^{-5} M$, but deviations were observed in the more concentrated solutions. In Figure 1, the apparent molar absorptivities, $a_{pp} = A/bC$, at room temperature of 10^{-3} and $10^{-5} M$ solutions are compared. A is the measured absorbance, b is the path length, and C is the nominal dye concentration if there were no dimerization. The absorption maximum, which occurs at $453 m\mu$ in the dilute solution, is shifted to $444 m\mu$ in the concentrated solution. In addition, there is increased absorption on both sides of the absorption maximum in the concentrated solution as compared with the dilute solution. We postulate that the failure of Beer's law in the solutions studied is due to aggregation of the molecules of acriflavine to form dimers as the concentration of the solution is increased



where A_2 = dimer and A = monomer.

$$K_{eq} = [A]^2/[A_2] \quad (2)$$

If α is the fraction of the dye existing as monomer, a_{app} at any wavelength is a linear function of α .⁶ An iterative process was used to calculate α values for various assumed K values over the concentration range 10^{-5} to

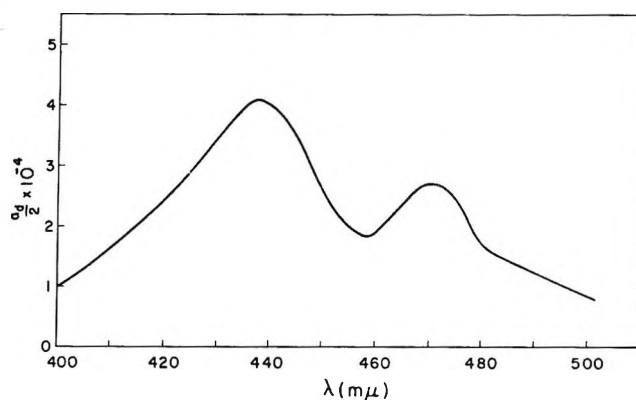


Figure 2. Absorption spectrum of aqueous acriflavine dimer. a_d is the molar absorptivity of the dimer, calculated by the procedure described in the text.

$10^{-2} M$.⁶ The value of the equilibrium constant giving the best lines at various wavelengths was found to be $(5.0 \pm 0.5) \times 10^{-3}$ mole/l.

Since the concentration study revealed that Beer's law was obeyed from 10^{-6} to $5 \times 10^{-5} M$ concentrations, the molar absorptivity indices of the monomer were obtained directly from the $10^{-5} M$ solution. The spectrum of the dimer was then obtained by resolving the total absorbance of a solution into the separate contributions of monomer and dimer and by using values for the concentrations of the two components computed from K_{eq} . The spectrum obtained from this procedure is shown in Figure 2. Dimerization in solution is seen to result in a splitting of the monomeric band into two bands with the stronger absorption occurring in the blue band.

Triplet Decay in Silica Gel Adsorbates of Acriflavine. Kato and Koizuma reported that the decay of acriflavine triplets in a baked-out, evacuated gel adsorbate consisted of two first-order processes.⁴ Rosenberg and Shombert also reported the nonexponential, but first-order nature of the decay.³ In both of the above studies, the major observations did not begin until 0.25 sec had elapsed from the onset of the decay. Our initial observations showed that as much as 90% of the decay was missed in those observations. We consequently constructed a flash phosphoroscope with a General Electric FT 230 flash lamp, which allowed observations of luminescence free of scattering from the flash as early as 5 msec after the onset of the flash. The decay was followed to 500 msec, and 95% of the entire luminescence curve, measured as the current in the detector photomultiplier tube, was displayed on a single oscillogram.

(6) K. Bergmann and C. T. O'Konski, *J. Phys. Chem.*, **67**, 2164 (1963).

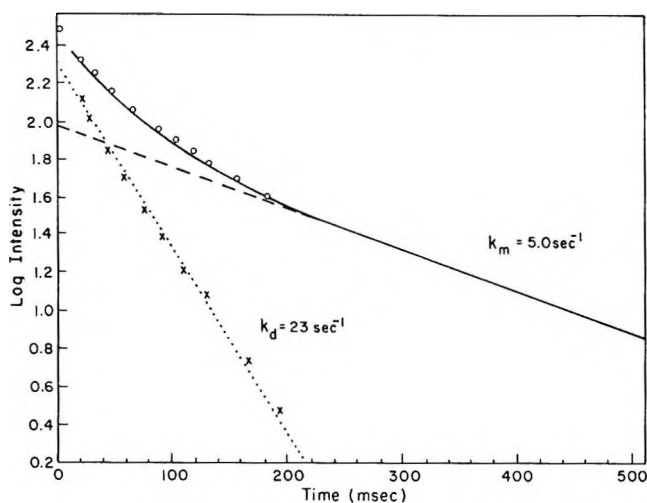


Figure 3. A typical decay curve for phosphorescence of acriflavine, observed in β band, above $600\text{ m}\mu$, following flash excitation, $430\text{--}600\text{ m}\mu$, at room temperature. Sample, 1.25×10^{-7} mole dye per g of silica gel; —, log of observed intensity; - - -, extrapolation of the linear portion of the solid line, giving the slow first-order component; X, computed point representing log (observed intensity minus the extrapolated intensity of the slow component); . . . , best line through X's, giving the fast first-order component; O, computed point synthesizing log of total intensities from sum of two first-order components.

In all cases, the luminescence decay was represented as the sum of two first-order processes, designated symbolically as d and m. At room temperature, the rate constants for decay in dilute adsorbates (less than 2×10^{-7} mole of dye/g of silica gel) were: $k_d = (24 \pm 2)\text{ sec}^{-1}$, $k_m = (5.0 \pm 0.5)\text{ sec}^{-1}$. For any adsorbate, each rate constant had the same value, within experimental error, whether measured in the α -, at $520\text{ m}\mu$, or in the β -phosphorescence, at wavelengths above $600\text{ m}\mu$. The luminescence was excited at wavelengths between 430 and $600\text{ m}\mu$. Over a concentration range from 5×10^{-8} to 1×10^{-5} mole/g, the greatest variation in k_m from the mean cited above was 8% and in the case of k_d , 16% . A typical experimental decay curve, along with its resolution into the two components, is shown in Figure 3. The relative contributions of the d and m processes depended on the filters used to monochromatize the exciting flash lamp. For example, d contributed 51% of the extrapolated β -phosphorescence at zero time for excitation at $420\text{ m}\mu$, 58% at $447\text{ m}\mu$, and 76% at $480\text{ m}\mu$. The rate constants, k_d and k_m , on the other hand, remained the same for all wavelengths of excitation. A similar phenomenon was observed in the systematic variation of filters used to monochromatize the emitted light admitted to the detector. When α -phosphorescence was observed at $520\text{ m}\mu$, d contributed 80% of the zero-time intensity, I^0 ; at 480

$\text{m}\mu$, it contributed only 70% . A slight decrease in the k 's was observed at the lower observation wavelength because of the greater reabsorption at this wavelength.

The relative contributions of d and m were drastically altered by varying the illumination regime, without any change in the separate rate constants. The adsorbate was subjected to an intermittent excitation from a tungsten lamp in a rotating-disk phosphoroscope until a steady state was reached. The light was then turned off and the decay of phosphorescence was observed. A comparison of the decay following single-flash and steady-state excitation is given in Table I for experiments with the same sample and the same sets of monochromatizing filters.

Table I: Rate Constants and Relative Contributions of the Two Components from Flash Excitation as Compared with Steady-State Excitation^a

	k_d , sec ⁻¹	k_m , sec ⁻¹	% I_d^0	% I_m^0
Observation, β				
Single flash	23 ± 2	5.0 ± 0.5	70 ± 3	30 ± 3
Steady state	22 ± 2	4.0 ± 0.5	47 ± 4	53 ± 4
Observation, α				
Single flash	23 ± 2	5.0 ± 0.5	68 ± 3	32 ± 3
Steady state	22 ± 2	4.0 ± 0.5	42 ± 4	58 ± 4

^a Sample, 1.25×10^{-7} mole/g; temperature, 25° ; excitation, $430\text{--}600\text{ m}\mu$. I^0 is the observed intensity extrapolated to zero time.

For a two-component system, steady-state excitation is expected to favor the slowly decaying component (m in our case) as compared with the single-flash excitation. In a single nonsaturating flash that is short compared with the triplet state lifetime, the two components are populated in proportion to the relative contributions to the absorption of the exciting light. In the steady-state experiment, however, the long-living triplet state of the more slowly decaying component accumulates to a larger relative extent because of the additive effect of successive flashes. For small relative triplet populations, I_{ss}^0 for each component in a steady-state experiment should be proportional to $I_f^0(1 - e^{-kt})^{-1}$, provided that the spectral distributions of the light admitted to the sample by the steady and flashing lamps are the same,⁷ where I_{ss}^0 and I_f^0 are the observed zero-time intensities in a steady-state and a single-flash experiment, respectively, and t is the length of a whole dark-light cycle, 11.8 msec in the case of our rotating-

(7) F. S. Humphries, Dissertation, University of Pittsburgh, 1964.

disk phosphoroscope. On the basis of the observed 30% contribution of *m* to I_f^0 in the β -phosphorescence, we predict a 64% contribution to I_{ss}^0 , and we observed 53%. The discrepancy is probably due to a difference in the spectral distribution between the filament lamp for the steady-state experiment and the gas-filled discharge lamp for the flash which was not completely compensated for by using the same set of filters. The experimental qualitative verification of the predicted increase in the relative contribution of the slowly decaying component in the steady-state experiment and the constancy of the *k*'s over a wide variation of experimental arrangements may be taken as a confirmation of our two-component analysis of the decay curves.

The solution studies suggested that the two components of the dye in the adsorbate may be monomers and dimers. There is some evidence from the literature that the aggregation of dyes in the adsorbed state may be even more pronounced than in solution.^{6,8} Direct experimental proof by spectrophotometry was not possible in our case because of the difficulty of preparing optically homogeneous samples of the adsorbate. We could show, at least qualitatively, that concentrated samples had an absorption spectrum different from dilute samples, the concentrated showing the increased absorption on both the long and short wavelength sides of the maximum, similar to the absorption by the dimer in solution.⁷

Additional evidence for the monomer-dimer assignments on the gels came from concentration effects in the luminescence experiments. The more concentrated adsorbates had a larger contribution of the fast-decaying (*d*) component in the luminescence. This suggests assignment of this component to the dimer by reference to the relative rate constants in solution. Actually, the total variation in percentage of *d* in the various adsorbates was not as great as would have been predicted on the basis of a simple mass action law. Another interesting finding was that an adsorbate baked out under vacuum at 250° for several hours at 10⁻⁶ mm had a larger relative amount of *d* than did an unbaked sample. Apparently, the dye molecules show both mobility and increased tendency to aggregate on the gel surface at elevated temperatures. An additional proof of this is that a baked-out sample shows increased absorbance, as compared with an unbaked sample, on both the long and short wavelength sides of the absorption maximum, in a manner similar to the dimer in solution. The state of the dye molecules on the gel is independent of their state in the solution from which they were prepared, as shown by the resolution into the same *d* and *m* components of the luminescence

curves for adsorbates prepared from a 10⁻⁴ *M* solution in dimethyl sulfoxide, in which Beer's law was shown to hold.

The wavelength discrimination effects in the luminescence experiments described above also support the assignment of the fast-decaying component as dimer. This component was found to be excited preferentially on the long wavelength side of the absorption maximum and was also found to constitute a larger relative percentage of the α -luminescence observed at the longer wavelength edge of the emission band. These findings are in accord with the increased absorbance at the long wavelength side of the absorption maximum in concentrated solutions.

Oxygen Quenching of Phosphorescence. Although the quenching of dye phosphorescence by oxygen has been known as an experimental phenomenon for some time, its mechanism has not been thoroughly understood. One of the puzzling systems has been the silica gel acriflavine adsorbate, whose phosphorescence intensity has been measured as a function of oxygen pressure in a rotating-disk phosphoroscope. A simple kinetic scheme involving a quenching collision of oxygen with the dye triplet state has not accounted for the results satisfactorily.⁹ Typically, quenching parameters chosen to give the best fit of the data at low oxygen pressures (10⁻⁵ mm) led to a predicted quenching at higher oxygen pressures (10⁻² mm) greater than the experimental quenching. Since previous experiments had been performed with unfiltered luminescence, we redetermined the quenching curves, observing the α - and β -phosphorescence in separate experiments. Figure 4 shows the experimental results obtained from the plot $100I(O_2)/I(\text{vac})$ vs. log of the oxygen pressure, for α - and β -phosphorescence at room temperature. $I(O_2)/I(\text{vac})$ is the ratio of the steady-state intensity for a given pressure of oxygen to the steady-state intensity under vacuum. It is readily seen that there is very little difference in the effect of oxygen on the two processes. This same similarity of the two processes in their dependence on oxygen was observed in all samples studied, regardless of concentration.

Our next set of experiments bearing on the quenching by oxygen was a study of the decay process in the presence of oxygen by the single-flash technique. The general procedure for recording the effect of oxygen on decay of phosphorescence was to add to the sample tube a premeasured amount of oxygen and then flash-excite the mixture with sufficiently weak flashes to pre-

(8) D. F. Bradley and M. K. Wolf, *Proc. Natl. Acad. Sci. U. S.*, **45**, 944 (1959).

(9) S. Lipsky, Dissertation, University of Chicago, 1954.

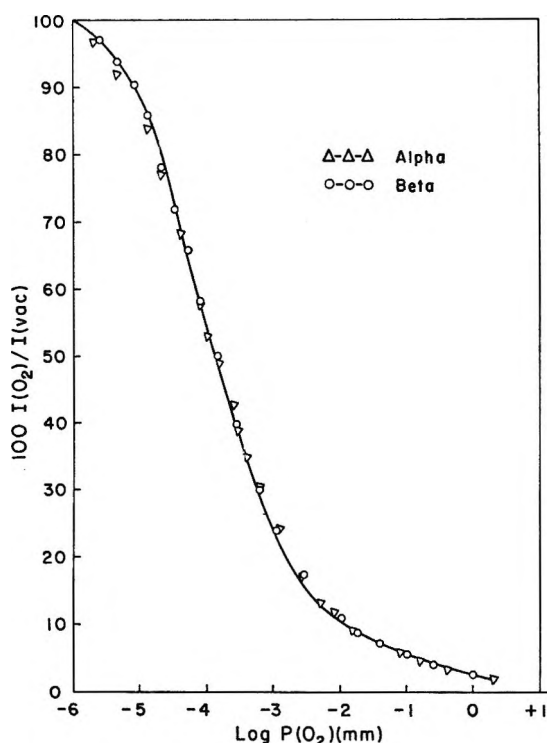


Figure 4. Phosphorescence quenching by oxygen at room temperature. Sample: 1.0×10^{-5} mole acriflavine/g of silica gel; excitation: 430–600 $m\mu$; observation: α , 520 $m\mu$; β , above 600 $m\mu$. $I(\text{vac})$ and $I(\text{O}_2)$ are luminescence intensities observed in the Becquerel phosphoroscope, under vacuum and in O_2 at the indicated pressure.

serve proportionality between the incident and phosphorescent intensities. The mixture was usually excited through Corning blue and sharp cut-off yellow filters to provide a broad band of radiation within the absorption spectrum of the adsorbates. α -Phosphorescence was observed through the usual 520 interference filter. The time interval investigated fully was

Table II: Rate Constants and Extrapolated I^0 Values for the Two Components as a Function of the Pressure of Oxygen for the α Process^a

Pressure, mm	k_d , sec ⁻¹	k_m , sec ⁻¹	I^0_d , rel units	I^0_m , rel units
0	20 ± 2	4.6 ± 0.5	225 ± 7	91 ± 3
1.62×10^{-4}	16 ± 2	6.2 ± 0.5	170 ± 8	44 ± 2
7.1×10^{-4}	20 ± 2	5.3 ± 0.5	116 ± 6	16 ± 2
1.43×10^{-3}	20 ± 2	5.7 ± 0.5	76 ± 5	13 ± 2
3.0×10^{-3}	20 ± 2	5.0 ± 0.5	52 ± 4	7 ± 1
6.8×10^{-3}	20 ± 2	5.0 ± 0.5	44 ± 4	5.4 ± 0.5
1.42×10^{-2}	20 ± 2	4.6 ± 0.5	32 ± 4	3.4 ± 0.4

^a Sample: 1.0×10^{-5} mole/g; temperature: 25°; flash excitation: 430–600 $m\mu$; observation: α , 520 $m\mu$.

the 20 to 500-msec region. Each decay curve, like those observed under vacuum, could be resolved into two first-order components. Table II records the data obtained from the resolution of the decay curves into two components for α -phosphorescence, observed at 520 $m\mu$. There were two significant results from these experiments and from similar observations of the β -phosphorescence: (1) the m (monomer) component is quenched by oxygen much more than the d (dimer) component, and (2) the rate constants for decay of phosphorescence are independent of the extent of quenching.

Discussion

Dimerization of the Dye. The splitting of the visible absorption of the dye into two bands separated by 1650 cm^{-1} , together with the intensity distribution between the two bands, as shown in Figure 2, are consistent with an exciton coupling model¹⁰ in which the transition moments of the two moieties make an angle of 70° with respect to each other and the distance between molecular centers is 8.2 Å.⁷

The forces responsible for the ground-state stabilization of such dimers are not well understood. Mukerjee and Ghosh recently presented evidence that hydrophobic bonding may be responsible for aggregation of dyes in aqueous solution.

It is interesting to note that the value of the association constant (the reciprocal of $K_{c,q}$ in eq 2) for acriflavine at room temperature is only $1/200$ of that for the tetramethyl derivative, acridine orange.¹¹ Similarly, from data in the literature, thionine¹² associates less than its tetramethyl derivative, methylene blue,⁶ and fluorescein¹³ less than its tetrabromo derivative, eosin.¹⁴ These correlations tend to support the recent proposal of Mukerjee and Ghosh that hydrophobic bonding may be responsible for aggregation of dyes in aqueous solution.¹⁵ Our observations of a decreased tendency of acriflavine to dimerize in ethanol and of the absence of measurable dimerization in dimethyl sulfoxide even at $10^{-3} M$ are also consistent with this view.

It does not follow that the shape of the dimer or the driving force for dimerization is the same in solution as on the gel. The hydrophobic bond concept, useful for understanding the solution results, cannot be very helpful in interpreting the experiments with the adsorbates. Perhaps the dimerization on the anionic gel

(10) M. Kasha and E. G. MacRae, *J. Chem. Phys.*, **28**, 72 (1958)

(11) V. Zanker, *Z. Physik. Chem.*, **199**, 225 (1952).

(12) E. Rabinowitch and L. Epstein, *J. Am. Chem. Soc.*, **63**, 69 (1941).

(13) J. Lavorel, *J. Phys. Chem.*, **61**, 1600 (1957).

(14) Th. Förster and E. König, *Z. Elektrochem.*, **61**, 344 (1957).

(15) P. Mukerjee and A. K. Ghosh, *J. Phys. Chem.*, **67**, 193 (1963).

involves charge delocalization in the dye, in accordance with the model of Levinson, Simpson, and Curtis.¹⁶ A Hückel molecular orbital calculation was carried out, with auxiliary inductive parameters but without overlap. Parameters were those recommended by Streitwieser.¹⁷ The computations, performed on the IBM 7090 at the University of Pittsburgh Computing Center, indicate a positive charge of only 0.30 on the hetero-N of the acriflavinium cation, 0.27 on the C opposite the hetero-N, and 0.11 on each of the amino N's. The extensive charge delocalization indicated by these calculations would result in electrostatic stabilization if a single negative site on the gel could be close to positively charged points in both moieties of the dimer.

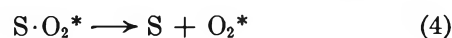
Our finding that the phosphorescence decay of acriflavine on silica gel is the sum of two first-order processes, the experimental basis for our interpretation of dimerization in the adsorbates, was not confirmed by Weiner and Seliger.¹⁸ They claim to have found strictly exponential decay curves in seemingly similar preparations with reported lifetimes at room temperature similar to those of our m, or slow, component. The d, or fast, component showed up in our work as a result of measurements in the first 50 msec, as indicated in Figure 3. No decay curve was shown by Weiner and Seliger, and it is possible that their observations could not have detected the fast component that we observed, especially since their 0-100 cycle recorder could not be expected to respond to the early moments as well as the oscilloscope used in our work. The failure to begin observations soon enough after excitation cut-off was certainly responsible for the earlier inability in our own laboratory to recognize the d component.³ Other experimental differences should be pointed out. Weiner and Seliger used 100-200 mesh silica gel whose pores they felt are impenetrable to acriflavine;¹⁸ accessibility of the internal pores to dye in our 14-28 mesh silica gel was definitely proved.¹⁹ Restriction of adsorption sites to the outer surface might also be related to a restriction in the size of a polymeric unit that might be found. Perhaps a more significant experimental difference is the use by Weiner and Seliger of an excitation, 407 m μ , far on the high-energy tail of the main absorption band. We purposely avoided excitation components at wavelengths below 430 m μ because it had previously been shown that silica gel itself absorbs in such regions and gives rise to a luminescence having quite distinct properties from that of photoexcited acriflavine phosphorescence.^{3,20} Such extraneous excitation processes would have been given added relative weight in the experiments of Weiner and Seliger since their sample was only one-tenth as concentrated as our most dilute adsorbate. Finally, the observation

implied by Weiner and Seliger that simple first-order decay was not observed at temperatures where α - and β -phosphorescence were of comparable intensity¹⁸ cannot be interpreted on the basis of their scheme but requires the assumption that either the dye itself has more than one component on the gel or that a second type of excitation other than photoexcitation to the first excited singlet state of the dye is occurring.

Mechanism of Quenching. If oxygen were quenching phosphorescence by collisions with the triplet state, the lifetime of phosphorescence would be shortened in the presence of oxygen but the initial intensity of phosphorescence following a single short nonsaturating flash would be independent of oxygen. Neither of these conditions was observed in our experiments (Table II). A simple interpretation of our results is that oxygen reacts with the ground state of the dye, S, rather than with the excited state. A loose complex, S \cdot O₂, between O₂ and the dye in its ground state, may be described by an equilibrium constant of formation, K_{eq} .

$$K_{eq} = \frac{[S \cdot O_2]}{[S][O_2]} \quad (3)$$

From the absence of any observed oxygen effect on the absorption spectrum we postulate that both the complexed and uncomplexed dye molecules absorb radiation equally but that phosphorescence arises only from T, the triplet of the uncomplexed dye. The excited complex, S \cdot O₂^{*}, decomposes very quickly by a radiationless process into S and O₂^{*}, an excited form of O₂.



In the absence of collisional processes between O₂ and T, the lifetime of the observed phosphorescence is then independent of the oxygen pressure, being simply the lifetime of T. The intensity of the observed phosphorescence, $I(O_2)$, is proportional to the fraction of the dye which is uncomplexed.

$$\frac{I(O_2)}{I(vac)} = (1 + K_{eq}[O_2])^{-1} \quad (5)$$

Equation 5 was tested by plotting the extrapolated zero dark-time intensities of phosphorescence as a function of oxygen pressure, measured at room tem-

(16) G. S. Levinson, W. T. Simpson, and W. T. Curtis, *J. Am. Chem. Soc.*, **79**, 4314 (1957).

(17) A. Streitwieser, Jr., "Molecular Orbital Theory for Organic Chemists," John Wiley and Sons, Inc., New York, N. Y., 1961, p 135.

(18) R. F. Weiner and H. H. Seliger, *Photochem. Photobiol.*, **4**, 1207 (1965).

(19) J. L. Rosenberg and F. S. Humphries, *ibid.*, **4**, 1185 (1965).

(20) D. J. Shombert, Dissertation, University of Pittsburgh, 1959.

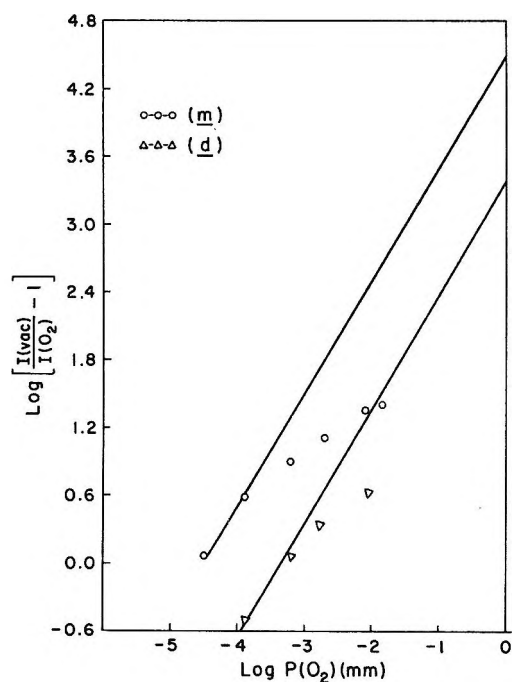


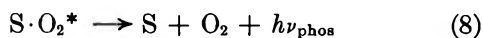
Figure 5. Evaluation of static quenching parameters. Sample: 1.0×10^{-5} mole acriflavine/g of silica gel. Intermittent excitation: 430–600 $m\mu$; observation: 520 $m\mu$. $I(\text{vac})$ and $I(\text{O}_2)$ are instantaneous luminescence intensities under vacuum and in O_2 , extrapolated to zero time from decay curves following intermittent illumination.

perature. The data used were similar to those shown in Table II but were obtained by following the decay of phosphorescence after cutting off the light in a rotating-disk phosphoroscope. This method was used rather than flash excitation in order to test the mechanism with other types of experimental results obtained with the Becquerel phosphoroscope. A plot for each component of $\log \{ [I(\text{vac})/I(\text{O}_2)] - 1 \}$ vs. $\log [\text{O}_2]$ is shown in Figure 5. Reasonable lines with unit slope could be drawn through the two experimental points at the lowest pressures for each component, and the intercepts of the unit-slope lines at 1 mm of O_2 give the following values for the equilibrium constants.

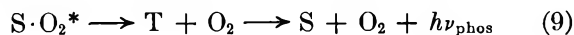
$$K_{\text{eq}}^{\text{m}} = 3.2 \times 10^4 \text{ mm}^{-1} \quad (6)$$

$$K_{\text{eq}}^{\text{d}} = 2.5 \times 10^3 \text{ mm}^{-1} \quad (7)$$

The points for higher oxygen pressures, however, fell below the unit-slope lines drawn through the low-pressure points. The deviations suggest that the $\text{S} \cdot \text{O}_2^*$ might have a radiative alternative to (4) for deexcitation to the ground state, either by a delayed radiation from $\text{S} \cdot \text{O}_2^*$ or some other excited state of the complex



or by a decomposition into the triplet state of the uncomplexed dye



Process 8 is ruled out for the following reason. Both α - and β -phosphorescences are quenched equally by O_2 , as shown in Figure 4; this is best understood if all the delayed light derives from a single long-living state, T. We thus accept process 9, with the proviso that the first stage, the decomposition into T and O_2 , is fast compared with the second stage. The effect of (9) is to limit the fractional quenching at high oxygen pressures to $(1 - \gamma)$, where γ is the ratio of quantum yields of T formation for the complex compared to the uncomplexed dye. This leads to the following modified prediction of the phosphorescence intensity.

$$\frac{I(\text{O}_2)}{I(\text{vac})} = (1 + \gamma K_{\text{eq}}[\text{O}_2])(1 + K_{\text{eq}}[\text{O}_2])^{-1} \quad (10)$$

The values of γ selected to give the best fit with the data are

$$\gamma_{\text{m}} = 0.042 \pm 0.005 \quad (11)$$

$$\gamma_{\text{d}} = 0.14 \pm 0.04 \quad (12)$$

To substantiate our mechanism, we used the above K and γ parameters determined for monomer and dimer from the analysis of the decay curves in predicting the entire phosphorescence quenching curves determined during steady-state illumination in a rotating-disk phosphoroscope. The prediction is

$$\frac{I(\text{O}_2)}{I(\text{vac})} = \frac{1 + \gamma_{\text{m}} K_{\text{eq}}^{\text{m}}[\text{O}_2]}{1 + K_{\text{eq}}^{\text{m}}[\text{O}_2]} \times \frac{I(\text{vac})^{\text{m}}}{I(\text{vac})^{\text{m}} + I(\text{vac})^{\text{d}}} + \frac{1 + \gamma_{\text{d}} [K_{\text{eq}}^{\text{d}}[\text{O}_2]]}{1 + K_{\text{eq}}^{\text{d}}[\text{O}_2]} \times \frac{I(\text{vac})^{\text{d}}}{I(\text{vac})^{\text{m}} + I(\text{vac})^{\text{d}}} \quad (13)$$

It had been noted in the course of our work that the over-all quenching efficiency of a given amount of oxygen was less when the phosphorescence was excited at 500 $m\mu$ than at 450 $m\mu$. Similarly, the quenching of α -phosphorescence was less when observed at 520 $m\mu$ than at 480 $m\mu$. These results are understandable, since the longer wavelength is associated to a greater extent with the dimer (Figure 2) than with the monomer, and since the dimer complexes less readily with oxygen than does the monomer (eq 6 and 7). Accordingly, we compared eq 13 with two phosphoroscope quenching curves differing widely in the relative contributions of the two components. The curves were observed with different exciting wavelengths and the percentage contribution of monomer to the observed luminescence intensity under vacuum was

either 30 or 65%, as determined from the resolution of the curves of decay following steady-state excitation into their two components. Figure 6 shows the agreement of the observed points with the calculated. It should be noted that all the parameters used to calculate the curves for these steady-state phosphorescence curves were taken from nonsteady-state decay experiments.

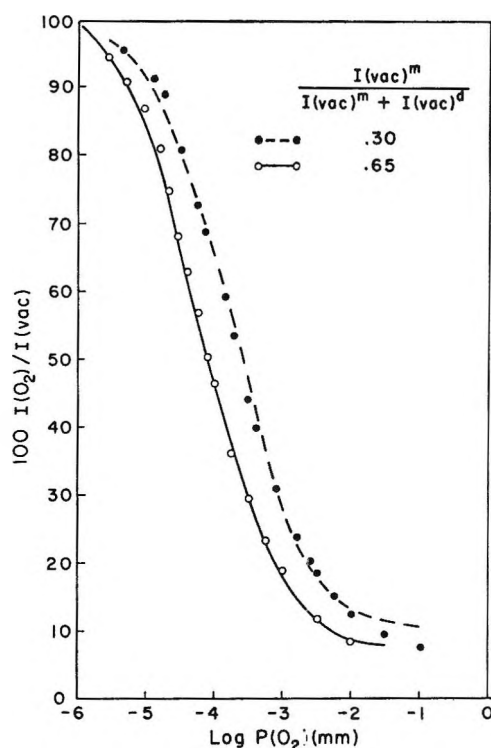


Figure 6. Phosphorescence quenching by oxygen at room temperature. Sample: 1.0×10^{-5} mole acriflavine/g of silica gel. Excitation and emission both under intermittent conditions. The circles represent experimental points. The curves are calculated from eq 13. The relative contribution of the monomer to the observed intensity (extrapolated to zero dark time for an evacuated sample) was 30% in the case of the filled circles and the dashed curve, and 65% in the case of the open circles and the solid curve.

The excellent agreement between theory and experiment over the pressure region 3.16×10^{-5} to 1×10^{-2} mm of oxygen pressure serves as added evidence for the validity of the proposed model of static quenching with a slight contribution to luminescence from the complex. The failure of the model to predict the proper amount of quenching for pressures greater than 10^{-2} mm of oxygen pressure is due to the failure to include the quenching of fluorescence, which begins to occur above 10^{-2} mm of oxygen pressure.^{21,22}

The significant process connecting phosphorescence

quenching with photosensitized oxidations is eq 4, the escape of oxygen from the excited complex with excess energy. The energy redistribution within the excited complex depends on the details of the potential energy surfaces, about which very little is known. It is interesting that the dimer complex shows a smaller chance for this redistribution of the excitation energy into the oxygen than does the monomer complex. (γ , a measure of the inefficiency of the energy transfer, is over three times as great for the dimer as for the monomer.) This might reflect the excitation delocalization in the dimer and suggests that a localized interaction between oxygen and the excited dye may be involved. It would be interesting to conduct systematic experiments to determine whether luminescence quenching by oxygen can be correlated with any of the localized molecular orbital parameters of the excited state, such as free valence.

We should point out that quenching requires not only that energy of excitation should flow into the complexed O₂, but also that the O₂* should escape from the complex before a reverse flow occurs followed by a radiative deexcitation of the dye. Rosenberg and Shombert indeed found that quenching does not occur below -182° because the O₂* cannot escape during the natural lifetime of the dye triplet.²³ A discussion of the nature of O₂* has been given elsewhere.¹⁹

There is a respectable body of evidence in the literature that O₂ quenches triplet states of aromatic substances in fluid solution by a collisional mechanism. Most of the reported systems have been studied by the triplet-triplet absorption technique, with oxygen concentrations considerably above those used here.²⁴⁻²⁶ If the static model is satisfactory for the dye-gel adsorbate reported here, why is it not appropriate for fluid media? One possible explanation is that the ground-state dye-oxygen complex might be too unstable in fluid media. Another possibility is that the time required for the energy redistribution in the excited state of the complex might not be short compared with the *actual* lifetime of the triplet in fluid media, where adventitious impurities reduce the lifetime to between 10^{-4} and 10^{-3} times the natural lifetime by a

(21) J. Franck and P. Pringsheir, *J. Chem. Phys.*, **11**, 21 (1943).

(22) S. Kato, *Bull. Chem. Soc. Japan*, **30**, 34 (1957).

(23) J. L. Rosenberg and D. J. Shombert, *J. Am. Chem. Soc.*, **82**, 3257 (1960).

(24) E. Fujimori and R. Livingston, *Nature*, **180**, 1036 (1957).

(25) R. Livingston and D. W. Tanner, *Trans. Faraday Soc.*, **54**, 765 (1958).

(26) G. Jackson, R. Livingston, and A. C. Pugh, *ibid.*, **56**, 1635 (1960).

dynamic mechanism. Probably, an experimental exclusion of a static quenching mechanism operative in fluid solutions (that might be in addition to the well-established dynamic quenching) has not yet been made, since most of the experiments recorded in the literature have been carried out with very intense saturating light flashes. It would be interesting to measure the relative quantum yield of triplet formation in weaker flashes as a function of oxygen pressure. This would be a more crucial test for the existence of nonphosphorescent $S \cdot O_2$ complexes.

We believe that Weiner and Seliger,¹⁸ like Rosenberg and Shombert,²³ erred in reporting oxygen-dependent triplet lifetimes by confining their analysis

to a later interval of time than in the present work. We showed that oxygen interacts more strongly with the slow component of decay, *i.e.*, $K_{eq}^m > K_{eq}^d$. Therefore, the observed decay at later times, when forced into an exponential formalism, will appear faster owing to the increased relative contribution of the dimer. Weiner and Seliger's report that the lifetime of triplets does not decrease indefinitely with increasing oxygen pressure indeed tends to support the mechanism presented in this paper. Their data on the "saturation" of the collisional decay constant at high oxygen pressure cannot be interpreted on the basis of their own mechanism, especially if a simple exponential decay is a parallel requirement, as they maintain.

Electron Paramagnetic Resonance Studies of Vitamin K

and Vitamin E Quinones¹

by John M. Fritsch, Shankar V. Tatwawadi, and Ralph N. Adams

Department of Chemistry, University of Kansas, Lawrence, Kansas 66044 (Received July 25, 1966)

A detailed study has been made of the electron paramagnetic resonance (epr) spectra of the anion radicals of vitamin K and E type quinones. In addition, the rates of electron transfer (homogeneous electron exchange) between the anions and the parent compounds were measured *via* epr line broadening. The epr spectra show that the characteristic side chain of vitamin K type quinones has relatively little effect on over-all chemical reactivity but materially influences the rate of simple chemical reactions such as electron transfer.

Despite intensive study over many years, the exact roles played by biologically important quinones in such processes as blood clotting and oxidative phosphorylation are still unknown. The final solution of such problems clearly will come from *in vivo* studies. Much remains to be known, however, about the oxidation-reduction characteristics, reactivities, etc., of biologically important quinones at the molecular level. This study is concerned with a detailed description of the electron paramagnetic resonance (epr) spectra of the monoanion radicals of several vitamin

K and E type quinones, their electron transfer rates (homogeneous electron exchange), and predictions of their rates of reaction in oxidation-reduction processes. The specific compounds investigated are shown in Figure 1.

(1) This work was supported by the Petroleum Research Fund administered by the American Chemical Society and the University of Kansas through its operation of computer facilities. The work was initiated while one of the authors (R. N. A.) was a J. S. Guggenheim Fellow and this support is gratefully acknowledged.

Experimental Section

The solutions of the radical ions were obtained by standard electrochemical reduction at a mercury-plated platinum gauze external to the epr cavity.² The solvents, *N,N*-dimethylformamide (DMF) and dimethyl sulfoxide (DMSO) were purified by conventional methods. Solutions were 0.5 to 1.0 mM in the various quinones and contained 0.1 M tetraethylammonium perchlorate (TEAP) as supporting electrolyte unless otherwise noted. The epr spectra were obtained with a Varian V-4500 spectrometer with a 6-in. magnet and Fieldial attachment. The reduction potentials for radical ion generation were chosen between the one- and two-electron polarographic waves. Half-wave potentials (essentially identical with the formal reduction potentials) for the one-electron process in DMF are listed in Table I.

Table I: Polarographic Half-Wave Potentials in *N,N*-Dimethylformamide^a

Compound	$E_{1/2}$
1,4-Naphthoquinone	-0.60 ± 0.02
Vitamin K ₃	-0.69 ± 0.03
Vitamin K _{1(120)}}	-0.76 ± 0.02
<i>p</i> -Benzoquinone	-0.48 ± 0.02
Duroquinone	-0.76 ± 0.02
Vitamin E quinone	-0.75 ± 0.03

^a For the first reduction step, a one-electron process. ^b In volts vs. a saturated calomel reference electrode.

Interpretation of Epr Spectra. Epr spectra of some of the vitamin quinone anions have been reported previously but without complete interpretation of the hyperfine splittings.³⁻⁸ From the structural viewpoint vitamin K₃ or menadione may be considered the simplest of the vitamin K quinones. Under moderately high resolution even the vitamin K₃ anion spectrum is quite complicated as seen in Figure 2. In general it was not possible to readily assign a single interpretation of splitting constants for the spectra of the vitamin K₃ and K_{1(120)}} anions. This was also true for vitamin E quinone anion. To establish which combinations of possible coupling constants and line widths could apply, each plausible approximate combination was computer plotted. For each of the spectra studied there was only one combination of coupling constants and line widths which yielded a reasonable approximation to the experimental spectrum. The precision of the coupling constants was then improved by varying the approximate values over small ranges

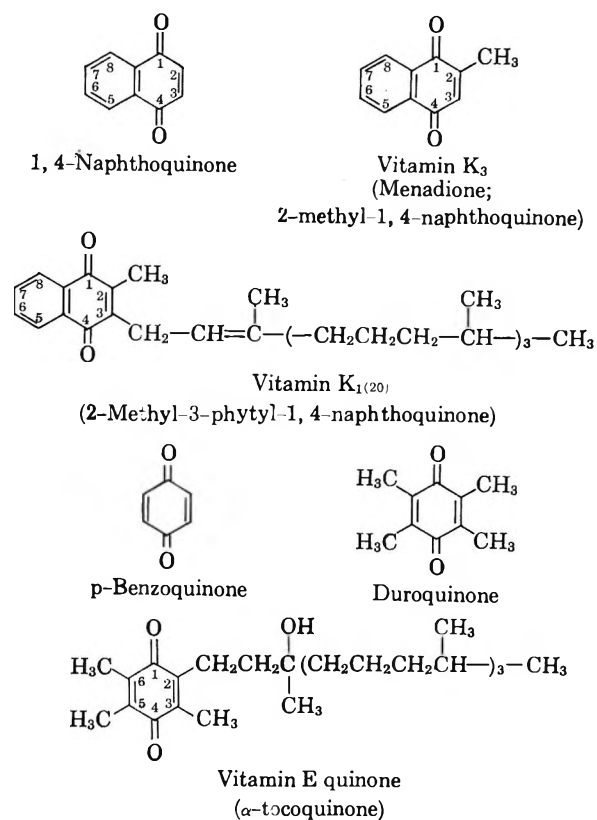


Figure 1. Vitamin quinones and related molecules studied by epr.

until optimum fittings of computer and experimental spectra were attained.

Unequivocal assignments for the ring protons in positions 5, 6, 7, and 8 of vitamins K₃ and K_{1(120)}} and the smaller methyl splittings in vitamin E cannot be made. These were assigned to be in best agreement with couplings predicted by McLachlan-modified Hückel MO calculations. The parameters used for these calculations are given in the Appendix.

The long side chain in vitamin K_{1(120)}} and vitamin E quinone was treated in the MO calculations as a methyl group with a slightly increased inductive effect. This treatment alters the coulomb integral of the carbon to which the side chain is attached as indicated in the Appendix. This approach is justified by the epr spec-

- (2) R. N. Adams, *J. Electroanal. Chem.*, **8**, 151 (1964).
- (3) S. Blois, *Biochim. Biophys. Acta*, **18**, 165 (1955).
- (4) J. E. Wertz and J. L. Vivo, *J. Chem. Phys.*, **24**, 479 (1956).
- (5) M. Adams, M. S. Blois, Jr., and R. H. Sands, *ibid.*, **28**, 774 (1958).
- (6) M. S. Blois, Jr., and J. E. Maling, *Biochem. Biophys. Res. Commun.*, **3**, 132 (1960).
- (7) Y. Matsunaga, *Bull. Chem. Soc. Japan*, **33**, 1436 (1960).
- (8) R. W. Brandon and E. A. C. Lucken, *J. Chem. Soc.*, 4273 (1961).

Table II: Proton Coupling Constants for the Vitamin K Semiquinone Radicals

Semiquinone	Solvent	Proton couplings (gauss) at position numbers ^a					
		2	3	5	6	7	8
1,4-Naphthoquinone	DMSO ^b	3.31	3.31	0.300	0.633	0.633	0.300
	DMF	3.27	3.27	0.26	0.57	0.57	0.26
	EtOH-H ₂ O ^c	3.23	3.23	0.513	0.655	0.655	0.513
	Alk ^d	3.22	3.22	0.57	0.57	0.57	0.57
Vitamin K ₃ · ⁻	DMSO	2.69 ^e	2.69	0.22	0.76	0.62	0.37
	DMF	2.69 ^e	2.69	0.22	0.78	0.61	0.36
	DMF-10% H ₂ O	2.80 ^e	2.51	0.40	0.69	0.69	0.40
	EtOH-H ₂ O ^f	3.01 ^e	2.38	0.64	0.64	0.64	0.64
	Alk ^d	2.94 ^e	2.40	0.59	0.59	0.59	0.59
Vitamin K ₁₍₂₀₎ · ⁻	DMSO	2.63 ^e	1.41 ^g	0.30	0.74	0.74	0.26
			1.22 ^g				
	DMF	2.63 ^e	1.39 ^g	0.30	0.74	0.74	0.26
			1.23 ^g				
	Alk ^d	2.2 ^e	1.1	0.55	0.55	0.55	0.55

^a The precision of the coupling constants is ± 0.02 gauss. ^b Data from E. W. Stone and A. H. Maki, *J. Chem. Phys.*, **36**, 1944 (1962). ^c A basic alcohol-water mixture, data from G. Vincow and G. K. Fraenkel, *ibid.*, **34**, 1333 (1961). ^d Alkaline aqueous solution with some alcohol or acetone, data from ref 5 and 6. ^e Methyl proton couplings. ^f 50% v/v alcohol-water buffer, apparent pH 8. ^g Nonequivalent proton couplings at methylene carbon of side chain.

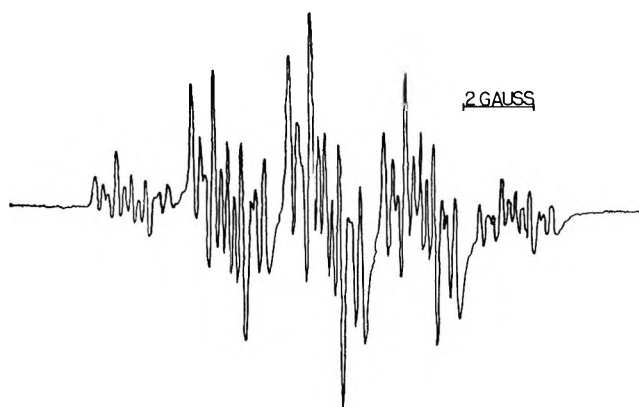


Figure 2. Epr spectrum of vitamin K₃ monoanion in dimethyl sulfoxide.

tra which show that within the present resolution there is no unpaired electron density in the side chain beyond the first methylene group. Blois and Maling earlier predicted and verified that interactions with protons further out on the side chain would be very weak if, indeed, they existed.⁶ It is very interesting that, with the increased resolution of the present study, it can be shown clearly that the methylene protons of vitamin K₁₍₂₀₎ semiquinone are nonequivalent. This lack of equivalence has also been noted in the nmr spectra of the parent molecule.⁹ Steric interactions between the phytol chain and the adjacent 2-methyl group might cause this. However, it is felt more likely due to hydrogen bonding of the ethylenic proton to the carbonyl oxygen in the anion radical. The infrared

spectrum indicates any such hydrogen bonding in the parent compound must be weak.¹⁰ In favor of the hydrogen bonding argument for the semiquinone are (1) increased electron charge on the carbonyl oxygen in the anion radical, (2) potential formation of a six-membered ring, and (3) a decrease in the nonequivalency of the methylene protons with increasing temperature. For even a weak hydrogen bond, a molecular model clearly shows the methylene protons would be nonequivalent due to twisting of the methylene carbon out of the plane of the aromatic system. As far as can be ascertained, the methylene protons of vitamin E semiquinone are equivalent. Tables II and III summarize all of the coupling constants for the vitamin K and vitamin E type compounds studied and compare them with some previous literature data.

The proton couplings at positions five and eight in the naphthoquinone system are markedly solvent dependent. This is also true, to a lesser extent, for positions two and three. These differences in coupling constants for aqueous and DMF DMSO systems are clearly seen in Table II. All the couplings are essentially invariant between DMF and DMSO. However, the intrinsic line width for the K₃ anion is considerably larger in DMF. The line width for K₁₍₂₀₎ anion is large in both solvents and may reflect a small

(9) C. von Planter, E. Billeter, and M. Kofler, *Helv. Chim. Acta*, **42**, 1278 (1959).

(10) O. Ister and O. Wiss in "Vitamins and Hormones," R. S. Harris, G. F. Marrian, and K. V. Thimann, Ed., Vol. 17, Academic Press, New York, N. Y., 1959, p 62.

Table III: Proton Coupling Constants for Vitamin E and Related Semiquinones^a

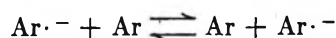
Semiquinone	Solvent system	Proton coupling, gauss
<i>p</i> -Benzoquinone	DMF	2.41
	DMSO ^b	(2.419)
	EtOH-H ₂ O ^c	(2.368)
Duroquinone	DMF	Methyl H's 1.91
	EtOH-H ₂ O ^c	Methyl H's (1.897)
Vitamin E quinone	DMF	Methyl, position 5 and 6 2.21
		Methyl, position 3 1.60
	Methylene ^d	0.81

^a The precision of the coupling constants is ± 0.01 gauss, previous literature data in parenthesis. ^b Data of Stone and Maki, see footnote *b* in Table I. ^c Data of B. Venkataraman, B. G. Segal, and G. K. Fraenkel, *J. Chem. Phys.*, **30**, 1006 (1959). ^d For two equivalent methylene protons on side chain at position 2.

(0.05–0.1 g) unresolved coupling of the ethylenic proton.

The point of examining the epr spectra of the vitamin quinone anions in detail was to see if there might be important differences in unpaired electron distribution between members of the series which would reflect differences of chemical reactivity in the aromatic portion of the molecules. It is quite clear that the effects of substitution, even of large side chains, is minimal with respect to the aromatic portion of the 1,4-naphthoquinone nucleus. Certainly, positions for chemical reactivity become blocked as one proceeds in substitution from 1,4-naphthoquinone and vitamin K₁₍₂₀₎. Both MO calculations and the experimental electrochemical and epr results support this view. The conclusions with regard to the K₁ vitamin series can be transposed to the K₂ compounds since these differ only in the length and nature of isolated double bonds in the side chain. In the next section, the above conclusions are contrasted to the marked differences in rates of chemical reactions of these compounds where the large side chains do play an important role.

Electron Transfer Rates. The electron transfer process of present interest is given for a neutral molecule Ar and its radical anion Ar^{•-} by the equation



This is the simplest of chemical reactions in which the reactants are identical with the products. (This process is commonly called homogeneous electron exchange. The terminology electron transfer is used here to differentiate it from such processes as spin-spin electron

exchange in which radical ions also participate under other conditions.) For the present study Ar represents the parent quinone and Ar^{•-} the semiquinone anion radical. Since one of the two species is paramagnetic, the rate constant k_{exc} can be determined from the epr line broadening as a function of the concentration of the parent quinone.^{11,12}

Table IV lists the values of k_{exc} determined. A major difficulty in evaluating these rate constants is the heavily overlapped spectra of the vitamin K type molecules. The problem was solved by a computer technique which accounts for merging of lines concurrent with the broadening process.

Table IV: Electron Transfer Rates in N,N-Dimethylformamide

Compound	k_{exc}^a
1,4-Naphthoquinone	$(4.2 \pm 0.3) \times 10^8$
Vitamin K ₃	$(4.0 \pm 0.5) \times 10^8$
Vitamin K ₁₍₂₀₎	$(1.3 \pm 0.5) \times 10^8$
<i>p</i> -Benzoquinone ^b	$(3.8 \pm 0.2) \times 10^8$
Duroquinone ^b	$(6.2 \pm 0.3) \times 10^7$
Vitamin E quinone	$(1.6 \pm 0.3) \times 10^7$

^a In l./mole-sec. ^b Data from ref 12.

Contrary to the previous effect on electron distribution and reactivities of the aromatic nucleus, in the rate studies a long side chain has a considerably greater effect than a simple methyl substitution. The value of k_{exc} for the K₁₍₂₀₎ system is one-third that of the K₃ and vitamin E quinone has a rate constant one-fourth that of duroquinone. From the precision of the k_{exc} values in Table IV it can be seen that these differences are quite real.

The k_{exc} values can be used to predict the cross reaction rates of compounds in a conventional oxidation-reduction reaction *via* the theory and prediction of Marcus.¹³ In the one-electron oxidation-reduction reaction



with an equilibrium constant of K_{12} and a forward rate of k_{12} , one denotes the individual k_{exc} values as k_{11} for Ox₁/Red₁ and k_{22} for Ox₂/Red₂. If k_{11} and k_{22}

(11) R. I. Ward and S. I. Weissman, *J. Am. Chem. Soc.*, **79**, 2086 (1957).

(12) T. Layloff, T. Miller, R. N. Adams, H. Föh, A. Horsfield, and W. Proctor, *Nature*, **205**, 4969 (1965).

(13) R. A. Marcus, *J. Chem. Phys.*, **43**, 679 (1965).

as well as K_{12} are known, according to Marcus, the forward rate of the cross reaction is given by

$$k_{12} = (k_{11}k_{22}K_{12}f)^{1/2} \quad (2)$$

where the quantity f is given by

$$\ln f = \frac{(\ln K_{12})^2}{4' \ln (k_{11}k_{22}/10^{22})} \quad (3)$$

Equation 2 has been found valid for quite a few inorganic oxidation-reduction reactions especially by Sutin and co-workers.¹⁴

Rather than predict the values of k_{12} for the compounds studied herein, it is of more interest to compare the relative ratios of predicted k_{12} values. If one considers a series of reductants Red₂, Red₃, Red₄, etc., all reacting with the same Ox₁ (or the opposite process of several oxidation species reacting with a common reduction species) then the relative values k_{12} , k_{13} , k_{14} , etc., can be calculated readily *via* eq 2 and 3. Thus, consider the situation where Red₃ is used in eq 1 and assume k_{33} equals $4k_{22}$ for which the equilibrium constant is unchanged. From eq 3, the effect of the change on f is very small but the over-all value of k_{13} is increased by a factor of 2. This applies to the reactions of vitamin E quinone as compared to duroquinone where the k_{exoc} values are in this ratio and their formal potentials are so close that any difference in equilibrium constants with a common reactant are small.

For vitamins K₃ and K₁₍₂₀₎ the predicted cross-reaction rates are more influenced by the relative equilibrium constants since their formal potentials differ somewhat. From these potentials if K₃ and K₁₍₂₀₎ react with a common reductant, the equilibrium constants should differ by a factor of about 12. This enters into eq 2 but still does not materially affect the value of f (frequently close to unity) in eq 3. Hence, it can be predicted that vitamin K₃ should react six to seven times faster than vitamin K₁₍₂₀₎ with a common reductant.

Summary

The epr hyperfine spectra show clearly that from the reactivity viewpoint, the aromatic nuclei of the vitamin K type compounds are practically uninfluenced by the nature of the side chain. (This argument cannot be applied indiscriminately to vitamin E quinone

because of intramolecular interactions of its side chain with the ring and the further discussion is limited to the K type compounds.) Thus, vitamin K₃, or certainly 2,3-dimethyl-1,4-naphthoquinone, is an acceptable substitute for the K₁ or K₂ vitamin series in terms of intrinsic reactivity. On the other hand, the rates of the simple chemical reactions are affected by the size of the side chain. Two attitudes may be taken with regard to the rate differences. If the differences in rates are considered significant, then they may well play a role in biological electron transport processes. For instance, the exact role of ubiquinone in mitochondrial electron transport is open to question because its oxidation-reduction rate differs somewhat from that of the over-all electron transport rate in the respiratory chain.¹⁵ If, alternately, the rate differences, which are indeed small, are considered non-influential in this sense, then the only biological significant differences in the vitamin K compounds are that the side chains provide lipid solubility or spatial characteristics significant for proper participation in the complexity of oriented *in vivo* reactions. The latter, of course, may be considered as a type of specific reactivity.

Appendix

In the MO calculations,¹⁶ the fairly standard value of $\lambda = 1.2$ was used. The coulomb integral for oxygen was taken as $\alpha_O = \alpha_C + 1.26\beta_{CC}$ and the resonance integral for the carbonyl bond was $\beta_{CO} = 1.55\beta_{CC}$.¹⁷ For those carbons to which a methyl is attached, the coulomb integral used was $\alpha_{CC(\text{Me})} = \alpha_C - 0.3\beta_{CC}$.¹⁸ For the side chain treated as a methyl group, the coulomb integral of the ring carbon to which the side chain is attached was taken as $\alpha_{C(\text{C-R})} = \alpha_C + h\beta_{CC}$. The value of h was varied between -0.2 and -0.8 in a sequence of calculations employing the other mentioned parameters. A value of -0.4 was found to fit best, as would be expected from this model.

(14) R. J. Campion, N. Purdie, and N. Sutin, *Inorg. Chem.*, **3**, 1091 (1964).

(15) B. Chance in "Biochemistry of Quinones," R. A. Morton, Ed., Academic Press, New York, N. Y., 1965, Chapter 14.

(16) A. D. McLachlan, *Mol. Phys.*, **3**, 233 (1960).

(17) J. Gendell, J. H. Freed, and G. K. Fraenkel, *J. Chem. Phys.*, **37**, 2832 (1962).

(18) J. P. Colpa, C. Maclean, and E. L. Mackor, *Tetrahedron*, **19**, Suppl. 2, 65 (1963).

Infrared Spectra of Carbon Monoxide Adsorbed on Some Evaporated Metal Films

by J. F. Harrod,¹ R. W. Roberts, and E. F. Rissmann

General Electric Research and Development Center, Schenectady, New York (Received July 26, 1966)

Infrared spectra of CO adsorbed on evaporated thin films of Rh, Pd, Ir, and Pt have been measured. A technique was devised for measuring such spectra by transmission through several very thin films (ca. 100 Å each) onto which CO was adsorbed. Initial studies to prove the feasibility of the method and to determine effects of contaminants such as H₂O, O₂, and H₂ on the spectra were performed with films evaporated at ca. 10⁻⁶ torr and reduced with H₂ prior to adsorption of CO. The spectra of H·COOH and H·CHO on Rh, Pd, Ir, and Pt were also measured in such a system. After the feasibility of the multiple-transmission technique was established, it was adapted for use with an ultrahigh-vacuum system and spectra of CO adsorbed on atomically clean Rh, Pt, and Ir were successfully measured. The latter spectra leave little doubt that those observed on contaminated samples of these metals are primarily due to CO and not some reaction product of CO with surface contaminants. Some preliminary kinetic studies of the oxidation of CO adsorbed on Ir are also discussed.

Introduction

During the past decade, many studies have been reported concerning the infrared spectra of carbon monoxide adsorbed on highly dispersed metal particles.²⁻⁹ Such studies provide information on the structure of chemisorbed carbon monoxide, the effects of coadsorbates on the metal-CO interaction, the effect of the support material on metal-CO interaction, and the kinetics of a variety of chemical reactions involving either gaseous or adsorbed CO.

Our initial interest in this subject was directed toward the use of infrared spectroscopy for studying rates of, and intermediates in, surface chemical reactions. The high extinction coefficient and strong chemisorption of CO made it particularly attractive for such studies, but there was serious doubt in our minds that the various methods used for preparing surfaces and observing spectra would be suitable for meaningful kinetic studies. The pressed-pellet method, first described by Eischens,¹⁰ suffered two possible serious disadvantages: (1) the rate of gas diffusion into and out of the pellet may be rate controlling, and (2) it is virtually impossible to obtain an atomically clean surface in this type of system.

Our ultimate objective was to make measurements on

CO that had been adsorbed onto an atomically clean metal. Eischens had reported² the successful observation of the transmission spectrum of CO adsorbed on a sputtered platinum film. Since the preparation of similar films, followed by the adsorption of CO onto them, seemed feasible as an ultrahigh-vacuum (<10⁻⁸ torr) experiment, we decided to investigate the utility of such a method.

(1) To whom correspondence should be addressed at Chemistry Department, McGill University, Montreal, Can.

(2) R. P. Eischens and W. A. Pliskin, *Advan. Catalysis*, **10**, 1 (1958).

(3) (a) A. C. Yang and C. W. Garland, *J. Phys. Chem.*, **61**, 1504 (1957); (b) C. E. O'Neill and D. J. C. Yates, *ibid.*, **65**, 931 (1961).

(4) J. B. Sardisco, *Perkin-Elmer Instrument News*, **15**, No. 1, 13 (1963).

(5) G. Blyholder, *J. Chem. Phys.*, **36**, 2036 (1962).

(6) H. L. Pickering and H. C. Eckstrom, *J. Phys. Chem.*, **63**, 512 (1959).

(7) R. A. Gardner and R. H. Petrucci, *J. Am. Chem. Soc.*, **82**, 50 (1960).

(8) C. W. Garland, R. C. Lord, and P. F. Troiano, *J. Phys. Chem.*, **69**, 1188 (1965).

(9) N. N. Kavtaradze, E. G. Borekova, and V. I. Lygin, *Kinetika i Kataliz.*, **2**, 378 (1961).

(10) R. P. Eischens, S. A. Francis, and W. Pliskin, *J. Chem. Phys.*, **22**, 1786 (1954).

Since we began our study, other workers have reported the difficulty that may be encountered in observing the transmission spectrum of CO adsorbed on metal films which have been evaporated under good vacuum conditions.⁸ These workers resorted to evaporating the metal in the presence of CO in order to obtain detectable spectra. Because occlusion and disproportionation of CO on hot metal filaments are possible under these conditions, we chose the alternative method of obtaining detectable spectra by means of stacking a number of very thin clean metal films in series in the beam of the spectrometer. We shall refer to this method as "multiple transmission" as opposed to the multiple-reflection method used by Pickering and Eckstrom.⁶

Experimental Section

All measurements were made on a Model 21 Perkin-Elmer spectrometer, with variable attenuation in the reference beam.

High-purity wires for filaments were obtained from Sigmund Cohn Inc., Mt. Vernon, N. Y. Minimum purities were Pd, 99.5% and Pt, Rh, and Ir, 99.9%. Gases were obtained from Airco Reduction.

Preliminary Observations on Contaminated Metal Films. Preliminary experiments to determine the feasibility of using the multiple-transmission technique were performed using the apparatus shown in Figure 1.

Films of the desired metal were evaporated onto 10-mm \times 1-mm circular NaCl disks. The films were evaporated from filaments in a bell jar at *ca.* 10^{-6} torr in such a way that both sides of the disks were coated with a film *ca.* 100 Å thick. A stack of ten such disks was found to have a transmission of *ca.* 10% compared to ten uncoated disks at 2000 cm^{-1} .

After deposition of the films, the disks were removed from the bell jar and ten of them were stacked in the aluminum holder (A) with a ring spacer 0.5-mm thick between each disk. The holder was placed inside the Pyrex cell and the cell was attached to a conventional vacuum system capable of rapidly achieving *ca.* 10^{-6} torr. The cell was made from a standard $29/42$ Pyrex ground-glass joint (F). The ends were flanged and closed by sealing on 1.75-in. rock salt windows (E) with epoxy resin.

A piece of heating tape wrapped around the cell in the vicinity of the aluminum disk holder, and about 15 mm removed from the window, allowed heating of the sample to *ca.* 150° .

All pressures were measured with electronic gauges (1.0–760 torr, Alphatron gauge; 0.001–1.0 torr, thermistor gauge; and <0.001 torr, ionization gauge) to avoid mercury contamination.

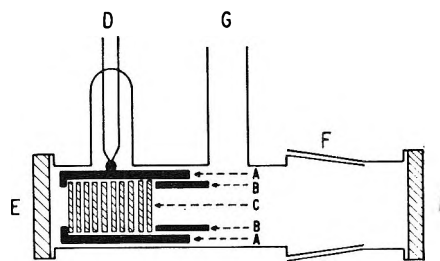


Figure 1. Cell system for preliminary investigation of multiple transmission spectra of CO on evaporated metal films: A, cylindrical aluminum disk holder; B, retaining sleeve; C, NaCl disks; D, thermocouple; E, NaCl windows; F, $29/42$ ground-glass joint; G, attachment to vacuum system.

Observations on Atomically Clean Metal Films. The apparatus used for generating and making measurements on clean films will be described in detail elsewhere.¹¹ Two major problems had to be overcome before the experiments could be performed. The first problem was to design a window system capable of withstanding repeated bakeout at *ca.* 200° and the second was to devise a system for the mechanical manipulation of the sodium chloride disks under high vacuum.

The apparatus used is illustrated schematically in Figure 2. The outer part (Figure 2a) consisted of a stainless steel tower the lower portion of which served as the infrared cell and the upper portion as a chamber for the evaporation of the metal films. The lower portion of the tower was fitted with 1-in. LiF windows (A) and the upper portion with 1-in. Pyrex observation ports (D).

The inner part of the apparatus (Figure 2b) consisted of a set of five disk holders (E) which could be moved up and down in parallel tracks by a magnetically activated vertical screw (F). Only one of the disk holders was coupled to the screw, but as it traveled upwards it picked up the second by an overlap of flanges at the bottom of the first and top of the second holder. Then flanges at the bottom of the second picked up the third and so on until by the time the first holder reached the top of the screw all five disk holders were strung out, one below the other, in the upper part of the tower. In this position, metal could be evaporated onto both sides of the disks from filaments supported by posts (G) attached to the lid of the tower. Also attached to the lid of the tower was a magnetically activated shutter system (H) for protecting the observation ports during evaporation of the filaments.

After the evaporation, the disk holders were lowered by reversing the screw, each holder coming to rest on

(11) R. W. Roberts and J. F. Harrod, to be published.

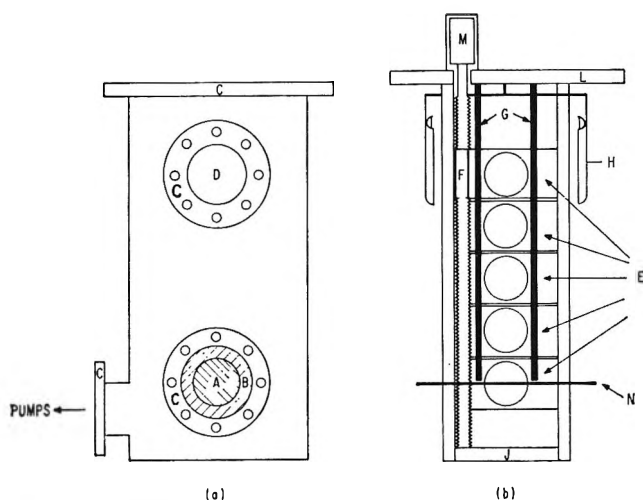


Figure 2. Ultrahigh vacuum cell for clean metal film studies. (a) Outer cannister: A, LiF windows; B, Ag spinning; C, press-seal flanges; D, Pyrex observation port. (b) Evaporation and disk manipulation assembly: E, disk holders; F, traveling nut; G, filament support posts; H, observation port shutters; J, base plate; L, lid; M, magnetic drive for screw.

the base plate (I) until by the time the uppermost holder reached the base plate they were all in series with each other and with the windows of the cell compartment. In these experiments five 25×2 -mm NaCl disks were used.

The windows of the cell were of a special design. A thin gold film was applied to the outer $1/8$ -in. of a 1-in. LiF disk. The disk was sealed with AgCl to a silver spinning which was in turn welded to a stainless steel flange which could be bolted to the outer can of the apparatus and sealed with conventional annealed copper shear gaskets. Of six such windows, two failed after the first bakeout and four have had extensive use without failure (one pair has survived twenty 24-hr bakeouts to 200° without failure).

The cell was attached to a conventional bakeable ultrahigh-vacuum system on a movable table. After bakeout the cell could be moved in and out of the spectrometer beam, when required, by moving the whole system.

A typical experiment was conducted as follows. Five freshly polished NaCl disks were mounted in the holders, and two filaments of the required metal, each consisting of 14 cm of 10-mil, high purity wire, were strung diagonally from the conductor posts opposite both faces of the disks. The apparatus was assembled and baked out for 24 hr with the cell assembly at 200° and the gas handling system at 300° . During the bakeout, the filaments were electrically heated to *ca.* 200 – 300° below their melting point and the disks were kept in

the lowered position. After the first bakeout, the system would normally pump down to *ca.* 10^{-8} torr. However, operation of the screw to raise and lower the disks resulted in considerable release of gas, the pressure rising sometimes as high as 10^{-5} torr. The screw was operated until the disks could be raised and lowered without raising the pressure of the system above 5×10^{-7} torr. During this period the filaments were also pulsed to evaporating temperature until they no longer raised the pressure above 5×10^{-7} torr.

After the above degassing procedure, a second bakeout under the same conditions as the first usually resulted in the achievement of a pressure of *ca.* 10^{-8} torr which could be maintained while operating both the screw and the filaments. After achieving such a vacuum, the disks were raised into the filament chamber and coated with metal. The evaporation rate was adjusted so that the total transmission of the disks would be reduced to *ca.* 10% at 2000 cm^{-1} , relative to the same disks before coating, after 1–2 min evaporation time. This corresponded to film thicknesses of *ca.* 100–200 Å and was found to give optimum resolution and intensity of spectra.

After coating, the disks were lowered into the cell, the spectrometer was returned to zero with a variable attenuator in the reference beam, and a base line was recorded. After recording the base line, CO (0.1 torr) was admitted to the cell and spectra were recorded periodically for a period of 1 hr.

After the initial spectrum was established, the system was pumped out and further spectra were recorded. At this point, the adsorbed CO was usually removed by oxidation or reduction (10 torr of O_2 or H_2), the system was pumped out and CO re-adsorbed, and the spectrum was recorded again. The latter procedure was usually repeated several times.

Results

1. *Spectra of CO Adsorbed on Contaminated Films.* Investigations were carried out using rhodium, palladium, iridium, and platinum films. Spectra were obtained of CO adsorbed on each of these metals. The CO spectra varied consistently in intensity on these four metals, with iridium $>$ rhodium \sim platinum $>$ palladium. Twenty 1-cm films of iridium usually gave a CO band with absorbance ~ 0.2 , platinum ~ 0.1 , and palladium < 0.1 . Rhodium gave two bands with roughly equal absorbance ~ 0.05 .

Effects of Hydrogen on Spectra of Adsorbed CO. The absorption maxima of the CO spectra are sensitive to the presence of other species adsorbed on the metal surface. When CO was adsorbed on a hydrogen-covered iridium film (CO pressure *ca.* 1 torr), the growth of the

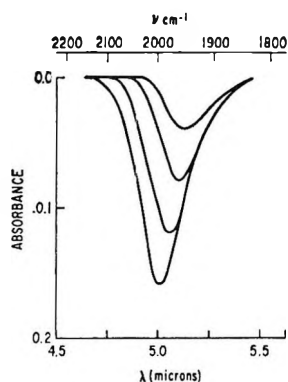


Figure 3. Removal of CO on Ir by H_2 . $T = 50^\circ$; $P_{H_2} = 10$ torr; 5-min intervals between scans.

CO peak could be observed. As the peak grew, the absorption maximum moved progressively to higher frequency. If the gaseous CO was pumped off and hydrogen (~ 10 torr) admitted, the peak decayed, moving to a lower frequency as it disappeared (Figure 3). The total shift between maximum and minimum observable intensities was generally *ca.* 50 cm^{-1} , and in the case of iridium the peak never shifted outside the envelope of the maximum intensity band.

Similar shifts in direction and magnitude were observed in the spectra of CO on Rh, Pd, and Pt. With these metals, however, the peaks initially shifted outside the envelope of the maximum intensity bands.

Effects of Oxygen on Spectra of Adsorbed CO. If oxygen (1.0–10 torr) was added at room temperature to films of Ir, Rh, Pd, or Pt covered with CO, the infrared bands disappeared at a measurable rate. In the cases of Ir, Rh, and Pt, there was virtually no shift of the absorption maxima as the bands disappeared. In the case of Pd, there was a significant shift (*ca.* 50 cm^{-1}) of the band to lower frequency, but it did not move outside the envelope of the maximum intensity band.

The reaction of gaseous CO with oxygen-covered films of the four metals was very dependent on the history of the samples. In all cases, if freshly prepared films were exposed to CO, the growth of an infrared band due to adsorbed CO could be observed in the course of 1–2 hr at room temperature. If the films were aged in oxygen for 24 hr, the growth of the CO peak was usually very slow (24–48 hr) and sometimes could not be observed at all. The shifts in the absorption maxima on appearance of the CO peaks corresponded to those observed on oxidation of adsorbed CO.

Effects of Water on Spectra of Adsorbed CO. Exposure of CO adsorbed on Pt and Ir films to water vapor (*ca.* 10 torr) produced small but reproducible changes in the spectrum. In both cases the CO peak underwent a slight increase in intensity (*ca.* 5–10% ab-

sorbance) and a slight shift ($10\text{--}20\text{ cm}^{-1}$) to lower frequency. If the water vapor was pumped off, the peak returned to its original position and intensity.

The effect of water on CO adsorbed on Rh was more complicated than with Ir and Pt. Exposure of a CO-covered Rh sample to water vapor (10 torr) resulted in a decrease in the intensity of the 2000 cm^{-1} peak to *ca.* 50% initial absorbance and a shift of *ca.* 20 cm^{-1} to lower frequency. At the same time, the 1850 cm^{-1} peak approximately doubled in intensity and shifted *ca.* 30 cm^{-1} to lower frequency. Removal of the water vapor by pumping resulted in a further considerable decrease in the 2000 cm^{-1} band, but only a small decrease in the intensity of the 1850 cm^{-1} band. A second exposure of the sample to water resulted in a further decrease in the 2000 cm^{-1} band and a further enhancement of the 1850 cm^{-1} band. These effects are illustrated in Figure 4.

Exposure of CO adsorbed on palladium to water vapor (10 torr) led to rapid disappearance of the CO peak. On disappearing, the peak shifted progressively to lower frequency in the same manner as observed with hydrogen reduction of CO on palladium.

Effects of Acetylene on the Spectra of Adsorbed CO. Two series of experiments were performed, one in which adsorbed CO was exposed to gaseous acetylene and another in which adsorbed acetylene was exposed to gaseous CO. In both series the initial adsorption was onto hydrogen-covered surfaces.

In the cases of Rh, Ir, and Pt, gaseous acetylene was not found to have any effect on the spectra of adsorbed CO, but CO was found to adsorb on acetylene-covered surfaces to give spectra identical with those of CO adsorbed on hydrogen-covered surfaces.

CO was also found to adsorb onto an acetylene-covered Pd surface, but contrary to the observations on the other three metals, gaseous acetylene was found to cause the disappearance of the spectrum of CO adsorbed on palladium.

Spectra of Formaldehyde and Formic Acid Adsorbed on Rh, Pd, Ir, and Pt Films. Exposure of hydrogen-covered Pt and Ir films to a few millimeters of formaldehyde or formic acid vapor at room temperature resulted in the appearance of infrared bands indistinguishable from those observed on adsorption of CO onto hydrogen-covered films of the same metals. Evacuation did not result in any measurable changes in the spectra.

In the case of rhodium, formaldehyde resulted in the appearance of a major band in the 1850 cm^{-1} region, which moved to higher frequency as it grew to maximum intensity, and a considerably smaller peak in the 2000 cm^{-1} region. Formic acid also gave two peaks on Rh, a small one at 2000 cm^{-1} and a larger one at 1780

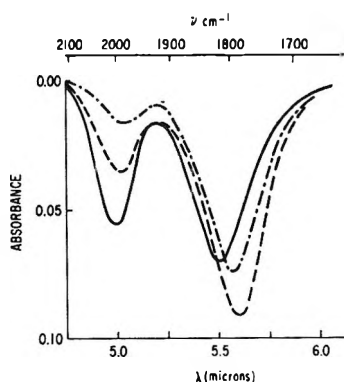


Figure 4. Effect of H_2O on spectrum of CO adsorbed on Rh: —, initial spectrum; ---, after exposure to H_2O (10 torr, 30 min); - · - ·, after pumping at 10^{-6} torr for 30 min.

cm^{-1} at maximum intensity. The latter peak, in addition to being at lower frequency than any observed with CO or formaldehyde, was considerably broader than those observed with other adsorbates.

Adsorption of formaldehyde or formic acid onto palladium films did not give rise to any detectable infrared bands in the CO region.

2. *Spectra of CO Adsorbed on Clean Metal Films.* The infrared spectra of CO adsorbed on clean films of Rh, Ir, and Pt were successfully recorded. No spectrum due to CO adsorbed on palladium was detected in four attempts.

Figure 5 shows the spectrum of CO adsorbed on a clean Rh film compared to the spectrum obtained with a contaminated, hydrogen-covered film. The spectra are both characterized by peaks at *ca.* 2000 and 1850 cm^{-1} . In fact, the spectrum shown for the contaminated film was chosen randomly from many samples and the variations between the many spectra observed on contaminated films are as great as the apparent differences between the spectra shown in Figure 5.

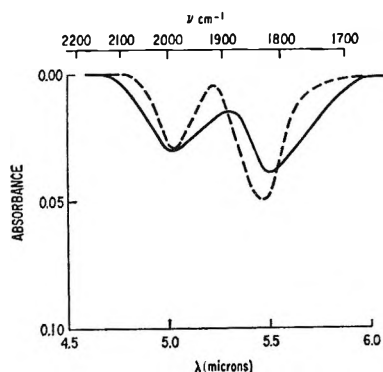


Figure 5. Spectra of CO adsorbed on clean (—) and contaminated (---) Rh films.

The spectra of CO adsorbed on clean Pt and Ir films are almost identical and are shown in Figures 6 and 7. The spectra are characterized by a sharp absorption edge at *ca.* 2050 cm^{-1} , a definite peak at 2030 cm^{-1} , and a broad, structureless absorption tailing out to *ca.* 1500 cm^{-1} . Removal of CO by exposure to oxygen (10 torr) for 1 hr followed by removal of gaseous oxygen and re-adsorption of CO resulted in slightly different spectra. The broad structureless absorption had largely disappeared and instead there was a single large peak at *ca.* 2000 cm^{-1} with both Ir and Pt and a suggestion of a second broad, weak peak at *ca.* 1750 cm^{-1} in the case of Pt (Figures 6 and 7).

After the first oxidation and re-adsorption of CO, the oxidation-re-adsorption cycle could be repeated many times without significantly altering the CO spectrum.

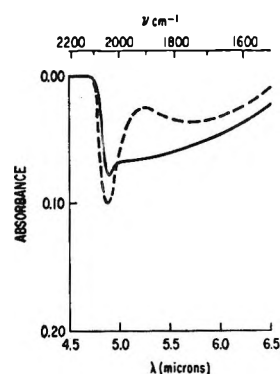


Figure 6. Spectra of CO on evaporated Pt: —, freshly evaporated, clean Pt; ---, after oxidation and re-adsorption of CO.

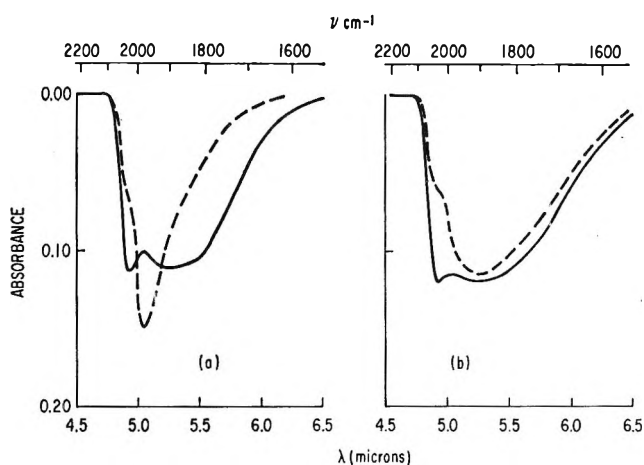


Figure 7. Spectra of CO adsorbed on evaporated Ir. (a) —, CO on freshly evaporated, clean Ir, and ---, after oxidation and re-adsorption of CO. (b) —, CO on freshly evaporated, clean Ir, and ---, same sample after exposure to H_2 (700 torr) for 20 min.

Rather unusual behavior was noted for CO adsorbed on clean Ir when the sample was exposed to hydrogen (100 torr). The peak at 2050 cm^{-1} disappeared almost immediately, but the broad absorption at lower frequency was virtually unaffected after 1 hr. Such resistance to hydrogen reduction was contrary to the behavior of CO adsorbed on contaminated Ir films.

3. *Kinetic Studies on the Oxidation of CO on Ir.* An extensive study of the oxidation of CO on contaminated Ir films was undertaken. Although the infrared technique promised to provide a relatively simple method for observing the surface oxidation of adsorbed CO, the results proved to be plagued by the usual problems of irreproducibility that are characteristic of many surface reactions.

In the first place, there is a variation in both position of the absorption maximum and the absorbance in going from one set of films to another. In Figure 8 we show a display of the results of 40 separate observations of the position of the absorption maximum and the absorbance per film for CO adsorbed on iridium films. Since there is considerable variation between different film samples (thickness, surface area, etc.) it is not surprising that there is considerable scatter in these data. However, we do feel that the pronounced tendency for samples with the absorption maximum at lower frequency to have lower absorbance is real and reflects varying degrees of contamination of the metal surface.

Many experiments were performed in which the disappearance of CO was followed in the presence of oxygen. The absorbance data from these experiments could be plotted as shown in Figure 9. In this figure, the logarithm of the absorbance (A) relative to the initial absorbance (A_0) is plotted *vs.* time. It can be

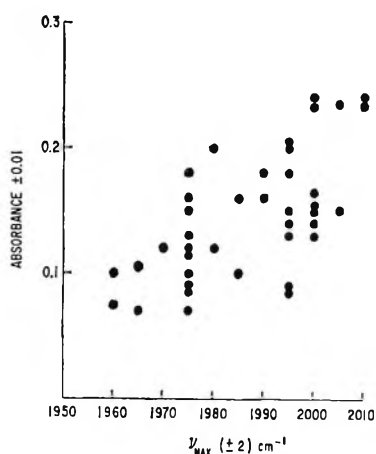


Figure 8. Absorbance at maximum coverage *vs.* frequency of absorbance maximum for CO on Ir for 40 separate experiments on contaminated films.

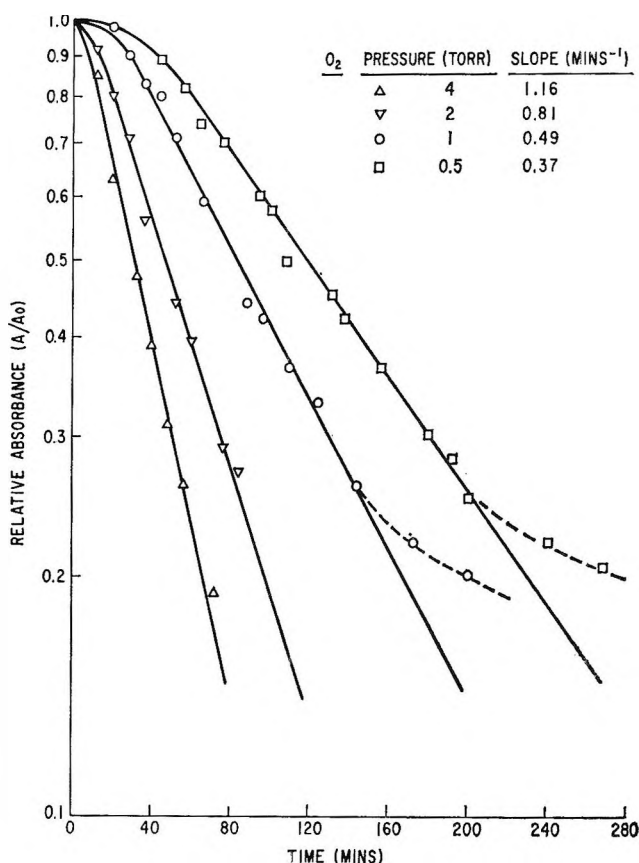


Figure 9. Oxidation of CO on Ir. Plots of absorbance (A) relative to absorbance at maximum CO coverage (A_0) *vs.* time ($T = 50^\circ$).

seen that each curve has a considerable linear portion for several different oxygen pressures. A log-log plot of the slopes of the curves in Figure 9 *vs.* oxygen pressure is shown in Figure 10. It can be seen that the data lay close to the line of slope 0.5.

All of the data shown in Figures 9 and 10 were obtained with a single set of films and represent the best obtained by us. The digits adjacent to the points in Figure 10 represent the chronological order in which the data were gathered and the point at 4 torr of oxygen pressure was reproduced after the other points were obtained. The whole series of measurements were taken during a period of 4 days and the initial intensity of the CO peak had not changed by more than 10% during these five sets of measurements. Whenever it was necessary to leave the disks overnight, they were stored under 10 torr of CO.

The details of the last paragraph were stressed because they were not typical of all of the oxidation rate measurements. They were in fact typical of several experiments in which high initial absorbance and a high frequency absorption maximum were observed. How-

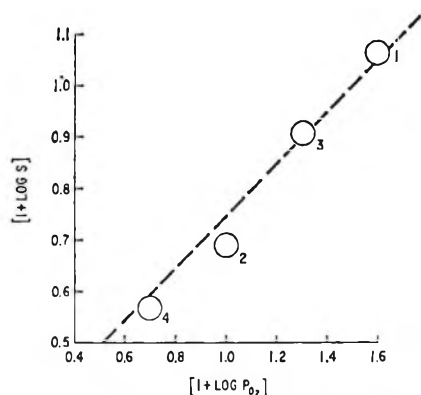


Figure 10. Oxidation of CO on Ir. Log-log plot of slopes S (Δ) vs. oxygen pressure P_{O_2} (P). The numbers on the data points represent the chronological order of the measurements. The broken line has a slope = 0.5.

ever, even with these most favorable runs, there was a spread of a factor of 2 in the rate (as measured by the slope of curves such as those shown in Figure 9) of oxidation at the same oxygen pressure on four different sets of iridium films.

In many other experiments in which the initial absorbance was lower, we observed (1) very much lower rates of oxidation, (2) very pronounced sigmoid curvature in plots analogous to Figure 9 with essentially no linear portion, (3) extremely irreproducible rates on the same set of films, and (4) progressive decline in the initial absorbance of the CO peak with repeated oxidation cycles.

4. *The Structure of the Metal Films.* Many of the evaporated metal films used in this work were examined by electron microscopy. The films were easily floated onto water from the sodium chloride crystals and could be picked up on electron microscope grids. Several transmission micrographs are shown in Figure 11. The films appear to be made up of clusters of particles *ca.* 50 Å in diameter and may be anywhere from one to several particles thick. There seems to be no obvious difference between these films and those employed by Garland, *et al.*⁸ Thus the reasons for the greater opacity of films evaporated under high vacuum, relative to those evaporated in 1–10 torr of inert gas or CO, are not obvious.

The craquelure apparent in the iridium film (Figure 11) was observed in many but not all samples, and may be due to partial collapse of the film on flotation from the supporting NaCl.

Discussion

The Nature and Position of the Infrared Bands of Adsorbed CO. The spectra obtained by us on thin evaporated films are in general an order of magnitude less in-

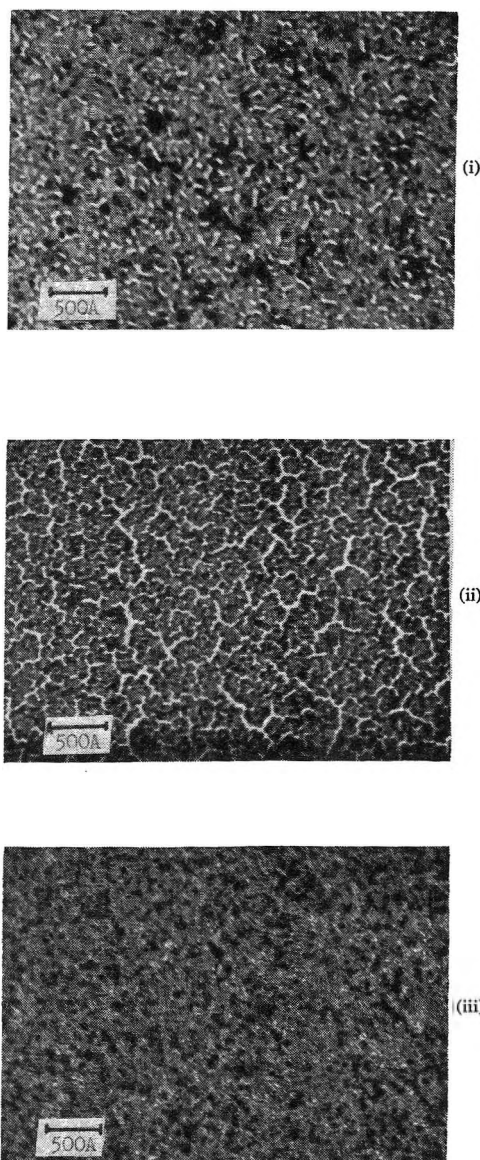


Figure 11. Electron micrographs of metal films: i, Pd; ii, Ir; iii, Pt ($\times 231,000$).

tense than the spectra obtained by other methods, such as the pressed silica pellet. One result of this is that only the more intense absorption bands are observed.

In the case of platinum the observation of a single peak at *ca.* 2040 cm^{-1} agrees well with most other values reported in the literature.^{2,4,8,12} We have also frequently observed a second weak band at *ca.* 1800 cm^{-1} on both clean and contaminated films, as have several other workers.^{2,8}

The spectrum of CO adsorbed on contaminated palladium films consisted of a single broad peak at 1890

(12) R. P. Eischens, S. A. Francis, and W. A. Pliskin, *J. Phys. Chem.*, **60**, 194 (1956).

cm^{-1} . The case of CO on palladium seems to have given rise to the most diverse set of results reported in the literature. Kavtaradze, *et al.*,⁹ observed the principal absorption band of CO on silica-supported palladium to be at *ca.* 2000 cm^{-1} , and this CO proved to be remarkably resistant to reduction by H_2 at 200°. Eischens and Pliskin, using the same system, observed the principal band at *ca.* 1930 cm^{-1} .¹² Sardisco,⁴ using sputtered films, and Nash and DeSieno,¹³ using films generated from exploding wires, observed single bands at 1960 and 1920 cm^{-1} respectively. Garland, *et al.*,⁸ observed the principal band at 1900 cm^{-1} , using films evaporated in the presence of CO. Since we have not yet succeeded in observing the spectrum of CO on clean palladium and since we have observed CO adsorbed on contaminated palladium to be very reactive toward H_2 , O_2 , and H_2O , we intend to reserve judgment as to whether the spectrum of CO adsorbed on contaminated palladium is that of CO or not. The experience with other systems does strongly suggest that it is.

Our observation of two bands of roughly equal intensity at *ca.* 2000 and 1820 cm^{-1} for CO on Rh agrees well with the results of Garland, *et al.*,⁸ for Rh films evaporated in the presence of CO. The latter workers reported two strong bands at *ca.* 2050 and 1850 cm^{-1} . Using highly dispersed Rh on alumina, Yang and Garland^{3a} observed two strong bands at *ca.* 2030 and 2090 cm^{-1} . With higher Rh loadings (presumably giving microcrystalites comparable to those in evaporated films), bands were observed at *ca.* 1900 and 2060 cm^{-1} , in fair agreement with observations on evaporated films. Of particular interest was the observation that a strong band appeared at *ca.* 1860 cm^{-1} with some samples in the presence of water vapor. The significance of this observation will be discussed further below.

Because of the problem of satisfactorily reducing iridium complexes to the metal, the evaporated film techniques are particularly suited to studies involving iridium. The only report of studies on this metal is by Baker, *et al.*,¹⁴ but no values for the positions of the absorption bands are yet available in the literature.

Effects of Surface Contamination on the Frequency of the Absorption Maxima. The position of the CO infrared absorption maximum for adsorbed CO is dependent on the fraction of surface occupied by CO. This fact has previously been observed^{2,3a,9,12} and was confirmed in the present study. In all studies, with the exception of those designed to produce atomically clean surfaces, it may be assumed that the fraction of surface not occupied by CO is occupied to some degree, if not completely, by some other species.

In some instances, such as experiments involving oxidation or hydrogenation of adsorbed CO, the second

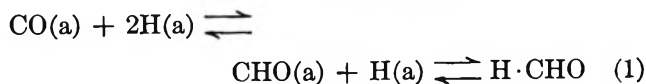
species coexisting with CO on the surface may be fairly specifically defined. For instance, there seems to be a general agreement that the absorption maximum for CO moves to lower frequency with decreasing coverage in the presence of coadsorbed hydrogen. This appears to be true of Pt,² Pd,⁹ Rh,^{3a} and Ir (present study) under a wide variety of experimental conditions.

In contaminated systems (such as those working at pressures $\geq 10^{-6}$ torr with greased stopcocks and no special precautions to exclude mercury or oil vapor), the presence of undefined surface contaminants may give rise to the kind of irreproducibility illustrated by Figure 8.

The Nature of the Adsorbed Species on Contaminated Films. Most of the attempts to interpret the infrared spectra of CO adsorbed on metals has centered around the question as to whether the multiplicity of bands is best explained by the assumption of linear and bridged surface carbonyls or by the assumption of adsorption on a variety of surface sites,^{2,15} each with a characteristic infrared absorption frequency. In our case, the prime concern was to establish whether the observed spectra were due to carbon monoxide or to other carbonyl species, *e.g.*, CHO, produced by reaction of CO with surface contaminants.

Doubt that the observed bands were due solely to CO was first aroused by the sensitivity of the spectrum of CO on Rh to the presence of water vapor. Indeed, both our observations and those of Yang and Garland^{3a} clearly show that water reacts with CO adsorbed on Rh at room temperature, giving rise to surface species with spectra quite different from those initially obtained, and also that water can even remove the carbonyl species from the surface. The reactivity of water with CO adsorbed on palladium was even more dramatic.

Doubt that the observed bands were due solely to carbon monoxide was further emphasized when it was observed that both formaldehyde and formic acid gave essentially the same spectra as CO when adsorbed onto hydrogen-covered films of Rh, Ir, or Pt. Thus, the contention that these spectra were due to adsorbed CO was no more tenable than that they were due to adsorbed species of a more complex chemical composition. One may postulate many reactions such as



(13) C. P. Nash and R. P. DeSieno, *J. Phys. Chem.*, **69**, 2139 (1965).

(14) F. S. Baker, J. Pritchard, and K. W. Sykes, Meeting of the Chemical Society of London, Nottingham, England, Sept 21-22, 1965, paper No. C18.

(15) G. Blyholder, *J. Phys. Chem.*, **68**, 2772 (1964).



where (a) = adsorbed species, which may occur at the surfaces in question. Since we do not know the strengths of the various metal-adsorbate bonds, it is not possible to draw *a priori* conclusions regarding in which directions these equilibria may lie.

The results obtained with clean metal films indicate that both sets of equilibria 1 and 2 lie very much to the left for Pt and Ir. Thus, the spectrum obtained with CO on a clean film is essentially the same as that obtained on a hydrogen-covered, contaminated film, which is the same as the spectra of adsorbed formaldehyde and formic acid.

The same is almost true of Rh except that the observed effects of water vapor on the spectrum of CO adsorbed on this metal suggest that equilibrium 2 does move appreciably to the right. In the case of Pd, the results indicate that equilibrium 2 lies largely to the right.

These results are in accord with the observations of Hinshelwood and Topley,¹⁶ who found that the relative rates of the two modes of decomposition of formic acid varied depending on the catalyst. Palladium was found to be 25 times and rhodium 10 times more effective than platinum in catalyzing the dehydrogenation of formic acid. All of these metals simultaneously catalyze the dehydration and dehydrogenation of formic acid under the high temperatures used to study the catalytic reaction using gas-phase techniques.¹⁶

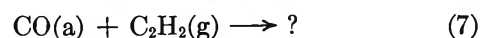
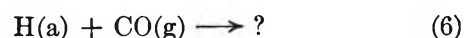
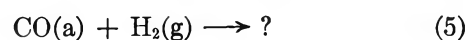
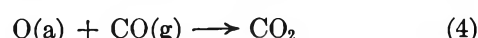
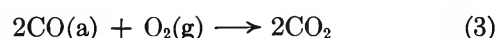
Characteristics of CO Spectra on Fresh, Clean Metal Films. The most outstanding characteristic of the spectrum of CO on freshly evaporated, clean films was the broad tailing of the absorption band toward lower frequencies observed with Ir and Pt films. Such tailing is exactly what would be expected of CO adsorbed onto a highly disordered, microcrystalline substrate. The sharpening of the band following oxidation and re-adsorption of CO may be attributed to two possible effects. Either the heat of reaction on oxidation is sufficient to sinter the disordered microcrystals or the more reactive of the surface sites are poisoned permanently by oxygen. The fact that other workers using evaporated metals under less rigorous vacuum conditions have not reported such tailing of spectra suggests that the latter poisoning effect may be of some importance.

Also of interest is the observation of a sharp band edge at the high-frequency end of the absorption. This band edge corresponds closely to the high-frequency edge of the spectrum of CO on contaminated films,

which indicates that there is a certain critical minimum in the interaction energy of chemisorbed CO on these metals. The existence of such a critical minimum may be interpreted in terms of chemisorption of CO onto the most stable crystal plane (or planes of very similar stability) of the metal crystal.

The Value of the Infrared Technique for Kinetic Studies. The value of any spectroscopic determination of concentration rests on the possibility of relating the concentration of a species to its spectroscopic absorbance. What little evidence is available thus far suggests that the extinction coefficient for the stretching fundamental of chemisorbed CO depends on surface coverage. However, for the case of CO on Pt, Eischens¹² observed a linear relation between absorbance and surface coverage up to a considerable fraction (*ca.* 60%) of total coverage.

The reliable determination of extinction coefficients for adsorbed CO is extremely difficult experimentally and we were unable to determine any using our systems. The results obtained by us for the oxidation of CO adsorbed on Ir suggest that the task of determining extinction coefficients would be well worth the effort. Even using only the spectrum of CO a large number of different reactions are available for study, *e.g.*



With a knowledge of true extinction coefficients, it is theoretically possible to obtain real rate constants for such simple reactions, and the use of the infrared method is relatively simple compared to gas-phase techniques previously employed.¹⁷

Conclusions

1. The infrared spectra of CO adsorbed on evaporated metal films can be measured, even when the films are evaporated under high-vacuum conditions, by using a number of very thin films in series.

2. Although spectra may be observed using atomically clean metal films, differences between such spectra and spectra obtained using contaminated films are probably due to the unusual structure of unsintered films rather than impurity effects. The spectra ob-

(16) C. N. Hinshelwood and B. Topley, *J. Chem. Soc.*, 1014 (1923).

(17) S. J. Stephens, *J. Phys. Chem.*, **63**, 188 (1959).

served in the present and previous studies, using contaminated Pt, Rh, and Ir, are due primarily to CO and not some species resulting from interaction of CO with surface contaminants.

3. The infrared method shows promise as a tool for studying the kinetics of surface reactions, but it is first of all necessary to obtain reliable values for extinction coefficients.

Phase Equilibria in Solutions of Liquid Sulfur. II. Experimental Studies in Ten Solvents: Carbon Disulfide, Carbon Tetrachloride, Benzene, Toluene, *o*-Xylene, Naphthalene, Biphenyl, Triphenylmethane, *cis*-Decalin, and *trans*-Decalin

by John A. Larkin, Jeffrey Katz, and Robert L. Scott

Contribution No. 1964 from the Department of Chemistry, University of California, Los Angeles, California 90024 (Received July 27, 1966)

Liquid-liquid phase diagrams and critical polymerization lines (from viscosity measurements) have been determined for solutions of liquid sulfur in ten solvents: carbon disulfide, carbon tetrachloride, benzene, toluene, *o*-xylene, naphthalene, biphenyl, triphenylmethane, *cis*-decalin, and *trans*-decalin. In six of these (three of them new), both an upper critical solution temperature (t_1) and a lower critical solution temperature (t_2) were found: benzene, 163 and 230°; toluene, 180 and 221°; *o*-xylene, 164 and 221°; biphenyl, 108 and 221°; triphenylmethane, 151 and 198°; *cis*-decalin, 160 and 212°; between these temperatures there is a region of complete miscibility. Several "quasi-binary" systems formed by mixtures of *cis*- and *trans*-decalin with sulfur were studied. For mixtures which are 55% *trans*, 45% *cis*, t_1 and t_2 coalesce at about 202°; mixtures which are richer in *trans*-decalin show partial miscibility with sulfur at all temperatures. The results are in reasonably good qualitative agreement with the theory presented in the first paper of this series, except that the lower critical solution temperature t_2 is never found below the upper one, t_1 . A dependence of the critical composition and the critical polymerization line upon the molar volume of the solvent is found, in agreement with the qualitative predictions of solution theory.

Introduction

In the first paper (I) of this series,¹ the Flory-Huggins equations for high polymer solutions were used to extend the Gee-Tobolsky-Eisenberg treatment of liquid sulfur to binary solutions. A "critical polymeri-

zation line" was deduced, below which the amount of open-chain sulfur is negligibly small, but above which increasing amounts of very long sulfur chains are

(1) R. L. Scott, *J. Phys. Chem.*, **69**, 261 (1965).

found. With a single adjustable parameter, an interchange energy w , the theory accounted for the two critical solution temperatures (upper, t_1 , and lower, t_2) previously observed in three solvent + sulfur systems; the lower critical solution temperature is a consequence of the ring-chain transition. The calculated phase diagrams seemed to be in qualitative agreement with the early experimental measurements (1905–1928).

We now report some new experimental measurements upon solutions of sulfur in ten solvents, three of which (benzene, toluene, and triphenylmethane) have been previously studied. Lower critical solution temperatures have been found in three additional solvents: *o*-xylene, biphenyl, and *cis*-decalin.

Experimental Section

Apparatus and Procedure. Phase boundaries and viscosities were determined by visual observation of mixtures of solvent + sulfur in a sealed ampoule prepared in the following manner. A glass ball (2.5 mm in diameter) was placed in a Pyrex glass tube (6 mm in diameter and about 15 cm long). Sulfur was added, the weight (0.5–2.5 g) being determined by difference afterward; then solvent (0.02–1.7 g) was added and the ampoule was sealed off. The ampoule was flushed with nitrogen at each stage to remove oxygen which might react with sulfur on heating.

The sealed ampoule was placed in a 4-l. Pyrex vessel containing silicone oil. This was fitted with three 750-w heaters, a copper cooling coil for the circulation of tap water, a mechanical stirrer, and a calibrated mercury-in-glass thermometer. The oil bath was totally surrounded by a stout wooden box fitted with a window made from 0.25-in. Plexiglass sheet and placed in a fume hood (the silicone oil fumed considerably at our maximum working temperature of 290°). The ampoule was agitated by rotation back and forth through about 120° of arc by means of a system of wire and pulleys which was operated manually.

The solvent + sulfur mixture was heated rapidly up to the first phase boundary, where the temperature (which we call Θ_1 to distinguish it from the critical solution temperature t_1) was measured carefully, passing back and forth through the boundary several times; the second boundary Θ_2 was measured in the same way. Viscosity measurements were recorded throughout by measuring the time taken for the glass ball to fall through the liquid. Since the viscosity decreases slowly and approximately linearly with temperature until the critical polymerization temperature t_{cp} is reached and then increases sharply (Figure 1), determination of t_{cp} (from the intersection of two straight lines) within $\pm 1^\circ$ is easy.

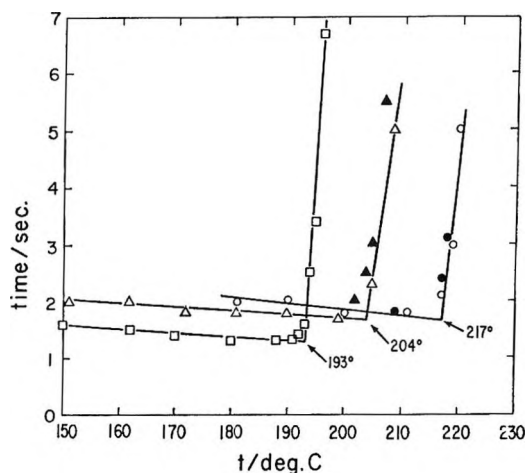


Figure 1. Example of determination of the critical polymerization line. Time of fall of glass ball in system biphenyl + sulfur: \circ , $x_s = 0.745$ ($t_{cp} = 217^\circ$); Δ , $x_s = 0.800$ ($t_{cp} = 204^\circ$); \square , $x_s = 0.846$ ($t_{cp} = 193^\circ$). Open points (\circ , Δ , \square) are for increasing temperatures; solid points (\bullet , \blacktriangle) for the subsequent decreasing temperatures.

The first phase boundary Θ_1 was reproducible to about $\pm 0.5^\circ$. The second phase boundary Θ_2 and the critical polymerization temperature t_{cp} were reproducible to about $\pm 1^\circ$. However, after the mixture had been heated to high temperatures ($t > \Theta_2$) for a few minutes, the temperature Θ_1 was usually found to increase and Θ_2 to decrease, sometimes by several degrees. The critical polymerization temperature was unaffected.

The greatest amount of irreversible change (presumably chemical reaction) was found with carbon tetrachloride; conversely the triphenylmethane and biphenyl systems were almost completely reversible.

Materials. The sulfur used in most of the experiments was American Smelting and Refining Co. special high-purity sulfur (99.999+%), Grade ASARCO A-58. Some early experiments (with *o*-xylene, naphthalene, biphenyl, carbon tetrachloride, and a few with carbon disulfide) were done with Baker sublimed sulfur; no discrepancies between results with the two different samples of sulfur were observed.

The carbon tetrachloride was Merck ACS specification grade "suitable for spectrophotometric use." The carbon disulfide, triphenylmethane, and biphenyl were Eastman Organic Chemicals White Label. Matheson Coleman and Bell supplied the benzene (Spectroquality), toluene and *o*-xylene (Chromatoquality), and naphthalene; the last was recrystallized from alcohol. The *cis*- and *trans*-decalin were supplied by K and K Laboratories, Inc. All of the solvents were examined by gas-liquid chromatography;

except for the decalins, no impurities were detected. The gpc measurements showed that the "cis-decalin" contained about 9% *trans*; the "trans-decalin" contained less than 2% *cis*.

Results

Figure 2 shows the measured critical polymerization lines for the systems carbon disulfide + sulfur and naphthalene + sulfur. The critical polymerization temperature t_{cp} is plotted against the formal mole fraction of sulfur x_s (always based upon S_8). The solid line is the prediction of the theory of paper I with the simplifying assumption that there is no configurational ("entropy") contribution to the polymer-solvent local free energy of interaction (*i.e.*, $\alpha = 0$) and that the differences in molar volume between the solvent and ring sulfur (S_8) can be neglected (*i.e.*, $r = 1$). The good agreement for $CS_2 + S$ is at least partly fortuitous; as shown in paper I, other assumptions yield equally good agreement.

Figures 3-10 show the liquid-liquid phase diagrams and the critical polymerization lines for carbon tetrachloride + sulfur, benzene + sulfur, toluene + sulfur, *o*-xylene + sulfur, biphenyl + sulfur, triphenylmethane + sulfur, *cis*-decalin + sulfur, and *trans*-decalin + sulfur. No phase separation was observed in the systems carbon disulfide + sulfur and naphthalene + sulfur (Figure 2). Also shown in Figures 4, 5, and 8 are early measurements by other workers.²⁻⁴ Considering the possible uncertainties in the earlier work (temperature calibration, purity of materials, etc.), the agreement in most cases is perhaps satisfactory. However, the lower solution curve, which is in excellent agreement for triphenylmethane (Figure 6), shows possibly significant

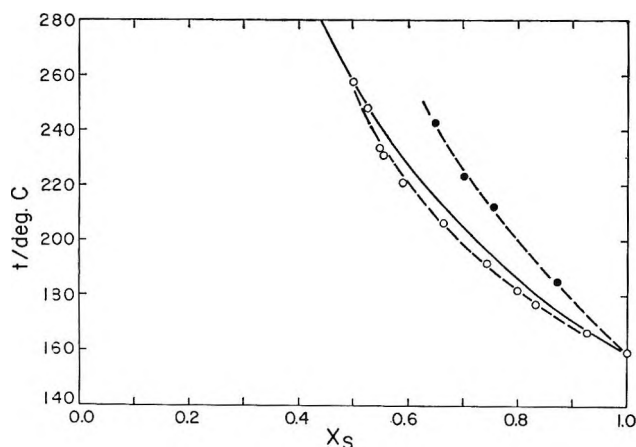


Figure 2. Critical polymerization lines for carbon disulfide + sulfur, O, and naphthalene + sulfur, ●. The solid line is that predicted from the simple theory of paper I (eq 20, with $\alpha = 0$, $r = 1$).

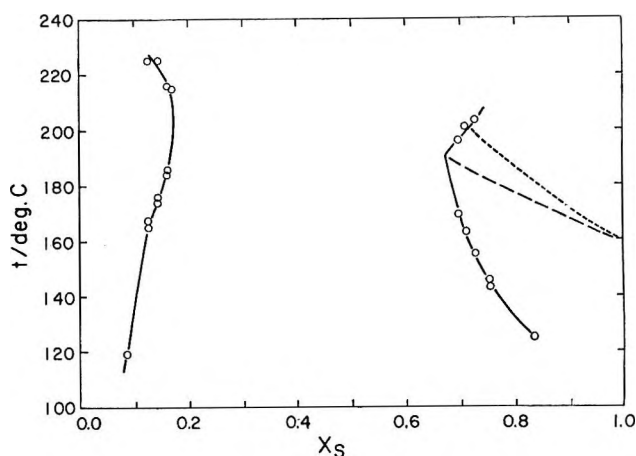


Figure 3. Phase diagram for carbon tetrachloride + sulfur. Phase boundary, O. Critical polymerization line not measured. Dotted line is theoretical curve (Figure 2), undoubtedly too high; dashed line is estimate to fit phase diagram.

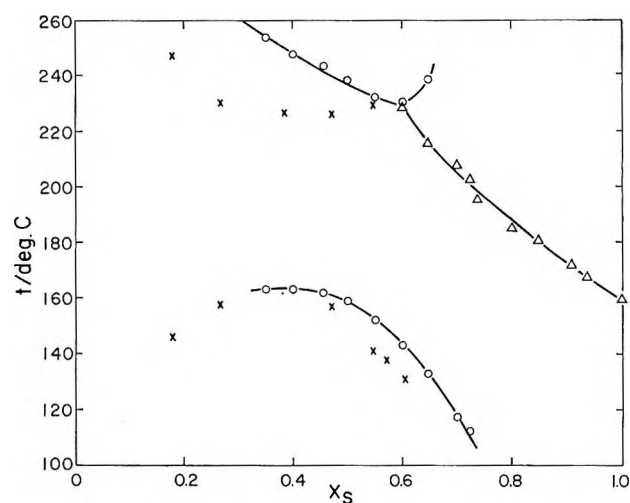


Figure 4. Phase diagram for benzene + sulfur. Phase boundary: O, this paper; X, Krut.³ Critical polymerization line: Δ.

variations for toluene (Figure 5) and marked disagreement for benzene (Figure 4). Our new measurements are much more nearly in accord with the theoretical predictions. In addition, the very crude viscosity measurements of Mondain-Monval and Schneider yield a poorer critical polymerization line.

Table I summarizes the critical solution parameters (temperature and composition) for these systems, and Table II contains a list of symbols used in the text and

(2) A. Smith, W. B. Holmes, and E. S. Hall, *Z. Physik. Chem.*, **52**, 602 (1905); *J. Am. Chem. Soc.*, **27**, 797 (1905).

(3) H. R. Krut, *Z. Physik. Chem.*, **65**, 486 (1909).

(4) P. Mondain-Monval and P. Schneider, *Bull. Soc. Chim. France*, [4] **43**, 1302 (1928).

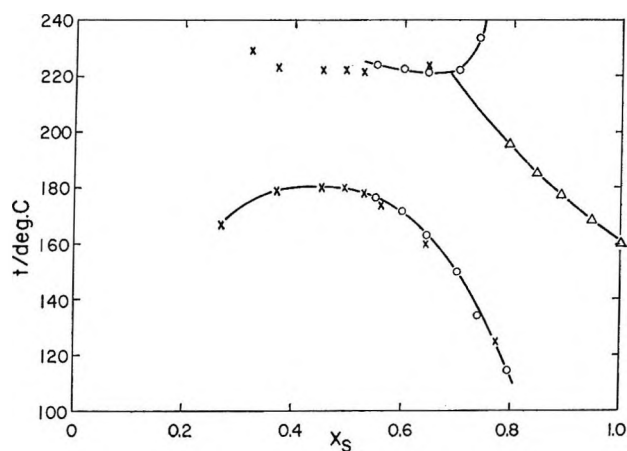


Figure 5. Phase diagram for toluene + sulfur. Phase boundary: O, this paper; X, Kruyt.³ Critical polymerization line: Δ.

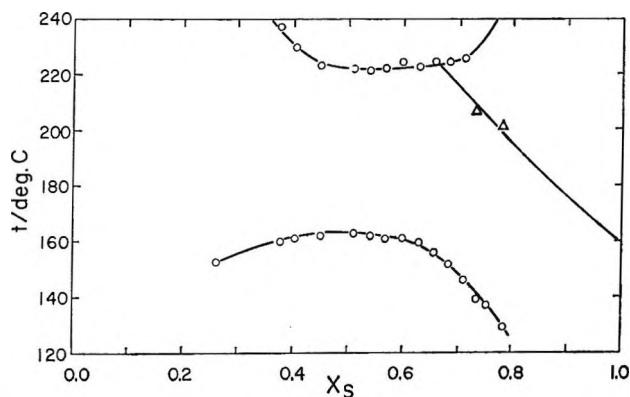


Figure 6. Phase diagram for *o*-xylene + sulfur. Phase boundary: O. Critical polymerization line: Δ.

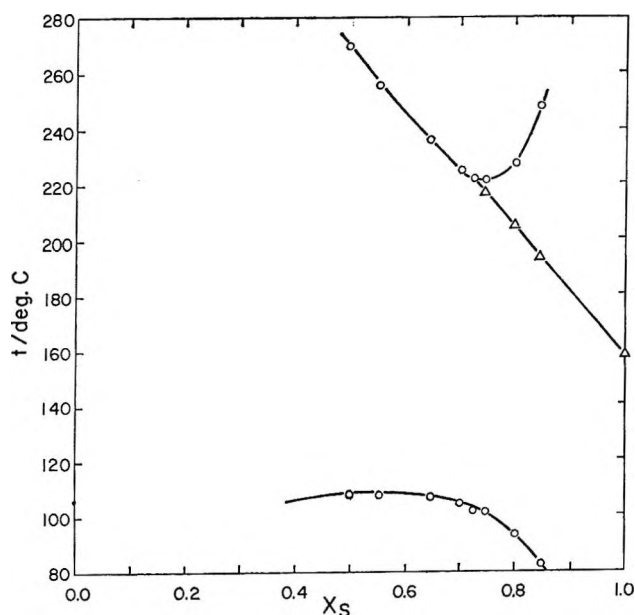


Figure 7. Phase diagram for biphenyl + sulfur. Phase boundary: O. Critical polymerization line: Δ.

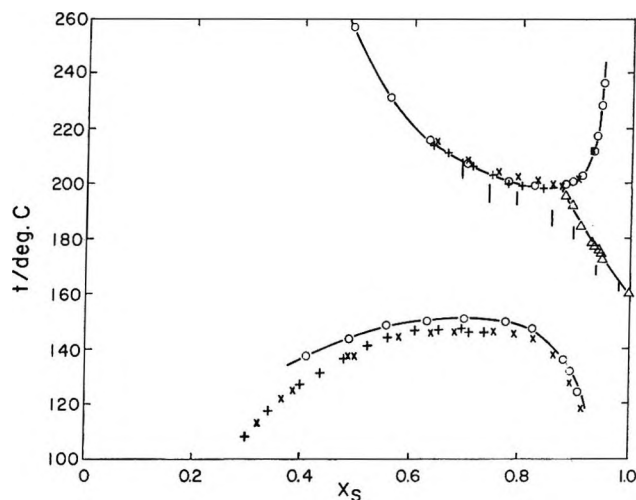


Figure 8. Phase diagram for triphenylmethane + sulfur. Phase boundary: O, this paper; +, Smith, Holmes, and Hall;² X, Kruyt.³ Critical polymerization line: Δ, this paper; I, from viscosity data of Mondain-Monval and Schneider⁴ (length of line is estimated uncertainty).

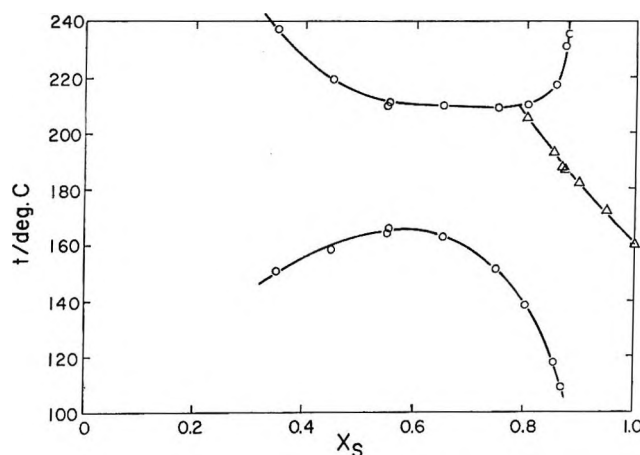


Figure 9. Phase diagram for *cis*-decalin (actually about 9% *trans*) + sulfur. Phase boundary: O. Critical polymerization line: Δ.

figures. The critical mole fraction of sulfur x_c at the lower critical solution temperature is not always easy to determine. The theory of paper I requires that the critical polymerization line intersect the phase boundary at the lower critical solution point. Table I lists values of x_c from this intersection x_{cp} and from an extrapolation x_{rd} based upon the law of the rectilinear diameter. In most cases the two extrapolations agree within the fairly large experimental error, but in the system *cis*-decalin + sulfur, the difference ($\Delta x = 0.1$) is hard to account for.

Since *cis*-decalin has a region of temperature in which it is completely miscible with liquid sulfur while *trans*-

Table I: Critical Solution Parameters in Solvent + Sulfur Systems

Solvent	Solvent solubility parameter, $\delta_0/\text{cal}^{1/2}/\text{cm}^{-3/2}$	Solvent molar volume at 25°, \bar{V}_0/cm^3	Upper critical		Lower critical			Critical polymerization x_S at $t_{ep} = 190^\circ$
			$t_1/^\circ\text{C}$	x_{upper}	$t_2/^\circ\text{C}$	x_{rd}	x_{cp}	
Naphthalene	10.2 ^a	123 ^a	None observed		None			C. 85
Carbon disulfide	10.0	61	None observed		None			C. 77
Biphenyl	10.0 ^a	150 ^a	108	...	221	0.76	0.73	C. 86
Triphenylmethane	9.4 ^a	270 ^a	151	(0.70)	198	0.85	0.87	C. 90
Benzene	9.2	89	163	(0.37)	230	0.60	0.60	0.76
<i>o</i> -Xylene	9.0	121	164	0.51	221	...	0.65	(0.84)
Toluene	8.9	107	180	0.45	221	0.66	0.7	0.82
<i>cis</i> -Decalin	8.8	155	160 ^b	0.58	212 ^b	0.69	0.78	0.86
<i>trans</i> -Decalin	8.6	160	Partially miscible at all temperatures					0.86
Carbon tetrachloride	8.6	97	Partially miscible at all temperatures					...

^a Estimated. ^b Measurements were made with "*cis*-decalin" containing about 9% *trans*-decalin, for which $t_1 = 165^\circ$ and $t_2 = 210^\circ$. Extrapolation to 0% *trans* (Figure 11) yields the figures in the table. The compositions x_S are for the measured "*cis*-decalin."

Table II: Symbols Used in Text and Figures

t_1	Upper critical solution temperature
t_2	Lower critical solution temperature
t_{cp}	Critical polymerization temperature (the temperature above which—for given composition—appreciable amounts of polymeric sulfur are present)
θ_1	Temperature of upper phase boundary—for given composition
θ_2	Temperature for lower phase boundary—for given composition
x_S	Mole fraction of total sulfur (always referred to S_8 , regardless of actual molecular species present)
x_{upper}	x_S at upper critical solution point (t_1)
x_{rd}	x_S at lower critical solution point (t_2) estimated from the law of the rectilinear diameter
x_{cp}	x_S at lower critical solution point (t_2) estimated from intersection of the phase boundary with critical polymerization line

decalin is only partially miscible at all temperatures, mixtures of *cis*- and *trans*-decalin should show intermediate phase diagrams and permit investigation of the region in which the two critical solution temperatures t_1 and t_2 approach each other. In such ternary systems, the ratio of *cis* to *trans* is unlikely to differ much between two conjugate phases, so we may describe them as "quasi-binary." Figure 11 shows the data for six such mixtures, all with a mole fraction of S_8 between 0.547 and 0.553 ($x_{\text{upper}} \cong 0.58$ at t_1 for *cis*-decalin + sulfur). Since the phase diagrams are very nearly flat in the critical region, the temperatures of phase separation, θ_1 and θ_2 , are very nearly critical solution temperatures.

From Figure 11 we infer that any quasi-binary mixture of *cis*- and *trans*-decalin containing more than

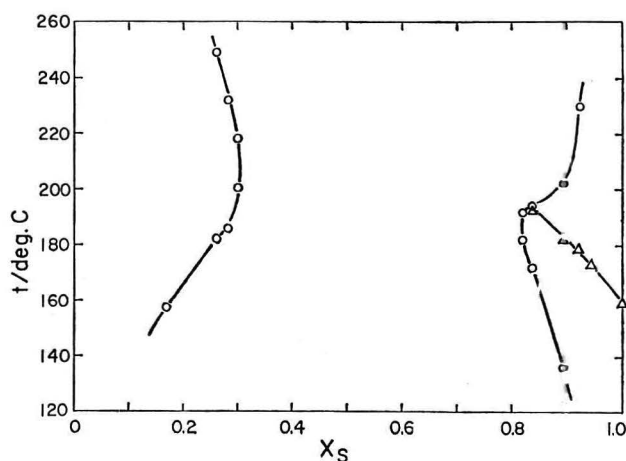


Figure 10. Phase diagram for *trans*-decalin + sulfur. Phase boundary: O. Critical polymerization line: Δ .

about 55% *trans* will be only partially miscible with sulfur at all temperatures. (Measurements with 68 and 77% *trans* showed two liquid phases at all temperatures.)

The near coalescence of the two phase boundaries was studied more carefully with one particular mixture of decalins (48% *cis* and 52% *trans*) with the results shown in Figure 12. The higher temperature ("lower critical") curve is much more nearly flat in the critical region than is the lower curve ("upper critical"). The critical composition cannot be determined unequivocally since the two extrapolation methods yield radically discordant results ($x_{\text{rd}} \cong 0.63$; $x_{\text{cp}} = 0.82$, while $x_{\text{upper}} \cong 0.55$). However, there is no suggestion that the lower critical solution temperature t_2 can lie below the upper one t_1 as predicted in paper I.

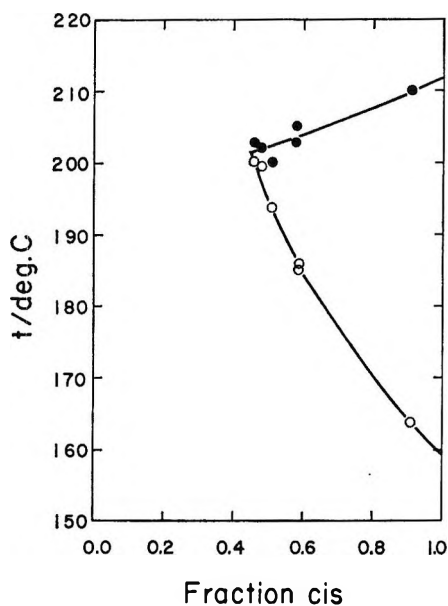


Figure 11. Upper, O, and lower, ●, critical solution temperatures for quasi-binary systems of decalin mixtures + sulfur. ($x_s = 0.55$.)

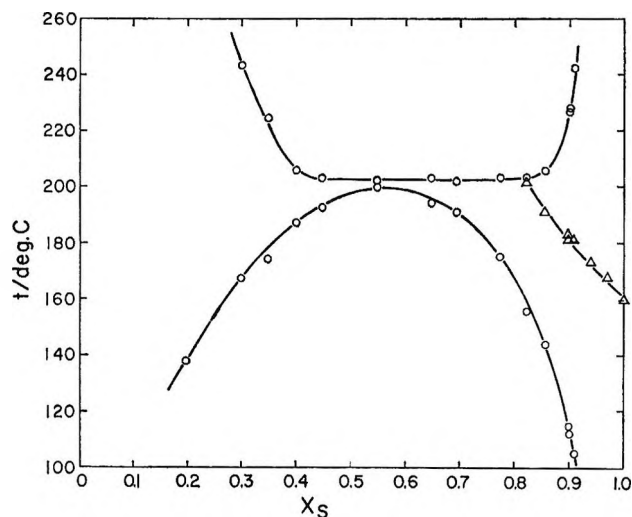


Figure 12. Quasi-binary phase diagram for a mixture (52% *trans*-decalin and 48% *cis*-decalin) + sulfur. Phase boundary: O. Critical polymerization line: Δ.

Discussion

The experimental results can be considered in the light of solution theory in general and the simple theory of paper I in particular. Four general conclusions suggest themselves.

1. While many of the qualitative predictions of the simple theory are borne out by the experimental phase diagrams (e.g., the association of the lower critical solution point with the critical polymerization line), there are some serious discrepancies in detail. Most im-

portant of these is the failure to observe a system in which the lower critical solution temperature t_2 is in fact a lower temperature than the upper critical solution temperature t_1 (cf. paper I, Figures 6b and 7a).

Whether t_1 and t_2 actually coalesce at the same critical composition is not clear. The evidence of the quasi-binary system (Figure 12) is inconclusive, since the two methods of extrapolation yield such discordant values of the lower critical composition. Further experimental studies are needed as well as more refined theory.

2. A dependence upon the molar volume of the solvent (ignored in the simple theory) is clearly indicated. In Figure 13 we plot the upper critical composition and the critical polymerization composition at $t = 190^\circ$ against molar volume \bar{V}_0 of solvent. The larger \bar{V}_0 , the more both are shifted in the direction of solutions richer in sulfur. A more convenient method of comparison (as suggested in paper I) would be to use volume fraction φ_s of sulfur as the independent variable; this is in accord with much evidence from other systems and is supported by theoretical considerations. Regular solution theory⁵ yields a relation between x_c and \bar{V}_0/\bar{V}_s ; for $\bar{V}_s = 135 \text{ cm}^3$, this gives the dashed line in Figure 13; the agreement is remarkably good.

3. In the simple theory, the upper critical solution temperature t_1 and the lower critical solution temperature t_2 are both functions only of w , the solvent + sulfur interchange energy, which by solubility parameter theory⁵ should be proportional to $(\delta_s - \delta_0)^2$ where δ_s and δ_0 are the solubility parameters of liquid sulfur

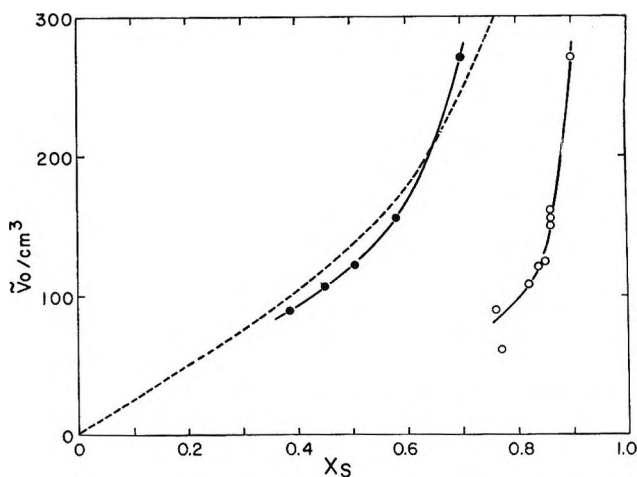


Figure 13. Correlation of upper critical solution composition x_{upper} , ●, and critical polymerization composition at $t = 190^\circ$; O, with molar volume of the solvent \bar{V}_0 . Dashed line is regular solution theory prediction of x_{upper} .

(5) J. H. Hildebrand and R. L. Scott, "Regular Solutions," Prentice-Hall, Inc., Englewood Cliffs, N. J., 1962, pp 143, 147.

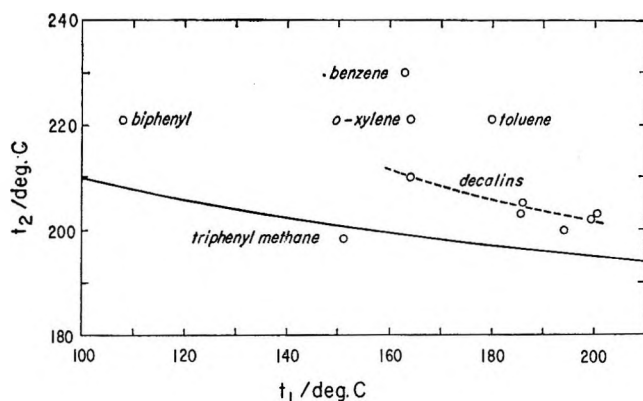


Figure 14. Correlation of upper and lower critical solution temperatures. Solid line is derived from simple theory of paper I ($r = 1$). Dashed line represents the quasi-binary systems decalin + sulfur (cf. Figure 11).

and solvent. Table I shows that t_1 increases regularly as δ_0 decreases; only *cis*-decalin is out of line. (The difference in solvent power of *cis*- and *trans*-decalin is in accord with the difference in their solubility parameters; the solubility of iodine in the two solvents shows similar differences.⁶)

Moreover, t_1 and t_2 should be directly related. The solid line in Figure 14 is the prediction of the simple theory ($\bar{V}_0 = \bar{V}_{S_8}$; *i.e.*, $r = 1$). The experimental points for the systems here reported scatter rather badly around this line, but it should be noted that the displacements from the theoretical line correlated rather well with the solvent molar volumes. Benzene with the smallest \bar{V}_0 lies the highest; triphenylmethane with the largest \bar{V}_0 lies lowest.

4. For many of the systems, the phase boundary in the vicinity of the lower critical solution temperature t_2 is very nearly flat, much more so than in typical critical

regions (*e.g.*, the upper critical region around t_1 ; compare the two curves in Figure 12). This may be due to small amounts of impurities produced by chemical reactions with the diradical chain sulfur. It is interesting to note that the curvature of this phase boundary is sharpest for the two solvents, triphenylmethane (Figure 8) and biphenyl (Figure 7), which show almost complete reproducibility after heating (presumably no chemical reaction).

The phase diagrams calculated in paper I were based upon an oversimplified model obviously at variance with the actual situation in at least four respects. (a) The molar volumes of the solvent and of S_8 rings were assumed to be equal. (b) Only two types of sulfur molecules were assumed: S_8 rings and long open chains. (c) For simplicity the molecular weight of the chain was taken to be infinite ($K_1^0 = 0$). (d) The polymer-solvent interaction parameter χ was assumed to depend only upon an interchange energy w , and not upon an additional configurational contribution α (*i.e.*, $\alpha = 0$).

The influence of molar volume is clearly demonstrated in the experiments reported here, and the deviation from the simple theory is in the direction expected. Refinements which take account of b, c, and d may eliminate the apparently incorrect prediction t_2 can be lower than t_1 , but until we carry out detailed calculations on a refined model, this is an open question.

Acknowledgments. Our research on liquids and solutions, of which this is a part, is supported by the National Science Foundation. We wish to thank Professor A. Eisenberg for suggesting the simple method for determining the critical polymerization temperature.

(6) K. Shinoda and J. H. Hildebrand, *J. Phys. Chem.*, **69**, 605 (1965).

The Enthalpy of Dissociation of Nitrogen Trifluoride

by G. C. Sinke

Thermal Research Laboratory, Dow Chemical Co., Midland, Michigan (Received July 29, 1966)

The enthalpies of explosion of mixtures of hydrogen and excess NF_3 were measured in a bomb calorimeter. From the measurements is derived the enthalpy of dissociation of the excess NF_3 and an enthalpy of formation of -31.44 ± 0.30 kcal/mole.

Introduction

In working with NF_3 as an oxidizer in calorimetry, it was noted¹ that when mixtures of NF_3 and an oxidizable substance are detonated, excess NF_3 is dissociated to the elements. This suggested the feasibility of determining the enthalpy of dissociation of NF_3 by measuring the enthalpy of explosion of mixtures of an oxidizable substance and a large excess of NF_3 . For the present work, mixtures of hydrogen and NF_3 were used to define successfully the enthalpy of dissociation of NF_3 .

Experimental Section

Materials. Materials were the same as those employed in previous work.¹

Procedure. An improved platinum-lined combustion bomb of 350-ml volume was developed in cooperation with the Parr Instrument Co. The bomb cylinder and head were dried at 110° for 1 hr, assembled, connected to a vacuum line, and evacuated while still hot. After cooling to room temperature, the bomb was surrounded by a constant-temperature water bath and pumped until a pressure of at least 1μ was achieved. The bomb was then charged with 799.0 mm of hydrogen as measured by a Wallace and Tiernan precision dial manometer which could be read to 0.1 mm. Nitrogen trifluoride was contained in a small stainless steel cylinder which could be weighed on a 200-g capacity analytical balance. The cylinder was connected to the vacuum line and the bomb charged with about 0.75 g of NF_3 (10% excess) or 1.38 g of NF_3 (100% excess) in alternate runs. Sample remaining in the connecting lines was recondensed in the cylinder with liquid nitrogen and the exact amount charged determined by reweighing. In the 10% excess runs, an additional 0.5 g of research grade N_2 was charged to the bomb in order

to make the final state of the bomb products as similar as possible in the two cases.

The bomb was placed in a conventional combustion calorimeter and the charge was fired by discharging a condenser through a fine platinum fuse wire. The condenser voltage before and after firing was a measure of the ignition energy. The calorimeter was calibrated with National Bureau of Standards benzoic acid 39i. An average of 0.55 g of acid was used and the bomb was charged with 1 ml of water and 30.3 atm of oxygen. In the notation of Hubbard, Scott, and Waddington,² the calorimeter equivalent \mathcal{E} (calor) was 3436.18 cal/deg with a standard deviation of 0.52 cal/deg for five experiments.

After the calorimetry was completed, the gaseous reaction products were passed over a NaF trap to remove HF and into a bulb containing mercury to react out the fluorine. The remaining gas was examined by infrared and mass spectroscopy. Only nitrogen and a small amount of CF_4 (from reaction of fluorine with a fluorocarbon gasket) was found. In some of the 100% excess NF_3 runs a trace of NF_3 (less than 0.05% of the original sample) was observed. The bomb was flushed with nitrogen and then opened and the surfaces washed with 6 *N* HCl to dissolve small amounts of PtF_4 and AuF_3 formed by fluorine attack on the fuse wire and electrodes. The solutions were analyzed for platinum and gold by atomic absorption techniques.

Results

The results of six 10% excess NF_3 experiments are given in Table I and of seven 100% excess NF_3 experiments in Table II. The final temperature of the

(1) G. C. Sinke, *J. Phys. Chem.*, **70**, 1326 (1966).

(2) W. N. Hubbard, D. W. Scott, and G. Waddington, "Experimental Thermochemistry," Vol. I, F. D. Rossini, Ed., Interscience Publishers, Inc., New York, N. Y., 1956, Chapter 5, pp 75-128.

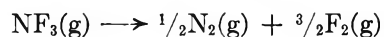
Table I: Results for 10% Excess NF₃ Runs

Mass of NF ₃ , g	Tot. cal	Corrections in calories					Net cal
		CF ₄	PtF ₄	AuF ₃	Ign	Adj	
0.7559	-1744.0	0.8	1.6	0.1	0.2	-2.6	-1743.9
0.7581	-1740.0	1.0	1.1	0.3	0.7	-3.5	-1740.4
0.7485	-1745.6	0.7	1.0	0.4	0.2	0.7	-1742.6
0.7584	-1737.2	0.5	1.0	0.1	0.7	-3.6	-1738.5
0.7401	-1749.2	0.6	1.3	0.3	0.2	4.3	-1742.5
0.7486	-1745.4	0.6	1.5	0.1	0.2	0.6	-1742.4
							Av -1741.7

Table II: Results for 100% Excess NF₃ Runs

Mass of NF ₃ , g	Tot. cal	Corrections in calories					Net cal
		CF ₄	PtF ₄	AuF ₃	Ign	Adj	
1.3754	-1477.0	5.4	2.5	0.2	0.4	2.0	-1466.5
1.3880	-1471.5	6.5	2.9	0.2	0.2	-3.5	-1465.2
1.3961	-1473.9	5.7	2.6	0.2	0.2	-7.0	-1472.2
1.3783	-1478.2	4.6	2.6	0.3	0.2	0.8	-1469.7
1.3765	-1475.7	5.0	1.8	0.2	0.2	1.5	-1467.0
1.3655	-1483.2	5.6	1.8	0.1	0.2	6.4	-1469.1
1.3775	-1474.0	4.6	1.5	0.1	0.2	1.1	-1466.5
							Av -1468.0

bomb was $25.00 \pm 0.01^\circ$ in all experiments. The total calories column in the notation of Hubbard, Scott, and Waddington² is equal to $\mathcal{E}(\text{calor})(t_i - t_f + \Delta t_{\text{cor}}) + \mathcal{E}^i(\text{cont})(t_i - t_h) + \mathcal{E}^f(\text{cont})(t_h - t_f + \Delta t_{\text{cor}})$. The correction for fluorine attack on the fluorocarbon was taken as 123.7 kcal/mole of CF₄ formed.³ The enthalpy of formation of PtF₄ was estimated at -180 kcal/mole and of AuF₃ as -130 kcal/mole. The runs were adjusted to an exact quantity of 0.7500 g of NF₃ in Table I and 1.3800 g of NF₃ in Table II by means of an iterative procedure for the energy of dissociation of NF₃. The difference between the two sets of experiments, 273.7 cal, is then the energy of dissociation of 0.6300 g of NF₃. Atomic weights of 14.0067 and 18.9984 for nitrogen and fluorine, respectively, are employed to derive $\Delta E_{r_{298}} = 30.85$ kcal for the reaction



The reverse process when calculated to constant pressure conditions is the enthalpy of formation of NF₃

$$\Delta H_{f_{298}}(\text{NF}_3, \text{g}) = -31.44 \text{ kcal/mole}$$

The complex final state of the experiments makes es-

timates of corrections to standard states of dubious value. The experiments were designed to keep such corrections to a minimum. The corrections are believed to be small compared to the over-all uncertainty of 0.3 kcal/mole based on twice the standard deviation.

Conclusions

The present value can be combined with previous work⁴ on the enthalpy of reaction of H₂ and NF₃ to derive an enthalpy of formation of HF (1 in 123 H₂O). The result, -77.0 ± 0.2 kcal/mole, lies between the latest "selected best value" of the National Bureau of Standards⁵ and the recent study by Cox and Harrop.⁶

Acknowledgment. This work was sponsored by the U. S. Air Force under Contract No. AF04(611)-11202.

(3) E. S. Domalski and G. T. Armstrong, *J. Res. Natl. Bur. Std.*, **A69**, 137 (1965).

(4) G. C. Sinke, *J. Chem. Eng. Data*, **10**, 295 (1965).

(5) D. D. Wagman, W. H. Evans, I. Halow, V. B. Parker, S. M. Bailey, and R. H. Schumm, National Bureau of Standards Technical Note 270-1, U. S. Government Printing Office, Washington, D. C., Oct 1, 1965.

(6) J. D. Cox and D. Harrop, *Trans. Faraday Soc.*, **61**, 1328 (1965).

The Enthalpy of Reaction of Sulfur and Nitrogen Trifluoride¹

by Lynn C. Walker

Thermal Research Laboratory, Dow Chemical Co., Midland, Michigan (Received July 29, 1966)

Rhombic sulfur has been burned in $\text{NF}_3(\text{g})$ using a nickel combustion bomb and static calorimeter to yield $\text{SF}_6(\text{g})$ and $\text{N}_2(\text{g})$. Combining the measured heat of reaction, -228.26 ± 0.2 kcal/g-atom of sulfur, with the published value for $\Delta H_f^\circ_{298.15}(\text{SF}_6, \text{g})^2$ we obtain $\Delta H_f^\circ_{298.15}(\text{NF}_3, \text{g}) = -31.75$ kcal/mole.

Introduction

Nitrogen trifluoride has become increasingly useful in the past few years as a calorimetric fluorinating agent mainly owing to its ease of handling. Volatile hydrides and fluorocarbons can be mixed with NF_3 without prereaction until the mixture is sparked, thereby eliminating the double-compartment type of bomb necessary when elemental fluorine is used. Also, solid inorganics which spontaneously burn in F_2 may be treated with NF_3 under combustion conditions again eliminating the need for complicated reactor designs. While simplicity of design is possible due to the "inert nature" of NF_3 , precision calorimetry requires a well-established value for the $\Delta H_f^\circ_{298.15}(\text{NF}_3, \text{g})$. Most experiments reported in the literature have involved $\text{HF}(\text{associated gas})$ or $\text{HF}(\text{aq})^{3,4}$ as a product. The $H_f^\circ_{298.15}(\text{HF}, \text{aq})$ is not yet well established,^{5,6} making its choice as a product in NF_3 calorimetry a serious source of systematic error. The uncertainty involved when $\text{HF}(\text{associated gas})$ is produced is described by Armstrong and Jessup.⁷

Experimental Section

Calorimetric System. The calorimeter used for this study was a conventional 25° isothermal jacket static bomb type. A nickel combustion bomb of 0.3522-l. volume was equipped with O-ring seal valves for vacuum work. The energy equivalent of the system was measured by combustion of benzoic acid (National Bureau of Standards sample 39i) in oxygen under the prescribed conditions. Eight determinations gave a value of $\varepsilon(\text{calor}) = -3200.7$ cal/deg with a standard deviation of the mean equal to ± 1.7 cal/deg (1 cal = 4.1840 absolute joules). The following expression was employed to calculate combustion heats from tempera-

ture measurements. $Q_v = \varepsilon(\text{calor})(t_i - t_f + \Delta t_{\text{cor}}) + \varepsilon^i(\text{contents})(t_i - t_h) + \varepsilon^f(\text{contents})(t_h - t_f + \Delta t_{\text{cor}})$.

Materials. Two samples of sulfur were burned in NF_3 . The first, laboratory designation DOW 1-S, was supplied by the Inorganic Research Group of the analytical laboratories at the Dow Chemical Co. X-Ray analysis showed the sample to be of the orthorhombic crystal structure and neutron activation analysis indicated 40 ppm of oxygen and a maximum of 0.1% chlorine. Infrared analysis showed no chlorine-containing organics. The purity was taken as 99.9%. A second sample, USBM-47, was supplied by W. D. Good, U. S. Bureau of Mines, Bartlesville, Okla. This material was of the same batch that was used in ref 2 for the determination of the $\Delta H_f^\circ_{298.15}(\text{SF}_6, \text{g})$. An accompanying analysis showed the sulfur sample to be of the orthorhombic variety and to contain total impurities amounting to 109 ppm. The sample purity was taken as 99.99%.

Research grade NF_3 was purchased from Air Products Corp. Mass and infrared spectral analysis showed the only impurity to be 0.15% CF_4 . By difference, the NF_3 was taken to be 99.85% pure.

(1) Presented at the 21st Annual Calorimetry Conference, Boulder, Colo., June 22-24, 1966.

(2) P. A. G. O'Hare, J. L. Settle, and W. N. Hubbard, *Trans. Faraday Soc.*, **62**, 558 (1966).

(3) O. Ruff and H. Wallauer, *Z. Anorg. Allgem. Chem.*, **196**, 421 (1931).

(4) G. T. Armstrong, S. Marantz, and C. F. Coyle, *J. Am. Chem. Soc.*, **81**, 3798 (1959).

(5) D. D. Wagman, W. H. Evans, I. Halow, V. B. Parker, S. M. Bailey, and R. H. Schumm, National Bureau of Standards Technical Note 270-1, U. S. Government Printing Office, Washington, D. C., Oct 1, 1965.

(6) J. D. Cox and D. Harrop, *Trans. Faraday Soc.*, **61**, 1328 (1965).

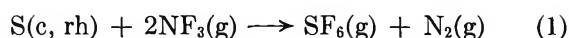
(7) G. T. Armstrong and R. S. Jessup, *J. Res. Natl. Bur. Std.*, **A64**, 49 (1960).

Table I: S-NF₃ Combustion Data

Run no.	S, g	Q _v , tot. cal	Corrections in calories			ΔE, gas	-ΔE _c ^o /M, cal/g ^a
			NF ₃	Mo	Ign		
7	0.95642	-6714.7	-115.0	31.4	1.6	0.2	7106.2
8	0.48179	-3249.3	-213.3	31.4	1.6	-0.3	7119.1
9	0.47001	-3160.0	-231.2	43.2	1.5	-0.3	7120.7
11	0.96877	-6813.7	-116.4	37.7	1.4	0.2	7112.9
12 ^b	0.92868	-6536.3	-128.6	41.1	1.4	0.2	7130.8
14 ^b	0.91896	-6452.4	-126.6	42.6	1.0	0.2	7111.5
17 ^b	0.93002	-6536.3	-115.8	28.9	1.0	0.2	7120.3
18 ^b	0.93922	-6639.8	-97.1	38.6	1.1	0.2	7130.4
							Av 7119.0

^a Std dev of mean = 6.6 cal/g. ^b Denotes Bureau of Mines sulfur.

Nature of the Reaction. Pelletized samples of sulfur were found to burn smoothly and completely in 5 atm of NF₃ when ignited by electrical fusion of an 8-10-cm length of 0.005-in. molybdenum fuse wire. The reaction is shown below.



Mass and infrared spectral analysis showed SF₆ gas as the only fluoride of sulfur. A small amount of NF₃ was thermally dissociated to the elements and necessitated a correction. The molybdenum fuse wire burned quantitatively to MoF₆(g) with the exception of a small, easily weighed piece. Data for this correction were available.⁸ Reaction with the crucible apparently did not occur as weight checks showed a constant mass. Ignition energy was measured by discharging a standardized capacitor. The sum of the above corrections amounted to approximately 1-2% of the measured heat in reaction 1.

Procedure. After the benzoic acid calibration experiments were carried out, the nickel bomb was passivated by carrying out several of the initial exploratory determinations. Between runs the bomb was kept under vacuum to preserve the nickel fluoride coating and all loading operations were carried out in a nitrogen-atmosphere glove box.

Sulfur was pelletized on 0.5- and 1-g quantities, weighed in air on a microgram balance, and transferred to the drybox with the evacuated bomb and fuse. After placing the pellet in the nickel crucible the molybdenum fuse was placed around the pellet and attached securely to two electrode posts. The bomb was then evacuated to less than 5 μ and charged with 5 atm of NF₃. The bomb was weighed before and after charging on a 10-kg capacity balance to determine the mass of NF₃. The loaded bomb was then placed in the calorimeter and the heat of combustion measured.

Immediately after the heat measurement the product gases were analyzed for free fluorine by reaction with mercury. The analysis vessel consisted of a 250-ml Pyrex flask with a tube extension on the bottom to contain 3-5 ml of mercury. The flask was evacuated, then filled to 1 atm with product gases from the bomb. The gases were allowed to condition the bulb and vacuum system for a minimum of 4 hr before a gas sample was taken for quantitative analysis. This technique was checked out both with mixtures of fluorine and nitrogen and with fluorine of 99.5% purity. Recoveries of fluorine on these gases averaged ±0.2% of theory. "Blank" experiments showed that NF₃ and SF₆ did not react with the system. From the gas sampling one could calculate the grams of F per gram of gas and from this the moles of NF₃ decomposed. The residual gases SF₆, NF₃, and N₂ were then checked by mass and infrared spectroscopy.

Results and Discussion

In Table I (S-NF₃ combustion data) we have listed eight determinations. The first four are on the Dow sulfur sample, the last four are on the Bureau of Mines sulfur. Columns 4-7 are thermochemical corrections to Q_v, the total observed heat. These have been discussed earlier. ΔE gas is a correction to standard state involving critical constants⁹ for the gases NF₃, SF₆, N₂, and F₂. The correction was calculated in the usual manner.¹⁰

The standard state enthalpy of reaction is calculated using 32.064 for the atomic weight of sulfur.

(8) J. L. Settle, H. M. Feder, and W. N. Hubbard, *J. Phys. Chem.*, **65**, 1337 (1961).

(9) M. Stacey, J. C. Tatlow, and A. G. Sharpe, *Advan. Fluorine Chem.*, **4**, 189 (1965).

(10) W. N. Hubbard, "Experimental Thermochemistry," Vol. II, H. A. Skinner, Ed., Interscience Publishers Ltd., London, 1962, Chapter 6.

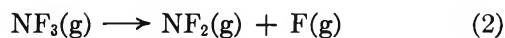
$\Delta E_c^{\circ}_{298.15} = \Delta H_c^{\circ}_{298.15} = -228.26 \pm 0.2$ kcal/g-atom of sulfur. The uncertainty interval, 2σ , is twice the over-all standard deviation of the mean as determined from calibration experiments and the S-NF₃ combustions. Taking $\Delta H_f^{\circ}_{298.15}(\text{SF}_6, \text{g}) = -291.77 \pm 0.24$ kcal/mole², we calculate $\Delta H_f^{\circ}_{298.15}(\text{NF}_3, \text{g}) = -31.75 \pm 0.2$ kcal/mole.

The work by Sinke on the enthalpy of dissociation of NF₃ appearing in the preceding paper is in agreement within experimental error.

Ludwig and Copper¹¹ carried out the combustion of boron using NF₃ as an oxidizer. Their measured ΔH_c° yields -32 kcal/mole for $H_f^{\circ}_{298.15}(\text{NF}_3, \text{g})$ using the latest BF₃ heat of formation = -271.65 kcal/mole.¹²

Derived Bond Energy. The average (N-F) bond energy of 67.1 kcal is calculated from the above result and "JANAF" values for heats of atomization. Armstrong and co-workers have measured¹³ the heats of reaction of NF₃ and N₂F₄ with NH₃ to yield NH₄F(c). Their data is combined with the present work for $\Delta H_f^{\circ}_{298.15}(\text{NF}_3, \text{g})$ to derive $\Delta H_f^{\circ}_{298.15}(\text{N}_2\text{F}_4, \text{g}) = -5$ kcal/mole. This value is combined with the heat of dissociation¹³ to two NF₂ radicals to give $\Delta H_f^{\circ}_{298.15}$

$(\text{NF}_2, \text{g}) = 8.5 \pm 2$ kcal/mole. From this we calculate the energy required for the dissociation of the first F from NF₃.



$D(\text{NF}_2\text{-F}) = 59.1 \pm 2$ kcal/mole. This is considerably less than the average and is in agreement with the electron paramagnetic resonance work by Kennedy and Colburn¹⁴ in which they report $D(\text{NF}_2\text{-F}) = 57.1 \pm 2.5$ kcal/mole. Thus both spectral and thermal evidence shows that NF₃ differs widely from NH₃ in that it first forms NF₂ radicals which are apparently stabilized by some bond hybridization.

Acknowledgment. This work was supported by the U. S. Air Force under Contract No. AF04(611)-11202.

(11) J. R. Ludwig and W. J. Cooper, *J. Chem. Eng. Data*, **8**, 76 (1963).

(12) G. K. Johnson, H. M. Feder, and W. N. Hubbard, *J. Phys. Chem.*, **70**, 1 (1966).

(13) "JANAF Thermochemical Tables," The Dow Chemical Co., Midland, Mich.

(14) A. Kennedy and C. B. Colburn, *J. Chem. Phys.*, **35**, 1892 (1961).

The Monomer-Dimer Equilibria of Liquid Aluminum Alkyls.

I. Triethylaluminum

by Martin B. Smith

Chemical Research and Development, Ethyl Corporation, Baton Rouge, Louisiana (Received July 29, 1966)

Experiments are described demonstrating the feasibility of determining the position of the monomer-dimer equilibrium of a liquid aluminum alkyl as a function of temperature by measuring its heat of dilution. Using a calorimeter developed especially for the purpose, the heat of dilution of a small quantity of triethylaluminum (TEA) with a relatively large quantity of *n*-hexadecane was measured at four temperatures from 60 to 150°. Equations were derived expressing the heat of dilution in terms of four parameters, two pertaining to the heat absorbed due to dissociation and two to the heat of physical mixing. A computer program determined values of the parameters which minimized the rms difference between calculated and observed heats of dilution. The values obtained for the heat and entropy of dissociation of 1 mole of TEA dimer are 16.93 ± 0.23 kcal and 32.19 ± 0.63 cal/deg. Degrees of dissociation of TEA in the pure liquid state and at various mole fractions in hydrocarbon solution are tabulated over a wide temperature range. The results obtained show satisfactory agreement with literature values. The ΔH of physical mixing of TEA with *n*-hexadecane is small and positive and decreases with rising temperature.

Introduction

Trimethylaluminum (TMA), triethylaluminum (TEA), and at least the next few aluminum tri-*n*-alkyls are primarily dimeric in dilute hydrocarbon solution.¹⁻³ In addition, TMA and TEA are partially dimerized in the vapor state.⁴ It is therefore appropriate to regard these compounds as dimeric according to the formula R_6Al_2 with partial *dissociation* to monomeric units, R_3Al . A bridge structure has been established for the dimers.⁵

Monomeric molecules, because of the electron deficiency of the aluminum atom, would be expected to be far more reactive than their dimeric counterparts. Indeed, kinetic studies⁶ of the addition of ethylene to TEA, the commercially important "growth reaction," have confirmed a suggestion by Ziegler⁵ that the monomeric form of the alkyl is the active species in the reaction. Dissociation to monomer and recombination provides a mechanism, perhaps the principal one under certain conditions, for the rapid exchange of alkyl groups which occurs when two aluminum alkyls are mixed. Monomeric molecules may undergo thermal

decomposition much more readily than dimeric molecules. In this case, it may be possible to correlate thermal decomposition rates with degrees of dissociation. A knowledge of the degrees of dissociation of liquid aluminum trialkyls at various temperatures and dilutions is therefore important.

Literature data on the degrees of dissociation of aluminum trialkyls are meager. Molecular weight measurements on tri-*n*-butylaluminum and tri-*n*-hexylaluminum² have indicated that these compounds are appreciably dissociated in dilute hydrocarbon solution

(1) K. S. Pitzer and H. S. Gutowsky, *J. Am. Chem. Soc.*, **68**, 2204 (1946).

(2) K. Ziegler, Special Publication No. 13, The Chemical Society, London, 1959.

(3) E. G. Hoffman, *Ann. Chem.*, **629**, 104 (1960).

(4) A. W. Laubengayer and W. F. Gilliam, *J. Am. Chem. Soc.*, **63**, 477 (1941).

(5) K. Ziegler in "Organometallic Chemistry," H. Zeiss, Ed., Reinhold Publishing Corp., New York, N. Y., 1960.

(6) C. S. Smith, Ph.D. Thesis, Chemical Engineering Department, Purdue University, Lafayette, Ind.; *Dissertation Abstr.*, **26**, 1540 (1965).

at 5°. The values obtained could be used to calculate equilibrium constants at this one temperature. However, similar measurements on TMA and TEA¹⁻³ have shown only that their degrees of dissociation under these conditions are too small for satisfactory evaluation by this method. The monomer-dimer equilibrium existing in TMA vapor has been determined from 100 to 160° by vapor density measurements,⁴ the heat of dissociation of 1 mole of dimer being evaluated as 20.2 kcal.

This investigation is the first of a series conducted to determine the degrees of dissociation of liquid aluminum trialkyls as functions of concentration and temperature. The experimental method selected consists of measuring the heat of dilution of a small quantity of alkyl with a relatively large quantity of saturated hydrocarbon. The heat of dilution, after subtracting the heat due to "physical mixing," is used to calculate the degree of dissociation of the pure alkyl.

Experimental Section

Materials. To avoid exposure to oxygen and moisture, all materials were stored in a nitrogen dry-box, and transfers to other containers were conducted there.

TEA was prepared by sodium reduction of ethylaluminum sesquichloride followed by distillation. Chemical analysis showed it to contain 97.42% (C₂H₅)₃Al, 0.41% (C₂H₅)₂AlH, and 2.17% (C₂H₅)₂Al-OC₂H₅. Thus the TEA contained 2.98 ethyl groups per aluminum atom. Normal hexadecane was ASTM grade (99% minimum) supplied by the Humphrey Chemical Co. It was deoxygenated by bubbling dry nitrogen through it for 2 hr and was stored over molecular sieves. Triply distilled mercury was deoxygenated similarly.

Apparatus. The calorimeter consisted of a 300-ml, 7-cm i.d. silvered borosilicate glass dewar (H. S. Martin & Son) provided with a Teflon cover (Figure 1). Temperatures were read to the nearest 0.0002° with a platinum resistance thermometer used in conjunction with a G-2 Mueller bridge and a Leeds and Northrup dc null detector. The stainless steel turbine stirrer, 19 mm in diameter at the base, was driven at 1800 rpm by a constant-speed electric motor. A rubber band 3 mm wide served as a belt. It passed around a Teflon pulley attached to the top of the 3/16-in. stirrer shaft and around a section of Tygon tubing slipped over the motor shaft. The liquids were brought to the test temperature and maintained there by means of a 165-w Chromalox cartridge heater controlled with two powerstats connected in series, one of which was plugged into a Sola constant-voltage transformer. The

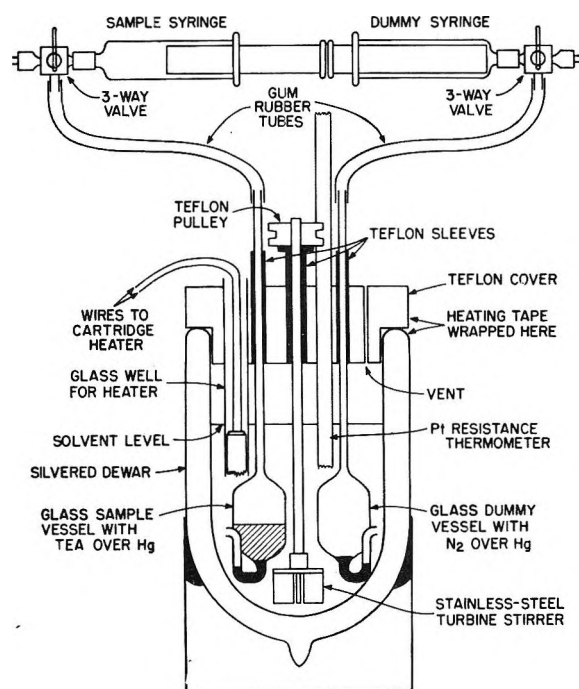


Figure 1. Calorimeter.

heater fit loosely inside a 10-mm i.d. glass well containing just enough silicone oil (Dow-Corning No. 200) to cover the heater. Auxiliary heating was provided by a 24 × 0.5-in. heating tape (Electrothermal HT-340, 0.5 amp). The tape was wrapped around the top of the dewar and the adjacent portion of the cover and was controlled by a powerstat.

The aluminum alkyl sample was contained in the 23-mm o.d. bulb of a glass vessel made from 3-mm i.d. tubing. The alkyl was held in the bulb by a small quantity of mercury in the side arm of the vessel. The neck of the vessel, which projected several centimeters above the Teflon cover, was connected by gum rubber tubing to a three-way valve (Becton, Dickinson & Co., MS08) attached to a 10-ml hypodermic syringe containing an appropriate volume (about 4 ml) of dry nitrogen. A second glass vessel, termed the "dummy" vessel, was rigged identically except that (1) it contained dry nitrogen instead of sample and (2) the plunger of its syringe was fully inserted. The sample and dummy syringes were mounted in a line, back to back, with the plungers touching. When the plungers were manipulated simultaneously, the alkyl was forced out the side arm of its vessel into the solvent. At the same time, an equal volume of solvent was drawn into the dummy vessel, thereby maintaining a constant liquid level in the calorimeter (this was found to be essential in order to obtain small, reproducible blanks).

A small vertical vent hole through the cover ensured equalization of pressure inside and outside the calorimeter. The calorimeter, syringes, and the electric motor were enclosed in a Plexiglas nitrogen drybox which provided full visibility.

Procedure. The hexadecane (184 ml) was added to the dewar and its weight was determined to 0.01 g. An appropriate volume of TEA (2 ml for "A" experiments and 10 ml for "B" experiments) was added to the hexadecane by syringe and its weight was measured to 0.0001 g (from the loss in weight of the syringe). The purpose of this preaddition was to destroy any traces of reactive materials still present in the solvent. In the case of the "B" experiments, an additional purpose was to reduce the magnitude of the heat absorbed due to dissociation relative to the heat of physical mixing and thereby provide a more accurate evaluation of the latter. The dewar was closed tightly with a rubber stopper. Mercury was added to the side arms of both the sample vessel and the dummy vessel and the side arms were closed with small rubber plugs. TEA (4 ml) was added to the sample vessel by syringe and its weight was determined to 0.0001 g. The necks of both vessels were plugged. The dewar and the vessels were transferred to the Plexiglas drybox.

The calorimeter syringes and their rubber tubes were flushed with nitrogen and the ends of the rubber tubes were plugged. The drybox was closed and thoroughly flushed with nitrogen. The calorimeter was assembled and the heating tape was tied in place. The syringe valves were set at the proper positions to open the rubber tubes to the box (to keep pressures equalized during the heating period). The calorimeter and contents were heated rapidly toward the desired test temperature (60, 90, 120, or 150°) using high settings of the cartridge heater powerstats. The powerstat for the tape heater was given an appropriate setting which varied with the test temperature. As the temperature approached the test temperature, the cartridge heater powerstats were cut back. They were adjusted until the temperature leveled out at the desired value ($\pm 0.2^\circ$). The syringe valves were then set at the proper positions to connect the syringes to the vessels.

Temperatures were read at regular intervals for several minutes until the rate of change became constant at 0.002° or less per minute. The TEA was forced from the sample vessel into the solvent by moving the syringe plungers to the second position. The plungers were moved back to the first position, causing solution to be drawn into the sample vessel (and discharged from the dummy vessel), and then returned to the second position. This rinsing of the sample

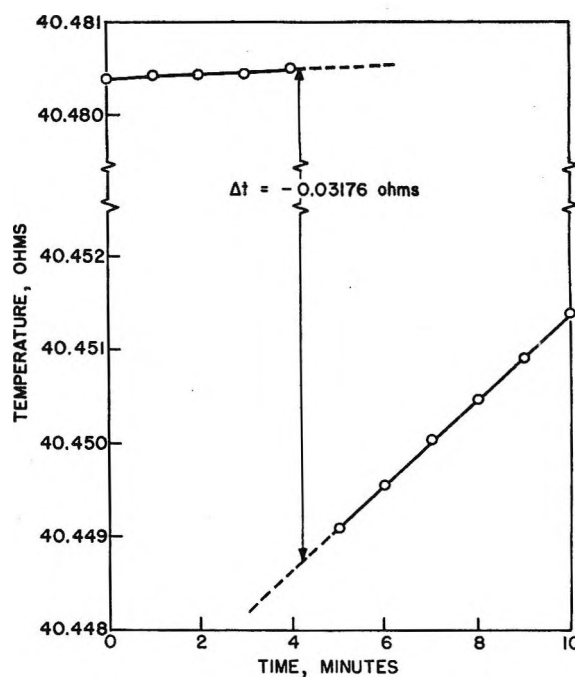


Figure 2. Typical temperature-time curve; experiment 150A1; time at which mixing occurred: 4.0 min.

vessel was repeated twice. Temperature readings were resumed and continued until a steady trend was again established. A blank experiment was performed by manipulating the plungers through the same sequence as before.

The temperature change was determined from a temperature-time plot, an example of which is given in Figure 2, and the blank correction applied (blank corrections varied from $-0.0030 \pm 0.0003^\circ$ at 60° to $0.0040 \pm 0.0006^\circ$ at 150°). The heat of dilution (Q_T) was calculated from the temperature change, the total heat capacity, and the weight of alkyl (corrected for buoyancy, as were all weights of materials). The heat of dilution was corrected to the target temperature ($60, 90, 120, \text{ or } 150^\circ$). These small corrections, which did not exceed 0.5%, were made with the aid of a plot of $\log Q_T$ vs. temperature.

Numerical Constants. The energy measurements were expressed in terms of the thermochemical calorie (1 cal = 4.1840 absolute joules). Temperature conversions were based on the relation $0^\circ\text{C} = 273.15^\circ\text{K}$. The 1961 International Atomic Weights were used, the gram formula weight of triethylaluminum being 114.168.

Heat Capacity Data. The specific heat of *n*-hexadecane was read from a plot obtained by extrapolating the measurements of Finke and others.⁷ The specific heat of triethylaluminum was determined over a wide

temperature range in this laboratory (data not published).

The heat capacity of the calorimeter (with mercury in the vessel side arms) was evaluated by draining a measured quantity (about 130 ml) of *n*-hexadecane at a known temperature near ambient into the calorimeter, which already contained some *n*-hexadecane (about 54 ml) and had been preheated to a somewhat higher, known temperature. The value obtained for the heat capacity at 25° (30.85 ± 0.25 cal/deg) was extended to higher temperatures using known temperature coefficients of heat capacity for the various materials present.

Discussion of Errors. Besides the 0.41% (C₂H₅)₂-AlH and 2.17% (C₂H₅)₂AlOC₂H₅ already present in the TEA, small additional amounts of impurities (estimated as less than 0.2%) were formed owing to contact with traces of moisture and oxygen in the nitrogen blanket. The amount of TEA decomposed thermally during an experiment was also insignificant (less than 0.2% at 150°). The heat of addition at 120° was not changed measurably upon substituting a sample of TEA containing about twice as much impurity, mostly (C₂H₅)₂AlOC₂H₅. Therefore, no corrections were applied.

The amount of TEA reacted in destroying traces of reactive materials in the solvent used in an experiment was calculated from calorimetric data as 0.033 g. When this amount was subtracted from each of the TEA preaddition weights, the calculated values of the heat and entropy of dissociation were increased by only 0.22 and 0.09%, respectively. Accordingly, no corrections were made.

If all of the TEA vapor in the sample vessel (about 5 cc) were condensed immediately upon mixing at 150°, the observed heat absorbed would be lowered by 1.1%. The actual error is much less since (1) only a portion of the vapor is condensed and (2) the condensation presumably occurs over a period of several minutes so that the error is partially eliminated by plotting and extrapolating the temperature readings. Again, no corrections were applied.

Derivation of Equations

The heat of dilution of an aluminum alkyl with a hydrocarbon (already containing some of the alkyl in solution) has two components: the heat due to dissociation of the alkyl and the heat due to physical mixing. This is expressed by the equation

$$Q_T = Q_D + Q_P \quad (1)$$

where each *Q* is heat absorbed in calories per gram formula weight of alkyl added. *Q_D* denotes heat due

to dissociation, *Q_P* is heat due to physical mixing, and *Q_T* is total (experimental) heat of dilution.

Heat Due to Dissociation. The following assumptions are made. (1) Triethylaluminum, either as the pure liquid or in hydrocarbon solution, consists of an ideal mixture of monomer and dimer. The equilibrium constant for the dissociation of the dimer into the monomer is therefore given by the expression

$$K_D = X_{\text{monomer}}^2 / X_{\text{dimer}} \quad (2)$$

where *X* is mole fraction. (2) *K_D* does not vary with the concentration of the alkyl in the solvent, its value being the same as in the pure alkyl. (3) The variation of the molar heat of dissociation with temperature is small and can be taken as zero.

Consider the addition of *f*₀ gfw of TEA to a solution containing *f*₁ gfw of TEA dissolved in *n_h* moles of *n*-hexadecane. Let *f*₂ = gram formula weight of TEA in final solution = *f*₀ + *f*₁; *r*₁ = *n_h*/*f*₁; *r*₂ = *n_h*/*f*₂; *β* = weight fraction of alkyl dissociated; *β*₀ = *β* for pure alkyl; *β*₁ = *β* for initial solution; *β*₂ = *β* for final solution; and *ΔH_D*^o = heat of dissociation, cal/mole of dimer dissociated.

For either solution (or the pure alkyl), moles of monomer = *βf*, moles of dimer = (1 - *β*)*f*/2, and total moles = *βf* + (1 - *β*)*f*/2 + *n_h* =

$$(f/2)(1 + \beta + 2r)$$

X_{monomer} = 2*βf*/(1 + *β* + 2*r*); *X_{dimer}* = (1 - *β*)/(1 + *β* + 2*r*); and

$$K_D = \frac{X_{\text{monomer}}^2}{X_{\text{dimer}}} = \frac{4\beta^2}{(1 - \beta)(1 + \beta + 2r)}$$

For the pure alkyl *r* = 0 and the expression becomes

$$K_D = \frac{4\beta^2}{(1 - \beta)(1 + \beta + 2r)} = \frac{4\beta_0^2}{1 - \beta_0^2} \quad (3)$$

Solution of the latter equation gives

$$\beta/\beta_0 = \sqrt{\beta_0^2 r^2 + 2r + 1} - \beta_0 r \quad (4)$$

Heat absorbed in experiment (due to dissociation) = *f*₀*Q_D* = (Δmoles of monomer)(*ΔH_D*^o/2).

Δmoles of monomer = *β*₂*r*₂ - (*β*₀*f*₀ + *β*₁*f*₁) =

$$f_0(\beta_2 - \beta_0) - f_1(\beta_1 - \beta_2)$$

$$f_0 Q_D = [f_0(\beta_2 - \beta_0) - f_1(\beta_1 - \beta_2)] \Delta H_D^o / 2$$

Q_D = (*β*₀*ΔH_D*^o/2)[(*β*₂/*β*₀) - 1 - (*f*₁/*f*₀)((*β*₁/*β*₀) - (*β*₂/*β*₀))]

Substitution of values of *β*₂/*β*₀ and *β*₁/*β*₀ from eq 4 gives

(7) H. L. Finke, M. E. Gross, G. Waddington, and H. M. Huffman, *J. Am. Chem. Soc.*, **76**, 333 (1954).

Table I: Heats of Dilution of Liquid Triethylaluminum with *n*-Hexadecane

Temp, °C	Expt no.	Initial solution		Grams of TEA added	-Δ _t , °C	Q _T , cal/gfw		Calcd values, cal/gfw	
		Grams of hexadecane	Grams of TEA			Exptl	Calcd	Q _P	Q _D
60.00	60A1	142.41	1.7088	3.3750	0.0395	153	156.9	60.5	96.4
	60A2	142.00	1.7823	3.3550	0.0430	156	153.7	60.4	93.3
	60B1	141.82	8.7667	3.4656	0.0257	97	95.9	55.1	40.8
	60B2	141.82	8.3375	3.4774	0.0236	91	97.6	55.4	42.2
90.00	90A1	142.37	1.6899	3.4186	0.0826	320	318.4	41.4	277.0
	90A2	141.59	1.6942	3.4015	0.0826	320	317.5	41.4	276.1
	90B1	141.75	8.1642	3.4790	0.0403	163	160.8	37.9	122.9
	90B2	142.08	8.4600	3.3281	0.0394	166	158.8	37.8	121.0
120.00	120A1	141.35	1.7694	3.4996	0.1650	672	676.2	22.2	654.0
	120A2	141.50	1.7999	3.4762	0.1647	673	673.6	22.2	651.4
	120B1	141.80	8.3718	3.4664	0.0736	313	315.5	20.3	295.2
	120B2	142.08	8.2547	3.4369	0.0751	321	319.1	20.4	298.7
150.00	150A1	141.65	1.7266	3.4521	0.3229	1387	1388.4	3.1	1385.3
	150A2	141.53	1.7875	3.4892	0.3227	1371	1366.5	3.1	1363.4
	150B1	141.42	8.3126	3.4947	0.1438	634	631.2	2.8	628.4
	150B2	141.75	8.3363	3.5071	0.1412	624	630.9	2.8	628.1

$$Q_D = (\beta_0 \Delta H_D^\circ / 2) [\sqrt{\beta_0^2 r_2^2 + 2r_2 + 1} - \beta_0 r_2 - 1 - (f_1/f_0)(\sqrt{\beta_0^2 r_1^2 + 2r_1 + 1} - \beta_0 r_1 - \sqrt{\beta_0^2 r_2^2 + 2r_2 + 1} + \beta_0 r_2)] \quad (5)$$

Application of basic thermodynamic formulas leads to the equation

$$\ln K_D = (\Delta S_D^\circ / R) - (\Delta H_D^\circ / RT) \quad (6)$$

where ΔS_D° = entropy of dissociation, cal/mole of dimer deg and T = temperature, °K.

Heat of Physical Mixing. The molar heat of mixing of two hydrocarbons at a particular temperature is given approximately by the relation $\Delta H_m = CX_1X_2$, where X is mole fraction. The measurements of McGlashan and others^{8,9} indicate that for pairs of hydrocarbons the proportionality constant C is linear with temperature to a first approximation. The physical mixing of TEA with *n*-hexadecane may be expected to resemble the mixing of two hydrocarbons. Since TEA is primarily dimeric, even in dilute solution (except at high temperatures where the heat of physical mixing is small), it is treated here as though it were all dimeric. It is therefore assumed that the heat of physical mixing of n_a moles of $(C_2H_5)_2Al_2$ with n_h moles of hexadecane is given by the expression

$$Q = (n_a + n_h)(A + Bt)X_aX_h = (A + Bt)n_a n_h / (n_a + n_h)$$

where A and B are constants to be determined and t is temperature. Differentiating with respect to n_a

$$\partial Q / \partial n_a = (A + Bt)n_h^2 / (n_a + n_h)^2 = (A + Bt)X_h^2$$

For a small addition of alkyl (Δn_a), as in the present experiments, the expression becomes, to a good degree of approximation

$$\Delta Q / \Delta n_a = (A + Bt)\bar{X}_h^2$$

where \bar{X}_h is the average X_h in the solution before and after the addition. Since $\Delta n_a = 1/2f_0$, it follows that

$$Q_P = \frac{\Delta Q}{f_0} = \frac{\Delta Q}{2\Delta n_a} = \left(\frac{A}{2} + \frac{B}{2}t\right)\bar{X}_h^2 \quad (7)$$

Results and Discussion

The endothermic process accompanying each dilution was completed within 1 min (and probably much sooner) as shown by the temperature-time curves (see Figure 2). The experimental results are listed in the first seven columns of Table I. At each temperature the total heat absorbed (Q_T) is roughly half as great for a "B" experiment (in which the initial solution contained about 10 ml of TEA) as it is for an "A" experiment (in which the initial solution contained about 2 ml of TEA). The net dissociation occurring in a "B" experiment is therefore much less than that occurring in an "A" experiment at the same temperature. This would be predicted from the monomer-dimer equilibrium; the presence of additional monomer molecules in the initial solution should have an inhibiting effect on the dissociation of added TEA. Within

(8) M. L. McGlashan in "Experimental Thermochemistry," Vol. II, H. A. Skinner, Ed., Interscience Publishers Ltd., London, 1962, Chapter 15, pp 337-339.

(9) J. A. Friend, J. A. Larkir, A. Maroudas, and M. L. McGlashan, *Nature*, 198, 683 (1963).

either the "A" series or the "B" series Q_T and therefore the net amount of dissociation occurring increase exponentially with temperature. This result would also be expected from the monomer-dimer equilibrium.

Values of the parameters ΔH_D° , ΔS_D° , A , and B were determined using a nonlinear least-squares computer program based on eq 1, 3, 5, 6, and 7. This routine solves for the values of the parameters for which the sum of the squares of the differences between calculated and observed heats of dilution (Q_T) is a minimum. The values obtained using a Scientific Data System 910 computer are listed in Table II with their

Table II: Values of Parameters Derived by Computer Program

ΔH_D° , cal/mole of dimer	$16,930 \pm 230$
ΔS_D° , cal/mole of dimer deg	32.19 ± 0.63
A , cal/mole	207 ± 14
B , cal/mole deg	-1.34 ± 0.12

estimated accuracy limits. Calculated values of Q_T based on the above numbers are given in column 8 of Table I where they are compared with experimental values (column 7). The rms difference between experimental and calculated values is 3.9 cal/gfw.

Calculated values of the heat of physical mixing (Q_P) and the heat due to dissociation (Q_D) given in the last two columns are all positive in sign. With increasing temperature, Q_D increases exponentially while Q_P decreases. At each temperature Q_P is larger relative to Q_D for a "B" experiment than for an "A" experiment. For two of the experiments (60B1 and 60B2), the heat of physical mixing exceeds the heat due to dissociation. The contributions of "chemical heat" (Q_D) and "physical heat" (Q_P) to the total heat absorbed (Q_T) at 90° are shown graphically for the entire composition range in Figure 3. At this temperature, Q_P exceeds Q_D at hexadecane mole fractions up to 0.6.

When the program was performed without the parameters A and B describing the heat of physical mixing, a much poorer fit of the experimental data was obtained. An analysis of variance of the fits of the data with and without parameters A and B indicated that the inclusion of the parameters is significant at better than the 97.5% level. The molar heat of mixing of $(C_2H_5)_6Al_2$ with n -hexadecane at $X = 0.5$, calculated as $\Delta H_m = 45.1$ cal at 25°, decreases with increasing temperature. This small positive heat of mixing decreasing with rising temperature is typical for pairs of similar hydrocarbons.⁸ The assumption made in deriving the equations that the physical

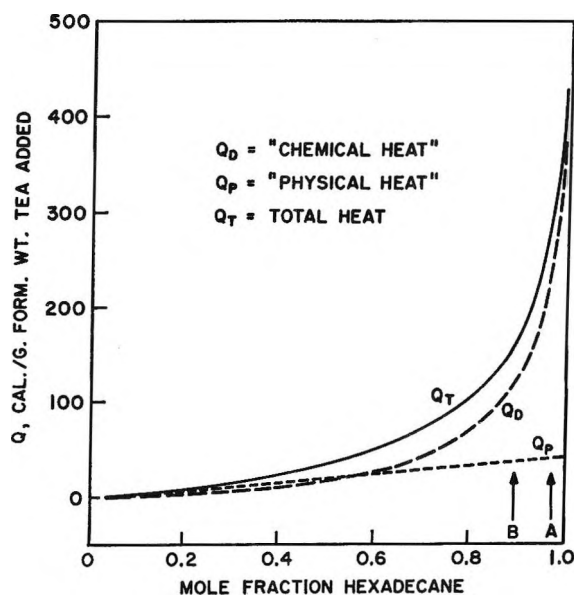


Figure 3. Contributions of chemical and physical heat to total heat absorbed at 90° as functions of composition. These calculated values are for the addition of 4 ml of TEA to various TEA-hexadecane mixtures, each containing 184 ml of hexadecane. Compositions designated as A and B are those employed in the "A" and "B" experiments, respectively. TEA was taken as the monomer in computing mole fractions.

mixing of TEA with n -hexadecane resembles the mixing of two hydrocarbons therefore appears to have been justified.

On substituting the values obtained for ΔH_D° and ΔS_D° in eq 6, the expression for the equilibrium constant becomes

$$\log K_D = 7.0344 - 3700.4/T \quad (8)$$

Values of K_D calculated from this equation at 10° intervals are given in column 1 of Table III. The degree of dissociation of pure TEA at each of these temperatures was calculated from the equilibrium constant using the equation $\beta_0 = \sqrt{K_D/(4 + K_D)}$ which is derived from eq 3. These values, expressed as per cent of TEA dissociated, are given in column 3 of Table III. Degrees of dissociation at various mole fractions in hydrocarbon solution, calculated from eq 4, are listed in the remaining columns of the table.

From their vapor density measurements, Laubengayer and Gilliam⁴ calculated the heat of dissociation of TMA vapor as 20.2 ± 1.0 kcal/mole of dimer. The corresponding value for the heat of dissociation of liquid TEA obtained in this investigation (16.93 ± 0.17 kcal/mole of dimer) is lower by 3.3 kcal. This seems reasonable since TEA is known to be less strongly associated than TMA.^{4,5,10}

Table III: Equilibrium Constant and Degree of Dissociation of Liquid Triethylaluminum^a

Temp, °C	K_D	% of TEA dissociated in hydrocarbon solution at TEA mole fraction ^b of							
		1	0.5	0.2	0.1	0.01	0.001	0.0001	0.00001
0	3.072×10^{-7}	0.02771	0.04799	0.08310	0.1207	0.3901	1.231	3.843	11.65
10	9.243×10^{-7}	0.04807	0.08324	0.1441	0.2093	0.6758	2.126	6.571	19.31
20	2.580×10^{-6}	0.08031	0.1390	0.2407	0.3495	1.127	3.527	10.73	30.04
30	6.729×10^{-6}	0.1297	0.2245	0.3884	0.5639	1.813	5.634	16.74	43.57
40	1.651×10^{-5}	0.2032	0.3515	0.6079	0.8819	2.825	8.681	24.90	58.52
50	3.832×10^{-5}	0.3095	0.5351	0.9247	1.341	4.272	12.91	35.23	72.54
60	8.456×10^{-5}	0.4598	0.7942	1.371	1.985	6.280	18.55	47.23	83.51
70	1.782×10^{-4}	0.6674	1.152	1.984	2.869	8.984	25.72	59.82	90.75
80	3.599×10^{-4}	0.9485	1.634	2.810	4.054	12.52	34.36	71.55	94.99
90	6.994×10^{-4}	1.322	2.273	3.897	5.608	17.00	44.18	81.16	97.29
100	0.001312	1.810	3.103	5.302	7.602	22.50	54.57	88.15	93.52
110	0.002380	2.439	4.165	7.082	10.11	29.01	64.76	92.77	99.17
120	0.004190	3.235	5.500	9.295	13.19	36.44	73.92	95.63	99.53
130	0.007173	4.231	7.151	12.00	16.90	44.54	81.49	97.36	99.72
140	0.01196	5.461	9.165	15.23	21.27	52.98	87.27	98.38	99.83
150	0.01948	6.961	11.58	19.04	26.29	61.32	91.42	98.99	99.90
160	0.03101	8.770	14.44	23.41	31.93	69.13	94.27	99.36	99.94
170	0.04833	10.93	17.77	28.35	38.08	76.04	96.17	99.59	99.96
180	0.07387	13.47	21.58	33.79	44.60	81.85	97.43	99.73	99.97
190	0.1109	16.42	25.87	39.65	51.31	86.49	98.26	99.82	99.98
200	0.1636	19.82	30.62	45.79	57.99	90.07	98.81	99.88	99.99
210	0.2374	23.67	35.78	52.05	64.41	92.75	99.17	99.92	99.99

^a Values at 0–50° and 160–210° are extrapolated. ^b TEA was taken as the monomer in computing mole fractions.

Smith⁶ conducted kinetic studies on the addition of ethylene to TEA in hydrocarbon solution. Assuming the monomeric form of TEA to be the only active species in the reaction, he derived dissociation constants for TEA at three temperatures. These constants are compared in Table IV with corresponding values ob-

Table IV: Comparison of Dissociation Constants with Literature Values

Temp, °C	K_D	
	This work	Lit. ^a
120	0.00419	0.0060
140	0.0120	0.021
160	0.0310	0.062

^a Calculated from related equilibrium constants given in ref 6.

tained in the present investigation. Considering the indirectness of Smith's method and the assumptions involved, the agreement is rather good.

Extrapolated values of the degree of dissociation of TEA at 5° range from 0.36 to 1.15% as the TEA mole fraction (computed with TEA as the monomer) is decreased from 0.02 to 0.002. Such low degrees of dissociation could scarcely be detected with certainty by cryoscopic molecular weight measurements. The (extrapolated) results of the present investigation therefore agree with the results of cryoscopic measurements reported in the literature.^{2,3}

Similar studies are planned of the monomer-dimer equilibria of other aluminum alkyls including triisobutylaluminum.

Acknowledgments. The author wishes to thank Mr. G. E. Bass for assistance in the design and construction of the apparatus and in the performance of preliminary experiments, Dr. G. J. Brendel for preparation of the TEA sample, Mr. G. A. Daniels for computational assistance and helpful discussions, and Mr. A. E. Harkins for programming the equations for the computer.

(10) The mixing of TMA and TEA is exothermic presumably because of the replacement of ethyl bridges with methyl bridges (unpublished data, Ethyl Corp).

A Study of the Chemiluminescence from Oxygen Atom-Hydrazine Flames

by K. H. Becker¹ and K. D. Bayes

Department of Chemistry, University of California, Los Angeles, California 90024
(Received August 8, 1966)

The behavior of the γ bands of NO, observed in emission from low-pressure oxygen atom-hydrazine flames, suggests that the electronically excited NO is formed by energy transfer rather than directly in a chemical reaction. The addition of NO to the flame increased the emission intensity of the γ bands and decreased the emission from NH. The energy carrier appears to have a lifetime longer than 3×10^{-5} sec, suggesting a metastable state. The most likely energy carrier is the lowest triplet state of nitrogen, $N_2(A^3\Sigma)$. Two additional experiments support this assignment: the addition of mercury vapor to the flame results in emission of the 2537-A mercury line and addition of NO to a system known to contain $N_2(A^3\Sigma)$ resulted in the almost exclusive emission of the γ bands of NO.

Introduction

Mixtures of gaseous hydrazine and atomic oxygen undergo a rapid chemiluminescent reaction. The emitting species have been identified as the NH, NH_2 , OH, and NO molecules.^{2,3} The excitation mechanism for any of these species is unknown.

A variety of radicals and intermediates are known to be formed from hydrazine. The photolysis of N_2H_4 can form both the NH and the NH_2 radicals.⁴ In addition, the OH and NO molecules were observed when N_2H_4 was photolyzed in the presence of O_2 .⁵ Intermediates such as NH_2 , N_2H_3 , and N_2H_2 have been observed mass spectrometrically in the N_2H_4 photolysis,⁶ in a hydrazine decomposition flame,⁷ and in the products from a high-frequency discharge in hydrazine.^{8,9} Recently, the N_2H_2 molecule has been observed by infrared absorption in a matrix following the decomposition of N_2H_4 or HN_3 .^{10,11}

The only observed emission from the NO molecule in the O- N_2H_4 flame is the γ bands, corresponding to the transition $A^2\Sigma \rightarrow X^2\pi$. Excitation of the $A^2\Sigma$ state requires 126 kcal/mole. There is no obvious reaction between any of the known intermediates and an oxygen atom that is sufficiently exothermic to form NO directly in this excited state. The current investigation concerns primarily this chemiluminescence of the NO molecule.

Experimental Section

A schematic diagram of the apparatus is shown in

Figure 1. The oxygen atoms were generated by flowing a mixture of Ar and O_2 through a microwave discharge in a cylindrical cavity (2450 MHz)¹² operated at a power of 80 w. The oxygen atom concentration in the reaction chamber was controlled by varying the O_2 content of the argon up to a maximum of 2%. Relative oxygen atom concentrations were measured by adding a known amount of NO through one of the inlets A or B and observing the intensity of the NO_2 emission with a photomultiplier (RCA 6199). A simple red filter in front of the photomultiplier removed wavelengths shorter than 6000 Å. It has been shown that the NO_2 emission intensity is proportional to $(O)(NO)$

(1) Requests for reprints should be directed to this author at the Institut für Physikalische Chemie, Universität, Bonn, West Germany.

(2) (a) G. E. Moore, K. E. Shuler, S. Silverman, and R. Herman, *J. Phys. Chem.*, **60**, 813 (1956); (b) A. R. Hall and H. G. Wolfhard, *Trans. Faraday Soc.*, **52**, 1520 (1956).

(3) H. Guenebaut, *Bull. Soc. Chim. France*, **26**, 962 (1959).

(4) D. A. Ramsay, *J. Phys. Chem.*, **57**, 415 (1953).

(5) D. Husain and R. G. W. Norrish, *Proc. Roy. Soc. (London)*, **A273**, 145 (1963).

(6) F. I. Vilesor, B. L. Kurbator, and A. N. Terenin, *Dokl. Akad. Nauk SSSR*, **122**, 94 (1958).

(7) K. H. Homann, D. I. MacLean, and H. G. Wagner, *Naturwissenschaften*, **52**, 12 (1965).

(8) S. N. Foner and R. L. Hudson, *J. Chem. Phys.*, **28**, 719 (1958).

(9) S. N. Foner and R. L. Hudson, *ibid.*, **29**, 442 (1958).

(10) E. J. Blau and B. F. Hochheimer, *ibid.*, **41**, 1174 (1964).

(11) K. Rosengren and G. C. Pimentel, *ibid.*, **43**, 507 (1965).

(12) Cavity 2A described by F. C. Fehsenfeld, K. M. Evenson, and H. P. Broida, *Rev. Sci. Instr.*, **36**, 294 (1965).

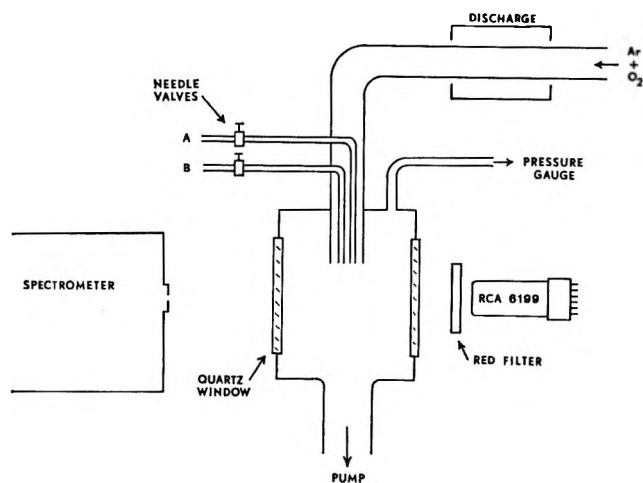


Figure 1. Schematic diagram of the apparatus.

in this pressure range.¹³ However, for a given oxygen atom flow in the above apparatus, it was observed that the continuum intensity was less than linear in (NO) at the higher addition rates of nitric oxide due to the consumption of oxygen atoms within the reaction vessel. But for a given NO concentration the NO₂ emission intensity was proportional to the inlet oxygen atom concentration, since the fraction of O atoms consumed within the vessel depended only on the NO pressure, the total pressure, and the residence time, all of which were constant. Thus the continuum intensity, at a constant NO partial pressure of 11.5 mtorr, was used as a measure of the relative oxygen atom concentration.

This relative atom concentration was converted into an absolute concentration at the inlet by titrating with NO₂, using the disappearance of the NO₂ emission as the end point.¹⁴ It is this absolute concentration, in terms of partial pressure of atomic oxygen at the inlet, which is of significance, since the fast O-N₂H₄ reaction should be confined to the vicinity of the inlet.

Small partial pressures of the added gases (NO, NO₂, and N₂H₄) were controlled in the following way. Known mixtures of the added gas or gases were made with argon in a 3-l. bulb up to a total pressure near 1 atmosphere. After thorough mixing a controlled flow of this mixture was admitted through inlets A or B sufficient to increase the total pressure in the reaction chamber from 5.0 to 6.0 torr as measured with the 0-20-torr Wallace and Tiernan diaphragm gauge. The partial pressure of the added gas in the chamber was then 1 torr times its original mole fraction in the 3-l. bulb, since the volume flow rate was approximately constant. All quantitative experiments were carried out at a total pressure of 6.0 torr. The reaction cham-

ber volume was approximately 0.3 l. and the flow rate 0.7 l./sec at 6 torr.

The chemiluminescence of the O-N₂H₄ reaction was investigated qualitatively with a 1-m Ebert spectrometer (Jarrell-Ash Co.) having a dispersion of 1 mm/16 Å and an effective aperture $f/8.6$. A search for emission below 2000 Å was made with a 1-m McPherson vacuum spectrometer. Quantitative intensity measurements of the NO emission were made with a 0.25-m monochromator (Bausch and Lomb) using a RCA 1P28 photomultiplier. A band pass of about 200 Å centered on 2500 Å allowed both the 0,2 and 0,3 γ bands to be measured. Time constants of 0.5-2 sec were used. Intensity measurements of the NH and OH bands were taken from peak heights on the scanned spectrum using the Ebert spectrometer.

Gaseous hydrazine was taken directly from the commercial liquid (Matheson Coleman and Bell, 95% anhydrous) and used after degassing at Dry Ice temperature. Further purification was unnecessary since it was shown that small amounts of NH₃ and H₂O did not affect the flame. Both the NO and NO₂ were purified by repeatedly distilling at low temperatures in the vacuum system. Commercial argon (Liquid Carbonic, 99.99%) and oxygen (Gordon Duff, 99.975%) were used without further purification.

Results

Figure 2 shows a typical emission spectrum of the O-N₂H₄ flame. The observed bands can be assigned to electronic transitions of the NH molecule, ($A^3\pi \rightarrow X^3\Sigma$), the OH molecule, ($A^2\Sigma \rightarrow X^2\pi$), and the γ bands of NO, ($A^2\Sigma \rightarrow X^2\pi$). The NO₂ continuum, due to the reaction of O with NO, is also present at longer wavelengths. No great efforts were made to observe the NH₂ emission since, at the resolution used, it would be easily lost in the NO₂ continuum.

The addition of argon, up to a total pressure of 150 torr, had little effect on the intensity of the NH, OH, or NO bands. The addition of NO, however, increased the NO and the NO₂ emission strongly and decreased the NH emission, as can be seen in Figure 3. The OH emission was relatively constant, decreasing only slightly with large additions of NO. For small addition rates of NO, the NO and NO₂ emission intensities were approximately linearly dependent on the NO partial pressure. These two intensities can be extrapolated to a common zero at about -3 mtorr (Figure 3): this is interpreted simply as the amount of NO

(13) F. Kaufman, *Proc. Roy. Soc. (London)*, **A247**, 123 (1958).

(14) F. Kaufman, *J. Chem. Phys.*, **28**, 352 (1958).

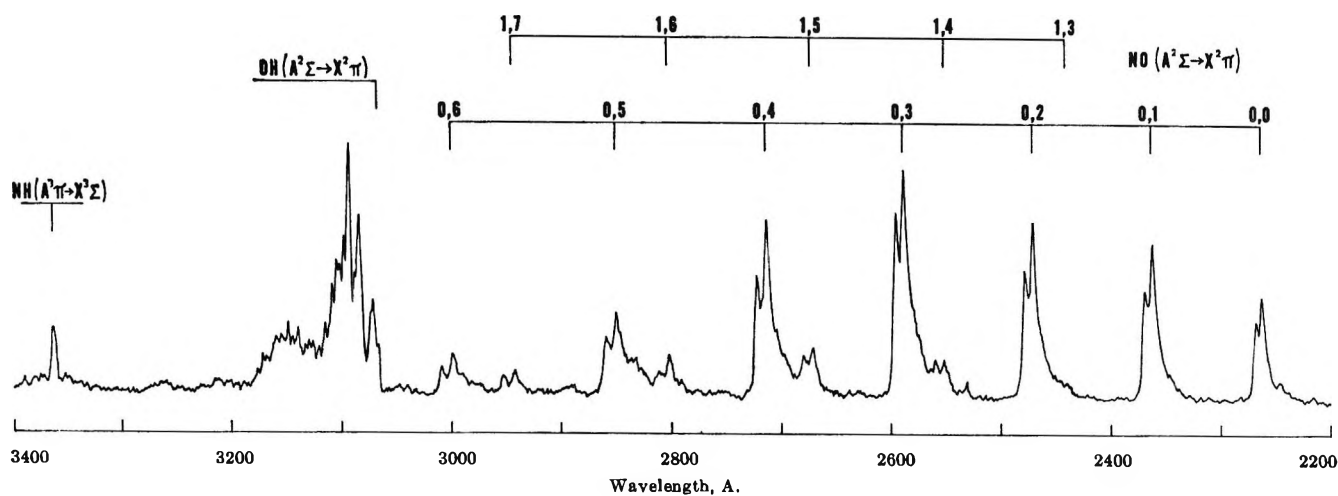


Figure 2. Emission spectrum from the oxygen atom-hydrazine flame. Partial pressures before reaction: (O) = 14 mtorr; (N_2H_4) = 6.7 mtorr. No added (NO). Total pressure 6 torr. Ebert spectrometer, 0.2-mm slits, EMI 6256S detector.

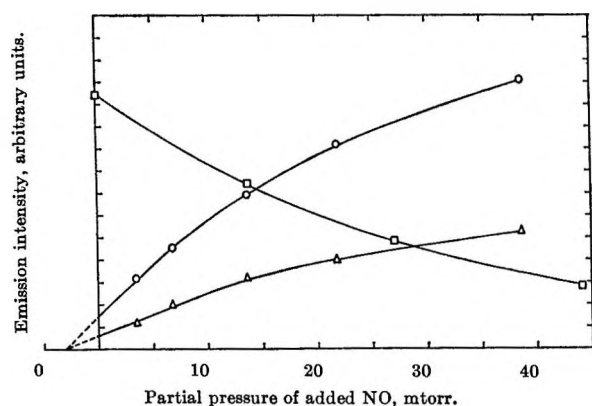


Figure 3. Emission intensity as a function of the partial pressure of added nitric oxide: O, $\text{NO}(\text{A}^2\Sigma \rightarrow \text{X}^2\Pi)$; □, $\text{NH}(\text{A}^3\Pi \rightarrow \text{X}^2\Sigma)$; Δ, NO_2 continuum. Each emission in different arbitrary units. The original hydrazine pressure was 3.5 mtorr for the NO and NO_2 measurements and 13 mtorr for the NH measurements. Total pressure 6 torr.

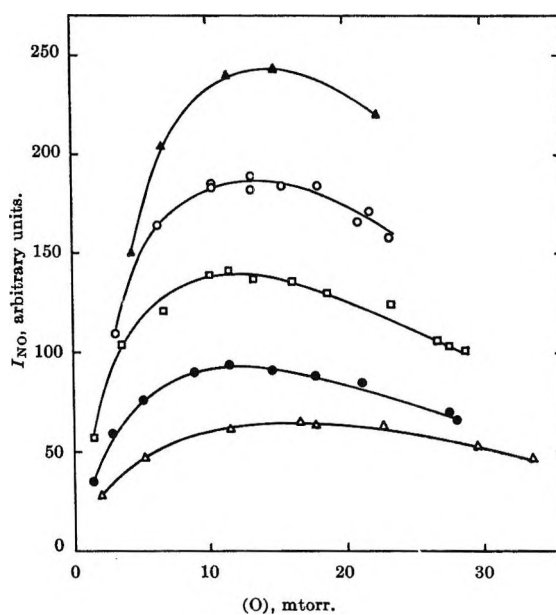


Figure 4. Emission intensity of the $\text{NO} \gamma$ bands as a function of the original oxygen atom pressure for different amounts of added NO: Δ, 3.5 mtorr; ●, 6.8 mtorr; □, 13.6 mtorr; ○, 21.9 mtorr; ▲, 38.6 mtorr. Original hydrazine pressure was 3.5 mtorr for all data.

which is formed by the complete oxidation of the original 3.5 mtorr of hydrazine.

The intensity of the $\text{NO} \gamma$ bands, I_{NO} , is plotted in Figure 4 and Figure 5 for a variety of conditions. The abscissa represents the absolute oxygen atom concentration at the inlet with no hydrazine present. The curves show a distinct maximum in the NO emission at an oxygen atom partial pressure of about 14 mtorr. Measurements on the NO_2 emission during the hydrazine addition indicate that very few oxygen atoms survive the flame until there is an excess over that needed to completely oxidize the hydrazine. This

confirms the earlier observation^{2a} that the $\text{O}-\text{N}_2\text{H}_4$ reaction is very fast.

The reaction of hydrazine with hydrogen atoms, made in a manner similar to the oxygen atoms, resulted in no observable light emission. Very weak emission (<1% of the oxygen atom flame), especially from NH_2 , could have been overlooked. The addition

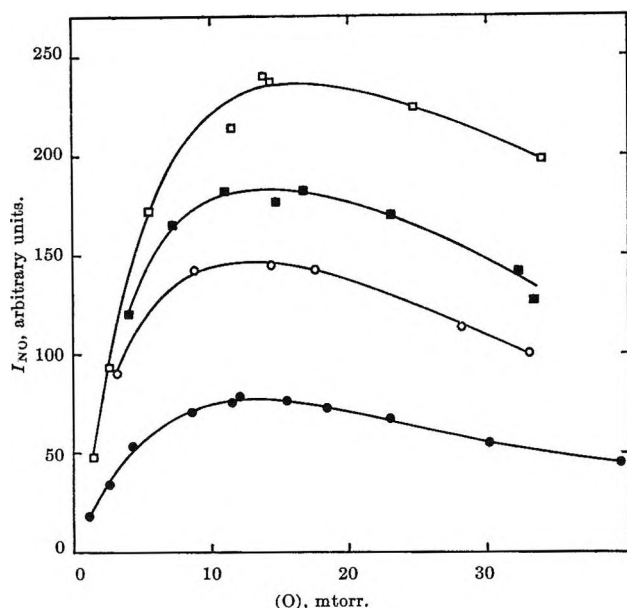
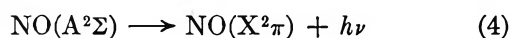
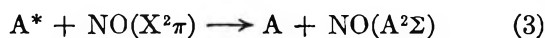
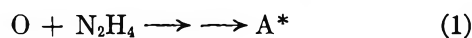


Figure 5. Emission intensity of the NO γ bands as a function of the original oxygen atom pressure for different original hydrazine pressures: \bullet , 0.7 mtorr; \circ , 2.0 mtorr; \blacksquare , 3.4 mtorr; \square , 6.8 mtorr. All data taken with 14.2 mtorr of added NO.

of NO to the $H + N_2H_4$ reaction did not result in NO emission.

Discussion

A major finding of this study is that the intensity of the NO bands is increased strongly by the addition of NO. This suggests that the excited NO is not formed directly in a chemical reaction but rather acquires its electronic excitation by energy transfer from another molecule. Since the observed increase in intensity may be substantial, the energy-rich molecules, in the absence of excess NO, lose their energy by some other means. Thus the kinetics may be simplified as



where A^* represents some energy-rich molecule formed during the oxidation of hydrazine. Step 2 is the non-luminescent deactivation of A^* which is in competition with energy transfer to NO, step 3. NO may also deactivate A^* without becoming electronically excited, but this will not alter the kinetic behavior of the relative light intensity. For a given hydrazine and oxygen atom flow, the intensity of the γ bands, I_{NO} , should obey the equation

$$I_{NO} \propto \frac{k_3(NO)}{k_2 + k_3(NO)} \quad (5)$$

where k_2 and k_3 refer to steps 2 and 3 above and (NO) is the partial pressure of nitric oxide, including that formed from the oxidation of hydrazine. Equation 5 was rearranged and tested on the data of Figure 3, as shown in Figure 6. The reciprocal of I_{NO} for an atomic oxygen concentration of 14 mtorr is plotted against the reciprocal of the added partial pressure of NO plus 2.7 mtorr. The latter value is somewhat arbitrary since the linearity shown in Figure 6 depends on the exact value used. However, 2.7 mtorr is consistent with the extrapolation to zero I_{NO} shown in Figure 3. Similar plots at other oxygen atom concentrations show comparable slope to intercept ratios. From the slope in Figure 6, the value of $k_3(NO)$ equals k_2 at an NO pressure of 43 mtorr. At this pressure, the direct electronic quenching of the γ bands by ground-state NO can still be neglected.¹⁵ Making the reasonable assumption that A^* is not deactivated by NO more rapidly than every gas kinetic collision, then the normal lifetime of A^* , in the absence of large amounts of NO, is equal to or greater than about 3×10^{-6} sec. Since the diffusion time to the walls is much longer than this at 6 torr (being about 10^{-2} sec), it is unlikely that the deactivation of A^* is by wall collisions.

Deactivation of A^* by radiation would produce an emission comparable in intensity to the NO bands. No unaccountable emission was observed over the wavelength range 1250–6000 Å. Since the actual lifetime of A^* is 3×10^{-6} sec or longer and since an emission which was 10% as intense as the strongest γ -band emission could have been easily detected, it is concluded that the radiative lifetime of the A^* state is longer than 3×10^{-5} sec. This means that A^* is in a metastable state.

Reaction 2 probably takes place by collisional deactivation. Both ammonia and water vapor reduce the NO emission significantly when present at partial pressures of about 20 mtorr. When added in very small amounts atomic hydrogen reduced the NO emission sharply, which may represent participation in steps 1 or 2. Almost certainly atomic hydrogen is present during the normal oxidation of hydrazine. The dependence of the NO emission, for an excess of atomic oxygen and added NO, on the hydrazine addition rate (Figure 7) also suggests that hydrazine or its oxidation products are quenching A^* . Increasing the

(15) H. P. Broida and T. Carrington, *J. Chem. Phys.*, **38**, 136 (1963).

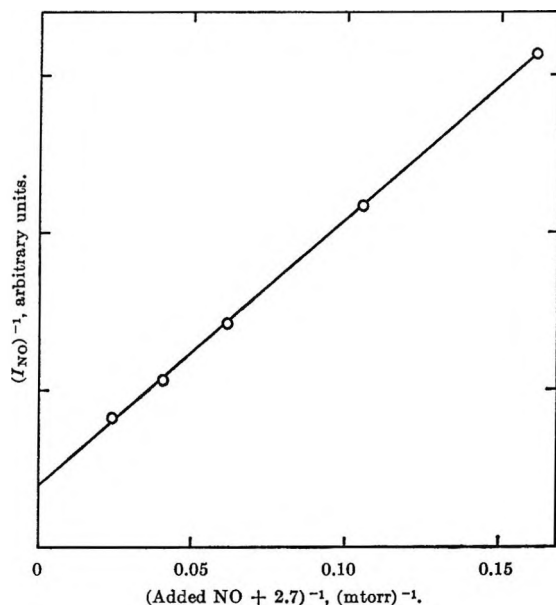


Figure 6. Test of eq 5 on the data shown in Figure 3.

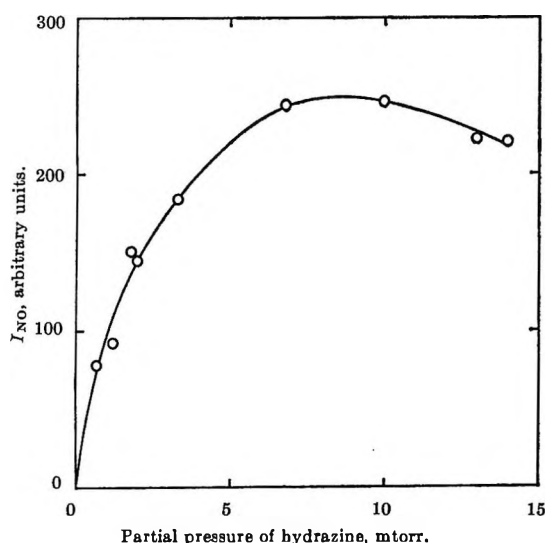


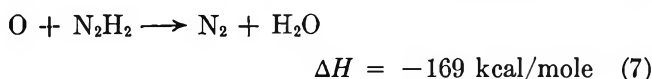
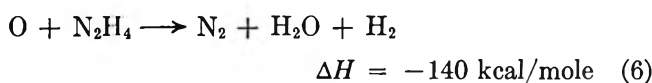
Figure 7. Emission intensity of the NO γ bands as a function of the original hydrazine pressure. All data taken with 14 mtorr of added NO and original oxygen atom pressure of 14 mtorr.

hydrazine flow rate initially generates increasing amounts of A^* . But as hydrazine or its oxidation products build up to concentrations comparable to the added NO, the intensity approaches a limit because the increased rate of formation of A^* is counterbalanced by the increased rate of quenching.

Additional conclusions about the nature of A^* may be derived from energy considerations. Simple reactions of ground-state NH and NH_2 radicals with atomic oxygen are not sufficiently exothermic to form NO

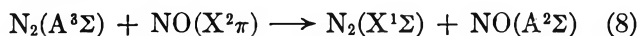
in its $A^2\Sigma$ electronic state. It is understandable, therefore, that the atomic oxygen-ammonia reaction does not cause emission of the γ bands^{2a} even though NO is formed during the oxidation.¹⁶ There is no evidence for the simultaneous reaction of two oxygen atoms with a radical, since I_{NO} depends linearly, not quadratically, on (O) at low atom concentrations (Figures 4 and 5).

Reactions of atomic oxygen with N_2H_4 or the lower hydrides, N_2H_x , are exothermic by more than 126 kcal/mole only if the large binding energy of N_2 is retained; for example¹⁷



But the formation of N_2 precludes the formation of NO in the same exothermic step. Again, energy transfer is suggested for the formation of $NO(A^2\Sigma)$.

Considering the above reasoning, the most likely candidate for A^* is N_2 . This is known to have a metastable state, the $A^3\Sigma$, which lies 142 kcal/mole above the ground state and has a radiative lifetime on the order of 1 sec.¹⁸ Because of its large exothermicity, reaction 7 is the most likely source of $N_2(A^3\Sigma)$, although the reactions $O + N_2H_4$ and $O + N_2H_2$ are also possibilities. Since N_2H_4 and probably N_2H_2 have singlet ground states, the formation of triplet N_2 would be favored by the spin conservation rule. Reaction 3 would then become



This reaction has been proposed recently by Welge¹⁹ to account for emission of the γ bands when NO was added to N_2O or HN_3 and the mixture was photolyzed by vacuum ultraviolet radiation.

The possibility that $N_2(A^3\Sigma)$ molecules are present in the atomic oxygen-hydrazine flame was tested in two additional experiments. Brennen and Kistiakowsky have shown that the 2537-A line of mercury is readily excited in active nitrogen.²⁰ By studying a variety of metals, they concluded that $N_2(A^3\Sigma)$ molecules are responsible for the excitation. When Hg

(16) E. L. Wong and A. E. Potter, *J. Chem. Phys.*, **43**, 3371 (1965).

(17) The necessary thermodynamic quantities are conveniently tabulated in J. G. Calvert and J. N. Pitts, Jr., "Photochemistry," John Wiley and Sons, Inc., New York, N. Y., 1966.

(18) C. G. Freeman and L. F. Phillips, *J. Phys. Chem.*, **68**, 362 (1964); L. F. Phillips, *Can. J. Chem.*, **43**, 369 (1965).

(19) K. H. Welge, *J. Chem. Phys.*, **45**, 166 (1966).

(20) W. R. Brennen and G. B. Kistiakowsky, *ibid.*, **44**, 2695 (1966).

vapor was introduced into the atomic oxygen-hydrazine flame, strong emission of the 2537-A line was observed, thereby supporting the presence of $N_2(A^3\Sigma)$ in this flame. The similar addition of Hg vapor to atomic oxygen with no hydrazine present did not result in 2537-A emission.

The independent generation of $N_2(A^3\Sigma)$ was attempted by the method developed by Phillips.¹⁸ Nitrogen was partially dissociated in a microwave discharge and then combined with argon containing iodine vapor. A vigorous reaction consumes the atomic nitrogen and generates a metastable molecule which has been shown to be the $A^3\Sigma$ state of N_2 .²¹ When NO was introduced into such a system downstream from the iodine inlet the NO γ bands were observed in emission with much weaker intensities of the β bands ($B^2\pi \rightarrow X^2\pi$). As the rate of I_2 addition was increased the intensity of the β bands decreased relative to the γ bands, indicating that they were probably the result of small amounts of unreacted atomic nitrogen²² ($N + NO \rightarrow N_2 + O$ followed by $N + O + M \rightarrow NO(B^2\pi)$). These observations, demonstrating the almost exclusive excitation of the $A^3\Sigma$ state of NO by metastable nitrogen, again lends support to the identification of A^* with $N_2(A^3\Sigma)$.

The fact that the NH emission decreases as the NO pressure is increased (see Figure 3) could be explained if NH is also being excited by A^* . Recent studies of the NH emission in several systems²³ have proposed such an energy transfer from $N_2(A^3\Sigma)$ to NH.

A second finding of the current study is that the NO emission reaches a maximum and then declines as the oxygen atom concentration is increased. The maximum occurs at a partial pressure of oxygen atoms of about 14 mtorr, approximately independent of the NO pressure (Figure 4) or the hydrazine pressure (Figure 5). At the highest addition rate of hydrazine (34 mtorr) no maximum in the NO emission was observed for the highest oxygen atom concentrations available. The cause of this maximum is not obvious.

The possibility that a change in flame geometry was causing the maximum was tested by observing the reaction zone along the axis of the hydrazine inlet with the entrance slit of the monochromator removed to a distance of 1 m. Again a maximum was observed, and the intensity decreased by a similar amount, although the atom concentration was not measured in this experiment. At this distance, even major changes in flame geometry should not alter the light intensity at the monochromator significantly. Visual observation of the flame was not possible since the major emissions are not in the visible region and the NO_2 masked any weak visible chemiluminescence. It is concluded

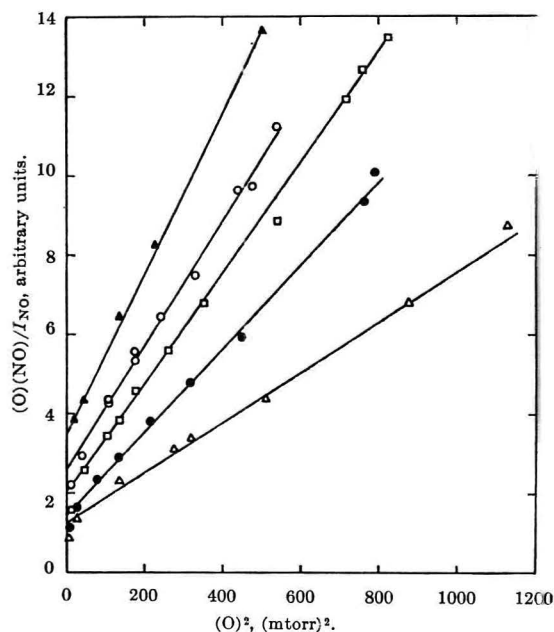


Figure 8. Test of eq 9 on the data shown in Figure 4. Key to symbols given in Figure 4.

that the maximum in the chemiluminescence curve is probably a real kinetic effect.

Another possible explanation of the emission maximum is that the products of the oxidation of hydrazine are quenching the energetic precursor of the γ bands. This possibility was tested by adding small amounts of various gases to the $O-N_2H_4$ flame and observing the intensity of the γ bands. The addition of partial pressures of approximately 20 mtorr of H_2 , N_2O , and N_2 caused little or no decrease in the NO emission. Adding similar amounts of H_2O and NH_3 reduced the emission intensity by approximately 15 and 40%, respectively. Small amounts of hydrogen atoms, generated in an auxiliary discharge and admitted in a stream of argon through the second inlet, were very effective in suppressing the NO emission. The partial pressure of H was not measured in these experiments, but it was certainly less than 20 mtorr. Thus some of the products do quench the NO chemiluminescence to the extent observed here. This explanation of the maximum is not very satisfactory, however, since oxidizing different amounts of hydrazine, which leads to different concentrations of products, gave approx-

(21) D. I. Walton, M. J. McEwan, and L. F. Phillips, *Can. J. Chem.*, **43**, 3095 (1965).

(22) R. A. Young and R. L. Sharpless, *Discussions Faraday Soc.*, **33**, 228 (1962).

(23) G. G. Mannella, *J. Chem. Phys.*, **37**, 678 (1962); H. E. Avery, J. N. Bradley, and R. Tuffnell, *Trans. Faraday Soc.*, **60**, 335 (1964); H. E. Avery and J. N. Bradley, *ibid.*, **60**, 850 (1964).

mately the same fractional decrease in Figure 5. Also, any simple kinetic scheme based on quenching by the products does not lead to the observed dependence on oxygen atom concentration.

Various analytical expressions were fitted to the measurements of I_{NO} and equations of the form

$$I_{NO} \propto \frac{c(O)(NO)}{1 + b(O)^2} \quad (9)$$

were found to fit the data of Figure 4 and Figure 5 quite well, as can be seen in Figure 8. The dependence on $(O)^2$ rather than on $(O)(1 + c(O))$ is noteworthy, for it indicates a specific second-order dependence on oxygen atoms rather than two independent first-

order quenching steps. Although it is not difficult to think of mechanisms that could give such an intensity expression, there is not sufficient evidence at present to seriously propose a specific mechanism. Studies under a greater variety of conditions are required for an understanding of the atomic oxygen-hydrazine flame.

Acknowledgments. The authors wish to thank the U. S. Air Force Office of Scientific Research, Directorate of Chemical Sciences, for support of this research through Grant AF-AFOSR-687-64. We are grateful to Dr. K. H. Welge for informing us of his results before publication.

Low-Pressure Physical Adsorption and Electron Microscope Study of the Surface of Annealed Pyrolytic Graphite^{1,2}

by L. B. Harris,³ J. B. Hudson, and S. Ross

Rensselaer Polytechnic Institute, Troy, New York (Received August 10, 1966)

A modification of the "flash filament" technique was used to measure the adsorption isotherms of krypton on annealed pyrolytic graphite at pressures between 10^{-10} and 10^{-6} torr at liquid nitrogen and liquid oxygen temperatures. The graphite surface was also studied by means of electron microscopy. The measured isosteric heats of adsorption vary from 5.6 to 3.5 kcal/mole over the range of pressures investigated. These values and the electron microscope results suggest that adsorption takes place in interlamellar crevices less than 10 Å wide.

Introduction

In recent years the technique of using the physical adsorption of a noble gas to characterize the energetic heterogeneity of a solid surface has received considerable attention.⁴ Most of this work has been done at pressures in the range above 10^{-4} torr on finely divided samples having high specific surface areas (*e.g.*, carbon blacks), although recently some work has been done on glass and on evaporated metal films at low pressures.⁵

In the present work, a technique has been developed for the measurement of physical adsorption at pressures

(1) This work was supported in part by the National Science Foundation under Grant No. 4430.

(2) Based in part on a thesis submitted by one of us (L. B. H.) in partial fulfillment of the requirements for the Ph.D. degree, June 1966, at Rensselaer Polytechnic Institute, Troy, N. Y.

(3) To whom correspondence should be addressed at Xerox Corporation, Rochester, N. Y.

(4) S. Ross and J. P. Olivier, "On Physical Adsorption," Interscience Publishers, Inc., New York, N. Y., 1964.

as low as 10^{-10} torr on small solid samples of very low surface area (a few square centimeters) whose structure can be characterized independently by X-ray diffraction and electron microscopy. This technique permits experimental correlation of adsorptive behavior with surface morphology.

Experimental Method

The method used in this investigation is a variation of the so-called "flash filament" technique, which has heretofore been used primarily to study chemisorption on metals.⁶⁻⁹

In this method the sample is placed in a steady flow of adsorbate gas in which the steady-state pressure is established by admitting the adsorbate into the sample-containing vessel at the same rate as that at which it is being removed by the pumping system.

The sample is then cooled to a temperature at which appreciable adsorption will take place. In this situation it then "pumps" molecules out of the flow stream until steady state is again established. If this pumping is fast enough, it will produce an observable transient pressure dip that is a direct measure of the amount of gas adsorbed. After the low-temperature steady state is established, the sample is warmed ("flashed") to a higher temperature and gives up the previously adsorbed gas, thus causing a transient pressure rise that is a measure of the amount of gas desorbed. If the "flashing" temperature is sufficiently high, the amount desorbed will equal the total amount adsorbed at the lower temperature. For the desorption of krypton from graphite, 150°K is a sufficiently high flash temperature; the adsorption equilibration temperature is 100°K or lower. In the present case the adsorption was relatively slow (partly due to thermal equilibration) so no measurable dip in pressure was observed during cooling. The transient pressure rise during desorption was therefore used to measure the amount adsorbed. If the amount adsorbed on the walls of the apparatus were the same after the transient as before then the amount adsorbed, G_{ads} (torr l.) would be given by

$$G_{\text{ads}} = \dot{S}I \quad (1)$$

where \dot{S} is the pumping speed in l./sec and I is the area (in torr sec) under the desorption pressure transient.

Materials. The annealed pyrolytic graphite used in this study was generously supplied by Dr. R. J. Diefendorf of the General Electric Co. Research Laboratory, Schenectady, N. Y. The piece from which the samples were taken had been annealed under vacuum at 3600° several times for about a half hour each time. X-Ray examination (by Dr. Diefendorf's associates at the

GE Research Laboratory) of other pieces of graphite from the same batch showed a complete set of reflections characteristic of crystalline graphite, with no detectable line broadening due to crystallite size or misorientation. The piece used here was approximately 1-in. square and a few tenths of an inch thick, the largest faces being C-face. Samples were obtained from this piece by sticking a strip of Scotch tape to the C-face along one end and then slowly raising the tape so as to separate a thin sheet of graphite from the rest of the block along the edge. With care this sheet could then be peeled from the block by pulling up on the tape. In this manner it was possible to obtain sheets of graphite about a hundredth of a millimeter thick and a few square centimeters in area with freshly cleaved surfaces on both sides. The piece was then cut to size with a scalpel and mounted on the sample holder.

Twelve sheets of the graphite prepared in this way were sent to Dr. V. R. Deitz of the U. S. Naval Research Laboratory, who ran a BET area determination on them using krypton at liquid nitrogen temperature. He found the total BET area to be 622 cm^2 . Since the total apparent area was 172 cm^2 , the average roughness factor was 3.6 for the 12 sheets tested by Dr. Deitz.

The adsorbate gas used was reagent grade krypton supplied by either Linde or Matheson in Pyrex break-seal flasks.

Apparatus. The experimental apparatus is shown in Figure 1, in which all but the sample vessel is shown schematically. The admission of adsorbate gas into the system was controlled by means of the metal valves V1 and V2 (Granville-Phillips, Type C). The pressure in the system was monitored with the ionization gauge, IG2 (GE Type 226T102), and sometimes with the small bakeable mass spectrometer, MS (GE Model 514 partial pressure analyzer). The sample, S, which was a sheet of annealed pyrolytic graphite approximately $12\text{ mm} \times 20\text{ mm} \times 0.01\text{ mm}$, was clamped by means of a small tantalum clip to a piece of tungsten wire, W, fastened to the Kovar slider, K, which was raised and lowered by means of a magnet. To cool the sample, this assembly was lowered until the slider made contact with the Kovar cup, C. The tube, TU,

(5) J. P. Hobson, *Can. J. Phys.*, **37**, 300 (1959); (b) J. P. Hobson, *ibid.*, **37**, 1105 (1959); (c) N. Hansen, *Vakuum Tech.*, **11**, 70 (1962); (d) J. P. Hobson and R. A. Armstrong, *J. Phys. Chem.*, **67**, 2000 (1963); (e) B. G. Baker and P. G. Fox, *Trans. Faraday Soc.*, **61**, 2001 (1965).

(6) J. A. Becker and C. D. Hartman, *J. Phys. Chem.*, **57**, 157 (1953).

(7) J. A. Becker, *Advan. Catalysis*, **7**, 135 (1955).

(8) G. J. Ehrlich, *J. Phys. Chem.*, **60**, 1388 (1956).

(9) P. Kisliuk, *J. Chem. Phys.*, **30**, 174 (1959).

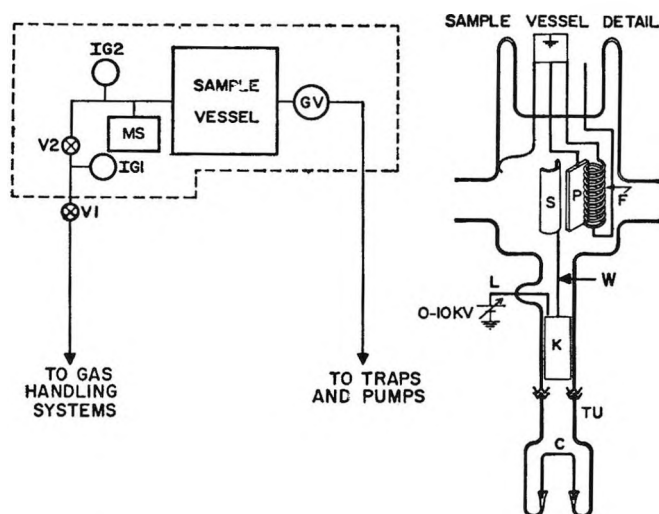


Figure 1.

was immersed in either liquid nitrogen or liquid oxygen up to the lead, L. To effect desorption the sample was raised to the position shown in Figure 1; sometimes the warming process was hastened by illuminating the upper position of the sample with a microscope lamp. GV is a glass slider valve which could be opened and closed by means of a magnet to regulate the system pumping speed.

System Calibration. To test whether the area under the observed desorption pressure transient was proportional to the amount desorbed from the sample under experimental conditions, the desorption was simulated by filling the tube between valves V1 and V2 (refer to Figure 1) with krypton at a given pressure and then opening the valve V2 rather quickly to admit the krypton into the vacuum system. If eq 1 were valid, then the ratio

$$r = \Delta v \Delta p / I \dot{S} \quad (2)$$

would be equal to unity, where Δv is the volume of the tube between valves V1 and V2 and Δp is the difference in pressure in that tube before opening V2 and after equilibrium was established with V2 open. The ratio, r , was measured with the sample tube at room temperature, at liquid nitrogen temperature, and at liquid oxygen temperature. In the last two cases, the actual experimental situation was simulated as closely as possible by adjusting valves V1 and V2 so that before opening V2 the krypton pressure near the sample tube, measured with gauge IG2, was approximately that which prevailed in an actual desorption run in which the amount desorbed from the sample was the same as that admitted through valve V2 for calibration purposes. In calculating the ratio, r , a cor-

rection was made for the ratio of the sensitivity of gauge IG1 to that of IG2; this ratio was measured and found to be 1.6 for pressures between 10^{-8} and 10^{-5} torr, which is the range of pressures that is of importance in measuring the desorption pressure transient. The volume, Δv , was estimated geometrically from the dimensions of the tubing between valves V1 and V2. The pumping speed was measured over the range of pressures from 10^{-9} to 10^{-5} torr and found to be almost constant, differing by less than 5% from its average value for pressures between 10^{-8} and 10^{-5} torr.

The ionization gauges were not calibrated; the sensitivity for dry nitrogen was taken from the manufacturer's specifications. For calculation of absolute pressure the gauge was corrected to krypton by using the ratio of 1.86 given by Dushman¹⁰ as the relative ionization gauge sensitivity for krypton vs. nitrogen. To correct the pressure for thermal transpiration, the formula $p/p' = (T/T')^{1/2}$, suitable for molecular flow conditions, was used.

Desorption Measurements. To prepare for desorption measurements, the apparatus (including traps) was baked overnight and the ionization gauges and mass spectrometer were outgassed before and after baking. Before each series of experiments the sample was cleaned by electron bombardment heating. Bombardment was carried out with an electron energy of 6–8 kv at a current of 5–10 ma. This raised the sample temperature to 1000–1500°. When the sample was first heated the pressure rose above 10^{-8} torr, but after several hours it dropped to 2×10^{-9} torr with the sample temperature about 1500° as measured with an optical pyrometer. The electron bombardment was then stopped and within several hours the background pressure returned to its usual value (2×10^{-10} torr). The system was then ready for operation.

During a series of experiments the tube, TU, was surrounded by a cylindrical dewar flask which was continuously kept full of liquefied gas up to the level of L. The level was controlled by a Fisher regulator and normally did not differ by more than a few millimeters from its average position.

After adjusting valve V2 so that the pressure in the system was at the desired value, the sample was left in its lower position long enough for equilibrium to be established. This required 1–2 hr at the higher pressures and 6–12 hr at the lower pressures. The desorption measurement was made by raising the sample to its upper position while simultaneously recording the pressure indicated by ion gauge IG2. Figure 2 shows

(10) S. Dushman, "Scientific Foundations of Vacuum Technique," 2nd ed, John Wiley and Sons, Inc., New York, N. Y., 1962.

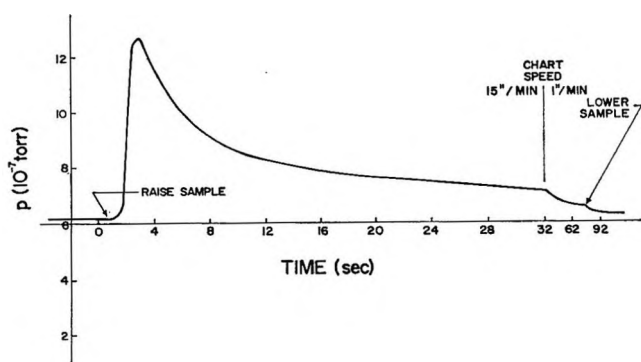


Figure 2.

the record of pressure *vs.* time for a typical desorption. The area under the curve was measured with a planimeter and converted to torr sec by suitably correcting for chart speed and the size of the chart divisions.

The procedure described above was then repeated many times, adjusting the equilibrium pressure to a different value each time to measure the adsorption *vs.* pressure.

In order to determine whether a correction was required to compensate for desorption from the sample holder, a series of desorption experiments was conducted using only the empty holder. These measurements showed that the amount of gas desorbed from the holder was negligible.

Electron Microscopy. To determine the surface configuration associated with adsorption sites, several sheets of graphite were studied by electron microscopy. A batch of samples (batch A) was first prepared as described previously. After shadowing with chromium, the samples were thinned by gluing the shadowed side to a glass slide with PVP (polyvinylpyrrolidone) and stripping the rest of the sample away with Scotch tape.¹¹ In some cases a thin translucent layer of graphite was left over the chromium on the PVP and in other cases only the chromium remained. In the first case, the thinned, chrome-shadowed graphite was floated off the PVP onto distilled water and then picked up on a grid. In the second case, the chromium on the PVP was first reinforced by depositing a layer of carbon over it and the composite chrome-carbon replica was then floated off the PVP and picked up on a grid. The specimens were then viewed in a Hitachi H-7 electron microscope and the fluorescent images recorded photographically.

A second batch of samples (batch B) was prepared in the same way as batch A but floated on hot water at 80° for several hours and then dried before preparing samples for the microscope. The reason for this procedure will appear later.

Results

The results of the calibration described previously showed that the amount of gas calculated from the area under the pressure transient was in all cases less than the amount actually released into the system. The ratio, r (defined by eq 2), was found to vary between 1.2 and 2.0, being higher when the sample tube was at lower temperature. This effect is probably due to the walls of the system adsorbing some of the krypton during the pressure transient and later desorbing it so slowly that the desorption causes no measurable pressure change. It was observed that even with the sample tube at room temperature, overnight pumping is required to reduce the krypton partial pressure below the residual gas pressure after closing valve V2; this indicates that even at room temperature krypton was captured by the walls of the apparatus and was released and pumped away very slowly when gas admission was cut off.

Table Ia reports desorption data at liquid nitrogen temperature and Table Ib reports data at liquid oxygen temperature for a sample of pyrolytic graphite, prepared as previously described. The indicated equilibrium pressure is in column 1; the area under the pressure transient is in column 2. In column 3 is the data of column 1 corrected for krypton sensitivity and thermal transpiration. In column 4 is the amount desorbed in torr l. at 0°, obtained by multiplying the data in column 2 by the correction factor previously obtained and correcting to 0° and for krypton sensitivity. All the figures shown in Table I refer to the manufacturer's stated nitrogen sensitivity for gauge

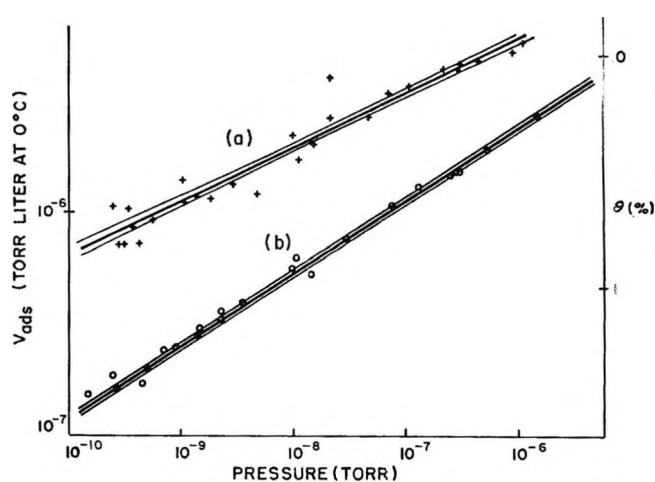


Figure 3.

(11) This technique is due to the late Dr. G. R. Hennig of Argonne National Laboratory.

Table I

P , torr	I , torr sec	P cor, torr	Gads, torr l. at 0°
(a)			
9.00×10^{-10}	1.23×10^{-6}	2.483×10^{-10}	1.051×10^{-6}
1.10×10^{-9}	7.98×10^{-7}	3.035×10^{-10}	7.118×10^{-7}
1.12×10^{-9}	7.96×10^{-7}	3.090×10^{-10}	7.100×10^{-7}
1.20×10^{-9}	1.20×10^{-6}	3.311×10^{-10}	1.028×10^{-6}
1.35×10^{-9}	9.46×10^{-7}	3.725×10^{-10}	8.300×10^{-7}
1.55×10^{-9}	8.04×10^{-7}	4.277×10^{-10}	7.162×10^{-7}
2.05×10^{-9}	1.03×10^{-6}	5.657×10^{-10}	8.962×10^{-7}
3.70×10^{-9}	1.65×10^{-6}	1.021×10^{-9}	1.370×10^{-6}
3.80×10^{-9}	1.28×10^{-6}	1.048×10^{-9}	1.090×10^{-6}
5.00×10^{-9}	1.37×10^{-6}	1.379×10^{-9}	1.159×10^{-6}
6.60×10^{-9}	1.35×10^{-6}	1.821×10^{-9}	1.144×10^{-6}
1.05×10^{-8}	1.58×10^{-6}	2.897×10^{-9}	1.318×10^{-6}
1.70×10^{-8}	1.42×10^{-6}	4.691×10^{-9}	1.197×10^{-6}
2.30×10^{-8}	2.08×10^{-6}	6.347×10^{-9}	1.686×10^{-6}
3.55×10^{-8}	2.71×10^{-6}	9.796×10^{-9}	2.136×10^{-6}
4.00×10^{-8}	2.10×10^{-6}	1.103×10^{-8}	1.701×10^{-6}
4.50×10^{-8}	2.59×10^{-6}	1.241×10^{-8}	2.052×10^{-6}
5.40×10^{-8}	2.48×10^{-6}	1.490×10^{-8}	1.974×10^{-6}
7.50×10^{-8}	3.34×10^{-6}	2.069×10^{-8}	2.575×10^{-6}
7.50×10^{-8}	5.28×10^{-6}	2.069×10^{-8}	3.865×10^{-6}
1.65×10^{-7}	3.33×10^{-6}	4.553×10^{-8}	2.568×10^{-6}
2.55×10^{-7}	4.38×10^{-6}	7.037×10^{-8}	3.276×10^{-6}
3.90×10^{-7}	4.80×10^{-6}	1.076×10^{-7}	3.553×10^{-6}
7.60×10^{-6}	5.70×10^{-6}	2.097×10^{-7}	4.136×10^{-6}
1.03×10^{-6}	5.70×10^{-6}	2.842×10^{-7}	4.136×10^{-6}
1.09×10^{-6}	6.06×10^{-7}	3.008×10^{-7}	4.366×10^{-6}
1.60×10^{-6}	6.31×10^{-6}	4.415×10^{-7}	4.524×10^{-6}
3.15×10^{-6}	7.10×10^{-6}	8.693×10^{-7}	5.020×10^{-6}
3.85×10^{-6}	7.69×10^{-6}	1.062×10^{-6}	5.385×10^{-6}
(b)			
4.79×10^{-10}	1.98×10^{-7}	1.427×10^{-10}	1.500×10^{-7}
7.96×10^{-10}	2.46×10^{-7}	2.371×10^{-10}	1.837×10^{-7}
8.40×10^{-10}	2.13×10^{-7}	2.502×10^{-10}	1.606×10^{-7}
1.50×10^{-9}	2.28×10^{-7}	4.469×10^{-10}	1.711×10^{-7}
1.60×10^{-9}	2.63×10^{-7}	4.767×10^{-10}	1.955×10^{-7}
2.40×10^{-9}	3.22×10^{-7}	7.151×10^{-10}	2.360×10^{-7}
2.82×10^{-9}	3.34×10^{-7}	8.402×10^{-10}	2.442×10^{-7}
4.59×10^{-9}	3.97×10^{-7}	1.367×10^{-9}	2.868×10^{-7}
4.80×10^{-9}	4.12×10^{-7}	1.430×10^{-9}	2.968×10^{-7}
7.40×10^{-9}	4.68×10^{-7}	2.204×10^{-9}	3.341×10^{-7}
7.95×10^{-9}	5.10×10^{-7}	2.368×10^{-9}	3.619×10^{-7}
1.16×10^{-8}	5.50×10^{-7}	3.456×10^{-9}	3.881×10^{-7}
3.20×10^{-8}	8.10×10^{-7}	9.535×10^{-9}	5.556×10^{-7}
3.50×10^{-8}	9.00×10^{-7}	1.042×10^{-8}	6.125×10^{-7}
4.78×10^{-8}	7.52×10^{-7}	1.424×10^{-8}	5.187×10^{-7}
9.55×10^{-8}	1.12×10^{-6}	2.845×10^{-8}	7.493×10^{-7}
2.50×10^{-7}	1.60×10^{-6}	7.449×10^{-8}	1.041×10^{-6}
4.28×10^{-7}	1.99×10^{-6}	1.275×10^{-7}	1.273×10^{-6}
7.95×10^{-7}	2.25×10^{-6}	2.368×10^{-7}	1.425×10^{-6}
9.65×10^{-7}	2.36×10^{-6}	2.875×10^{-7}	1.489×10^{-6}
1.76×10^{-6}	3.00×10^{-6}	5.244×10^{-7}	1.856×10^{-6}
4.70×10^{-6}	4.34×10^{-6}	1.400×10^{-6}	2.604×10^{-6}

IG2 as standard. The data are plotted in Figure 3 in which the group of points marked (a) is the liquid nitrogen temperature data taken from columns 3 and 4 of Table Ia and the group of points marked (b) is the liquid oxygen temperature data taken from columns 3 and 4 of Table Ib. The limits shown in Figure 3 were obtained by point-by-point RMS addition of the effect of statistical uncertainties in both the desorption data and the calibration data. The values of coverage indicated at the right of the figure are based on a sample area of 22 cm² obtained by multiplying the apparent area (6 cm²) by the roughness factor of 3.6 measured by Deitz. The area of an adsorbed krypton atom was taken as 20×10^{-16} cm².

Several micrographs of samples prepared from batch A (see above) are shown in Figure 4. Plates a and b show high-magnification micrographs of a bumpy area and a smooth area, respectively, and plate c is a lower magnification micrograph of the boundary between two such areas. The magnification in each case is indicated in the plate. The shadowing ratio (the ratio of length of shadow to height of prominence) is 3:1 in all cases. The final detail visible in most of the plates is due to the nucleation pattern of the chromium. This was verified by depositing chromium at 90° incidence on a test sample, in which case no specimen from that sample showed any detail except fine-grained mottling similar in appearance to that in plates a and b.

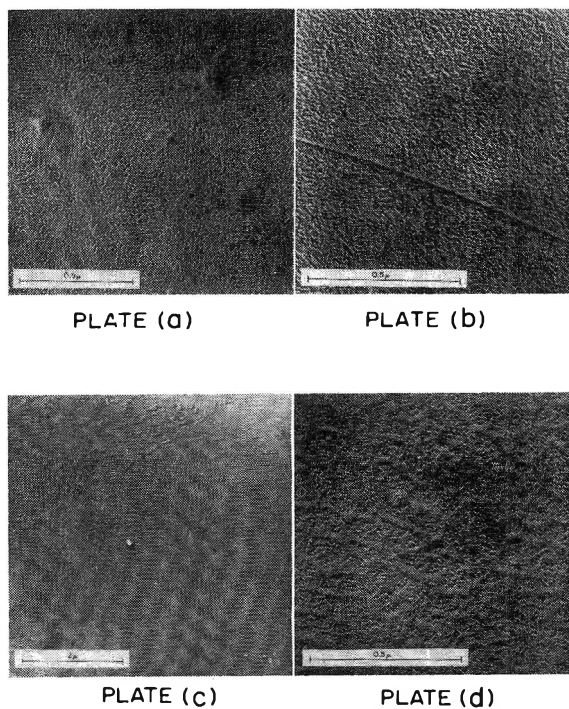


Figure 4.

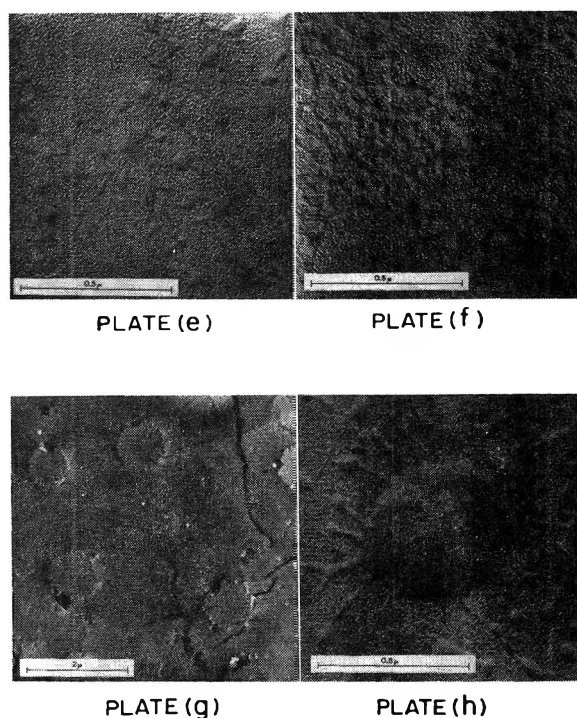


Figure 5.

The ridge visible in plate b is approximately 30 Å high as indicated by the width of the shadow above it (note that shadowed areas appear *lighter* than chrome-covered areas). The smallest shadows that can easily be distinguished on any of the micrographs correspond to features about 20 Å high, although some even lower surface relief (probably due to a slight separation of the topmost graphite layers from those beneath) can be distinguished by a difference in the nucleation pattern in the chromium. This effect is noticeable in plate a, in which the foothills of the larger bumps exhibit finer grains than the surrounding areas. These areas of relatively low relief are probably less than 10 Å high. The smooth area of plate b is representative of most of the specimens prepared from batch A. Only one specimen from the batch showed the features in plates a and c. A significant number of specimens showed topography of intermediate roughness such as that in plate d.

Although the micrographs show no evidence of surface irregularities other than slightly raised areas, the presence of very low and/or closely spaced steps or corrugations cannot be ruled out, since such features probably could not be distinguished from the chromium grains.

Micrographs of specimens from the water-floated samples of batch B are shown in Figure 5. All specimens from batch B showed striking evidence of delami-

nation due to water penetration. Plates e-g show the delamination at successive stages in its development. In plate e blisters can be seen except on three fairly well-defined patches which may have been separated from the water by air bubbles. In plate f the blistering has developed further and plate g shows a large area, all delaminated except for several round patches. Plate h shows an exceptionally large and well-formed blister.

Discussion

It now remains to establish a correlation between the coverage and heat of adsorption data derived from the flash filament studies and the surface topographic information obtained by electron microscopic observation.

Consider first the adsorption data. The coverages at various pressures may be compared with that observed by Ross and Winkler¹² on a sample of the graphitized carbon black P-33 (2700°) having a monolayer capacity of about 4 cc (STP) of krypton. At 10⁻³ torr the carbon black adsorbed 0.2 cc (STP) at liquid nitrogen temperature. This is a coverage of 5%. Table II shows a comparison of the approximate coverage in the present work (see Figure 3) and the coverage on the graphitized carbon black, assuming that adsorption on the carbon black obeys Henry's law at pressures below 10⁻³ torr. As can be seen from Table II, the difference in coverage between the pyrolytic graphite and the carbon black is three to five orders of magnitude, becoming larger at the extreme low pressures.

Table II: Comparative Krypton Coverage at Liquid Nitrogen Temperature on Graphitized Carbon Black P-33 (2700°) and on Pyrolytic Graphite

P, torr	% Coverage	
	P-33 (2700°) ^a	Pyrolytic graphite, sample D
10 ⁻³	5	..
10 ⁻⁶	5 × 10 ⁻³	10
10 ⁻⁹	5 × 10 ⁻⁶	2

^a Data from Ross and Winkler (ref 12) extrapolated toward zero pressure along a straight line.

A comparison may also be made between the isosteric heats of adsorption

$$q_{st} = R \left[\frac{\partial \ln P}{\partial \frac{1}{T}} \right]_{\theta} \quad (3)$$

(12) S. Ross and W. Winkler, *J. Colloid Sci.*, **10**, 319 (1955); S. Ross and W. Winkler, *ibid.*, **10**, 330 (1955).

(which were calculated from the isotherms in Figure 3 and are shown in Figure 6) with those measured by Ross and Winkler.¹² In Figure 6 the heavy line gives the heats obtained from the best straight lines in Figure 3. The lighter lines show the 90% confidence limits obtained by using the inner and outer limits in Figure 3. At the lowest coverage obtained at liquid nitrogen temperature q_{st} is about 5.6 kcal/mole, about 60% higher than the Ross–Winkler value for the heat of adsorption on graphitized carbon black near half-coverage.¹² With increasing coverage q_{st} falls rapidly and is down to 3.6 kcal/mole at coverages of the order of 10%. This observed high relative coverage and high isosteric heat of adsorption, which are consistent with each other, are indicative of a high degree of surface heterogeneity in the present case relative to the previous work on P-33 (2700°), which has been shown to possess a highly uniform (energetically) surface.

To elucidate the origin of the high degree of heterogeneity observed in the present work, we must turn to the results of the electron micrographic study. Plates a–d in Figure 4 show that the sheets of graphite peeled from the parent block are slightly delaminated (probably due to stresses developed while peeling), but that the resulting separation of the graphite layers is almost always less than 10 Å. Plates e–h in Figure 5 show that when the surface of a graphite sheet is brought into contact with hot water for several hours, the water makes its way through openings in the surface into the very narrow interlamellar cavities and widens them so that they are easily distinguished in the electron microscope after chromium shadowing. Furthermore, the dimensions of the water blisters indicate that the blistered graphite layers must be extremely thin in order to be so severely bent without fracturing. This argues against any invisible pattern of closely spaced steps on the surface, for one would

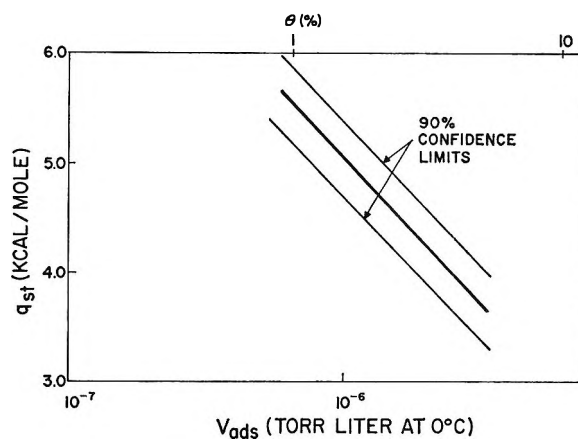


Figure 6.

expect that under the stress of blistering such a surface would come apart and present a “shredded” appearance after the water treatment. Thus it appears that the sample used for the adsorption studies was permeated with a series of very narrow crevices having lateral dimensions of the order of 10 Å.

Calculation indicates that the heat of adsorption in such a crevice would reach a maximum value of a little less than twice that on the basal plane, or about 6.5 kcal/mole rather than 3.5 kcal/mole as measured by Ross and Winkler.¹² This is in good agreement with the measured heats of adsorption, which lie between 3.6 and 5.6 kcal/mole, corresponding to crevices having widths between 2.5 and 2.0 times the equilibrium krypton-to-carbon spacing on the uniform C-face of graphite. Thus we have a clear correlation of the physical structure of the surface as determined by electron microscopy and the energetic heterogeneity of the surface as revealed by measurement of the heat of adsorption at low coverage.

Pulse Radiolysis Studies. IX. Reactions of the Ozonide Ion in Aqueous Solution¹

by W. D. Felix, Bonnie L. Gall, and Leon M. Dorfman

Department of Chemistry, The Ohio State University, Columbus, Ohio (Received August 12, 1966)

The radiation chemistry of strongly basic aqueous solutions containing oxygen and nitrous oxide has been investigated by the pulse radiolysis method with particular attention to the decay kinetics of the ozonide ion. The apparent discrepancies in the literature concerning the kinetic order of the ozonide decay may be understood as an effect of pulse intensity and oxygen concentration. Absolute rate constants have been determined for the following reactions at 25°: $O_3^- + HO_2^-$ (8.9 ± 1.1) $\times 10^6 M^{-1} sec^{-1}$ pH 13.1 and 13.5, $e_{aq}^- + HO_2^-$ (3.5 ± 0.4) $\times 10^9 M^{-1} sec^{-1}$ pH 13.0, and $O^- + HO_2^-$ (7 ± 3) $\times 10^8 M^{-1} sec^{-1}$ pH 13.0, as determined by competitive kinetics based on a rate constant of $2.5 \times 10^9 M^{-1} sec^{-1}$ for the reaction $O^- + O_2$. The rate constant for the reaction $O_3^- + O_3^-$ is substantially lower than previously reported² and shows an inverse functional dependence on the oxygen concentration. At $[O_2] = 3.1 \times 10^{-3} M$, the highest oxygen concentration attained, and pH 13.5 this rate constant has the value $2k = (0.9 \pm 0.2) \times 10^6 M^{-1} sec^{-1}$ where it seems to be leveling off. This value is based on our determination of $\epsilon_{O_3^-}^{4300} = 1900 \pm 120 M^{-1} cm^{-1}$ for the molar extinction coefficient of the ozonide ion at 4300 Å.

Introduction

The recent investigations²⁻⁴ of transient species in irradiated oxygenated aqueous solutions at high pH are in agreement in identifying the observed absorption band at 4300 Å with the ozonide ion, O_3^- . The identification of this band seems reliably established on the basis of: (a) its pH-dependent formation,^{2,3} correlating with the pK of 11.9 for the hydroxyl radical,⁵ which is apparently the precursor; (b) its suppression by the addition of hydroxyl radical scavengers; (c) its absence in deaerated solutions; (d) its formation rate which is first order in oxygen with a rate constant² of $2.5 \times 10^9 M^{-1} sec^{-1}$ at room temperature; (e) its correspondence with the 4300-Å band observed in the flash photolysis⁶ of oxygenated alkaline solutions of hydrogen peroxide; and (f) its similarity to the stable ozonide band in liquid ammonia⁷ and the band in alkaline aqueous glass⁸ containing hydrogen peroxide.

These authors^{2,3} have reported on the decay kinetics of the ozonide ion with apparently discordant results. Czapski and Dorfman³ found the decay to be first order, an observation which has been confirmed and extended by Czapski⁹ in a current investigation covering a

broad range of conditions. Adams, *et al.*,² report substantial deviation from first order in oxygenated solutions and a decay which is second order in solutions saturated with N_2O . They attribute this second-order decay to the reaction of the ozonide ion with itself, for which they report a rate constant of $2k = 1.1 \times 10^8 M^{-1} sec^{-1}$ at room temperature.

The present investigation is concerned principally with the decay kinetics of the ozonide ion, which we

(1) Based on work performed under the auspices of the U. S. Atomic Energy Commission.

(2) G. E. Adams, J. W. Boag, and B. D. Michael, *Proc. Roy. Soc. (London)*, **A289**, 321 (1966).

(3) G. Czapski and L. M. Dorfman, *J. Phys. Chem.*, **68**, 1169 (1964).

(4) J. W. Boag and G. E. Adams, 18th Annual Symposium on Cellular Radiation Biology, Houston, Texas, 1964; (also see Williams and Wilkins, 19th Symposium, Baltimore, Md., 1965).

(5) J. Rabani and M. S. Matheson, *J. Am. Chem. Soc.*, **86**, 3175 (1964).

(6) L. J. Heidt and V. R. Landi, *J. Chem. Phys.*, **41**, 176 (1964).

(7) A. J. Kacmarek, J. M. McDonough, and I. J. Solomon, *Inorg. Chem.*, **1**, 659 (1962).

(8) A. D. McLachlan, M. C. R. Symons, and M. G. Townsend, *J. Chem. Soc.*, 952 (1959).

(9) G. Czapski, *J. Phys. Chem.*, in press.

have investigated over greater than a hundredfold variation in initial concentration up to a maximum of $2.4 \times 10^{-4} M$. The results permit us to resolve the apparent discrepancies in the literature and provide absolute rate constants for some of the reactions. The rate constant for the reaction of the ozonide ion with itself is substantially lower than previously reported² and is an inverse function of the oxygen concentration.

Experimental Section

The general methods of pulse radiolysis used here are, for the most part, the same as those previously described in this series of reports.^{3,10,11} The principal differences are in the pulsed electron source and the irradiation cells used. The detection equipment is very nearly identical with that previously described.

Pulse Irradiation. A Varian V-7715A linear accelerator was used as the source of the electron pulse. This accelerator is useful over the energy range 2–6 Mev. The pulse width is continuously variable from 1.6 to 0.005 μsec . For the 1.6- μsec pulse the maximum current is approximately 290 ma at 4 Mev and about 400 ma at 2.2 Mev. Most of the work was done at 3–4 Mev. Runs at the highest dose rate were done at 2.2 Mev where the 1.6- μsec pulse delivers a dose of approximately 2.5×10^{18} ev/g. The dose was generally varied by changing the pulse width from the maximum to less than 0.02 μsec . The electron beam diverges slightly from the accelerator window to a diameter of approximately 2.5 cm at the point of incidence on the cell for the arrangement used.

Optical Detection. The transient species were detected by observing their optical absorptions spectrophotometrically. A 1P28 photomultiplier tube was used to monitor the light passing through the irradiation cell. A 500-w Osram xenon lamp, Type XBO 450 W, was used as the light source. Either a double pass or a single pass of the analyzing light beam was used at right angles to the electron beam.

An arrangement of two Bausch and Lomb grating monochromators, Type 33-86-25, $f/3.5$, was used with the light beam split by a partially reflecting mirror. This was particularly useful for mapping spectra as well as for observing kinetics simultaneously at two different wavelengths. The grating used in most of the work had a dispersion of $6.4 \text{ m}\mu/\text{mm}$. The exit slit was generally set between 0.1 and 0.3 mm so that the band width was usually less than $1.8 \text{ m}\mu$. For kinetic studies between 2200 and 2400 Å, interference filters were used together with the monochromator to eliminate problems of scattered light.

Reaction Cells. Two types of rectangular quartz

cells with high-purity silica windows were used. For all the runs at atmospheric pressure the cell used was 2.89 cm (along the optical path) by 1.5 cm by 0.8 cm. The cell had two entry tubes, and the solutions were prepared and handled by the syringe technique.¹² The broad window through which the electron beam entered was ground down to approximately 0.5 mm. A second cell was used for high-pressure runs up to 6 atm. in order to attain high concentrations of oxygen. This cell was 2.03 cm (along the optical path) by 0.8 cm by 0.8 cm. It was used for the high-intensity runs at 2.2 Mev. For these runs the back half of the cell was blanked off and only the first 4 mm of liquid behind the electron window were monitored because of the electron range at this energy. The electron beam window was ground down to less than 1 mm. The cell had a single entry tube connected to a degassing bulb. The high pressures of N_2O and O_2 were attained by sealing off the cell with connecting bulbs at liquid nitrogen temperature. The arrangement, which is shown in Figure 1, is useful in that it permits some 10–15 runs to be carried out on fresh solutions at high pressure with the preparation of a single batch of solution. The solution is simply transferred by tipping from the degassing bulb to the cell and then to the waste solution bulb.

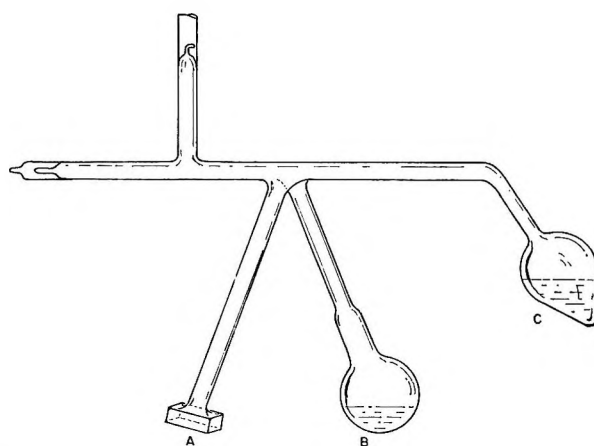


Figure 1. Reaction cell used for irradiation of systems under high-pressure conditions: A, quartz irradiation cell with optical windows perpendicular to the long axis; B, waste storage; C, sample storage vessel. The pear bulb facilitates degassing and freezing. The upper arm with break seal is for post-irradiation analysis of pressurizing gases.

(10) L. M. Dorfman, I. A. Taub, and R. E. Bühler, *J. Chem. Phys.*, **36**, 3051 (1962).

(11) I. A. Taub and L. M. Dorfman, *J. Am. Chem. Soc.*, **84**, 4053 (1962).

(12) C. B. Senvar and E. J. Hart, *Proc. Intern. Conf. Peaceful Uses At. Energy*, **29**, 19 (1958).

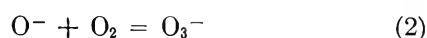
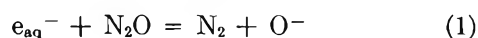
Dosimetry. The dose was required for the determination of the extinction coefficient of the ozonide ion. The *in situ* dosimetry method previously described¹³ was used. The dosimeter solution consisted of 10^{-2} M ferrous ion and 0.8 N sulfuric acid saturated with oxygen and containing no chloride ion. The yield of ferric ion at high dose rates^{14,15} is 15.6 molecules/100 ev. The optical density of ferric ion was measured at two wavelengths depending on the pulse intensity. At low dose it was determined at 304 m μ and the dose calculated from an extinction coefficient of $2200 M^{-1} \text{cm}^{-1}$. At high intensity it was measured at 366 m μ and the calculation of dose based on $\epsilon^{304}/\epsilon^{366} = 8.9$, the mean of two previously determined values.^{3,13} With unchanged accelerator settings the pulse power was found to be constant to within $\pm 1\%$, so that no pulse monitoring was necessary.

Materials. The water was triply distilled in a quartz still. The potassium hydroxide, barium hydroxide, and ferrous sulfate used were Baker Analytical reagent. The ferrous sulfate was recrystallized. Hydrogen peroxide from two sources was used: 30% Baker Analyzed reagent containing no stabilizer and 90% FMC hydrogen peroxide. For several of the runs, sodium was doubly distilled *in vacuo*. Ceric sulfate was from G. F. Smith Chemical Co. Oxygen and nitrous oxide were both passed through strongly alkaline solution.

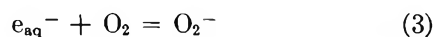
Analytical. Hydrogen peroxide was analyzed using the ceric ion method.¹⁶ The N₂O and O₂ composition was determined by pressure measurement and selective condensation at liquid nitrogen temperature. The gas concentration in the liquid was calculated assuming Henry's law at the specific pH.

Results and Discussion

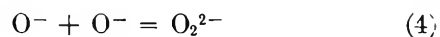
The decay kinetics of the ozonide ion were investigated in solutions containing both nitrous oxide and oxygen over a pH range of 12.5–14. As has been pointed out² if the N₂O concentration is sufficiently high a desirable simplification in the kinetics results from the conversion of the reducing species to O⁻ and hence to O₃⁻. The N₂O concentration in this work was usually on the order of 10^{-2} M with the N₂O/O₂ ratio ranging from 10 to 100. In most of the runs the ratio N₂O/O₂ was at least 20. Under these conditions the hydrated electron is converted predominantly but not exclusively to ozonide ion



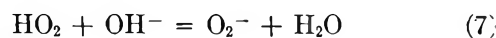
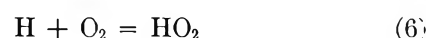
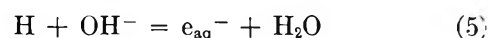
rather than to O₂⁻



Taking the values^{17,18} $k_1 = 8.7 \times 10^9 M^{-1} \text{sec}^{-1}$ and $k_3 = 1.9 \times 10^{10} M^{-1} \text{sec}^{-1}$ the ratio $k_1[\text{N}_2\text{O}]/k_3[\text{O}_2]$ becomes 9.2 for our experimental conditions with $[\text{N}_2\text{O}]/[\text{O}_2] = 20$. In addition the ratio $[\text{O}_2]/[\text{O}^-]$ was sufficiently high so that the reaction



did not take place to an appreciable extent. At the highest pH, any hydrogen atom yield is also converted largely to ozonide ion rather than to O₂⁻



Taking $k_5^{19} = 1.8 \times 10^7 M^{-1} \text{sec}^{-1}$ and $k_6^{20} = 2 \times 10^{10} M^{-1} \text{sec}^{-1}$ the ratio $k_5[\text{OH}^-]/k_6[\text{O}_2]$ becomes 2 for our experimental conditions. On the basis of $G_{\text{O}^-} = 3.4$ molecules/100 ev at²¹ pH 13.5, $G_{\text{H}+e_{\text{aq}}^-} = 3.85$ molecules/100 ev²¹ and $G_{\text{H}} = 0.6$ molecule/100 ev,²² the yields of O₃⁻ and O₂⁻ will be, respectively, 6.7 and 0.49 molecules/100 ev giving the ratio $G_{\text{O}_3^-}/G_{\text{O}_2^-} = 14$. At the higher N₂O/O₂ ratios the yield of O₂⁻ becomes vanishingly small. The system thus consists almost entirely, in the first few microseconds after the pulse, of the single transient species O₃⁻. There is in addition, a molecular yield of hydrogen peroxide amounting to²¹ $G_{\text{H}_2\text{O}_2} = 0.58$.

The correctness of this interpretation may be seen from the observation of the absorption band at 4300 Å in solutions containing N₂O and O₂ and from the doubling of the yield by the addition of N₂O which has already been noted.^{2,9} Figure 2 shows that the 4300-Å absorption band in N₂O–O₂ solutions is identical with that observed in the absence of N₂O. The ratio of the yield of O₃⁻ in N₂O–O₂ solution to that in O₂ solution was found from optical density measurement

(13) L. M. Dorfman and I. A. Taub, *J. Am. Chem. Soc.*, **85**, 2370 (1963).

(14) J. Rotblat and H. C. Sutton, *Proc. Roy. Soc. (London)*, **A255**, 49 (1960).

(15) J. K. Thomas and E. J. Hart, *Radiation Res.*, **17**, 408 (1962).

(16) H. H. Willard and P. Young, *J. Am. Chem. Soc.*, **55**, 3260 (1933).

(17) S. Gordon, E. J. Hart, M. S. Matheson, J. Rabani, and J. K. Thomas, *Discussions Faraday Soc.*, **36**, 193 (1963).

(18) S. Gordon, E. J. Hart, M. S. Matheson, J. Rabani, and J. K. Thomas, *J. Am. Chem. Soc.*, **85**, 1375 (1963).

(19) M. S. Matheson and J. Rabani, *J. Phys. Chem.*, **69**, 1324 (1965).

(20) S. Gordon, E. J. Hart, and J. K. Thomas, *ibid.*, **68**, 1262 (1964).

(21) F. S. Dainton and W. S. Watt, *Proc. Roy. Soc. (London)*, **A275**, 447 (1963).

(22) G. E. Adams, J. W. Boag, and B. D. Michael, *Trans. Faraday Soc.*, **61**, 492 (1965).

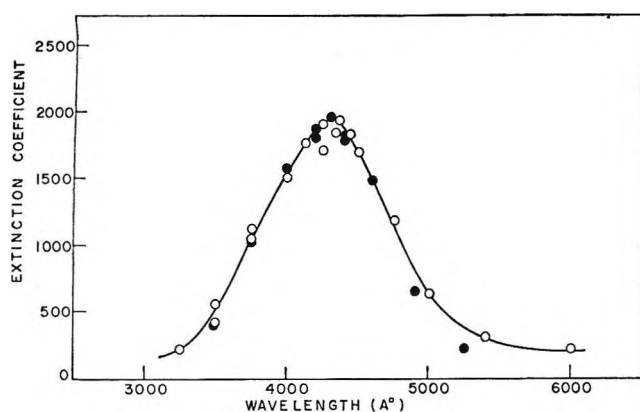


Figure 2. Transient absorption spectra in oxygenated alkaline water: ●, the spectrum of a solution containing N_2O ($N_2O/O_2 = 20:1$) is compared to ○, that of the ozonide obtained in solution free of N_2O from Czapski and Dorfman.

at 1 μsec after the pulse to be 1.9₆ at pH 13.5, in excellent agreement with the prediction of 1.9₇ from the foregoing.

Extinction Coefficient of O_3^- . The molar extinction coefficient of the ozonide ion at 4300 Å was obtained from optical density measurement in oxygen saturated solutions and from dosimetry measurement using the Fricke dosimeter. The ferric ion formation curve and the initial optical density of ozonide ion were both measured over a fourfold intensity range using pulses of 0.4, 0.8 and 1.6 μsec . For the 0.4- and 0.8- μsec pulse the ferric formation curve was obtained at 3040 Å and for the 1.6- μsec pulse at 3660 Å. The extinction coefficient of ozonide ion is obtained from

$$\epsilon_{O_3^-} = \frac{G_{Fe^{3+}} \times \epsilon_{Fe^{3+}} \times D_0^{O_3^-}}{G_{O^-} \times D_{\infty}^{Fe^{3+}}} \quad (8)$$

taking $G_{Fe^{3+}} = 15.6$ molecules/100 ev and $G_{O^-} = 3.3$ molecules/100 ev at²¹ pH 13.1. The values obtained, each an average of many runs, are shown in the following table. The mean is $\epsilon_{O_3^-}^{4300} = 1900 \pm 120 M^{-1} \text{cm}^{-1}$, which is within experimental agreement with the value of Adams, *et al.*² The indicated error limit does not include the uncertainty in the G values.

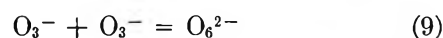
The Reaction $O_3^- + O_3^-$. The apparent differences in the literature^{2,3,9} concerning the kinetic order of the

Table I: Extinction Coefficient of O_3^-

Pulse, μsec	$\epsilon_{O_3^-}^{4300}$, $M^{-1} \text{cm}^{-1}$
1.6	1980
0.8	1850
0.4	1700
0.4	2030

ozonide decay may be understood largely as an effect of intensity and oxygen concentration, the observed order being a function of the initial concentration of ozonide ion. At concentrations of ozonide ion below about $5 \times 10^{-6} M$ the decay is first order as reported.³ Czapski⁹ has confirmed this and our observations, as will be seen, are in accord.

At concentrations in excess of $10^{-5} M$ of O_3^- there is, as Adams, *et al.*,² have pointed out, a substantial second-order contribution. The extent of this increases with intensity. However, even at concentrations of 2×10^{-5} to $5 \times 10^{-5} M$ the first-order decay still constitutes a large part of the observed decay. Figure 3 shows a second-order plot of two of our ozonide ion decay curves in this concentration region. There is a marked deviation from a second-order rate law. The same is true of the rate curves in Figure 10 of ref 2 from which Adams, *et al.*,² have derived the value $1.1 \times 10^8 M^{-1} \text{cm}^{-1}$ for the rate constant of the reaction



The interpretation of the initial portion of the rate curves in this concentration region in N_2O solution as consisting only of reaction 9 is clearly incorrect and the value of $1.1 \times 10^8 M^{-1} \text{sec}^{-1}$ seriously in error. As the initial concentration of ozonide ion is increased the

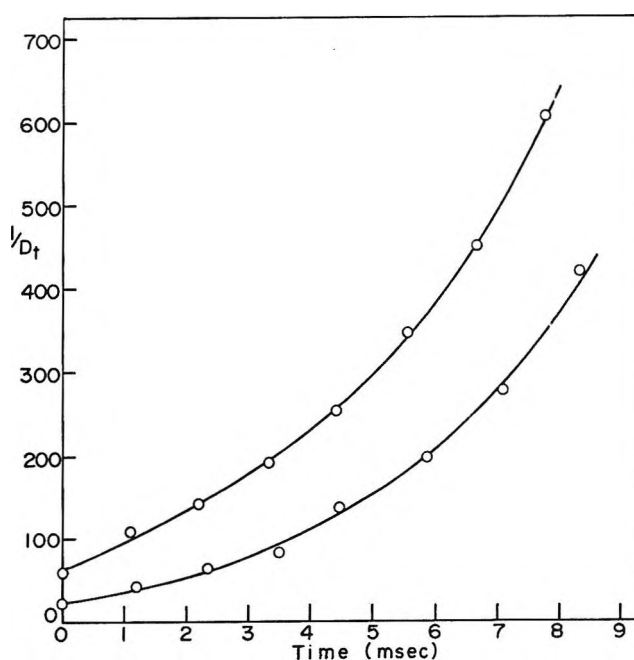


Figure 3. Test of second-order rate law for the decay of ozonide ion at 4300 Å in alkaline water containing oxygen and nitrous oxide. The optical density, D_t , has been corrected to 1-cm path length. Both curves represent medium intensity runs at an O_2 concentration of $3 \times 10^{-4} M$.

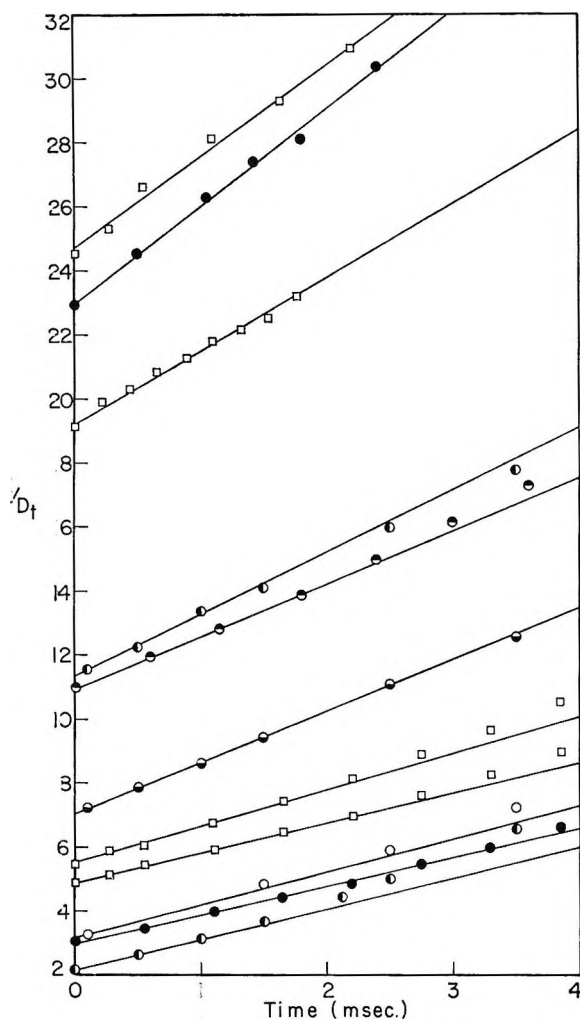


Figure 4 Test of the second-order rate law for the decay of the ozonide ion at 4300 Å showing effect of initial ozonide concentration. Concentrations of oxygen and nitrous oxide, respectively, were: □, 1.32×10^{-3} and $1.5 \times 10^{-2} M$; ○ and ●, 1.81×10^{-3} and $2.67 \times 10^{-2} M$; ●, 3.13×10^{-3} and $5.27 \times 10^{-2} M$, pH 13.5.

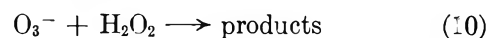
slope of the initial linear portion of the second-order plot continues to decrease. This may be seen from Figure 4 which includes initial concentrations of ozonide ion up to $2.4 \times 10^{-4} M$, the highest we were able to reach. To attain concentrations of $10^{-4} M$ it was necessary to have higher oxygen concentrations to avoid the loss of O_3^- by reaction 4. Consequently, the higher intensity runs were done in a pressurized cell at oxygen concentrations up to $3.1 \times 10^{-3} M$ and N_2O concentrations to $5.3 \times 10^{-2} M$.

The slopes of the straight lines in Figure 4 decrease with increasing optical density and appear to be leveling off in the region $1/D_0 = 2-5$ for these high-pressure runs. The slope here, taking $\epsilon_{O_3^-} = 1900$

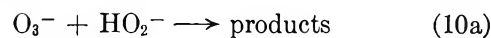
and assuming that only reaction 9 is occurring indicates a value of about $1.6 \times 10^6 M^{-1} \text{sec}^{-1}$ for the rate constant. However, the following consideration of the observed initial rate of reaction and of the first-order decay rate indicates that the contribution of the first-order decay, even at these high concentrations, is not negligible. For the foregoing estimate of $2k_9$ and an observed first-order decay constant $k_f = 100 \text{sec}^{-1}$ in these solutions, the initial rates of the second-order and first-order decay at $[O_3^-]_0 = 2.4 \times 10^{-4} M$ are $R_9 = 0.098 \text{ml}^{-1} \text{sec}^{-1}$ and $R_f = 0.024 \text{ml}^{-1} \text{sec}^{-1}$, respectively. The first-order decay must therefore constitute at least 20% of the observed initial rate and the value of $2k_9$ would therefore appear to be more nearly equal to $1 \times 10^6 M^{-1} \text{sec}^{-1}$.

The value of $2k_9$ is best determined from a computer analysis of the rate curves which has been done by curve fitting of the entire rate curve using an analog computer.

The three concurrent reactions under these conditions were taken into account. They are reaction 9 which predominates at the highest intensities, the first-order decay which constitutes about 20% or more of the observed initial rate depending upon the intensity, and the reaction of ozonide ion with hydrogen peroxide formed as a molecular yield



Since the pK for hydrogen peroxide^{23,24} is 11.8 reaction 10 should be written in the form



The contribution of this latter reaction to the observed decay is relatively small since the rate constant, which is discussed in the next section, is $k_{10a} = 8.9 \times 10^5 M^{-1} \text{sec}^{-1}$ at 25°.

A Heath electronic analog computer was used to integrate the two kinetic rate equations in ozonide ion and hydrogen peroxide

$$\frac{-d[O_3^-]}{dt} = 2k_9[O_3^-]^2 + k_{10a}[O_3^-][HO_2^-] + k_f[O_3^-] \quad (11a)$$

$$\frac{-d[HO_2^-]}{dt} = k_{10a}[O_3^-][HO_2^-] \quad (11b)$$

The time-dependent output voltage, directly proportional to the concentration of the ozonide ion, was plotted on an x-y recorder. An experimental data

(23) M. G. Evans and N. Uri, *Trans. Faraday Soc.*, **45**, 224 (1949).

(24) J. Jortner and G. Stein, *Bull. Res. Council Israel*, **A6**, 239 (1957).

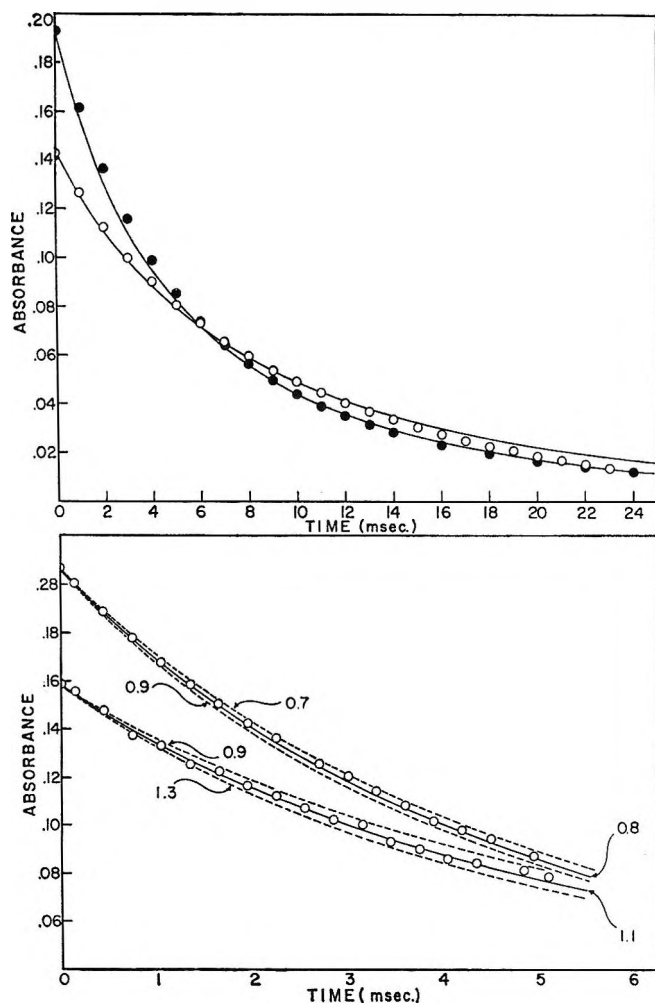


Figure 5. Examples of analog computer fit to the decay of the ozonide ion: upper figure, fit at two different intensities over nearly total decay range; lower figure, sensitivity of fit to changes in the second-order rate constant. Notations are $2k_9 \times 10^{-6} M^{-1} \text{sec}^{-1}$.

curve was superimposed on the synthesized curve for comparison. The parameter $k_{10a} = 8.9 \times 10^5$ was taken from our data. The rate constant, k_f , was determined for each particular data set from first-order decay curves at low pulse intensities. The values ranged from 40 to 590 sec^{-1} depending upon the oxygen concentration. The parameter $2k_9$ was then varied by changing its analogous potentiometer setting on the computer so as to give the best fit to the experimental data.

The sensitivity of the computer fit to a given rate curve was such that differences of 5% in $2k_9$ were readily detected. Although the first-order decay comprises a small proportion of the over-all decay rate at the highest intensities, the variation in the value of k_f contributes an additional uncertainty in the determination of $2k_9$.

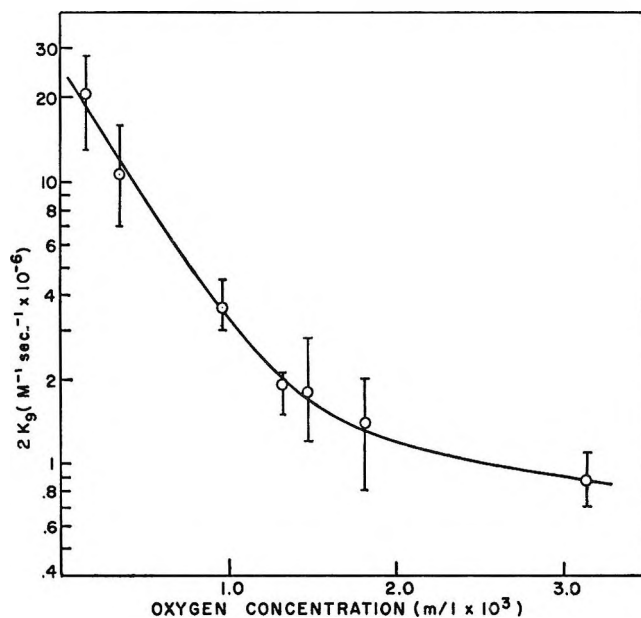


Figure 6. Oxygen dependence of second-order rate constant, $2k_9$. I, spread; O, mean of the constant as determined by analog computer methods.

Analog computer fits were done for data over a tenfold range in initial ozonide concentration and a twentyfold range in oxygen concentration. Representative plots for some of these fits are shown in Figure 5. The numerical results of the computer analyses showed an inverse functional dependence upon the oxygen concentration with a value of $2k_9 = (0.9 \pm 0.2) \times 10^6 M^{-1} \text{sec}^{-1}$ at $[\text{O}_2] = 3.1 \times 10^{-3} M$, the highest oxygen concentration attainable with our equipment. The indicated error limit in $2k_9$ includes the uncertainty in our determination of $\epsilon_{\text{O}_3^-} = 1900 M^{-1} \text{cm}^{-1}$. From the data in Figure 6 it appears that the value of $2k_9$ is leveling off at the highest oxygen concentrations.

The Reaction $\text{O}_3^- + \text{H}_2\text{O}_2$. The rate constant for reaction 10a was determined from ozonide decay curves at a sufficiently high concentration of added hydrogen peroxide so that the decay was pseudo first-order and the occurrence of reaction 9 negligible. The runs were carried out in solutions saturated with oxygen. The hydrated electron reacts with both hydrogen peroxide, producing additional O^- , and with oxygen. The quality of the first-order fit of some typical rate curves is shown in Figure 7. The values of the rate constant are shown in Table II. The average value is $k_{10a} = (8.9 \pm 1.1) \times 10^5 M^{-1} \text{sec}^{-1}$ at 25°, pH 13.1 and 13.5. The value is somewhat lower than that reported by Czapski.⁹ In determining the above values, the appropriate correction for the concurrent first-order decay without added peroxide, as determined experimen-

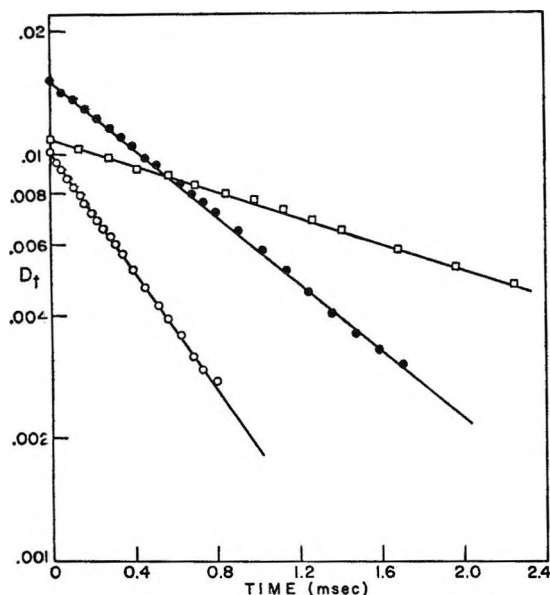


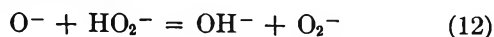
Figure 7. Test of the first-order rate law for the reaction of ozonide ion with hydrogen peroxide in oxygen saturated solution. Concentrations of hydrogen peroxide at pH 13.1: O, 1.78×10^{-3} ; ●, 1.01×10^{-3} ; □, 2.92×10^{-4} .

Table II: Rate Constant for $O_3^- + HO_2^-$ at 25°

Concn of H_2O_2 , $M \times 10^3$	pH	k_{10a} , $M^{-1} \text{sec}^{-1}$ $\times 10^{-5}$
0.29	13.1	9.79
		10.8
		10.0
		13.5
		8.72
0.36	13.5	8.67
		9.50
		7.78
0.54	13.5	8.30
		8.69
1.01	13.1	8.25
1.54	13.5	6.50
		6.90
		6.98
		7.10
		8.97
1.78	13.1	9.00
		9.20
		9.62
Mean:		8.9 ± 1.1

tally in these solutions, was made at all concentrations. It ranged from 6 to 30%.

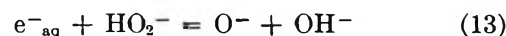
It was necessary to work at low peroxide concentrations because the reaction



begins to occur appreciably at $[H_2O_2] \geq 3 \times 10^{-3} M$. As the concentration of peroxide is increased, the optical density of O_3^- at 4300 Å decreases and there is an additional anomalous effect which we do not understand. The decay curves conform to a first-order rate law, but the observed rate is no longer proportional to the peroxide concentration. This is a subject for further investigation.

The Reaction $O^- + HO_2^-$. The decrease in the yield of ozonide ion at the higher concentrations of hydrogen peroxide results from the competition between reactions 12 and 2. It is therefore possible to determine k_{12} relative to k_2 from the difference in the relative yield of O_3^- as a function of hydrogen peroxide concentration.

In strongly basic solution containing only oxygen, the ozonide ion is formed only from reaction 2 with a yield corresponding to G_{O^-} . With added hydrogen peroxide the hydrated electron is converted to O^-



thus increasing the yield of O_3^- . The yield of ozonide ion is then a function of k_{12} , k_{13} , k_2 , k_3 and the concentrations of oxygen and hydrogen peroxide. The ratio of the yields of ozonide ion with and without added hydrogen peroxide is

$$\frac{G_{O_3^-}^{H_2O_2}}{G_{O_3^-}} = \frac{D_{O_3^-}^{H_2O_2}}{D_{O_3^-}} = \left\{ G_{O^-} + G_{e^-_{aq}} \left(\frac{k_{13}[H_2O_2]}{k_{13}[H_2O_2] + k_3[O_2]} \right) \right\} \times \frac{\left(\frac{k_2[O_2]}{k_2[O_2] + k_{12}[H_2O_2]} \right)}{G_{O^-}} \quad (14)$$

where $G_{O_3^-}^{H_2O_2}$ and $G_{O_3^-}$ represent the yields of ozonide ion with and without added peroxide and D is the initial optical density at 4300 Å. Data were obtained over an eightfold range in hydrogen peroxide concentration in oxygen saturated solution at pH 13.0. The rate constant for reaction 13 had been determined to be $k_{13} = 3.5 \times 10^9 M^{-1} \text{sec}^{-1}$ at pH 13.0 and 25°. The data for k_{12} , obtained relative to k_2 in this way, are shown in Table III.

The value for k_{12} depends principally upon $k_2 = 2.5 \times 10^9 M^{-1} \text{sec}^{-1}$ and to a lesser extent upon k_{13} and k_3 . The data give $k_{12} = (7 \pm 3) \times 10^8 M^{-1} \text{sec}^{-1}$ at 25°. The complexities of the system preclude any significant comparison with the value $4.5 \times 10^7 M^{-1} \text{sec}^{-1}$ in neutral solution.²⁵

Because of the complex form of eq 14 a substantial uncertainty which is unavoidable has been indicated in

(25) H. A. Schwarz, *J. Phys. Chem.*, **66**, 255 (1962).

Table III: Rate Constant for $O_3^- + HO_2^-$ at pH 13.0 and 25°

Concn of H_2O_2 , $M \times 10^2$	k_{12} from eq ⁿ 14, $M^{-1} \text{sec}^{-1} \times 10^{-8}$
0.61	7.2
0.61 ^a	8.2
1.9	7.1
4.7	6.3

^a The pulse intensity for this set of runs is 50% of that of all the others. Each indicated value for k_{12} is the average of several runs.

the value of k_{12} . The direct determination by observation of the O_2^- formation curve in deaerated hydrogen peroxide solution would be desirable but is very difficult because of the strong overlapping absorption of the hydrogen peroxide.

The Reaction $e_{aq}^- + HO_2^-$. The rate constant for the reaction of the hydrated electron with hydrogen peroxide²⁶ has been determined as $1.3 \times 10^{10} M^{-1} \text{sec}^{-1}$ in neutral solution. At pH greater than 11.8, the pK of hydrogen peroxide, the value may be different. We have therefore determined k_{13} at pH 13.0 by observation of the hydrated electron decay curve at 7200 Å over a fourfold range in hydrogen peroxide concentration chosen such that reaction 13 predominates. The data are shown in Table IV. The mean value is $k_{13} = (3.5 \pm 0.4) \times 10^9 M^{-1} \text{sec}^{-1}$.

The First-Order Decay. As we have already mentioned the decay of the ozonide ion at low concentration

Table IV: Rate Constant for $e_{aq}^- + HO_2^-$ at pH 13.0 and 25°

Concn of H_2O_2 , $M \times 10^4$	k_{13} , $M^{-1} \text{sec}^{-1} \times 10^{-9}$
4.10	4.09
	2.73
	3.82
	3.15
	3.32
6.02	3.43
	3.94
	4.04
	2.93
13.0	3.20
	3.22
	3.33
	4.11
	Mean: 3.48 ± 0.38

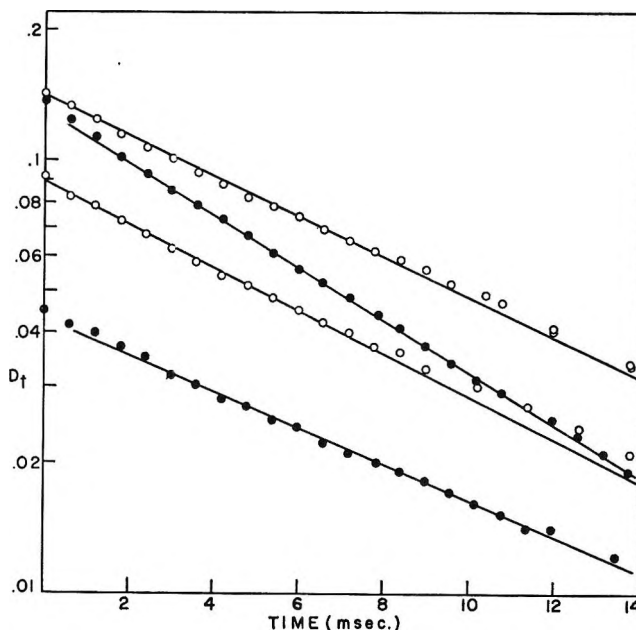
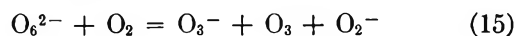


Figure 8. Test of first-order rate law for the decay of the ozonide ion at pH 13.5: O, $1.81 \times 10^{-3} M O_2$, $2.67 \times 10^{-2} M N_2O$; ●, $3.13 \times 10^{-3} M O_2$, $5.27 \times 10^{-2} M N_2O$. For the four curves shown pulse widths vary from 300 to 600 nsec at 350–400 ma.

obeys a first-order rate law as observed by Czapski.⁹ Examples are shown in Figure 8 for the two highest oxygen concentrations. We are in agreement with Czapski⁹ with respect to an observed inverse dependence of the first-order decay upon oxygen concentration. However, the half-time for the first-order decay appears to be leveling off at oxygen concentrations greater than $2 \times 10^{-3} M$. It is interesting to note from Figure 6 that the second-order decay constant also appears to be leveling off in this region.

Mechanism. The stabilizing effect of oxygen upon the ozonide ion suggests a mechanism in which an equilibrium and back reaction involving oxygen may occur. Czapski⁹ has suggested an equilibrium with the dimer O_6^{2-} which may decompose further. The reaction of O_6^{2-} directly with oxygen seems plausible



and may be part of the over-all mechanism. The possibility of ozone formation is suggested by our observation of an absorption band at 2500 Å with a lifetime of at least several seconds. The absorption maximum of ozone in basic aqueous solution⁶ is at 2600 Å. A crude estimate from our preliminary data in-

(26) L. M. Dorfman and M. S. Matheson, *Progr. Reaction Kinetics*, 3, 237 (1965).

icates a G value of approximately 1 for ozone formation based on this interpretation of the absorption band.

Our current investigations of the spectra and kinetics in the far-ultraviolet have shown at least one other band with a maximum at about 2250 Å. Preliminary observations indicate different lifetimes for these bands which must therefore be attributed to different species. The investigations in this spectral region are being continued.

Acknowledgment. We are grateful to Mr. E. G. Wendell whose operation and maintenance of the ac-

celerator and assistance with the electronic equipment is vital to these investigations. Miss R. Casey's contribution to the investigation was greatly appreciated. We are indebted to Professor R. F. Firestone for the use of the analog computer and to Mr. W. Bishop for his helpful advice. Mr. R. Sadler of Argonne National Laboratory kindly provided us with the partially reflecting mirrors. The assistance of Battelle Memorial Institute, Pacific Northwest Laboratories, in supporting W. D. F. as a visiting scientist from Battelle to Ohio State University is gratefully acknowledged.

The Kinetics of Oxalate Ion Pyrolysis in a Potassium Bromide Matrix^{1,2a}

by K. O. Hartman^{2b} and I. C. Hisatsune

Department of Chemistry, Whitmore Laboratory, The Pennsylvania State University, University Park, Pennsylvania 16802 (Received August 15, 1966)

The thermal decomposition of the oxalate ion dispersed in a KBr matrix was observed to follow first-order kinetics with a rate constant of $0.7 \times 10^{13} \exp[(-60,000 \pm 6000)/RT]$ sec⁻¹. The principal reaction product was the carbonate ion, but traces of formate and monomeric bicarbonate ions were detected as by-products. The yields of the by-products were significant when the initial solute concentrations were low, but at higher concentrations the carbonate ion yield was $90 \pm 10\%$. A reaction mechanism in which the oxalate dissociates into two CO₂⁻ radicals is proposed.

Introduction

The thermal decompositions of relatively complex oxalate salts have been studied widely, but those of sodium and potassium salts have received much less attention. For example, Glasner and Steinberg³ have carried out extensive studies of the decompositions of rare earth oxalates, and Yankwich and Zavitsanos⁴ have reported similar studies on magnesium, manganese, and zinc oxalates. Apparently, the only investigation of the kinetics of the pyrolysis of alkali metal oxalates is that reported by Akalan.⁵

In the present study the infrared disk technique⁶ was used to follow the decomposition kinetics of the oxalate ion. Our results show that the pyrolysis kinetics in the KBr matrix are different from those in the alkali earth

or rare earth oxalate environment reported by earlier investigators. On the basis of kinetic parameters determined in this study, a mechanism for the oxalate ion decomposition is proposed.

(1) This work was supported by the National Science Foundation, Grant NSF-G17346, and by the Directorate of Chemical Sciences, Air Force Office of Scientific Research, Grant AF-AFOSR-907-65.

(2) (a) Abstracted in part from the Ph.D. Thesis of K. O. Hartman; (b) Mellon Institute, 4400 Fifth Avenue, Pittsburgh, Pa. 15123.

(3) A. Glasner and M. Steinberg, *J. Inorg. Nucl. Chem.*, **22**, 39 (1961); **26**, 525 (1964).

(4) P. E. Yankwich and P. D. Zavitsanos, *J. Phys. Chem.*, **69**, 442 (1965).

(5) S. Akalan, *Rev. Fac. Sci. Univ. Istanbul*, **21**, 184 (1956); *Chem. Abstr.*, **51**, 9273 (1957).

(6) K. O. Hartman and I. C. Hisatsune, *J. Phys. Chem.*, **69**, 583 (1965); **70**, 1281 (1966).

Experimental Section

Kinds and sources of matrix salts used in the present study have been described before.⁶ Sodium oxalate, a Baker and Adamson product, was recrystallized from water, but potassium oxalate monohydrate from Matheson Coleman and Bell was used directly. The procedures for preparing the pressed disks, for obtaining the kinetic data, and for determining the reaction stoichiometry also have been described before.⁶ The apparatus for disk fabrication, heating ovens, and infrared instruments were the same as those used in earlier studies. Most of the spectra were obtained on the Perkin-Elmer Model 21 spectrometer.

Results

Disks were prepared by both the freeze-dry and grinding methods. In the freeze-dried samples, the oxalate infrared bands were much sharper than those in the ground samples. As shown in Table I, these two preparative methods resulted in slight frequency variations. The initial spectra of sodium oxalate dispersed in different matrix salts by grinding were essentially the same. Some frequencies varied by a few wavenumbers, but this deviation was within experimental error. When the disks were heated a short time at 500° frequency shifts were observed in KBr, KCl, and KI, but not in NaBr, CsBr, and CsI (Table II). In those matrices where the shift was observed both sodium and potassium oxalates gave the same set of frequencies after heating. Also, the doublets observed at approximately 1330 and 775 cm^{-1} in the ground samples coalesced into singlets upon heating.

Further heating led to the decomposition of the oxalate ion. During the decomposition, a number of bands in addition to those of the major product, carbonate, were generated. From the correlations of the optical densities of these additional bands and from their behavior when the disks were ground or freeze-dried, the extra bands were found to fall into two sets as shown in Table III. Since these frequencies agreed well with those of the monomeric bicarbonate ion⁷ and distorted formate ion,⁶ the identification of the two by-products of the reaction was unequivocal. These by-products were demonstrated, in the following way, to originate from the reaction of the oxalate ion with traces of water present in the disk. A potassium oxalate sample was freeze-dried from a D_2O solution and heated at 510° for 1 min. The by-products in this case were identified as bicarbonate-*d* and formate-*d* from their characteristic infrared spectra.

The quantity of formate and bicarbonate ions produced in different disks was approximately constant and appeared to be independent of the initial oxalate con-

Table I: Sodium and Potassium Oxalate Frequencies (cm^{-1}) in Unheated KBr Matrix^a

Mode ^b	Na ₂ C ₂ O ₄		K ₂ C ₂ O ₄ ·H ₂ O
	Freeze-dried	Ground	
H ₂ O	3410 m	3420 m	3400 s
	2900 w	2935 w	2900 w
	1882 w		
$\omega_\alpha(\text{CO}_2)$	1639 vs	1647 s	1645 s
	1416 m	1421 w	1410 w
	1400 sh		
$\omega_\sigma(\text{CO}_2)$	1335 sh	1339 sh	1325 sh
	1329 s	1321 s	1310 s
$\omega_\omega(\text{CO}_2)$	779 s	781 s	780 s
		774 s	
$\nu_\beta(\text{CO}_2)$		(515 w) ^c	

^a Spectra recorded at 25°, sh = shoulder. ^b α = antisymmetric stretch, β = bending, σ = symmetric stretch, ω = out-of-plane wag; assignment from G. M. Begun and W. H. Fletcher, *Spectrochim. Acta*, **19**, 1343 (1963). ^c Spectrum on Perkin-Elmer Model 521.

centration. This fact suggested that the secondary reaction was limited by the amount of water present in the disk. This water was very difficult to eliminate. Even when a freeze-dried powder was heated at 100° under vacuum for 24 hr, cooled to room temperature under a dry nitrogen atmosphere, and transferred to the disk die with a maximum of 30-sec exposure to the laboratory air, this sample still produced a detectable quantity of these by-products.

A sequence of spectra obtained from a typical kinetic run is illustrated in Figure 1. The initial spectrum is the upper curve, and the second spectrum was obtained after a short heating. Further heating gave the lower spectrum in which the absorption bands of the primary product, carbonate, and the more prominent bands of the minor products, formate and bicarbonate, are present. When the disks were heated for longer periods of time, the oxalate bands disappeared completely followed by the decay of bicarbonate and formate bands. At the commonly employed reaction temperatures (Table V), it was surprising to observe that the carbonate ion absorption bands also decayed slowly. The carbonate ion half-life was about 700 hr at 508°.

In addition to the absorption bands of the principal and minor reaction products, we also observed weak

(7) D. L. Bernitt, K. O. Hartman, and I. C. Hisatsune, *J. Chem. Phys.*, **42**, 3553 (1965).

Table II: Frequencies of Heated Sodium Oxalate in Alkali Halide Matrices (cm^{-1})^a

Mode ^b	KCl	KBr	KI	NaBr	CsBr	Cs ⁻
$\omega_2(\text{CO}_2)$	1580 s	1600 s	1595 s	1640 s 1418 w	1640 s 1420 w	1645 s 1420 w
$\omega_7(\text{CO}_2)$	1308	1316 s	1315 s	1336 s 1320 s	1336 s 1320 s	1340 s 1320 s
$\omega_3(\text{CO}_2)$	755 s	758 s	760 s	780 s 773 s	780 s 772 s	780 s 773 s

^a Spectra recorded at 25°. ^b See footnote b of Table I.

Table III: Frequencies (cm^{-1}) of By-Products Produced in Oxalate Decomposition in KBr Matrix^a

Species 1	Monomeric bicarbonate ^b	Species 2	Distorted formate ^c
3380	3390	2660	2666
1700	1697	1630	1633
1339	1338	1445	1445
1210	1211	1350	1352
960	960	753	752
335	835		
712	712		

^a Spectra recorded at -190° . ^b Reference 7. ^c Reference 6.

bands at 2170 and 2331 cm^{-1} which are due, respectively, to the cyanate ion and to carbon dioxide. Trace amounts of cyanate ion were observed in the pyrolyses of nearly all common solid reagents as we reported earlier.⁷ The origin of the carbon dioxide in the matrix is the disproportionation reaction of the carbon monoxide evolved by the oxalate decomposition.⁶ Our disks, after completion of the reaction, were generally dark gray in color.

The stoichiometry of the reaction was determined by comparing the final absorbance of the carbonate bands with calibration curves constructed from disks containing known amounts of carbonate. From more than 20 runs in which the initial oxalate concentration was varied from 0.4 to 2.1 mg/g (milligrams of oxalate per gram of matrix salt), the carbonate yield was 90% \pm 10. Hence, the primary reaction is



The less than 100% yield of carbonate may in part be accounted for by the slow decomposition of the potassium carbonate as described earlier. The major cause, however, was the formation of the by-products, formate and bicarbonate. It was observed that the yield of carbonate markedly declined when the initial oxalate concentration was decreased below about 0.8 mg/g.

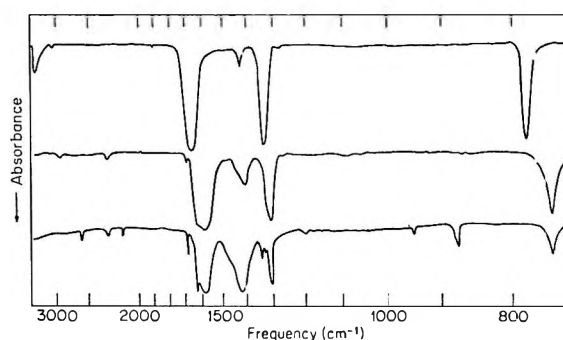


Figure 1. Infrared spectrum of sodium oxalate in KBr matrix: concentration, 1.5 mg/g; upper spectrum, freeze-dry sample before heating; middle spectrum, after 5-min heating at 508°; lower spectrum, after 100-min heating at 508°. All spectra recorded at 25°.

The yield was only 50% when the initial oxalate concentration was 0.403 mg/g and 25% when it was 0.313 mg/g. This reduction in yield was due to the consumption of a higher percentage of the oxalate in the reaction with water to produce the by-products.

The reaction order was determined graphically from plots of log rate *vs.* log concentration for the reactant and product absorption bands. The order was found to be 1.0 ± 0.2 in oxalate ion.

The occurrence of the side reaction with water caused some difficulty in the determination of consistent rate constants for the oxalate decomposition. In Table IV the variation of the first-order rate constants with initial oxalate concentrations is shown. At lower concentrations where most of the oxalate was consumed by the reaction with water, the rate constant for the loss of oxalate is larger. At such concentrations, the rate of formate and bicarbonate formation was about equal to the rate of oxalate decomposition. Since the amounts of formate and bicarbonate are relatively smaller in higher concentration samples, the rate constants from such disks should represent the correct constants for the primary reaction. This expectation is

in fact borne out by the values shown in Table IV. The rate constants are more nearly invariant at higher concentrations and are equal to the constants determined from the carbonate bands.

Table IV: Effect of Oxalate Concentration on Rate Constants (KBr Matrix)^a

Initial oxalate concn, mg/g	Rate constants, $10^4 k$, sec^{-1}		
	1600 cm^{-1}	1316 cm^{-1}	758 cm^{-1}
1.50	1.8	1.7	1.5
1.50	2.0	1.8	1.6
1.51	1.2	1.3	1.6
1.05	1.8	2.0	1.8
0.866	2.2	2.3	1.7
0.866	3.0	2.5	2.5
0.403	3.2	3.8	2.3
0.403	3.0	3.0	2.5
0.313	6.3	6.3	6.3
0.313	6.2	6.2	6.2

^a All samples were prepared by the freeze-dry method. Reaction temperature = 508°.

To maintain a check on the internal consistency of the results, rate constants were determined throughout the work from both the oxalate 758- cm^{-1} band and the carbonate bands at 1430 and 880 cm^{-1} . The rate constants for the 1430- cm^{-1} carbonate band were higher than those for the other bands, but the discrepancy was within experimental error. Average rate constants determined from these bands are summarized in Table V. The data obtained in the present study are less precise than those obtained in earlier investigations⁸ because the reaction temperature was not closely controlled. Also, in some runs the 880- cm^{-1} carbonate band split into a doublet with peaks at 883 and 878 cm^{-1} , and this introduced some error in the rate constants. The Arrhenius activation energies and frequency factors determined from different bands are also listed in Table V.

For matrices other than KBr, rate constants were determined from single runs at 508°. The rate constant obtained using the CsI matrix was the same as that from KBr, while the constants from CsBr and NaBr were about 40% less than this value. Since these runs extended only to 60% reaction this deviation may well be within experimental error.

Discussion

The frequencies of the sodium oxalate absorption bands observed in the KBr matrix before heating are in reasonable agreement with those reported by Schmelz,

Table V: Average Rate Constants for Oxalate Ion Decomposition in KBr Matrix

Temp, °C	$10^5 k$, sec^{-1}		
	1430 cm^{-1} CO_3^{2-}	880 cm^{-1} CO_3^{2-}	758 cm^{-1} $\text{C}_2\text{O}_4^{2-}$
490 ± 5	6.8	5.7	4.5
508 ± 8	18.5	13.0	16.0
518 ± 8	29.0	13.5	19.0
566 ± 8	220.0	150.0	175.0
582 ± 7	405.0	350.0	290.0
Activation energy, kcal/mole	60 ± 6	63 ± 6	60 ± 6
Frequency factor, sec^{-1}	0.91×10^{13}	4.3×10^{13}	0.68×10^{13}

*et al.*⁸ The shifts in these frequencies produced by short heating of the disk indicate that the oxalate ion has diffused into the matrix salt and that its environment is now the KBr lattice. Additional evidences which support this interpretation are: the same set of final frequencies was obtained by starting with potassium or sodium oxalate, the frequency shifts were dependent on the matrix salt, and no frequency shifts were observed when undiluted oxalate salts were heated. We may also conclude from the fact that shifts were not observed in NaBr, CsBr, and CsI matrices that the extent of diffusion of the solute ion into these matrices is negligible.

The kinetic data obtained in this study thus can be associated with the decomposition of oxalate ions isolated in the KBr matrix. The observed first-order rate law, the experimental activation energy, and the calculated frequency factor all suggest that this decomposition can be regarded as a unimolecular reaction. A simple mechanism which accounts for the experimental data is one in which the rate-determining step is the unimolecular dissociation of the oxalate ion into two carbon dioxide anion radicals. This step is followed by a rapid bimolecular reaction of the two free radicals to form the products carbonate ion and carbon monoxide. A possible transition complex for the second step may be the carbonyl carbonate ion, OCOCO_2^{2-} which is iso-electronic with a known isomer of N_2O_4 .⁹ The formation of bicarbonate and formate as by-products of the decomposition reaction is not inconsistent with this free-radical mechanism since the CO_2^- radical has been observed to react readily with water to form just these

(8) M. J. Schmelz, T. Miyazawa, S. Mizushima, T. J. Lane, and J. V. Quagliano, *Spectrochim. Acta*, **9**, 51 (1957).

(9) I. C. Hisatsune, J. P. Devlin, and Y. Wada, *J. Chem. Phys.*, **33**, 714 (1960).

products.¹⁰ However, our experimental data do not allow us to determine whether these by-products were formed by a concerted attack on the oxalate ion by water or through the direct reaction of the CO_2^- radicals with water. We also examined several disks for the presence of the CO_2^- radical but found no esr signal that can be attributed to this species. This negative result however, does not contradict our mechanism because previously we found the CO_2^- radical to be unstable at temperatures above about 100° in alkali halide matrices.¹⁰ The only esr signal observed in our pressed disks was a sharp line with $g = 2.0028$. The same signal was observed previously in our formate kinetic studies.⁶ This free radical appears to be an ion containing only oxygen atom or atoms since no hyperfine structures were observed with H, D, and ^{13}C isotopic samples.

The observed Arrhenius activation energy of 60 ± 6 kcal/mole is considerably higher than 32 and 43 kcal/mole reported by Akalan,⁵ respectively, for the sodium

and potassium salts. However, our present value is in agreement within experimental error with the 68 ± 5 kcal/mole determined for calcium oxalate pyrolysis by both the infrared and thermogravimetric methods.¹¹ Also, the calculated rate constant of $3.2 \times 10^{-4} \text{ min}^{-1}$ at 450° is in reasonable agreement with $1.7 \times 10^{-4} \text{ min}^{-1}$ found recently by Wing and Harris¹² for the decomposition of undiluted potassium oxalate. In addition, the reaction mechanism proposed by the latter authors involved a step similar to our rate-determining dissociation of an oxalate ion into two CO_2^- free radicals.

Acknowledgments. We are pleased to acknowledge the financial support from the National Science Foundation and the Air Force Office of Scientific Research.

(10) K. O. Hartman and I. C. Hitsatsune, *J. Chem. Phys.*, **44**, 1913 (1966).

(11) F. E. Freeberg, K. O. Hartman, I. C. Hisatsune, and J. W. Schempf, *J. Phys. Chem.*, **71**, 397 (1967).

(12) R. M. Wing and G. M. Harris, *ibid.*, **69**, 4328 (1965).

The Kinetics of Calcium Oxalate Pyrolysis^{1,2}

by F. E. Freeberg, K. O. Hartman, I. C. Hisatsune,³ and J. M. Schempf

Department of Chemistry, Whitmore Laboratory, The Pennsylvania State University,
University Park, Pennsylvania 16802 (Received August 15, 1966)

The pyrolysis of calcium oxalate was studied by employing differential thermal analysis, thermogravimetric analysis, and the infrared disk technique. Both reagent grade oxalate and some oxalate samples prepared in our laboratory were investigated. The over-all reaction was found to be $\text{CaC}_2\text{O}_4 = \text{CaCO}_3 + \text{CO}$. A first-order rate constant of $9.3 \times 10^{14} \exp[(-68,000 \pm 5000)/RT] \text{ sec}^{-1}$ was found. Arrhenius activation energies by the thermogravimetric method and from the infrared technique agreed within experimental error. Anomalous spectral, thermal, and kinetic behavior was observed during the decomposition of some of the prepared oxalate salts, and it was attributed to the internal rotation of the carboxyl group about the C-C bond during the pyrolysis.

Introduction

Calcium oxalate monohydrate was among the first compounds studied by the thermogravimetric analysis. Because of the regular and apparently invariant thermogram shown by this compound, Duval⁴ suggested its use as a calibration standard. However, a recent work by Simons and Newkirk⁵ showed that experimental variables such as the reaction atmosphere, the shape of the sample container, etc., must be carefully controlled in order to obtain reproducible thermograms. It was also shown recently that the method of preparation of the calcium oxalate monohydrate greatly affects its decomposition parameters.⁶ A quantitative kinetic study of the decomposition of calcium oxalate has been reported by Freeman and Carroll,⁷ who employed only the thermogravimetric technique. In the present investigation, the thermogravimetric analysis (TGA), the differential thermal analysis (DTA), and the infrared disk technique were used to examine in detail the chemical kinetics of the pyrolysis of calcium oxalate.

Experimental Section

Reagent grade calcium oxalate monohydrate obtained from Matheson Coleman and Bell was used as received. Additional samples were prepared by reacting reagent grade calcium bromide with oxalic acid and drying the precipitate at 110° for 2 hr. A few samples were prepared with other salts— $\text{Ca}(\text{NO}_3)_2$, CaCl_2 , and CaI_2 . Harshaw optical grade KBr was used for the infrared disks.

Details of the infrared disk preparation and its use in kinetic studies have been described in previous papers.^{8,9} Band frequencies and optical densities were measured on both the Perkin-Elmer Model 21 (NaCl prism) and Model 521 spectrometers.

A Chevenard automatic recording thermobalance was used to obtain the TGA data. The balance arm in this instrument was extended to increase its sensitivity, and the recorder was modified to indicate both the weight loss and the furnace temperature. The DTA apparatus was constructed in our laboratories.¹⁰ In general, undiluted calcium oxalate was used in DTA and TGA runs. Samples weighing about 160 and 20 mg were used, respectively, for TGA and DTA. Kinetic analyses were made by both the dynamic (temperature programmed) and the isothermal methods in the TGA runs.

(1) This work was supported in part by the Directorate of Chemical Sciences, Air Force Office of Scientific Research, Grant AF-AFOSR-907-65 and by the National Science Foundation Grant NSF-G17346.

(2) Abstracted in part from the Ph.D. Theses of F. E. Freeberg and K. O. Hartman.

(3) To whom correspondence should be addressed.

(4) C. Duval, *Anal. Chem.*, **23**, 1271 (1951).

(5) E. L. Simons and A. E. Newkirk, *Talanta*, **11**, 549 (1964).

(6) J. M. Schempf, F. E. Freeberg, and F. M. Angeloni, *Anal. Chem.*, **37**, 1704 (1965).

(7) E. A. Freeman and B. Carroll, *J. Phys. Chem.*, **62**, 394 (1958).

(8) K. O. Hartman and I. C. Hisatsune, *ibid.*, **69**, 583 (1965).

(9) K. O. Hartman and I. C. Hisatsune, *ibid.*, **70**, 1281 (1966).

(10) F. M. Angeloni, Ph.D. Thesis, The Pennsylvania State University, 1965.

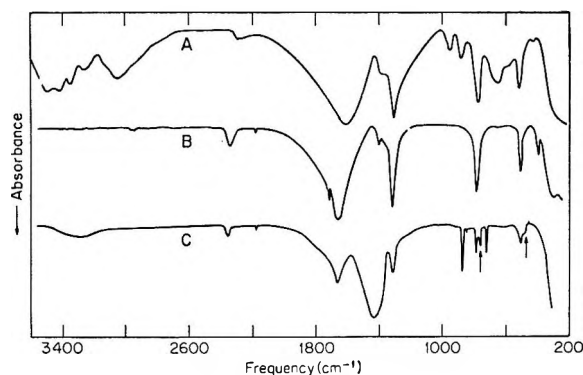


Figure 1. Infrared spectrum of calcium oxalate in KBr matrix. Ground sample with a concentration of 2.1 mg/g. A, unheated; B, 2 min at 490°; C, 543 min at 490°.

Results

The initial infrared spectrum of both reagent grade calcium oxalate and the material prepared from calcium bromide was similar to trace A shown in Figure 1. Short heating at the pyrolysis temperatures (480–560°) dehydrated the oxalate salt and caused a large change in the spectrum (trace B). On further heating, the intensities of the oxalate bands decreased and carbonate bands were generated as shown by trace C. In the case of the reagent grade material, the oxalate bands continued to decrease and the carbonate bands increased until the reaction was complete. However, with the salt prepared from calcium bromide new bands, indicated by arrows in spectrum C, appeared during the pyrolysis. These bands disappeared with further heating. They were also observed in the infrared spectrum of prepared salt which had been partially decomposed before being pressed in a KBr disk. With the exception of a small amount of CO₂ and cyanate the final spectrum showed only calcium carbonate.

A difference between the reagent grade salt and the salt prepared from calcium bromide was also observed in the DTA runs as shown in Figure 2. Here, endothermic peaks one, two, and three are due to the decomposition of the oxalate to carbonate. The appearance of these peaks was accompanied by the evolution of carbon monoxide when the pyrolysis was carried out in an inert atmosphere. Peak one, which corresponded to less than 10% reaction, was found from earlier studies⁶ to be due to sodium ion impurity in the sample. In addition to peak two which appeared in all oxalate samples, materials prepared from calcium bromide, iodide, and nitrate showed peak three. Furthermore, only oxalate samples showing peak three gave the anomalous infrared bands pointed out in trace C of Figure 1. Under identical experimental conditions, the tempera-

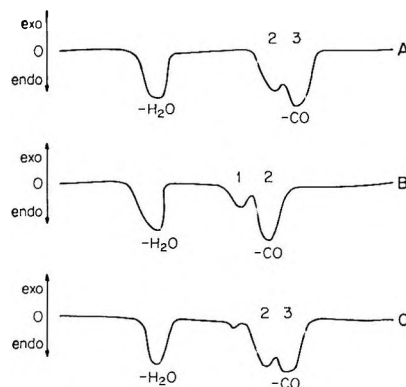
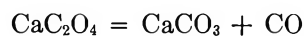


Figure 2. DTA traces of various calcium oxalate samples. Sample size, 20 mg; heating rate, 20°/min; atmosphere, He, 60 cc/min; A, prepared from Ca(NO₃)₂; B, reagent grade; C, prepared from CaBr₂.

tures at which the DTA peaks appeared were reproducible. At a programmed heating rate of 20°/min, these temperatures were 462° (peak one), 510° (peak two), and 525° (peak three).

In contrast to the DTA and spectroscopic data, the thermograms of all oxalate salts showed no qualitative differences. It was observed, however, that the rate of decomposition and the temperature at which it was initiated varied according to the method of preparation of the salt.

In Table I the frequencies of the initial and heated calcium oxalate are listed. The monohydrate frequencies are in agreement with those reported by Schmelz, *et al.*¹¹ The assignments given in Table I for the dehydrated ion are based on a planar symmetry for the oxalate ion. The frequencies of the product calcium carbonate were the same as those of calcite. The yield of the carbonate, according to the calibration curves constructed from disks containing known amounts of calcium carbonate, was 92 ± 6%. Isothermal TGA on undiluted oxalate salt gave 99 ± 1% yield of carbonate. Thus the reaction stoichiometry is



The order of the reaction was determined in a number of ways. For the undiluted oxalate it was deduced from the DTA data by the method of Kissinger.¹² In both air and nitrogen atmospheres, the rate was first order in oxalate. Isothermal TGA also showed the decomposition to be first order since the log of the oxalate weight was a linear function of time. The reaction order from the infrared data was obtained by

(11) M. J. Schmelz, T. Miyazawa, S. Mizushima, T. J. Lane, and J. V. Quagliano, *Spectrochim. Acta*, **9**, 51 (1957).

(12) H. E. Kissinger, *Anal. Chem.*, **29**, 1703 (1957).

Table I: Calcium Oxalate Frequencies in KBr Matrix (cm^{-1})

Mode ^a	CaC ₂ O ₄ ·H ₂ O	CaC ₂ O ₄ ^b
$\nu(\text{H}_2\text{O})$	348 $\bar{5}$	
	3420 ^s	
	3340 sh	
	3250 sh	
	3040 s	2950 w
$\nu_\alpha(\text{CO}_2)$	228 $\bar{5}$ vw	
		1705 w
	161 $\bar{5}$ vs	1638 s
$\nu_\sigma(\text{CO}_2)$	1380 w	1362 sh
	1312 vs	1313 s
$\nu_\omega(\text{CO}_2)$	94 $\bar{5}$ w	
	880 w	
	77 $\bar{8}$ s	782 s
	65 $\bar{5}$ s	
$\nu_\beta(\text{CO}_2)$	580 sh	
	510 s	518 m
$\nu_\rho(\text{CO}_2)$	41 $\bar{5}$ vw	388 m
$\nu(\text{Ca-O})$	290 m	304 m

^a α , antisymmetric stretch; σ , symmetric stretch; ω , out-of-plane wag; β , deformation; ρ , in-plane rock. ^b Heated.

plotting log rate against log optical density of the oxalate band and log optical density against time. The order was 1.0 ± 0.1 , and linear first-order plots were obtained over about 80% of the reaction.

In general rate constants were determined spectroscopically for the oxalate in KBr disks and thermogravimetrically for undiluted calcium oxalate. Infrared measurements on the reagent grade salt showed an induction period of 5–10% of the reaction. This induction period was difficult to detect by means of TGA isothermal runs because of shorter reaction times. Lack of thermal equilibrium at the initial stage of the pyrolysis also was a factor which obscured the induction period. Neither the infrared nor the TGA data showed an induction period in the pyrolysis of the oxalate samples prepared from calcium bromide.

Reaction rate constants were determined from several infrared bands of both oxalate and carbonate in order to test for internal consistency of our infrared data. The reagent grade calcium oxalate gave good experimental data, and first-order rate constants obtained from all infrared bands agreed within experimental error. In

contrast to this, the rate constants determined from the oxalates prepared from CaBr_2 were anomalous. At lower reaction temperatures, the 782-, 518-, and 388- cm^{-1} oxalate bands decreased faster than did the 1638- and 1313- cm^{-1} bands. Although all bands still decayed by the first-order rate law, only the rate constants from the latter bands agreed with those determined from the carbonate bands. Two of the three oxalate bands which decayed faster were quite close to the transient bands at 755 and 490 cm^{-1} .

The TGA data also indicated a difference between the reagent grade salt and the oxalate prepared from calcium bromide. The former was observed to decompose twice as fast as the latter salt. In order to test the agreement between the TGA and infrared methods, an isothermal TGA run was made on a KBr disk with a 10 mg/g oxalate concentration. A rate constant of $1.7 \times 10^{-4} \pm 5 \times 10^{-5} \text{ sec}^{-1}$ was found, and this agreed well with the spectroscopic value of $1.3 \times 10^{-4} \pm 2.5 \times 10^{-5} \text{ sec}^{-1}$. However, TGA measurements, both isothermal and dynamic, on undiluted oxalate gave rate constants a factor of about 80 higher than those obtained from the infrared data.

Rate constants and reaction activation energies determined from the infrared, TGA, and DTA data are summarized in Tables II and III. Calculation of the kinetic parameters from the dynamic TGA data was based on the method suggested by Newkirk¹³ and modified by Freeberg.²

Discussion

Since the pyrolyses of the prepared and reagent grade oxalates showed first-order kinetics with activation energies of about 67 kcal/mole, both salts must have

Table II: Rate Constants for Calcium Oxalate Pyrolysis in KBr Matrix ($10^5 k$, sec^{-1})

Temp, °C	1638 and 1315 cm^{-1} , $\text{C}_2\text{O}_4^{2-}$	1435 and 872 cm^{-1} , CO_3^{2-}	782 cm^{-1} , $\text{C}_2\text{O}_4^{2-}$
Prepared material from CaBr_2			
490 \pm 1	3.2	3.7	4.4
490 \pm 1	2.8	3.4	4.3
512 \pm 1	6.7	7.7	8.5
512 \pm 1	11.0	11.0	12.5
556 \pm 1	90.0	78.0	92.0
556 \pm 1	...	98.0	...
Reagent grade			
481 \pm 2	2.2	2.0	

(13) A. E. Newkirk, *Anal. Chem.*, **32**, 1558 (1960).

Table III: Activation Energy of Calcium Oxalate Decomposition

Frequencies, cm ⁻¹	E _a , kcal/ mole	A, sec ⁻¹
KBr matrix—prepared material ^a		
163℄ 131℄ } C ₂ O ₄ ²⁻	68 ± 5	9.3 × 10 ¹⁴
143℄ 87℄ } CO ₃ ²⁻	66 ± 5	3 × 10 ¹⁴
DTA and TGA undiluted oxalate		
Prepared material ^a		
Temp programmed	66 ± 6	450 × 10 ¹⁴
Reagent grade		
Isothermal	66 ± 6	1 × 10 ¹⁷
Temp programmed	67 ± 6	2 × 10 ¹⁷
DTA prepared material ^a	62 ± 6	

^a Preparation from CaBr₂ described in Experimental Section.

essentially the same over-all decomposition mechanism. The observed kinetic data can be interpreted by the same reaction mechanism proposed for the decomposition of the oxalate ion isolated in a KBr matrix.¹⁴ According to this mechanism the rate-determining step is the unimolecular dissociation of the oxalate ion into two carbon dioxide anion radicals. The products carbonate and carbon monoxide are formed by the subsequent rapid bimolecular reaction of the two radicals. The activation energy and frequency factor in calcium oxalate are larger than those of potassium oxalate, respectively, by 8 kcal/mole and by a factor of about 20, but these differences are well within the estimated experimental errors. However, the rate constants in the potassium salt were generally larger than those in the calcium salt by a factor of about 2, which is slightly greater than the estimated uncertainty. Thus, the differences between the present results and those obtained in the potassium oxalate decomposition appear to be real and can be attributed to the dependence of the decomposition kinetics on the reaction environment. Such an effect may be the reason for the difference by a factor of about 80 between the rate constants determined from the infrared disks and those obtained from TGA measurements on the undiluted calcium oxalate. The fact that a rate constant from a TGA run with a KBr disk was in good agreement with the infrared result is also consistent with the above interpretation.

The infrared data obtained in this study provide a possible interpretation of the anomalous kinetic results obtained from the calcium oxalate prepared from calcium bromide, iodide, and nitrate. The transient in-

frared bands observed in these samples with short heating periods cannot be due to formation of a solid solution with the KBr matrix or to the exchange of the cations since the same bands were observed in undiluted samples and since no potassium carbonate was observed as the reaction product. These extra absorption bands can be assigned to an oxalate ion having a nonplanar structure on the basis of the following arguments. The crystal structure of calcium oxalate monohydrate is not known, but the dihydrate structure¹⁵ has been determined and in this case the oxalate ion is planar. Indeed the observed spectrum obtained by short heating and consequent dehydration of the monohydrate salt is consistent with the expected spectrum of a D_{2h} symmetry ion. According to this symmetry, five infrared-active fundamentals are expected, and five medium to strong bands are indeed observed as shown in Table I. The lowest observed frequency of 306 cm⁻¹ was not assigned to the oxalate since calcium carbonate also was found to exhibit a band at this position. These five observed bands have frequencies near those found in sodium oxalate¹¹ which has a D_{2h} symmetry.¹⁶ However, Begun and Fletcher¹⁷ have shown that the structure of the oxalate ion changes into a nonplanar form when sodium oxalate is dissolved in water. The frequencies reported by these authors from the Raman and infrared spectra of aqueous oxalate ion are in reasonably good agreement with the earlier results of Ito and Bernstein¹⁸ although the latter authors interpreted their solution spectra on the basis of a D_{2h} symmetry for the ion. When we combine the frequency data from these two sources, we noted that both the 782- and 518-cm⁻¹ solid bands show a red shift of about 20 cm⁻¹ when the salt is dissolved in water. This shift is comparable to a frequency difference of about 28 cm⁻¹ between the transient bands and the normal oxalate bands. Although these frequency shifts in sodium oxalate may well be due to dielectric effect, similar changes in frequency have been observed in the spectrum of isoelectronic N₂O₄ when its structure changed from a D_{2h} to a nonplanar form in the solid phase.¹⁹ If our interpretation is correct, the fact that no new bands were detected in the CO bond stretch region and

(14) K. O. Hartman and I. C. Hisatsune, *J. Phys. Chem.*, **71**, 392 (1967).

(15) C. Sterling, *Acta Cryst.*, **18**, 917 (1965).

(16) G. A. Jeffery and G. S. Parry, *J. Am. Chem. Soc.*, **76**, 5283 (1954).

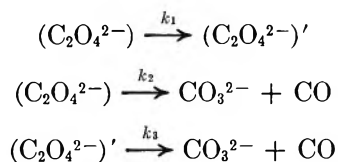
(17) G. M. Begun and W. H. Fletcher, *Spectrochim. Acta*, **19**, 1343 (1963).

(18) K. Ito and H. J. Bernstein, *Can. J. Chem.*, **34**, 170 (1956).

(19) I. C. Hisatsune, J. P. Devlin, and Y. Wada, *J. Chem. Phys.*, **33**, 714 (1960).

near 388 cm^{-1} must be explained. A shift in the anti-symmetric stretch band at 1638 cm^{-1} would be difficult to detect since this fundamental remained very broad throughout the reaction as shown in Figure 1. The symmetric stretch band is sharper, but its frequency difference between the two isomers in sodium oxalate¹⁷ was only about 5 cm^{-1} . Finally, the 388-cm^{-1} band was not very intense to begin with, and it had disappeared by the time the two transient bands were detectable as shown in trace C of Figure 1.

According to the interpretation of the transient bands described, above, we may take the intensities of the 782- , 518- , and 388-cm^{-1} bands as being proportional to the concentration of the planar oxalate in the sample, and the 1313- and 1638-cm^{-1} bands to represent the total oxalate concentration. Experimentally, we observed that the former set of three bands decayed more rapidly than the latter two bands and that all five bands followed a first-order rate law. These observations may be accounted for by the following mechanism.



where $(\text{C}_2\text{O}_4^{2-}) =$ planar oxalate, $(\text{C}_2\text{O}_4^{2-})' =$ nonplanar oxalate, and the total oxalate concentration is given by $(\text{C}_2\text{O}_4^{2-})^T = (\text{C}_2\text{O}_4^{2-}) + (\text{C}_2\text{O}_4^{2-})'$. The disappearance rate of the planar oxalate is then

$$-d(\text{C}_2\text{O}_4^{2-})/dt = (k_1 + k_2)(\text{C}_2\text{O}_4^{2-})$$

where the rate constant $(k_1 + k_2)$ corresponds to the numbers listed under the 782-cm^{-1} band in Table II. The rate constants for the total oxalate decomposition are those given under the $1638\text{--}1313\text{-cm}^{-1}$ bands and these are associated with the rate equation

$$\begin{aligned}-d(\text{C}_2\text{O}_4^{2-})^T/dt &= k_2(\text{C}_2\text{O}_4^{2-}) + k_3(\text{C}_2\text{O}_4^{2-})' \\ &= k^T(\text{C}_2\text{O}_4^{2-})^T\end{aligned}$$

Thus, within experimental error $k^T \cong k_2 \cong k_3$ which appears reasonable since the decompositions of both isomers of oxalate still involve the C-C bond rupture as the rate-determining step and since we expect the difference in energy between the two isomers to be small. Although the experimental error in the rate constants does not allow us to calculate the activation energy for the isomerization reaction with precision, our data give an estimated value of about $12 \pm 20\text{ kcal/mole}$ for the activation energy of step 1. In the isoelectronic N_2O_4 the estimated rotational barrier is only about 3 kcal/

mole¹⁹ while in nitrous acid the isomerization barrier is about 9 kcal/mole .²⁰

The proposed mechanism was also tested in the following way. The predicted rate equation for the nonplanar oxalate concentration, $d(\text{C}_2\text{O}_4^{2-})'/dt = k_1(\text{C}_2\text{O}_4^{2-}) - k_3(\text{C}_2\text{O}_4^{2-})'$, was integrated and gave $(\text{C}_2\text{O}_4^{2-})' = k_1(\text{C}_2\text{O}_4^{2-})^0/k_3 - k_1 - k_2[e^{-(k_1+k_2)t} - e^{-k_2t}]$ where $(\text{C}_2\text{O}_4^{2-})^0$ is the initial oxalate concentration. By substituting the measured values of the rate constants in the equation, the absorbance of the nonplanar oxalate band at 755 cm^{-1} was calculated. The absorption coefficients of this band and the planar oxalate band at 782 cm^{-1} were assumed to be equal. The calculated values agreed with observed values within 30%. This agreement is quite reasonable when the error which accumulates in the evaluation of the expression $k_1/k_3 - k_1 - k_2$ is considered. The calculated values were usually though not always higher than the observed values.

The DTA data obtained from undiluted oxalate samples are also consistent with the decomposition mechanism proposed in the preceding paragraphs. As we stated previously, only oxalate samples which showed the transient infrared bands gave the extra peak in their DTA records (peak three, Figure 2). By carrying out the DTA run in air, this extra peak was shown not to be due to a phase transition. The decomposition of the oxalate in air produced carbonate and carbon dioxide, and the reaction was exothermic. Peak three, as well as peaks one and two, was still observed under this reaction condition and was exothermic. Thus, both the main peak two and the extra peak three arise from the decomposition of oxalates with peak two representing the planar form and three representing the nonplanar form. The fact that peak three occurs at a higher temperature than that of peak two indicates that k_2 and k_3 are not exactly equal and that k_3 is slightly lower than k_2 at temperatures near 500° . This condition would cause the deviation described in the previous paragraph, *i.e.*, the calculated nonplanar oxalate concentration was higher than the observed.

The interpretation of the shifted oxalate infrared bands proposed here suggests that frequency shifts, observed when oxalate ions diffused into potassium halide matrices,¹⁴ may be due also to a change in structure of the ion from a D_{2h} symmetry to a nonplanar form. If this is true, then the rate constants obtained from the decomposition of oxalate ions isolated in KBr matrix will be k_3 , the rate constant for reaction 3 in the

(20) R. T. Hall and G. C. Pimentel, *J. Chem. Phys.*, **38**, 1889 (1963).

above mechanism. Unfortunately, the experimental uncertainty is too large to make any meaningful interpretation of our combined kinetic data on this basis.

Acknowledgments. We are grateful to Dr. F. M.

Angeloni for obtaining the DTA data and for valuable discussions. We are pleased to acknowledge the financial support from the National Science Foundation and the Air Force Office of Scientific Research.

A Study of the Adsorption of Thiourea on Mercury by Chronocoulometry

by Brian Case and Fred C. Anson¹

Contribution No. 3412 from the Gates and Crellin Laboratories of Chemistry, California Institute of Technology, Pasadena, California (Received August 17, 1966)

Chronocoulometry, a newly developed faradaic procedure for measuring reactant adsorption at electrodes, has been applied to the study of thiourea adsorption at mercury electrodes. The results of these experiments compare very favorably with those from independent thermodynamic measurements on the same system. The chronocoulometric method appears to offer significant advantages as a complementary technique for the determination of surface concentrations of electroactive substances.

In view of an anticipated increase in the use of chronocoulometry² to study the adsorption of electroactive species on mercury, it was thought desirable to make an extensive comparison of the results obtained by this technique with those found by entirely independent methods.

The classical approach to the determination of surface excesses of adsorbed material has been by thermodynamic analysis of electrocapillary and double-layer capacity measurements. Most of the existing information concerning adsorption at electrode surfaces has been obtained in this way.³

Anson and Payne⁴ have shown that their chronocoulometric results on the adsorption of thiocyanate ion agree fairly well with the values of surface excesses calculated by extrapolation of an adsorption isotherm for SCN^- which was derived from electrocapillary work by Wroblowa, Kovac, and Bockris.⁵ However, the uncertainties involved in the extrapolation of the isotherm from 10 mM were considerable and a further chronocoulometric study of a system which had been more thoroughly treated by thermodynamic methods seemed desirable.

Thiourea fulfills this criterion very well. It has been the subject of several previous investigations.⁶⁻⁸ It is very strongly adsorbed and, fortunately, polarographic work⁹ has shown that it gives rise to a reversible anodic wave to form predominantly $[\text{Hg}(\text{thiourea})_2]^{2+}$. In this respect thiourea is very similar to the thiocyanate ion.

Experimental Section

The theory and practice of chronocoulometry have

(1) Alfred P. Sloan Research Fellow.

(2) (a) F. C. Anson, *Anal. Chem.*, **38**, 54 (1966); (b) R. W. Murray and D. J. Gross, *ibid.*, **38**, 392 (1966).

(3) Paul Delahay, "Double Layer and Electrode Kinetics," Interscience Publishers, Inc., New York, N. Y., 1965.

(4) F. C. Anson and D. A. Payne, *J. Electroanal. Chem.*, **13**, 35 (1967).

(5) H. Wroblowa, F. Kovac, and J. O'M. Bockris, *Trans. Faraday Soc.*, **61**, 1523 (1965).

(6) F. W. Schapink, M. Oudeman, K. W. Leu, and J. N. Helle, *ibid.*, **56**, 415 (1960).

(7) R. Parsons, *Proc. Roy. Soc. (London)*, **A261**, 79 (1961).

(8) M. A. V. Devanathan, *ibid.*, **A264**, 133 (1961).

(9) C. J. Nyman and E. P. Parry, *Anal. Chem.*, **30**, 1255 (1958).

been described in detail.^{2a,10-13} The instrumentation was essentially the same as that used previously,^{2a,4} except that the unavoidable, uncompensated resistance in the cell was largely compensated for electronically with the circuit described by Lauer and Osteryoung.¹⁴ The output from the current-measuring amplifier was fed back through a variable potentiometer to the input of the potential control amplifier. The required amount of compensation applied *via* this potentiometer was determined experimentally by observing the current pulse following application of the potential step and by increasing the feedback to a point where the system was just about to break into oscillation.

This compensation was indispensable when making measurements with 5 and 10 mM thiourea solutions. Marked nonlinearity of the chronocoulometric plots (Q vs. $t^{1/2}$) was observed at times less than 1 msec after the application of the potential step unless this compensation was employed. A comparison of compensated and uncompensated plots for 5 mM thiourea solution is shown in Figure 1. With compensation the $Q-t^{1/2}$ plots were usually linear down to about 250 μ sec after the potential step was applied. At still shorter times the compensation was not adequate to prevent the Q values from falling below the linear extrapolation. There was some indication that the compensation circuit was not capable of eliminating all of the uncompensated resistance. The slopes of the Q vs. $t^{1/2}$ plots with 5 and 10 mM thiourea solutions tended to be slightly less than 2.5 and 5 times as great as the slopes with the 2 mM solutions. Although this effect could have reflected an increasing contribution from mercury(II)-thiourea complexes containing three or four thiourea molecules, the constancy of the diffusion current to concentration ratios obtained by Nyman and Parry⁹ for the same concentration range indicate that this was not the source of the effect observed in these experiments and we attribute it primarily to the residual uncompensatable resistance in the cell.

For the experiments in which the rate of adsorption of thiourea was measured it was necessary to employ a potentiostat with a faster response than could be obtained with our operational amplifier-based circuit. In these experiments a commercial potentiostat and pulse generator (Chemical Electronics Co., Newcastle, England) designed for very fast response were employed. This potentiostat is designed to operate with differential input so that no electronic compensation of the uncompensated resistance was possible.

Charge-time traces were recorded on a Tektronix Type 564 storage oscilloscope and data were read directly from Polaroid photographs of the traces.

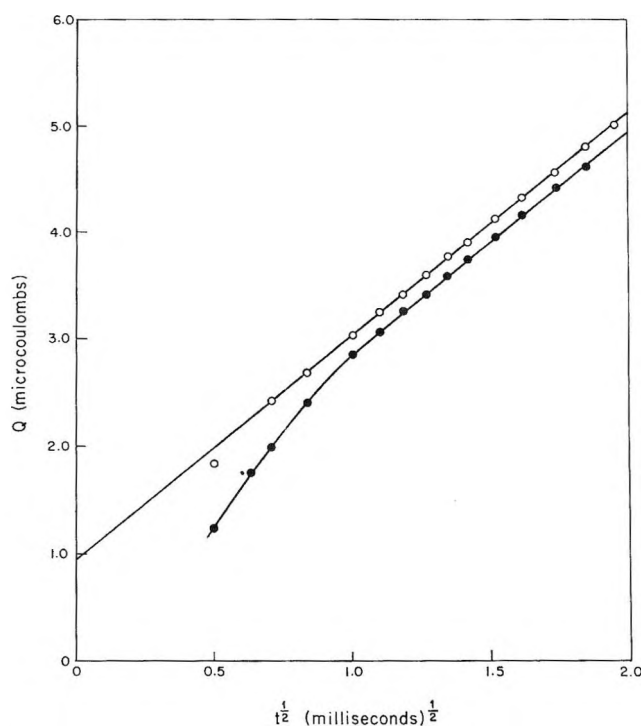


Figure 1. Chronocoulometric charge-(time)^{1/2} plot for 5 mM thiourea. O, with compensation; ●, without compensation. The potential step was from -400 to +300 mv vs. sce. Electrode area was 0.032 cm².

Reagent grade sodium nitrate was recrystallized once from water. Thiourea was triply recrystallized. The final product was white plate crystals with a melting point of 181-182°. Triply distilled water was used throughout for the recrystallizations and preparation of solutions. A commercially available (Brinkman Instruments, Inc.) hanging mercury drop electrode was used together with a platinum wire counter electrode and a saturated calomel reference electrode which contacted the experimental solution *via* a 1 M sodium nitrate salt bridge. Results obtained with the cell thermostated at 25° appeared identical, within experimental error, with those at ambient room temperature. All potentials were measured and are reported with respect to a saturated calomel electrode (sce).

(10) J. H. Christie, G. Lauer, R. A. Osteryoung, and F. C. Anson, *Anal. Chem.*, **36**, 975 (1963).

(11) J. H. Christie, G. Lauer, and R. A. Osteryoung, *J. Electroanal. Chem.*, **7**, 60 (1964).

(12) J. H. Christie, R. A. Osteryoung, and F. C. Anson, *ibid.*, **13**, 236 (1967).

(13) F. C. Anson, J. H. Christie, and R. A. Osteryoung, *ibid.*, in press, 1967.

(14) G. Lauer and R. A. Osteryoung, *Anal. Chem.*, **38**, 1106 (1966).

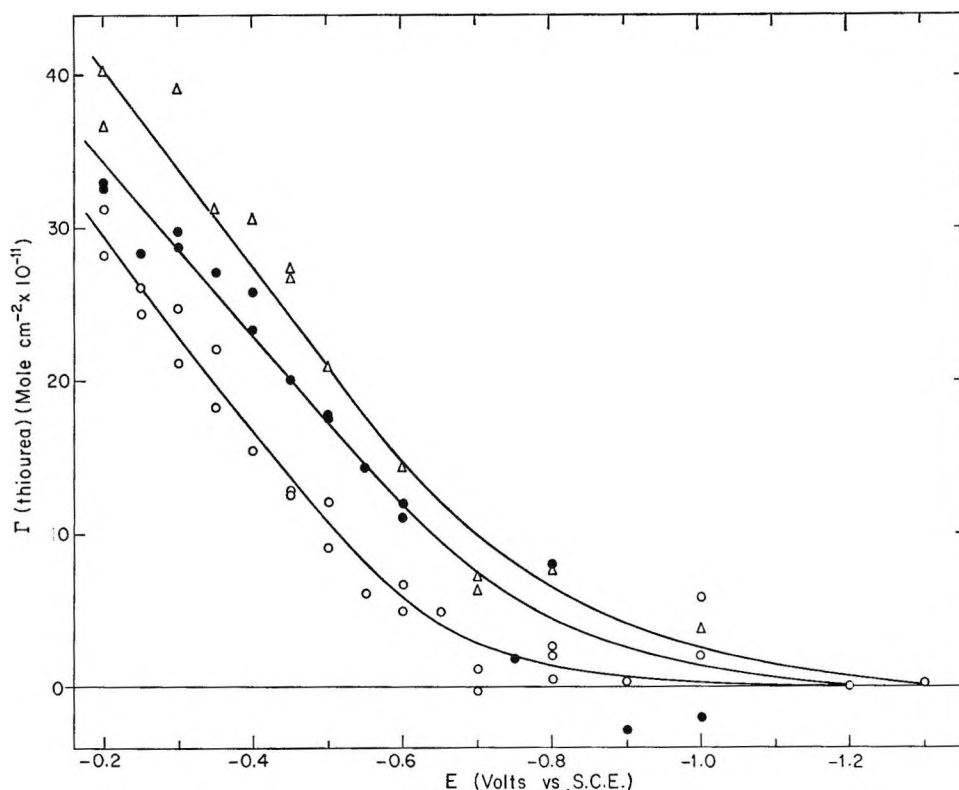


Figure 2. Chronocoulometric values for adsorbed thiourea as a function of the initial electrode potential in 1 *M* NaNO₃ containing: O, 2 *mM* thiourea; ●, 5 *mM* thiourea; Δ, 10 *mM* thiourea. Potential step was from the potential plotted to +300 *mv vs. sce.*

Results and Discussion

Chronocoulometric plots were made for single potential steps from various initial potentials to a potential 300 *mv* anodic of that of the saturated calomel electrode for solutions of 2, 5, and 10 *mM* thiourea in 1 *M* NaNO₃. It was not possible to estimate the double-layer contribution to the intercept of these plots by the direct method of drop extrusion^{2a} because solutions of the oxidation product, [Hg(thiourea)₂]²⁺, were not sufficiently stable. Addition of a thiourea solution to a slightly acidic solution of a mercuric salt produced immediate cloudiness and rapid precipitation of HgS. The solutions appeared more stable at lower pH values but even in the most stable medium tested, 9 *M* HClO₄, discoloration of the solutions appeared 5–10 *min* after mixing.

To obtain the double-layer charging correction the procedure used in the previous work on thiocyanate ion adsorption⁴ was adopted. Chronocoulometric plots were first made for potential steps from initial potentials negative enough to ensure that adsorption of thiourea was negligible. (From the results of double-layer capacity studies^{7,8} it was known that there would be negligible adsorption at -1200 *mv* for 2 and 5 *mM*

thiourea solutions and at -1300 *mv* for 10 *mM* solutions.) The intercepts of these plots, $\Delta Q_{dl}(E_0 \rightarrow +300)$, were taken as the true difference in double-layer charge between E_0 , *i.e.*, -1200 or -1300 *mv*, and the final potential (+300 *mv*). The charge, $\Delta Q_{dl}(E_0 \rightarrow E_i)$, required to step the electrode potential from -1200 or -1300 *mv* to the initial potentials employed in the subsequent experiments where thiourea adsorption did occur was also measured. The appropriate double-layer charging correction, $\Delta Q_{dl}(E_i \rightarrow +300)$, to be applied to potential steps from E_i to +300 was then calculated from

$$\Delta Q_{dl}(E_i \rightarrow +300) = \Delta Q_{dl}(E_0 \rightarrow +300) - \Delta Q_{dl}(E_0 \rightarrow E_i) \quad (1)$$

Values of the amount of thiourea adsorbed at the initial potentials, E_i , were calculated from the expressions

$$\Gamma_{\text{thiourea}} = Q_{\Gamma}(E_i)/nF \quad (2)$$

where $n = 1$ and $Q_{\Gamma}(E_i)$ is given by

$$Q_{\Gamma}(E_i) = \Delta Q_{\text{exp}}(E_i) - [\Delta Q_{dl}(E_0 \rightarrow +300) - \Delta Q_{dl}(E_0 \rightarrow E_i)] \quad (3)$$

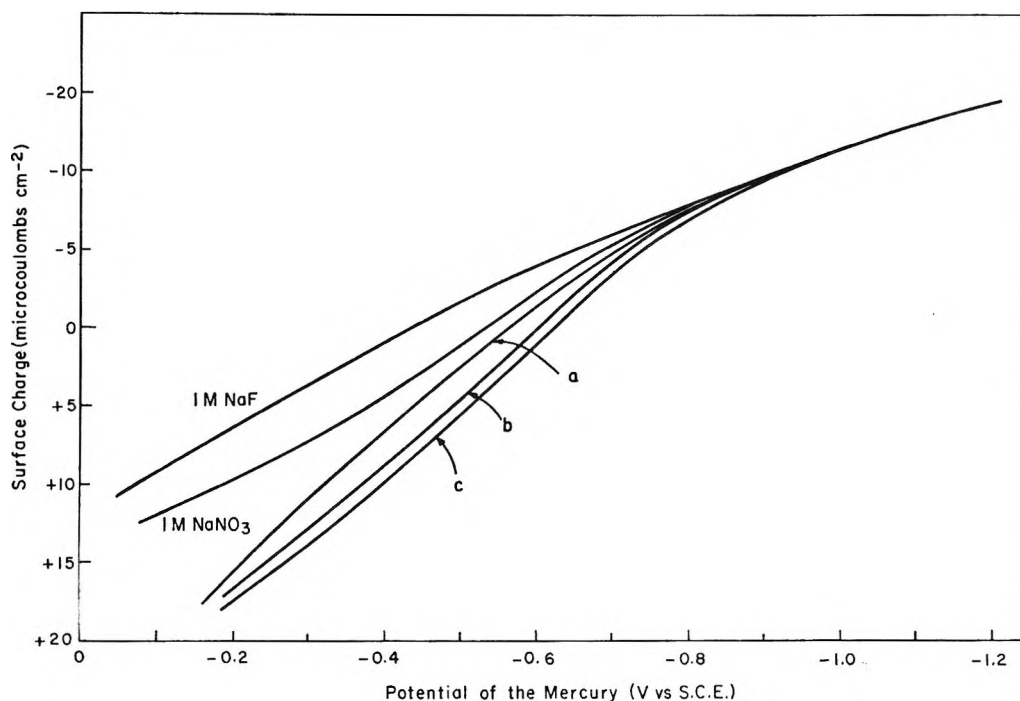


Figure 3. Surface charge-potential curves for mercury electrode in 1 M NaF, 1 M NaNO₃, and 1 M NaNO₃ containing (a) 2 mM thiourea, (b) 5 mM thiourea, (c) 10 mM thiourea.

$\Delta Q_{\text{exp}}(E_i)$ is the experimentally observed intercept of the chronocoulometric plot for a potential step from E_i to 300 mv and the other terms are defined as in eq 1. The values of $\Delta(E_i)$ obtained for the three thiourea concentrations are plotted as a function of E_i in Figure 2.

The absolute value of the charge on the electrode at at least one of the negative starting potentials is required if the absolute value of the charge at E_i is desired. In the previous study with thiocyanate⁴ this was obtained by integration of the current that flowed when a mercury drop was extruded at a constant potential. In the present study this technique was found to be rather imprecise at potentials markedly cathodic of the electrocapillary maximum and the charges so evaluated could not be reliably reproduced to better than $\pm 3 \mu\text{coulombs cm}^{-2}$. A more satisfactory procedure was to assume that the charge on the electrode at a very negative potential is the same as the value for mercury in sodium fluoride solution at the same concentration as the base electrolyte. The charge-potential curves illustrated in Figure 3 were evaluated on this assumption. The electronic charge on the electrode, q^M , at -1300 mv vs. sce was taken from the tables of Russell¹⁵ as $-16.12 \mu\text{coulombs cm}^{-2}$.

The values of q^M in Figure 3 were then obtained by stepping the electrode potential from -1300 mv to the potential plotted on the horizontal axis while inte-

grating the resulting current. The step change in charge that resulted was subtracted algebraically from the value of q^M at 1300 mv and the result was plotted on the vertical axis.

For the 10 mM thiourea solution the values of q^M were determined by stepping from both -1500 ($q^M = 19.60 \mu\text{coulombs cm}^{-2}$)¹⁶ and -1300 mv . The results agreed to within $0.35 \mu\text{coulomb cm}^{-2}$ —well within experimental error.

The electrode charge at potential E may be read directly from Figure 3 and hence plots of Γ_{thiourea} against electrode charge may be constructed as shown in Figure 4. For comparison, also shown in Figure 4, are values of Γ_{thiourea} calculated by Schapink, *et al.*,⁶ from their capacity data for thiourea in 0.1 M NaF solution and surface excesses of thiourea given by Parsons and Symons¹⁶ from analysis of capacity results for thiourea in 0.1 M KNO₃ solution. So long as the base electrolyte is not appreciably specifically adsorbed it would not be expected to affect markedly the adsorption of thiourea. The agreement between the chronocoulometric results and the values obtained from these two rather different analyses of double-layer capacity measurements is very gratifying.

The chronocoulometric and double-layer capacity

(15) C. D. Russell, *J. Electroanal. Chem.*, 6, 489 (1963).

(16) P. C. Symons, Thesis, University of Bristol, England, 1963.

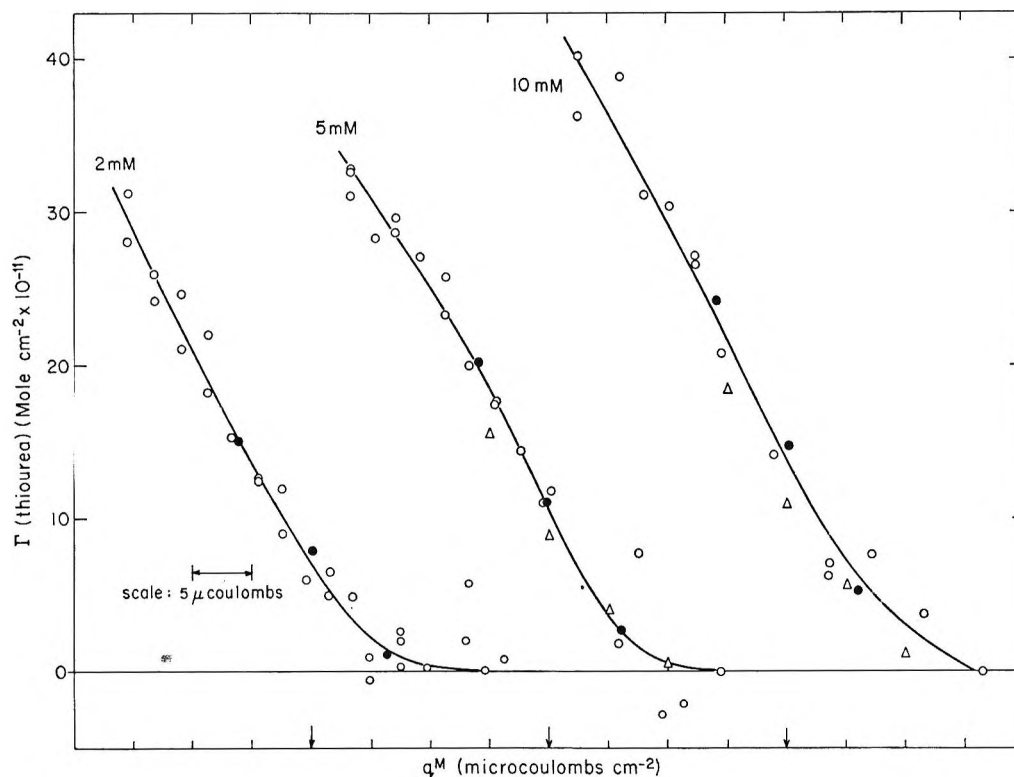


Figure 4 Adsorbed thiourea vs. electronic charge on the mercury electrode for 2, 5, and 10 mM thiourea solutions in 1 M NaNO₃. The point of zero charge for each solution is indicated by the arrows on the q^M axis: O, chronocoulometric data from this study; ●, data of Parsons and Symons¹⁷ (0.1 M KNO₃); Δ, data of Schapink, *et al.*⁸ (0.1 M NaF).

results are to some extent complementary in that the former technique allows adsorption at somewhat higher positive electrode charges to be studied, although (with the present instrumentation) it does not permit measurements at as high reactant concentrations as are suitable in double-layer work.

Kinetics of the Adsorption of Thiourea. In principle, one should be able to apply chronocoulometry to the study of the kinetics of adsorption by stepping the potential from a value where adsorption is negligible to a potential where adsorption does occur, pausing there for varying times to allow reactant to adsorb, and then determining the amount adsorbed after each pause time by stepping to a potential where the reactant is reduced or oxidized and plotting Q against an appropriate function of time, $f(t)$. The form of $f(t)$ would depend on the adsorption isotherm since this determines the concentration profile of the adsorbing material near the electrode and hence the current- and charge-time relationships in the subsequent chronocoulometric experiments.

An exact mathematical solution for the form of $f(t)$ is extremely difficult to derive even for the simplest case of a linear adsorption isotherm. However, a quali-

tative picture of the limiting behavior to be expected is not hard to provide.¹⁷

Consider the following experiment. An electrode is potentiostated at a potential, E_0 , where no reactant is adsorbed. The potential is stepped to a new value, E_1 , where reactant does adsorb but where no faradaic reaction takes place. The electrode is maintained at potential E_1 for time τ . Finally the potential is stepped to a potential, E_2 , where the reactant is reduced or oxidized at a diffusion-limited rate. The total charge, $Q(\tau + t)$, that has passed at potential E_2 is measured at some time, t , after the second potential step, *i.e.*, at time $\tau + t$ after the first potential step. A pictorial representation of the various quantities is given in Figure 5.

Now it is instructive to consider the *faradaic* charge that has passed at time $\tau + t$, $Q_f(\tau + t)$, and the *faradaic* charge, $Q_f(\tau)$, that would have passed at time τ if the initial potential step had been from E_0 to E_2 .

$$Q_f(\tau + t) = Q(\tau + t) - \Delta Q_{dl}(E_0 \rightarrow E_2) \quad (4)$$

(17) We are indebted to J. H. Christie of these laboratories for providing a rigorous but more complicated quantitative analysis on which the following qualitative discussion is based.

and

$$Q_f(\tau) = Q(\tau) - \Delta Q_{d.l.}(E_0 \rightarrow E_2) \quad (5)$$

where $\Delta Q_{d.l.}(E_0 \rightarrow E_2)$ is the observed intercept of a chronocoulometric plot (Q vs. $t^{1/2}$) for a single potential

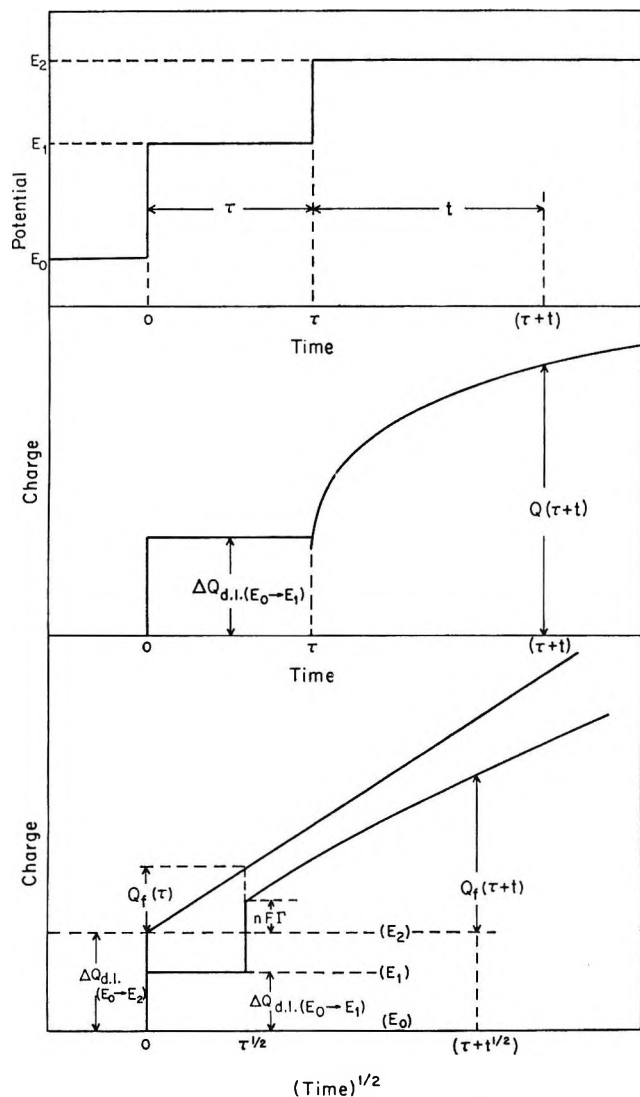


Figure 5. Pictorial representation of the potential-time, charge-time, and charge-(time)^{1/2} variations during a chronocoulometric experiment to study the rates of adsorption. No reactant is adsorbed at the initial potential, E_0 . No faradaic reaction occurs at the pause potential, E_1 , but reactant is adsorbed. A diffusion-limited faradaic reaction proceeds at the final potential, E_2 .

step from E_0 (where there is no adsorption) to E_2 . The ratio $Q_f(\tau + t)/Q_f(\tau)$ must approach certain values in the limit of very small or very large pause times, τ .

For small values of τ

$$\frac{Q_f(\tau + t)}{Q_f(\tau)} \rightarrow \frac{Q_{diff}(\tau + t)}{Q_{diff}(\tau)} = \sqrt{\frac{\tau + t}{\tau}} \text{ as } \tau \rightarrow 0 \quad (6)$$

(where $Q_{diff}(t)$ is the charge passed by a diffusion-limited current in time t) because for sufficiently small pause times all of the reactant that reaches the electrode will adsorb and then be instantaneously reduced (or oxidized) when the potential is stepped from E_1 to E_2 . At this point the electrode will be exposed to a concentration gradient of reactant indistinguishable from the one that could have been produced by stepping

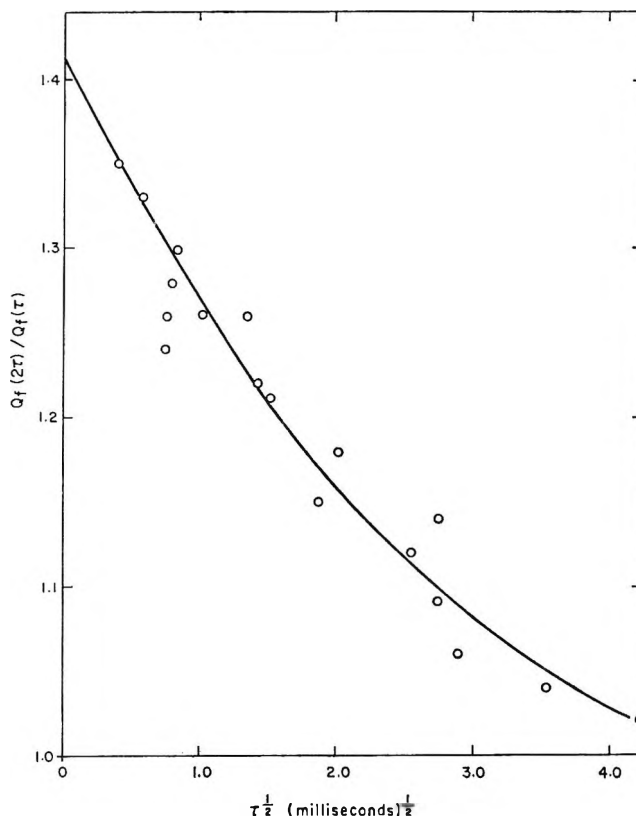


Figure 6. Plot of $Q_f(t + \tau)/Q_f(\tau)$ vs. $\tau^{1/2}$ (see text for definitions). Data are for a 2 mM thiourea solution in which the electrode potential was stepped from -1300 to -200 mv for τ msec and then to $+300$ mv for another τ msec.

the potential from E_0 to E_2 in the first place, and the ratio of the charges passed up to two different times during such a single-step chronocoulometric experiment is given by the ratio of the square root of the two times.¹¹

For large values of τ

$$\frac{Q_f(\tau + t)}{Q_f(t)} \rightarrow \frac{Q_{diff}(t) + nF\Gamma}{Q_{diff}(\tau)} = \left(\frac{t}{\tau}\right)^{1/2} + \frac{nF\Gamma}{Q_{diff}(\tau)} \rightarrow \left(\frac{t}{\tau}\right)^{1/2} \text{ as } \tau \rightarrow \infty \quad (7)$$

Equation 7 follows from the fact that for sufficiently long pause times Γ will essentially attain its equilibrium value. For still longer times both the concentration gradient at the electrode surface and the term $nF\Gamma/Q_{diff}(\tau)$ will become progressively smaller.

Thus the ratio of $Q_f(\tau + t)$ to $Q_f(\tau)$ should vary from $\{(t + \tau)/\tau\}^{1/2}$ to $(t/\tau)^{1/2}$ as τ goes from 0 to ∞ . For example, if t is chosen to be equal to τ , then the ratio of $Q_f(\tau + t)$ to $Q_f(\tau)$ should vary from the square root of 2 to unity. Figure 6 shows a set of data points obtained with a 2 mM thiourea solution in which the electrode potential was stepped from -1300 mv (where thiourea is not adsorbed) to -200 mv where it was held for τ msec and then to $+300$ mv where the total charge passed after another interval of τ msec was recorded. The data all fall reasonably close to a smooth curve drawn between the two theoretical limits for $Q_f(\tau + t)/Q_f(\tau)$.

It is, in principle, possible to extract information about the isotherm parameters from data such as that in Figure 6, but the present limits on the accuracy of the data that can be obtained, coupled with the rather major assumptions about the form of the isotherm that must be made to analyze the data, make this an unattractive possibility.

Conclusions

The objective of this study was to determine if the amounts adsorbed, determined by chronocoulometry, agreed with those resulting from classical double-layer capacity measurements. In the case of thiourea the answer is clearly affirmative. This result, coupled with the rather complementary character of the two methods, leads us to conclude that the chronocoulometric method can be of considerable value in the determination of surface concentrations of electroactive substances.

Acknowledgment. This work was supported in part by the U. S. Army Research Office (Durham). We are grateful to Dr. Roger Parsons and P. C. Symons for sending us data from the latter's thesis before publication.

SCF-MO Calculations of Heteroatomic Systems with the Variable- β

Approximation. II. Electronic Spectra of Hydroxy

Aza-aromatic Molecules¹

by Kichisuke Nishimoto and Leslie S. Forster

Department of Chemistry, University of Arizona, Tucson, Arizona (Received August 19, 1966)

The spectra of the pyridinols, quinolinols, isoquinolinols, quinolones, and isoquinolones have been calculated by a variable- β procedure within the Pariser-Parr-Pople SCF approximation. The relative positions and intensities of the lower excited states in hydroxy aza-aromatics vary considerably with substituent position, and the calculations are in good agreement with experiment. The vector addition of spectroscopic moments leads to transition moments that differ little from those obtained directly from the SCF-MO calculations.

Introduction

It is desirable to have available a rapid, reliable, semiempirical method for the calculation of π -electron structures. This method should be applicable to a wide variety of systems of varying complexity and should involve a single parameterization scheme irrespective of the number and type of heteroatoms present. The technique should not require detailed geometrical information. An SCF-MO (Pariser-Parr-Pople approximation) method in which the core resonance integrals, $\beta_{\mu\nu}$, and the two-center repulsion integrals, $\gamma_{\mu\nu}$, are expressed in terms of π -bond orders and adjusted iteratively until self-consistency is obtained, has been successful in the calculation of ground-state properties of hydrocarbon and heteroatomic π systems.^{2,3} The suitability of a similar scheme for the computation of spectral energies has been demonstrated and it has been found that the iterative adjustment of the $\gamma_{\mu\nu}$ is unnecessary.^{4,5} The parameterization within this "variable- β " SCF procedure has been tested on molecules containing only one kind of heteroatom (nitrogen or oxygen).⁵ Extension to more complex systems has been made in only one case, isoalloxazine,⁶ and a more systematic validation is necessary. In the present report we deal with molecules containing one nitrogen and one oxygen atom.

The pyridinols, quinolinols, isoquinolinols, quino-

lones, and isoquinolones are systems in which the relative positions of the oxygen and nitrogen atoms may be varied. The spectra of most of the quinolinols and isoquinolinols are known; therefore, the applicability of the parameterization may be evaluated and the extent to which interactions between heteroatoms vitiate the calculations may be assessed.

Method

The method and parameterization used in this work have been described elsewhere.⁵ As nearly the same results were obtained with the Nishimoto-Mataga (NM) integrals as with the "theoretical" integrals reduced for nearest neighbors (R integrals) the former set was used for simplicity.

All bond lengths and angles were set at 1.395 Å and 120°, respectively. Configurations within 3.5 eV of the lowest excited state were included in the configuration

(1) Supported by the U. S. Atomic Energy Commission (Contract No. AT(11-1)-773).

(2) M. J. S. Dewar and G. J. Gleicher, *J. Am. Chem. Soc.*, **87**, 1459 (1965).

(3) M. J. S. Dewar and G. J. Gleicher, *J. Chem. Phys.*, **44**, 759 (1966).

(4) K. Nishimoto and L. S. Forster, *Theoret. Chim. Acta*, **3**, 407 (1965).

(5) K. Nishimoto and L. S. Forster, *ibid.*, **4**, 155 (1966).

(6) J. L. Fox, K. Nishimoto, and L. S. Forster, *Biochim. Biophys. Acta*, **109**, 626 (1965).

Table I: Singlet Transition Energies (ev) and Oscillator Strengths (f)

Energy			Energy			Energy					
Calcd	Obsd	f	Calcd	Obsd	f	Calcd	Obsd	f			
2-Pyridinol			3-Pyridinol			4-Pyridinol					
4.6 ξ	4.61 ^a	0.125	4.65	4.44 ^b	0.119	4.86	5.27 ^a	0.061			
5.9 ξ	>6.04 ^a	0.257	5.78	5.77 ^b	0.242	5.83	5.58 ^a	0.174			
7.0 ξ	...	0.978	6.82	...	0.829	6.65	...	0.884			
7.0 ξ		0.917	7.06		1.025	6.82		1.128			
2-Quinololin			3-Quinololin			4-Quinololin					
3.9 ξ	3.90 ^b	0.131	3.84	3.71 ^b	0.137	4.03	...	0.066			
4.4 ξ	4.68 ^b	0.110	4.33	4.46 ^b	0.117	4.30	4.35 ^d	0.274			
5.24		0.751	5.19	5.27 ^c	0.461	5.39		0.051			
5.5 ξ		0.615	5.41		0.658	5.50		1.624			
5.91		0.690	5.71		0.863	5.56		0.064			
6.02		0.463	5.93		0.450	5.75		0.126			
6.12		0.055	6.04		0.115	6.11		0.551			
5-Quinololin			6-Quinololin			7-Quinololin					
3.91	3.84 ^b	0.197	3.81	3.75 ^b	0.133	3.81	3.72 ^b	0.139			
3.96	...	0.003	4.27	4.52 ^b	0.087	4.29	4.71 ^b	0.087			
5.08	5.12 ^b	0.922	5.21	5.46 ^b	0.731	5.22	5.46 ^b	0.614			
5.57		0.078	5.56		0.587	5.52		1.077			
5.81		0.207	5.73		0.565	5.62		0.079			
5.92		0.636	6.04		0.007	6.05		0.734			
6.31		1.014	6.14		0.732	6.15		0.233			
8-Quinololin			1-Isoquinolinol			3-Isoquinolinol			4-Isoquinolinol		
3.90	4.06 ^b	0.186	3.95	...	0.114	3.80	...	0.145	3.90	3.76 ^b	0.163
3.95		0.006	4.31		0.229	4.36		0.122	4.15	4.20 ^b	0.171
5.05	5.12 ^b	0.933	5.26		0.496	5.25		0.311	5.17	5.39 ^b	0.555
5.52		0.042	5.51		0.062	5.30		0.661	5.36		0.014
5.69		0.329	5.63		0.625	5.60		0.852	5.64		0.433
5.98		0.526	5.94		0.573	6.02		0.315	5.81		0.768
6.31		1.047	6.26		0.507	6.25		0.305	6.19		0.499
5-Isoquinolinol			6-Isoquinolinol			7-Isoquinolinol			8-Isoquinolinol		
3.86	3.80 ^b	0.125	3.95	3.89 ^b	0.001	3.79	3.67 ^b	0.124	3.86	3.71 ^e	0.165
4.13	4.10 ^b	0.186	4.26	4.43 ^b	0.212	4.42	4.79 ^b	0.107	4.17	4.08 ^e	0.125
5.24	5.27 ^b	0.577	5.31	5.51 ^b	1.455	5.27		0.313	5.22		0.427
5.43		0.043	5.35		0.201	5.47	5.51 ^b	1.447	5.45		0.098
5.71		0.764	5.68		0.283	5.50		0.117	5.66	5.32 ^e	1.063
5.74		0.403	5.95		0.123	5.93		0.500	5.78		0.251
6.24		0.468	5.98		0.408	6.09		0.069	6.23		0.499
2-Quinolone			4-Quinolone			5-Quinolone			7-Quinolone		
3.88	3.81 ^b	0.222	3.98	3.80 ^c	0.206	2.42	2.68 ^f	0.231	2.57	3.05 ^f	0.312
4.50	4.56 ^b	0.152	4.33	4.43 ^c	0.167	3.64	3.81 ^f	0.274	3.77	3.99 ^f	0.018
5.19	5.06 ^b	0.382	5.00		0.245	4.59	4.54 ^f	0.384	4.37	4.75 ^f	0.985
5.32	5.44 ^b	0.951	5.20	5.16 ^c	0.383	5.10	5.23 ^f	0.437	4.65		0.048
5.75		0.230	5.39		0.024	5.33		0.026	5.37		0.675
6.18		0.130	5.89		0.542	5.58		0.092	5.69		0.011
6.37		0.584	6.23		0.032	6.22		0.779	5.83		0.533

Table I (Continued)

Energy			Energy			Energy			Energy		
Calcd	Obsd	<i>f</i>	Calcd	Obsd	<i>f</i>	Calcd	Obsd	<i>f</i>	Calcd	Obsd	<i>f</i>
1-Isoquinolone			3-Isoquinolone			6-Isoquinolone			8-Isoquinolone		
4.01	3.87 ^c	0.111	3.11	...	0.318	2.75	3.46 ^f	0.250	2.64	2.82 ^f	0.206
4.32	4.43 ^c	0.363	4.15	...	0.144	3.55	4.64 ^f	0.237	3.33	3.71 ^f	0.323
5.10		0.392	4.58		0.122	4.38		0.599	4.68	...	0.037
5.43		0.361	4.73		0.008	4.76		0.094	5.10	4.82 ^f	0.268
5.68		0.008	5.33		1.609	5.39	5.39 ^f	0.872	5.31		0.180
6.14		0.675	6.14		0.001	5.61		0.610	5.52		0.034
6.21		0.289	6.28		0.271	5.90		0.231	5.83		0.437
6.49		0.003	6.46		0.382	6.44		0.074	6.38		0.539

^a Reference 11. ^b Reference 10. ^c Reference 12. ^d G. F. Tucker, Jr. and J. L. Irvin, *J. Am. Chem. Soc.*, **73**, 1923 (1951). ^e Reference 14. ^f S. F. Mason, private communication.

interaction calculation. Transition energies within approximately 2.5 eV of the lowest energy transition should be meaningful.

Notation

The Platt classification scheme, widely used to designate the excited states of hydrocarbons, has been extensively employed in the labeling of excited states of derivatives of the hydrocarbons.⁷ The states, designated as ¹L_a, ¹L_b, ¹B_a, and ¹B_b, are characterized by the nodal patterns of the transition dipole maps derived from the perimeter model. The two lowest energy transitions, ¹L_a and ¹L_b, are distinguished by intensity, the ¹L_b being the weakest. In LCAO-MO calculations for alternant hydrocarbons with $2n$ π electrons, ¹L_a corresponds to the orbital transition $n \rightarrow n + 1$ while ¹L_b and ¹B_b are related to the states produced by configuration interaction between $n - 1 \rightarrow n + 1$ and $n \rightarrow n + 2$. Hummel and Ruedenberg have shown that the LCAO-MO and the perimeter models lead to the same transition dipole maps for ¹L_a but differ for the ¹L_b transition.⁸ Furthermore, they question the applicability of the Platt notation to nonlinear polyacenes. The α -naphthol states resemble the corresponding naphthalene states and it is appropriate to continue the use of the Platt symbols in this case.⁹ The designation of the β -naphthol states by the Platt symbols does not seem justified; the β -naphthol excited-state wave functions bear little resemblance to those of naphthalene. In the light of this discussion we adopt the following convention: when the relative intensities of the two lowest transitions resemble those of naphthalene, we label the weaker transition ($f < 0.05$) ¹L_b and the stronger ¹L_a. In all other cases these states are simply labeled ¹L₁ and ¹L₂.

Results

The calculated transition energies and oscillator strengths are assembled in Table I. Comparison with experiment is often complicated by the possibility of zwitterion and keto-enol tautomerism.^{10,11} Where such equilibria are important, reference to the spectrum of the corresponding methoxy derivative has been used to eliminate the uncertainty.

Pyridinols. The measured spectra of 2- and 3-methoxypyridine correspond closely to the phenol spectrum with the ¹L₁ peak somewhat intensified by the aza substitution.¹⁰ The calculated transition energies are in good accord with experiment. The spectrum of 4-methoxypyridine is quite different; the ¹L₁ seems to be shifted until it becomes a shoulder on ¹L₂. If this shoulder is due to the ¹L₁ transition the calculations do not reproduce this blue shift. There is a possibility, however, that the ¹L₁ transition does lie at lower energy and has not been reported because of the low intensity.

Quinolins. It is useful to classify these molecules as derivatives of α - and β -naphthol.¹² The spectra of the quinolins derived from α -naphthol (4-, 5-, and 8-) resemble the parent. The long-wavelength bands are much broader and intense than the corresponding absorption bands in the β -naphthol derivatives and it appears that both the ¹L_a and ¹L_b transitions contribute

- (7) J. R. Platt, *J. Chem. Phys.*, **17**, 484 (1949).
- (8) R. L. Hummel and K. Ruedenberg, *J. Phys. Chem.*, **66**, 2334 (1962).
- (9) L. S. Forster and K. Nishimoto, *J. Am. Chem. Soc.*, **87**, 1459 (1965).
- (10) S. F. Mason, *J. Chem. Soc.*, 5010 (1957).
- (11) S. F. Mason, *ibid.*, 1256 (1959).
- (12) G. W. Ewing and E. A. Steck, *J. Am. Chem. Soc.*, **68**, 2181 (1946).

to these bands in 4-, 5-, and 8-quinolinol. The calculations support this interpretation; the 1L_a and 1L_b transitions are predicted to be very close in energy. The calculations also indicate that 1L_b is the lowest energy state in 4-quinolinol, but inversion of the 1L_a and 1L_b order occurs in 5- and 8-quinolinol. Therefore, it is expected that the fluorescence of 5- and 8-quinolinol will be 1L_a whereas that of 4-quinolinol will be 1L_b . Perkampus and Kortüm have proposed this same assignment for the 8-quinolinol spectrum.¹³

The SCF calculations underestimate the 1L_1 - 1L_2 splitting in β -naphthol by about 0.3 eV.⁵ A similar situation is encountered in these calculations for the β -naphthol derivatives, 2-, 3-, 6-, and 7-quinolinol, with the discrepancy increasing to 0.5 eV in the case of 7-quinolinol.

Isoquinolinols. The intensity patterns in the spectra of the isoquinolinols derived from α -naphthol differ from the corresponding quinolinols. The two lowest transitions (1L_1 and 1L_2) are now nearly equally intense. A similar situation obtains in the spectra of the isoquinolinols derived from β -naphthol with one exception, 6-isoquinolinol. In this latter spectrum the lowest energy absorption band is relatively weak.¹¹ The calculations parallel experiment for this entire class of molecules.

The ϵ -isoquinolinol spectrum reported by Mason¹¹ could not be confirmed.¹⁴ Our calculations support the results of Nakanashi, *et al.*

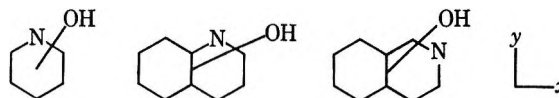
Quinolones and Isoquinolones. With the exception of 6-isoquinolone, the measured spectra are consonant with the calculations, even for those species (5- and 7-quinolone and 3- and 8-isoquinolone) where 1L_1 is shifted markedly to low energies.

Discussion

In general, the method and the specific parameterization reproduce the experimental results rather well with respect to transition energies and relative intensities. The calculation of polarization directions presents a problem for the very weak transitions such as the ${}^1L_b \leftarrow {}^1A$ in 4-, 5-, and 8-quinolinol. The transition moment direction may depend upon the parameterization and/or the extent of configuration interaction in such cases.⁹ Consequently, our agreement with the 8-quinolinol 1L_b - 1L_a assignment of Perkampus and Kortüm¹³ should not be construed as support for their designation of 1L_b as long-axis polarized. The present results indicate the 1L_b absorptions are short-axis polarized (Table II). At the present time only experiment can provide a reliable answer to this question. It is of some interest to note that the aforementioned dependence of the computed α -naphthol 1L_b transition

moment upon parameterization was not obtained when the variable- β procedure was utilized.⁵

In Table II we compare the x and y (long and short axes) components of the transition moments computed by the SCF method with the vector sums (Platt's spec-



troscopic moments) of the appropriate phenol or naphthol and aza-aromatic molecules. In obtaining the vector sums, the transition dipole maps based on the perimeter model were used.¹⁵ The benzene 1L_b dipole maps are the same in both the perimeter and LCAO-MO

Table II: Comparison of SCF and Vector Addition Transition Moments Associated with the Lowest Transitions, $D = D_x\hat{i} + D_y\hat{j}$ (e Å)

Molecule	D_x		D_y	
	SCF	Vector sum	SCF	Vector sum
Pyridine	0.364	...	0	...
Phenol	0.309	...	0	...
2-Pyridinol	0.517	0.519	-0.194	-0.268
3-Pyridinol	0.463	0.519	0.281	0.268
4-Pyridinol	-0.018	0.055	0	0
Quinoline	0.385	...	-0.007	...
Isoquinoline	-0.112	...	0.424	...
α -Naphthol	-0.322	...	-0.025	...
β -Naphthol	0.186	...	-0.346	...
4-Quinolinol	0.127	0.063	-0.012	+0.018
5-Quinolinol	-0.153	...	-0.743	<i>a</i>
8-Quinolinol	0.015	0.063	0.099	-0.032 ^e
	0.111	...	-0.730	<i>a</i>
2-Quinolinol	0.003	0.063	-0.134	0.018 ^e
	0.569	0.571	-0.245	-0.353
3-Quinolinol	0.536	0.571	0.349	0.359
6-Quinolinol	0.491	0.571	-0.396	-0.353
7-Quinolinol	0.552	0.571	0.332	0.339
1-Isoquinolinol	-0.250	-0.434	0.517	0.399
4-Isoquinolinol	-0.411	-0.434	0.556	0.449
5-Isoquinolinol	-0.355	-0.434	0.494	0.399
8-Isoquinolinol	-0.409	-0.434	0.568	0.449
3-Isoquinolinol	0.035	0.074	0.660	0.770
6-Isoquinolinol	-0.047	0.074	0.005	0.078
7-Isoquinolinol	0.110	0.074	0.601	0.770

^a The lowest transition is 1L_a ; the comparison is made for 1L_b .

(13) H. H. Perkampus and K. Kortüm, *Z. Anal. Chem.*, **190**, 111 (1962).

(14) K. Nakanashi, M. Ohashi, S. Kumaki, and H. Koike, *Bull. Chem. Soc. Japan*, **34**, 533 (1961).

(15) J. Petruska, Ph.D. Thesis, University of Chicago, reprinted in "Systematics of the Electronic Spectra of Conjugated Molecules," John Wiley and Sons, Inc., New York, N. Y., 1964, paper 30.

models, but the naphthalene 1L_b dipole maps differ; only one nodal plane, perpendicular to the long axis, occurs in the LCAO-MO treatment.⁸ Both models lead to the same vector sums for the α -naphthol derivatives, but the LCAO-MO vector addition is not unambiguous for the β -naphthol derivatives. If the relative orientation of the naphthol and quinoline vectors is established in one case (*e.g.*, 2-quinolinol) by reference to the SCF-MO results, then for the remainder of the molecules the procedure is straightforward, and the results are then the same as obtained from the perimeter model.

A comment regarding the polarizations of the quinoline and isoquinoline transitions is appropriate. The small perturbation produced by the aza substitution permits the use of the same conventions applied to naphthalene, *viz.*, 1L_a corresponds to $n \rightarrow n + 1$ and 1L_b to a state derived from $n \rightarrow n + 2$ and $n - 1 \rightarrow n + 1$. On this basis, the lowest transition in quinoline is labeled 1L_b (long-axis polarized) while the 1L_a is short-axis polarized. 1B_b is also long-axis polarized. The computed polarizations are consistent with those inferred from fluorescence polarization measurements.¹⁶ However, the calculations indicate that both 1L_a and 1L_b are nearly short-axis polarized in isoquinoline, but are directed $\sim 25^\circ$ from one another. 1B_b is again long-axis polarized. Zimmermann and Joop observed perpendicular polarization for 1B_b and the longest wavelength transition, as expected from our calculations. They also found the same polarization for 1L_b and the

O-O band of the 1L_a (for reasons given above we reverse their labeling) but on the basis of decreasing polarization in the vibronic region of 1L_a believed that 1L_a and 1L_b are not parallel. Our results are not in accord with the latter conclusion.

The success of the vector addition process in reproducing the full SCF-MO results can be understood by comparing the molecular orbitals of the parent species (α - or β -naphthol and quinoline or isoquinoline) with the quinolinols or isoquinolinols. If the corresponding parent orbitals (*e.g.*, the highest occupied) are added and renormalized, the resultant orbital closely resembles the SCF orbital of the derivative. Incidentally, it was not necessary to adjust the vector lengths in the manner Petruska has suggested for the naphthalene derivatives.¹⁵

It should be noted that the intensities of 1L_b transitions of 4-pyridinol, 4-, 5-, and 8-quinolinol, and 6-isoquinolinol are expected to be very weak because the spectroscopic moments tend to cancel.

Finally, the variation of the 1L_a and 1L_b order in the quinolinols related to α -naphthol indicates this ordering is sensitive to slight perturbations. The fluorescence quantum yields of 8-quinolinol derivatives vary with substituents.¹⁷ Some of the variation may be related to the inversion of the 1L_a - 1L_b order.

(16) H. Zimmermann and N. Joop, *Z. Elektrochem.*, **55**, 61 (1961).

(17) D. C. Bhatnagar and L. S. Forster, *Spectrochim. Acta*, **21**, 1803 (1965).

Estimations of the Dispersion and Polar Force Contributions to Heats of Immersion and Interaction Energies of Organic Molecules with Rutile and Graphon Surfaces

by J. A. Lavelle and A. C. Zettlemoyer

Center for Surface and Coatings Research, Lehigh University, Bethlehem, Pennsylvania
(Received August 23, 1966)

The theory of additivity of intermolecular forces as proposed by Fowkes has been applied to studies of the heats of immersionsal wetting of rutile and Graphon in organic liquids of varying polarity. For Graphon the average dispersion force contribution to the heat of immersion (h_i^d) in a series of *n*-butyl derivatives was calculated to be 110 ergs/cm². Dispersion forces alone are sufficient to account for the heat liberated in forming the Graphon-organic liquid interface. For rutile, h_i^d was calculated to be 146 ergs/cm², but this value includes a minor contribution due to polarization of the liquid by the electrostatic field of the solid. The average electrostatic force field extending from the rutile surface was calculated to be 2.72×10^5 esu/cm² in good agreement with previously reported values. For butanol and heptane on Graphon, the interaction energy was calculated to be due entirely to dispersion forces. Approximately 70% of the interaction energy for heptane on rutile was calculated to be due to dispersion forces and 30% due to polarization of the hydrocarbon by the rutile. For butanol on rutile, the major contribution to the adsorption energy is due to dipole-dipole interactions. The contribution due to hydrogen bonding of butanol with rutile is estimated to be less than 10% of the total interaction energy.

Introduction

The heats of immersion of rutile and Graphon in organic liquids have been reported.^{1,2} For a series of *n*-butyl derivatives, the heats of immersion with rutile were shown to be an approximate linear function of the dipole moment of the wetting liquid.² For a polar solid interacting with a polar molecule, a major contribution to the total energy of interaction is due to the interaction of the dipole of the wetting liquid molecules with the electrostatic field of the solid as given by the equation

$$E_\mu = -\mu F \quad (1)$$

where E_μ is the interaction energy between the permanent dipole of the liquid and the electrostatic field of the solid surface, μ is the dipole moment of the adsorbate and, F is the average electrostatic field of the solid.

Zettlemoyer, *et al.*,² assumed that contributions from the London dispersion forces to the net energy of adsorption were approximately constant. They attributed differences in heat of immersion values primarily to E_μ . The slope of the linear plot of net energy of interaction *vs.* dipole moment was taken to be a first approximation of the average electrostatic field strength of the rutile surface. This approach for obtaining F has been critically assessed in this laboratory.³

Based on the theory of the additivity of intermolecular forces, Fowkes has recently developed an approach for estimating the dispersion force contribution to

(1) F. H. Healey, J. J. Chessick, A. C. Zettlemoyer, and G. J. Young, *J. Phys. Chem.*, **58**, 887 (1954).

(2) J. J. Chessick, A. C. Zettlemoyer, F. H. Healey, and G. J. Young, *Can. J. Chem.*, **33**, 251 (1955).

(3) J. J. Chessick, *J. Phys. Chem.*, **66**, 762 (1962).

heats of immersion.^{4,5} This theory suggests a method of checking the assumption that the dispersion force contribution was indeed constant for the systems rutile-organic liquids.

Application of Theory

Assuming the additivity of intermolecular forces, the experimentally determined heats of immersional wetting per unit area can be expressed as the sum of the dispersion force contribution (h_i^d), a polarization force contribution (h_i^α), and a contribution due to the interaction of the permanent dipole with the solid (h_i^μ)

$$h_i = h_i^d + h_i^\alpha + h_i^\mu \quad (2)$$

The dispersion force contribution to heats of immersion is given by Fowkes⁵ as

$$h_i^d = \gamma_L - 2\sqrt{\gamma_s^d \gamma_L^d} - T \left[\frac{d\gamma_L}{dT} - 2\sqrt{\gamma_L^d} \frac{d\sqrt{\gamma_s^d}}{dT} - 2\sqrt{\gamma_s^d} \frac{d\sqrt{\gamma_L^d}}{dT} \right] \quad (3)$$

γ_L^d , the dispersion force component of the surface tension of the liquid, was taken to be equal to γ_L , the surface tension of the liquid. This assumption is not unreasonable since Fowkes has calculated γ_L^d values from contact angles and found for some polar organic molecules, such as bromonaphthalene, that the values are not too different from γ_L .⁵ The term γ_s^d is the dispersion force component of the surface free energy of the solid. The temperature dependence of γ_s^d was estimated from the coefficient of thermal expansion using the relation that the surface tension increases as the $2/3$ power of the density. Thus $d\sqrt{\gamma_s^d}/dT$ is very small and generally amounts to about 2% of the total heat of immersion. The term γ_s^d for Graphon is given by Fowkes as 108 ergs/cm² and for rutile as 143 ergs/cm².⁵ All of the values needed for solving eq 3 for the dispersion force contribution to the heat of immersion are therefore available.

It is important to note that the γ_s^d value for rutile as reported by Fowkes was obtained from heats of immersion with hydrocarbons and contains the contribution due to polarization of the liquids by the rutile surface. Heats of immersion calculated by eq 3, therefore, give values representing both the dispersion and polarization components of the heat of immersion, but as Fowkes points out,^{5,6} both the dispersion and polarization forces are proportional to the polarizability of the molecule and these two forces should be additive. Equation 2 may then be rewritten as

$$h_i = h_i^{d+\alpha} + h_i^\mu \quad (4)$$

where $h_i^{d+\alpha}$ is calculated from eq 3 neglecting any polarization contribution to γ_L^d .

Results

Tables I and II show the results of the calorimetrically determined heats of immersion of rutile and Graphon in organic liquids of varying polarity.¹ The calculated dispersion and polarization force component is given and the contributions due to permanent dipole interactions are obtained using eq 4.

Table I: van der Waals Components of the Heats of Immersional Wetting of Rutile (TiO₂) at 25° (ergs/cm²)

Liquid	h_i , measd	$h_i^{d+\alpha}$, calcd	h_i^μ , eq 4
Heptane	-144 ± 9	-144	0
Octane	-140 ± 5	-147	0
Butylamine	-330 ± 40	-145	-185
Butyl alcohol	-410 ± 1	-139	-271
Butyl chloride	-502 ± 8	-143	-359
Butyric acid	-506 ± 11	-143	-363
Nitropropane	-664 ± 6	-159 ^b	-505
Water ^a	-550 ± 18	-65	-485

^a $\gamma_L^d = 21.8$ for water, ref 4. ^b Calculated for nitromethane.

Table II: Comparison of Calculated and Measured Heats of Immersional Wetting of Graphon at 25° (ergs/cm²)

Liquid	h_i , measd	h_i^d , calcd
Heptane	-103 ± 3	-112
Butylamine	-106 ± 6	-112
Butyl alcohol	-114 ± 5	-107
Butyl chloride	-106 ± 2	-111
Butyric acid	-115 ± 1	-110
Water ^a	-32.2 ± 0.1	-34.0

^a $\gamma_L^d = 21.8$ ergs/cm².

Figure 1 is a plot of the net energy of adsorption ($h_i - h_L$) vs. the dipole moment of the wetting liquid. The experimental values and the calculated dispersion and polarization values are shown. It is significant to note that the slope of the line is unchanged after subtracting the dispersion and polarization force component from the net interaction energy. The average electrostatic field strength (F) of the rutile surface is

(4) F. M. Fowkes, *ASTM Tech. Publ.*, **360**, 20 (1963).

(5) F. M. Fowkes, *Ind. Eng. Chem.*, **56**, No. 12, 40 (1964).

(6) F. M. Fowkes, *Advances in Chemistry Series*, No. 43, American Chemical Society, Washington, D. C., 1964, p 99.

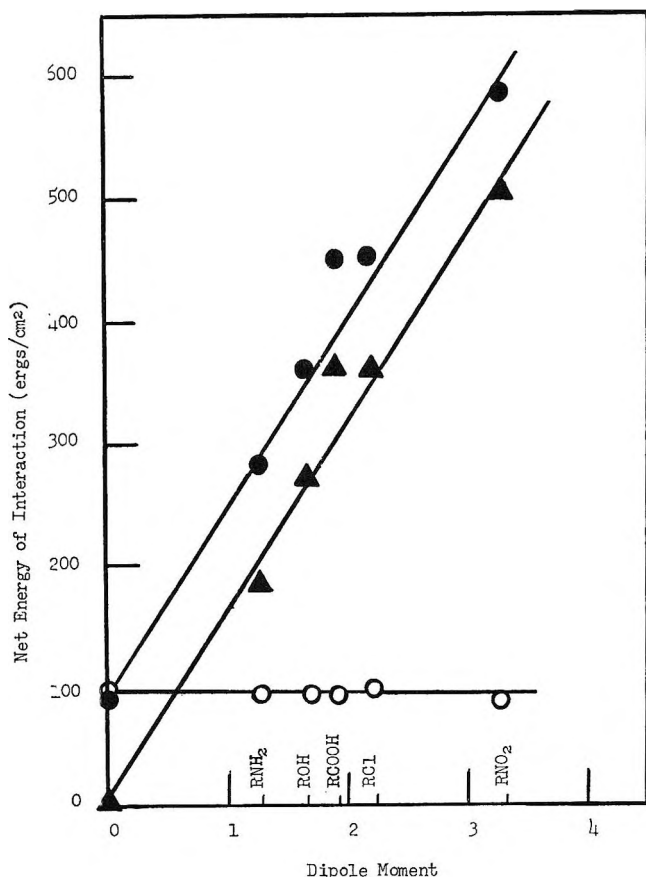


Figure 1. Polar and dispersion force components of the net interaction energy as a function of dipole moment of various polar molecules on rutile:

●, experimental; ▲, E_{μ} ; ○, $E_{\alpha} + E_{\alpha}$.

calculated to be 2.72×10^5 esu/cm² as previously determined by Zettlemoyer² and estimated by de Boer.⁷

The Contributions of van der Waals Forces to the Adsorption Energy

With the assumption that vertical, lateral, and other internal interactions of the molecules in the adsorbed state are the same as in the liquid state, the total energy of interaction between adsorbed polar molecules and a heteropolar surface is given by²

$$E_A - E_L = E_d + E_{\mu} + E_{\alpha} \quad (5)$$

where $E_A - E_L$ is the net integral energy of adsorption, E_d is the contribution due to London dispersion forces, E_{α} is the contribution due to polarization of the molecule by the field of the solid, and E_{μ} is defined by eq 1. The various expressions developed for these energies have been summarized by de Boer.⁷ The most useful forms of these equations for the purpose of this paper are

$$E_d = \frac{N_v \pi}{-4r_0^3} \alpha_1 \alpha_2 \frac{I_1 I_2}{I_1 + I_2} \quad (6)$$

$$E_{\mu} = -\mu F \quad (1)$$

$$E_{\alpha} = -\frac{\alpha_1 F^2}{2} \quad (7)$$

Since the calculated average electrostatic force field for rutile was found to be the same as that calculated by Zettlemoyer, values for E_{α} and E_{μ} are the same as previously reported. When the values of E_{α} are subtracted from $E_{d+\alpha}$ (obtained from $h_i^{d+\alpha} - h_L$), E_d values for rutile systems are obtained. There is no detectable electrostatic force field for Graphon; therefore, the E_d values may be calculated directly from h_i^d . Table III shows E_d values for Graphon in heptane and in butanol. These values were calculated by Zettlemoyer² by subtracting $E_{\alpha} + E_{\mu}$ from the net energy of adsorption. These values are compared with those obtained directly from calculated heats of immersion using the method of Fowkes. Considering the assumptions made, the agreement is quite good.

Table III: Comparison of Calculated Dispersion Energies for Heptane and *n*-Butyl Alcohol on Graphon (ergs/cm²)

System	Zettlemoyer, <i>et al.</i> ²	Method of Fowkes
Heptane on graphon	67	64
Butanol on graphon	66	68

Table IV shows the various calculated interaction energies for the rutile-heptane and rutile-butanol systems. For heptane on rutile, the quantity $E_{d+\alpha}$ obtained by the method of Fowkes is 95 ergs/cm². E_{α} , as calculated from eq 7, is 30 ergs/cm² and upon subtracting this quantity from $E_{d+\alpha}$, an E_d value of 65 ergs/cm² is obtained. This value compares favorably with the 62 ergs/cm² obtained by Zettlemoyer.²

For *n*-butyl alcohol on rutile, E_{μ} (obtained from $E_{NET} - E_{d+\alpha}$) is 271 ergs/cm². This result represents an energy liberation of 25 ergs/cm² in excess of that calculated from eq 1. This excess in the polar contribution is attributed to a hydrogen bonding interaction of the butanol with the rutile surface (E_{HB}). Based on this assumption, E_d has a value of 70 ergs/cm², which is consistent with the magnitude of the other E_d values. When 25 ergs/cm² is subtracted from E_d given by Zettlemoyer, who did not assess the hydrogen-bonding contribution, a value of 69 ergs/cm²

(7) J. H. de Boer, *Advan. Colloid Sci.*, **3**, 1 (1950).

Table IV: Comparison of Calculated Interaction Energies for Heptane and *n*-Butyl Alcohol on Rutile (ergs/cm²)

System	E_d	E_α	E_μ	E_{HB}	Method
Heptane on rutile	62	30	0	0	Zettlemoyer ²
Heptane on rutile	65	30	0	0	Fowkes
Butanol on rutile	94	21	246	0	Zettlemoyer
Butanol on rutile	69	21	246	25	Corrected for H bonding
Butanol on rutile	70	21	246	25	Fowkes

cm² is obtained for E_d . This result is in excellent agreement with our E_d value of 70 ergs/cm². When allowance is made for hydrogen bonding, better agreement of Zettlemoyer's original E_d value with the assumption that E_d is approximately constant is obtained. When 20–25 ergs/cm² as the hydrogen bonding contribution is subtracted from the E_μ values in Table I, the slope of the linear curve in Figure 1 is not significantly altered. In fact, it can be argued that this procedure gives a better fit for butanol and butyric acid.

From studies of water adsorption on high-area rutile (72 m²/g), Micale⁸ has estimated the minimum number of hydroxyl sites to be about 1×10^{14} sites/cm². The proposed mechanism for this adsorption is that one water molecule reacts with one oxygen atom on the rutile surface to give two hydroxyl sites. Thus the minimum number of oxygen sites per cm² of surface is about 5×10^{13} . Allowing 5 kcal/mole for the energy

liberated during the formation of a hydrogen bond at these sites, a value of 17 ergs/cm² is estimated for the minimum contribution of hydrogen bonding to the total interaction energy. This result is in the range of the value of 20–25 ergs/cm² that we suggest is involved in the interacting of butanol with rutile.

Heats of Immersion in Water

As shown in Table I, the polar contribution (h_i^d) to the heat of immersion of rutile in water is considerably higher than one would predict on the basis of its dipole moment. This result is strong evidence for the presence of an additional polar interaction between water and rutile most probably in the form of hydrogen bonding.

In Table II, the excellent agreement between measured and calculated heats of immersion for Graphon in water indicate that only dispersion force interactions are operative at this interface. Indirectly, then, the value of 21.8 ergs/cm² calculated by Fowkes⁵ as the dispersion component of the surface tension of water appears to be an excellent approximation.

Acknowledgment. The authors wish to express their appreciation to F. M. Fowkes for his aid in determining the temperature coefficient of γ_s^d for rutile and to the Technical Association of the Graphic Arts and the Litho Chemical and Supply Co. for their financial support in the form of the Thomas R. Caton Fellowship for J. A. L.

(8) F. J. Micale, Ph.D. Thesis, Lehigh University, 1965.

The Dialysis of Sodium Dodecyl Sulfate, Its Activity above the Critical Micelle Concentration, and the Phase-Separation Model of Micelle Formation¹

by Mohammad Abu-Hamdiyyah and Karol J. Mysels²

Department of Chemistry, University of Southern California, Los Angeles, California 90007
(Received September 6, 1966)

The phase-separation theory of micelle formation assumes that the activity of monomers becomes independent of concentration when micelles are present. Dialysis, however, continues at all concentrations though slower when micelles are present on both sides. Hence, activity increases with concentration and this increase can be accounted for on a simplified mass action model. The measurements were performed in a new kind of dialysis cell which permitted continuous monitoring of the composition of the dialyzate and a large number of separate kinetic experiments using the same membrane. Thus, the permeability of a particular membrane to various solutes could be studied, and, in particular, its permeability to micelles could be estimated using solubilized dye as a tracer.

It is generally agreed that micelles of surfactants are formed from monomeric molecules or ions above a certain rather well-defined critical micelle concentration (cmc). Below the cmc, the activity of the solute is to a good approximation similar to that of other low molecular mass molecules or ions, but above the cmc it certainly varies much less rapidly with concentration. This has led to the point of view that micelle formation is akin to a phase separation^{3,4} and to the proposal that the phenomenon can, and should, be treated as corresponding to zero change of the activity of monomers above the cmc. It has even been stated that the other approach which assumes a mass action equilibrium between micelles and monomers is incorrect.⁴ This phase-separation approach has the great merit of simplicity and has been supported by experimental results dealing with surface tension measurements,⁵ ultrafiltration,⁶ and dialysis.⁷

General arguments against the validity of the phase-separation approach and in favor of the mass action approximation have been given⁸⁻¹⁰ and will not be repeated. More recently, ultrafiltration experiments of Schott¹¹ on a purified nonionic surfactant showed that the monomer concentration—and therefore activity—increases significantly above the cmc. Surface tension measurements of Elworthy and Mysels¹⁰ show that if proper experimental precautions are taken, the ac-

tivity of sodium dodecyl sulfate clearly increases above the cmc band that this increase can be accounted for very well by a simplified mass action theory.¹² A preliminary report on dialysis experiments⁹ showed that dialysis continued above the cmc through a membrane impervious to micelles, which means that the activity of monomers continued to increase with concen-

(1) Based on part of the Ph.D. Thesis of M. Abu-Hamdiyyah, University of Southern California, Los Angeles, Calif., 1965.

(2) Research Department, R. J. Reynolds Tobacco Co., Winston-Salem, N. C. 27102.

(3) (a) G. Stainsby and A. E. Alexander, *Trans. Faraday Soc.*, **46**, 527 (1950); (b) K. Shinoda, *Bull. Chem. Soc. Japan*, **26**, 101 (1953); (c) K. Shinoda, T. Nakagawa, B. Tamamushi, and T. Isemura, "Colloidal Surfactants," Academic Press Inc., New York, N. Y., 1963, p. 6.

(4) E. Hutchinson, A. Inaba, and L. G. Bailey, *Z. Physik. Chem. (Frankfurt)*, **5**, 344 (1955).

(5) K. Shinoda and E. Hutchinson, *J. Phys. Chem.*, **66**, 577 (1962).

(6) E. Hutchinson, *Z. Physik. Chem. (Frankfurt)*, **21**, 38 (1959).

(7) J. T. Yang and J. F. Foster, *J. Phys. Chem.*, **57**, 628 (1953).

(8) P. Mukerjee, *ibid.*, **66**, 1375 (1962).

(9) K. J. Mysels, P. Mukerjee, and M. Abu-Hamdiyyah, *ibid.*, **67**, 1943 (1963).

(10) P. Elworthy and K. J. Mysels, *J. Colloid Interface Sci.*, **21**, 331 (1966).

(11) H. Schott, *J. Phys. Chem.*, **68**, 3612 (1964).

(12) (a) R. C. Murray, *Trans. Faraday Soc.*, **31**, 207 (1935); (b) K. J. Mysels, *J. Colloid Sci.*, **10**, 507 (1955); (c) P. Mukerjee, K. J. Mysels, and P. Kapauan, unpublished data.

tration. We are now reporting details of these and additional experiments along with a fuller interpretation confirming the original conclusion.

The first dialysis experiments⁷ on a surfactant suggested that the dialyzate and retentate did not reach the same concentration. This result was criticized¹³ as being due to impurities and indeed later experiments^{14,15} agree that equilibrium is reached more or less rapidly.^{15a} The authors of these later experiments suggest, however, that this is due to a slow permeation by micelles rather than to an activity gradient of monomers. In no case, however, has the permeability of the membranes to micelles been measured directly and only in one case¹⁵ could the same membrane be used for both pore size determinations and surfactant dialysis. The difficulty of repeatedly determining the concentration during an experiment in the conventional dialysis apparatus also limited the value of the kinetic data obtained.

Our results have been obtained using an apparatus which permitted the use of the same membrane through a long series of experiments. In fact, one of them was used intermittently for 3 years and showed no detectable change in permeability to either surfactant or dye during that time. (Another membrane was also used and gave very similar results.) The apparatus also permitted continuous monitoring of the concentration of the dialyzate during an experiment and good control over all experimental variables. The dye-tagging technique of Hoyer¹⁶ was used to study any transport of micelles through the membrane and showed, along with other evidence, that it was negligible.

We shall consider the theory involved in the dialysis experiments, then experimental tests of their validity, and finally the results obtained for sodium dodecyl sulfate or NaLS.

Experimental Section

Apparatus. The dialysis membrane was a section of Visking cellophane sausage casing $20/32$ in. flat width and about 10 cm long. After thorough washing, its ends were forced along with the platinum rings upon the Teflon cones as shown in Figure 1. The cones were then mounted on the central glass rod to give a rigid assembly. One of the cones was fixed by means of the screw cap in one arm of the glass cell. A screw plug in this cone also allowed filling and emptying the retentate without removing the assembly from the cell. The other arm of the cell had an opening for handling the dialyzate. In this arm there was also a small conductivity cell whose electrode seals served as the axis around which the cell was rocked at 1 cps by means of a string attached to the larger screw cap and to a motor-driven eccentric. This position of the elec-

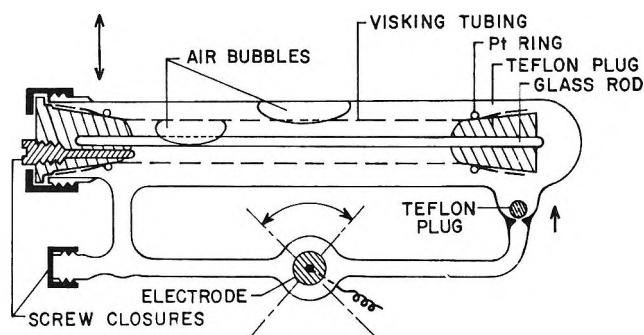


Figure 1. Dialysis cell permitting repeated use of same membrane and continuous conductometric monitoring of the dialyzate.

trodes minimized the strain on the wiring, despite the energetic mixing of both compartments. A Teflon sphere acted as a one-way valve in one of the connections between the two arms and ensured continuous and quite rapid circulation of the dialyzate between the two arms of the cell during the rocking motion. Concentration gradients within the dialyzate dissipated completely in less than 1 min.

The cell was mounted in an air bath maintained at $25 \pm 0.05^\circ$. Conductivity was determined using a precision bridge with an accuracy much exceeding our requirements. Conductance data were translated into concentration using previously obtained values^{17,18} for the same sample and several new points obtained in the dialysis cell.

Materials. Distilled water equilibrated with the laboratory air was used to minimize conductance fluctuations due to atmospheric CO_2 . Reagent grade chemicals, National Bureau of Standards standard sucrose, and a high-purity sample of NaLS previously described¹⁷ were used.

Two samples of Orange OT (1-*o*-tolylazo-2-naphthol) were used. One was a purified commercial sample and has been described earlier;¹⁷ the other was freshly synthesized and purified by reprecipitating twice from acetone with water (mp 131° , $\epsilon_{\text{max}} 1.91 \times 10^4$ independent of pH at λ 493–494 m μ). The optical density of

(13) K. J. Mysels in discussion of ref 7.

(14) B. S. Harrap and I. J. O'Donnel, *J. Phys. Chem.*, **58**, 1097 (1954).

(15) H. B. Klevens and C. W. Carr, *ibid.*, **60**, 1245 (1956).

(15a) NOTE ADDED IN PROOF. However, G. Bobalek and E. G. Bell, *Offic. Dig. Federation Soc. Paint Technol.*, **35**, 423 (1963), support ref 7.

(16) H. W. Hoyer and K. J. Mysels, *J. Phys. Colloid Chem.*, **54**, 966 (1950); H. W. Hoyer, K. J. Mysels, and D. Stigter, *J. Phys. Chem.*, **58**, 385 (1954).

(17) K. J. Mysels and R. J. Otter, *J. Colloid Sci.*, **16**, 462 (1961).

(18) R. J. Williams, J. N. Phillips, and K. J. Mysels, *Trans. Faraday Soc.*, **51**, 728 (1955).

saturated aqueous solutions of the two dye samples was undetectable in 1-cm cells and amounted to 0.002 in a 10-cm cell. Assuming that molar absorptivity is the same as in acetone solutions, this corresponds to a solubility of about $1 \times 10^{-7} M$ or 0.03 mg/l., which is several times lower than some earlier reports¹⁹ but in agreement with the value found previously in this laboratory.¹⁷ A Carey Model 11 spectrophotometer was used in this last determination.

Procedure. In experiments with solubilized dye, the concentration of the dye varied between 40 and 70% of saturation. These solutions were prepared by gently shaking part of an NaLS solution with excess dye for several hours, filtering through Whatman No. 41 filter paper, diluting with the same NaLS solution, and shaking for several hours to dissolve any remaining dye particles. The optical density was determined in a Beckman DU spectrophotometer at 494 or 498 m μ , which corresponds to the maximum of the new and old dye samples, respectively. Preliminary tests showed that in neither case (contrary to previous indications²⁰) was the result dependent on pH and no acid was added prior to the measurement. The samples were withdrawn from and then returned as promptly and as completely as possible to the dialyzate compartment of the cell.

In the dialysis of sucrose, very small samples were withdrawn, and their concentration was determined using a Bryce²¹ type of differential refractometer.

Except for special experiments, a standardized procedure was followed, namely, through rinsing of both compartments, draining, and then introducing 6 ml of solution into the casing and 23 ml into the other compartment of the cell. A syringe with a thin Teflon tubing attached to the needle was used to introduce and withdraw solution from the casing through the narrow opening in the Teflon cone without danger of damaging the casing. The exact values of volumes used were determined by weighing the cell and, where needed, the results corrected for small deviations.

Theory

Dialysis of Monomer. Experimentally, we can measure C , the concentration of the dialyzate as a function of time t . We can also determine the initial volumes V_i and V_d and concentrations C_i^0 and C^0 of the retentate (inside) and the dialyzate (outside) the membrane. Assuming that these volumes remain constant during the experiment, conservation of mass gives the difference of concentrations ΔC between the two compartments as

$$\Delta C/V_d = (C_i^0/V_d) + (C^0/V_i) - \alpha C \quad (1)$$

where

$$\alpha = (V_i + V_d)/V_i V_d \quad (2)$$

At equilibrium $\Delta C = 0$, and both compartments have a concentration C_{eq} given by

$$\alpha C_{eq} = (C_i^0/V_d) + (C^0/V_i) \quad (3)$$

With the usual assumptions of irreversible thermodynamics²² about linear coupled flows, we can write for our system

$$J_i = L_{i1}F_1 + L_{i2}F_2 + L_{i3}F_3 \quad (4)$$

where $i = 1, 2$, and 3 for the anion, cation, and water respectively, F_i are the forces exerted on species i , and the phenomenological coefficients L_{ij} obey Onsager's relations $L_{ij} = L_{ji}$. We now assume that the transport of ions is not affected by the transport of water, *i.e.* $L_{i3} = 0$; that the gradient of electrochemical potential is the only driving force, *i.e.*, that the pressure difference between the two sides of the membrane is negligible; and that the charges on the membrane have a negligible effect; *i.e.*, the concentration of anions and cations is equal to every point in the membrane. In view of electroneutrality, the membrane potential can then be eliminated to give

$$J = \frac{(L_{11}L_{22} - L_{12}^2)}{(L_{11} + L_{22} - 2L_{12})} \left[\frac{d\mu_1}{dx} + \frac{d\mu_2}{dx} \right] \quad (5)$$

We further assume that the solution is sufficiently dilute so that the only interaction between the flows of ions is due to electroneutrality, hence $L_{12} = 0$. Introducing the values of $L_{ii} = u_i C_i$ (where u is the mobility and C the concentration of our 1-1 electrolyte), of $d\mu_i = RT \ln a_i$, and of $d\mu_1 + d\mu_2 = RT \ln a_{\pm}$ gives

$$J = 2URTC \, d \ln a_{\pm}/dx = 2URT(dC/dx)(d \ln a_{\pm}/d \ln C) = D \, dC/dx \quad (6)$$

where the reduced mobility $U = u_1 u_2 / (u_1 + u_2)$ and D is by definition the diffusion coefficient. Thus $D = D_{ideal} \, d \ln a_{\pm}/d \ln C$ where $D_{ideal} = 2RTU$.

Since we are dealing with ϵ membrane whose accessible cross section A is unknown, we can only measure experimentally the permeation $P = AJ$. Furthermore, the membrane and its stagnant layers represent a

(19) I. M. Kolthoff and W. F. Graydon, *J. Phys. Chem.*, **55**, 699 (1951); M. W. Rigg and F. W. Liu, *J. Am. Oil Chemists' Soc.*, **30**, 14 (1953).

(20) D. Stigter, R. J. Williams, and K. J. Mysels, *J. Phys. Chem.*, **59**, 330 (1955).

(21) B. Brice and M. Halwer, *J. Opt. Soc. Am.*, **41**, 1033 (1951).

(22) I. Prigogine, "Thermodynamics of Irreversible Processes," C. C. Thomas, Springfield, Ill., 1955, p. 40.

system of unknown thickness Δx within which concentration gradients are unknown but have to sustain a constant permeation. However, the over-all concentration difference ΔC can be determined. The experimentally accessible permeation corresponds therefore not to the differential diffusion coefficient D as derived above, but to a semiintegral diffusion coefficient D' which is a weighted average of D over ΔC . Hence

$$dC/dt = P/V_0 = AJ/V_0 = (AD'/V_0)\Delta C/\Delta x \quad (7)$$

Introducing the expression obtained earlier for ΔC , this equation can be integrated if one makes the approximation that D' remains constant, which is often reasonable because the two concentrations change in opposite direction so that the center of the ΔC range involved in the averaging of D remains fixed. In other words, there is always a point in the membrane where $C = C_{eq}$. This gives, after introducing the initial conditions

$$(2.3/\alpha) \log [(C_{eq} - C)/(C_{eq} - C_i^0)] = (A/\Delta x)D't \quad (8)$$

In this equation, the left side contains only measurable quantities, the right-hand side the duration of the experiment t , the unknown ratio of membrane dimensions $(A/\Delta x)$ which has been assumed to be constant, and D' . Hence, if the experiment conforms to the above reasoning and assumptions, a semilogarithmic plot of $(C_{eq} - C)/(C_{eq} - C_i^0)$ vs. t should give a straight line. The slope of this line $k = (\alpha A/2.3\Delta x)D'$ is a measure of the rate of dialysis and, as long as $A/\Delta x$ and α remain constant, is proportional to D' . This should be the case for any given substance provided experimental conditions remain constant.

Dialysis of Tracer Dye. We now consider an experiment in which both compartments contain the same concentration of micelles C_m , but one side contains initially also some dye whose concentrations will be denoted by c . The dye is mainly solubilized by the micelles, but a small fraction will be present "free" in simple solution in water. The equilibrium between these two fractions can be advantageously described in terms of a partition coefficient r between the "micellar" and aqueous "phases." In view of the very small amount of dye present, we can make the approximation that this partition coefficient is independent of dye concentration and also that the presence of dye does not cause any net dialysis of micelles (or that if it does this has no effect upon the dialysis of the dye). The fact that the solubility of the dye increases linearly with concentration¹⁸ indicates also that the partition coefficient is independent of total concentration of micelles. Hence

$$c_w/(c_m/C_m) = r; \quad c_m + c_w = c \quad (9)$$

if we denote by c_m and c_w the amount of solubilized and of free dye per milliliter of solution. This gives

$$c = c_m(1 + r/C_m) \approx c_m \quad (10)$$

where the approximation is justified if the dye is sufficiently water-insoluble to give a very small r ($\approx 10^{-5}$ equiv/l. in our case) and the concentration of micelles is not too low.

It is then easy to show by following the reasoning of the preceding section that if the dye has an over-all (total) diffusion coefficient D'_t in the membrane, one can experimentally measure an over-all rate of dye dialysis k_t by measuring dye concentration as a function of time according to the equivalent of eq 8

$$\log [(c_{eq} - c)/(c_{eq} - c_i^0)] = (\alpha A_t/2.3\Delta x)D'_t t = k_t t \quad (11)$$

As the dye may cross the membrane in one of two states, solubilized or free, we may assign two separate diffusion coefficients, D_m and D_w , to these two modes of transport. The problem is to separate the two, since D_m is an indication of the permeability of the membrane to micelles.

The total flux of the dye is the sum of its fluxes in the two forms

$$J_t = J_m + J_w \quad (12)$$

and by definition

$$J_i = D_i dc_i/dx \quad (13)$$

Following the above reasoning, we obtain

$$dc/dt = (AD'_t/V_0)\Delta c_t/\Delta x = (A_m D'_m/V_0)\Delta c_m/\Delta x + (A_w D'_w/V_0)\Delta c_w/\Delta x \quad (14)$$

This equation is based on the assumption that whereas the thickness of the membrane and of its stagnant layer, Δx , is the same for free and solubilized dye, the effective cross section A may differ. In fact, because of the heterogeneity of the membrane and the great difference in size between the kinetic unit of solubilized and free dye, this difference may be expected to be much larger than that between their diffusion coefficients. Simplifying and introducing the values of c_m and c_w from (9) gives

$$A_t D'_t = A_m D'_m + (A_w D_w r)(1/C_m) \quad (15)$$

Equation 15 shows that one cannot separate the corresponding pairs of $A_i D'_i$ terms and that if these products for the solubilized and for the free dye are assumed to be constant, the product for the total transport must

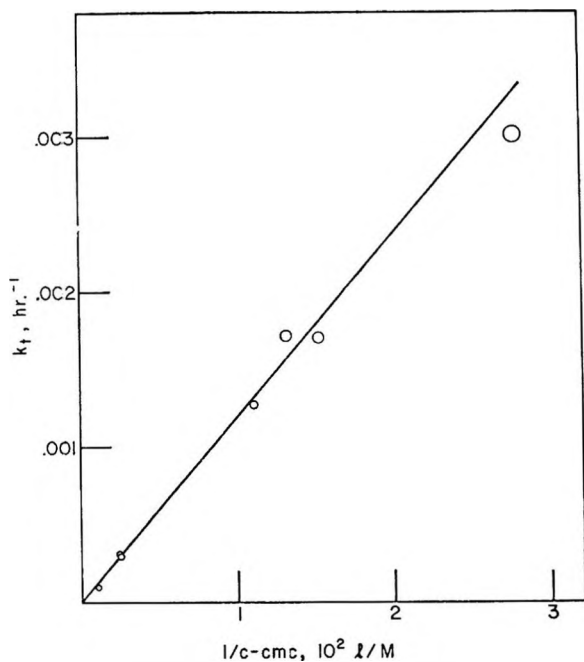


Figure 2. The total rate of dialysis of Orange OT as a function of concentration of sodium dodecyl sulfate at 25°.

vary with the concentration of micelles present during the experiment. This corresponds to the fact that as the concentration of micelles increases, the fraction of dye which is free decreases and so does the importance of its transport. In view of the assumption that Δx is the same, we can rewrite eq 15 as

$$k_t = k_m + k_w r / C_m \quad (16)$$

which shows that a plot of the experimentally measured over-all rate of dye dialysis *vs.* the inverse of the concentration of micelles should give a straight line. Its intercept gives the rate of dialysis of solubilized dye, its slope that of the free dye times the distribution ratio r . Figure 2 shows that the experimental points indeed define a line with a very small intercept. A least-squares calculation of the intercept from this plot over-emphasizes the points at low C_m . It is, therefore, better to rearrange eq 16 into

$$k_t C_m = k_m C_m + k_w r \quad (17)$$

and to calculate the slope of the straight line thus defined. We thus find $k_m = 3.6 (\pm 3.3) \times 10^{-4} \text{ hr}^{-1}$ which will be compared later to $k \approx 1.6 \times 10^{-2}$ for NaLS above the cmc.

The slope of the line of Figure 2 is $1.1 \times 10^{-4} \text{ l./equiv hr}$. The value of r can be estimated from the findings of Williams, *et al.*,¹⁸ that the optical density of saturated Orange OT in NaLS is given by $6.00(C - \text{cmc})$

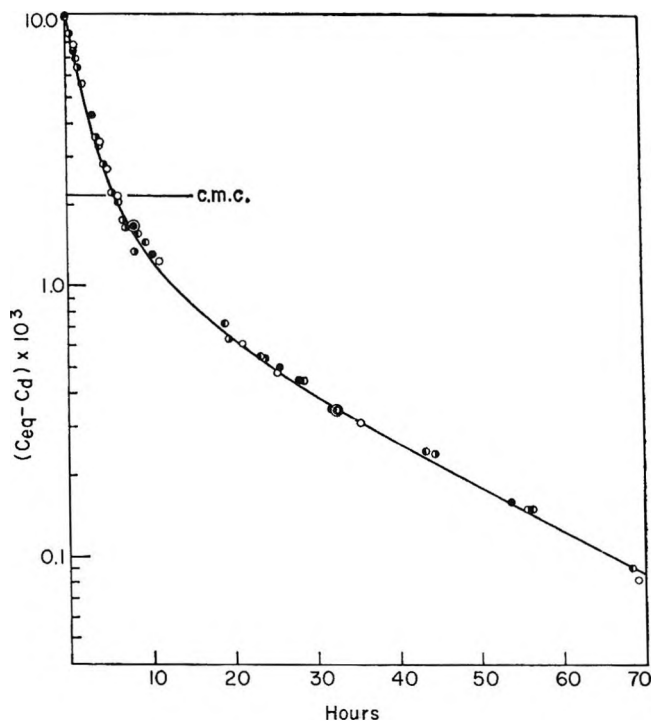


Figure 3. Dialysis of solutions initially at $6 \times \text{cmc}$ against water showing continuous change of rate in the cmc region, continuation of dialysis when both sides are above the cmc, and reproducibility of the measurements: taut membrane, \bullet ; slack membrane, \circ ; normal membrane, \circ ; second membrane, \bullet .

g/cm 100 ml, *i.e.*, 173 equiv/cm l. We have found the optical density of water saturated with Orange OT to be 0.002 cm^{-1} ; hence, if we assume that the molar absorptivity of the dye does not vary much between the solvents, $r = 1.15 \times 10^{-5} \text{ equiv/l}$. Hence, k_w for Orange OT is approximately 1.0 hr^{-1} , which is the value used later in discussing the permeability of the membrane to various solutes.

Results

Validity of the Method. In discussing the theory, a number of assumptions were made which can be checked experimentally. Among these were that the total effects upon the rate of dialysis of the initial volumes were properly taken into account by conservation-of-mass eq 1. In fact, second-order effects were present, but they were small as a 25% change in V_d and a 15% change in V_i produced 1.6 and 2.8% changes in D' (eq 8), respectively. In all experiments, these volumes were kept within 1.5% of 23.0 and 6.0 ml and were corrected for in calculating k when needed. Hence, this assumption seems well justified.

Another assumption is that hydrostatic pressure produced by osmotic flow during dialysis has no effect of

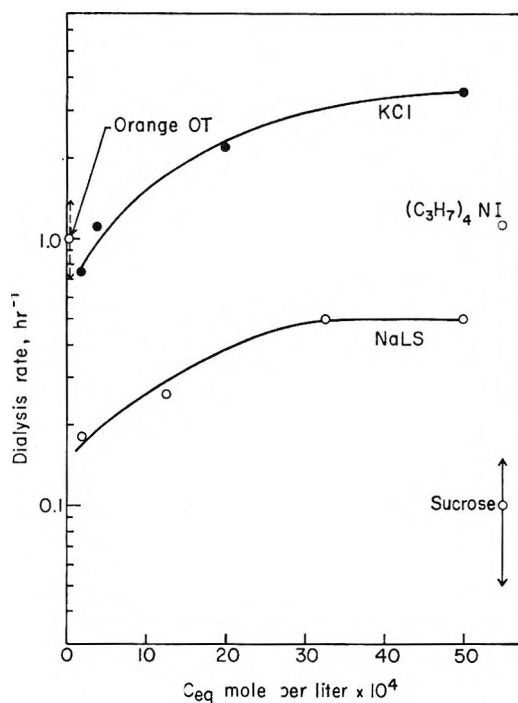


Figure 4. Effect of concentration and size upon the rate of dialysis through the same membrane at 25°.

the latter. As the dialysis tubing normally has a considerable slack, a certain amount of osmotic flow can occur without changing the pressure within it. To test whether this was a critical factor, the tubing was made initially as taut as possible and as slack as possible in some experiments, but as shown in Figure 3 there was no detectable effect. As a further control, the size of the air bubble within the casing was observed from time to time as an indication of the pressure prevailing within the tubing. For the experiments reported, no significant changes were noted. In these experiments the initial concentration difference does not exceed $6 \times \text{cmc}$ and is often less. In one experiment in which a solution at $32 \times \text{cmc}$ was dialyzed against initially pure water, the situation was different, however. The air bubble decreased in size until it disappeared and the tubing bulged conspicuously. The rate of dialysis did not seem to be affected significantly until the disappearance of the bubble, which was a very different situation from the rest of the experiments. Incidentally, the properties of the membrane were not affected measurably by this mistreatment. Figure 3 also shows the over-all reproducibility of the measurements.

A further assumption is that electroneutrality is the only charge effect, *i.e.*, that the effect of charges in the membrane is swamped by the electrolyte concentration present as far as dialysis of *monomers* is concerned. (This last limitation is important as these same charges

may well be decisive in preventing the dialysis of micelles which are not only larger but also carry much higher charges.) To study the effect of membrane charges upon small particles, the dialysis of KCl and NaLS was measured as a function of concentration and that of tetra-*n*-butyl iodide and of sucrose was measured at one concentration. The results are shown in Figure 4. It may be seen that at higher dilutions dialysis is significantly slower but that the rate levels off at higher concentration and for NaLS becomes constant above 3×10^{-3} , which is about one-third of the cmc. Hence, no significant rate effect from this source is expected at the cmc or above.

If the membrane were homogeneous in pore size and presented the same effective cross section A to all small particles, the ratio of dialysis rates would be equal to the ratio of free diffusion coefficients once membrane-charge effects have been swamped. The free diffusion coefficients are known or can be calculated from limiting conductivities of the ions and show that this is not the case. The larger particles are slowed increasingly by the membrane. Taking KCl as the standard, the effect is 1.3 for tetrabutyl iodide, 2.8 for NaLS, and 16.5 for sucrose. The dialysis rate of Orange OT is much more uncertain but appears to be high in comparison with sucrose, suggesting the presence of an alternative transport mechanism for more hydrophobic particles.

This inhomogeneity of the membrane made it unpromising to attempt any calculation of absolute values of diffusion coefficients from our experiments by comparison with a standard.

An assumption which is not always expected to be valid is that of the constancy of $D' = [D_{\text{ideal}} d \ln a_{\pm} / d \ln c]_{\text{av}}$ over the span of concentrations involved in an experiment and therefore in the integration leading to eq 8. The differential term can be expected *a priori* to change as the cmc is crossed and this should result in a curve instead of a straight line after integration with a marked change in the cmc region. Figure 3 shows that this is indeed the case. On the other hand, as shown by Figure 5, excellent straight lines are obtained when the retentate and the dialyze both remain either above or below the cmc as equilibrium is approached. (This is also the case for the lower part of Figure 3.) Depending on the analytical precision, good to excellent straight lines could also be obtained for solubilized dye and for the other solutes as shown in Figure 6.

The Behavior of Sodium Dodecyl Sulfate. As pointed out in the preliminary communication,⁹ the curve of Figure 3 shows clearly that NaLS continues to dialyze, though at a reduced rate, after its concentration on both sides of the membrane is above the cmc, and the

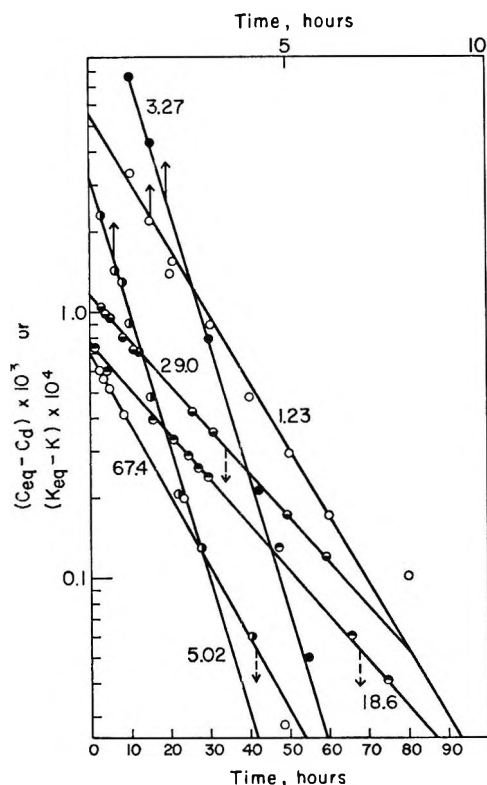


Figure 5. The dialysis of sodium dodecyl sulfate when both sides are either above or below the cmc and straight lines are obtained. Note large difference of time scales. The conductances are a linear function of concentration above the cmc and are plotted for this region. The numbers indicate C_{eq} in mmoles/l.

process continues until an equilibrium is reached. This equilibrium can be calculated from the initial conditions or measured after dialysis has proceeded long enough for the concentration not to change perceptibly further. Table I shows that the two values agree very well.

Table I: Dialysis of Sodium Dodecyl Sulfate at 25° (All Concentrations in mmoles/l.)

C_i^0	C^0	C_{eq}		Slope, hr^{-1}
		Exptl	Calcd	
1.00	0		0.20	0.18
5.95	0		1.26	0.26
16.25	0	3.27	3.32	0.50
24.75	0	5.01	5.02	0.50
48.00	0	9.82	9.82	0.0165
50.6	0	10.05	10.14	0.0165
16.06	8.03	9.70	9.75	0.034
31.98	15.99	18.40	18.64	0.0170
47.97	23.98	29.14	29.40	0.0164
80.16	64.02	67.72	67.72	0.027

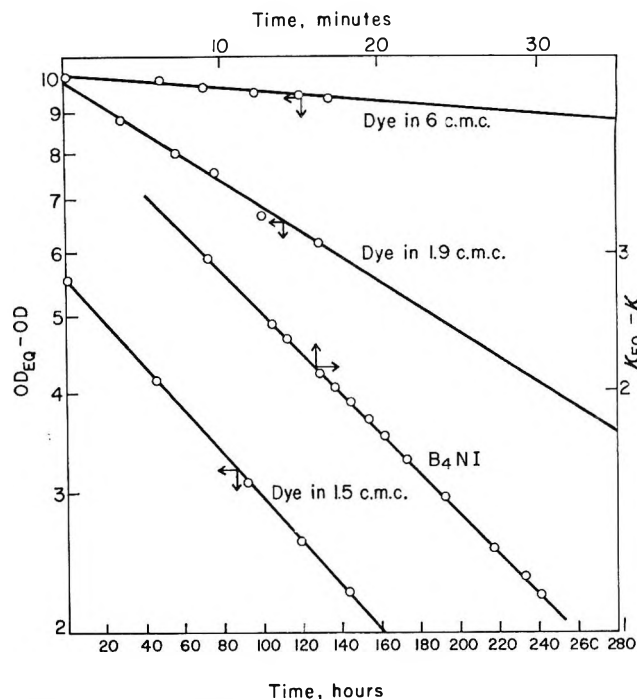


Figure 6. Dialysis of solubilized dye and of tetra-*n*-propyl iodide through the same membrane at 25°.

As pointed out above, when the points lie on a straight line extending to lowest concentrations, a meaningful dialysis rate is given by its slope and this is the case when both solutions are above or below the cmc. In the immediate neighborhood of the cmc, no straight line is obtained. Hence only the slopes, k , of such straight lines are listed in Table I.

Figure 7 shows these slopes and the range of concentrations over which they were obtained as a function of concentration. The slow increase at low concentrations which we attribute to swamping effects, the sudden change in the cmc region, and the low but clearly nonzero rates above the cmc, which increase at higher concentrations, are clearly seen.

Even the lowest of these rates, $164 \times 10^{-4} hr^{-1}$, is much larger than the rate k_m found above for the dialysis of dye solubilized within micelles, *i.e.*, $3.6 (\pm 3.3) \times 10^{-4} hr^{-1}$ which may, in fact, not differ significantly from zero. If it is really zero then, of course, our membrane was truly impervious to micelles and the observed rates are due to monomers alone. If the rate is nonzero, however, this could be due to the presence of some small but macroscopic leak in our system. In that case, the transport of dye would be an exact measure of the transport of any solute including untagged micelles and this would then be negligible. This type of leak is unlikely, however, because the transport of dye was exactly the same for a second piece of cello-

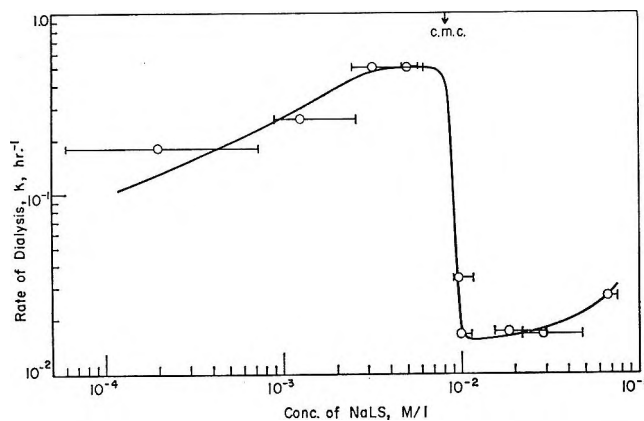


Figure 7. The rate of dialysis of sodium dodecyl sulfate as a function of concentration. Horizontal segments show the range of linear behavior leading to the rate shown.

phane tubing after the apparatus had been completely disassembled and reassembled again.

It is more likely, therefore, that the transport, if any, occurs through pores of molecular dimensions in the membrane. In this case, it is probable that untagged micelles will dialyze faster than the tagged ones and the question arises whether they could account for the observed transport. As is shown elsewhere,²³ the size distribution of the tagged micelles is very likely to be weighed toward large micelles according to the size; *i.e.*, their number distribution is equal to the weight distribution of the untagged ones. Thus, if the membrane permitted the passage of a micelle only $1/10$ as large as the average one, this size would be only $1/10$ as frequent among the tagged ones and the rate for the untagged ones would be ten times larger than measured by the dye technique. This is a rather extreme possibility, since a micelle of about seven monomers is highly unlikely, and still it would account for only a small part of the transport above the cmc.

A strong argument against any significant contribution by the small micelle lies in the fact that at highest concentrations the rate increases, whereas the proportion of the smaller micelles must decrease radically according to the law of mass action.

Thus it is likely that the permeability of our membrane to micelles was negligible and the observed transport is due entirely or predominantly to monomers (and any dimers²⁴ present). This is further supported by the semiquantitative explanation of the transport above the cmc using a simple mass action approach as shown below.

It should be noted, however, that whether transport by micelles is postulated or not, the complete and relatively rapid equilibration at all concentrations shows

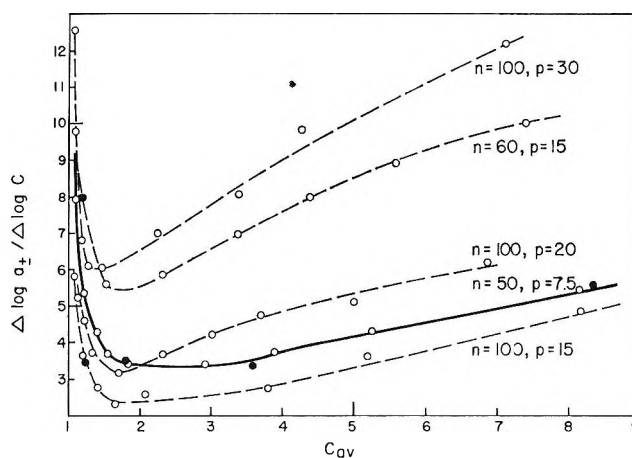


Figure 8. Comparison of averaged experimental value of $\phi = d \ln a_{\pm} / d \ln C$ with those calculated for several models of micelles: experimental, ●; calculated, ○; p from ref 12b has same meaning as s in text and in ref 12c.

clearly again that the chemical potential of NaLS continues to increase above the cmc at a significant rate. Solely monomeric transport permits, however, a more complete analysis and a test of that part of the phase separation theory which assumes⁵ that the activity of the monomers remains practically constant above the cmc.

The Activity Change above the Cmc. As shown above, the rate of dialysis is proportional to $D_{ideal} d \ln a_{\pm} / d \ln C$ averaged over the membrane thickness and if this is reasonably constant, the experimental points lie on a straight line in a semilogarithmic plot according to eq 8. Thus, the rates obtained from the straight lines under comparable conditions permit an intercomparison of these averages. If we define experimentally

$$\phi = k_{above\ cmc} / k_{just\ below\ cmc}$$

this should be also given by

$$\phi = (D_{ideal} d \ln a / d \ln C)_{above} / (D_{ideal} d \ln a_{\pm} / d \ln C)_{below}$$

If we assume transport by monomers only, the D_{ideal} term should cancel and any nonideality existing both just below and above the cmc (including contributions by dimers) will also cancel. Hence, ϕ will measure the change in the differential term due solely to the formation of micelles and to accompanying changes in ionic strength, etc. The solid points of Figure 8 show the experimental values of ϕ from our measurement.

(23) K. J. Mysals, unpublished data.

(24) P. Mukerjee, *J. Phys. Chem.*, **62**, 1404 (1958).

The lines of Figure 8 have been calculated on the assumption that the system is ideal, *i.e.*, neglecting ionic strength effects, etc., that the micelles are monodisperse and characterized by a degree of association n and an effective charge s which is constant but takes into account^{12c} all nonidealities of the system. Values previously computed^{12b} using a simple law of mass action approach have been utilized. The computed points are $\Delta \ln a_{\pm} / \Delta \ln C$ taken between the tabulated values and plotted at the midpoint of C . Thus, the averaging process is not necessarily analogous to the experimental one and may account for some of the discrepancies.

It may be noted that the calculated curves all show the rise at higher concentrations which is also shown by our experiment and corresponds to the double curvature of the activity-log C plot and of the experimental surface tension results.¹⁰ Over the range of parameters used, the curves differ markedly and the one for $n = 50$

and $s/n = 0.15$ comes closest to the experimental results. It does not seem likely that significantly better agreement can be obtained by other choice of the parameters and these are also reasonably close to, *e.g.*, $n = 62$ and an effective ionization of 0.17 obtained from light scattering.²⁵

Thus dialysis results are not only in disagreement with the phase separation theory, but are in fair agreement with values estimated using a highly simplified mass action approach. In view of the difficulty of comparing the theory with the experiment, the agreement may be as good as could be expected.

Acknowledgment. This work was supported in part by fellowships sponsored by the Continental Oil Co. and awarded to Mohammad Abu-Hamdiyyah.

(25) K. J. Mysels and L. H. Princen, *J. Phys. Chem.*, **63**, 1966 (1959).

Reactions of 40-kev Tritiated Ions with Solid Organic Compounds

by Sergio Ascoli, Fulvio Cacace, Giordano Giacomello, and Elvira Possagno

*Centro di Chimica delle Radiazioni del C.N.R., Istituto di Chimica Farmaceutica dell'Università, Rome, Italy
(Received September 27, 1966)*

The labeled products formed from the reactions of 40-kev tritiated ions with solid organic targets, such as sodium *m*-iodobenzoate, sodium phenylacetate, and sodium benzoate, have been determined. The results indicate that the radiochemical yield and the intramolecular tritium distribution correspond within the analytical errors with the values obtained in experiments involving the use of the much more energetic recoil tritons, as expected on the basis of the current theories on the "hot" chemistry of tritium. In addition, it has been experimentally demonstrated that mono- and polyatomic tritiated ions react with a given target to give the same products, a result consistent with the view that high-energy polyatomic species dissociate into the constituent atoms in their initial collisions with the target molecules, before their energy is sufficiently lowered to make the formation of stable products possible.

Introduction

Most of the investigations in the field of "hot" chemistry so far have been carried out using nuclear reactions as a source of the high-energy species.

In 1954, Croatto and Giacomello¹ described a different approach, subsequently employed by a number of other workers,²⁻⁷ based on the use of radioactive ions accelerated with an energy of a few tens kev against solid targets.

This "beam technique," while similar to recoil methods as to the kinetics, analytical procedures, and limitations, offers, in principle, two advantages: the possibility to vary over a rather extended range the energy of the "hot" species and to reduce the radiation damage to the target, eliminating the unwanted effects of the extraneous radiations invariably associated with the nuclear production of "hot" atoms.

According to the prevailing theories,⁸ no significant difference should exist between the chemical reactivity of a "hot atom" produced by nuclear means, with an energy up to several Mev, and the corresponding ion electrically accelerated to several tens kev. In fact, both the recoil "atom" and the ion must collide many times with the target molecules before their energy is sufficiently lowered to make the formation of chemical bonds possible. In the slowing down process, both the reactive species necessarily cross the same energy region

and therefore the charge-exchange processes should play the same role in both cases.

Therefore, independently of the efficiency of such charge-exchange processes,⁸ one should expect that both recoil tritons and electrically accelerated ions are in the same charge state when they reach the energy region where they can undergo combination, through reactions whose study is the objective of "hot" chemistry.

From the generally accepted views on the chemically significant energy range and charge state, another consequence follows: polyatomic "hot" species, for instance T_2^+ or T_3^+ ions, should dissociate in their initial collisions with the molecules of a given target to give "hot" atomic species, whose reactions are expected to

(1) U. Croatto and G. Giacomello, *Atti del XLV Congresso della SIPS*, Naples, 1954.

(2) B. Aliprandi *et al.*, *Ric. Sci.*, **26**, 3029 (1956).

(3) B. Aliprandi and F. Cacace, *Ann. Chim. (Rome)*, **46**, 1204 (1956).

(4) B. Aliprandi *et al.*, "Radioisotopes in Scientific Research," Vol. 2, Pergamon Press Inc., New York, N. Y., 1958, p 146.

(5) F. Cacace, *et al.*, *Energia Nucleare*, **5**, 387 (1958).

(6) R. M. Lemmon, *et al.*, *J. Am. Chem. Soc.*, **78**, 6415 (1956).

(7) R. M. Lemmon, *et al.*, "Chemical Effect of Nuclear Transformations," Vol. 2, International Atomic Energy Agency, Vienna, 1961, p 27.

(8) R. Wolfgang, *Progr. Reaction Kinetics*, **3**, 106 (1965).

be identical with the reactions of monoatomic ions of equivalent energy.

No experimental evidence regarding the chemical equivalence of a recoil atom and the corresponding accelerated ion has been so far obtained, nor has the behavior of any polyatomic "hot" species been investigated. It was decided to undertake the comparative study of the reactions of recoil tritons, having a maximum energy of 2.7-Mev and 40-kev tritium-containing ions, such as T^+ and HT^+ , with the same solid targets, at carefully controlled levels of radiation damage.

The isotope separator recently built at Rome University^{9,10} was used as a source of accelerated ions.

Experimental Section

Materials. The inactive compounds used were reagent grade chemicals. The *m*-iodobenzoic acid was prepared from *m*-aminobenzoic acid¹¹ and crystallized from acetone to a melting point of 187°.

Tritium gas from C.E.A., France, was employed in the ion source of the isotope separator, neat and mixed with neon.

Irradiation. All of the acids were irradiated in the form of the corresponding sodium salt, owing to the necessity of using compounds of sufficiently low volatility.

The solid targets were prepared by evaporation of concentrated alcoholic solutions of sodium benzoate, sodium phenylacetate, and sodium *m*-iodobenzoate on metallic plates (approximately 10 × 25 cm), in such a way as to obtain a uniform layer about 1 mm thick.

The targets were thoroughly dried under vacuum before being mounted in the bombardment chamber of the isotope separator, on a support that could be rotated away from the ion beam at the beginning of the experiment during the necessary adjustments of the separator.

The tritiated ions were obtained from tritium gas or from appropriate tritium-neon and tritium-hydrogen mixtures.

In order to avoid an excessively concentrated beam and therefore locally intense radiation damage to the target, the beam was swept onto the target surface making use of a suitable modulation of the acceleration voltage.

The intensity of the beam was adjusted at the beginning of the irradiation and continuously monitored with a model 610 B Keitley electrometer. Typical current intensities ranged from 10^{-8} to 10^{-7} amp, with irradiation times from 2 to 60 min, the conditions chosen being, of course, a compromise between the need to introduce into the target an activity sufficient

for the subsequent analysis and the necessity to keep the radiation damage of the target surface at the lowest level.

Analysis of the Products

Purification. After the irradiation, the organic sample was recovered from the metallic support, the appropriate carriers were added, and the purification procedure was undertaken.

The benzoic, phenylacetic, and *m*-iodobenzoic acid sodium salts were dissolved in water, the solution was acidified, and the crude acids were repeatedly crystallized before being converted into the corresponding methyl esters with an excess of diazomethane in ether.

The esters were purified by preparative gas chromatography using a Fractovap Model B from Soc. Carlo Erba, Milan, equipped with stainless steel columns. The following conditions were chosen for the purification of the aromatic esters: methyl benzoate and methyl phenylacetate: 1-m long column, packed with Bentone 34 (25% w/w on Celite) at 160°; methyl *m*-iodobenzoate: 2-m long column, packed with sodium dodecyl benzyl sulfonate (25% w/w on Chromosorb) at 165°.

In order to avoid the mixing of the eluted fractions and their contamination with traces of the stationary phase, separate glass collection traps were directly inserted into the detector block of the gas chromatograph.¹² Helium was used as the carrier gas in all of the separations.

Intramolecular Tritium Distribution. The purified phenylacetic acid (I) was degraded with permanganate in alkaline solution to benzoic acid, which was in turn converted to the methyl ester with diazomethane and purified by preparative glpc (II). The difference between the molar activity of II and I gave the tritium content of the methylene positions.

The benzoic acid was nitrated with concentrated nitric acid at 20–30°. The *o*- and *m*-nitrobenzoic acids formed were converted to the corresponding methyl esters. They were separated and purified by preparative glpc using the sodium dodecyl benzyl sulfonate column at 190°. The molar activity of the *o*- and *m*-nitrobenzoates, subtracted from the molar activity of the methyl benzoate, gave the tritium content of the *ortho* and *meta* positions in the ring. Control experiments were undertaken when required to check that no signifi-

(9) S. Ascoli, *et al.*, *Ric. Sci.*, **35** (II-A), 15 (1965).

(10) S. Ascoli and F. Cacace, *Nucl. Instr. Methods*, **38**, 202 (1965).

(11) F. Cattelain, *Bull. Soc. Chim. France*, (4) **41**, 1547 (1913).

(12) B. Aliprandi, F. Cacace, and G. Ciranni, *Anal. Chem.*, **36**, 2445 (1964).

cant tritium exchange occurred in the degradation and purification procedures.

Tritium Activity Assay. The activity of the purified samples was determined according to the procedure described by Wilzbach.¹³ The samples were combusted over zinc and nickel oxide at 650°, obtaining a mixture of HT and CH₃T, whose activity was determined with a 250-ml ionization chamber connected to a Victoreen Model 475 A vibrating-reed electrometer. No difficulty was experienced in the quantitative combustion of the aromatic compounds analyzed according to Wilzbach's original procedure.

Results and Discussion

In order to verify through the analysis of the final products the identical nature of the reactions of two different "hot" species with the same target molecule, it is desirable to compare the absolute yields of all the labeled products formed and to determine the intramolecular distribution of the radioactive atoms within the major products.

Unfortunately, such a comparison is difficult in the present case, owing to the fact that the bombardments with accelerated ions are carried out at pressures of 10⁻⁵ torr and the volatile products are therefore likely to escape from the target, to be lost in the vacuum pumps of the isotope separator.

While a technique to trap and recover volatile products from the reaction of accelerated ions, using solid adsorbents and differential pumping has recently been described,¹⁴ the quantitative recovery of the HT, the main gaseous product, is quite difficult and requires the development of different and more elaborate irradiation facilities.

The comparison therefore had to be restricted to compounds of low volatility and the logical choice was to measure the radiochemical yield of the labeled parent molecule.

Again, the determination of the *absolute* yield of the products obtained from the bombardment of a solid target with tritiated ions is far from accurate, since the measurement of the ion current impinging on the target is affected by considerable errors, mainly associated with the emission of secondary electrons from the target surface.

It was therefore concluded that the *ratio of the yields* of the major reaction products, instead of the absolute yields, could afford a suitable criterion for a comparison between the reactions of nucleogenic and electrically accelerated tritons.

The results obtained are compared, in Tables I and II, with the corresponding values reported by White and Rowland¹⁵ and Elatrash and Johnsen¹⁶ in their study

of the interactions of recoil tritons with, respectively, *m*-iodobenzoic acid and phenylacetic acid.

Table I: Irradiation of *m*-Iodobenzoic Acid with Recoil and 40-keV ³H⁺ Ions

	2.73-MeV recoil tritons ^a	40-keV ³ H ⁺ ions ^b
Radiochemical yield ^c of the parent	0.36 ± 0.3	~30 ^d
Ratio of the benzoic and <i>m</i> -iodobenzoic acid yields	0.40	0.43 ± 0.02
Intramolecular tritium distribution in benzoic acid:		
<i>ortho</i> positions	2 ± 3	6.2 ± 2
<i>meta</i> positions	86 ± 3	32.5 ± 2
<i>para</i> position	12 ± 3	11.2 ± 4

^a Data from ref 15. ^b Irradiation of sodium *m*-iodobenzoate. ^c Fraction of the total tritium activity introduced into the system found in the parent molecule. ^d See text.

Table II: Irradiation of Phenylacetic Acid with Recoil Tritons and 40-keV Tritiated Ions

Intramolecular distribution	2.73-MeV recoil tritons ^a	40-keV T ⁺ ions ^b	40-keV HT ⁺ ions ^b
<i>ortho</i> positions	37.0	41.2 ± 3	33.8 ± 3
<i>meta</i> positions	37.6	36.8 ± 3	36.8 ± 3
<i>para</i> position	23.4	18.8 ± 5	25.9 ± 5
α position	2.0	3.6 ± 1	4.2 ± 2

^a Data calculated from ref 16 without taking into account the labile activity. The accuracy of the activity distribution is probably similar to that given in ref 15. ^b Irradiated as sodium phenyl acetate.

Table I shows that the ratios of the yields of the benzoic and *m*-iodobenzoic acids obtained, respectively, in the experiments with accelerated ions and recoil tritons are very close. Further, the intramolecular tritium distribution in the benzoic acid is practically identical, within the rather large experimental errors involved in this type of analysis.

The close correspondence between the tritium content in the *meta* positions of the labeled benzoic acids

(13) K. E. Wilzbach, *et al.*, *Science*, **118**, 522 (1953).

(14) J. M. Paulus and J. P. Adloff, *Radiochim. Acta.* **4**, 146 (1965).

(15) R. M. White and F. S. Rowland, *J. Am. Chem. Soc.*, **82**, 4713 (1960).

(16) A. M. Elatrash and R. H. Johnsen, "Chemical Effects of Nuclear Transformations," Vol. 2, International Atomic Energy Agency, Vienna, 1961, p 123.

obtained in both types of experiments seems particularly noticeable. In addition, the peculiar feature of the intramolecular distribution obtained from the recoil experiments, *i.e.*, the rather large percentage of activity contained *outside* the position originally occupied by the iodine atom, is faithfully reproduced.

This feature has been explained¹⁵ with the "hot" substitution of T for H at an adjacent ring position, followed by intramolecular hydrogen shift and displacement of the iodine atom, a mechanism that is likely to depend to a large extent on the energy of the tritium atoms responsible for the replacement reactions.

The similarity of the distribution obtained in the experiments carried out with 40-keV ions provides further evidence that the energy level of the species responsible for the substitution processes is the same in both cases.

As to the phenylacetic acid, Table II shows that there is a striking similarity (within the rather large experimental errors) in the intramolecular tritium distribution obtained with recoil tritons by Elatrash and Johnson¹⁶ and in the present irradiation with 40-keV T⁺ ions.

The irradiation of sodium phenylacetate with a biatomic "hot" species, *i.e.*, 40-keV HT⁺ ions, gave the distribution shown in the last column of Table II. A comparison with the second column of the same table shows that the intramolecular tritium distribution is reasonably close in experiments carried out with T⁺ and HT⁺ ions having the same energy.

The source of the discrepancies observed cannot, however, be safely traced to experimental errors only, and a more precise determination was therefore deemed necessary in order to establish on a firmer experimental

basis the equivalence of mono- and polyatomic accelerated ions.

Table III shows the results of such experiments carried out with 40-keV T⁺ and HT⁺ ions accelerated on a sodium benzoate target. A considerable effort was made to improve the accuracy of the analysis, essentially by increasing the activity contained in the labeled benzoic acid. This was achieved combining the irradiated targets from a large number of runs until a sufficient amount of crude material was obtained to

Table III: Irradiation of Sodium Benzoate with 40-keV T⁺ and HT⁺ Ions

Intramolecular distribution	40-keV T ⁺ ions	40-keV HT ⁺ ions
<i>ortho</i> positions	38.2 ± 2	39.0 ± 2
<i>meta</i> positions	32.4 ± 2	32.6 ± 2
<i>para</i> position	29.4 ± 2	28.4 ± 2

carry out the subsequent purification and degradation steps without the need to dilute the sample with inactive sodium benzoate. These improved experiments demonstrate beyond any doubt that both types of ions given an identical intramolecular distribution within the parent compound. As a whole, the present results indicate that radioactive ions accelerated at relatively low energy can afford a useful and versatile tool in the study of "hot" atom chemistry.

Acknowledgments. The authors are indebted to B. Aliprandi for the analysis of several irradiated samples and to D. Carrara for his skillful assistance.

Spectroscopic Moments and the Question of d-Orbital Participation in the Elements of Groups IV and VII

by W. Kenneth Musker and George B. Savitsky

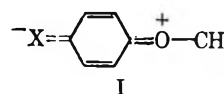
Department of Chemistry, University of California, Davis, California 95616 (Received March 8, 1966)

The question of d-orbital participation by $M(\text{CH}_3)_3$ groups ($M = \text{C, Si, Ge, Sn}$) and the halogens is discussed on the basis of an analysis of the change in intensity of the symmetry-forbidden $A_{1g} \rightarrow B_{2u}$ transition in the ultraviolet spectrum of benzene derivatives. The extent of overlap between the d orbitals of the group IV metals and the π orbital of the benzene ring in *para*-substituted anisoles appears to decrease in the series silicon > germanium > tin. The decrease in spectroscopic moment with increasing size of M which is observed for the group IV elements seems to parallel the trend observed in the group VII elements.

Introduction

The spectroscopic moment¹ of benzene substituents can be measured by an analysis of the change in intensity of the symmetry-forbidden $A_{1g} \rightarrow B_{2u}$ transition² which appears near 2600 Å in the ultraviolet absorption spectrum. The sign of the moment may be either positive or negative depending on whether the group is an electron donor or an electron acceptor by resonance interaction with the benzene ring. However, the sign of the moment of certain groups may be changed as a result of the donor or acceptor ability of another substituent in *para* position.

An inversion or change of sign of the moment of bromine and iodine was observed by Goodman and Frolen³ in a study of *p*-haloanisoles. In monosubstituted benzenes, bromine and iodine have positive spectroscopic moments indicating that they are electron donors. However, the oscillator strength⁴ of *p*-bromo- and *p*-iodoanisoles was found to be smaller than the oscillator strength of anisole itself indicating that the bromo- and iodo-groups behaved as electron-withdrawing groups when a very strong donor such as the methoxy group was present in the *para* position. Consequently the sign of the spectroscopic moment of the halogens was inverted. This inversion was attributed to d-orbital participation by the halogens involving resonance structures of type I.



The oscillator strengths were estimated by these authors on the basis of the absorption maximum (ϵ_{max}) of these compounds in the 2600-Å region. Using this estimate the spectroscopic moment of chlorine appeared to be reduced to zero, but not inverted. However, a more accurate estimate of the oscillator strength was determined by one of us⁵ which was based on the integrated intensity of the absorption band. This method revealed that an actual inversion of the spectroscopic moment was observed for the chloro group. This can be seen from the results recorded in Table I which lists the ratio of the oscillator strength of the *p*-haloanisoles to that of anisole.

- (1) J. R. Platt, *J. Chem. Phys.*, **19**, 263 (1951).
- (2) A. L. Sklar, *ibid.*, **7**, 984 (1939); *ibid.*, **10**, 135 (1942).
- (3) L. Goodman and L. J. Frolen, *ibid.*, **30**, 1361 (1959).
- (4) The oscillator strength is related to the spectroscopic moment by the equation $|\vec{m}_x|^2 = m_x^2 = k(f_x - f_x^0)$ where \vec{m}_x is the spectroscopic moment of substituent x, f_x is the experimentally measured oscillator strength of the monosubstituted benzene, $\text{C}_6\text{H}_5\text{X}$, f_x^0 is the vibrational contribution to the oscillator strength, and k is a constant of proportionality.
- (5) G. B. Savitsky, "Some Studies on Spectroscopic Moments of Polysubstituted Benzene," University Microfilms, Ann Arbor, Mich., S.C. Card No. Mic. 59-6108.

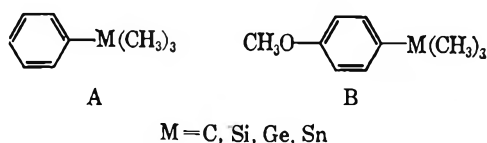
Table I: Ratio of the Oscillator Strength of *p*-Haloanisoles to Anisole

Group X	$\frac{f(p\text{-X-C}_6\text{H}_4\text{-OCH}_3)}{f(\text{C}_6\text{H}_5\text{OCH}_3)}$
F	1.58
Cl	0.92
Br	0.91
I	0.91 ^a

^a Corrected for the atomic absorption by iodine which also falls in the same region: T. M. Dunn and T. Iredale, *J. Chem. Soc.*, 1592 (1952).

Only in the case of the fluoro group is the ratio of intensities greater than unity. Therefore among the halogens only fluorine retains its positive spectroscopic moment in the presence of a strong donor in *para* position. This observation is consistent with the fact that there are no low-lying d orbitals available in fluorine which could interact with the benzene nucleus.

Recently, d-orbital participation in *p*-methoxyphenylsilane was observed by Goodman, Konstam, and Sommer⁶ and the theory of this interaction was thoroughly analyzed. The ratio of the intensity of the silane to that of anisole was found to be 0.89 which is of the same order of magnitude as the ratio of the halogen compounds. In this work the scope of d-orbital participation⁷ by the group IV elements has been examined by measuring the oscillator strength of two series of compounds.



Experimental Section

Materials. Most of the compounds used in this study were synthesized by modifications of reported procedures. Isolation and purification were accomplished by gas-liquid chromatography using a 3-ft silicone column. The appropriate fraction was collected and rechromatographed prior to ultraviolet analysis to ensure that decomposition had not occurred. All products were determined to be >99% pure by this technique. The infrared spectrum of all products was consistent with the structure of expected compounds.

Trimethylphenylsilane,^{8,9} n_{D}^{25} 1.4906, lit.,⁹ n_{D}^{20} 1.4880; trimethylphenyl germane, $n_{\text{D}}^{25.5}$ 1.5044, lit.,¹¹ n_{D}^{25} 1.5045; trimethylphenylstannane,¹⁰ n_{D}^{25} 1.5365, lit.,¹¹ n_{D}^{25} 1.5330; *p*-*t*-butylanisole, n_{D}^{28} 1.5002,

lit.,¹² n_{D}^{20} 1.5030; *p*-methoxyphenyltrimethylsilane,¹³ $n_{\text{D}}^{24.5}$ 1.5038, lit.,¹³ n_{D}^{13} 1.5073; *p*-methoxyphenyltrimethylstannane,¹⁴ $n_{\text{D}}^{25.5}$ 1.5385, lit.,¹⁴ n_{D}^{20} 1.5430; *m*-bistrimethylsilylbenzene,¹⁵ n_{D}^{25} 1.4870, lit.,¹⁵ n_{D}^{25} 1.4867.

***p*-Methoxyphenyltrimethylgermane.** The synthesis used for the germane was identical with the process used in the preparation of the corresponding stannane.¹⁴ Trimethylbromogermane was prepared according to the procedure of Dennis and Patnode¹⁶ from tetramethylgermane (City Chemical Corp., New York, N. Y.) and bromine. A solution of *p*-methoxyphenyllithium in diethyl ether was prepared¹⁷ and added slowly at room temperature to a solution of trimethylbromogermane in diethyl ether. After neutralization and ether extraction the *p*-methoxyphenyltrimethylgermane was collected, chromatographed, and analyzed, $n_{\text{D}}^{25.5}$ 1.5158. *Anal.* Calcd for $\text{C}_{13}\text{H}_{16}\text{OGe}$: C, 53.42; H, 7.17. Found: C, 53.66; H, 7.16.

Tris-1,3,5-trimethylsilylbenzene. This compound was prepared by a modification of the methods of Burkhard¹⁸ and of Clark¹⁵ for the preparation of bistrimethylsilyl-substituted benzenes.

1-Trimethylsilyl-3,5-dichlorobenzene, bp 117–123° (20 mm), was synthesized from 1-bromo-3,5-dichlorobenzene (K and K Laboratories) by preparing the Grignard reagent in diethyl ether and treating this intermediate with trimethylchlorosilane in the usual way. Further silylation was accomplished by treatment of 1-trimethylsilyl-3,5-dichlorobenzene with sodium and excess trimethylchlorosilane in refluxing toluene. After stirring for 5 hr the solution was filtered while hot and neutralized with 10% NH_4Cl . The toluene layer was separated and dried with sodium sulfate. The

(6) L. Goodman, A. H. Konstam, and L. H. Sommer, *J. Am. Chem. Soc.*, **87**, 1012 (1965).

(7) It is convenient to refer only to d-orbital participation; however, in heavier atoms other low-lying orbitals may be available for interaction with the benzenoid system.

(8) R. A. Benkeser and A. Torkelson, *J. Am. Chem. Soc.*, **75**, 1252 (1954).

(9) J. D. Roberts, E. A. McElhill, and R. Armstrong, *ibid.*, **71**, 2923 (1949).

(10) R. H. Bullard and W. B. Robinsor, *ibid.*, **49**, 1368 (1927).

(11) D. Seyferth and D. L. Alleston, *Inorg. Chem.*, **2**, 417 (1963).

(12) W. T. Olson, H. F. Hipsher, C. M. Buess, I. A. Goodman, I. Hart, J. H. Lamneck, Jr., and L. C. Gibbons, *J. Am. Chem. Soc.*, **69**, 2451 (1947).

(13) C. Eaborn, *J. Chem. Soc.*, 3148 (1953).

(14) O. Buchman, M. Grosjean, and N. Nasielski, *Bull. Soc. Chim. Belges*, **71**, 467 (1962).

(15) H. A. Clark, A. F. Gordon, C. W. Young, and M. J. Hunter, *J. Am. Chem. Soc.*, **73**, 3798 (1951).

(16) L. M. Dennis and W. I. Patnode, *ibid.*, **52**, 2779 (1930).

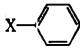
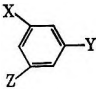
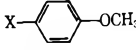
(17) H. Gilman and R. A. Benkeser, *ibid.*, **69**, 123 (1947).

(18) C. A. Burkhard, *ibid.*, **68**, 2103 (1946).

toluene was removed by means of a rotary evaporator and the residue was injected into the gas chromatograph. The major component was collected, rechromatographed, and analyzed. $n_{25.5D}^{25}$ 1.4834. *Anal.* Calcd for $C_{15}H_{30}Si_3$: C, 61.13; H, 10.26. Found: C, 62.16; H, 10.37. The infrared spectrum (liquid film) was consistent with the highly symmetrical structure expected for tris-1,3,5-trimethylsilylbenzene.

Spectral Measurements. The ultraviolet absorption spectra were obtained in cyclohexane solvent (Fisher Spectroquality) using a Cary Model 14 recording spectrophotometer. The spectrum obtained for each compound was replotted in wavenumbers (cm^{-1}) vs. absorbance and the area under the curve in the 38,500- cm^{-1} (2600-A) region was determined with a planimeter. There is some inaccuracy inherent in this treatment owing to the presence of a much stronger band at about 50,000 cm^{-1} (2000 A). The overlap between these bands was generally small and the tail of the 2600-A band could be extrapolated to zero absorbance. The shape of the curves for the series of *para*-substituted anisoles and for the series of monosubstituted derivatives are similar and the uncertainty within each of these series should be small. For this reason the ratio of the oscillator strength is generally discussed. In most compounds the λ_{0-0} band was well resolved and its position is reported in Table II.

Table II: Spectral Properties of Substituted Benzenes

	$f \times 10^3$	λ_{0-0} , cm^{-1}	$-\Delta\nu$, cm^{-1}
X = H	1.6 ^a	37,850 ^a	0
X = C(CH ₃) ₃	1.92 ^b	37,450 ^a	400 ^a
X = Si(CH ₃) ₃	3.32	36,970	880
X = Ge(CH ₃) ₃	3.42	37,740	110
X = Sn(CH ₃) ₃	2.85	37,690	260
			
X = Y = Z = Si(CH ₃) ₃	4.93	37,240 ^c	(610)
			
X = H	22.9	35,950	1900
X = C(CH ₃) ₃	23.2	35,310	2540
X = Si(CH ₃) ₃	18.3	35,590	2260
X = Ge(CH ₃) ₃	19.8	35,550	2300
X = Sn(CH ₃) ₃	23.1	35,510	2340

^a J. Petruska, *J. Chem. Phys.*, **34**, 1120 (1961). ^b Reference 5.

^c The reported value represents the maximum of the band envelope.

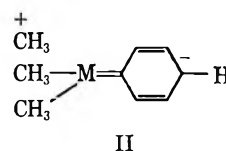
Results

Listed in Table III is the ratio of the oscillator strength of the 2600-A bands of *para*-substituted anisole derivatives to that of anisole. All of the group IV derivatives have an oscillator strength higher than that of benzene, and even if a correction for the vibra-

Table III: Ratio of the Oscillator Strength of *p*-Substituted Anisoles to Anisole

M	$\frac{f(\text{CH}_3\text{O}-\text{C}_6\text{H}_4-\text{M}(\text{CH}_3)_3)}{f(\text{CH}_3\text{O}-\text{C}_6\text{H}_5)}$
C	1.00
Si	0.80
Ge	0.86
Sn	1.00

tional contribution of the oscillator strength is made (see discussion below), a small, finite, spectroscopic moment is associated with these groups. If these compounds involve only hyperconjugative electron-donor structures of type II, then the moment can be assumed to have a positive sign. In *para*-substituted anisoles



the positive sign of the moment for all the elements of group VII is inverted except for fluorine; however, all of the elements in group IV show either a significant inversion or a reduction to zero. The extent of overlap between the d orbital of the metal and the π orbital of the benzene ring would be expected to decrease in the series silicon > germanium > tin. Therefore silicon should exhibit a higher negative moment than the rest of the group IV elements in the presence of a strong donor as observed in Table III. This would indicate that resonance structures of type I are decreasingly important in the series silicon > germanium > tin.

The trend of spectroscopic moment of the $M(\text{CH}_3)_3$ groups, where M = carbon, silicon, germanium, and tin, is of interest since apparently few systematic physical measurements related to the resonance parameters of these groups have been made. The oscillator strengths of phenyltrimethyl derivatives are listed in Table II.

These values are relatively small and seem to pass through a maximum at germanium. However, to

estimate that part of the oscillator strength which is associated with the actual spectroscopic moment, a vibrational contribution must be subtracted from the observed oscillator strength. These vibrational contributions for various groups are never known accurately, but they can be estimated from the oscillator strength of 1,3,5-trisubstituted benzenes. The oscillator strength of benzene is 1.6×10^{-3} and that for most 1,3,5-trisubstituted benzenes is from 2.0×10^{-3} to 2.1×10^{-3} indicating a negligible vibrational contribution of about 0.15×10^{-3} per substituent to the oscillator strength. However, for the *t*-butyl group the oscillator strength of the 1,3,5-trisubstituted benzene is significantly higher, amounting to 2.9×10^{-3} ¹⁹ and indicating a vibrational contribution of about 0.4×10^{-3} per *t*-butyl group to the oscillator strength.

We have prepared only one trisubstituted benzene, tris-1,3,5-trimethylsilylbenzene, and found that its oscillator strength is even higher (4.93×10^{-3}) than the *t*-butyl analog. This would indicate that the vibrational contribution amounts to about 1.1×10^{-3} per trimethylsilyl group. Thus the oscillator strengths corrected for the vibrational contribution of the *t*-butyl group and the trimethylsilyl group are about 0.9 and 0.6, respectively. If it is assumed that the vibrational contributions of the other $-M(\text{CH}_3)_3$ groups are similar to the silyl group or increase with an increase in the atomic weight of M, then the spectroscopic moments of the trimethylgermyl group be similar or slightly smaller than the trimethylsilyl

group and that of the trimethylstannyl group would be practically negligible.

The generally decreasing trend of the spectroscopic moment with an increasing size of the atom M, which is observed for the group IV elements, seems to parallel the trend observed in the group VII elements.

In Table III the maximum of the 0-0 band has been recorded as well as its frequency shift ($-\Delta\nu$) with respect to benzene. The red shift of this transition in substituted benzenes can be related to its intensification when there is constructive interference.^{6,19} However, when there is strong destructive interference the red shift-intensification rule will be violated.⁶ Although all of the *p*-substituted anisole derivatives exhibited a red shift with respect to anisole, this observation cannot be regarded as the most reliable criterion for d-orbital participation. The sign of the spectroscopic moment should be more definitive. The data on the methylated silanes reported here parallel the data reported by Goodman, Konstam, and Sommer⁶ for the simple silanes.

Acknowledgments. We thank Mr. E. M. Chen, Mr. J. Thomas, and Mr. L. A. Lafferty for synthesizing several of the compounds used in this study and for carrying out some of the spectroscopic measurements. We also thank the National Science Foundation (GP-5716) for support of part of this research.

(19) J. Petruska, *J. Chem. Phys.*, **34**, 1120 (1961).

Cation Exchange across Ion-Exchange Membranes

by A. S. Tombalakian,¹ C. Y. Yeh, and W. F. Graydon

Department of Chemical Engineering and Applied Chemistry, University of Toronto,
Toronto, Ontario, Canada (Received July 29, 1966)

A study of the exchange of inorganic cations of various valence for hydrogen ion has been made using polystyrenesulfonic acid ion-exchange membranes. The results indicate that the preference of the ion-exchange membrane for the various inorganic counterions increases with increasing valence and decreasing hydrated ionic size. A marked dependency of the selectivity coefficient on external solution concentration is noted only in the case of multivalent ions exchanging for hydrogen ion. From the ion-exchange equilibria data and cation-interchange fluxes obtained in counterdiffusion experiments across the same membrane, single-ion diffusion coefficients for the interdiffusing ion species in the membrane have been estimated using the Nernst-Planck equation. The dependence of the membrane interdiffusion coefficient on the ionic composition of the membrane for various ion pairs has been determined.

Introduction

Equilibria between synthetic ion exchangers and solutions of cations of various valence have been the subject of numerous investigations.²⁻¹⁰ A complete listing of these studies is given by Helfferich¹¹ in his comprehensive treatise on ion exchange. These studies of exchange equilibria with synthetic ion-exchange resins in granular form have revealed that the exchanging properties of a resin depend upon its macromolecular structure. The homogeneity of some of the ion-exchange resins used in these earlier investigations has been a matter of some doubt. Typical ion-exchange resins prepared by sulfonation of cross-linked resins, for example, contain sulfonate groups the environment of which differ markedly from that of other sulfonate groups. Ion-exchange resins of the polystyrenesulfonic acid type of improved homogeneity may be prepared by direct copolymerization of styrene, divinylbenzene, and the ester of *p*-styrenesulfonic acid. The ion-exchange behavior of such homogeneous ion-exchange membranes in solutions of cations of various valence is thus of interest.

The results of measurements of the selectivity of polystyrenesulfonic acid ion-exchange membranes for the exchange of inorganic cations of various valence for hydrogen ion are given in this report. The results are consistent with theoretical considerations of ion-exchange equilibria for synthetic ion-exchange resins.

The dependence of the ion diffusivities in the membrane on membrane properties and the interdiffusing ion species has been determined.

Experimental Section

(A) *Membranes.* Two polystyrenesulfonic acid ion-exchange membranes were prepared by the bulk copolymerization of the *n*-propyl ester of *p*-styrenesulfonic acid with styrene, divinylbenzene, and benzoyl peroxide as catalyst and subsequent hydrolysis in 5% caustic soda solution following the procedure described previously.¹²⁻¹⁴ Membranes one and two had a

(1) To whom correspondence should be addressed at Department of Chemistry and Engineering, Laurentian University, Sudbury, Ontario, Canada.

(2) T. R. E. Kressman and J. A. Kitchener, *J. Chem. Soc.*, 1190 (1949).

(3) T. R. E. Kressman and J. A. Kitchener, *ibid.*, 1201 (1949).

(4) D. Reichenberg, K. W. Pepper, and D. J. McCauley, *ibid.*, 493 (1951).

(5) H. P. Gregor, *J. Am. Chem. Soc.*, **73**, 642 (1951).

(6) H. P. Gregor, O. R. Abolafia, and M. H. Gottlieb, *J. Phys. Chem.*, **58**, 984 (1954).

(7) D. Reichenberg and D. J. McCauley, *J. Chem. Soc.*, 2741 (1955).

(8) G. E. Myers and G. E. Boyd, *J. Phys. Chem.*, **60**, 521 (1956).

(9) O. D. Bonner and L. L. Smith, *ibid.*, **61**, 326 (1957).

(10) H. C. Subba Rao and M. M. David, *A.I.Ch.E. J.*, **3**, 187 (1957).

(11) F. Helfferich, "Ion Exchange," McGraw-Hill Book Co., Inc., Toronto, 1962.

Table I: Separation Factors and Selectivity Coefficients for the Exchange of Various Cations for H⁺

Counterion	Membrane no.	Moisture content at 100% RH at 25°, moles of H ₂ O/equiv	Equiv ionic fraction of counterion in resin	Separation factor, α_B^A	Selectivity coeff, K_B^A
H	1	18.8			
	2	19.8			
Li	1	19.0	0.431		0.760
	2	20.0	0.421		0.729
Na	1	17.3	0.509		1.04
	2	18.7	0.507		1.02
K	1	16.2	0.554		1.21
	2	17.5	0.549		1.20
Cs	1	13.6	0.564		1.26
	2	15.0	0.560		1.25
Mg	1	12.0	0.878	7.22	0.825
	2	16.6			
Ca	1	11.3	0.892	8.26	1.03
	2	14.8			
Sr	1	10.3	0.910	10.1	1.31
	2	12.9			
Ba	1	9.2	0.926	12.5	1.71
	2	11.2			
Al	1	11.5	0.936	14.6	3.03
	2	14.5			

nominal cross linking of 4 mole % of DVB, an exchange capacity of 2.01 and 2.61 mequiv/g of dry resin H form, and a thickness of 0.0545 and 0.0670 ± 0.0002 cm, respectively.

(B) *Exchange Capacity.* Samples of the membranes in the hydrogen form were added to 50-ml portions of 0.1 N sodium chloride (or the salt of a different counterion) solution and the solution was titrated with 0.1 N sodium hydroxide using brom cresol green.

(C) *Ion-Exchange Equilibrium Determination.* Weighed samples of the membranes in the hydrogen form were equilibrated at 25° in solution containing hydrochloric acid and the salt of the counterion (LiCl, NaCl, KCl, CsCl, MgCl₂, Ca(NO₃)₂, SrCl₂, BaCl₂, and AlCl₃). After equilibration the membrane sample was removed from the solution and the solution analyzed for hydrochloric acid and chloride ion content by titration. The difference between these titration results gave the counterion content of the solution. The membrane sample was thoroughly rinsed with conductivity water and the hydrogen ion on the membrane determined as in the capacity determinations. The counterion on the membrane was calculated from the difference between the hydrogen ion on the membrane

and the capacity. There was no change in the capacity of a membrane sample after each ion-exchange equilibrium determination for the different ion-pair exchange systems investigated.

Results and Discussion

The equilibrium data obtained for the exchange of various univalent and divalent inorganic cations for hydrogen ion across two typical polystyrenesulfonic acid ion-exchange membranes are given in Table I. These measurements were made with solutions (0.1 N total solution concentration) containing the same number of equivalents of the two cation species. The separation factors, α_B^A , and molal selectivity coefficients, K_B^A , for the membranes were calculated from the experimental data using eq 1 and 2, respectively.

$$\alpha_B^A = \frac{\bar{X}_A X_B}{\bar{X}_B X_A} \quad (1)$$

(12) W. F. Graydon and R. J. Stewart, *J. Phys. Chem.*, **59**, 86 (1955).

(13) A. S. Tombalakian, H. J. Barton, and W. F. Graydon, *ibid.*, **66**, 1006 (1962).

(14) P. Rosenblum, A. S. Tombalakian, and W. F. Graydon, *J. Polymer Sci.*, **A1**, 1703 (1966).

$$K_B^A = \frac{\bar{M}_A^{Z_B} M_B^{Z_A}}{\bar{M}_B^{Z_A} M_A^{Z_B}} \quad (2)$$

where \bar{X} and X are the equivalent ionic fractions of the ion species in the membrane and external solution, respectively; \bar{M} and M are the molalities of the ion species in the membrane and external solution, respectively; and Z is the valence of the ion species. For the exchange of univalent ions the above equations yield the same numerical value for the separation factor and the selectivity coefficient.

The data in Table I show that the preference of the ion-exchange membrane for the various inorganic counterions increases with increasing valence and also in the order lithium, sodium, potassium, cesium, magnesium, calcium, strontium, barium, and aluminum. This latter effect is consistent with the variation in the effective radii of these ions of the same valence in solution in their hydrated forms. These results may be compared, for example, with data for sulfonated styrene-divinylbenzene copolymer beads of comparable capacity and cross linking which showed higher values.^{4,8,9} This variation may be due to differences in detail structure between the polystyrenesulfonic acid ion-exchange membranes and the sulfonated styrene-divinylbenzene copolymer beads.

The effects of variation of the composition and concentration of the external solution on the exchange properties of the membranes also were determined. No significant variation in the selectivity coefficient (for membrane one, 1.06 ± 0.03 ; membrane two, 1.04 ± 0.03) for the exchange $\text{Na}^+ - \text{H}^+$ was observed using solutions of varied composition (0.1 *N* total solution concentration).¹⁵ The results obtained using solutions of different concentration are given in Table II. It can be seen that although both univalent and divalent counterions exhibit an increase in the selectivity

Table II: Selectivity Coefficients for the Exchange of Na^+ and Mg^{2+} for H^+

Membrane no.	Exchange system	Tot. normality of ext soln	Equip ionic fraction of counterion in resin	Selectivity coeff
1	$\text{Na}^+ - \text{H}^+$	0.001	0.523	1.08
		0.01	0.515	1.04
		0.1	0.510	1.03
		1.0	0.505	1.02
1	$\text{Mg}^{2+} - \text{H}^+$	0.001	0.988	0.927
		0.01	0.952	0.860
		0.1	0.878	0.825
		1.0	0.661	0.644

of the membrane with dilution of the external solution, this effect is much greater for divalent than monovalent counterions.

In counterdiffusion experiments of two cation species across an ion-exchange membrane, the cations exchange in equivalent quantities. If the cation-interchange flux is described by a special form of Fick's first law, we may write

$$J_A = -J_B = -\frac{\bar{C}_i + \left(\frac{Z_B}{Z_A} - 1\right)(\bar{C}_A)_{av}}{\bar{C}_i} D_{AB} \frac{\Delta \bar{C}_A}{L} \quad (3)$$

The flux in a diaphragm diffusion cell having solutions of equal volume and normality is

$$J = Vdc/2dt \quad (4)$$

Using the approximation

$$dc = d(\Delta C_A) = \frac{(\Delta C_A)_{t=0}}{(\Delta \bar{C}_A)_{t=0}} d(\Delta \bar{C}_A) \quad (5)$$

Substitution of eq 4 and 5 in eq 3 and integration lead to the relationship

$$D_{AB} = K_i L \frac{(\Delta C_A)_{t=0}}{(\Delta \bar{C}_A)_{t=0}} \frac{\bar{C}_i}{\bar{C}_i + \left(\frac{Z_B}{Z_A} - 1\right)(\bar{C}_A)_{av}} \quad (6)$$

where J is the interchange flux, equiv/cm² sec; D_{AB} is the membrane interdiffusion coefficient, cm²/sec; K_i is the over-all ion-interchange mass-transfer coefficient ($= (V/2At) \ln (\Delta C_0/\Delta C_t)$),^{16,17} cm²/sec; L is the membrane thickness, cm; ΔC_A is the difference in concentration of the counterion between half-cells,

Table III: Membrane Interdiffusion Coefficients

System	Normality of ext soln	Interchange coeff (K_i), (cm sec ⁻¹ × 10 ⁵)		D_{AB} calcd by eq 6, cm ² sec ⁻¹ × 10 ⁵	
		Membrane 1	Membrane 2	Membrane 1	Membrane 2
$\text{MgCl}_2 - \text{HCl}$	0.01	38.6	61.0	1.07	2.88
	0.1	13.2	20.9	1.22	3.20
	1.0	4.58	7.32	1.36	3.35
				Av 1.26	3.14

(15) I. H. Spinner, J. Ciric, and W. F. Graydon, *Can. J. Chem.*, **32**, 143 (1954).

(16) A. S. Tombalakian, C. Y. Yeh, and W. F. Graydon, *Can. J. Chem. Eng.*, **42**, 61 (1964).

(17) M. Worsley, A. S. Tombalakian, and W. F. Graydon, *J. Phys. Chem.*, **69**, 883 (1965).

Table IV: Membrane Interdiffusion Coefficients

Membrane no.	Ion-pair exchange system	Normality of ext soln	Exptl D_{AB} calcd by eq 6, $\text{cm}^2 \text{sec}^{-1} \times 10^6$	Single-ion diffusion coeff calcd by eq 6 and 7, $\text{cm}^2 \text{sec}^{-1} \times 10^6$
1	$\text{Cs}^+ - \text{H}^+$	0.1	1.42	Cs^+ , 0.798 H^+ , 3.62
	$\text{Na}^+ - \text{H}^+$	0.1	1.24	Na^+ , 0.697 H^+ , 4.88
	$\text{Ba}^{2+} - \text{H}^+$	0.1	2.69	Ba^{2+} , 0.533 H^+ , 2.93
	$\text{Sr}^{2+} - \text{H}^+$	0.1	2.53	Sr^{2+} , 0.481 H^+ , 2.84
	$\text{Ca}^{2+} - \text{H}^+$	0.1	2.18	Ca^{2+} , 0.416 H^+ , 2.45
	$\text{Mg}^{2+} - \text{H}^+$	0.1	1.22	Mg^{2+} , 0.219 H^+ , 1.45

equiv/ml; $\Delta \bar{C}_A$ is the difference in concentration of the counterion in the membrane between the membrane faces ($= 2\bar{X}_B \bar{C}_i$ at zero time), equiv/ml; \bar{C}_i is the membrane internal ion concentration, equiv/ml; and $(\bar{C}_A)_{av} = \bar{X}_A \bar{C}_i$ equiv/ml. Adherence of the experimental data to eq 6 is illustrated by the close agreement in the values of the membrane interdiffusion coefficient for the interchange of magnesium with hydrogen over a 100-fold increase in external solution concentration gradient as shown in Table III. The results indicate an increase of about 20% in the value of the interdiffusion coefficient for the $\text{Mg}^{2+} - \text{H}^+$ exchange as the external solution concentration is increased from 0.01 to 1.0 *N*.

It is of interest to determine the dependence of the membrane interdiffusion coefficient for the various exchange systems on the ionic composition of the membrane. The equilibrium data (Table I) together with cation-interchange fluxes measured previously¹⁶ in mass-transfer experiments across the same membrane equilibrated with isotonic solutions were used in eq 6 to obtain membrane interdiffusion coefficients for our experimental conditions given in Table IV. The membrane interdiffusion coefficients obtained by the above method were used in eq 7 together with the assumption that limiting ionic mobility ratios in water apply in the membrane solution to estimate single-ion diffusion coefficients for hydrogen and the various counterions.

$$D_{AB} = \frac{\bar{D}_A \bar{D}_B (Z_A^2 \bar{C}_A + Z_B^2 \bar{C}_B)}{Z_A^2 \bar{C}_A \bar{D}_A + Z_B^2 \bar{C}_B \bar{D}_B} \quad (7)$$

where \bar{D} is the single-ion diffusion coefficient of the exchanging ion species in the membrane, cm^2/sec . Equation 7 is an evaluation of the membrane interdiffusion coefficient (D_{AB}) from the Nernst-Planck equation¹⁸ for the exchange of two cations. The limiting evaluations of D_{AB} from eq 7 are $D_{AB} = D_A$ for $\bar{C}_A \sim 0$ and $D_{AB} = D_B$ for $\bar{C}_B \sim 0$. These single-ion diffusion coefficients of the two exchanging cations in the membrane

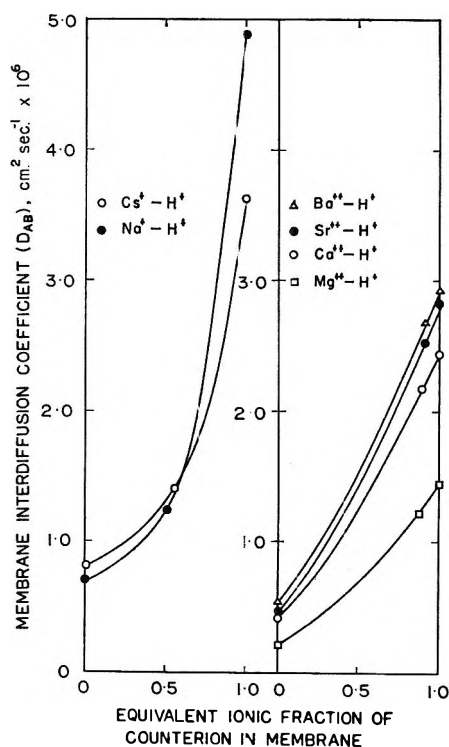


Figure 1. The variation of the membrane interdiffusion coefficient with variation of the equivalent ionic fraction of counterion in the membrane for the exchange of various univalent and divalent inorganic counterions with hydrogen ion.

represent the limiting evaluations of the membrane interdiffusion coefficient.

Samples of such values of single-ion diffusion coefficients (limiting evaluations of D_{AB}) calculated by combination of eq 6 and 7 for the exchange of various univalent and divalent inorganic cations with hydrogen ion are also given in Table IV. These single-ion diffusion coefficients serve to correlate interdiffusion

(18) F. Helfferich and M. S. Plesset, *J. Chem. Phys.*, **28**, 418 (1958).

behavior for various ion pairs and also describe the range of membrane interdiffusion coefficients predicted from the experimental data by the Nernst-Planck equation, eq 7. The observed dependence of the interdiffusion coefficient on the ionic composition of the

membrane for the various exchange systems across membrane one is shown in Figure 1.

Acknowledgment. The authors are indebted to the National Research Council, Ottawa, Ontario, Canada, for financial support.

Self-Diffusion in Simple Fluids

by John A. Palyvos and H. Ted Davis

*Department of Chemical Engineering, University of Minnesota, Minneapolis, Minnesota
(Received September 22, 1966)*

Application of the formula for the friction coefficient derived independently by Helfand and by Rice and Allnatt yields generalized charts comparing hard-core interaction contributions to the friction constant to contributions arising from soft interactions as predicted by the linear trajectory approximation. Numerical calculations based on the theoretical pair correlation functions of Kirkwood, *et al.*, are presented for liquid argon, krypton, and xenon. On the basis of these calculations it is concluded that the use of the linear trajectory approximation in the Rice-Allnatt theory yields fairly reliable predictions (to within 10-40% over the entire liquid range) for the self-diffusion coefficients of simple liquids.

Introduction

Rice and Allnatt¹ have developed a theory of transport in dense fluids based on the assumptions that (1) the interaction potential can be split into a hard-core repulsive part and a longer range soft part and (2) the dissipative effects of the hard and soft parts are additive. According to their model, a molecule moving through a dense fluid will undergo a motion in which it experiences a hard-core collision followed by a "Brownian motion" caused by soft interactions with the potential field of the neighboring molecules. Under these assumptions Rice and Allnatt obtained a modified Boltzmann equation in which the hard-core collisions were treated as in Enskog's theory² of a dense rigid-sphere fluid while the soft interactions were handled by Ross's weak coupling theory³ which leads to the Fokker-Planck approximation for these interactions.

In order to predict values of transport coefficients from the formulas of Rice and Allnatt, one must have,

in addition to the parameters of the interaction potential, values for the equilibrium pair correlation function. Several numerical comparisons, discussed in detail in the text by Rice and Gray,⁴ between experimental and theoretical viscosities and thermal conductivities of the noble liquids indicate that the Rice-Allnatt theory gives a quantitative description of transport in simple liquids. In obtaining the theoretical predictions, the Lennard-Jones potential was used as the soft part of the potential. The theoretical pair correlation function for this potential model has been computed by Kirkwood, Lewinson, and Alder using the superposition approximation on the Born-Green-Yvon integral equation.⁵

(1) S. A. Rice and A. R. Allnatt, *J. Chem. Phys.*, **34**, 2145 (1961).

(2) S. Chapman and T. G. Cowling, "The Mathematical Theory of Nonuniform Gases," Cambridge University Press, Cambridge, 1964.

(3) J. Ross, *J. Chem. Phys.*, **24**, 375 (1956).

(4) S. A. Rice and P. Gray, "The Statistical Mechanics of Simple Liquids," John Wiley and Sons, Inc., New York, N. Y., 1964.

In view of the success with viscosity and thermal conductivity predictions, we feel it is worthwhile to test in detail the self-diffusion coefficient predicted by the Rice-Allnatt theory. According to the theory the self-diffusion coefficient is given by the relation

$$D = kT/(\zeta^H + \zeta^S) \quad (1)$$

where ζ^H is a friction coefficient arising from the hard-core collisions and ζ^S is a friction coefficient arising from the soft interactions. Explicit formulas for the friction coefficients will be given in the following section.

The quantity ζ^S in the Rice-Allnatt theory is identical with the friction coefficient obtained by Helfand by applying the linear trajectory approximation to Kirkwood's formula for the friction coefficient.⁶ Using the theoretical pair correlation functions computed by Kirkwood, *et al.*,⁵ Helfand calculated the self-diffusion coefficient of liquid argon at 84°K and 1 atm of pressure. He found 3.0×10^{-5} cm²/sec compared to the latest experimental⁷ value of 2.0×10^{-5} cm²/sec (older values obtained by Cini-Castagnoli and Ricci⁸ at 84.6°K and 0.9 atm and Corbett and Wang⁹ at 84.3°K and 0.8 atm are 1.53×10^{-5} and 2.07×10^{-5} cm²/sec, respectively). The agreement is not too bad.

In the following section, comparisons over wide ranges of temperature and density of theory and experiment for the liquids argon, krypton, and xenon indicate that the agreement is more than fortuitous. We have also compared predictions of this theory with those of other models and have given the separate contributions ζ^H and ζ^S as functions of temperature and density.

Numerical Computations

The friction coefficient arising from hard-core collisions has been found to be^{2,6,10}

$$\zeta^H = (8/3)\rho_N\sigma^2(\pi m/\beta)^{1/2}g_2(\sigma) \quad (2)$$

where ρ_N is the number density, m is the molecular mass, $\beta = 1/kT$, σ is the hard-core diameter, and $g_2(\sigma)$ is the contact pair correlation function. The corresponding coefficient due to soft interactions, evaluated by Helfand,⁶ is given by

$$\zeta^S = -\rho_N(m\beta/144\pi^3)^{1/2} \int_0^\infty k^3 \bar{V}(k) \bar{G}(k) dk \quad (3)$$

where $\bar{V}(k)$ and $\bar{G}(k)$ are the Fourier transforms of the potential and of the quantity $[g_2(r) - 1]$, respectively. Helfand inverted eq 3 using the modified Lennard-Jones pair potential

$$V(x) = V_0(x) + V_1(x) \quad (4)$$

where

$$V_0(x) = \infty, V_1(x) = 0 \quad x \leq 1$$

$$V_0(x) = 0, V_1(x) = 4\epsilon[x^{-12} - x^{-6}] \quad x > 1 \quad (5)$$

in which x is the ratio of the intermolecular separation, r , to the molecular diameter, σ , and ϵ is the depth of the potential well. His result is

$$\zeta^S = 8/3\rho_N\sigma^2(\pi m/\beta)^{1/2}(\beta\epsilon) \int_0^\infty [g_2(\sigma x) - 1][11f_{12}(x) - 5f_6(x)]dx \quad (6)$$

where

$$f_n(x) = 2 \sum_{l=1}^{n/2} \frac{x^{2l-n}}{2l-1} - x^{1-n} \ln \left| \frac{x+1}{x-1} \right| \quad (7)$$

Since $g_2(\sigma x)$ vanishes in the region $0 < x < 1$, the integration in eq 6 may be performed analytically yielding

$$- \int_0^1 [11f_{12}(x) - 5f_6(x)]dx = 0.599 \quad (8)$$

In the region $1 < x < \infty$ the same integration can be performed numerically using the pair correlation function

$$g_2(x) = \exp \left\{ \frac{\psi_0(x) + (\beta\epsilon)\psi_1(x) + (\beta\epsilon)^2\psi_2(x)}{x} \right\} \quad (9)$$

where the $\psi_i(x)$ are given by Kirkwood, *et al.*⁵

For the purpose of numerical calculations, eq 2 and 6 were written as

$$\zeta^H/\zeta^* = \zeta_r^H \quad (10)$$

$$\zeta^S/\zeta^* = \zeta_r^S \quad (11)$$

where

$$\zeta^* \equiv (8\rho_N\sigma^2/3)(\pi m/\beta)^{1/2} \quad (12)$$

$$\zeta_r^H \equiv g_2(\sigma) \quad (13)$$

$$\zeta_r^S \equiv (\beta\epsilon) \int_0^\infty [g_2(\sigma x) - 1][11f_{12}(x) - 5f_6(x)]dx = (\beta\epsilon) \left\{ 0.599 + \int_1^\infty [g_2(\sigma x) - 1] \times [11f_{12}(x) - 5f_6(x)]dx \right\} \quad (14)$$

(5) J. G. Kirkwood, V. A. Lewinson, and B. J. Alder, *J. Chem. Phys.*, **20** (6), 929 (1952).

(6) E. Helfand, *Phys. Fluids*, **4** 681 (1961).

(7) J. Naghizadeh and S. A. Rice, *J. Chem. Phys.*, **36**, 2710 (1962).

(8) G. Cini-Castagnoli and F. P. Ricci, *ibid.*, **32**, 19 (1960).

(9) T. W. Corbett and J. H. Wang, *ibid.*, **25**, 422 (1956).

(10) H. C. Longuet-Higgins and J. A. Pople, *ibid.*, **25**, 884 (1956).

Using the theoretical pair correlation function as given by eq 9, we have calculated ζ_r^S for values of $\beta\epsilon$ ranging from 0.10 to 1.50 and for the three values of $\rho_N\sigma^3$, 0.443, 0.674, and 0.818. The calculated values are presented in Tables I-III and Figure 1. From the plots in Figure 1 one sees that the hard-core contribution dominates in the high-temperature gas and the soft interaction contribution dominates in the low-temperature liquid (or low-temperature gas if the

Table I: Predicted Values of the Reduced Hard-Core and Soft Interaction Contributions to the Friction Constant as a Function of $\beta\epsilon$ for $\rho_N\sigma^3 = 0.443$

$\beta\epsilon$	ζ_r^S	ζ_r^H
0.10	0.133	1.663
0.15	0.203	1.599
0.20	0.274	1.538
0.25	0.349	1.479
0.30	0.425	1.423
0.35	0.505	1.369
0.40	0.587	1.317
0.45	0.671	1.267
0.50	0.759	1.220
0.55	0.849	1.174
0.60	0.942	1.130
0.65	1.038	1.088
0.70	1.138	1.048
0.75	1.240	1.009
0.80	1.346	0.972
0.85	1.456	0.937
0.90	1.569	0.902
0.95	1.686	0.869
1.00	1.807	0.838
1.05	1.932	0.807
1.10	2.061	0.778
1.15	2.194	0.750
1.20	2.331	0.723
1.25	2.473	0.698
1.30	2.620	0.673
1.35	2.771	0.649
1.40	2.928	0.626
1.45	3.089	0.604
1.50	3.256	0.583

density is low). At the critical temperature, $\beta\epsilon \approx 0.7-0.8$ for the noble liquids. Thus the division between the liquid and gaseous state is roughly where the curves for ζ_r^H intersect the curves for ζ_r^S in Figure 1. Near the critical point ζ_r^S accounts for about 50% of the total friction coefficient of a liquid; it accounts for 85% near the melting point ($\beta\epsilon \sim 1.45$ for argon at its melting point). The soft contribution is a more rapidly varying function of temperature than is the hard-core contribution.

As a specific application, the relative contributions of

Table II: Predicted Values of the Reduced Hard Core and Soft Interaction Contributions to the Friction Constant as a Function of $\beta\epsilon$ for $\rho_N\sigma^3 = 0.674$

$\beta\epsilon$	ζ_r^S	ζ_r^H
0.10	0.172	2.153
0.15	0.260	2.055
0.20	0.349	1.961
0.25	0.439	1.871
0.30	0.531	1.785
0.35	0.624	1.703
0.40	0.719	1.624
0.45	0.815	1.549
0.50	0.912	1.476
0.55	1.010	1.407
0.60	1.110	1.341
0.65	1.210	1.278
0.70	1.312	1.217
0.75	1.415	1.159
0.80	1.520	1.104
0.85	1.625	1.051
0.90	1.732	1.000
0.95	1.839	0.952
1.00	1.948	0.906
1.05	2.058	0.862
1.10	2.169	0.820
1.15	2.281	0.779
1.20	2.394	0.741
1.25	2.507	0.704
1.30	2.622	0.670
1.35	2.738	0.636
1.40	2.854	0.604
1.45	2.972	0.574
1.50	3.090	0.545

ζ_r^H and ζ_r^S for liquid argon are compared in Table IV for various temperatures along the vapor pressure curve. In the table the data presented are in the range $0.77 \leq \beta\epsilon \leq 1.47$. The results for krypton and xenon are quite similar. We see that the relative contribution of ζ_r^H to the total friction constant ranges from 19% near the melting point to 41% near the critical point. It is interesting to note that even halfway between the melting point and the critical point ζ_r^S still accounts for 70% of the total friction coefficient. Thus, in this temperature range a description such as Kirkwood's, ignoring completely the hard-core terms, provides a good-sized portion of the total picture.

The predicted self-diffusion coefficients of liquid argon, krypton, and xenon calculated on the basis of eq 1 are presented in Figures 2-4. As illustrated in these figures the predicted values exhibit a temperature dependence similar to that observed by Naghizadeh and Rice⁷ up to temperatures corresponding to $\beta\epsilon \approx 0.95$; at higher temperatures the predicted self-diffusion coefficients increase sharply with temperature. The

Table III: Predicted Values of the Reduced Hard-Core and Soft Interaction Contributions to the Friction Constant as a Function of $\beta\epsilon$ for $\rho_N\sigma^3 = 0.818$

$\beta\epsilon$	ζ_r^S	ζ_r^H
0.10	0.198	2.420
0.15	0.299	2.306
0.20	0.401	2.197
0.25	0.504	2.092
0.30	0.608	1.992
0.35	0.713	1.896
0.40	0.820	1.804
0.45	0.927	1.716
0.50	1.035	1.632
0.55	1.145	1.552
0.60	1.255	1.476
0.65	1.366	1.403
0.70	1.477	1.333
0.75	1.590	1.266
0.80	1.703	1.203
0.85	1.816	1.142
0.90	1.930	1.084
0.95	2.045	1.029
1.00	2.160	0.976
1.05	2.276	0.926
1.10	2.392	0.878
1.15	2.508	0.833
1.20	2.624	0.790
1.25	2.741	0.748
1.30	2.858	0.709
1.35	2.975	0.672
1.40	3.091	0.636
1.45	3.208	0.602
1.50	3.325	0.570

Table IV: Comparison of ζ^H and ζ^S for Liquid Argon as a Function of Temperature along the Vapor Pressure Curve

T , °K	ρ_M , g/cc	$\zeta^H \times 10^{10}$, g/sec	$\zeta^S \times 10^{10}$, g/sec	$\zeta^H/(\zeta^H + \zeta^S)$
90	1.374	0.71	3.02	0.19
95	1.343	0.77	2.85	0.21
100	1.309	0.81	2.67	0.23
110	1.238	0.89	2.30	0.28
120	1.160	0.93	1.99	0.32
130	1.065	0.94	1.68	0.36
140	0.940	0.88	1.37	0.39
148	0.773	0.74	1.04	0.42

experimental values have been obtained by use of Naghizadeh and Rice's interpolation formulas.⁷

In the temperature region corresponding to the range $0.7 < \beta\epsilon \leq 0.95$ the predicted coefficients lie above experimental values by 9–20% for argon and by 15–40% for krypton; the corresponding predicted coefficients for xenon, on the other hand, remain within

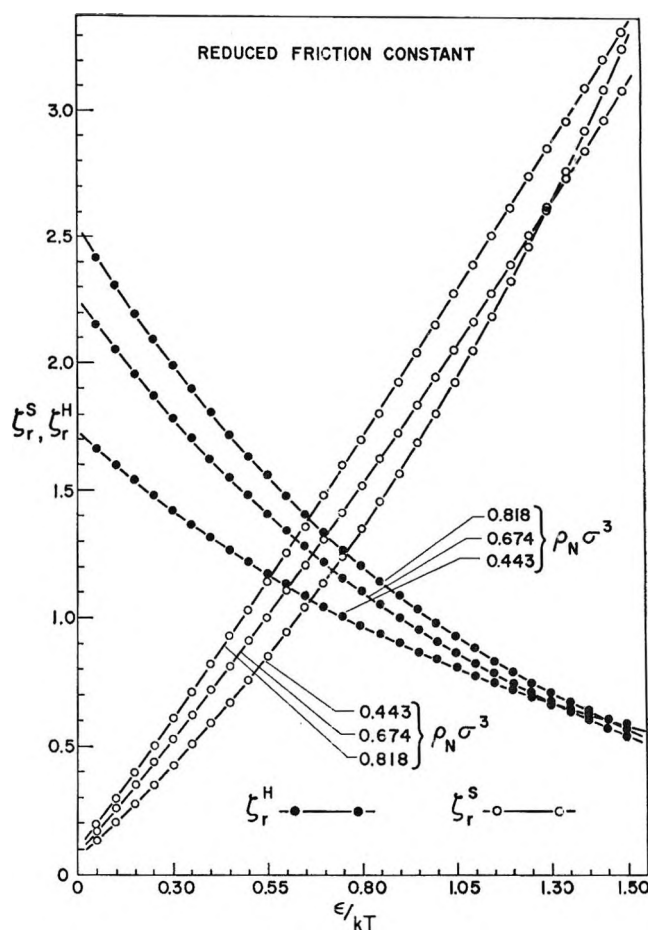


Figure 1. Reduced hard-core and soft interaction contributions to the friction constant as a function of $\beta\epsilon$ and $\rho_N\sigma^3$.

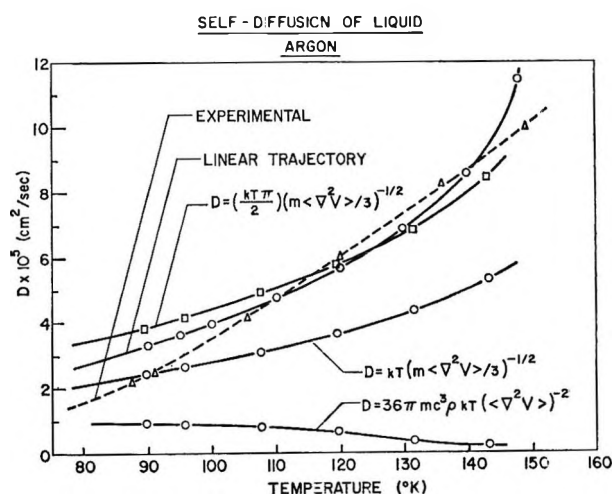


Figure 2. Comparison of predicted and experimental self-diffusion coefficients of liquid argon along the vapor pressure curve. (The curves based on eq 15–17 were taken from ref 15.)

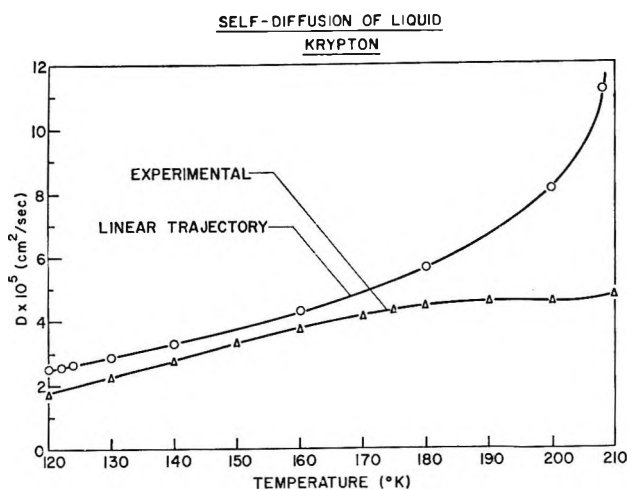


Figure 3. Comparison of predicted and experimental self-diffusion coefficients of liquid krypton along the vapor pressure curve.

11% above the observed values throughout the same temperature range.

In addition to experimental values and to our predicted values, Figure 2 includes values for the self-diffusion coefficient of argon predicted from the following.

(1) The acoustical model of Rice^{11,12} states that the fluid around the diffusing molecule is treated as a structured continuum in the sense that the density field is taken to be the product of the macroscopic density and the pair correlation function. Then the molecule acts as a distributed force center which affects the amplitude and propagation of acoustic disturbances in the structured continuum. On the basis of this model the diffusion coefficient is

$$D = 36\pi mc^3 \rho_N kT (\langle \nabla^2 V \rangle)^{-2} \quad (15)$$

where c is the velocity of sound.

(2) The formula

$$D = kT(m\langle \nabla^2 V \rangle/3)^{-1/2} \quad (16)$$

was predicted first by Kirkwood¹³ on the basis of dimensional arguments and later by several investigators (see ref 11) using other arguments. In particular Rice¹⁴ has shown that, aside from a factor of $(\pi/2)^{1/2}$, eq 16 may be derived under the assumption that the velocity autocorrelation function is gaussian in time.

(3) The formula

$$D = (\pi kT/2)(m\langle \nabla^2 V \rangle/3)^{-1/2} \quad (17)$$

is based on a theory by Douglass^{15,16} wherein it is assumed that the velocity autocorrelation function, $F(t)$, is given by $(kT/m) \operatorname{sech}(t/\tau)$. The relaxation time,

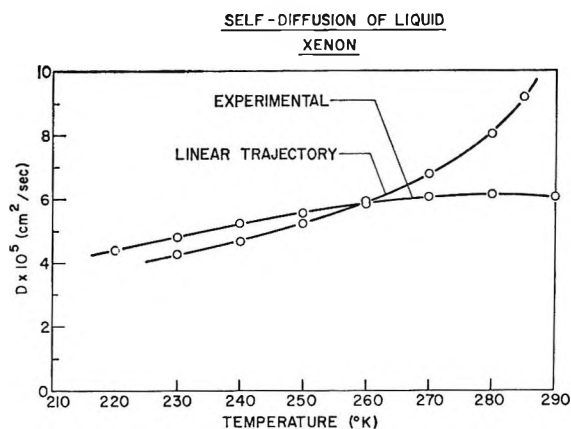


Figure 4. Comparison of predicted and experimental self-diffusion coefficients for liquid xenon along the vapor pressure curve.

τ , is obtained from the short-time expansion of $F(t) = \langle v(0)v(t) \rangle / \langle v^2 \rangle$.

The formulas 15–17 involve the ensemble average of the Laplacian of the intermolecular potential, $\langle \nabla^2 V \rangle$; values of $\langle \nabla^2 V \rangle$ are taken from experiments¹⁶ on isotope separation for the comparisons shown in Figure 2. Of these formulas eq 17 gives the best predictions for the self-diffusion coefficient of liquid argon, the predicted curve showing a temperature dependence similar to that of the linear trajectory curve. Over-all the linear trajectory approximation yields better values than any of eq 15–17.

On the basis of the numerical results presented in this section, it is concluded that the use of the linear trajectory approximation in the Rice–Allnatt theory gives fairly reliable predictions for the self-diffusion coefficients of simple liquids over wide ranges of temperature and density. It should of course be kept in mind that our conclusion rests on calculations based on the pair correlation function obtained from the superposition approximation. Unfortunately, this is the best we can do at present since an exact, tractable theory of the pair correlation function is lacking. Gray and Rice¹² have improved the predictions based on eq 15 by multiplying the velocity of sound by a numerical factor. However, it is as of yet not possible to justify this factor theoretically.

Acknowledgments. We wish to thank K. D. Luks and C. C. Wei for their assistance and comments in

(11) S. A. Rice, *Mol. Phys.*, **4**, 305 (1961).

(12) P. Gray and S. A. Rice, *J. Chem. Phys.*, **40**, 3671 (1964).

(13) J. G. Kirkwood, *ibid.*, **14**, 180 (1946).

(14) S. A. Rice, *ibid.*, **33**, 1376 (1960).

(15) D. C. Douglass, *ibid.*, **35**, 81 (1961).

(16) G. Boato, G. Casanova, and A. Levi, *ibid.*, **40**, 2419 (1964).

connection with this article. We are also grateful for financial support of this research furnished by the National Science Foundation (NSF GP 3789), the

Army Research Office (Durham) (DA 31 124 ARO D 241), and a NASA grant (NGR-24-005-063) to the Space Science Center of the University of Minnesota.

NOTES

Hydrogen-Bonding Interaction between Alcohols and Ethylene Trithiocarbonate

by Sadhan Kumar De and Santi R. Palit

Department of Physical Chemistry,
Indian Association for the Cultivation of Science,
Jadavpur, Calcutta 32, India (Received March 25, 1966)

Hydrogen-bonding interaction with C=S chromophore has been but little studied except for some preliminary investigations.¹⁻³ We report herein some results of our preliminary studies of the hydrogen-bonding interaction of ethylene trithiocarbonate (ETTC) with alcohols. Following the suggestion of Chandra and Sannigrahi,⁴ we have allowed for self-association of alcohols⁵⁻⁹ in calculating the stability constant of the hydrogen-bonded complexes.

Experimental Section

ETTC was obtained as a gift from Evans Chemetics, Inc. The nonhydrogen-bonding solvent used was Merck's *n*-heptane which showed cutoff at 220 m μ . The alcohols were purified by standard methods¹⁰ and distilled before use.

The solutions were made gravimetrically and all of the spectral measurements were taken on freshly prepared solutions in a Hilger UVspeck spectrophotometer using 1-cm stoppered quartz cells at 24° (a temperature constant within $\pm 0.5^\circ$ being maintained by circulating water through the cell holder).

Results

The observed blue shift of the $n-\pi^*$ transition of ETTC with increasing concentration of alcohols as shown in Figure 1 was utilized to calculate the equilibrium constant by determining the slope and intercept of an $[A]/D$ vs. $[A]$ plot (Figure 2) in accordance with the following equation due to Chandra and Sanni-

grahi.⁴ If the base B forms a 1:1 complex with a proton donor A, then

$$\frac{[A]}{D} = \frac{1}{K[B]_0\bar{\epsilon}} + \frac{[A]}{[B]_0\bar{\epsilon}}$$

where $D = OD - \epsilon_B[B]_0$, $\bar{\epsilon} = \epsilon_C - \epsilon_B$, K is the equilibrium constant of the complex, OD is the optical density of the mixture, $[B]_0$ is the formal concentration of solute, $[A]$ is the monomer concentration of alcohol, and ϵ_C and ϵ_B are the molar extinction coefficients of the complex and solute, respectively. Calculation of monomer concentration of alcohols requires dimerization constant values and these values of benzyl alcohol, *n*-propyl alcohol, and *n*-butyl alcohol were those as reported by Coggeshall and Saier,⁵ those of ethyl alcohol and *t*-butyl alcohol as reported by Becker,⁶ and of isopropyl alcohol as reported by Blanks and Prausnitz.⁹

The results are summarized in Table I where the average values of the equilibrium constants measured at several wavelengths near the shifted peak are given. The values of equilibrium constant for a given system are constant within 10%. In order to study any effect due to solute concentration, the ETTC-*n*-butyl al-

- (1) L. J. Bellamy and P. E. Rogasch, *J. Chem. Soc.*, 2218 (1960).
- (2) M. J. Janssen, *Rec. Trav. Chim.*, **79**, 454, 464 (1960).
- (3) A. Balasubramanian and C. N. R. Rao, *Spectrochim. Acta*, **18**, 1337 (1962).
- (4) A. K. Chandra and A. B. Sannigrahi, *J. Phys. Chem.*, **69**, 2494 (1965).
- (5) N. D. Coggeshall and E. L. Saier, *J. Am. Chem. Soc.*, **73**, 5414 (1951).
- (6) E. D. Becker in "Hydrogen-Bonding," D. Hadzi, Ed., Pergamon Press Ltd., London, 1959.
- (7) J. C. Davis, Jr., K. S. Pitzer, and C. N. R. Rao, *J. Phys. Chem.*, **64**, 1744 (1960).
- (8) B. D. N. Rao, P. Venkateswarulu, A. S. N. Murthy, and C. N. R. Rao, *Can. J. Chem.*, **40**, 387 (1962).
- (9) R. F. Blanks and J. M. Prausnitz, *J. Chem. Phys.*, **38**, 1500 (1963).
- (10) "Techniques of Organic Chemistry," A. Weissberger, Ed., Vol. VII, Interscience Publishers, Inc., New York, N. Y., 1955.

Table I: Equilibrium Constants of the Hydrogen-Bonded Complexes between ETTC and Alcohols

Alcohols	Concn of ETTC $\times 10^3$, M	Range of alcohol concn, ^a M	Range of monomer concn in the range of alcohol concn used, M	Equilibrium constant, M^{-1}	pK_a of alcohol at 25° ^b	Taft's σ^* of R in R-OH ^c
Benzyl alcohol	4.414	0.09649–0.4824	0.0804–0.2826	0.620	15.4	0.215
Ethyl alcohol	4.942	0.3422–1.711	0.2389–0.7352	0.286	15.93	–0.100
<i>n</i> -Propyl alcohol	4.406	0.2672–1.7368	0.1879–0.6850	0.245	16.1	–0.115
<i>n</i> -Butyl alcohol	3.692	0.3273–1.4183	0.2120–0.5741	0.198		
	6.572	0.7637–2.182	0.3848–0.7484	0.192	16.1	–0.130
Isopropyl alcohol	4.229	0.7806–1.9515	0.4595–0.8506	0.137	17.1	–0.190
<i>t</i> -Butyl alcohol	3.965	0.3177–2.645	0.2152–0.8906	0.038	19.2	–0.300

^a The concentration of benzyl alcohol was kept low because of its limited solubility in *n*-heptane. ^b J. Murto, *Acta Chem. Scand.*, 18, 1043 (1964). ^c See ref 14.

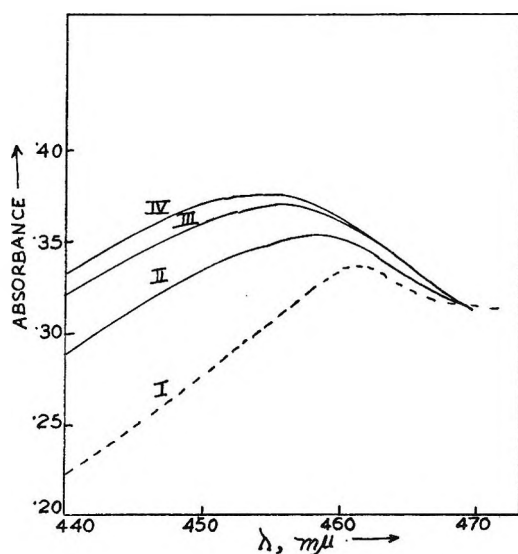


Figure 1. Absorption spectra of ETTC in 0 (I), 1.706 (II), 3.412 (III), and 4.265 (IV) M ethyl alcohol. Concentration of ETTC was $5.171 \times 10^{-3} M$ for all absorption curves.

cohol system was studied at two different concentrations of ETTC and no significant variation in the equilibrium constant was observed.

Discussion

It is evident from our data that alcohols form weak 1:1 hydrogen-bonded complexes with ETTC and the stability constants follow the order: benzyl alcohol >

ethyl alcohol > *n*-propyl alcohol > *n*-butyl alcohol > isopropyl alcohol > *t*-butyl alcohol. Balasubramanian and Rao³ found that the hydrogen-bond energies in an ETTC-alcohol system increase in the order: methyl alcohol > ethyl alcohol > isopropyl alcohol > *t*-butyl alcohol. However, these values of hydrogen-bond energies do not represent the energy of one hydrogen bond, since the concentration of the proton-donor solvents was very large in their experiments thereby leading to considerable self-association of the solvent molecules. A similar trend has also been observed in various base-alcohol systems. For example, Becker¹¹ found that the equilibrium constants for 1:1 complex formation between alcohols and different proton acceptors follow the order: methyl alcohol > ethyl alcohol > *t*-butyl alcohol. Chandra and Basu¹² and Murthy¹³ found that the equilibrium constants for the formation of 1:1 hydrogen-bonded complexes decrease in the order: primary, secondary, and tertiary alcohol. However, the equilibrium constants reported by Chandra and Basu as well as by Murthy do not correspond to any definite composition of the complexes since alcohols would exist appreciably as dimers and polymers in their working range of concentrations and no correction was

(11) E. D. Becker, *Spectrochim. Acta*, 17, 436 (1961).

(12) A. K. Chandra and S. Basu, *Trans. Faraday Soc.*, 56, 632 (1960).

(13) A. S. N. Murthy, Ph.D. Thesis, The Indian Institute of Science, Bangalore, 1964.

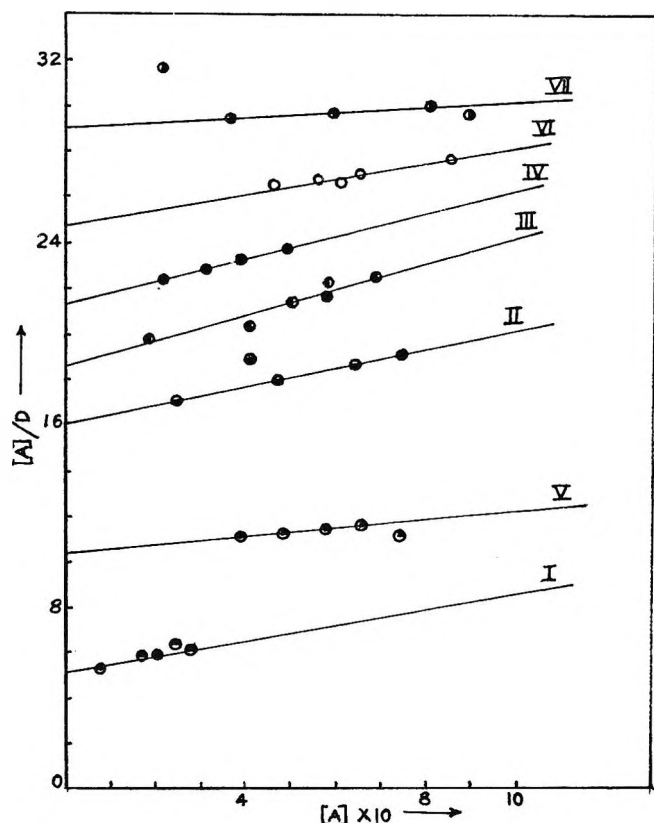


Figure 2. Plot of $[A]/D$ vs. $[A]$: I, benzyl alcohol ($4.414 \times 10^{-3} M$); II, ethyl alcohol ($4.942 \times 10^{-3} M$); III, *n*-propyl alcohol ($4.406 \times 10^{-3} M$); IV, *n*-butyl alcohol ($3.692 \times 10^{-3} M$); V, *n*-butyl alcohol ($6.572 \times 10^{-3} M$); VI, isopropyl alcohol ($4.229 \times 10^{-3} M$); VII, *t*-butyl alcohol ($3.965 \times 10^{-3} M$). The concentrations of $ET^{\circ}C$ are indicated in the parentheses. All of the spectral measurements were made at $454 m\mu$.

applied for the same. Nevertheless, all these trends are consistent with the concepts of acidities of the alcohols.

Table I shows that the equilibrium constants for hydrogen bond formation run parallel with the acidic strength or proton-donating power of alcohols and also with Taft's polar substituent constant (σ^*).¹⁴ Such a correlation between the acidity of proton donor and stability of the hydrogen-bonded complex shows in an indirect way the contribution of the electrostatic part in the over-all strength of a hydrogen bond.

Acknowledgments. The authors are grateful to Evans Chemetics, Inc., for a gift sample of ethylene trithiocarbonate. Thanks are due to the Council of Scientific and Industrial Research, India, for awarding a Junior Research Fellowship to S. K. D.

(14) R. W. Taft, Jr., in "Steric Effects in Organic Chemistry," M. S. Newman, Ed., John Wiley and Sons, Inc., New York, N. Y., 1956, Chapter 13.

Mass Spectrometric Studies at High Temperatures. XIV. The Vapor Pressure and Dissociation Energy of Silver Monofluoride

by K. F. Zmbov and J. L. Margrave

Department of Chemistry, Rice University, Houston, Texas
(Received July 22, 1966)

The vaporization behavior of AgCl, AgBr, and AgI has been studied,¹⁻⁴ but quantitative vapor pressure data have not been available for silver monofluoride. The object of the present work was to study the sublimation and vaporization of AgF and to determine the dissociation energy of $AgF(g)$.

Experimental Section

The mass spectrometer has been described.⁵ The AgF sample was obtained from Research Inorganic Chemicals Co., Sun Valley, Calif., and was used without further purification. The sample was evaporated from a platinum Knudsen cell; the temperature of the cell was measured with a Pt-Pt-10% Rh thermocouple, calibrated against a National Bureau of Standards standard thermocouple, and is believed accurate to $\pm 0.5^\circ$, although the maximum temperature gradient in the cell could be as great as $\pm 5^\circ$.

Results

The vaporization of AgF was studied over the temperature range $854-1024^\circ K$. The only ions formed by electron bombardment of the vapors effusing from the Knudsen cell were AgF^+ and Ag^+ in the ratio 0.25 to 0.17 at 75 ev. No polymeric species $(AgF)_n^+$ were observed in the mass spectrum. The appearance potentials of Ag^+ and AgF^+ ions, determined by the vanishing-current method and using background mercury as a standard, were found to be 11.5 and 11.4 ev, respectively, with probable errors of ± 0.3 ev.

The heat of vaporization of AgF was determined from the plot of $\log I^+T$ (for the AgF^+ ion) vs. $1/T$ as $\Delta H_{v,935.6} = 42.8 \pm 0.3$ kcal mole⁻¹, where the uncertainty given represents the standard deviation of the least-squares treatment of the data. The true uncer-

(1) H. Von Wartenberg and O. Besse, *Z. Elektrochem.*, **23**, 384 (1922).

(2) K. Jelinek and A. Rudat, *Z. Physik. Chem.*, **A143**, 55 (1929).

(3) A. V. Gusarov and L. N. Gorokhov, *Vestn. Mosk. Univ. Ser. II, Khim.*, **17**, No. 5, 14 (1962).

(4) H. M. Rosenstock, J. R. Walton, and L. K. Brice, U. S. Atomic Energy Commission Report ORNL-2772 (1959).

(5) G. Blue, J. W. Green, R. G. Bautista, and J. L. Margrave, *J. Phys. Chem.*, **67**, 877 (1963).

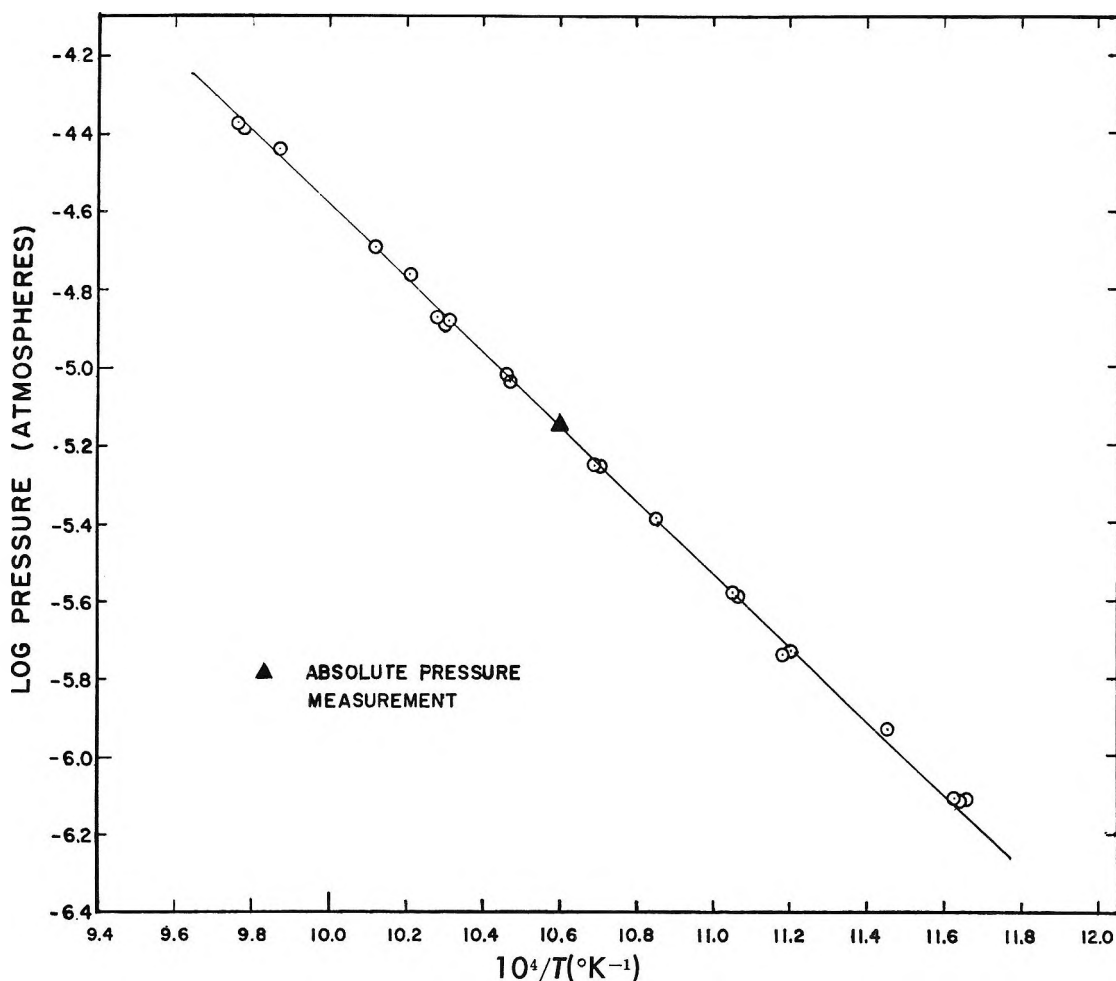


Figure 1. Vapor pressure data for AgF.

tainty, reflecting the errors in the temperature measurements, which are the major inherent errors in the second-law results, is estimated to be ± 1.0 kcal mole $^{-1}$.

Because of the lack of high-temperature heat capacity data for AgF, enthalpy increments were estimated by comparison with available data for CuCl, CuF, and AgCl.⁶ This procedure gave $\Delta H_{s, 298}^{\circ} = 50.9 \pm 3.0$ kcal mole $^{-1}$ for the heat of sublimation of silver monofluoride where the uncertainty now includes the additional error possible in the estimation of the thermodynamic functions. Since no high-temperature thermal functions for AgF(s) are known, there is no justification for a point-by-point third-law calculation.

An absolute pressure determination has been made by vaporizing a weighed amount of a well-outgassed silver monofluoride sample at a constant temperature. From a measured weight loss of 7.332×10^{-2} g at 953°K in 215 min through an orifice of area 8.50×10^{-3} cm 2 , the absolute pressure has been calculated and used to evaluate the machine constant k in the current-

pressure relationship $P = kI + T$. This value of k was combined with the least-square relationship for log $I + T$ vs. $1/T$ to give the vapor pressure equation

$$\log P = -(0.937 \pm 0.007) \times 10^4/T + 4.78 \pm 0.08 \quad (1)$$

where $854^{\circ} < T < 1024^{\circ}\text{K}$. By this absolute technique one eliminates the need for knowing the ionization cross sections and the multiplier gains. The vapor pressure data for AgF(l) are plotted in Figure 1.

An equation for the pressure over the solid phase can be obtained by employing the simplified vapor pressure equation

$$\log P_{MP} = -(A_s/T_{MP}) + B_s = -(A_l/T_{MP}) + B_l \quad (2)$$

where the subscripts s and l refer to the solid and liquid phases, respectively. The coefficients A_s and A_l are

(6) K. K. Kelley, U. S. Bureau of Mines Bulletin 584, U. S. Government Printing Office, Washington, D. C., 1960.

related to the heats of sublimation and of vaporization, $\Delta H_{s,T}$ and $\Delta H_{v,T}$ through the Clausius-Clapeyron equation, and $\Delta H_{\text{sub}} = \Delta H_{\text{fus}} + \Delta H_{\text{vap}}$. With ΔH_{fus} estimated as 4.0 ± 1 kcal mole⁻¹, one obtains the following vapor pressure equation for solid AgF

$$\log P_{\text{AgF}(s)} = -(1.023 \times 10^4/T) + 10.07 \quad (3)$$

where $T \leq 708^\circ\text{K}$, and thus, $\Delta H_s^\circ_{298} = 47 \pm 5$ kcal mole⁻¹.

The Dissociation Energies of AgF and AgF⁺. When the heat of sublimation of AgF, the heat of formation of AgF(s)⁷ ($\Delta H_{f,298} = -48.5$ kcal mole⁻¹), the heat of sublimation of silver = 67.97 ± 0.5 kcal/g-atom,⁸ and the dissociation energy of fluorine = 37.7 ± 0.3 kcal mole⁻¹⁹ are combined, one calculates $D^\circ_{298}(\text{AgF}) = 84.8 \pm 4$ kcal mole⁻¹.

An alternate method for getting the dissociation energy of AgF is to use appearance potential measurements. The appearance potential for the Ag⁺ ion formed in the dissociative ionization process



is the sum of the dissociation energy $D(\text{Ag-F})$ and the ionization potential of Ag

$$D(\text{Ag-F}) = \text{A.P.}(\text{Ag}^+/\text{AgF}) - \text{I.P.}(\text{Ag})$$

By using the experimental value of $\text{A.P.}(\text{Ag}^+/\text{AgF}) = 11.4 \pm 0.3$ ev, the spectroscopic value, $\text{I.P.}(\text{Ag}) = 7.574$ ev,¹⁰ and assuming no F⁻ is formed, one obtains a dissociation energy for AgF of 3.9 ± 0.3 ev (89.9 ± 7 kcal mole⁻¹). This is in agreement, within the limits of experimental error, with the thermochemical value and thus precludes F⁻ ions as significant products in the fragmentation since the electron-attachment process would be ~ 3.7 ev exothermic.

The dissociation energy of AgF⁺, as calculated through a thermochemical cycle, is in the range 0.1–0.5 ev.

Acknowledgment. This work was supported by the U. S. Atomic Energy Commission under Contract No. AT-(40-1)-2907.

(7) F. D. Rossini, D. D. Wagman, W. H. Evans, S. Levine, and I. Jaffe, "Selected Values of Chemical Thermodynamic Properties," National Bureau of Standards Circular 500, U. S. Government Printing Office, Washington, D. C., 1952, p 1266.

(8) (a) P. D. Zavitsanos, Space Science Laboratory, General Electric Co., Report R63SD06 (1963); (b) R. Hultgren, R. L. Orr, P. D. Anderson, and K. K. Kelley, "Selected Values of Thermodynamic Properties of Metals and Alloys," John Wiley and Sons, Inc., New York, N. Y., 1965, p 30.

(9) "JANAF Thermochemical Tables," The Dow Chemical Co., Midland, Mich.; now available as U. S. Government Document No. PB-168-370, Clearinghouse for Federal Scientific and Technical Information, Springfield, Va.

(10) C. E. Moore, National Bureau of Standards Circular 467, Vol. 3, U. S. Government Printing Office, Washington, D. C., 1958.

On the Application of the Scaled Particle

Theory to Aqueous Solutions of Nonpolar Gases¹

by A. Ben-Naim and Harold L. Friedman

Department of Chemistry, State University of New York,
Stony Brook, New York (Received July 25, 1966)

Recently, the scaled particle theory of fluids^{2,3} has been applied by Pierotti to calculate the thermodynamics of solution of nonpolar gases in nonpolar solvents⁴ and in water.⁵ The free energy increase in the process in which the gas is transferred from the hypothetical 1-atm gas state to the hypothetical unit mole fraction state in solution was expressed as

$$\Delta G = G_c + G_i + RT \ln (RT/V) \quad (1)$$

and G_c , the reversible work to form the cavity to accommodate the gas molecule in the solvent, was calculated from the scaled particle theory while G_i , the free energy of interaction of the solute molecule in the cavity with the surrounding solvent, was estimated on the basis of dispersion and dipole-polarizability interactions. The last term in (1) merely accounts for the change in standard states. By appropriate differentiation of this equation, changes in other thermodynamic functions were obtained. Good agreement of calculated and experimental values was obtained and, what is most striking, the calculations reproduce the large dependence of the thermodynamics of this process on whether the solvent is a nonpolar liquid or water.

It was assumed that G_i is independent of temperature so in the case of ΔS the seat of the solvent dependence is in the temperature coefficient of the cavity work, which is in turn determined mainly by difference in coefficient of thermal expansions of water (0.25×10^{-3} deg⁻¹) and the nonpolar liquids (*ca.* 1.2×10^{-3} deg⁻¹) at 25°. On the other hand, the same entropy effects have been taken as indications of major structural changes in the water due to the solute molecules.^{6,7} It seems surprising that such structural effects, if they exist, should be so completely accounted for *via* dif-

(1) This study was aided by a grant from the Office of Saline Water, U. S. Department of the Interior.

(2) (a) H. Reiss, H. L. Frisch, and J. L. Lebowitz, *J. Chem. Phys.*, **31**, 369 (1959); (b) H. Reiss, H. L. Frisch, E. Helfand, and J. L. Lebowitz, *ibid.*, **32**, 119 (1960); (c) F. Helfand, H. Reiss, H. L. Frisch, and J. L. Lebowitz, *ibid.*, **33**, 1379 (1960).

(3) H. Reiss, *Advan. Chem. Phys.*, **9**, 1 (1966).

(4) R. A. Pierotti, *J. Phys. Chem.*, **67**, 1840 (1963).

(5) R. A. Pierotti, *ibid.*, **69**, 281 (1965).

(6) H. S. Frank and M. W. Evans, *J. Chem. Phys.*, **13**, 507 (1945).

(7) A. Ben-Naim, *J. Phys. Chem.*, **69**, 3240 (1965).

ferences in macroscopic properties. As Pierotti points out,⁵ this suggests an almost thermodynamic independence of molecular structure. In order to elucidate this, we have included one more property of the solvents in these considerations.

The crucial assumption of the scaled particle theory is that G_c is given by a certain polynomial in the cavity radius if the cavity is larger than a certain minimal size (which is smaller than any of interest here). Therefore, Pierotti's expression for G_c with the parameters he chose must, if it is correct, also pertain to macroscopic cavities and therefore to the surface tension of the solvent.^{2,8} However, Mayer⁹ has found that such an expression does not yield the experimental temperature dependence of the surface tension of water, the surface entropy, unless a_1 , the parameter representing the hard-sphere diameter of the solvent molecule, is taken as temperature dependent. Pierotti took a_1 as independent of temperature.

Therefore, we have the following inconsistency: the scaled particle theory with the auxiliary assumptions employed by Pierotti correctly gives $-dG_c/dT = S_c$ as

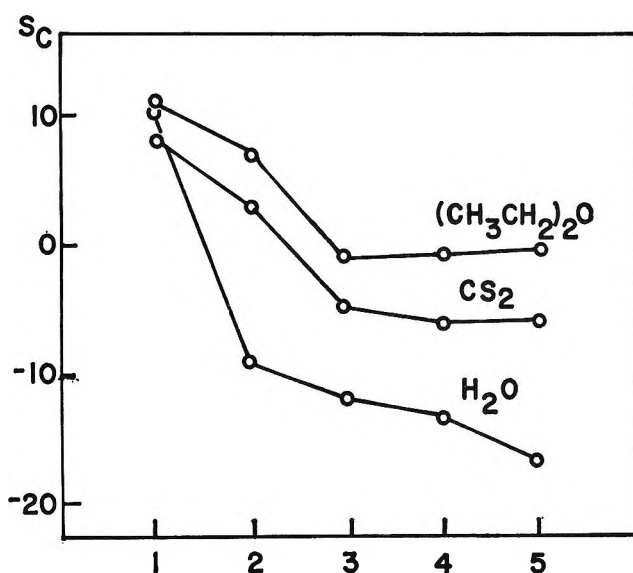


Figure 1. Values of the cavity entropy computed by the scaled particle theory for argon in the solvents Et₂O, CS₂, and H₂O at 25° on the basis of various assumptions about the hard-sphere diameter a_1 : (1) a_1 from second virial coefficient and da_1/dT chosen to fit surface entropy, using values given by Mayer;⁹ (2) same a_1 but da_1/dT chosen to fit temperature dependence of compressibility, using values given by Mayer;⁹ (3-5) $da_1/dT = 0$ and a_1 chosen in various ways with respective values (in angstroms) as follows: Et₂O: 4.87, 4.93, 5.00; CS₂: 4.44, 4.55, 4.53; H₂O: 2.71, 2.75, 2.93. For CS₂ and H₂O, the middle value (4) is the one used by Pierotti.^{4,5} In each case the calculation pertains to a cavity suitable for an argon atom and the parameters are, as far as possible, the same as he used.

a function of cavity size for cavities in water just large enough to accommodate the solute molecules in the range from He to C₆H₆, but not for cavities of macroscopic dimensions. However, the *basic* assumption of the theory requires that S_c be given by the same function throughout this range.

We note that for anisotropic molecules the equivalent hard-sphere diameter a_1 may be regarded as an average over orientations and therefore temperature dependent. Thus it is permissible to allow for temperature dependence, and one might hope to be able to choose da_1/dT to give the experimental surface entropy while not significantly affecting S_c for cavities of molecular dimensions. This has been tested by computations with the results shown in Figure 1. The computed values are very different from those obtained by Pierotti, and the agreement with experiment is destroyed if his assumption $S_i = 0$ is retained. Apparently, the inconsistency cannot be resolved in this way.

Also shown in Figure 1 are the results of computations using da_1/dT determined by the temperature dependence of the compressibility which reveals another inconsistency in this application of the theory. Finally, the figure also shows that for water, the computed value of S_c is rather strongly dependent on a_1 even for $da_1/dT = 0$.

Similar results are obtained in computations for other thermodynamic functions, but they do not give any further insight into this problem. Finally, we remark that it seems quite possible at this time that the correct S_c function is given by the scaled particle theory if one uses da_1/dT to fit the surface entropy and that there is an additional large and negative contribution to ΔS from dG_i/dT in the case of nonpolar solutes in water.

(8) The surface tension given by the theory in this way is for the interface between the liquid and a rigid plane wall, but it is not believed to be significantly different from that for the interface between the liquid and dilute vapor. See ref 2.

(9) (a) S. W. Mayer, *J. Chem. Phys.*, **38**, 1803 (1963); (b) S. W. Mayer, *J. Phys. Chem.*, **67**, 2160 (1963).

Improved Theoretical Calculation of the Stability Ratio for Colloidal Systems

by D. N. L. McGown and G. D. Parfitt

Department of Chemistry, University of Nottingham, Nottingham, England (Received July 6, 1966)

The stability of a colloidal dispersion is commonly expressed in terms of the stability ratio W , being the ratio

of the most rapid rate of coagulation to the actual, slower rate. In order to predict the magnitude of this quantity theoretically, it has been usual to compare the rapid rate derived by Smoluchowski¹ with a slower rate from Fuchs' equation,² thereby obtaining the expression³

$$W = 2 \int_2^{\infty} \frac{\exp(V/kT)}{s^2} ds$$

where V is the energy of interaction of two spherical particles of radius a and $s = R/a$; R is the distance between particle centers.

In using Smoluchowski's value for the rapid rate of coagulation, however, one is assuming that no attractive forces are in operation until the particles are in contact. It is this assumption which accounts for the fact that theoretical curves of W as a function of surface potential always fall below unity at low potentials and thus cannot easily be compared with experiment.^{4,5}

Fuchs provides a general equation for the flux of particles in a force field around a central particle, this force field not necessarily involving any element of repulsion. This leads to the following expression for the number of collisions J per second with one particle

$$J = \frac{8\pi DN a}{\int_2^{\infty} \frac{\exp(V/kT)}{s^2} ds}$$

where D is the diffusion coefficient for a primary particle and N is the number of particles per cubic centimeter. Thus, if we define a new rapid rate such that the energetic interaction between the particles is entirely attractive and compare the corresponding flux with that when there is a superimposed repulsive force, we obtain a new expression for W

$$W = \frac{\int_2^{\infty} \frac{\exp(V/kT)}{s^2} ds}{\int_2^{\infty} \frac{\exp(V_A/kT)}{s^2} ds}$$

where V_A is the attractive potential energy. When so defined, W falls to unity only when repulsion is entirely absent and would thus be expected to be more in accord with experimental reality. In terms of the magnitude of W , the new expression gives rise to values which are higher than previously predicted by a factor which is constant for a given particle radius and Hamaker constant.

The ratio f between corrected and uncorrected values of W is such that

$$1/f = 2 \int_2^{\infty} \frac{\exp(V_A/kT)}{s^2} ds$$

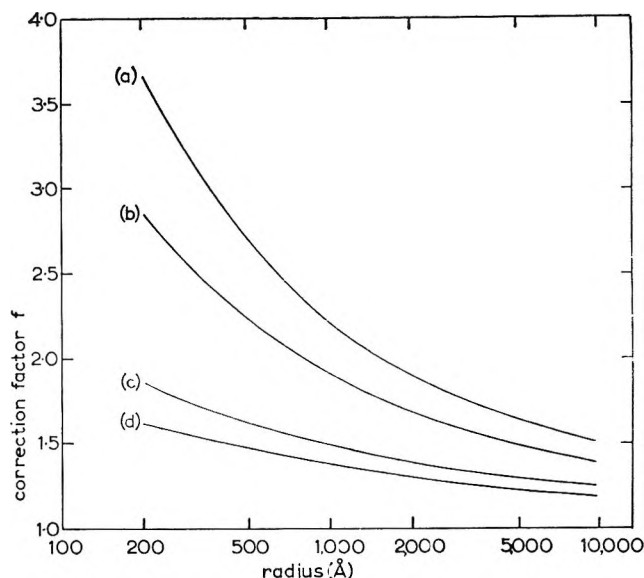


Figure 1. Correction factor as a function of particle radius: (a) 1×10^{-11} erg; (b) 5×10^{-12} erg; (c) 1×10^{-12} erg; and (d) 5×10^{-13} erg.

and in Figure 1 is shown plotted as a function of particle radius for four values of Hamaker constant. The attractive energy has been calculated using the limiting form of the Hamaker equation with the retardation corrections of Schenkel and Kitchener.⁶

- (1) M. Von Smoluchowski, *Z. Physik. Chem.*, **92**, 129 (1917).
- (2) N. Fuchs, *Z. Physik*, **89**, 736 (1934).
- (3) E. J. W. Verwey and J. Th. C. Overbeek, "Theory of Stability of Lyophilic Colloids," Elsevier Publishing Co., Amsterdam 1948, p 166.
- (4) See ref 3, p 176.
- (5) K. E. Lewis and G. D. Parfitt, *Trans. Faraday Soc.*, **62**, 1652 (1966).
- (6) J. H. Schenkel and J. A. Kitchener, *ibid.*, **56**, 161 (1960).

The Proton Magnetic Resonance Spectra of Ammonia Nickel Cyanide Clathrates

by Kimiko Umemoto and Steven S. Danyluk¹

Department of Chemistry, University of Toronto,
Toronto, Canada (Received July 25, 1966)

The wide-line proton magnetic resonance spectra for ammonia nickel cyanide clathrates of benzene, aniline, and pyridine have been reported recently by Nakajima, Bhatnagar, and Cole,² and by Nakajima.³ In each

(1) Address correspondence to this author at Argonne National Laboratory, Argonne, Ill.

case the derivative curves were found to be asymmetric and although the line width, ΔH , and second-moment, S_2 , variation with temperature were attributed qualitatively to the motional behavior of the enclathrated molecule, this interpretation is open to some question because of the difficulties inherent in evaluating these parameters for superimposed sets of signals, *i.e.*, those for ammonia protons and aromatic ring protons. The situation is further complicated by the possibility of electron-nucleus interaction between paramagnetic (octahedrally coordinated) Ni(II) atoms and the ammonia ligands. Such an interaction would act to shift the resonance frequency, H_0 , for the ammonia protons from the value expected for a purely diamagnetic compound. In order to assess the relative contribution of the host and enclathrated molecules to the observed signal, we have investigated the proton spectra for complexes in which the ammonia and aromatic molecules have been selectively replaced by their deuterio analogs. Since the observed signals are now solely due to the enclathrated molecules and host molecules, respectively, the determination of S_2 values for the individual components is simplified considerably.

Experimental Section

Details for the preparation of deuterated $\text{Ni}(\text{CN})_2 \cdot \text{ND}_3 \cdot \text{M}$ and $\text{Ni}(\text{CN})_2 \cdot \text{NH}_3 \cdot \text{C}_6\text{D}_6$ clathrates are reported elsewhere.⁴ Fully deuterated chemicals, except for the enclathrated molecules, were used in the preparative steps throughout and the preparations were carried out in a drybox. The nmr spectra were measured with a Varian DP 60 spectrometer and the field was calibrated with a Harvey-Wells G 502 gaussmeter. Care was taken to avoid modulation broadening of the signal and modulation amplitudes were usually maintained below 1.7 gauss.

Results and Discussion

The spectra observed for the $\text{Ni}(\text{CN})_2 \cdot \text{NH}_3 \cdot \text{C}_6\text{D}_6$ (I), $\text{Ni}(\text{CN})_2 \cdot \text{ND}_3 \cdot \text{C}_6\text{H}_6$ (II), and $\text{Ni}(\text{CN})_2 \cdot \text{NH}_3 \cdot \text{C}_6\text{H}_6$ (III) clathrates at 298 and 100°K are shown in Figure 1 (a-e) and a summary of ΔH , S_2 , and $(H^* - H_0)^5$ values derived from these spectra is given in Table I. The spectrum for $\text{Ni}(\text{CN})_2 \cdot \text{NH}_3 \cdot \text{C}_6\text{D}_6$ at 298°K (Figure 1a) is typical of a symmetric three-spin system,⁶ apart from the narrow signal located at the center. The latter is probably due to small amounts of H_2O which could not be removed from the starting NiSO_4 despite repeated attempts to prepare the anhydrous salt.⁷ From the line-width and second moment values, 12.6 ± 0.4 gauss² for I at 298°K, it can be concluded that the NH_3 groups are reorienting about the

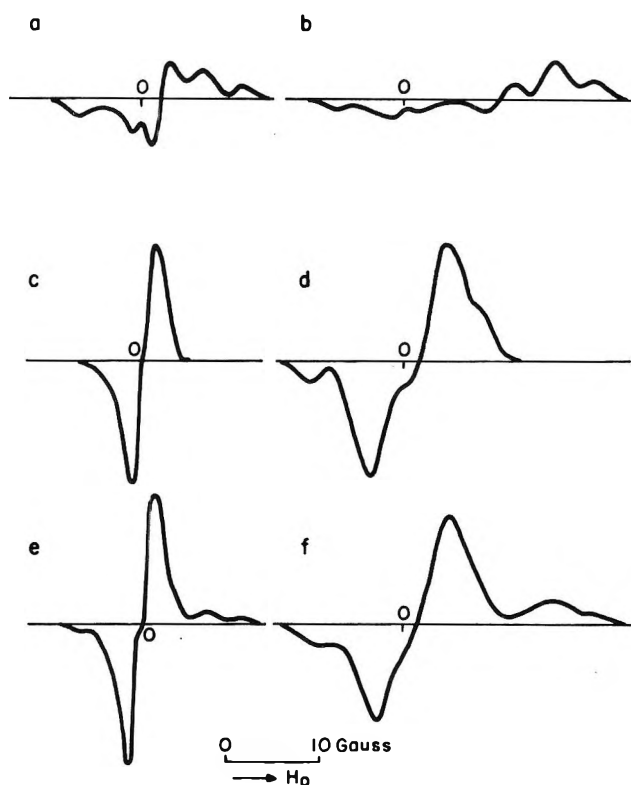


Figure 1. Proton magnetic resonance derivative curves of: (a) $\text{Ni}(\text{CN})_2 \cdot \text{NH}_3 \cdot \text{C}_6\text{D}_6$ at 298°K; (b) at 100°K; (c) $\text{Ni}(\text{CN})_2 \cdot \text{ND}_3 \cdot \text{C}_6\text{H}_6$ at 298°K; (d) at 100°K; (e) $\text{Ni}(\text{CN})_2 \cdot \text{NH}_3 \cdot \text{C}_6\text{H}_6$ at 298°K; (f) at 100°K. The zero field has been taken as the field value of a purely diamagnetic reference sample.

C_{3v} axis at this temperature.⁸ At 100°K both ΔH and S_2 for I are much larger than the values at 298°K. Although the S_2 value is less accurate at 100°K because of the marked asymmetry of the signal, the magnitude indicates that the NH_3 groups are most likely rigid at this temperature. The line-shape changes with

(2) H. Nakajima, V. M. Bhatnagar, and A. R. H. Ccle, *J. Phys. Soc. Japan*, **17**, 1194 (1962).

(3) H. Nakajima, *ibid.*, **20**, 555 (1965).

(4) K. Takahashi (Umemoto), Ph.D. Thesis, University of Toronto, 1965.

(5) H_0 represents the field value for a purely diamagnetic sample while H^* is the field value for the proton signal studied, *i.e.*, NH_3 or C_6H_6 .

(6) E. R. Andrew, "Nuclear Magnetic Resonance," Cambridge University Press, Cambridge, England, 1958, Chapter 6.

(7) A small residual signal of approximately the same line width and intensity was noted for the fully deuterated complex $\text{Ni}(\text{CN})_2 \cdot \text{ND}_3 \cdot \text{C}_6\text{D}_6$. Since the starting materials were all better than 95% deuterated the residual signal must be due to tightly bound hydrate water which does not exchange during the synthesis steps.

(8) The theoretical rigid lattice second-moment value for the NH_3 groups is 30.2 gauss².

temperature for I are similar to changes noted previously for nickel amines⁹ and can be attributed to an electron-nucleus interaction between paramagnetic nickel atoms and the ammonia protons in the clathrate. Magnetic susceptibility measurements have shown that more than 50% of the Ni atoms are paramagnetic in the Ni(CN)₂NH₃M clathrates.^{10,11} An electron-nucleus interaction of the Fermi contact type is further confirmed by the large shift of ~10 gauss of the resonance frequency upon lowering of the temperature.

Table I: Second Moments, Line Widths, and Field Shifts for Proton Signals in Ammonia Nickel Cyanide Benzene Clathrates^a

	Ni(CN) ₂ ND ₃ · C ₆ H ₆	Ni(CN) ₂ NH ₃ · C ₆ D ₆
S_2 (theoretical), gauss ²		
Rigid lattice	4.3	30.2
Rotation	Hexad axis, 1.1	C _{3v} axis, 7.6
S_2 (observed), gauss ²		
100°K	9.6	39.5
298°K	1.6	12.6
ΔH , gauss		
100°K	8.5	17.3
298°K	2.6	2.1
$H^* - H$, gauss		
100°K	1.2	9.8
298°K	0.0	2.0

^a Observed S_2 values are accurate to ± 0.4 gauss;² line widths are given as the distance between the maximum and minimum of the derivation curves and are accurate to ± 0.2 gauss; H^* denotes the field value at the zero value of the derivative spectrum.

The spectrum for the benzene protons in II at 298°K, Figure 1e, shows a single slightly asymmetric derivative curve with a second-moment value of 1.6 ± 0.2 gauss². This value is appreciably less than the rigid lattice value, 4.3 ± 0.2 gauss², and the benzene molecules are therefore reorienting about their hexad axis^{12,13} at 298°K. At 100°K, the signal for II shows a pronounced asymmetry and the line width increases to 8.5 gauss. The second moment, $S_2 = 9.6 \pm 0.2$ gauss², evaluated by the method of Andrew and Tunstall¹⁴ for asymmetric lines, is more than twice the value calculated for a rigid lattice, Table I. This difference can be attributed to an "indirect" electron dipole-nuclear dipole interaction between the Ni(II) atoms and the benzene protons. The mechanism for this interaction differs from that for the Ni(II)-NH₃

interaction since the latter is due to the presence of unpaired electron spin density at the ammonia protons, a situation which is unlikely for the nickel-benzene interaction. The present second-moment value for benzene in clathrate II at 100°K is appreciably larger than the value reported by Nakajima³ for benzene in the fully protonated clathrate, III at 77°K. The discrepancy cannot be attributed to the temperature difference or to an additional intermolecular contribution in III since both effects would act in the opposite direction to the observed discrepancy. Since the values given by Nakajima³ were apparently derived from line shapes obtained by fitting the observed curve to two assumed component curves, it is likely that at least part of the discrepancy arises from this procedure.

The spectra for the fully protonated clathrate, III (Figure 1e, f), are markedly asymmetric at both of the temperatures reported with the asymmetry most pronounced at 100°K. The present spectra also show considerably more detail at both temperatures than the earlier spectrum reported at 90°K by Nakajima.² Comparison of the spectra in Figure 1a, c, and e shows that the asymmetry for III is due to a superposition of two signals, *i.e.*, NH₃ and C₆H₆, with different H^* values.¹⁵ The difference of approximately 2 gauss is presumably due to the electron-nucleus contact interaction between Ni(II) and NH₃ which acts to shift the NH₃ protons upfield. Because of the asymmetry, a satisfactory estimate of the second moments is not feasible. However, it is not likely that the magnitude will differ very much from the sum of the values for the two deuterio clathrates. The motional properties of the enclathrated benzene in III are not expected to differ from those in the deuterated cases.

Acknowledgments. The financial support of the National Research Council of Canada and the Ontario Research Foundation is gratefully acknowledged. Part of this work was completed at Argonne National Laboratory with the support of the U. S. Atomic Energy Commission.

(9) P. H. Kim, *J. Phys. Soc. Japan*, **15**, 445 (1960).

(10) M. Kondo and M. Kubo, *J. Phys. Chem.*, **61**, 1648 (1957).

(11) R. S. Drago, J. R. Kwon, and R. D. Archer, *J. Am. Chem. Soc.*, **80**, 2667 (1958).

(12) Other modes of reorientation, *e.g.*, about the twofold axis are restricted by the geometry of the cavity.¹³

(13) H. M. Powell, G. Huse, and P. W. Cooke, *J. Chem. Soc.*, 153 (1943).

(14) E. R. Andrew and D. P. Tunstall, *Proc. Phys. Soc.*, **81**, 986 (1963).

(15) H^* is taken as the field at the zero of the derivative curve for the given signal.

Effect of Pretreatment on the Two-Dimensional Condensation of Adsorbed Krypton on Alkali Chlorides

by T. Takaishi and Masashi Saito

Institute for Atomic Energy, Rikkyo (St. Paul's) University, Yokosuka, Japan (Received August 2, 1966)

It has been found that two-dimensional condensation takes place in the adsorption of krypton on NaBr,¹ LiF,² and NaF.² It is proposed that such condensations are facilitated by easy formation of homotactic crystal surfaces and appropriate distances between adsorption sites. The interaction potential between a pair of krypton atoms has its minimum at a distance of 4.074 Å.³ Hence, it is anticipated that two-dimensional condensation may also occur on alkali halide crystals which have the NaCl-type structure and lattice constant around 4.074 Å. With this in view, the adsorption of krypton on NaCl, KCl, and RbCl at liquid nitrogen temperature was studied with special reference to the effect of heat treatment of crystals.

Experimental Section

The crystals were prepared by precipitation according to Marshall's method,⁴ and have a rather small surface area, *i.e.*, about 2 m²/g. Krypton gas with a purity of 99.9%, contained in a glass cylinder, was supplied by Takachiho Chemical Co. and used after distillation. The adsorption system, similar to that of Rosenberg,⁵ was equipped with a level controller for liquid nitrogen, and the krypton pressure was measured with an accuracy of 0.1% at 0.5 torr. The sample was heated under a vacuum of 10⁻⁶ torr or in an atmosphere of hydrogen of a few centimeters.

Adsorption isotherms obtained are shown in Figure 1. The step in the adsorption isotherm which is an indication of the two-dimensional condensation is vague for samples evacuated at such low temperatures as 120 ~ 130° and becomes progressively sharper with increasing temperature of pretreatment. It is worthy of notice that the amounts of adsorption in the regions before condensation are decreased by severe pretreatments, but those after condensation are increased. The annealing process diminished active sites which predominate in a lower pressure region, and promoted the two-dimensional condensation by offering flatter surfaces, without producing any serious sintering (except RbCl).

The adsorption isotherms with the sharp steps are

well described by a modified Fisher-McMillan equation

$$\ln \frac{P}{P_0} \frac{1 - \theta}{\theta(K + \theta)} = \frac{2w\theta}{kT} \quad (1)$$

where P , P_0 , θ , and kT have the usual meaning, $2w$ denotes the lateral interaction energy which krypton atoms may feel at $\theta = 1$, and K is a constant. In the original equation due to Fisher and McMillan,¹ K was neglected, but in general, K is to be included as can be seen from their derivation of the equation. The plots of eq 1 are shown in Figure 2, where the choice is made for the values of K to give the best linear lines.

Discussion

It may be said that the sharpness of the step in the adsorption isotherm is a measure of the surface homogeneity and is obtained by heating at temperatures fairly higher than the Tammann temperature. (The Tammann temperature is 265° for NaCl, 250° for KCl, and 221° for RbCl.) Powdery crystals, as usually recognized, sinter with a considerable rate at and above the Tammann temperature. In our case,

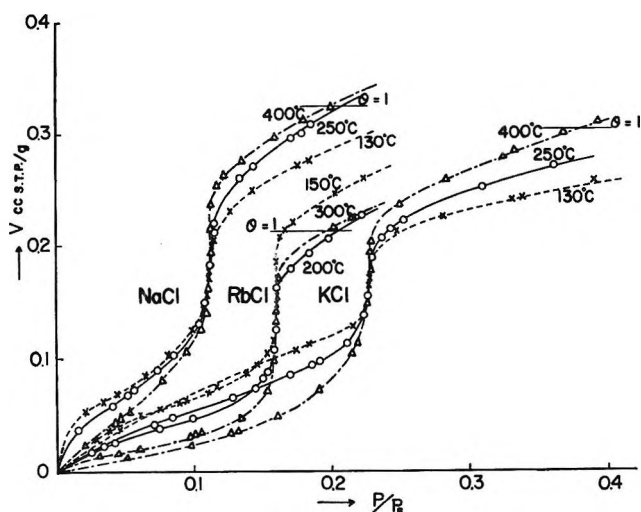


Figure 1. Adsorption isotherms of krypton on alkali chlorides at -195° . The temperatures in the figure denote pretreatment temperatures, and $\theta = 1$ is calculated by the use of eq 2. (As to RbCl, the surface area is decreased by heat treatment and the line of $\theta = 1$ is to be referred to the curve of 300° .)

- (1) B. B. Fisher and W. G. McMillan, *J. Chem. Phys.*, **28**, 549, 555, 562 (1958).
- (2) Y.-F. Yu Yao, *J. Phys. Chem.*, **69**, 2472 (1965).
- (3) A. K. Bawa and P. K. Chakraborti, *Physica*, **27**, 753 (1961).
- (4) F. H. Marshall, *Phys. Rev.*, **56**, 642 (1940).
- (5) A. J. Rosenberg, *J. Am. Chem. Soc.*, **78**, 2929 (1956).

however, relatively coarse powders are installed in a glass vessel without any compression, and hence the intercrystallite diffusion of constituent ions may probably be inhibited, but the surface diffusion in each crystallite may be rapid at and above the Tammann temperature. If the active adsorption sites originate from point defects on the surface, they would disappear by heating at 260°, while if they originate from

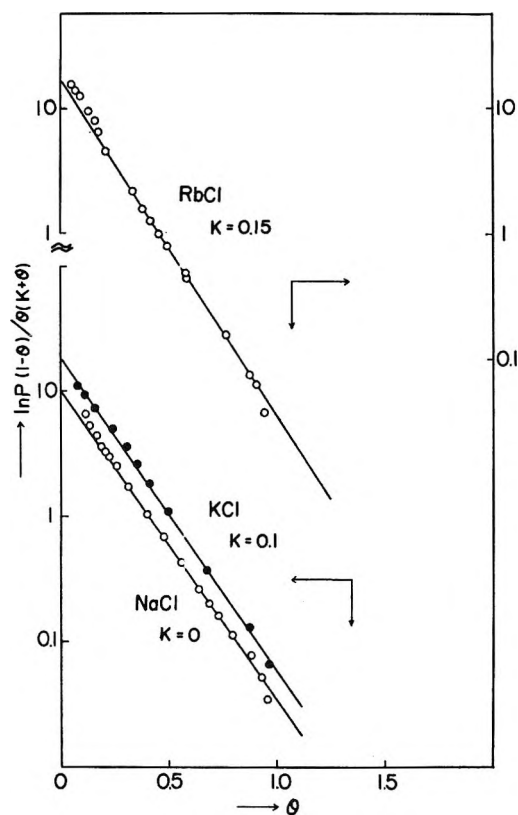


Figure 2. Fisher-McMillan plots of the adsorption of krypton on alkali halides at -195° . The points are obtained from the isotherms for the samples pretreated at highest temperatures in Figure 1.

the edges of a crystal, they would not diminish under the present condition since the absolute surface area remains almost constant. The experimental results show that neither of these is the case. Thus, the origin of active adsorption sites may be attributed either to the surface dislocation which persists even above the Tammann temperature, or to impurities on the surface. It is verified that the latter is the case by the following experiments. After getting a homotactic surface by evacuation at 400°, we removed the liquid nitrogen from the trap and after 1 day the surface returned to the original state; *i.e.*, the adsorption isotherm showed a vague step similar to that produced

when the sample was evacuated at about 130°. These results, as well as previous data on the difference between precipitated and anhydrous sodium bromide,⁶ suggest that water is the impurity adsorbate which affects the adsorption isotherm.

Because of their theoretical importance, surface properties of alkali chlorides have been studied from various points of view,⁷ and some experiments inevitably require large surface area, and hence heat treatments which diminish the surface must be avoided. However, the present results show that preevacuation, to at least 350°, is necessary to study homotactic surface properties. The physical adsorption is rather less structure-sensitive in comparison with chemisorption and other electronic processes. Hence, the sharp step in an adsorption isotherm of krypton is a minimum condition to be satisfied by the *cleaned* and *homotactic* surfaces of alkali chlorides.

Recently, Yao² suggested that the monolayer capacity, V_m , is obtained from the end point of the step in the adsorption isotherm when two-dimensional condensation takes place and the BET equation cannot be applied. This procedure, however, is open to some ambiguities, since the position of the end point depends on pretreatments of the adsorbent. On the other hand, the position of the middle point of the step is rather insensitive to pretreatments and may be used to measure the surface area. According to the Fisher-McMillan equation, the amount adsorbed at the middle point of the step, V_{mid} , differs only slightly from that at the critical point of the two-dimensional condensation, which corresponds to $\theta = 0.58$. Hence, by putting

$$V_m = V_{mid}/0.58 \quad (2)$$

we can obtain a good approximation for V_m . An error introduced due to uncertainties in the positions of the starting and end points of the step may not exceed 5% if a carefully measured isotherm is used.

Acknowledgment. The authors' thanks are due to Dr. K. M. Sancier of the Stanford Research Institute, who corrected the manuscript.

(6) S. Ross, J. P. Oliver, and J. J. Hinchey, "Solid Surfaces and the Gas-Solid Interface," *Advances in Chemistry Series*, No. 33, American Chemical Society, Washington, D. C., 1961, p. 317.

(7) D. M. Young, *Trans. Faraday Soc.*, **50**, 838 (1954); J. A. Morrison and D. Patterson, *ibid.*, **52**, 764 (1956); L. G. Harrison, J. M. Hoodless, and J. A. Morrison, *Discussions Faraday Soc.*, **28**, 103 (1959); R. Rudham, *Trans. Faraday Soc.*, **59**, 1853 (1963); G. C. Benson and G. W. Benson, *Can. J. Chem.*, **33**, 232 (1955); P. Balk and G. C. Benson, *J. Phys. Chem.*, **63**, 1009 (1959); R. J. Adams and L. G. Harrison, *Trans. Faraday Soc.*, **60**, 1792 (1964); J. A. Morrison and K. Nakayama, *ibid.*, **59**, 2560 (1963).

Gibbs Equation for the Adsorption of Charged Micelles

by D. K. Chattoraj

Department of Chemistry, Jadavpur University,
Calcutta 32, India (Received August 11, 1966)

The general forms of the Gibbs equation for the adsorption of the surface-active monovalent and polyvalent ions in the presence and absence of the neutral salt have recently been proposed.^{1,2} An attempt will be made here to extend this treatment for the adsorption of the charged micelle in equilibrium with its monomer at the air-water and oil-water interfaces.

Let C_R and C_B^M be the bulk concentrations of the monomeric soap (e.g., RNa) and their associated micelle, and let Z represent the number of the monomeric units aggregating within a micelle. In the usual experimental arrangement, the boundary tension is measured at varying soap concentrations in the presence of the constant concentration C of the neutral salt (e.g., NaCl). The Gibbs adsorption equation for such system will be given by³

$$-d\gamma = n_R d\mu_R + n_S^M d\mu_S^M + n_{Na^+} d\mu_{Na^+} + n_{Cl^-} d\mu_{Cl^-} \quad (1)$$

where γ is the boundary tension, n_R , n_S^M , n_{Na^+} and n_{Cl^-} are the surface concentrations of the monomer, micelle, sodium and chloride ions, respectively, per unit area; μ represents the equilibrium chemical potentials of the ions concerned. As before, since the neutral salt concentration is kept constant, the $n_{Cl^-} d\mu_{Cl^-}$ term in eq 1 may be neglected.²

Now within the bulk phase, the organic amphipathic ions will associate due to the dislike of their hydrocarbon tail toward water. When these surface-active ions come to the surface phase, their hydrophobic tail part will remain in the oil phase. The cohesive and hydrophobic forces responsible for the micellization in the bulk will disappear in the surface phase so that n_S^M in eq 1 may be put equal to zero. Adsorbed ions in the surface will remain only in the monomeric form and eq 1 will now become

$$-d\gamma = n_R \frac{dC_R}{C_R} KT \left[1 + \frac{n_{Na^+}}{n_R} \frac{C_R}{C_{Na^+}} \frac{dC_{Na^+}}{dC_R} \right] \quad (2)$$

Here C_R represents the bulk concentration of the monomer in equilibrium with bulk micelle concentration C_B^M .

Now assuming complete dissociation of the micelle and the monomer, we can write

$$C_{Na^+} = C_R + ZC_B^M + C \quad (3)$$

Since C is constant

$$dC_{Na^+} = dC_R + Z dC_B^M$$

or

$$\frac{dC_{Na^+}}{dC_R} = 1 + Z \frac{dC_B^M}{dC_R} \quad (4)$$

The bulk equilibrium constant K' for the micellar reaction will be given by the expression

$$K' = \frac{C_B^M}{[C_R]^Z} \quad (5)$$

or

$$\ln K' = \ln C_B^M - Z \ln C_R \quad (6)$$

Differentiating eq 6 and rearranging

$$\frac{dC_B^M}{dC_R} = Z \frac{C_B^M}{C_R} \quad (7)$$

Putting this result in eq 4

$$\frac{dC_{Na^+}}{dC_R} = 1 + Z^2 \frac{C_B^M}{C_R} \quad (8)$$

Assuming the structure of the double layer to be of the Helmholtz type

$$n_R = n_{Na^+} \quad (9)$$

Using relations 3, 8, and 9, the KT coefficient m , representing the expression within the bracket of 2, will be given by

$$\begin{aligned} m &= 1 + \frac{C_R}{C_R + ZC_B^M + C} \left[1 + \frac{Z^2 C_B^M}{C_R} \right] \\ &= 1 + \frac{1 + [Z^2 C_B^M / C_R]}{1 + x + [ZC_B^M / C_R]} \end{aligned} \quad (10)$$

Here x stands for the ratio C/C_R .

We can also eliminate C_B^M in eq 10 by using eq 5.

$$m = 1 + \frac{1 + K' Z^2 C_R^{Z-1}}{1 + x + K' Z C_R^{Z-1}} \quad (11)$$

If, however, a Gouy model is proposed for the interfacial double layer, then eq 12 results.

(1) D. K. Chattoraj, *J. Phys. Chem.*, **70**, 2687 (1966).

(2) D. K. Chattoraj, *ibid.*, **70**, 3743 (1966).

(3) J. T. Davies and E. K. Rideal, "Interfacial Phenomena," Academic Press, New York, N. Y., 1961.

$$n_R + n_{Cl^-} = n_{Na^+} \quad (12)$$

Putting relations 3, 8, and 12 in the bracketed term of eq 2 representing the KT coefficient m' , we shall obtain

$$m' = 1 + \frac{1}{1 - \frac{n_{Cl^-}}{n_{Na^+}}} \frac{C_R}{C_R + ZC_B^M + C} \left[1 + Z^2 \frac{C_B^M}{C_R} \right] \quad (13)$$

From the Boltzmann distribution principle¹

$$\frac{n_{Cl^-}}{n_{Na^+}} = \frac{C_{Cl^-}^S}{C_{Na^+}^S} = \frac{C e^{-\psi/KT}}{(C_R + ZC_B^M + C) e^{\psi/KT}} \quad (14)$$

where C_s stands for the surface concentration per unit volume and ψ is the potential for the Gouy double layer. Putting eq 14 in eq 13 and simplifying

$$m' = 1 + \frac{1 + Z^2 \frac{C_B^M}{C_R}}{1 + x(1 - e^{-2\psi/KT}) + Z \frac{C_B^M}{C_R}} \quad (15)$$

It is to be noted with interest that for the negligible bulk micelle formation ($C_B^M \rightarrow 0$), eq 10 and 15 will be converted to the simple forms already derived.¹ At very high salt concentration, the KT coefficient will be unity. In the absence of salt, however (x is zero)

$$KT \text{ coefficient} = 1 + \frac{1 + Z^2 \frac{C_B^M}{C_R}}{1 + Z \frac{C_B^M}{C_R}} \quad (16)$$

The coefficient in the absence of the salt seems to be dependent on the ratio C_B^M/C_R and for each concentration of soap, its value is to be calculated. Its value seems from eq 16 to be higher than 2 compared to the value 2 in the absence of the micelle. At critical micelle concentration, γ has been experimentally found to be almost independent of the soap concentration ($d\gamma \rightarrow 0$). The minimum value of the KT coefficient has been shown to be unity and n_R in eq 2 is a positive quantity at the cmc. So for $d\gamma$ to be zero, dC_R/C_R or $d \ln C_R$ in eq 2 must tend toward zero, which means that the concentration of the monomer will remain almost constant at the cmc whereas the concentration of the micelle will increase with the addition of soap further above the cmc.

Among the amphiphatic ions, the bulk micellar properties, as well as the boundary tension of sodium lauryl sulfate (NaLS) have been most widely studied. The excellent work of Mukherjee, *et al.*,^{4,5} has recorded that

even at the very high dilution, NaLS partly dimerizes (Z equal to 2). The dimerization constant has been estimated by them from which the equilibrium concentrations C_R and C_B^M for the monomer and dimer, respectively, can be calculated. Equations 10 and 15 can be fully utilized to calculate correctly the surface concentration or the area per adsorbed molecule for such a system with the help of the Gibbs equation. Calculation of the pressure-area values of the NaLS system in this way will be shown to remove many confusions existing in the estimation of the electrical free energy contribution of the surface pressure.^{6,7} Recently, considerable interest has also been found for the accurate measurement of the boundary tension of NaLS above the critical micelle concentration⁸ in the absence of the neutral salt. Equation 16 will be useful to interpret these data correctly from the prior accurate knowledge about the micellar constant and the micelle number.

In deducing eq 10 and 15, the absence of the micelles in the interfacial phase has been assumed. However, for the organic ions of considerable chain length within the monolayer at the air-water interface, the possibility of aggregation exists when the pressure due to inter-chain cohesion overcomes the pressure effect due to electrical repulsion.⁹ Let n_R' represent the total monomer concentration per unit area of the surface phase prior to this kind of interfacial micellization and let $p x_s$ fraction of this monomer aggregate p times to form x_s fraction of the micelle. The thermodynamic equilibrium for this micellization reaction will be expressed by

$$p\mu_R = \mu_s^M$$

or

$$pd\mu_R = d\mu_s^M \quad (17)$$

and

$$n_R' = n_R + pn_s^M \quad (18)$$

Inserting eq 17 and 18 in eq 1 and again setting $n_{Cl^-} d\mu_{Cl^-}$ equal to zero under the experimental condition results in eq 19.

(4) P. Mukherjee, K. J. Mysels, and C. I. Dulin, *J. Phys. Chem.*, **62**, 1390 (1958).

(5) P. Mukherjee, *ibid.*, **62**, 1397, 1404 (1958).

(6) A. K. Chatterjee, Thesis, Jadavpur University, 1966.

(7) G. M. Bell, S. Levine, and B. A. Pethica, *Trans. Faraday Soc.*, **58**, 904 (1962).

(8) P. H. Elworthy and K. J. Mysels, *J. Colloid Surface Sci.*, **21**, 331 (1966).

(9) D. K. Chatteraj and A. K. Chatterjee, *ibid.*, **21**, 159 (1966).

$$-d\gamma = n_t \frac{dC_R}{C_R} KT \left[1 + \frac{n_{Na^+}}{n_R^t} \frac{C_R}{C_{Na^+}} \frac{dC_{Na^+}}{dC_R} \right] \quad (19)$$

The electroneutrality conditions $n_R^t = n_{Na^+}$ for the Helmholtz double layer and $n_R^t + n_{Cl^-} = n_{Na^+}$ for the Gouy double layer will remain unchanged when the part of n_R^t aggregates in the surface phase. The value of the bracketed term in eq 19 representing the KT coefficient will be given again by either eq 10 or 15. However, from the plot of γ against C_R for this special case, it will be possible only to calculate n_R^t , the total number of monomeric ions per unit area prior to surface micellization. The real equilibrium value of the area per molecule is however, equal to $1/[n_R^t(1 - px_s + x_s)]$ since the number of molecules per unit area changes from n_R^t to $n_R^t(1 - px_s + x_s)$ due to micellization. When micelles exist in the surface phase, the calculation of the real area per molecule will be difficult due to the lack of information about p and x_s from the experimental data. Under special circumstances for the $C_{18}H_{37}N(CH_3)_3^+Br$ and $C_{26}H_{53}N(CH_3)_2^+Cl$ monolayers at the air-water interface, their values can be estimated from the data of cohesional pressure.⁹

Let us now consider the limitation of eq 10 and 15 when applied to an actual micellar system. These equations have been derived on the basis of the Helmholtz and Gouy models for the interfacial double layer. If, however, the validity of the Stern model is assumed, then ψ_d , the potential of the diffuse part of the double layer, should replace ψ in eq 15. For ψ above 25 mv, it has already been shown that $(1 - e^{-2e\psi/KT}) \rightarrow 1$, and eq 15 will be independent of the model of the double layer.

We have assumed in eq 3 that the micelle has been completely dissociated, whereas experimental evidence indicates about 30 to 50% dissociation.¹⁰⁻¹² The degree of dissociation, however, has been shown¹⁰⁻¹² to be independent of the neutral salt concentration. If this is the case, then Z in eq 15 will represent the number of the actual charge per micelle in the bulk and not the aggregation number. The charge may be assumed to be constant within the limited range of the soap concentration during the application of eq 15. Another limitation of eq 15 is that here the equilibrium concentration C_R is to be plotted against γ . Accuracy for the value of C_R will depend upon the accuracy of determining K' which is really a problem.¹³ The third point is that we have neglected the activity coefficients of the

monomer and the micelle in eq 2 and 5. Very little is, in fact, known about the activity coefficients of these substances above and even below the cmc,⁸ and in our future analysis, an attempt will be made to take this important factor into account.

Gaseous Oxides and Oxyacids of Iodine and Xenon: Mass Spectra¹

by Martin H. Studier

Chemistry Division, Argonne National Laboratory, Argonne, Illinois

and John L. Huston

Chemistry Department, Loyola University, Chicago, Illinois
(Received August 18, 1966)

Volatility of oxygen compounds of xenon and iodine decreases in the order: XeO_4 , XeO_3 , HIO_4 , I_2O_5 ; all are sufficiently volatile to allow their mass spectra to be observed by appropriate techniques. The mass spectra reported here were observed with a Bendix time-of-flight mass spectrometer equipped with a source² modified to allow continuous, as well as pulsed, operation of the ionizing electron beam. They are presented as photographs of oscilloscope displays. The small peaks at every mass, from trace hydrocarbon impurities, were used for precise mass determinations.

Xenon tetroxide is the most volatile, most reactive, and least stable of the three known volatile tetroxides: OsO_4 , RuO_4 , and XeO_4 . It has been made³ by reaction of concentrated sulfuric acid with the stable perxenate salts of sodium, rubidium, and barium, *i.e.*, with salts of octavalent xenon. We find that it is also generated by reaction of concentrated sulfuric acid with the explosive yellow alkali metal salts of the type $K_2XeO_4 \cdot 2XeO_3$ reported by Appelman and Malm,⁴ providing thereby confirmation of the presence of octavalent xenon in these compounds. On the other hand, when the recently prepared⁵ salt of hexavalent xenon, monocationic xenate, $CsHXeO_4$, is decomposed in sulfuric

(1) Based on work performed under the auspices of the U. S. Atomic Energy Commission.

(2) M. Studier, *Rev. Sci. Instr.*, **34**, No. 12, 1369 (1963).

(3) J. L. Huston, M. H. Studier, and E. N. Sloth, *Science*, **143**, 1161 (1964); H. Selig, H. H. Claassen, C. L. Chernick, J. G. Malm, and J. L. Huston, *ibid.*, **143**, 1322 (1964).

(4) E. H. Appelman and J. G. Malm, *J. Am. Chem. Soc.*, **86**, 2141 (1964).

(5) B. Jaselskis, T. M. Spittler, and J. L. Huston, *ibid.*, **88**, 2149 (1966).

(10) M. L. Corrin, *J. Colloid. Sci.*, **3**, 333 (1948).

(11) D. Stigter, *Rec. Trav. Chim.*, **73**, 771 (1954).

(12) D. Stigter and K. J. Mysels, *J. Phys. Chem.*, **59**, 452 (1955).

(13) B. A. Pethica, Proceedings of the Third International Congress of Surface Activity, Amsterdam, Vol. I, 1960, p 212.

acid, xenon and oxygen are observed in the evolved gases but no xenon compounds. Mass spectrographic observation of xenon tetroxide thus provides a simple verification of the presence of octavalent xenon in a compound.

The volatility of xenon tetroxide allows its mass spectrum readily to be observed if it is generated and conducted to the source of the mass spectrometer in a system sufficiently inert. Pyrex glass, fluorocarbon plastics, and fluorinated metal have been used successfully. The material can be purified by fractional distillation in such a system. Vapor from purified samples maintained at Dry Ice temperature has been valved to the mass spectrometer source maintaining therein sufficiently constant pressure to allow scans to be made of relative intensities of the various peaks, Xe^+ , 100, XeO^+ , 3.7, XeO_2^+ , 8.0, XeO_3^+ , 3.6, XeO_4^+ , 1.4 at an ionizing energy of 70 ev. The observed ratios were substantially constant and provided no evidence for formation in the spectrometer of lower xenon oxides such as XeO or XeO_2 .

Mass spectra of substances of lower volatility have been observed by means of an apparatus originally designed for study of surface ionization.² Samples were mounted on a platinum filament which could be electrically heated while inserted in the mass spectrometer source close to the ionizing electron beam. Samples of xenon trioxide have thus yielded mass spectra as shown in Figure 1. The spectrum displays the typical isotopic composition of xenon repeated at intervals of 16 mass units, corresponding to Xe^+ , XeO^+ , XeO_2^+ , and XeO_3^+ . Again, scans of the various peaks indicate substantial constancy of their relative intensities and no evidence for formation of lower oxides such as XeO or XeO_2 . The mass spectrum could be ob-

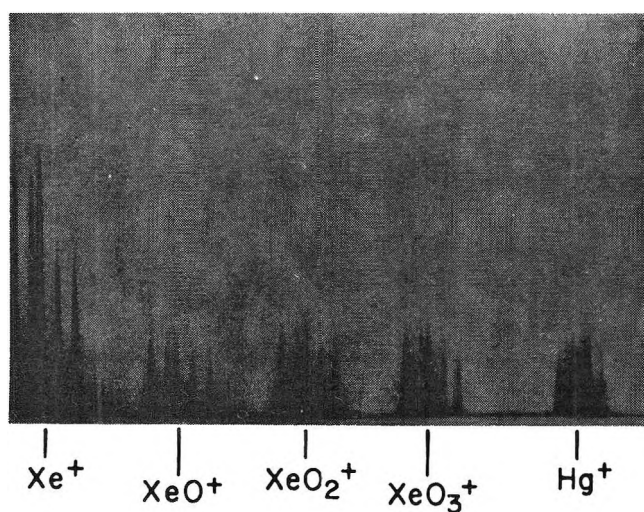


Figure 1. Mass spectrum of xenon trioxide.

served at room temperature when the sample (which had been mounted from aqueous solution) was sufficiently dehydrated to allow the mass spectrometer to be operated, and became more intense when the sample was heated.

No oxyacid of xenon such as H_2XeO_4 could be observed, indicating that whatever may be the extent of hydration of "xenic acid" in aqueous solution, no sufficiently strong association to the solvent exists to produce an oxyacid in the gas phase.

Observation of the existence of XeO_3 in the vapor phase encouraged us to try purification of the material by molecular distillation. The distillation proceeds with some decomposition to xenon and oxygen, yields of recovered XeO_3 ranging from 50 to 75% as shown by titration. The distillation takes place conveniently around 70° with the distilled material depositing as a white solid on the walls of the glass apparatus. In one experiment, it was distilled onto a surface ionization apparatus which was then inserted into the mass spectrometer to verify that the deposited material was in fact XeO_3 .

Most distillations have been done successfully when quantities of around 20 mg of material were used, but some have resulted in explosions which broke the containing glass apparatus. Two attempts were made to distil 100 mg, but in both cases explosions resulted.

Periodic acid samples were placed in the mass spectrometer in the same manner as xenon trioxide and the mass spectrum observed as shown in Figure 2. Somewhat higher filament temperature was required than for XeO_3 . The mass of parent HIO_4 was identified by reference to the mercury spectrum, counting down from

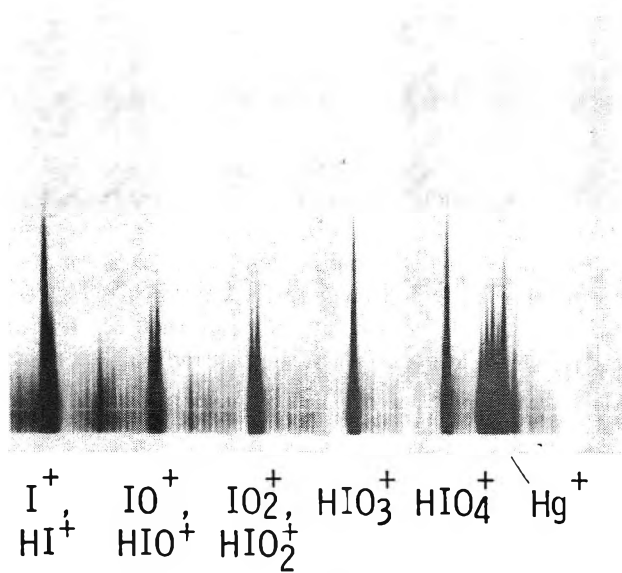


Figure 2. Mass spectrum of periodic acid.

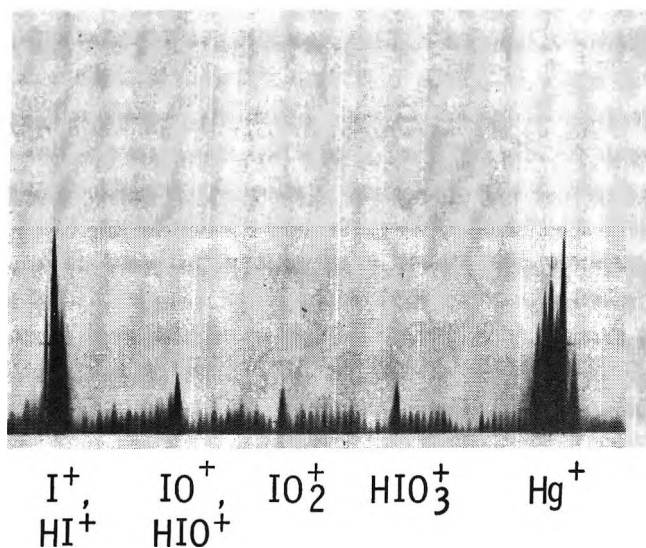


Figure 3. Mass spectrum of iodic acid.

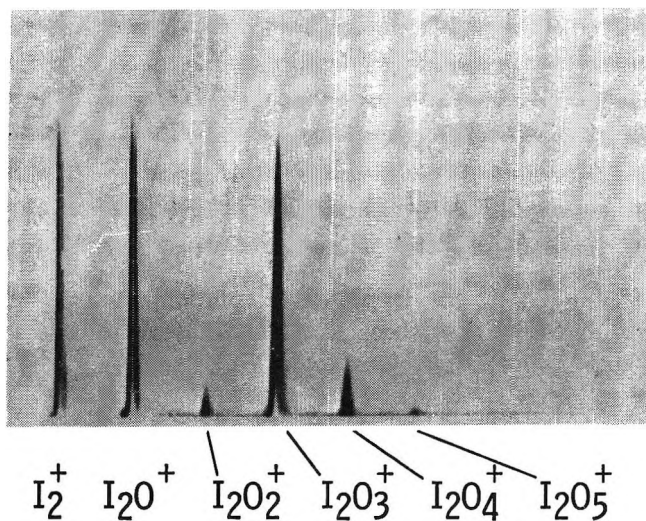


Figure 4. Mass spectrum of iodine pentoxide.

198 to 192. Hypiodous acid was formed as an independent species. It varied in intensity relative to the other peaks and persisted in the mass spectrometer after heating of the sample had been discontinued and the spectrum of HIO_4 itself could no longer be observed.

No evidence was obtained for periodic acid anhydride, I_2O_7 .

Iodic acid similarly mounted on a filament yielded the mass spectrum of HIO_3 as shown in Figure 3. After the sample was sufficiently dehydrated, heating of the filament caused sufficient volatilization of I_2O_5 to give the mass spectrum of Figure 4. Scans of these various peaks showed no substantial variation in relative intensities and no evidence for formation of such

lower oxides as I_2O . However, IO^+ and IO_2^+ were also observed along with the dimeric iodine species of Figure 4 and were seen to undergo marked fluctuations in intensity relative to the dimeric species, thus indicating an independent existence for IO_2 in the gases produced by vaporization of I_2O_5 .

Acknowledgment. We are grateful to Mr. Leon P. Moore for technical assistance.

Concerning the Spectroscopic Determination of the Structure of Water

by Gerhard Boettger, Hartwig Harders,

Rechenzentrum der Badischen Anilin- & Soda-Fabrik AG, Ludwigshafen am Rhein

and Werner A. P. Luck

Hauptlaboratorium der Badischen Anilin- & Soda-Fabrik AG, Ludwigshafen am Rhein, Germany (Received February 25, 1966)

In a former publication, it was attempted to estimate the approximate proportions of open and closed hydrogen bonds of water (from the change of infrared bands) in order to test the available theories concerning the structure of water.¹ By extensive measurements up to and above the critical point,²⁻⁶ it was attempted to increase the probability of the approximations. During these measurements, Buijs and Choppin⁷ reported a method of calculation in which, by use of measurements in a small area of temperatures, the relative concentrations of the individual species of water without H bonds, c_0 , with one H bond, c_1 , and with two H bonds, c_2 , and also the unknown extinction coefficients could be determined. Therefore, they took the gross molar extinction coefficients E_n^i at three wavelengths λ_n ($n = 1, 2, 3$) and at different temperatures T_i ($i = 1, 2, \dots$).

(1) W. A. P. Luck, Vortrag Tagung der Deutschen Bunsengesellschaft für Physikalische Chemie, Münster, Feb 6, 1962; *Z. Elektrochem.*, **66**, 766 (1962); *Ber. Bunsenges.*, **67**, 186 (1963).

(2) W. A. P. Luck, *Fortschr. Chem. Forsch.*, **4**, 653, 877 (1964).

(3) W. A. P. Luck, *Nachr. Chem. Technik*, **12**, 345 (1964).

(4) W. A. P. Luck, *Ber. Bunsenges.*, **68**, 895 (1964); **69**, 69 (1965).

(5) W. A. P. Luck, *ibid.*, **69**, 626 (1965).

(6) W. A. P. Luck, *Naturwissenschaften*, **52**, 25, 49 (1965).

(7) K. Buijs and G. R. Choppin, *J. Chem. Phys.*, **39**, 2035 (1963).

$$\begin{aligned}
 \epsilon_1^0 C_0^i + \epsilon_1^1 C_1^i + \epsilon_1^2 C_2^i &= E_1^i \\
 \epsilon_2^0 C_0^i + \epsilon_2^1 C_1^i + \epsilon_2^2 C_2^i &= E_2^i \\
 \epsilon_3^0 C_0^i + \epsilon_3^1 C_1^i + \epsilon_3^2 C_2^i &= E_3^i \\
 C_0^i + C_1^i + C_2^i &= 1
 \end{aligned}
 \quad (i = 1, 2, \dots) \quad (1)$$

For simplification of this problem, it was assumed that the ϵ_n^k is not a function of temperature. In the meantime, Goldstein and Penner,⁸ and Thomas, Scheraga and Schrier⁹ have followed this procedure and solved eq 1 using a least-squares procedure. For simplification of the problem, all three teams have introduced the following assumptions: $\epsilon_3^0 = 0$; $\epsilon_1^1 = \epsilon_3^1$; ϵ_n^2 known from ice spectra.

Under these assumptions, seven temperatures are required to make the number of equations at least equal the number of unknowns. The spectroscopic results found in this manner have already been discussed further. Therefore, we wish to point out that the nonlinear system of eq 1 (also by using the introduced assumption of approximations) may have more than one solution. In other words, the reported solutions are possible solutions but not the only ones. Using the solution reported by Scheraga,⁹ we calculated as an example the gross molar extinction coefficients E_n^i and received from (1) the additional systems of solutions shown in Table I.

Table I

T_i , °C	System 1			System 2		
	C_0	C_1	C_2	C_0	C_1	C_2
12.5	0.188	0.553	0.259	0.315	0.110	0.576
32.0	0.239	0.575	0.187	0.370	0.114	0.515
41.3	0.262	0.583	0.156	0.395	0.116	0.489
54.8	0.298	0.590	0.112	0.433	0.117	0.449
68.2	0.332	0.593	0.075	0.468	0.118	0.414
73.4	0.347	0.590	0.063	0.482	0.117	0.400
82.5	0.371	0.586	0.043	0.506	0.117	0.378
	$\epsilon_1^0 = 19.06$	$\epsilon_2^0 = 1.25$	$\epsilon_3^0 = 0$			
	$\epsilon_1^2 = 1.33$	$\epsilon_2^2 = 5.78$	$\epsilon_3^2 = 8.97$			

Together with the solution reported by Scheraga, *et al.*, there are already three possible solutions. According to the following formulas one can calculate any number of solutions. Therefore, by use of the method of Buijs and Choppin,⁷ it is not possible to reach unequivocal solutions without additional assumptions to the problem. The assumptions used by the three

teams only limit the variety of the possible solutions. Therefore, it seems that there exist certain ranges of concentration for possible solutions. Our two systems of solutions have been chosen near the limits of the free selectable parameter $d_{1,2}$. We did not vary $d_{1,1}$. Thus, we left the ϵ_n^0 unchanged. This corresponds with the status of our experiments which enable us by measurements at the critical point to estimate ϵ_1^0 , ϵ_2^0 , and ϵ_3^0 .

Now we demonstrate the possibility of getting additional solutions from one given solution of system 1. First, we write (1) as a matrix equation

$$AC = F$$

with

$$\begin{aligned}
 A &= (a_1, a_2, a_3), \quad a_{j+1} = \begin{pmatrix} \epsilon_1^j \\ \epsilon_2^j \\ \epsilon_3^j \\ 1 \end{pmatrix} \\
 C &= (c_1, c_2, \dots, c_n), \quad c_i = \begin{pmatrix} C_0^i \\ C_1^i \\ C_2^i \end{pmatrix} \\
 F &= (f_1, f_2, \dots, f_n), \quad f_i = \begin{pmatrix} E_1^i \\ E_2^i \\ E_3^i \\ 1 \end{pmatrix}
 \end{aligned}$$

If A and C already represent a solution, then $\bar{A} = AD$ and $\bar{C} = D^{-1}C$ because $ADD^{-1}C = AC$ is also a solution of (1).

$$D = d_{m,n} \quad (m = 1, 2, 3; \quad n = 1, 2, 3)$$

Clearly, with the additional assumptions introduced for several ϵ by the three teams, not every 3×3 matrix D , $\det D \neq 0$, is allowed. The elements of D must apply the following conditions

$$\sum_{k=1}^3 a_{m,k} \cdot d_{k,3} = a_{m,3}$$

because the ϵ_n^2 are given

$$\sum_{k=2}^3 a_{3,k} \cdot d_{k,1} = 0$$

because $\epsilon_3^0 = 0$

$$\sum_{k=1}^3 a_{1,k} \cdot d_{k,2} = \sum_{k=2}^3 a_{3,k} \cdot d_{k,2}$$

because $\epsilon_1^1 = \epsilon_3^1$ is required. In addition, there must be

(8) R. Goldstein and S. S. Penner, *J. Quant. Spectry.*, **4**, 441 (1964).

(9) M. R. Thomas, H. A. Scheraga, and E. E. Schrier, *J. Phys. Chem.*, **69**, 3722 (1965).

$$\sum_{k=1}^3 a_{4,k} \cdot d_{k,n} = \sum_{k=1}^3 d_{k,n} = 1$$

because of the structure of (1). Under this condition, the matrix D becomes

$D =$

$$\begin{bmatrix} d_{1,1} & & d_{1,2} & 0 \\ (1-d_{1,1})a_{3,3} & a_{1,3} - a_{3,3} - (a_{1,3} - a_{3,3} - a_{1,1})d_{1,2} & & 0 \\ a_{3,3} - a_{3,2} & a_{13} - a_{33} - a_{12} + a_{32} & & \\ \frac{(1-d_{1,1})a_{3,2} & a_{3,2} - a_{1,2} - (a_{3,2} - a_{1,2} + a_{1,1})d_{1,2}}{a_{3,3} - a_{3,2} & a_{1,3} - a_{3,3} - a_{1,2} + a_{3,2}} & & 1 \end{bmatrix}$$

Here $d_{1,1}$ and $d_{1,2}$ are free selectable parameters. The physical condition that the elements of the new solution \bar{A} and \bar{C} should be positive limits the two parameters to ranges the limits of which depend upon the

initial solution A, C in a clear manner. We choose $d_{1,1} = 1$ for the reason just pointed out and get

$$D = \begin{pmatrix} 1 & d_{1,2} & 0 \\ 0 & 1 - 3.4948d_{1,2} & 0 \\ 0 & 2.4948d_{1,2} & 1 \end{pmatrix}$$

with $-0.65 \leq d_{1,2} \leq 0.11$. $d_{1,2} = 0.1$ gives system 1, and $d_{1,2} = 0.65$ gives system 2 listed in Table I.

Our remark should not mean that it is impossible to say something on the structure of water by spectroscopic methods. A critical discussion of the previous spectroscopic papers give a joint model of the water structure according to present experimental knowledge.¹⁰

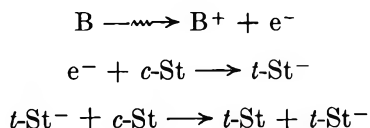
Acknowledgment. We thank Mr. and Mrs. W. Ditter for the translation of this paper.

(10) W. A. P. Luck, *Ber. Bunsenges.*, in press.

COMMUNICATIONS TO THE EDITOR

High-Energy Induced Isomerization of Stilbene in Benzene Solution¹

Sir: Recent work on ⁶⁰Co γ -induced isomerization of stilbene in this laboratory² has demonstrated that, in both cyclohexane and benzene solutions, the G values of *trans* \rightarrow *cis* isomerization, *i.e.*, $G(t \rightarrow c)$, attain approximate plateau values at a concentration of *trans*-stilbene near 0.1 M , while the G of *cis* \rightarrow *trans* continues to rise. The highest value of $G(c \rightarrow t)$ reported in that work, in the case of 1.8 M *c*-stilbene in benzene solution, was ~ 5.6 .³ These results were interpreted on the assumption of a very important contribution of an ionization-transfer chain, *e.g.*



(where B is benzene and St is stilbene) plus a chain-termination step involving neutralization by an ionizable impurity.

Ionizable impurity may be present in the original sample or be produced as a result of irradiation. In very recent work (part of an effort addressed toward

establishment of mechanism), we have checked the role of ionizable impurity (a) by working with *c*-stilbene from which a remnant of major impurity (suggested by the suppliers, Aldrich Chemical Co., Inc., to be β -methyl-naphthalene) was removed by distillation in a spinning-band column, and (b) by studying the effect of irradiation dose. The results pertinent for this report are summarized in Figure 1 which shows that for high-purity *cis*-stilbene irradiated for 2.5 min (*i.e.*, total dose = 2.98×10^{18} ev ml⁻¹), values of $G(c \rightarrow t)$ range up to *ca.* 210. By contrast, the maximum $G(t \rightarrow c) \cong 3.0$, reported in earlier work, was not significantly affected by further purification or by time of irradiation.

The import of this communication does *not* involve speculation regarding the ionization-chain mechanism.² The important fact is that a G value of *ca.* 210 cannot possibly be interpreted in terms of any nonchain process involving *any* single species producible in a high-

(1) This is U. S. Atomic Energy Commission Document COO-38-495.

(2) R. R. Hentz, D. B. Peterson, S. B. Srivastava, H. F. Barzynski, and M. Burton, *J. Phys. Chem.*, **70**, 2362 (1966).

(3) Cf. R. A. Caldwell, D. G. Whitten, and G. S. Hammond, *J. Am. Chem. Soc.*, **88**, 2659 (1966), who report a value of $G(c \rightarrow t) = 4.45$ at 1.045 M *c*-stilbene.

energy process. For example, a suggestion³ that $2.4 \times G(c \rightarrow t)$ corresponds to a value of G (triplets) is inadmissible in terms of these new results; *i.e.*, G (triplets) in benzene cannot be $>ca. 100 \text{ ev}/3.6 \text{ ev}$ (*i.e.*, ~ 28), where 3.6 eV is the excitation energy of the $^3B_{1u}$ state of benzene.⁴ The only reasonable inference from the

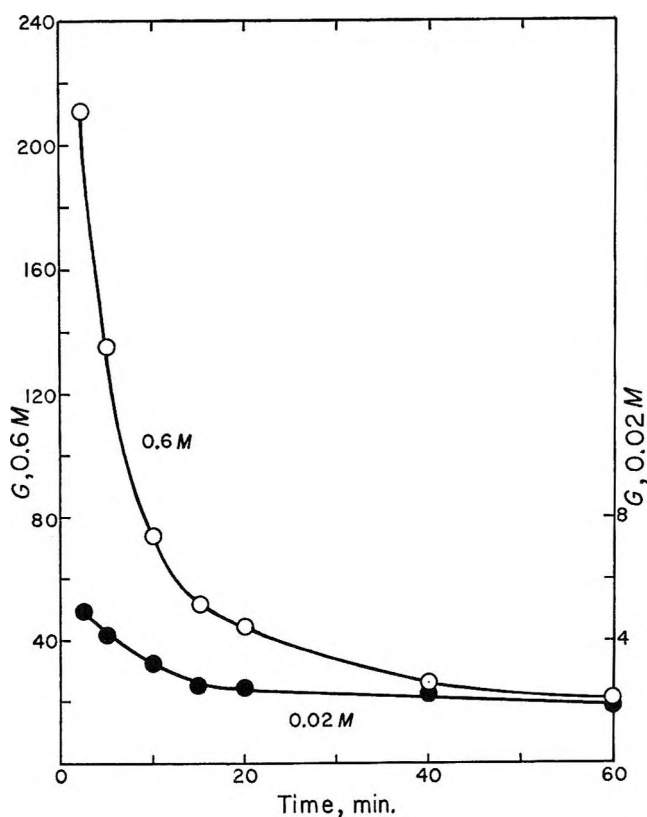


Figure 1. Yields of isomerization of *cis*-stilbene in benzene as functions of concentration and time of ^{60}Co γ irradiation at a dose rate of $\sim 1.2 \times 10^{18} \text{ ev ml}^{-1} \text{ min}^{-1}$.

present results is that in radiation-sensitized *cis* \rightarrow *trans* isomerization of stilbene in benzene solution a chain mechanism is involved. Further, if the suggestion of an ionic chain is accepted, the earlier described method of calculation² leads to a chain length of *ca.* 2000 on the basis of $G(c \rightarrow t) \sim 210$.

(4) Cf. N. J. Turro, *J. Chem. Educ.*, **43**, 13 (1966).

DEPARTMENT OF CHEMISTRY AND THE
RADIATION LABORATORY
UNIVERSITY OF NOTRE DAME
NOTRE DAME, INDIANA 46556

ROBERT R. HENTZ
K. SHIMA
MILTON BURTON

RECEIVED SEPTEMBER 20, 1966

Identification of a Specific Mode of Oxidation in the Radiolysis of the Purine Bases in Oxygenated Aqueous Solution

Sir: The pyrimidine and purine moieties represent major sites of chemical degradation in the radiolysis of nucleic acids in aqueous solutions containing molecular oxygen.^{1,2} Radiation chemical studies of representative pyrimidines such as cytosine, uracil, and thymine in dilute aqueous solution have shown that OH radicals formed in the radiation decomposition of water add preferentially to the 5,6 carbon-carbon double bond to form the hydroxypyrimidyl radical.^{1,3-5} In oxygenated solution, this radical is scavenged by oxygen and in subsequent steps yields the 5,6 glycol as a radiolysis product.^{1,3,4}

Reaction stoichiometries in the radiolysis of the purines in oxygenated solution remain to be established.^{2,6} Adenine has received the most attention and is reported by Scholes and Weiss^{1,6} to yield ammonia with $G(\text{NH}_3) = 0.5$ (molecule/100 ev) on radiolysis with γ -rays in dilute aqueous solution; they suggest that such deamination arises as a consequence of OH addition to the central 5,6 double bond.⁷ Conlay^{8a} and Ponnamperna, Lemmon, and Calvin^{8b} have isolated organic products from the same system and find 8-hydroxyadenine and 3,4,5-triaminopyrimidine derivatives are produced with G values of several tenths. The latter products provide evidence for OH attack at the 7,8 position of the imidazole ring. Such reaction is in accord with Pullman's molecular orbital calculations⁹ which indicate that the 7,8 bond of the purine nucleus has the highest mobile bond order. However, since the yield for OH production in the radiation decomposition of water corresponds to $G_{\text{OH}} = 2.4$ for γ -rays,¹⁰ it follows that no conclusions regarding the major locus of reaction of OH with the purine

(1) G. Scholes, J. F. Ward, and J. Weiss, *J. Mol. Biol.*, **2**, 379 (1960).

(2) G. Hems, *Radiation Res.*, **13**, 777 (1960).

(3) B. Ekert and R. Monier, *Nature*, **138**, 309 (1960).

(4) R. Latarjet, B. Ekert, and P. Demerseman, *Radiation Res. Suppl.*, **3**, 247 (1963).

(5) (a) A. Kamal and W. M. Garrison, *Nature*, **206**, 1315 (1965); (b) J. Holian and W. M. Garrison, *Radiation Res.*, **27**, 257 (1966).

(6) G. Scholes, *Progr. Biophys.*, **13**, 59 (1963).

(7) We use here the notation in which the carbon-carbon double bond of both the purine and pyrimidine nuclei is referred to as the 5,6 position.

(8) (a) J. J. Conlay, *Nature*, **197**, 555 (1963); (b) G. Ponnamperna, R. M. Lemmon, and M. Calvin, *Radiation Res.*, **18**, 540 (1963).

(9) B. Pullman and A. Pullman, "Comparative Effects of Radiation," M. Burton, *et al.*, Ed., John Wiley and Sons, Inc., New York, N. Y., 1960.

(10) E. Hayon, *Trans. Faraday Soc.*, **61**, 734 (1965).

nucleus can be made on the basis of the reported experimental yields.

Now, if glycol formation at the central 5,6 position is involved in the radiolytic oxidation of the purines, it is clear that such products on mild hydrolysis would liberate a reactive carbonyl function. Uric acid and xanthine, for example, would yield alloxan, whereas the corresponding products from hypoxanthine and adenine would be expected to undergo further hydrolysis with liberation of free mesoxalic acid.¹¹

Oxygen-saturated solutions of uric acid, xanthine, hypoxanthine, and adenine (Calbiochem, A grade, chromat. homogeneous) were irradiated with Co^{60} γ -rays at dosages in the range 2.8 to 5.6×10^{18} ev/ml. The irradiated solutions were made $2 N$ in hydrochloric acid, treated with 2,4-dinitrophenylhydrazine reagent at 70° for 1 hr, cooled, and extracted with chloroform. The hydrazones were then transferred to filter paper and chromatographed with a butanol-ammonia solvent system.¹² Control solutions containing known amounts of alloxan and mesoxalic acid were similarly treated and the authentic hydrazone derivatives were chromatographed in parallel with the irradiation products. Appropriate areas of the chromatogram were eluted and assayed spectrophotometrically. The indicated carbonyl products are formed in the yields given in Table I. Other as yet unidentified carbonyl products, probably dicarbonyls, are also formed, but in low yield.

Table I: Formation of Carbonyl Products in the γ -Radiolysis of Purine Bases in Oxygenated Solution^a

Purine	Concn, mm	Carbonyl product	Yield, % ^c
Xanthine	0.5 ^b	Alloxan	2.0
Hypoxanthine	2	Mesoxalic acid	1.5
Uric acid	0.4 ^b	Alloxan	1.2
Adenine	2	Mesoxalic acid	<0.1

^aYields of the indicated carbonyl products are essentially independent of pH over the range 3 to 7. ^bSolubility limit. ^cYields are essentially independent of dosage up to a maximum conversion of approximately 20% of the parent solute. Initial yields are shown.

In the case of xanthine, the evidence is that OH radicals are quantitatively removed at the 5,6 double bond to give $G(\text{alloxan}) = 2.0 \simeq G_{\text{OH}}$. The carbonyl yields from hypoxanthine and uric acid indicate that although the 5,6 position of these compounds also represents the major locus of OH attack, other competing sites are involved. Adenine, on the other hand, appears to be essentially unreactive at the 5,6 position. That adenine is, nevertheless, undergoing chemical

change is evidenced by the fact that the yield for base destruction under the conditions of Table I (pH 3) corresponds to $G(-B) = 1.8$. This value was obtained through chromatographic isolation (on Dowex 50) of unchanged base from an irradiated solution. Adenine is the only aminopurine of the four purines listed in Table I. The question of whether the amino group is exerting a directing influence or is actually involved chemically as a competing reaction locus remains to be elucidated.

Acknowledgment. This work was performed under the auspices of the U. S. Atomic Energy Commission.

(11) See, for example, G. A. Howard, "Chemistry of the Carbon Compounds," Vol. IV, E. H. Rodd, Ed., Elsevier Publishing Co., Amsterdam, 1967.

(12) B. M. Weeks and W. M. Garrison, *J. Phys. Chem.*, **69**, 4131 (1965).

LAWRENCE RADIATION LABORATORY
UNIVERSITY OF CALIFORNIA
BERKELEY, CALIFORNIA 94720

JOHN HOLIAN
WARREN M. GARRISON

RECEIVED OCTOBER 3, 1966

Thermodynamic Limiting Laws for Impurities in Semiconductors

Sir: The considerations advanced in a recent Note¹ and subsequent Communication² concerning the applicability of Henry's law to dilute solutions of electrically active impurities in metals and semiconductors prompt the following comments.

Henry's law expresses the insensitivity of the chemical environment of a particular solute species to changes in its concentration. Thus, in the example of a donor impurity, one would expect Henry's law to apply in the limit to neutral and ionized donors separately. What O'Keefe actually investigates is the relation between the concentration of neutral donors $[D]$, assumed equal to their activity a_D , and the total donor concentration $N_D = [D] + [D^+]$. His result that the thermodynamic activity of neutral donors in a typical semiconductor is not proportional to the sum of the concentrations of neutral and ionized donors, *i.e.*, $\partial \ln a_D / \partial \ln N_D \neq 1$, does not (except in a trivial way) signify a departure from Henry's law but, rather, is solely a consequence of the varying degree of ionization.³

(1) M. O'Keefe, *J. Phys. Chem.*, **70**, 596 (1966).

(2) M. O'Keefe, *ibid.*, **70**, 2065 (1966).

(3) Actually, for donor concentrations sufficiently small in comparison to n_i , the intrinsic carrier concentration, $N_D = [1 + (K'_D/n_i)] [D]$, a result which in the context of O'Keefe's treatment would be interpreted as conformance to Henry's law (K'_D is here the mass action product for donor ionization).

It has been recognized for some time that beyond the range of applicability of Boltzmann statistics, electrons and holes deviate from ideal solute behavior. In addition to quantum statistical causes of deviation from ideality,⁴ electrons and holes, in common with other imperfections, are subject to solute-solute interactions; under some circumstances the latter effects are determinative and operate to alter the energy gap.⁵ Impurity ionization energies are similarly altered,⁵ *viz.*, decreased by net attractive interactions experienced by occupied and unoccupied states.⁶ The consequent concentration dependence of the ionization energy must be included in calculating the range of applicability of a Henry's law relation to the total impurity concentration.

(4) For a recent discussion, see W. W. Harvey, *J. Phys. Chem. Solids*, **23**, 1545 (1962).

(5) W. W. Harvey, *Phys. Rev.*, **123**, 1666 (1961).

(6) W. W. Harvey, submitted for publication.

LEDGEMONT LABORATORY
KENNECOTT COPPER CORPORATION
LEXINGTON, MASSACHUSETTS 02173

W. W. HARVEY

RECEIVED OCTOBER 4, 1966

Hydrodynamic Shear Stress and the Tensile Strength of Covalent Bonds

Sir: Harrington and Zimm¹ have reported experiments on the degradation of polymers under controlled hydrodynamic shear. Similar experiments carried out previously by us² measured the flow rates in a capillary tube just sufficient to cause a monodisperse solution of DNA molecules of high molecular weight to be ruptured. We assumed that at the moment of rupture the molecule was maximally extended; the tensile stress suffered by the ruptured bond, which was assumed to be close to the center of the molecule, was calculated, and quite good agreement was found between this value and the tensile force which, it was calculated, a covalent bond could withstand. Harrington and Zimm,¹ employing a different formula, calculated critical stresses 30-fold lower than those we determined. Since that date, Pritchard, Hughes, and Peacocke³ have studied the degradation of DNA molecules under sonic irradiation, and the shearing stress they calculate required to break the covalent bond agrees reasonably well with that which we calculated if they employed our formula, but is 100-fold less if they calculate from the formula of Harrington and Zimm. Thus the differences between ourselves and the latter

authors lies not in the experimental results but rather in the interpretation of these results.

Although the results were stated in other terms, the essential assumption made by Harrington and Zimm was that the random coils relevant to static solution are the appropriate configurations to be considered in calculating the tension produced by the hydrodynamic shear. Despite their own findings which showed that the gaussian coil behavior was not consistent with their experimental observations, they applied this model to their calculation. The assumption made by us was that the molecule, when it is being broken, is in a more or less fully extended configuration. The difference between these two treatments is large because the effective tension of the molecule is proportional to the square of the dimension being considered.

One can make various *a priori* arguments as to the plausibility of these two treatments, but these arguments seem somewhat irrelevant since there is good experimental evidence that the molecules are in fact extended at the time of breakage. It is known from our experiments, as well as those of Hershey and Burgi,⁴ that if the hydrodynamic shear is controlled at a level just necessary to produce the first breakage product, the latter has a molecular weight very close to half that of the initial molecule. This is the result expected on our theoretical treatment and totally inexplicable by the treatment used by Harrington and Zimm.

At any instant a randomly coiled molecule in a medium in laminar flow can be expected to have several segments of the backbone traversing the plane through the center of gravity of the molecule across which the tensile stresses will be exerted. If the frictional forces across this plane suffice to break the molecule, there is no reason to suppose this break should be centrally located since any of the crossing points could be the most strained.

One could visualize a coiled molecule becoming extended into two coiled ends with the central region traversing the plane of the center of gravity. In this situation there would of course be a larger force exerted on the molecule than in the situation of a truly random coil, and rupture would be expected to occur toward the middle of the polymer, but the stresses calculated for this model certainly do not relate to dimensions pertaining to a random coil.

(1) R. E. Harrington and B. H. Zimm, *J. Phys. Chem.*, **69**, 161 (1965).

(2) C. Levinthal and P. F. Davison, *J. Mol. Biol.*, **3**, 674 (1961).

(3) N. J. Pritchard, D. E. Hughes, and A. R. Peacocke, *Biopolymers*, **4**, 259 (1966).

(4) A. D. Hershey and E. Burgi, *J. Mol. Biol.*, **2**, 143 (1960).

With the further extension of the molecule, this model leads to the one proposed by us, namely, where the molecule was fully extended. It is impossible to show that such complete extension as used in our calculation would take place in any finite time interval; however, we can see no reason to expect breakage in the center of the molecule without some orientation of the structure along the flow lines, and for such a situation the dimensions of the molecule must be greater than for a random coil. This statement is our major rebuttal to the criticisms of Harrington and Zimm. In spite of the fact that it is not possible to carry out the kinetic calculations in detail, it has been shown with model systems that flexible fibers in laminar flow will not maintain a random configuration,⁵ and in fact the shear dependence of the viscosity of many polymeric materials shows that they do not.

Recent experimental evidence shows that the preferential rupture of DNA molecules in the middle of the polymer under hydrodynamic shear holds even in the case of denatured molecules where the rigidity of the chains is much lower than in the case of native DNA.⁶ Thus, we would conclude that if at the moment of shear even flexible molecules are to some degree extended, then the stiff native DNA molecules may be close to full extension.

Our model would predict that the rupturing shear stress is independent of solvent but not of solvation, and we cannot deduce how a change of solvent would affect the rate at which the molecule can become extended in the brief periods it comes under tension as it is tumbling. In fact, Harrington and Zimm found that the molecules were more readily broken in a poor solvent than in a good solvent. Their observation is directly opposed to the behavior predicted by their model which would assume a greater extension and therefore a lower critical shear for molecules in a good solvent.

Finally, Harrington and Zimm criticized the use of the Lippencott and Schroeder potential function for calculating the breaking strength of the covalent bonds in the DNA backbone. It is true that the equation is properly applicable to the gas phase and its relevance to normal solvated reaction mechanisms can be questioned. However, there is no evidence that shearing proceeds by a hydrolytic process. For polymers in organic solvents, it is known that degradation induced by sonic irradiation and shearing with high speed stirrers proceeds extensively if not entirely with the liberation of the radicals at the points where the polymers break.⁷ There is also evidence for free radical phenomena in sonic degradation of polymers in aqueous solutions, and in view of the striking parallel

between sonic degradation and shearing,^{3,8} it is probable that shear scission in aqueous systems also occurs with the liberation of free radicals, clearly a highly energetic process. A free-radical generating process is, we believe, compatible with tearing the molecule asunder, scarcely with the facilitation of a hydrolytic process. Both the bond stress calculated on our model and the bond strength we calculated are maximal, but it appears to us that both values must be in the right order of magnitude. On the other hand, Harrington and Zimm are forced to postulate unknown mechanisms involved in shear degradation since the activation energy which they calculate is provided by the hydrodynamic forces is too weak to provide significant facilitation of normal hydrolysis. The difficulty in interpretation stems, we believe, from an inappropriate calculation.

(5) O. L. Forgacs and S. G. Mason, *J. Colloid Sci.*, **14**, 473 (1959).

(6) P. F. Davison and D. Freifelder, *J. Mol. Biol.*, **16**, 490 (1966).

(7) W. R. Johnson and C. C. Price, *J. Polymer Sci.*, **45**, 217 (1960).

(8) D. Freifelder and P. F. Davison, *Biophys. J.*, **2**, 235 (1962).

DEPARTMENT OF BIOLOGY
 MASSACHUSETTS INSTITUTE OF TECHNOLOGY
 CAMBRIDGE, MASSACHUSETTS 02139

CYRUS LEVINthal
 PETER F. DAVISON

RECEIVED OCTOBER 6, 1966

A 2:1 Solid-State Complex of HMB·TCNE¹

Sir: Although pyrene and pyromellitic dianhydride tend to form a 1:1 crystalline molecular complex, Ilmet and Kopp have recently discovered that, using rather extreme conditions, the 2:1 crystalline complex may be obtained.² They proposed that the 2:1 crystal is composed of alternating stacks of the 1:1 complex and pure pyrene, but this certainly has not been confirmed.

In a related study, we have found that well-defined needle-shaped crystals of a 2:1 complex of hexamethylbenzene (HMB) and tetracyanoethylene are easily deposited from an ether solution. In this case, however, the infrared spectra and, in particular, the infrared dichroism exhibited by these crystals show conclusively that the extra HMB molecules are incorporated into the complex stacks so that the simplest and most likely structure can be represented as $-D \cdot A \cdot D -$.

The 2:1 complex crystals were prepared by mixing 2 mmoles of HMB with 1 mmole of TCNE in 50 ml of ether within a standard 100-ml beaker followed by

(1) Supported by the National Science Foundation.

(2) I. Ilmet and L. Kopp, *J. Phys. Chem.*, **70**, 3371 (1966).

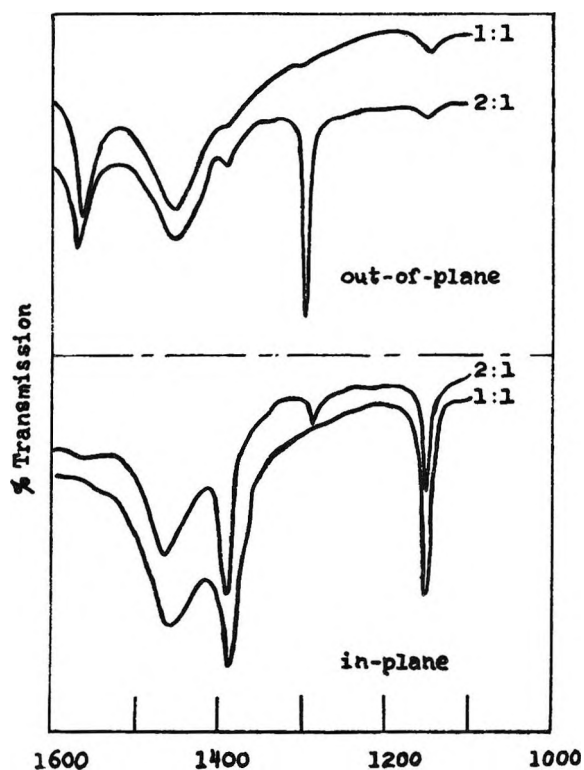


Figure 1. Infrared spectra in the 1100–1600- cm^{-1} range for the 1:1 and 2:1 crystalline complexes of HMB and TCNE.

evaporation at the rate of 10 ml/hr. During evaporation, parallel needle crystals of the 2:1 complex were continuously deposited on a polished NaCl window positioned upright in the center of the beaker. Under a microscope the resulting pattern appeared to be as well ordered as for the 1:1 crystal which had been studied previously.³

The infrared spectra in Figure 1 are confirmation of the orderly arrangement of the crystals, as nearly perfect separation of in-plane and out-of-plane infrared activity was invariably achieved by orienting the needle

axes alternately perpendicular to and parallel to the electric vector of the polarized infrared radiation. The most interesting spectral feature relates to the 1295- cm^{-1} totally symmetric C-CH₃ stretching mode of HMB. Ferguson and Chang have shown that this normally inactive mode is strongly activated in the HMB·I₂ complex in solution⁴ and have properly attributed this activity to a vibronic interaction unique to such complexes.⁵ The charge oscillation between donor and acceptor, characteristic of this vibronic interaction, is symmetry canceled in the -D·A·D·A-stacks in the 1:1 crystal of HMB·TCNE so that, as can be seen from Figure 1, no absorption occurs at 1295 cm^{-1} .

However, in the proposed structure for the 2:1 crystal, the symmetry about the donor molecules is lowered so that symmetry cancellation of the vibronic charge oscillation is no longer possible. One would thus predict and, in fact, observes strong activity at 1295 cm^{-1} in the 2:1 complex. The existence of this strong absorption, having the predicted out-of-plane character, plus the obvious stacked character of the crystal is considered strong evidence for the proposed crystal structure. It is also noteworthy that the infrared activity at 1560 cm^{-1} , attributable to the totally symmetric double bond mode of TCNE,³ is quite similar in the 2:1 and 1:1 crystals. This is consistent with the expectation that the symmetry about the acceptor is comparable in the two crystals.

(3) J. Stanley, D. Smith, B. Latimer, and P. Devlin, *J. Phys. Chem.*, **70**, 2011 (1966).

(4) E. E. Ferguson and I. Y. Chang, *J. Chem. Phys.*, **34**, 628 (1961).

(5) H. B. Friedrichs and W. B. Person, *ibid.*, **44**, 2161 (1966).

DEPARTMENT OF CHEMISTRY
OKLAHOMA STATE UNIVERSITY
STILLWATER, OKLAHOMA

BOBBY HALL
J. PAUL DEVLIN

RECEIVED NOVEMBER 21, 1966